DEVELOPMENT OF NOVEL MODULATORS OF PROTEIN-PROTEIN INTERACTIONS ASSOCIATED WITH CANCER

Alan Healy

A Thesis Submitted for the Degree of PhD
at the
University of St Andrews

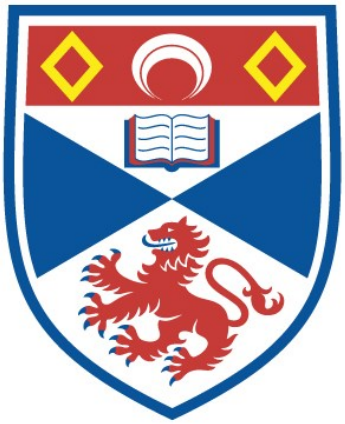

2014

Development of Novel Modulators of Protein-Protein Interactions Associated with Cancer

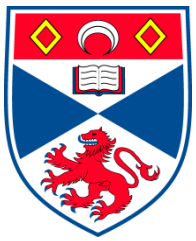

Alan Healy

This thesis is submitted in partial fulfilment for the degree of PhD

at the

University of St Andrews

August 2014

1. Candidate's declarations:

I, Alan Healy, hereby certify that this thesis, which is approximately 87,000 words in length, has been written by me, that it is the record of work carried out by me and that it has not been submitted in any previous application for a higher degree.

I was admitted as a research student in September 2011 and as a candidate for the degree of PhD in September 2012; the higher study for which this is a record was carried out in the University of St Andrews between 2011 and 2014.

Date 29th August 2014 Signature of candidate

2. Supervisor's declaration:

I hereby certify that the candidate has fulfilled the conditions of the Resolution and Regulations appropriate for the degree of PhD in the University of St Andrews and that the candidate is qualified to submit this thesis in application for that degree.

Date 29th August 2014 Signature of supervisor

3. Permission for electronic publication:

In submitting this thesis to the University of St Andrews I understand that I am giving permission for it to be made available for use in accordance with the regulations of the University Library for the time being in force, subject to any copyright vested in the work not being affected thereby. I also understand that the title and the abstract will be published, and that a copy of the work may be made and supplied to any bona fide library or research worker, that my thesis will be electronically accessible for personal or research use unless exempt by award of an embargo as requested below, and that the library has the right to migrate my thesis into new electronic forms as required to ensure continued access to the thesis. I have obtained any third-party copyright permissions that may be required in order to allow such access and migration, or have requested the appropriate embargo below.

The following is an agreed request by candidate and supervisor regarding the electronic publication of this thesis:
(iii) Embargo on both of printed copy and electronic copy for the same fixed period of 1 year on the following ground:
Publication of this thesis in either printed or electronic form would preclude future publication

Date 29th August 2014
signature of candidate signature of supervisor

Abstract

An understanding of the underlying mechanisms by which proteins engage and communicate within the complex cellular environment is critical to the elucidation of the molecular basis of disease states and the development of safer, more efficacious drug therapies. Diverse cellular functions, including replication, transcription, cell growth and intracellular signal transduction, are governed by extensive networks of protein-protein interactions (PPIs). Disruption of the finely-tuned cellular networks due to the formation of aberrant or unregulated PPIs is implicated in the development and progression of cancer. As a result, over the last decade, PPI modulation has developed as an attractive molecular target for novel cancer therapies and as a powerful research tool in chemical biology to provide insight into the cellular transformations involved in carcinogenesis.

Chapter 1 provides a review of the physiological importance of PPIs and the role they play in the development and progression of cancer. A summary of the challenges associated with targeting PPIs is given, highlighting the changing perception regarding the drugabbility of PPIs and the technological and conceptual advances driving this transformation. A brief overview of the approaches used to identify PPI modulators links the reader to the appropriate chapter for further discussion and utilisation of a selection of these methods.

Chapter 2 describes the application of a virtual screening approach to discover PPI modulators. In particular, the development of an *in silico* – *in vitro* screening method to identify modulators of the protein interactome of the AAA+ protein reptin. The synthesis and optimisation of two hit compounds is outlined, with a discussion of their predicted binding modes, mode of action, potential as chemical tools and lead molecules for an anti-cancer drug discovery programme.

Chapter 3 highlights the potential to discover PPI modulators from Nature's rich source of structurally complex, bioactive molecules. A synthetic approach to a sub-family of tetramic acid natural products is outlined, involving the development of a short, asymmetric synthesis of unnatural 4,4-disubstituted glutamic acid derivatives. The first total syntheses of the potent siderophore harzianic acid and the PAC3 PPI inhibitor JBIR-22 are reported. In addition, the potential role of a Diels-Alderase enzyme in the biosynthesis of JBIR-22 and the development of a chiral catalysed intramolecular Diels-Alder of an advanced JBIR-22 intermediate is investigated.

Chapter 4 discusses the use of structure based design techniques in the development of PPI modulators. The process involved in the design of two series of inhibitors of PICK PDZ domain mediated interactions is outlined. This leads to the development and optimisation of synthetic routes to both series of inhibitors, including the utilisation of a strategic sp^3-sp^2 cross coupling reaction. Finally, preliminary biological assessment of the inhibitors is reported.

Chapter 5 gives a brief overview of high-throughput screening (HTS) methods used to identify PPI modulators. The utilisation of a forward chemical genetics screen to identify the p53 activator MJ05 is described. A racemic and asymmetric route to MJ05 is developed and biochemical analysis of the two enantiomers of MJ05 is reported including the investigation of MJ05 as an adjuvant therapy for the treatment of cancer.

Chapter 6 provides a general overview of the outcome of the different approaches used in this research to discover PPI modulators. Particular emphasis is placed on the development of chemical tools for the elucidation and dissection of the physiological role of protein-protein interactions and the identification of novel drug targets, in addition to the identification of lead molecules for PPI drug development programmes.

Acknowledgements

Firstly, I would like to thank Prof Nick Westwood for giving me the opportunity to carry out my PhD in his laboratory as part of the CRUK medicinal chemistry training programme. Nick encouraged and supported my development as a scientist, in particular by giving me the opportunity and guidance to develop new projects and explore different ideas, which was a rare and fantastic learning experience.

I would also like to thank all the members of the Westwood group, both past and present for all their help and wisdom. In particular, Dr Fanny Tran who has done a very thorough and excellent job proof reading this thesis and many other documents over the years. I would also like to thank Chris Lancefield, Craig Johnston, Graeme Rogers and Ross Wilkie for being great sounding boards and sources of advice for some of my crazier ideas. And I cannot forget Agathe D'Hollander and Ciaran Lahive who sustained me through the last year with French sweets and tar-like coffee.

I am especially grateful to all the members of staff in the School of Chemistry, including Mrs Caroline Horsburgh (mass spectrometry), Dr Tomas Lebl and Mrs Melanja Smith (NMR spectroscopy) and Prof Alexandra Slawin and Dr David Cordes (small molecule X-ray crystallography).

I have had the opportunity to work with fantastic collaborators in numerous different fields of research which has provided a great learning experience. I would like to thank all of the collaborators mentioned in this thesis, and in particular, Prof Ted Hupp, Dr Sonia Lain, Dr Doug Houston and Prof Kenneth Masden.

I would like to thank all the people who have made the past four years in St Andrews a wonderful and fun experience. From rounds of golf on the Old Course to extensive whiskey tasting, it will not be forgotten. I am especially grateful for the love and support of my family, especially my parents Michele and Richard and my brothers Sean and Luke. They have been unwavering in their support and encouragement.

And finally, I owe a huge debt of gratitude to my wonderful partner Caroline, who has been my rock, my biggest supporter and my best friend. I could not have achieved what I have without her by my side and I can't wait for our next adventure together.

Abbreviations and Acronyms

3D	Three dimensional
AAA+	ATPases associated with various cellular activities
Ac	Acetyl group (-$COCH_3$)
AcOH	Acetic acid (CH_3CO_2H)
ADME	Absorption/distribution/metabolism/excretion
ADP	Adenosine diphosphate
AHL	*N*-acyl homoserine lactone
Ala	Alanine
AMPAR	α-Amino-3-hydroxy-5-methyl-4-isoxazolepropionic acid receptor
Arg	Arginine
Asp	Aspartic acid
ATP	Adenosine triphosphate
BLAST	Basic local alignment search tool
br.	Broad (NMR spectroscopy)
^{i}Bu	*iso*-Butyl group (-$CH_2CH(CH_3)_2$)
^{n}Bu	*n*-Butyl group (-$(CH_2)_3CH_3$)
^{t}Bu	*tert*-Butyl group (-$C(CH_3)_3$)]
^{t}BuOK	Potassium *tert*-butoxide
CAB	Chiral acyloxyborane
CADD	Computer aided drug discovery
CBD	Carboxylate binding domain
CCl_4	Carbon tetrachloride
Conc.	Concentrated
COSY	Correlation spectroscopy (NMR)
CML	Chronic myelogenous leukemia
(CT)-HMBC	Constant time - heteronuclear multiple bond correlation
d	Doublet
DA	Diels-Alder
DAT	Dopamine active transporter
DCM	Dichloromethane
DDQ	2,3-Dichloro-5,6-dicyano-1,4-benzoquinone
δ	Chemical shift in ppm (NMR)

DMF	*N*,*N*,-Dimethylformamide
DMSO	Dimethyl sulfoxide
ED_{50}	Effective dose for 50% of the population
ELISA	Enzyme-linked immunosorbent assay
equiv./eq.	Equivalents
ES	Electrospray (mass spectrometry)
Et	Ethyl group (-CH_2CH_3)
et al	*Et alia* (latin), and others
Et_2O	Diethyl ether
EtOAc	Ethyl acetate
EtOH	Ethanol
EXSY	Exchange spectroscopy
FCG	Forward chemical genetics
FP	Fluorescence polarisation
FRET	Fluorescence resonance energy transfer
FT	Fourier transform
GC	Gas chromatography
Gln	Glutamine
Gly	Glycine
GPCR	G protein-coupled receptors
h	Hour(s)
HIV	Human immunodeficiency virus
HMBC	Heteronuclear multiple bond correlation (NMR)
HMT	Histone-lysine-methyltransferase
HNDF	Human normal dermal fibroblasts
HPLC	High-performance liquid chromatography
HRMS	High resolution mass spectrometry
HSQC	Heteronuclear single quantum coherence (NMR)
HTS	High-throughput screening
IC_{50}	Half maximal inhibitory concentration
Ile	Isoleucine
IMDA	Intramolecular Diels-Alder
^{i}Pr	*iso*-Propyl group (-$CH(CH_3)_2$)
IR	Infrared

J	Coupling constant (NMR)
k_i	Dissociation constant of an inhibitor from an enzyme complex
Lit.	Literature
LLS	Longest linear sequence
LRMS	Low resolution mass spectrometry
Lys	Lysine
m	Multiplet (NMR spectrometry)
MD	Molecular dynamics
MDM2	Mouse double minute 2
Me	Methyl group ($-CH_3$)
MEME	Multiple EM for motif elicitation
MeOH	Methanol
min	Minute(s)
MLL1	Mixed lineage leukemia 1
Mp	Melting Point
MS	Mass spectrometry
m/z	Mass over charge ratio (mass spectrometry)
NMR	Nuclear magnetic resonance
NOE	Nuclear Overhauser effect
NRPS	Nonribosomal peptide synthetase
NTP	Nucleoside triphosphate
PAC3	Proteasome assembling chaperone 3
PAINS	Pan assay interference compounds
PBD	Polo-box domain
PBDD	Peptide-based drug discovery
PCA	Protein fragment complementation assay
PCC	Pyridinium chlorochromate
PDB	Protein data bank
PDZ	PSD-95/Discs-large/ZO-1 homology domain
PICK1	Protein interacting with C kinase
PIKK	Phosphatidylinositol-3 kinase–related kinase
PKS	Polyketide synthase
PP2A	Protein phosphatase 2
PPA	Polyphosphoric acid

PPI	Protein-protein interaction
^{n}Pr	*n*-propyl group (-$CH_2CH_2CH_3$)
Ph	Phenyl group (-C_6H_5)
Phe	Phenylalanine
ppm	Parts per million
q	Quartet (NMR spectroscopy)
R	Generic group
RMSD	Root-mean-square deviation
r.t.	Room temperature
RTK	Receptor tyrosine kinase
s	Singlet (NMR spectroscopy)
SAR	Structure activity relationship
SEC-MALS	Size exclusion chromatography – multiangle light scattering
Siam	Bis(sulfinyl)imidoamidine
snoRNP	small nucleolar Ribonucleoprotein
t	Triplet (NMR spectroscopy)
TD_{50}	Toxic dose for 50% of the population
TFA	Trifluoroacetic acid
TfOH	Triflic acid
THF	Tetrahydrofuran
TLC	Thin layer chromatography
TOF	Time of flight (mass spectrometry)
TPAP	Tetrapropylammonium perruthenate
Ts	Tosyl group (-$OSO_2C_6H_4CH_3$)
TKI	Tyrosine kinase inhibitor
Tyr	Tyrosine
UV	Ultraviolet
Val	Valine
vs	Versus
v	Wavenumber (IR spectroscopy)
VS	Virtual screening
XIAP	X-linked inhibitor of apoptosis protein

Contents

1 General Introduction

Landmark technological and conceptual advances in biochemistry, molecular cell biology and genomic technologies have progressively transformed contemporary understanding of the extensive and responsive protein interaction networks which regulate essential cellular processes.[1] Genome-wide proteomic studies have heightened awareness of the significant and ubiquitous role of protein-protein interactions (PPIs) in cellular physiology.[2] Critical cellular functions, including replication, transcription, cell growth and intracellular signal transduction, are all governed either by finely-tuned PPI mediated transient protein interactions or by the formation of dynamic multiprotein complexes.[3,4] An understanding of the underlying mechanisms of how proteins engage and communicate within the extensive cellular network has allowed the elucidation of the molecular basis of a number of disease states, especially complex multifactorial ones such as cancer.

1.1 PPIs and Cancer

A variety of genetic and epigenetic alterations induce the transformation of normal cells into cancer cells through the acquisition of physical and molecular characteristics that promote tumorigenesis. These hallmarks of cancer include sustained independent proliferation, evasion of growth suppressors and apoptotic signals and the ability to metastasise to distal sites.[5–7] The development and progression of cancer is at least in part determined by a combination of alterations in the operation of finely-tuned PPI networks.[8] It is now well established that aberrant protein-protein interactions, either from the loss of essential interactions, unchecked cellular signalling and formation and/or stabilisation of a protein complex at the wrong time or location can result in intracellular malfunctions, such as the uncontrolled cell growth that typifies cancer.[3,4,9] Several PPI complexes have been implicated in the acquisition of the hallmark characteristics of cancer, the relay of oncogenic signals and the progression and maintenance of the malignant phenotype.[10] Thus, over the last decade, PPI modulation has developed as an attractive molecular target for novel cancer therapies and as a powerful research tool in chemical biology to advance our understanding of the underlying mechanisms involved in carcinogenesis.[11,12]

1.2 PPI Modulators

The major motivation driving PPI drug discovery is the potential to provide safer and more effective therapies for complex diseases, given the ubiquitous importance of PPIs to cellular pathology, and their orthogonality to conventional drug targets.[1] Traditional drug development campaigns have primarily focused on conventional protein targets such as enzymes and transmembrane receptors, which have well defined active sites using a "static" protein model.[12] This approach has historically been highly effective and profitable, but an over-reliance on similar small molecules targeting related protein targets has resulted in increased cases of resistance, poor selectivity and often poor efficacy against complex multiprotein diseases. This crisis in the pharmaceutical industry has highlighted the need for innovative approaches to discover novel drug leads, particularly targeting the increasingly prevalent diseases such as cancer and neurodegenerative disorders.[1]

Several excellent reviews have been published which detail the challenges and successes of targeting PPIs,[1,3,12–16] particularly towards the development of cancer therapies.[2,4,8,10,11,17,18] Despite their pivotal role in carcinogenesis, the interest in PPIs as drug targets has historically been tempered by the pervasive view that the large and often noncontiguous nature of the PPI interface hampers their druggability. The shallow and often featureless interface surface is in sharp contrast to the well-defined, deep pockets of conventional enzyme and receptor drug targets. Furthermore, unlike traditional drug targets, the majority of PPIs do not have endogenous substrate or ligands which can be exploited as a natural chemical starting point. Despite these challenges, major inroads into discovering and developing PPI modulators have been made in recent years as a result of significant advances in screening technologies, computational modelling techniques and in particular the identification of hot spots on protein interaction surfaces. Large mutational studies revealed that the majority of PPI interfaces contain a critical interaction site which is responsible for a disproportionate contribution to the binding energy of the two proteins.[19,20] The binding of small molecule modulators to these hotspots can modulate a protein interaction which occurs over a much larger surface area. Additional innovative breakthroughs have demonstrated that a significant proportion of protein-protein interactions are driven by linear peptide motifs[21] which can be targeted using peptides or peptidomimetics. In addition to traditional PPI interface modulation, an increasing number of orthosteric or allosteric modulators have been reported which alter a target PPI by inducing a change in the conformation or oligomeric state of one or more of the protein partners.[11,22,23] This increasing and compelling body of evidence is dispelling the dogma that PPIs are intractable drug targets. This change in perception in the pharmaceutical industry is mirrored by the fact that there are more than 12 small molecule PPI modulators currently in clinical development as cancer therapeutics.[11] Examples of these include, Nutlin-3 (**1**) an inhibitor of the p53-MDM2 PPI,[24,25]

an important complex involved in the neutralisation of tumour suppressor functions and Navitoclax (**2**) an inhibitor of the BH3-domain mediated PPIs of Bcl-2, an important regulator of apoptosis (Figure 1.1).[26]

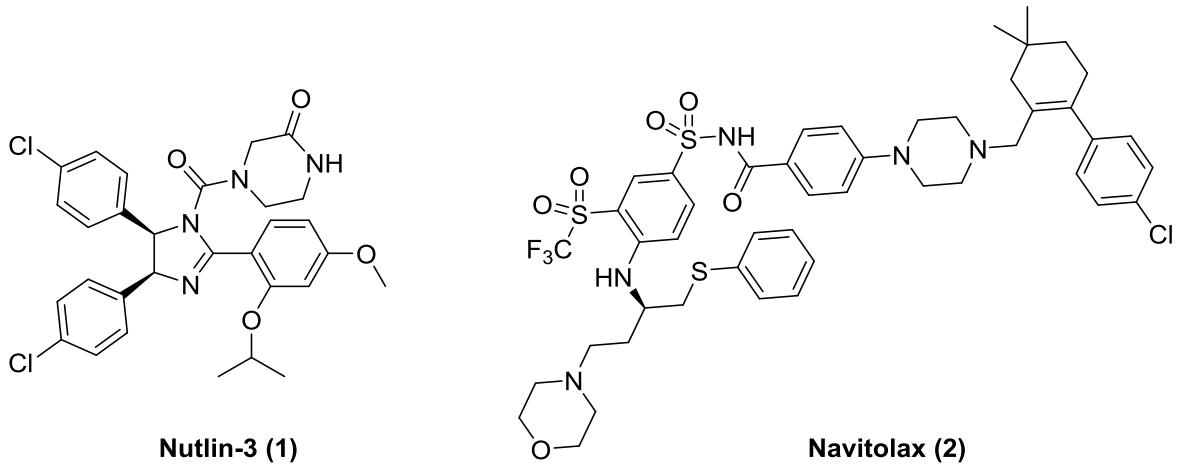

Figure 1.1. Examples of PPI modulators in clinical development as cancer therapeutics.

1.3 Approaches for the Identification of PPI Modulators

Traditional medicinal chemistry approaches which have been highly successful at addressing classical drug targets have proven to be less effective for the more unconventional PPI drug targets.[4] However, innovative approaches involving organic chemistry, chemical biology and computational modelling are valuable methods for the identification and development of novel PPI drug modulators. The main strategies used to discover modulators can be grouped into three inter-related groups – namely, 1.) compound library screening, 2.) natural product-inspired PPI modulation and 3.) structure-based design; which are discussed in an extensive review published by Milroy *et al*.[1] For the purpose of this thesis, a concise summary of these approaches will be outlined here and referenced to the appropriate chapter in which aspects will be described in further detail (Figure 1.2).

High-throughput screening (HTS) of large compound libraries can be a highly effective method to discover new PPI modulators (Figure 1.2). Typical methods involve screening commercial libraries of small molecules (see Chapter 5) or fragments against a target PPI. Increasing the diversity, complexity and biological relevance of the screening libraries can greatly improve the likelihood of identifying a new drug lead. However, significant challenges can arise as a result of increasing the library size with regards to sample handling, assay miniaturisation and the method of hit detection. *In silico* or virtual screening can provide a useful alternative, by identifying a smaller, focused subset

of predicted modulators of the target PPI from a large compound library prior to *in vitro* assessment (see Chapter 2).

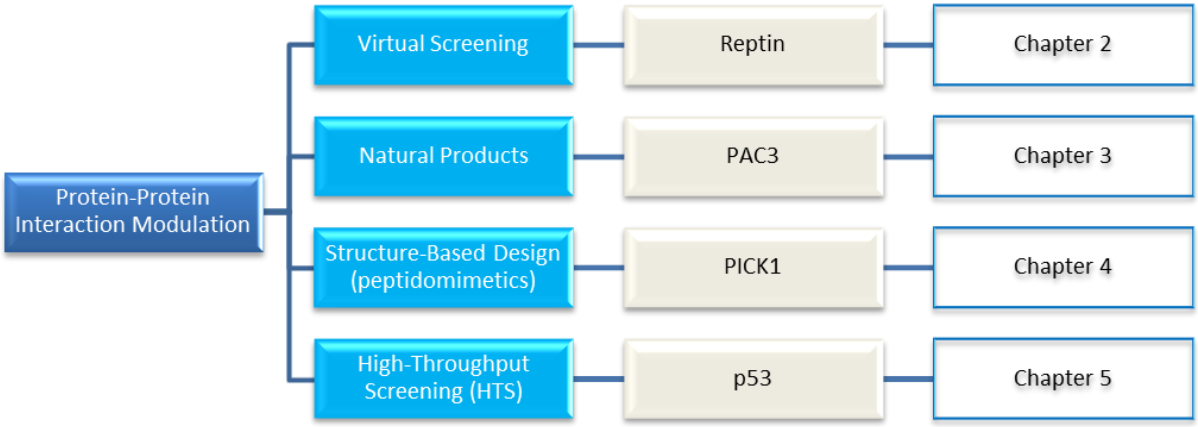

Figure 1.2. Overview of the methods utilised in this research towards the identification of PPI modulators.

Over the past century, natural products have provided a rich source of drug molecules due to their inherent biological activity, unrivalled structural complexity and the diversity of chemical space which they occupy (Figure 1.2). Challenges associated with accessing sufficient quantities of biologically active natural products and diverse analogue libraries have fostered a range of new techniques. These include semisynthesis (chemical modification of an advanced intermediate from nature), mutagenesis (reprogramming of a biosynthetic pathway or engineering an artificial cellular synthetic system to assemble natural products in a host organism) and biology-oriented synthesis (generation of a focused library of structurally diverse compounds based around validated scaffolds which predominate in drug molecules and natural products). However, the total synthesis of a complex natural product is frequently the principal approach used for structural elucidation/confirmation, and as a method to provide sufficient material for initial biological evaluation (see Chapter 3).

Structure-based design approaches exploit the peptide binding epitope of one of the protein partners as a chemical starting point for the development of a modulator (Figure 1.2). Numerous examples of three-dimensional X-ray crystallographic or NMR spectroscopic structures of proteins complexed with their biological partners have facilitated the rational structure-based design of conformationally constrained peptides, peptidomimetics (see Chapter 4) and mimetics of protein secondary structure as novel PPI modulators.

These approaches provide viable methods for the identification of PPI modulators as chemical tools to study a protein's role in oncogenesis or as validation of new drug targets. In this thesis (Figure 1.2), the utilisation of a range of screening approaches to identify chemical tools to study and validate novel anticancer targets such as reptin (Chapter 2), PAC3 (Chapter 3) and PICK1 (Chapter 4) are described. Furthermore, PPI modulators identified through these approaches could be optimised and developed as drug leads against these novel targets, or as improved therapies for well-validated cancer targets such as the tumour suppressor protein, p53 (Chapter 5).

2 A Virtual Screening Approach to the Discovery of PPI Modulators of the AAA+ Protein Reptin

2.1 Introduction

2.1.1 Virtual screening

Virtual screening (VS; also known as *in silico* screening) is a computer aided drug discovery (CADD) process which involves the fast computational screening of a library of chemical entities, in order to identify compounds that have the greatest potential to interact with a particular protein target[27] and, in this context modulate a specific PPI. VS can be used as a stand-alone method to identify a limited set of compounds for *in vitro* evaluation, thereby speeding up the drug discovery process and reducing costs. It can also be used as a prelude to high-throughput screening (HTS, see Chapter 5 for further discussion of HTS) to provide a more focused and selective compound collection for evaluation, which can reduce the cost of this process and increase hit rates.[11] *In silico* compound libraries are derived from several sources, such as commercial and non-commercial supplier databases which can contain marketed drugs, natural products or even sets of 'virtual' compounds that arise from *in silico* combinatorial chemistry.[28] For a VS project, the compound collection typically undergoes several *in silico* ADME/tox filtering steps in an attempt to remove compounds with undesirable physiochemical properties and promiscuous compounds (PAINS, Figure 2.1).[29]

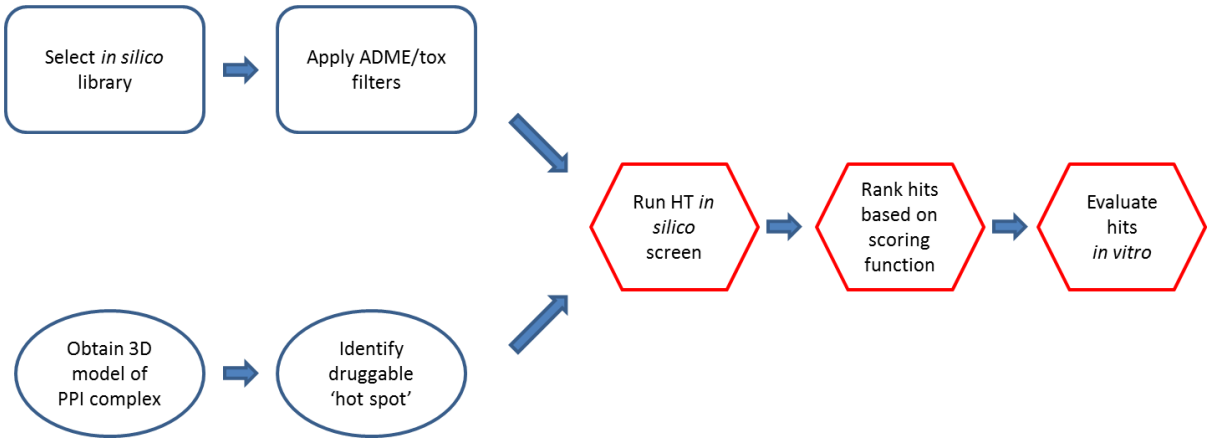

Figure 2.1. Virtual screening workflow.

The nature of the VS approach depends on the availability of a 3D structure of the target protein or protein-protein complex.[11] In cases where the structure has been obtained, either by X-ray crystallography, NMR analysis or homology modelling, potential modulators can be identified

through high-throughput docking strategies.[14] This method involves screening an *in silico* library to identify compounds with the ability to interact with an experimentally determined druggable pocket or 'hot spot' on the protein interaction surface (Figure 2.1). Molecular docking simulations use a computational algorithm (DOCK, Glide, GOLD, AutoDock, Vina, etc.) to assess a compound's ability to interact at the protein's hot spot, which is in turn ranked based on a scoring function (ChemScore, X-score, DrugScore).[14] Numerous examples of modulators identified by VS that target cancer-related PPIs have been published, including for XIAP–caspase 9.[11] X-linked inhibitor of apoptosis protein (XIAP) inhibits caspase mediated apoptotic cell death and is upregulated in many cancers, including breast, pancreas, prostate and solid tumours.[10] The programme DOCK[30] was used to screen a library comprised of 8,000 small molecules against the XIAP BIR3 domain.[31] The compounds were ranked using X-score and 36 of the top 200 hits were assessed in a fluorescence polarisation assay (FP). Five of the 36 compounds showed affinity for the XIAP BIR3 domain, with one compound, Embelin (**1**) having an IC_{50} value of 4.1 µM (Figure 2.2). Embelin (**1**) inhibits prostate cancer cell (PC-3 and LNCaP) growth with an IC_{50} value of 3.7 µM and 5.7 µM respectively, and induces apoptosis in PC-3 cells *via* activation of caspase 9.[31]

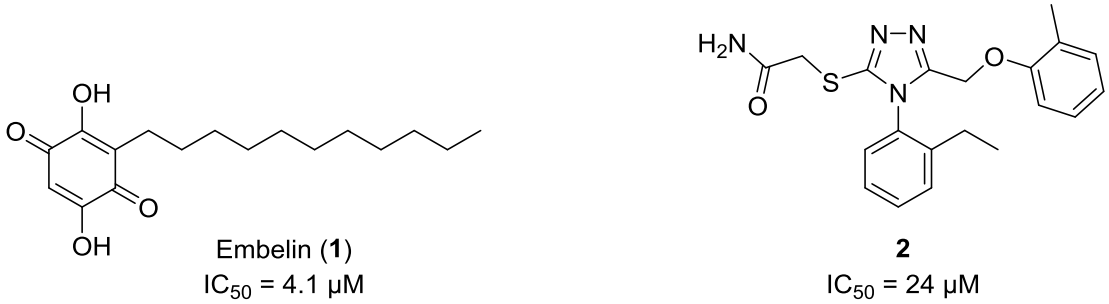

Figure 2.2. Structures of the PPI inhibitors Embelin (1)[31] and 2[32] identified through a VS approach.

An alternative VS approach involves the identification of the binding epitope of one of the proteins involved in a specific interaction and the representation of this motif as a pharmacophore.[11] This pharmacophore then enables the screening of an *in silico* compound library to identify compounds that contain the essential functional groups in the correct 3D conformation.[33] Compounds are then ranked and selected for further bioassay evaluation based on how well they satisfy the pharmacophore. The pharmacophore-based approach has been used successfully in the identification of substituted 1,2,4-triazoles as inhibitors of the S100A10-annexin A2 PPI, which is implicated in the process of neo-angiogenesis and the recruitment of macrophages to tumour sites.[34] In addition, S100A10 has recently been identified as a potential therapeutic target for the treatment of colorectal cancer.[35] The crystal structure of the S100A10-annexin A2 complex was used to generate a pharmacophore model which represented the amino acid interactions present at the annexin A2-binding site on the S100A10 protein.[32] This model was used to screen a virtual library of

704,000 commercially available compounds. The 586 compounds which satisfied the pharmacophore were subsequently docked using the programme GOLD[36] into the annexin A2-binding site. GOLD docking scores were used to select 190 compounds for further *in vitro* evaluation using a competitive FRET assay. This resulted in the identification of inhibitor **2**, which had an IC_{50} value of 24 µM against the S100A10-annexin A2 PPI (Figure 2.2), providing the basis for a medicinal chemistry optimisation programme.[32]

The identification of modulators of PPIs, in cases where the binding interface has not been identified or no 3D structure of the PPI complex is available, is considerably more challenging. This is particularly relevant for PPIs, involving a membrane bound protein or a signalling or chaperone protein which forms dynamic and transient interactions.[23] The identification of novel modulators in these cases has mainly been possible through HTS approaches.[11] However, a growing area of research has focused on the identification of small molecules, which bind to novel allosteric 'hot spot' on the target protein and affect its PPIs through modulation of its conformation or oligomeric state, e.g. TNF,[37] survivin,[38] iNOS[39].[40,41] It is with this approach in mind that we undertook a virtual screen to identify small molecules, which bind at the ATP pocket of the AAA+ protein reptin, and consequently modulate its protein-protein interactome.

2.1.2 The multifaceted AAA+ protein reptin

Reptin, also known as Ruvbl2 and Tip48, is a highly conserved member of the ATPases associated with various cellular activities (AAA+) family of proteins. The role of reptin as an important regulator of key cellular functions through a range of diverse PPIs has been extensively discussed in several excellent reviews.[42–45] Reptin is present in numerous protein and nucleoprotein complexes and is implicated in biological processes such as transcriptional regulation, chromatin remodelling, DNA damage response and ribonucleoprotein complex biogenesis (Figure 2.3). It is an integral subunit of several chromatin-modifying complexes, including Ino80 in yeast and animals,[46,47] Tip60 in animals,[48,49] Swr1 in yeast[50] and the equivalent SRCAP in animals.[51] Reptin is often coexpressed with pontin,[52] a highly conserved ortholog of reptin. Reptin and pontin frequently share common binding partners and help assemble complexes containing members of the phosphatidylinositol-3 kinase–related kinase (PIKK) family,[53] which participate in many signalling pathways, including those involved in regulating nutrient sensing, RNA metabolism, and DNA damage response. Reptin's participation in transcriptional regulatory complexes with a clear involvement in oncogenesis, such as those involving c-myc[54] or β-catenin[55,56] and its role in assembling the telomerase holoenzyme[57] will be discussed further in Section 2.1.4. Extensive research regarding the structural and oligomeric

organisation of reptin is likely key to understanding its diverse role in numerous biological processes.[42]

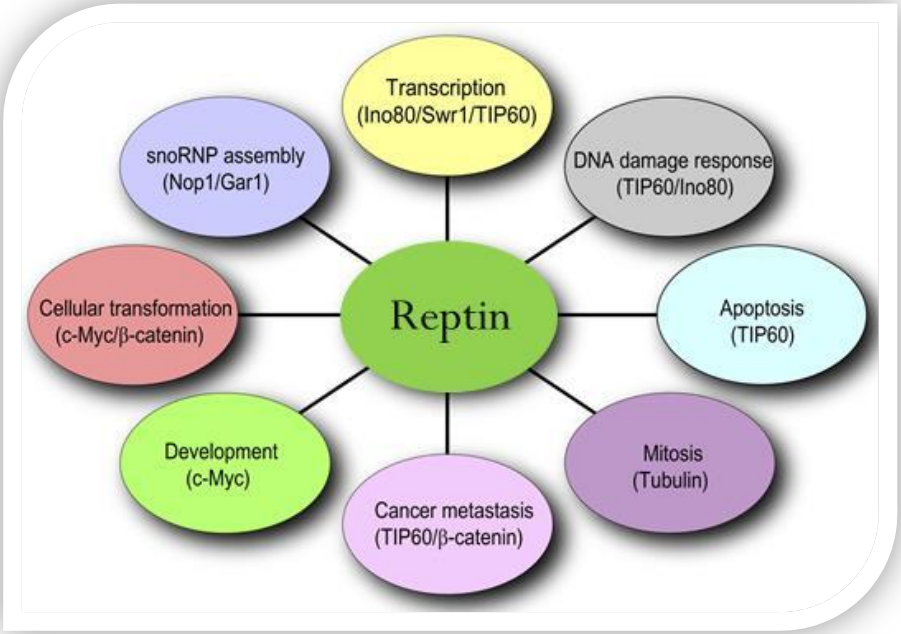

Figure 2.3. Reptin is involved in multiple cellular pathways. Schematic representation of reptin's involvement in transcription, DNA damage response, small nucleolar ribonucleotide protein (snoRNP) assembly, cellular transformation, cancer metastasis, apoptosis, mitosis, and development. Figure adapted from Jha *et al*.[43]

2.1.3 Structure and oligomeric nature of reptin

Recent X-ray crystal structures[58–60] and cryo-electron microscopy structures[61,62] have provided important details about the structure of human reptin and pontin. High-resolution X-ray crystal structures of hexameric pontin,[58] a dodecameric complex of reptin and pontin consisting of two heterohexameric rings (Figure 2.4A)[59] and hexameric reptin[60] have been reported to date. These have revealed that each reptin/pontin monomer consists of three distinct structural domains (Figure 2.4B). Domain I (DI, mainly N-terminal) and domain III (DIII, C-terminal) form the archetypical ATPase module of AAA+ proteins. The ATPase domain consists of two integral parts; the P-loop NTP binding motif (also known as the Walker A box) and the DEAD motif (also known as the Walker B box). The Walker A motif (consensus GxxGxK[S/T], where x is any amino acid) is involved in nucleotide binding and metal-ion coordination. The Walker B motif (consensus φφφφDE, where φ is a hydrophobic amino acid) plays an important role in ATP hydrolysis and metal-ion coordination. The ATPase domain also contains an arginine finger which coordinates ATP hydrolysis in the hexamer and the sensor I and II domains. The sensor I domain distinguishes between the nucleotide diphosphate and triphosphate bound states whereas a highly conserved arginine residue in the sensor II binds across

the nucleotide binding site differentiating between the nucleotide bound and unbound states. The Walker A and B motifs are separated by domain II; a 170 amino-acid insert which protrudes out of the hexameric ring and is proposed to function as a nucleic acid binding site (Figure 2.4B).[45]

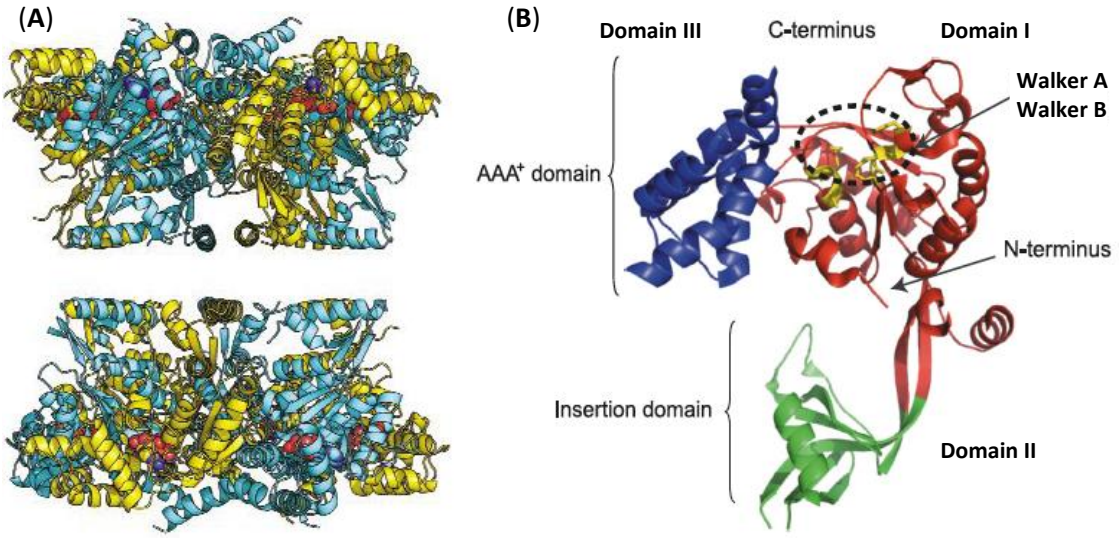

Figure 2.4. Structures of the pontin monomer and the reptin-pontin dodecamer. (**A**) Ribbon diagram of the reptin-pontin dodecamer with truncated domain II [PDB 2XSZ]. Pontin monomers are shown in yellow; reptin monomers are shown in light blue. ATP ligands represented as spheres with grey for carbon, blue for nitrogen, red for oxygen and orange for phosphorus. Figure adapted from Rosenbaum *et al*.[42] (**B**) Ribbon representation of the pontin monomer [PDB 2C90], showing its domain structure. Domains I-III are represented in a different colour. The Walker A and B motifs are shown in yellow. Figure adapted from Huen *et al*.[44]

Members of the AAA+ family of proteins usually self-assemble into oligomers, predominantly hexamers, and this ability appears to be required for their biological activity.[63] This is similarly the case for reptin, which has been observed in various oligomeric states using multiple biophysical techniques, including analytical ultracentrifugation, size exclusion chromatography, mass spectrometry and electron microscopy.[45] It has been demonstrated that reptin can exist as a dimer, trimer, hexamer and as heterohexamers and dodecamers in conjugation with pontin. An important consequence of reptin oligomerisation into a hexamer is the capping of the ATPase site by a neighbouring monomer.[64] The nucleotide binding site is completely blocked by the α5 helix of DIII, Arg400 of the sensor II (in reptin) and the neighbouring monomer, which makes the release of ADP impossible. This is consistent with the low ATPase activity experimentally observed for reptin.[64,61] Cryo-electron microscopy studies[62] and molecular dynamic studies[60] support the rationale that a nucleotide induced conformational change is required for ATPase activity. Reptin's diverse repertoire of biological activities suggests that its oligomeric nature may be dependent on the complex or cellular process in which it is involved. The observation that adenine nucleotides alter its oligomeric state, promoting hexamerisation, suggests that cofactors (including DNA binding) and other proteins might be involved in regulating its activty.[65,66]

2.1.4 Reptin as a major player in cancer

A growing body of evidence is highlighting reptin as a promising target for cancer therapies.[67,68] This research has focused around reptin's level of expression in cancer, its interactions with mediators of carcinogenesis and its role in cell death/viability. Reptin was shown by differential proteomic analysis to be overexpressed in human colorectal cancer (HCC) tumours when compared with the non-tumour-surrounding liver.[69] Elevated expression of both reptin and pontin at both the mRNA and protein levels in HCC compared to the non-tumour liver was also observed.[70] Reptin and/or pontin have since been shown to be overexpressed in a variety of human solid tumours including bladder, colorectal, gastric, mesothelioma, non-small cell lung cancer, as well as in several types of acute or chronic leukaemia, in multiple myeloma, high-grade lymphoma and Burkitt lymphoma.[68]

The role of reptin in transcriptional regulation *via* its interactions with Tip60, c-myc and β-catenin, highlights the potential effect of its overexpression on the pathogenesis of cancer. For example, reptin potentiates c-myc mediated repression of the p21 gene,[71] hence impeding cell cycle arrest. Additionally, reptin represses β-catenin-dependent reporters. This suggests that reptin may indirectly play a role in cellular transformation, since deregulation of β-catenin signalling, due to an activating mutation of β-catenin or its interacting partners, has been observed in several cancers.[72] In metastatic cells, the β-catenin-reptin complex is preferentially recruited to the KAI1 promoter where it inhibits KAI1 expression *via* histone deacetylation.[56] As KAI1 increases cell adhesion and thereby inhibits metastasis, this indicates that the reptin-mediated repression of KAI1 may be involved in the development of metastasis. Collectively, it appears that reptin in association with β-catenin, recruits histone deacetylases to different promoters and converts the chromatin to a repressive state. Reptin also interacts with several other proteins with strong involvement in carcinogenesis such as the oncoprotein AGR2[65] and the telomerase components TERT and dyskerin.[57]

Reptin's role in cell death/viability has been demonstrated in several *in vitro* and *in vivo* studies. Decreasing reptin expression *in vitro* reduces tumour cell growth and increases apoptosis.[73] In addition, doxycycline-dependent shRNA-induced *in vivo* silencing of reptin results in growth arrest of established tumours in mice xenograft experiments.[74,67] These studies in combination with the loss of growth viability in yeast and the inactivation of several functional properties of reptin as a result of loss-of-function mutants of the Walker A or B motifs,[43,67,68] further implicates reptin as a promising therapeutic target in cancer.

2.2 Aims of this work

Reptin is a highly conserved member of the AAA+ superfamily which functions as an important regulator of a diverse range of cellular processes. Its presence in numerous protein and nucleoprotein complexes implicated in biological processes such as transcriptional regulation, chromatin remodelling and DNA damage response underlines its significant physiological role. In particular, an emerging body of evidence has implicated reptin in oncogenesis *via* its interactions with mediators of carcinogenesis and its role in cell death/viability. Despite its increasing prominence, no modulators of reptin's functions or interactions have been reported to date. Herein, we aim to develop a chemical biology platform to discover novel small molecule regulators of reptin's protein interactome, *via* a cross-disciplinary process in collaboration with Prof. Malcolm Walkinshaw and Dr Doug Houston (University of Edinburgh) and Prof. Ted Hupp (CRUK centre, Edinburgh).

This discovery platform will involve the following stages:

- A high-throughput virtual screen (Walkinshaw & Houston) to identify small molecules which are predicted to bind in the reptin ATP binding pocket
- *In vitro* evaluation (Hupp group) of the allosteric effect of the top predicted hits from this process on reptin's PPIs
- Optimisation of active lead molecules through an SAR study guided by molecular modelling and biological evaluation
- Investigation of the mode of action, and physiological effect of a modulator on reptin's protein interactome

2.3 Virtual Screening and Hit Identification

2.3.1 *In silico* screening using pontin

As no X-ray crystal structure of reptin was available at the time these studies began, initial *in silico* screening efforts focused on the use of the X-ray crystal structure of pontin, a highly conserved ortholog of reptin (PDB 2C90;[75] solved to a resolution of 2.3 Å). The virtual library used for this screen contained commercially available compound libraries from ChemBridge, Asinex, Maybridge, Enamine, LifeChemicals, Specs, InterBioScreen, ChemDiv and KeyOrganics. The library was filtered according to Oprea lead-like rules (H-bond acceptors ≤ 9; H-bond donors ≤ 5; MW ≤460; -4.6 ≤ cLogP ≥ 4.2; cLogS ≥ -5; Number of rings ≤ 4; Number of rotatable bonds ≤ 9)[76] resulting in 1,137,587 molecules. A multiconformer version of the virtual library was produced using Multiconf-DOCK;[77] an average of approximately 4.25 conformers per compound were generated depending on flexibility; this resulted in a virtual library containing a total of 4,840,093 conformers (Figure 2.5). The docking of this conformer virtual library of 4.8 million compounds into the ATP pocket (the Walker A motif) of pontin was carried out using the rigid-body docking program LIDAEUS by Dr Doug Houston.[78]

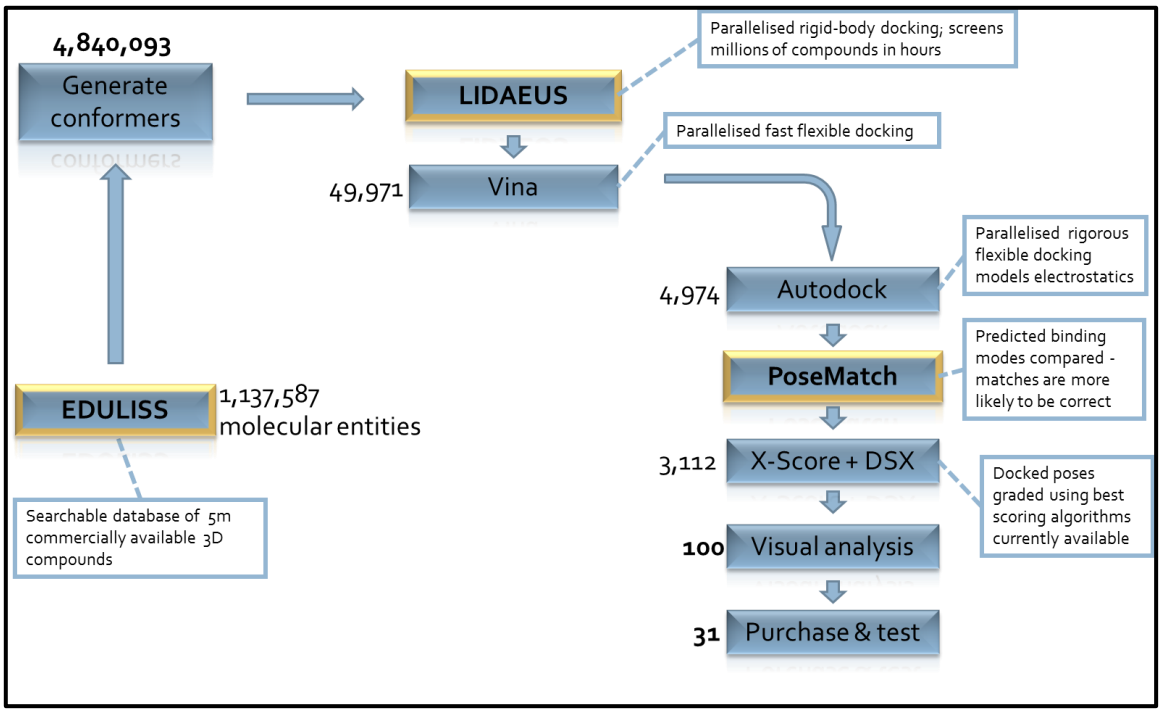

Figure 2.5. Workflow diagram of the virtual screening process. Numbers of molecular entities (compounds or conformers) are indicated at each stage. Figure created by Dr Doug Houston.

The results were ranked based on the LIDAEUS score and the top 49,971 compounds were then redocked using Vina. Docked poses were scored using both Vina's internal scoring algorithm and X-Score 1.2.[79] A "rank-by-rank" consensus protocol was then used to create a ranked list. The top

4,974 compounds were then docked using Autodock and the binding poses predicted by Autodock and Vina were compared *via* RMSD (root-mean-square deviation is a measure of the average distance between the backbone atoms of the superimposed binding poses[80]). Predicted binding poses that were similar (RMSD ≤ 2.0 Å) were also scored using DrugScore 1.2.[81] A final ranked list of the top 100 hits was prepared *via* a "rank-by-rank" scheme, taking the Vina, Autodock, X-Score and DrugScore (DSX) rank positions into account (Figure 2.5).

The binding mode of the top 100 highest scoring hits from the *in silico* screen underwent visual inspection and I subsequently subdivided them into different classes based on structural similarity. This visual analysis resulted in the identification of 14 different structural classes. The remaining analogues which did not contain a common structural core were grouped separately. A limited number of compounds (1-3) were purchased from each representative class based on their size and structural diversity. A further 7 compounds were purchased from the structurally unrelated group of hits, resulting in a final library of 31 compounds for testing (see Appendix A).

2.3.2 *In vitro* assessment of the top ranked *in silico* hits

As the focus of this work was to identify compounds that could, in some way, regulate reptin's protein-protein interactions, a previously validated PPI ELISA assay developed by the Hupp group[65] was used. In this assay, the binding of full-length reptin to a peptide (104-FVLLNLVY-111) representing the essential binding epitope of the reptin-binding protein AGR2[65] was assessed. This assay was initially used to demonstrate that binding of ADP to reptin modulates the reptin-AGR2 peptide interaction. A titration of ADP revealed that low levels of the nucleotide stimulate the AGR2 peptide binding activity of reptin, whilst higher levels of the nucleotide reduced and attenuated the reptin-AGR2 peptide interaction (Figure 2.6A). The biphasic effect of the nucleotide in this assay might be related to the stoichiometry of the nucleotide-bound hexamer or the ratio of the reptin monomer to hexamer at lower ADP concentrations. The 31 compounds purchased from the *in silico* screen's top 100 highest scoring hits were then assessed using this ELISA assay. Hits were defined in this assay as compounds that modified (increased or decreased) significantly the signal corresponding to reptin binding to the AGR2 peptide compared to the DMSO control (Figure 2.6B). Of the 31 compounds tested at a final concentration of 100 μM, 3 compounds (Figure 2.6B-C; **13**, **17** & **22**) resulted in a significant response and were therefore prioritised for further study.

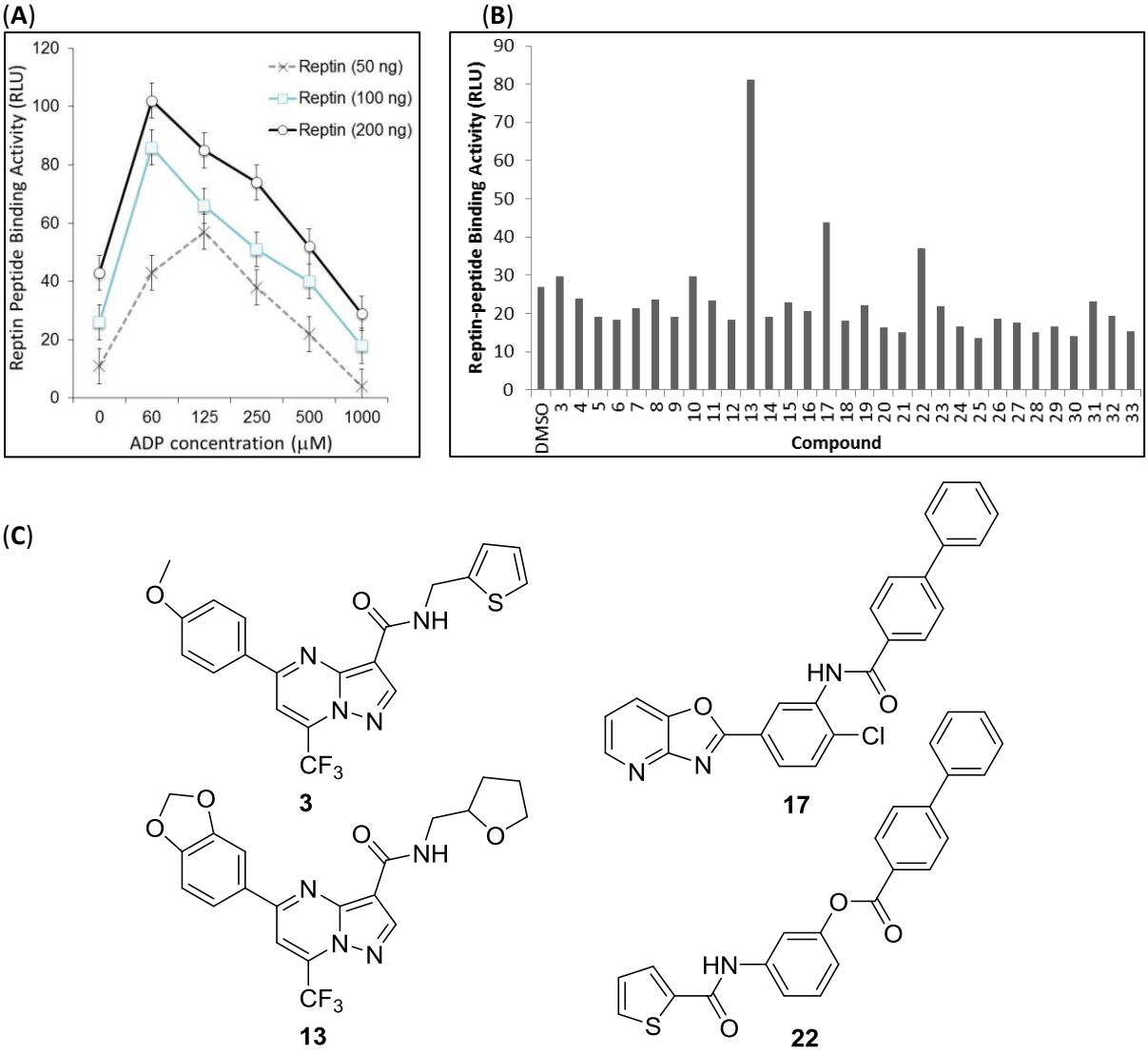

Figure 2.6. (A) The effect of ADP on the reptin-AGR2 peptide binding activity. A biotinylated version of the peptide binding motif from wild-type AGR2 (104-FVLLNLVY-111) was bound onto streptavidin coated wells and reptin was titrated followed by a primary antibody to reptin and a peroxidase linked secondary antibody to measure binding stability of reptin to the AGR2 peptide. The data are plotted as reptin binding activity (in RLU) as a function of reptin protein levels. Differing concentrations of reptin (50, 100, or 200 ng) were incubated with increasing concentrations of ADP. Low concentrations of ADP stimulated the AGR2-peptide binding function of reptin, in contrast with higher concentrations which attenuated its binding activity. **(B) Evaluation of the top 31 hits from the *in silico* screen in the peptide binding assay at 100 μM.** Data provided by the Hupp group. **(C) Structures of primary hits 13, 17 and 22, which significantly stimulated reptin's binding activity to the AGR2 peptide relative to the DMSO control. Structure of 3, an inactive analogue of hit 13.**

Interestingly compounds **17** and **22** appeared to be structurally related, both containing a biphenyl ring substituent (Figure 2.6C). In contrast, **3** which is a closely related analogue of **13** did not result in a significant response in the ELISA assay (Figure 2.6B). Based on these observations it was initially decided to focus on the class of compounds containing a biphenyl ring system, of which **17** had shown the most significant response (see Section 2.6 for the development of **13**).

2.3.3 Screen of the conformer library using reptin

Analysis of the predicted binding mode of **17** in the ATP binding pocket of pontin revealed that the biphenyl substituent of **17** sat deep in the Walker A pocket where the adenine of ADP/ATP has been shown to bind (Figure 2.7A). In addition, **17** contains a pyridine-oxazolo ring system which was predicted to extend out of the pocket. The computational studies progressed further following the report of an X-ray crystal structure of reptin in an alternating heterododecameric complex with pontin.[59] Comparison of this structure (PDB 2XSZ) with that of hexameric pontin (PDB 2C90) confirmed the high structural similarity between the reptin and pontin ATP-binding pockets (Figure 2.7B).

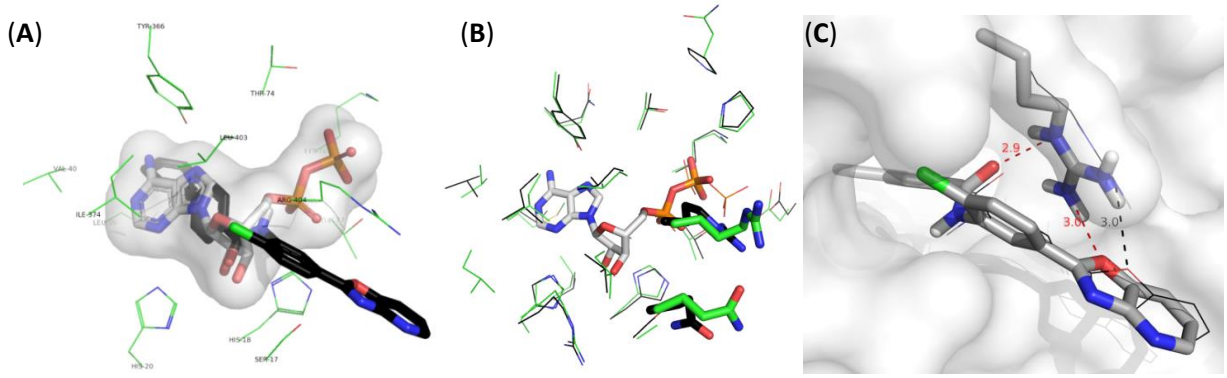

Figure 2.7. (**A**) The binding mode of **17** as predicted by Autodock is shown as black sticks. The side chains of residues that comprise the active site of pontin are shown as green lines and are labelled. The ADP molecule present in the pontin structure is coloured white and shown as sticks. The pocket is also shown as a transparent surface representation. In all cases nitrogen is coloured blue, oxygen red, phosphorous orange, and chlorine green**.** (**B**) Figure showing an overlay of the residues of the reptin and pontin ATP pockets, highlighting the difference in position of two key side chains (Arg404 and Gln408 in pontin and Arg400 and Gln404 in reptin). Reptin is coloured green, pontin black. The ADP molecule from the pontin structure is shown as sticks, the ATP from the superposed reptin structure as lines. (**C**) Original and optimised Autodock predictions of **17's** binding conformation. The predicted mode from the virtual high-throughput screen is shown as black lines and the hydrogen bonds it makes with Arg400 are shown as a black dashed line with its length in Å. The result of the docking with maximal parameters and flexible Arg400 activated is shown as grey sticks. Two hydrogen bonds shown in orange are predicted between the optimised **17** docking pose and the side chain. Data provided by Dr Doug Houston.

However, one important difference was observed between the position of the sensor II residue (Arg400) in reptin compared to its position in pontin (Arg404, Figure 2.7B). In the pontin structure, Arg404 is folded over the ATP binding pocket whereas in the reptin monomer Arg400 was located such that the Walker A binding site is more open and accessible (Figure 2.7B). Rescreening of the conformer library using the open structure of the reptin monomer present in this complex failed to identify **17** as a hit. Petukhov, M. *et al,* previously demonstrated using molecular dynamics methods that Arg400 in reptin and Arg404 in pontin are highly flexible and play an essential role as a R-valve controlling access to the ATP-binding pocket.[60] The *in silico* screen was then repeated for a third time with the side chain of Arg400 being computationally locked over the pocket. This modified screen predicted that **17** could bind to the Walker A site in reptin, suggesting that the correct positioning of

the sensor II arginine is essential for the binding of **17**. When **17** was docked into reptin keeping Arg400 flexible and using energy minimisation methods to identify the optimal interactions between **17** and Arg400, the side chain of Arg400 was predicted to fold over the pyridine-oxazolo ring system in **17** (Figure 2.7C). The formation of hydrogen bonds between the side chain of Arg400 and both the pyridine-oxazolo ring system and the amide oxygen in **17** was predicted, suggesting that these interactions may be essential for the experimentally observed activity of **17**.

2.4 SAR Optimisation of 17

2.4.1 SAR analysis of lead compound 17

SAR studies were carried out to further dissect and enhance **17**'s effect on reptin's binding activity. These studies aimed i) to assess whether **17** is likely to bind in the Walker A site as predicted and ii) to attempt to increase the biological activity of this series of compounds. First an efficient synthesis of **17** was developed to provide sufficient material for further validation of this hit (Scheme 2.1). This was achieved through a 2-step procedure from commercially available 2-amino-3-hydroxypyridine (**34**).

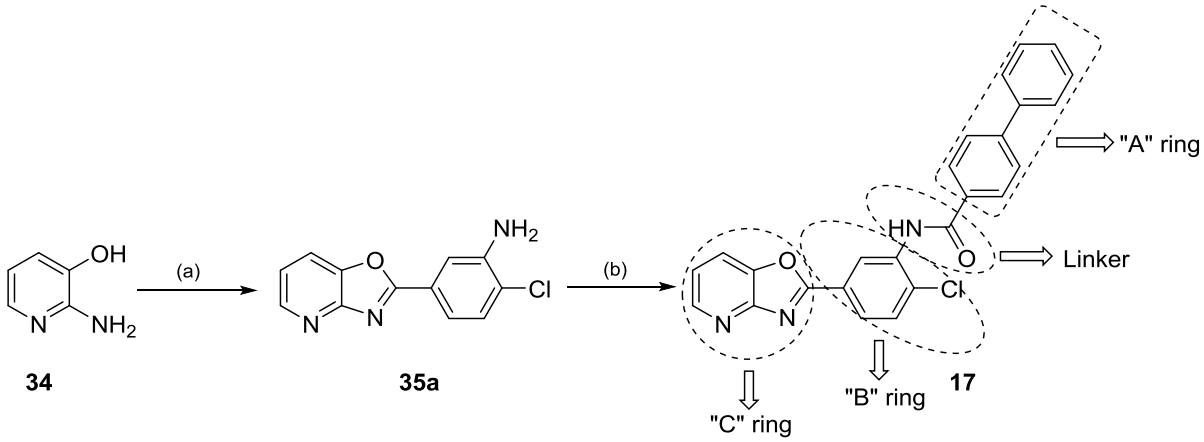

Scheme 2.1. Synthesis of 17. (**a**) (i) 3-Amino-4-chlorobenzoic acid (**34**), PPA, 200 °C, 4 h. (ii) H_2O, $NaHCO_3$, 55%. (**b**) Biphenyl-4-carbonyl chloride, DIPEA, DCM, r.t., 24 h, 57%.

Condensation of **34** and 3-amino-4-chlorobenzoic acid in polyphosphoric acid (PPA) at 200 °C for 4 hours provided the key intermediate **35a**. Compound **35a** was subsequently stirred with biphenyl-4-carbonyl chloride in DCM resulting in the precipitation of the desired compound **17** from the reaction. **17** was purified by recrystallisation from DCM. For the purposes of the SAR study, **17** was viewed as comprising of 4 distinct regions (labelled A-C rings and "linker", Scheme 2.1).

2.4.2 Modification of the "A" ring

Analysis of the predicted binding pose of **17** revealed that the biphenyl moiety binds deep in the Walker A pocket of pontin where the adenine of ADP/ATP has previously been shown to bind (Figure 2.7A). To probe this predicted binding mode, analogues of **17** containing modifications in the A ring were either purchased from Chembridge (Figure 2.8, **36**-**41**) or synthesised in an analogous manner to **17** (Figure 2.8, **42** & **43**).

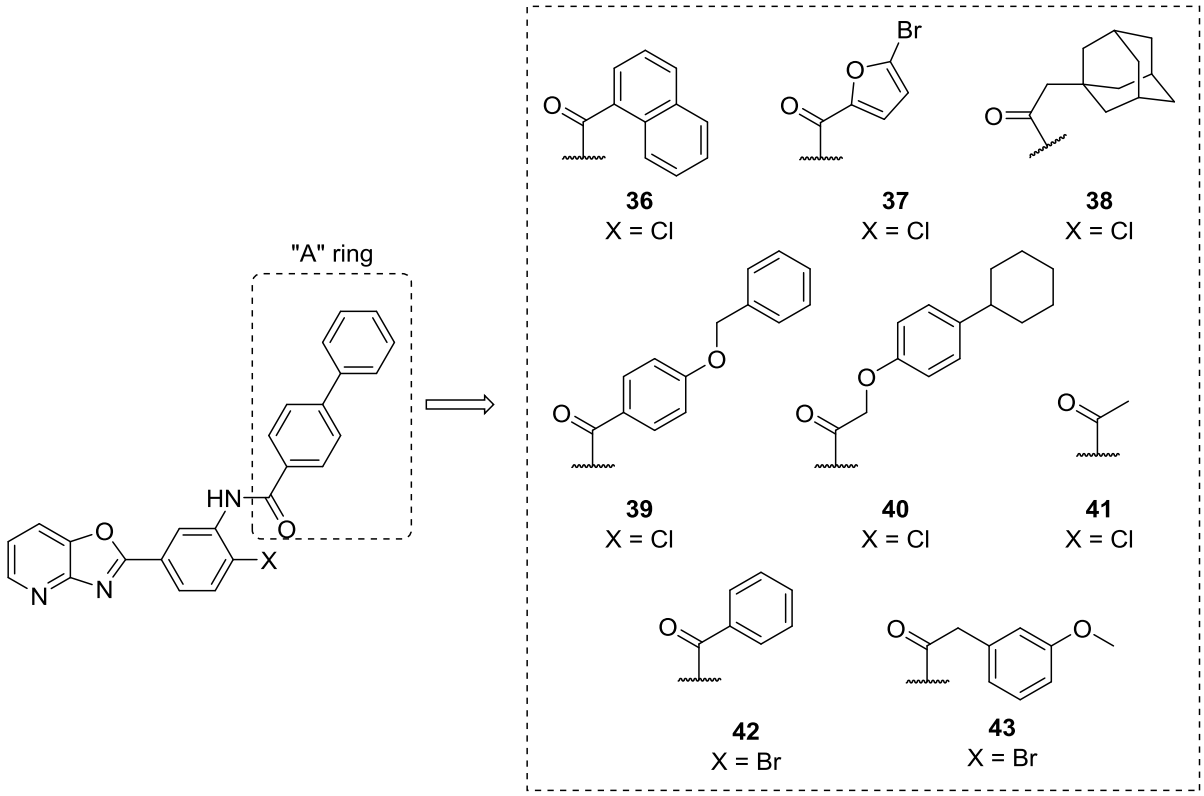

Figure 2.8. A ring analogues tested in the SAR study. Compounds **36**-**41** were purchased from Chembridge. Compounds **42** & **43** were synthesised in an analogous manner to **17** (Scheme 2.1). These analogues were inactive in the reptin-AGR2 peptide binding ELISA.

Biochemical analysis of analogues **36**-**43** showed that significant variations in the length and width of the substituent in the A region were not well tolerated, as they all proved to be inactive in the ELISA assay. This observation was consistent with the predicted position of the A ring of **17.** Interestingly, 10% of the top 100 *in silico* hits from both the pontin and second reptin screens contained the biphenyl system present in both initial hits **17** & **22**, suggesting this is an optimal functionality for the predicted binding.

2.4.3 Modification of the "B" ring

Analogues containing a modified B ring (**44**-**50**), which were synthesised in an analogous manner to **17**, explored two issues: i) the relative positions of the A and C rings and ii) the role of the halogen (Figure 2.9A). Changing the position of the amide group relative to the chlorine atom from the *meta*-

to the *ortho*-position (c.f. **17** vs. **44**) was not tolerated as expected based on the predicted binding mode. Replacement of the chlorine atom in **17** with a hydrogen atom resulted in complete loss of activity (**17** vs. **45**) and this could not be rescued by the repositioning of the amide group *para*- to the pyridine-oxazolo ring (in **46**). Variation of the halogen showed that an increase in atomic radius led to an increase in activity (**47**(F) < **17**(Cl) < **48**(Br)) with the bromine analogue **48** being the most active in the series (Figure 2.9B). Replacing the halogen with a methyl group (**49**) abolished activity.

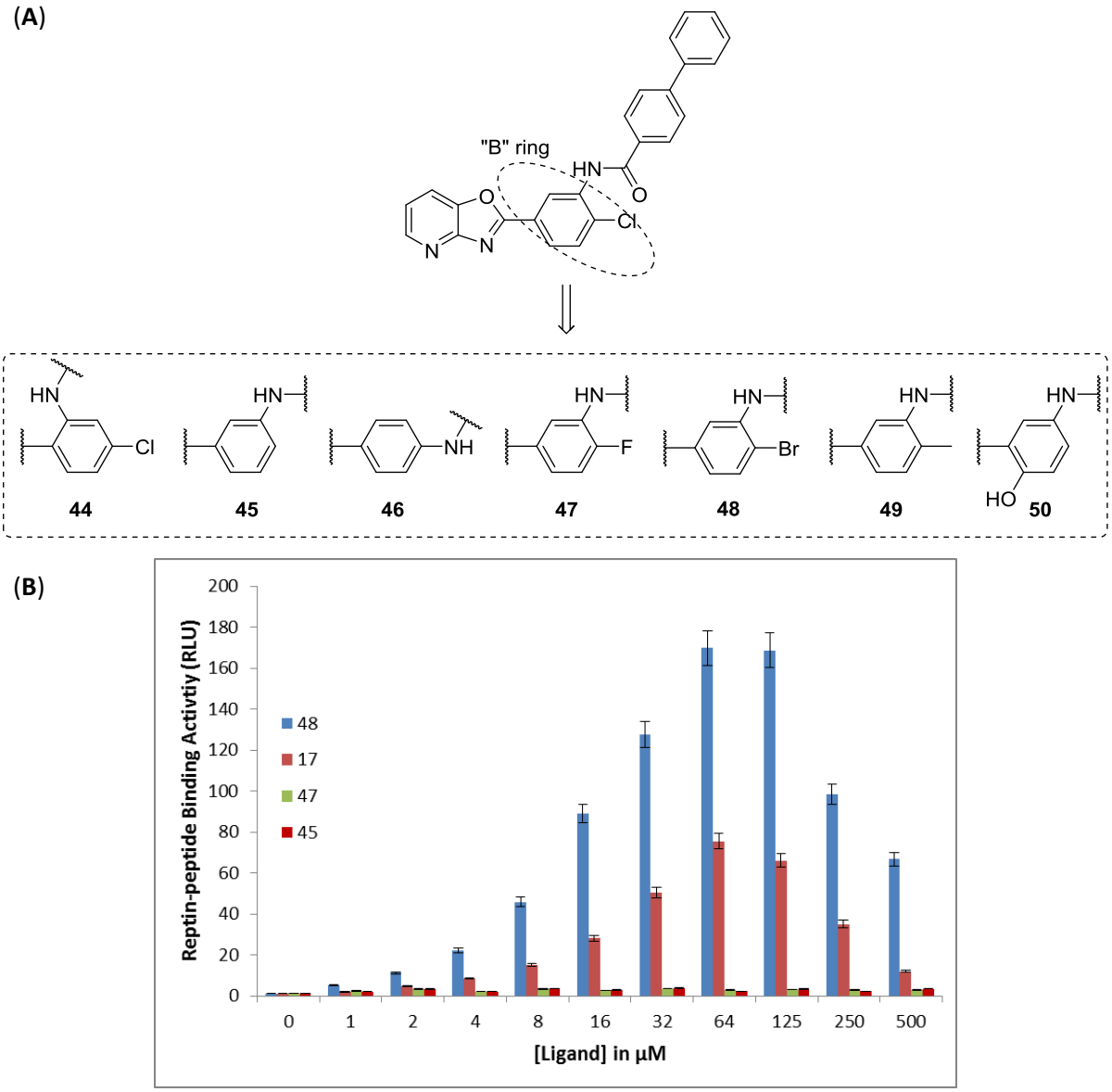

Figure 2.9. B ring analogues tested in the SAR study. (**A**) Compounds **44**-**50** were synthesised in an analogous manner to **17** (Scheme 2.1). (**B**) The effects of halogen substitution in ring B on the specific binding activity of reptin. Data was provided by the Hupp group (n = 3).

A dose titration of the halogen series confirmed a concentration dependent effect on the stimulation and attenuation of the specific reptin-AGR2 peptide binding activity, with as little as 1 µM of compound **48** showing stimulation (Figure 2.9B). The significant difference in activity between the

inactive non-halogenated analogue **45** and the most active analogue **48** (Figure 2.9B) would suggest that the bromine may have several roles, including van der Waals interactions, orientation of the "C" ring to best hydrogen bond with the Arg400 (Figure 2.7C) and a potential lowering of the barrier for rotation around the amide bond.

2.4.4 Modification of the linker region

Assessment of analogues **51** and **52** that contained modifications of the linker unit (Figure 2.10A) revealed that the activity increased with increasing linker flexibility (Figure 2.10B)**.** Interestingly, the ester-containing analogue **51** was more active than the sulfonamide **52**, whilst the amide **45** was inactive as previously mentioned (Figure 2.10B).

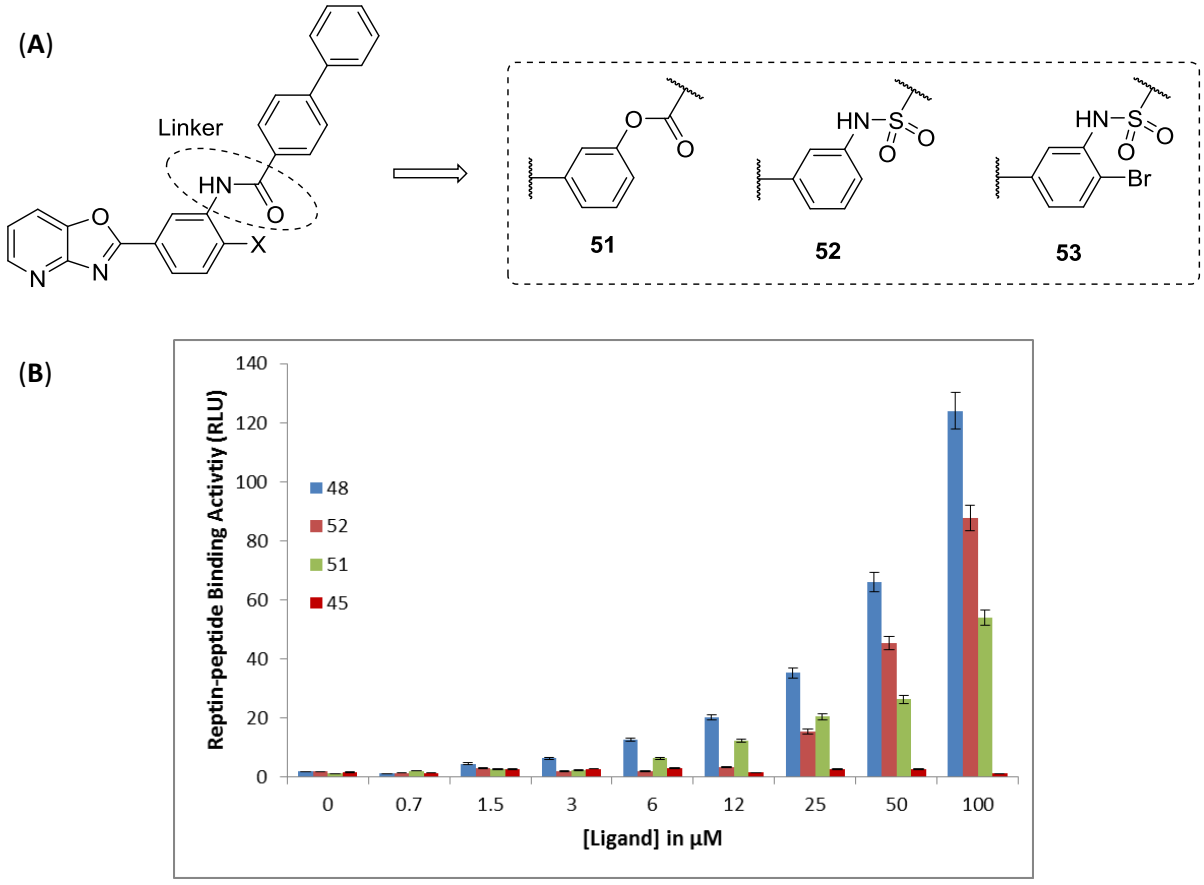

Figure 2.10. Linker unit analogues tested in the SAR study. (**A**) Compounds **51**-**53** were synthesised in an analogous manner to **17** (Scheme 2.1). (**B**) The effects of linker modification on the specific binding activity of reptin. Data was provided by the Hupp group (n = 3).

The correlation between increasing activity and increasing linker flexibility also supports the predicted binding mode which has **17** bound with the linker at right angles to the B ring. A lower energy barrier of rotation would allow the molecule to access the predicted binding conformation more easily, resulting in improved binding (Figure 2.7A). Incorporation of a bromine atom into the

sulfonamide analogue (**53**) abolished activity, suggesting the non-planar conformation of the sulfonamide results in a binding conformation for this analogue which does not tolerate a halogen atom.

2.4.5 Modification of the "C" ring

The final stage of the SAR analysis investigated the proposed binding of the C ring to R400. Docking studies combined with molecular dynamics revealed that potential hydrogen bonding between the C ring and Arg400 may play a key role in **17**'s mode of action (Figure 2.7C). The first aim of this study was to assess if it was possible to modify or remove this region and retain activity. To this end, two compounds **54** and **55** were synthesised using our previously developed route (Figure 2.11).

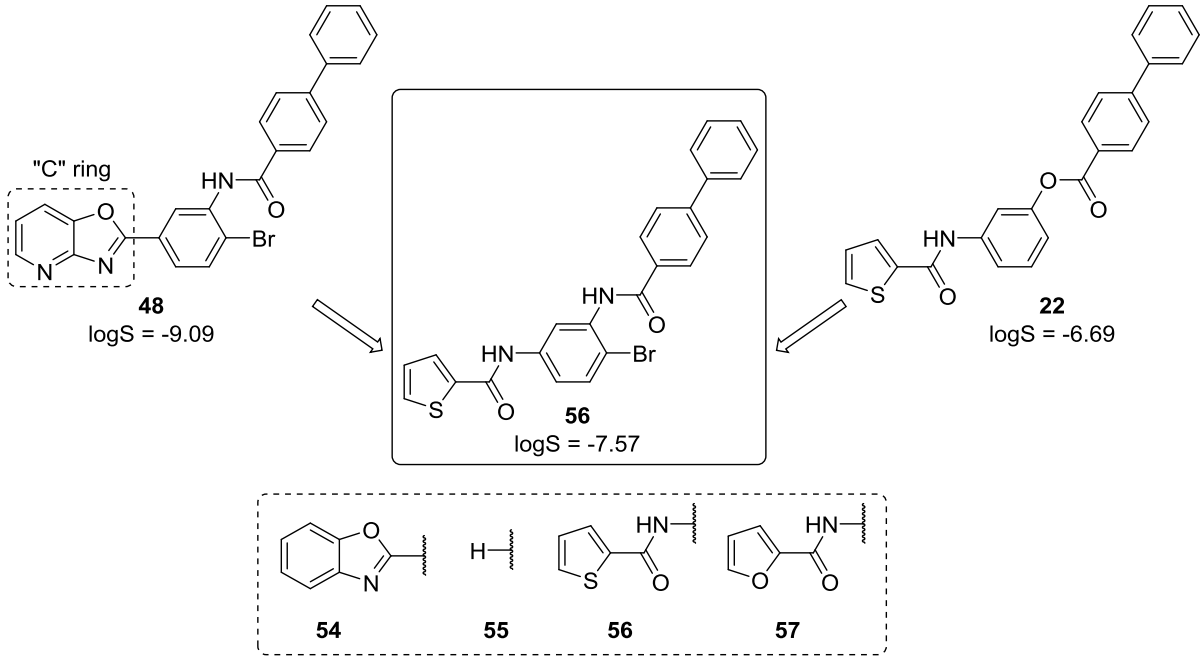

Figure 2.11. C ring analogues tested in the SAR study. Combination of the C ring of **22** and optimised A, B and linker regions of **48** resulted in compound **56** which showed an improved predicted logS value of -7.57 when compared to **48** (-9.09). Compounds **54** and **55** were synthesised in an analogous manner to **17** (Scheme 2.1). Compounds **56** and **57** were synthesised by an alternative route (Scheme 2.2). These analogues were inactive in the reptin-AGR2 peptide binding ELISA.

As predicted, removal of the C ring (**55**) abolished activity. Similarly, replacement of the pyridine nitrogen by a carbon (**54**) also abolished the activity of this compound. This suggested that it may be involved in a hydrogen-bonding network with R400 and neighbouring polar residues, although the observed inactivity could be a result of **54**'s poor solubility under the assay conditions. These preliminary results confirmed that the C ring is essential for activity, consistent with a requirement for hydrogen bonding of this heterocycle to Arg400.

Due to the inactivity and poor solubility of initial analogues of **17** containing a modified pyridine-oxazole ring, an alternative optimisation strategy was proposed which aimed to incorporate the C region of related *in silico* hit **22**, which contains a thiophene ring linked to the B ring *via* an amide group (Figure 2.11). The heteroatoms of the C region of **22** are in a similar spatial orientation to those present in the heterocyclic C ring of **17**, suggesting that they could form a similar hydrogen bonding network with R400 as predicted for **17**. However, **22** contains an ester linker connecting its B and A rings, which is prone to hydrolytic cleavage in aqueous environments, thus potentially restricting **22**'s utility as a chemical tool. Therefore, it was decided to combine the amide-linked thiophene of **22** with the optimised B ring, linker and A ring regions of **48** (Figure 2.11). This could potentially lead to an analogue with improved potency and pharmokinetic properties when compared to **22**, whilst also containing a C region which may be more amenable to further optimisation. Furthermore, it had been observed that our initial hit **17** and our most active bromine derivative **48** had poor solubility which is in agreement with their predicted logS values (-8.99 & -9.09 respectively[82]). The estimated logS value is a unit stripped logarithm (base 10) of the predicted solubility of a given compound in mole/litre. More than 80% of the drugs on the market have a logS value greater than -4.[82] The estimated logS values of less than -9 for our analogues suggest that they would have poor *in vivo* absorption and distribution. This poor aqueous solubility is presumably due to the relatively flat, hydrophobic nature of these compounds, which would promote the formation of a strong π-π interaction network. The replacement of the pyridine-oxazole heterocyclic ring system of **48** with the amide-linked furan functionality of **22**, resulted in a marked increase in the predicted solubility from –9.09 to –7.57 (Figure 2.11). Two analogues were selected, one which incorporated the amide-linked thiophene group from **22** and one which incorporated an amide-linked furan. To access these desired analogues, an alternative synthetic route was required.

The proposed synthetic route to access analogues **56** and **57** focused on a late-stage incorporation of the required C rings (Scheme 2.2). This versatile strategy began with the large scale synthesis of intermediate **59**, which could be readily acylated with a range of acid chlorides to form a diverse library of analogues if required. The synthesis of intermediate **59** involved the coupling of **58** and biphenyl-4-carbonyl chloride. Subsequent transfer hydrogenation (Fe in NH_4Cl) of the nitro group of **59** provided the corresponding amine **60**. Finally, **60** was acylated with 2-thiophene chloride or 2-furoryl chloride to furnish **56** and **57** respectively (Scheme 2.2).

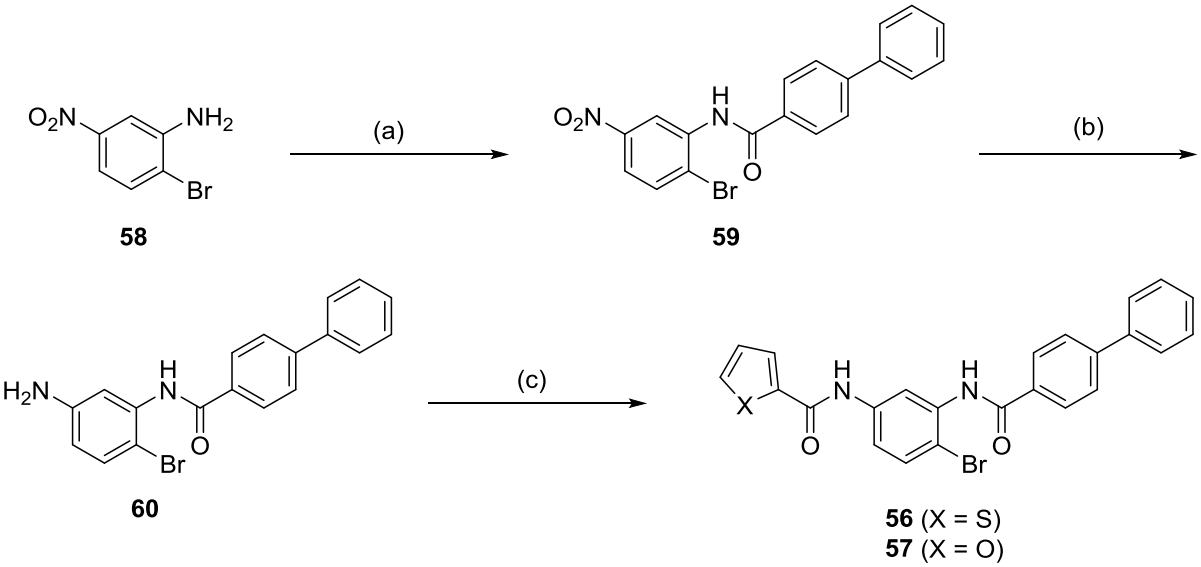

Scheme 2.2. Synthesis of C ring analogues 56 and 57. (**a**) Biphenyl-4-carbonyl chloride, pyridine, DCM, r.t., 18 h, 53%. (**b**) Fe, NH_4Cl, MeOH, H_2O, 100 °C, 3 h, 90%. (**c**) 2-Thiophene chloride or 2-furoyl chloride, pyridine, DCM, r.t., 18 h, **56** = 85%, **57** = 72%.

Disappointingly, neither **56** nor **57** were active in the reptin-AGR2 peptide binding assay. This would suggest that the role played by the amide and halogen in the correct alignment of the pyridine-oxazole ring of **48** for strong binding to Arg400 had an opposite detrimental effect on the corresponding amide-linked furan/thiophene ring. This is believed to result from a change in its spatial orientation, thereby disrupting its hydrogen bonding interactions with Arg400.

In summary, an *in silico* screen of a ~4.8 million conformer library against the ATP binding pocket of pontin and subsequently reptin, generated a ranked list of the top 100 predicted binders. A robust ELISA based protein-protein interaction assay was used to screen a selection of 31 compounds, which represented an overview of the chemical diversity present in the top 100 hits. **17** was identified from this *in vitro* assay to have a stimulatory/stabilisation effect on the formation of the reptin-AGR2 peptide interaction. **17** was modelled and subjected to SAR, guided by the ELISA based protein-protein interaction assay to generate a more active lead molecule **48**, which we have termed Liddean. The SAR study also supported the predicted binding mode of **17** in the ATP pocket of reptin, highlighting the correct orientation of the molecule and the formation of key hydrogen bonds with the amide and C ring to be essential for activity. With the chemical tool Liddean (**48**) in hand, further studies were undertaken to elucidate its mode of action and its effect on reptin's protein interactome.

2.4.6 Investigation of Liddean's mode of action

The investigation of Liddean (**48**)'s mode of action focused around two key observations. 1.) Liddean (**48**) produced a similar biphasic concentration dependent effect (Figure 2.9B) on the stimulation and attenuation of the specific reptin-AGR2 peptide binding as observed with ADP (Figure 2.6A). It stimulated the interaction at lower concentrations but attenuated it at higher concentrations. This would suggest that Liddean (**48**) has a similar physiological effect on reptin as ADP. 2.) The observation that the Arg400 loop needed to be closed over the ATP pocket for **17** to be identified as a hit from the *in silico* screen suggests that this could be important for its mode of action. This was further supported by the identification of possible hydrogen bonds with Arg400 through the use of molecular modelling (Figure 2.7C) and the observation that chemical modification of **17**, which resulted in a change of its preferred conformation or hydrogen bonding network, diminished or abolished its activity. Arg400 is a key residue involved in the sensor II domain. On binding of ATP/ADP to the ATP pocket of reptin, the Arg400 closes down over the pocket; binding to the phosphate chain.[60] This sensing of bound nucleotide could be essential for its resulting physiological effect.

Recent research has revealed that the predominant role of nucleotide binding to reptin is through modulation of its protein-protein interactome and the assembly/disassembly of multiprotein complexes.[43] This hypothesis is supported by the low levels of ATPase activity and the nucleotide dependent change in oligomerisation state observed for reptin.[61,64] The identification of a wide spectrum of oligomeric states, ranging from monomer to hexamer and dodecamer including hetero-oligomers with pontin is believed to underpin reptin's functional diversity and broad biological function.[45] It was therefore decided to assess whether like ADP, Liddean (**48**) could modify reptin's ability to form homo-oligomers. Reptin was subjected to SDS denaturing (0.1%) electrophoresis in the presence of varying amounts of SDS (0 - 1%) in the loading buffer resulting in the observation of both monomeric and dimeric forms of the protein (Figure 2.12A, lanes 1, 4, 7 and 10; dimeric reptin is typically observed as two SDS-resistant separate bands around 130 kDa). The preincubation of reptin with Liddean (**48**) induced the formation of a stable oligomeric form of reptin that was approximately 250 kDa (Figure 2.12A, lane 3, 6, 9 and 12) as well as additional slower running bands, possibly corresponding to even higher order oligomers. The Liddean (**48**)-induced oligomers were even stable when reptin was preincubated with 1% SDS prior to electrophoresis (Figure 2.12A, lane 12). ADP was able to induce the formation of a marginally stable oligomer (Figure 2.12A, lanes 2, 5, 8, and 11). These data suggest that Liddean (**48**) is able to trap reptin in a more stable oligomeric state.

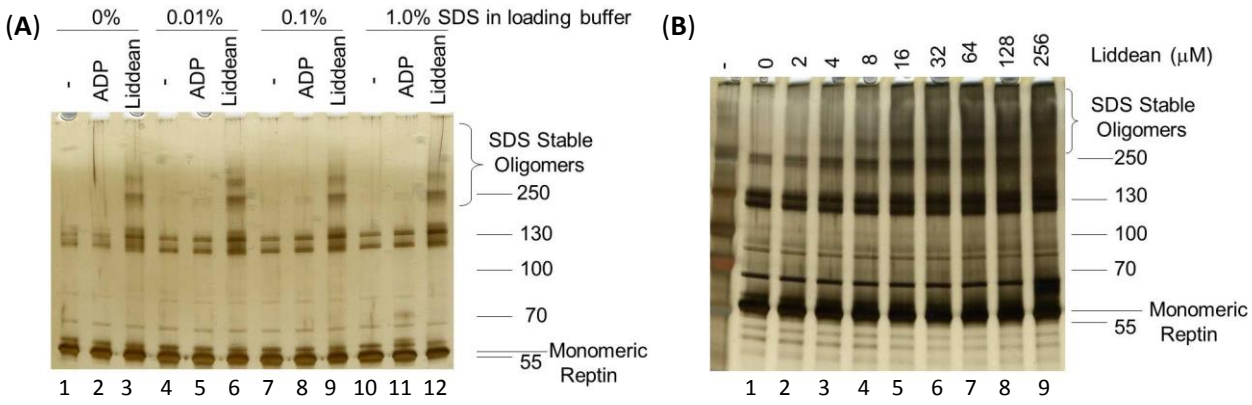

Figure 2.12. The effects of Liddean (48) on the oligomerisation of reptin. (**A**). Reptin (1 μg) was subjected to denaturing SDS (0.1%) gel electrophoresis in ADP binding buffer without or with ADP (100 μM) or Liddean (100 μM), as indicated. After 30 minutes of incubation at room temperature, gel loading buffer was added (with the indicated SDS concentrations from 0 to 1%), and electrophoresis was then carried out. Reptin protein was visualised by silver staining. (**B**). Reptin (1 μg) was subjected to denaturing SDS (0.1%) gel electrophoresis in ADP binding buffer with increasing concentrations of Liddean (**48**), as indicated. After 30 minutes of incubation at room temperature, gel loading buffer (0% SDS) was added and electrophoresis was carried out. Reptin protein was visualised by silver staining. Data provided by the Hupp group.

Liddean (**48**) was next titrated in this gel based assay to determine if there was a correlation between its ability to induce reptin homo-oligomerisation and a stimulation of reptin's binding to the AGR2 peptide. As little as 2 μM Liddean (**48**) was able to induce the formation of a stable oligomer (Figure 2.12B, lane 2), with maximal amounts of oligomers being induced between 64-256 μM (Figure 2.12B, lanes 7-9). This formation of SDS-resistant oligomer correlates with the specific reptin-AGR2 peptide binding activity induced by Liddean (Figure 2.9B, compound **48**).

2.5 Liddean as a Chemical Tool

2.5.1 Liddean induced modulation of reptin's protein interactome

Reptin can interact with a variety of signalling proteins and is often linked to oncogenesis.[68] Identifying reptin's protein interactome is crucial to understanding its role in oncogenesis and identifying novel targets for drug discovery programmes. Therefore, Liddean (**48**) was used as a synthetic ADP mimetic to determine whether novel interacting proteins could be identified for reptin. Liddean (**48**) behaves in a similar manner to ADP in that it produces a concentration dependent stabilisation or de-stabilisation of reptin-peptide or reptin-protein interactions. Importantly, Liddean (**48**) induced a more stable oligomer than ADP, suggesting that it indeed can function as a useful tool to dissect the protein interactome of reptin. It is in this more stabilised oligomeric state of Liddean (**48**)-bound reptin *in vitro* that "consensus binding motifs" were searched for using next generation deep-sequencing of a combinatorial peptide-phage library in the Hupp group.

Peptide phage display is a molecular technique, whereby a gene encoding a peptide of interest is inserted into the genome of the capsid proteins of a bacteriophage.[83–86] The encoded peptide is expressed or displayed in a functional form on the outer surface of the phage, creating a connection between the genotype (gene encoding the peptide) and the phenotype (the displayed peptide) within the phage particle.[87] In contrast to a synthetic small molecule library, a typical peptide phage combinatorial library can contain as many as 10^{10} phage-displayed peptides[88] (prey), which are screened simultaneously for their ability to bind to a target protein (bait) (Figure 2.13). The increased utilisation of this approach reflects the growing realisation that a majority of protein-protein interactions in higher eukaryotes are driven by linear motifs. [21,89]

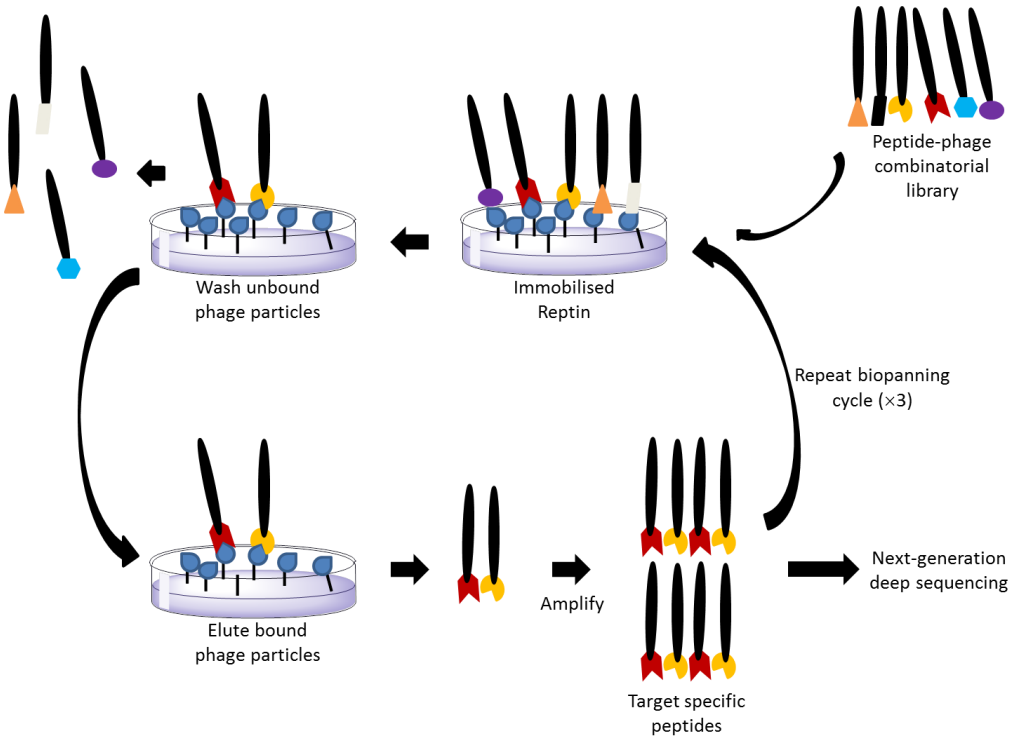

Figure 2.13. Peptide phage display platform. A peptide-phage library was added to immobilised reptin in the *apo*, ADP- or Liddean (**48**) bound forms (bait). Nonbinders were removed by extensive washing. Target-specific phage were eluted and amplified to provide an enriched pool. This biopanning cycle was repeated 3 times. The final target-specific, high-affinity phage were cloned and sequenced using next-generation deep sequencing.

A drawback to most protein-protein interaction discovery platforms such as yeast two hybrid or tap-tagging, is that they do not provide a robust opportunity for the identification of allosterically regulated or ligand-dependent PPIs. However, peptide phage display provides a method for discovering novel binding peptides for a ligand-bound target *in vitro*, where the bait conformation can be manipulated. Based on this concept, an alternative phage-based assay was developed to identify novel Liddean (**48**) induced/stabilised reptin-peptide interactions. A 12-mer peptide-phage combinatorial library was screened against immobilised (reptin) in its *apo*, ADP- or Liddean (**48**)-

bound state (Figure 2.13). Phage-particles displaying peptides capable of forming an interaction with reptin were isolated and subjected to three rounds of biopanning, an *in vitro* "natural selection" process.[83,85,86] This affinity selection procedure consists of the removal of unbound phages, the elution and amplification of interacting phages to create an enriched pool, which is subjected to two further rounds of biopanning under conditions of increasing stringency, resulting in the further enrichment of selective and high affinity binders.[88,87] The final phage-peptide pool was subjected to next generation deep sequencing (a high-throughput parallel DNA sequencing method) to identify the peptide sequences (Figure 2.13).[90–93]

The majority of peptides identified in the *apo*-reptin form (no bound ligand) were suppressed in the presence of ADP and Liddean (**48**), suggesting both ligands generally exert a similar effect on reptin's peptide binding activity. However, peptides which were enriched by ligand were prioritised as we were primarily interested in identifying reptin PPIs which were allosterically upregulated or stabilised by Liddean (**48**). A thousand of such peptides were identified and subjected to analysis using MEME (Multiple EM for Motif Elicitation), a bioinformatics tool used to identify conserved motifs that occur repeatedly within a pool of peptides, proteins or DNA sequences (Figure 2.14A).[94] The identified consensus peptide motifs were subsequently blasted (BLAST; Basic Local Alignment Search Tool is a bioinformatics algorithm for comparing amino acid sequences)[95] against the human proteome to identify known proteins which contain this particular motif.

(A)

12-MER
EXAMPLE CONSENSUS MOTIF ENRICHED WITH LIGAND

SEQUENCE	APO	ADP	Liddean
ARERINLSFINP	1	1	1
HAGLRERSIELT	1	2	1
RVQYDPTPLRER	0	0	1
SLQEANMMLRER	2	3	3
QGTSNGALRERL	2	0	5
NASSDDRERMNA	0	4	1
YFEPPLRSDRER	3	4	0
IATEGYRERQGN	1	0	3
SVDQSALRTRER	0	4	2
LPADSQQFPRER	0	1	3
ASFGAQLRERIT	1	1	2
QQIEESRERTPL	1	0	2
Total	12	20	24

(B)

Start	MOTIF	
7	ASFGAQ	LRERITG
4	HAG	LRERSIELTG
9	RVQYDPTP	LRERG
9	SLQEANMM	LRERG
8	QGTSNGA	LRERLG
6	NASSD	DRERMNAG
9	YFEPPLRS	DRERG
6	IATEG	YRERQGNG
9	SVDQSALR	TRERG
9	LPADSQQF	PRERG
1		ARERINLSFINPG
6	QQIEE	SRERTPLG

(C)

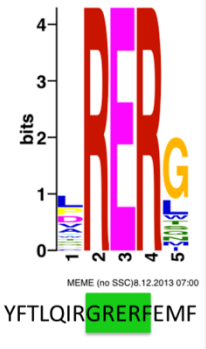

Figure 2.14. Identification of novel reptin binding peptides using peptide phage display linked with next-generation deep sequencing. (**A**) 1000 peptides which were enriched in the ligand bound state were processed using MEME to identify consensus motifs (http://meme.nbcr.net/meme/cgi-bin/meme.cgi). (**B**) The panel represents data from a 12-mer peptide screen where the core motif identified is highlighted as ϕRERϕ or LRER[L/G]. (**C**) A blast motif screen using the MEME derived peptide consensus sites gave rise to a peptide derived from the tumour suppressor protein p53. Data provided by the Hupp group.

Of particular interest was the ADP and Liddean (**48**) induced-enrichment of a motif containing a ϕRERϕ core (Figure 2.14B), which was identified in the tetramerisation domain of the p53 tumour

suppressor (Figure 2.14C), an important therapeutic target for the development of anticancer agents.The ϕRERϕ motif was also identified in the *apo*-reptin form suggesting it is a naturally occurring reptin PPI (Figure 2.14A). The interaction however, was enhanced by ADP, and to a greater extent by Liddean (Figure 2.14A), which is in agreement with our previously observed relative effect of these two different ligands on reptin. This novel reptin-p53 PPI was validated *in vitro* through an ELISA assay which demonstrated that purified p53 protein was able to bind to reptin (Figure 2.15A). Liddean (**48**) stabilised the p53-reptin complex (Figure 2.15B), which is similar to what was observed in the synthetic peptide-phage screen. In contrast to Liddean (**48**)'s stabilisation of the reptin-AGR2 peptide complex (Figure 2.9B), Liddean (**48**) was found to destabilise the binding of reptin to full-length AGR2 protein at low concentrations but stabilise it at higher concentrations (Figure 2.15B). This effect of Liddean (**48**) is similar to the effect of ADP on full-length AGR2-reptin complex stability.[65] These data confirm that Liddean (**48**)-responsive peptide-binding activities of reptin can be translated to the corresponding interactions with the full-length target proteins, and suggest that the reptin oligomer (induced by Liddean) has a higher specific activity towards p53 and AGR2 proteins.

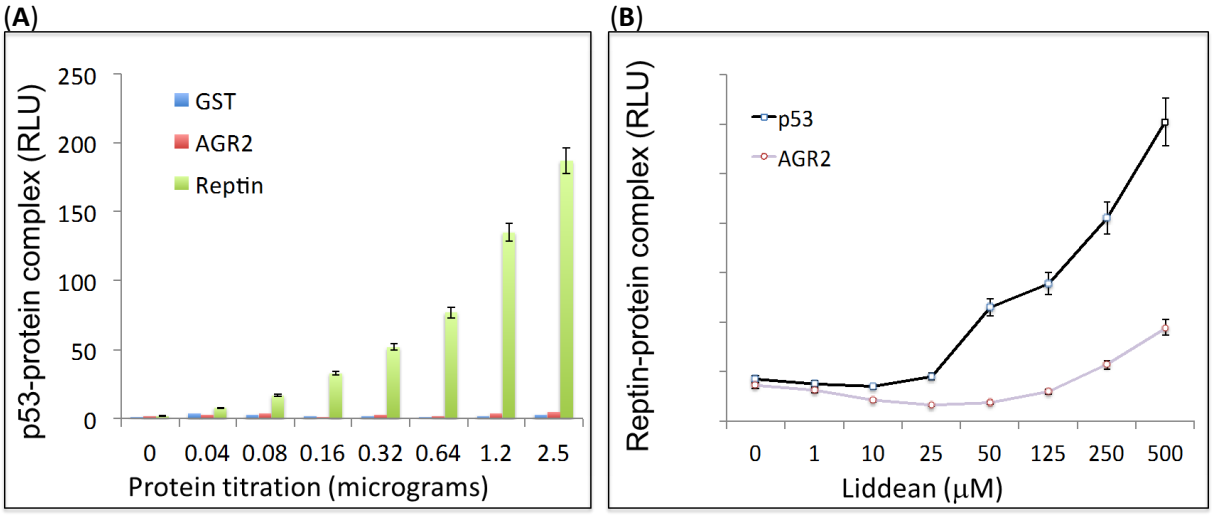

Figure 2.15. *In vitro* validation of the novel reptin-p53 PPI. (**A**) GST-tagged reptin and AGR2 proteins were assessed for their ability to bind to full length p53 using ELISA. p53 protein was absorbed onto the solid phase, and the indicated proteins were titrated in solution phase. The binding was detected using GST antibodies, followed by peroxidase conjugated secondary antibodies and processing using chemiluminescence. The data is plotted as binding activity as a function of protein amount (in RLU). (**B**). The effect of Liddean (**48**) on the reptin-AGR2 and reptin-p53 protein interactions was evaluated. Either p53 or AGR2 protein were absorbed onto the solid phase and reptin protein (200 ng) was added in 50 µL of buffer containing increasing amounts of the indicated ligand. After 60 minutes incubation at room temperature, reptin protein bound to its target was detected using a reptin antibody and a peroxidase linked secondary antibody. Binding activity was quantified by chemiluminescence using a Fluoroskan Ascent FL Labsystems. Data provided by the Hupp group.

2.5.2 Identification of a reptin binding site on p53

In order to fine map the reptin binding site on p53, overlapping biotinylated peptides derived from the open reading frame of human p53 protein (Figure 2.16A) were adsorbed onto a streptavidin coated solid phase and then evaluated for specific binding to the reptin protein. Two dominant peptides were identified which bound to reptin (Figure 2.16B). These peptide motifs overlap with the known MMD2 binding site (peptide 31) in the central domain of p53 and also with a motif in the tetramerisation domain of p53 (peptide 38).

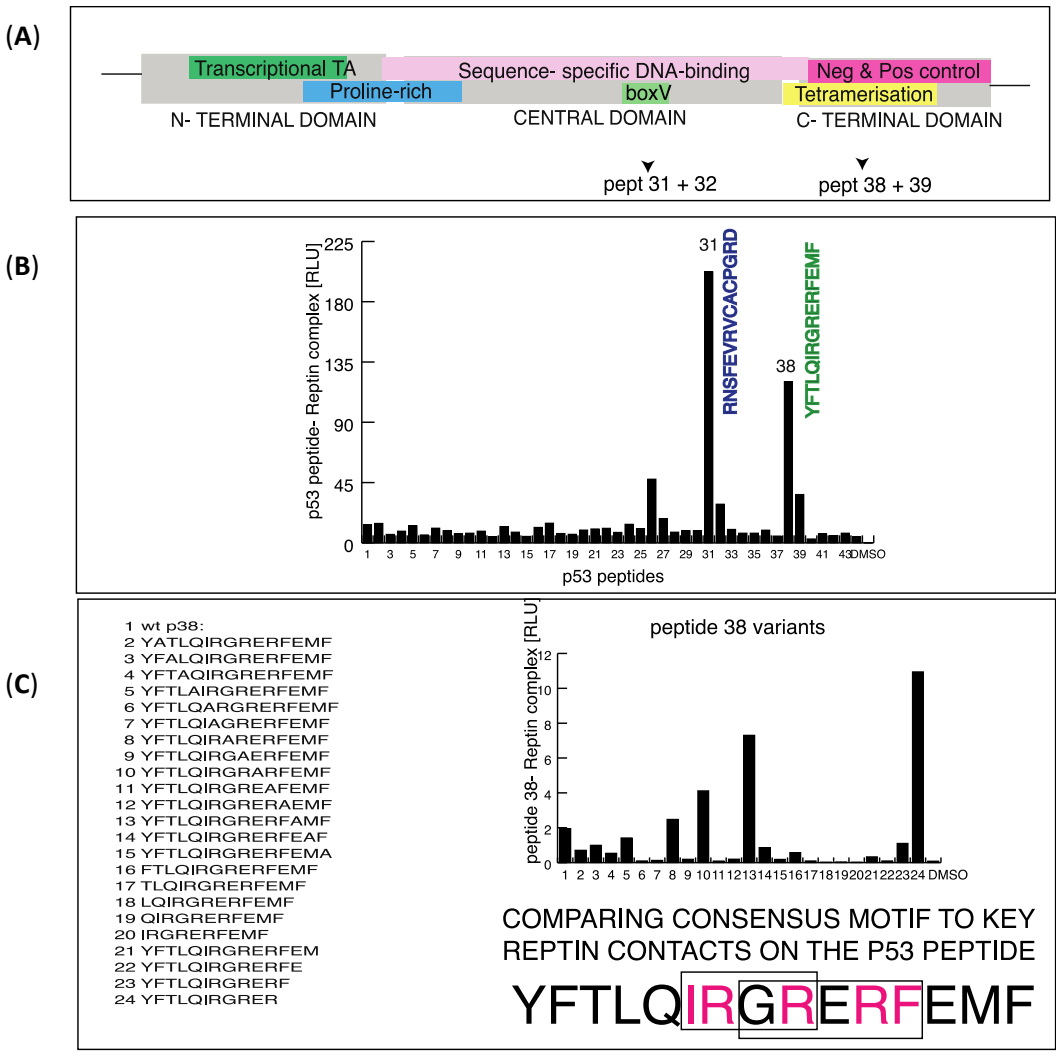

Figure 2.16. Fine mapping of the dominant linear peptide docking sites of reptin on p53. (**A**) The domain structure of p53 including the sites bound by MDM2 (in green), proline rich motif (blue), the specific DNA-binding domain (pink); tetramerisation domain (yellow); and the C-terminal regulatory domain (in red). The arrows highlight the two binding sites mapped for reptin (in panels below). (**B**). An overlapping series of synthetic biotinylated peptides derived from the open reading frame of p53 were captured on streptavidin coated solid phase and reptin binding was detected using a reptin antibody and a peroxidase linked secondary antibody. Binding activity was quantified by chemiluminescence using a Fluoroskan Ascent FL Labsystems. Two domain regions from p53 bound to reptin and were mapped to the BOX-V domain (RNS…GRD) and to the tetramerisation domain (YFT…EMF). The latter peptide contains two repeats of the ϕRERϕ or LRER[L/G] motifs identified from the ligand responsive peptides using MEME (Figure 2.15). (**C**) Alanine scan mutagenesis of peptide 38 (YFTLQIRGRERFEMF) identifies key amino acid side chains that are important for reptin binding to p53; in the core sequence IRGRERFEMF, mutating IRGR or the overlapping RERF motif abrogates reptin binding to p53. This functional alanine mutagenesis is consistent with the MEME derived peptide motif obtained from the deep sequencing analysis.

Alanine scan mutagenesis of p53 peptide 38 (YFTLQIRGRERFEMF) was performed to determine whether a minimum binding motif could be identified (Figure 2.16C). The key amino acid contacts required for efficient binding of the p53 peptide to reptin forms the core ϕRERϕ motif (Figure 2.16C), identified by the peptide-phage screen (Figure 2.15). These data further confirmed that the peptide combinatorial screen combined with next-generation sequencing can identify viable dominant docking sites for protein-protein interactions.

The identification of p53 as a novel reptin interactor further enhances the knowledge surrounding this multifunctional AAA+ protein. Research is continuing utilising the chemical tool Liddean (**48**) to further understand the role and significance of this novel PPI. The reptin-p53 interaction has since been validated *in vivo* using knockdown and pull-down experiments, and it appears to be involved in regulating p53-DNA binding. The essential role, which the p53-DNA interaction plays in regulating apoptosis and cell cycle homeostasis, highlights the reptin-p53 PPI as a novel and promising target for the development of new anticancer agents. The *in vivo* effect of Liddean (**48**) on the reptin-p53 interaction is currently being evaluated.

2.6 Development of the 2nd *In Silico* Hit 13

The power and utility of an *in silico* screen to identify novel small molecule PPI modulators was exemplified by the identification of the novel chemical tool Liddean (**48**). Encouraged by the success of the initial discovery programme, compound **13**, the 2nd hit identified from the *in silico* screen and subsequent ELISA assay was focused on (Figure 2.6). The main aim for the development of a second reptin modulator was towards the identification of a more water soluble lead compound to be used in a drug development programme. Although the development of Liddean (**48**) provided a useful chemical tool, its poor water solubility could prevent it from being a potential drug lead. In contrast, **13** has a predicted solubility (logS) of -5.42,[82] which is a good starting point for the development of a novel drug lead targeting reptin.

2.6.1 Analysis of the predicted binding mode of 13

Similarly to the Liddean precursor **17**, **13** was not identified in the first reptin *in silico* screen, but was present in the second screen when the Arg400 loop in reptin was manually closed over the pocket. Analysis of the predicted binding mode of **13** (in reptin with closed Arg400 loop) revealed that it is a much closer mimic of ADP than Liddean (**48**). The benzo[1,3]dioxole ring of **13** is predicted to be buried deep in the ATP pocket where the adenine of ADP resides (Figure 2.17A). The amine

substituent of the adenine ring is thought to adopt a similar position to one of the dioxole oxygens, potentially forming similar hydrogen bond interactions. The core (trifluoromethyl)pyrazolo-pyrimidine motif of **13** is predicted to be in the same position as the ribose ring of ADP (Figure 2.17A), where interestingly the CF_3 group is predicted to occupy the small hydrophobic pocket in which the bromine atom of Liddean (**48**) was predicted to bind (Figure 2.7A). In contrast to Liddean (**48**), **13** contains an amide-linked tetrahydrofuran moiety which is predicted to bind in the ATP/ADP phosphate channel. Most importantly, the nitrogen and oxygen atoms of the amide and the oxygen of the tetrahydrofuran ring overlay with oxygen atoms present in the phosphate chain of ADP (Figure 2.17B), suggesting the possible formation of a similar hydrogen bonding network with Arg400 as ADP.

(**A**) (**B**)

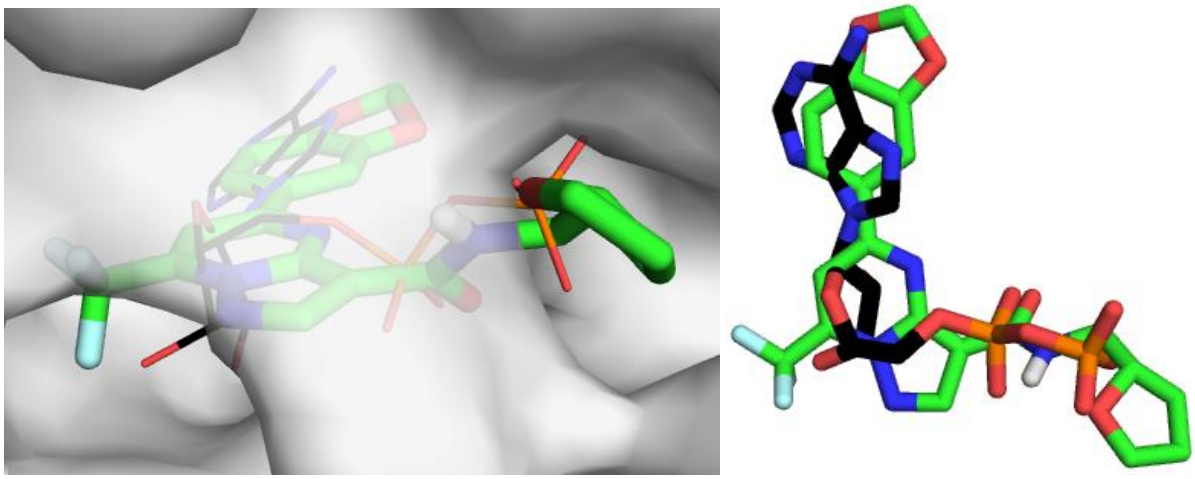

Figure 2.17. (**A**) The Autodock prediction of the binding mode of **13** is coloured green and shown as sticks. The ADP molecule present in the pontin structure is coloured black and shown as lines. The ATP pocket of reptin with the Arg400 manually closed over the ATP pocket is shown as a transparent surface representation. In all cases nitrogen is coloured blue, oxygen red, phosphorous orange, and chlorine green**.** Figure created using Pymol. (**B**) Overlay of ADP and **13**. Figure created using PyMOL.

Based on the surprising discovery that related analogue **3** (Figure 2.6C) was not active in the reptin-AGR2 peptide binding assay, the remaining members (**61** and **62**) of the structural class which contained **13** and **3** were purchased (Figure 2.18A). This would provide preliminary SAR data and determine whether there was scope to modify **13** without abolishing its biological activity. Assessment of **61** and **62** in the previously described reptin-AGR2 peptide binding ELISA revealed that they induced a similar stabilisation/upregulation in the interaction as **13** (Figure 2.18B).

The biological activity observed for analogues of **13** containing different functionalities at the 3-(amide-linked tetrahydrofuran) and 5-(benzo[1,3]dioxole) positions highlighted the potential to undertake an SAR study to optimise this lead compound. The synthesis of a diverse library of

analogues based around the 7-(trifluoromethyl)pyrazolo[1,5-a]pyrimidine core lends itself to a combinatorial chemistry approach.[96,97] The development of a solution-phase synthesis of **13** which would be amenable to a parallel library approach would provide access to a structurally diverse library of analogues. A suitable synthetic route would require simple purification, display a relatively high substituent tolerance and provide sufficient quantities of the desired analogues in a fast and cost efficient manner from readily available starting materials.[98]

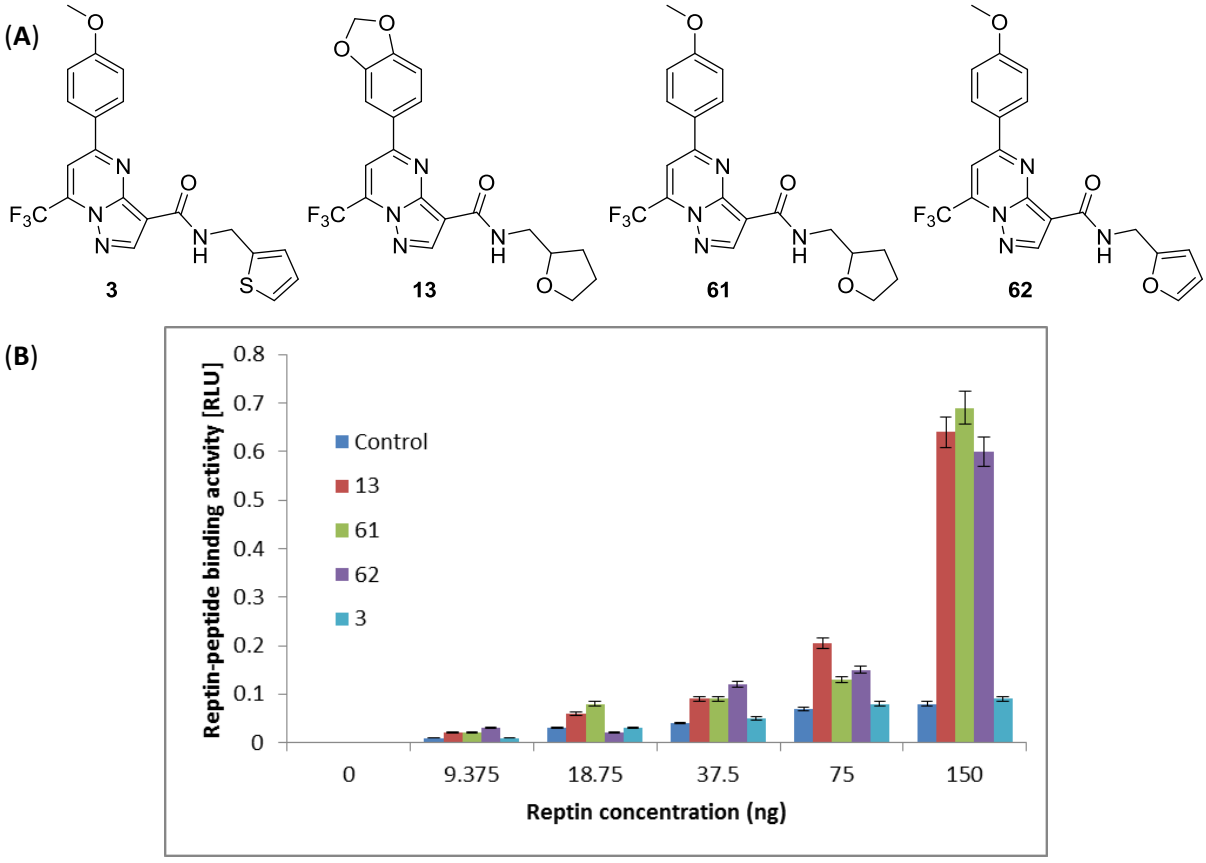

Figure 2.18. (A) The structures of lead compound 13, and related analogues 3, 61 and 62. (B) The effects of analogues of 13 on reptin-AGR2 peptide binding activity. AGR2 peptide was absorbed onto the solid phase and reptin protein was titrated from 0-150 ng as indicated with a fixed concentration (25 µM) of ligand (**3**, **13**, **61**, **62** and DMSO (control)).

2.6.2 Development of a combinatorial approach

The development of a suitable combinatorial approach was considerably aided by the extensive research undertaken to identify novel solution and solid phase combinatorial syntheses of heterocyclic compounds in medicinal chemistry.[99,100] In particular, the pyrazolo[1,5-a]pyrimidine structural motif is present in a large number of pharmaceutical agents encompassing a broad range of biological activities, including, antiepileptic agents, anxiolytics, antidepressants, agents for the treatment of sleep disorders and oncolytics.[101] Dalinger *et al*. reported a combinatorial approach to access a diverse library of 7-trifluoromethyl-substituted pyrazolo[1,5-a]pyrimidine analogues which

could potentially be adapted to provide our desired analogues.[101] The general synthetic approach involved the treatment of trifluoromethyl-β-diketones **63** with 5-aminopyrazolecarboxylic ester derivatives **64** to provide the substituted pyrazolo[1,5-a]pyrimidine carboxylate core **65**. These could be readily converted into the desired libraries of amides **66** *via* the corresponding acid chlorides (Scheme 2.3).

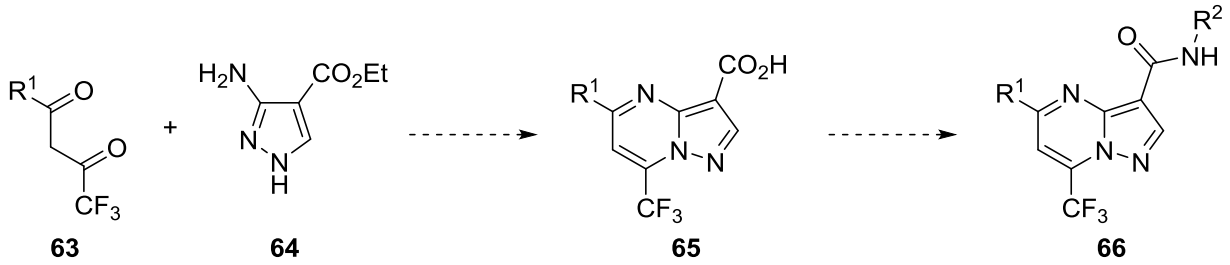

Scheme 2.3. General scheme for the synthesis of pyrazolo[1,5-a]pyrimidine carboxylate derivatives.[101]

Dalinger and coworkers accessed the required trifluoromethyl-β-diketone reagents **63** by trifluoroacetylation of the appropriate methyl ketones, using ^{t}BuOK in benzene.[101,102] However, this route was deemed not suitable for the large scale synthesis of a range of trifluoromethyl-β-diketones as it would require large quantities of toxic benzene and a column chromatographic purification step. Instead, a trifluoroacetylation procedure described by Danheiser *et al*., involving LiHMDS in THF (Scheme 2.4) was utilised to access the desired trifluoromethyl-β-diketone **68**.[103] This route provided **68** in quantitative yield after a simple aqueous work-up.

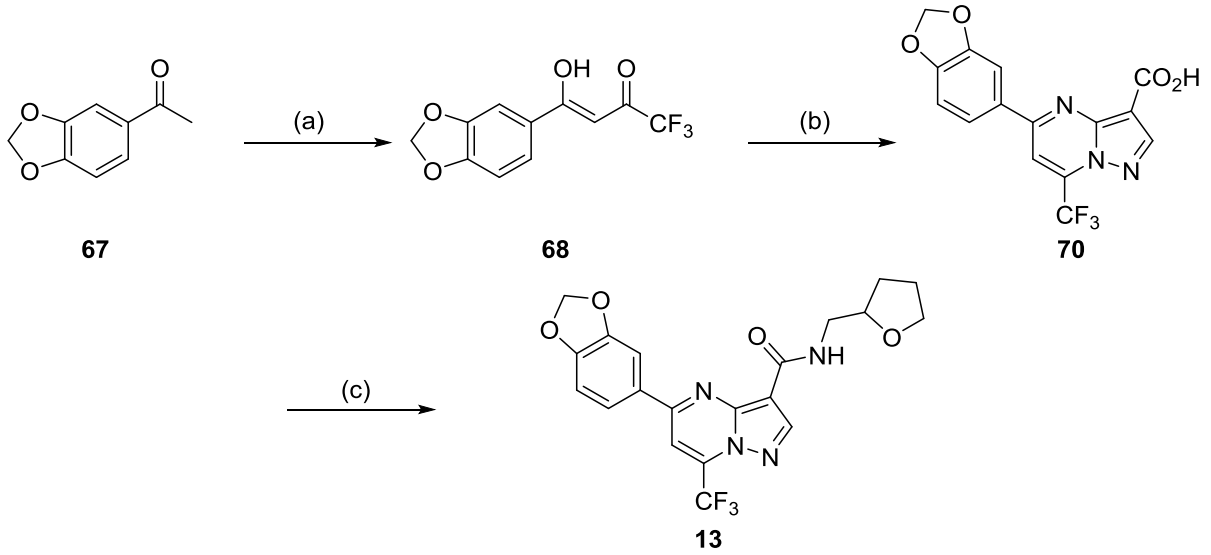

Scheme 2.4. Synthesis of 13. (**a**) LiHMDS, ethyl trifluoroacetate, THF, 0 °C → r.t., 3 h, quantitative. (**b**) (i) Ethyl 3-amino-1*H*-pyrazole-4-carboxylate **64**, acetic acid, reflux, 5 h, 90% (ii) NaOH, EtOH, H_2O, 65 °C, 4 h. (**c**) (i) Oxalyl chloride, DCM, DMF, 0 °C → r.t., 2 h. (ii) tetrahydrofurfurylamine, MeCN, r.t., 2 h, 72%.

68 was heated at reflux in the presence of commercially available ethyl 3-amino-*1H*-pyraxole-4-carboxylate **64** and acetic acid to furnish the desired pyrazolo[1,5-a]pyrimidine carboxylate **69** after simple precipitation from ice-water. **69** was subsequently treated with solid NaOH in a H_2O/EtOH mixture at 65 °C for 4 hours. Cooling to room temperature followed by acidification yielded the desired acid **70** in a 4:1 ratio to unreacted ethyl carboxylate **69** which was not removed until the final purification (Scheme 2.4). The final step involved conversion of the acid **70** into the desired amide **13** *via* the corresponding acid chloride. Dalinger *et al*. formed the acid chlorides by refluxing the acids with thionyl chloride in CCl_4.[101] Optimisation of this step targeted the removal of the toxic solvent CCl_4, which can result in adverse health effects[104] and ozone depletion.[105]

An alternative route was developed which involved the generation of the acid chloride using oxalyl chloride and DMF (cat.) in DCM, followed by concentration *in vacuo*, dilution with MeCN and stirring with tetrahydrofufurylamine for 2 hours. The pure product **13** was obtained after column chromatography (to remove unreacted ethyl carboxylate **69**) and recrystallisation from hot EtOH (Scheme 2.4). Further optimisation of the ester hydrolysis step is required to push it to completion which would remove the need for a column purification step at the end of the synthesis. The issue surrounding the hydrolysis of **69** appears to result from its relatively poor solubility under the reaction conditions. Altering the ratio of the H_2O/EtOH solvent system, reaction concentration and time should result in the complete conversion to the desired acid **70**.

In summary, we have developed a concise synthetic route to **13** which could be used in the parallel synthesis of a diverse library of analogues. This four step route utilises simple aqueous work-ups or precipitation to access the desired intermediates and recrystallisation to provide the pure desired product **13**. Optimisation of this route by the elimination of the column purification step in the synthesis of trifluoromethyl-β-diketone **68** and removal of the toxic solvents benzene and CCl_4, make it significantly more amenable to large scale parallel synthesis. Finally, incorporating a range of commercially available methyl ketones or amines would provide access to a diverse library of analogues.

2.6.3 Inhibition of HCT-116 cancer cell proliferation

As the main focus of developing this second series of compounds was towards the identification of a possible anticancer drug lead, **13** was assessed for its effect on the proliferation of HCT-116 cancer cells by the Hupp group.

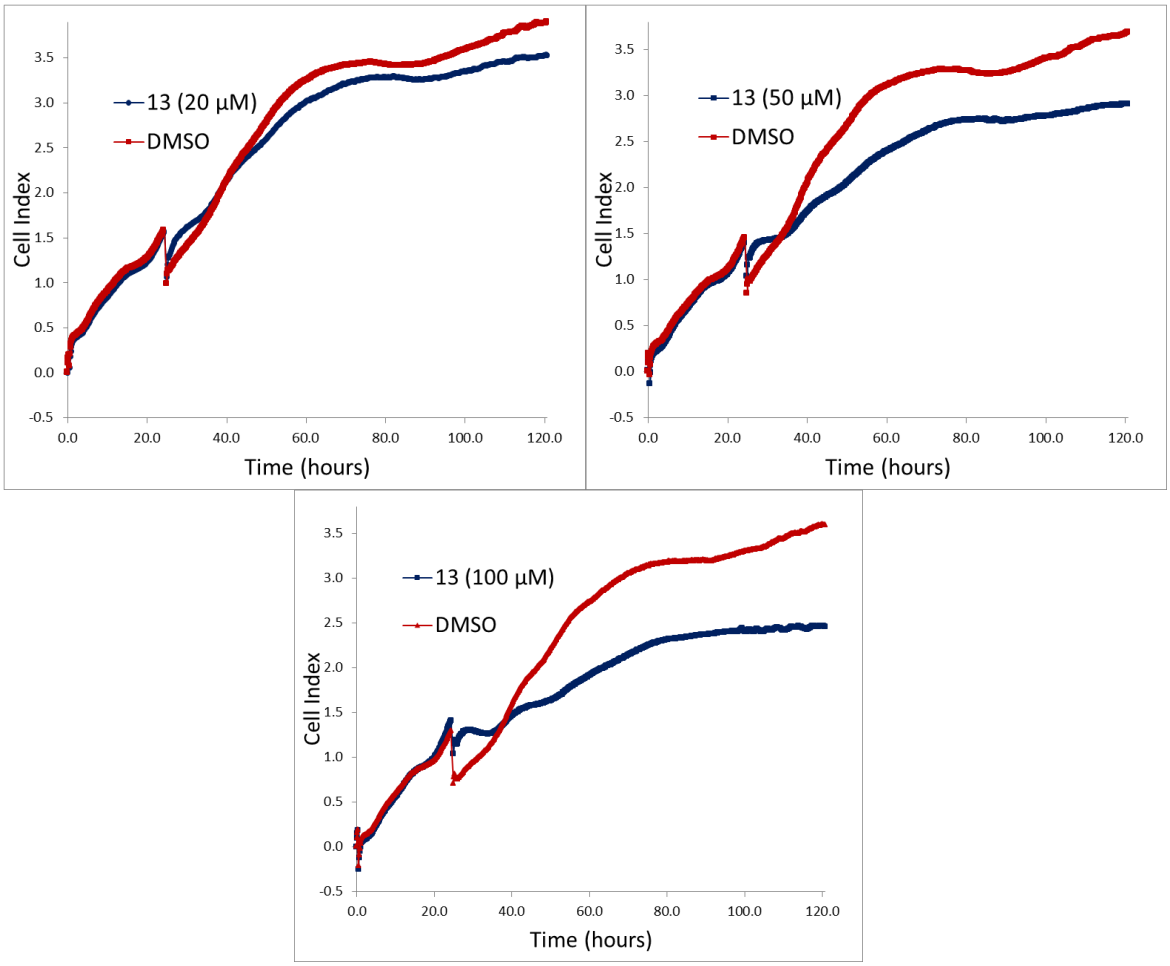

Figure 2.19. Effect of 13 on the proliferation of a HCT-116 +/+ cancer cell line. 13 was added after 24 hours and its effect monitored over 96 hours using iCELLigence (ACEA biosciences). Each data point is an average of 3 counts. Data provided by the Hupp group.

13 was found to inhibit cell proliferation in a dose dependent manner (0-100 µM) in both a HCT-116 (p53 +/+) cell line (Figure 2.19) and a HCT-116 (p53 -/-) cell line (data not shown). Further research is required to investigate if this is a cancer cell specific response and to explore if the observed cytotoxicity is a result of modulation of reptin's cellular functions or an alternative off-target effect. However, this preliminary result validates **13** as a promising cell permeable lead molecule for a medicinal chemistry drug development programme.

2.7 Conclusions and Future Work

Reptin is a central mediator of numerous cellular processes, mainly as a result of its role in the assembly of multiprotein complexes involved in the regulation of transcription, chromatin remodelling, DNA damage response and nutrient sensing. Reptin's involvement in cellular regulation, signalling and pathophysiology has identified it as a promising therapeutic target, particularly in the area of cancer research. However, little is known about factors that control its multiple functions and how the relevant signalling pathways are regulated. Herein we report the development of a multi-disciplinary chemical biology platform to discover and optimise small molecule modulators of reptin's protein interactome, thus providing chemical tools by which to further dissect reptin's role in oncogenesis.

This discovery platform involved the use of high-throughput virtual screening coupled to an *in vitro* PPI ELISA to identify two lead compounds, **13** and **17**, from an *in silico* 4.8 million conformer library. Synthetic optimisation of **17** guided by molecular modelling and biological evaluation resulted in the identification of a more active analogue, Liddean (**48**). The SAR optimisation process also provided valuable insight into the binding pose, conformation and potential mode of action of **17**. Future optimisation of Liddean (**48**) will focus on three areas: 1.) improved solubility 2.) optimisation of the C ring and 3.) generation of a tagged-derivative of Liddean (**48**).

1.) Improving the solubility of Liddean (**48**) will mainly focus on disruption of the π-system which stabilises the flat conformation of Liddean (**48**). Biphenyl ring systems are detrimental to solubility due to their planar hydrophobic nature, a larger screen of A ring derivatives could potentially lead to the identification a more optimal substituent. In addition, preliminary analysis of the effect of the pyridine-oxazole ring of Liddean (**48**) on its predicted solubility has highlighted this as an important region for optimisation.

2.) The expanding toolbox of C-H functionalisation methodology[106–108] provides an efficient and versatile method to access Liddean (**48**) analogues containing a diverse range of heterocyclic rings in place of the pyridine-oxazole.

3.) Finally, modification of the pyridine-oxazole ring of Liddean (**48**) or incorporation of a different substituent at this position would provide the opportunity to tag Liddean (**48**) with a photoaffinity label or a biotin linker. These Liddean (**48**) derivatives could facilitate the isolation of additional Liddean (**48**)-bound reptin PPIs using affinity chromatography.

Reptin's diverse range of biological functions are believed to be regulated in part, by its oligomeric state, which is currently known to exist from a monomer to a dodecamer. Liddean (**48**) was subsequently shown to induce the formation of higher order reptin oligomers. It is with this more stabilised oligomeric state of Liddean (**48**)-bound reptin, that peptides containing a ϕRERϕ motif were preferentially found to bind. The ϕRERϕ motif was subsequently validated as the core motif forming a reptin binding site on the tetramerisation domain of tumour suppressor protein, p53. The identification of this novel reptin-p53 PPI validates this platform as a valuable method for dissecting reptin's protein interactome. In particular, elucidation of reptin's role in regulating the essential tumour suppressor protein p53, could reveal a novel pathway involved in cancer development and provide a valuable new therapeutic target. Extensive research is underway to probe this interaction and to identify and validate further novel interacting proteins from the peptide-phage screen. In addition, a range of biochemical techniques are being used to analyse Liddean (**48**)'s effect on reptin and the resulting cellular responses, including, HD exchange, SEC-MALS, proximity ligation assay (PLA), fluorescence polarisation (FP) and cell growth assays.

The second hit compound **13** obtained from the *in silico* – *in vitro* screen was developed in parallel as a potential drug lead, due to its superior predicted solubility when compared to the chemical tool Liddean (**48**). A preliminary SAR study containing structurally related analogues identified from the virtual screen revealed that it was possible to modify the substituents connected to the (trifluoromethyl)pyrazolo-pyrimidine core, while maintaining its biological activity. A synthetic approach was developed to access **13**, which would in the future provide the opportunity to rapidly assemble a focused library of analogues containing the (trifluoromethyl)pyrazolo-pyrimidine core. The observed concentration dependent cytotoxicity of **13** against a HCT-116 cancer cell line validated it as promising cell permeable anticancer drug lead. Future work will focus on the development of a more potent lead compound through a combinatorial approach, and investigation if **13**'s observed cytotoxicity is a result of modulation of reptin's cellular functions.

The utility of this *in silico* – *in vitro* approach as a method to detect novel small molecule PPI modulators is exemplified by the expedient and cost efficient identification of the chemical tool Liddean (**48**) and drug-lead **13** from a 4.8 million conformer library. Furthermore, this platform could provide a powerful approach by which to identify modulators of other therapeutically relevant members of the AAA+ superfamily.

2.8 Experimental

2.8.1 General Considerations

All chemicals and solvents were purchased from Aldrich (UK), Alfa Aesar, or Acros Organics and used without further purification. All reactions involving moisture sensitive reagents were performed in oven or flame dried glassware under a positive pressure of nitrogen. Tetrahydrofuran (THF), dichloromethane (DCM) and hexanes were obtained dry from a solvent purification system (MBraun, SPS-800). Anhydrous *N*,*N*-dimethylformamide (DMF) was purchased from Aldrich.

Thin layer chromatography (TLC) analysis was performed using glass plates coated with silica gel (with fluorescent indicator UV_{254}). Developed plates were air dried and analysed under a UV lamp (254/365 nm) or by $KMnO_4$ dip staining. Flash chromatography was performed using silica gel (40-63 μm, Fluorochem).

Melting points were recorded in open capillaries using an Electrothermal 9100 melting point apparatus. Values are quoted to the nearest 1 °C and are uncorrected.

Fourier Transform infra-red spectra (FT IR) were acquired on a Perkin Elmer paragon 1000 FT spectrophometer (KBr disc) or a Shimadzu IRAffinity-1 FT spectrophotometer with a Pike MIRacle™ (solid or thin film). Absorption maxima are reported in wavenumbers (cm^{-1}).

Nuclear magnetic resonance (NMR) spectra were recorded at room temperature on Bruker Avance 500 (^1H, 499.9 MHz; ^{13}C, 125.7 MHz), Bruker Avance 400 (^1H, 400.1 MHz; ^{13}C, 100.6 MHz) and Bruker Avance 300 (^1H, 300.1 MHz; ^{13}C, 75.5 MHz) instruments. NMR spectra were recorded in deuterated solvents and internally referenced to the residual solvent peak, chloroform-*d* (δ_C 77.16, δ_H 7.26 ppm), acetone-d_6 (δ_C 29.8, δ_H 2.04 ppm), DMSO-d_6 (δ_C 39.52, δ_H 2.50 ppm) or methanol-d_4 (δ_C 49.0, δ_H 3.31 ppm). Chemical shifts are expressed as δ in units of ppm. ^{13}C NMR spectra were recorded using the PENDANT sequence mode. Data processing was carried out using the MestReNova 8.1.1 NMR program (Mestrelab Research S.L.). For ^1H NMR, the multiplicity used for assignment is indicated by the following abbreviations: s = singlet, d = doublet, t = triplet, q = quartet, p = pentet, h = sextet, hept = heptet, m = multiplet, br = broad. Signals of protons and carbons were assigned, as far as possible, by using the following two dimensional NMR spectroscopy techniques: [^1H, ^1H] COSY (Correlation Spectroscopy), [^1H, ^{13}C] HSQC (Heteronuclear Single Quantum Coherence) and long range [^1H, ^{13}C] HMBC (Heteronuclear Multiple Bond Connectivity).

Low resolution (LR) and high resolution (HR) electrospray mass spectral (ES-MS) analyses were acquired by electrospray ionisation (ESI). These were acquired by the EPSRC National Mass Spectrometry Service or within the School of Chemistry, University of St Andrews.

See Appendix B for the ^{1}H NMR spectra of the analogues of **13** and **17** purchased from Chembridge.

2.8.2 General Methods

General Method A: Synthesis of the Pyridine-oxazolo core

To polyphosphoric acid (~20 eq.) at 120 °C were added simultaneously 2-amino-3-hydroxypyridine **34** (1 eq.) and a range of substituted benzoic acids (1 eq.). The resulting mixture was heated to 200 °C for 4 hours. After cooling slightly, ice water was added to the reaction. The solution was neutralised by the slow addition of a saturated sodium hydrogen carbonate solution and the resulting precipitate collected by filtration. Drying in a vacuum oven yielded the pure product.

General Method B: *N*-acylation

To a solution of the appropriate aniline (**35a**-**j**) (1 eq.) in DCM (1 mL/mmol) was added a range of carbonyl chlorides (2.5 eq.). The mixture was stirred for 10 minutes before the dropwise addition of DIPEA (1.5 eq.). The reaction was stirred at room temperature for 24-72 hours. The resulting precipitate was filtered and dried to yield the desired compound. Recrystallisation from DCM afforded the product in high purity.

2.8.3 Experimental procedures

2-Chloro-5-(oxazolo[4,5-b]pyridin-2-yl)aniline (35a)[109]

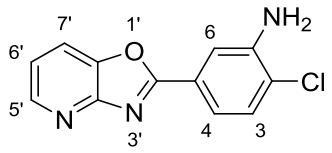

Prepared from 2-amino-3-hydroxypyridine **34** (4.00 g, 36.3 mmol, 1.0 eq.) and 3-amino-4-chlorobenzoic acid (6.23 g, 36.3 mmol, 1.0 eq.) using general method A. **35a** was obtained as a white solid (4.90 g, 55%). **mp** 205-208 °C; **IR** (solid) ν $_{max}$: 3453 (NH), 3345 (NH), 1614, 1406, 1261, 781 (C-Cl); **^{1}H NMR** (500 MHz, Chloroform-*d*) δ 8.57 (dd, *J* = 4.9, 1.5 Hz, 1H, C5'-H), 7.84 (dd, *J* = 8.1, 1.5 Hz, 1H, C7'-H), 7.73 (d, *J* = 2.0 Hz, 1H, C6-H), 7.61 (dd, *J* = 8.3, 2.0 Hz, 1H, C4-H), 7.40 (d, *J* = 8.3 Hz, 1H,

C3-H), 7.29 (dd, *J* = 8.1, 4.9 Hz, 1H, C6'-H), 4.30 (br s, 2H, NH_2); **^{13}C NMR** (126 MHz, Chloroform-*d*) δ 165.3 (C2'), 156.4 (C3'a), 146.9 (C5'), 143.6 (C1), 143.2 (C7'a), 130.2 (C3), 125.9 (C5), 123.6 (C2), 120.3 (C6'), 118.4 (C4), 118.3 (C7'), 114.8 (C6); ***m/z*** (ES^+) 246.04 ($[M+H]^+$, 100 %); **HRMS** (ES^+) Calcd for $C_{12}H_9ON_3Cl$ $[M+H]^+$: 246.0429, found 246.0431. Spectroscopic data are in accordance with the literature.[109]

2-Bromo-5-(oxazolo[4,5-b]pyridin-2-yl)aniline (35b)

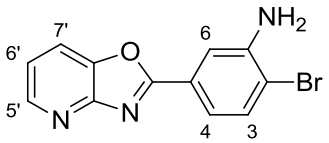

Prepared from 2-amino-3-hydroxypyridine **34** (600 mg, 5.45 mmol) and 3-amino-4-bromobenzoic acid (1.18 g, 5.45 mmol, 1.0 eq.) using general method A. **35b** was obtained as a pale brown solid (1.38 g, 87%). **mp** 211-212 °C; **IR** (solid) ν_{max}: 3418 (NH), 3287 (NH), 3171, 1736, 1620, 1597, 1543, 1404; **^{1}H NMR** (300 MHz, DMSO-d_6) δ 8.54 (dd, *J* = 4.9, 1.4 Hz, 1H, C5'-H), 8.23 (dd, *J* = 8.2, 1.4 Hz, 1H, C7'-H), 7.70 (d, *J* = 2.1 Hz, 1H, C6-H), 7.61 (d, *J* = 8.2 Hz, 1H, C3-H), 7.46 (dd, *J* = 8.2, 4.9 Hz, 1H, C6'-H), 7.31 (dd, *J* = 8.2, 2.1 Hz, 1H, C4-H), 5.79 (br s, 2H, NH_2); **^{13}C NMR** (75 MHz, DMSO-d_6) δ 164.7 (C2'), 155.5 (C3'a), 146.7 (C1), 146.5 (C5'), 142.7 (C7'a), 133.3 (C3), 125.8 (C5), 120.7 (C6'), 119.0 (C7'), 115.9 (C4), 113.5 (C6), 111.8 (C2); ***m/z*** (ES^+) 289.99 ($[^{79}BrM+H]^+$, 100 %), 291.99 ($[^{81}BrM+H]^+$, 100%); **HRMS** (ES^+) Calcd for $C_{12}H_9ON_3Br$ $[M+H]^+$: 289.9924, found 289.9927.

2-(Oxazolo[4,5-b]pyridin-2-yl)aniline (35c)

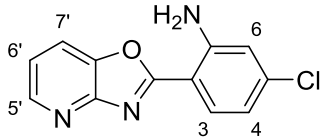

Prepared from 2-amino-3-hydroxypyridine **34** (600 mg, 5.45 mmol, 1.0 eq.) and 2-amino-4-chlorobenzoic acid (935 mg, 5.45 mmol, 1.0 eq.) using general method A. **35c** was obtained as a white solid (690 mg, 52%). **mp** 256-259 °C; **IR** (solid) ν_{max}: 3402 (NH), 3310 (NH), 3201, 1612, 1543, 1481, 1404, 772 (C-Cl); **^{1}H NMR** (500 MHz, DMSO-d_6) δ 8.51 (d, *J* = 5.2 Hz, 1H, C5'-H), 8.19 (d, *J* = 8.2 Hz, 1H, C7'-H), 7.94 (d, *J* = 8.3 Hz, 1H, C3-H), 7.50 – 7.35 (m, 3H, C6'-H, NH_2), 7.01 (s, 1H, C6-H), 6.73 (d, *J* = 8.3 Hz, 1H, C4-H); **^{13}C NMR** (126 MHz, DMSO-d_6) δ 164.2 (C2'), 155.2 (C3'a), 150.3 (C1), 146.2 (C5'), 141.1 (C7'a), 138.1 (C5), 129.9 (C3), 120.5 (C6'), 118.5 (C7'), 115.6 (C4), 115.1 (C6), 104.6 (C2); ***m/z*** (ES^+) 246.04 ($[M+H]^+$, 100%); **HRMS** (ES^+) Calcd for $C_{12}H_9ON_3Cl$ $[M+H]^+$: 246.0429, found 246.0430.

3-(Oxazolo[4,5-b]pyridin-2-yl)aniline (35d)[109]

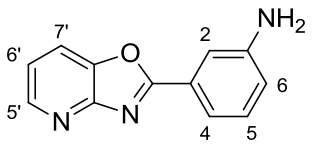

Prepared from 2-amino-3-hydroxypyridine **34** (300 mg, 2.70 mmol, 1.0 eq) and 3-aminobenzoic acid (370 mg, 2.70 mmol, 1.0 eq.) using general method A. **35d** was obtained as an off-white solid (500 mg, 88%). **mp** 186-189 °C; **^{1}H NMR** (300 MHz, DMSO-d_6) δ 8.52 (dd, *J* = 4.9, 1.5 Hz, 1H, C5'-H), 8.21 (dd, *J* = 8.1, 1.5 Hz, 1H, C7'-H), 7.48 (app. t, *J* = 2.0, 1H, C2-H), 7.44 (dd, *J* = 8.1, 4.9 Hz, 1H, C6'-H), 7.38 (ddd, *J* = 7.8, 2.0, 1.1 Hz, 1H, C4-H), 7.26 (app. t, *J* = 7.8 Hz, 1H, C5-H), 6.84 (ddd, *J* = 7.8, 2.0, 1.1 Hz, 1H, C6-H), 5.55 (br s, 2H, NH_2); **^{13}C NMR** (75 MHz, DMSO-d_6) δ 165.6 (C2'), 155.6 (C3'a), 149.5 (C1), 146.4 (C5'), 142.6 (C7'a), 129.9 (C5), 126.3 (C3), 120.5 (C6'), 118.9 (C7'), 118.1 (C6), 114.9 (C4), 112.3 (C2); ***m/z*** (ES^+) 218.08 ($[M+H]^+$, 100 %); **HRMS** (ES^+) Calcd for $C_{12}H_{10}ON_3$ $[M+H]^+$: 212.0818, found 212.0818. Spectroscopic data are in accordance with the literature.[109]

4-(Oxazolo[4,5-b]pyridin-2-yl)aniline (35e)[110]

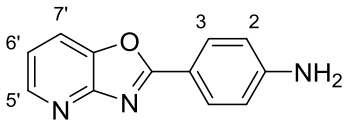

Prepared from 2-amino-3-hydroxypyridine **34** (600 mg, 5.45 mmol, 1.0 eq.) and 4-aminobenzoic acid (747 mg, 5.45 mmol, 1.0 eq.) using general method A. **35e** was obtained as a pale yellow solid (906 mg, 79%). **mp** 257-259 °C (lit. 252-254 °C[110]); **IR** (solid) ν_{max}: 3395 (NH), 3310 (NH), 3202, 1605, 1489, 1404; **^{1}H NMR** (500 MHz, DMSO-d_6) δ 8.41 (dd, *J* = 4.9, 1.3 Hz, 1H, C5'-H), 8.07 (dd, *J* = 8.1, 1.3 Hz, 1H, C7'-H), 7.91 (d, *J* = 8.6 Hz, 2H, C3-H), 7.31 (dd, *J* = 8.1, 4.9 Hz, 1H, C6'-H), 6.71 (d, *J* = 8.6 Hz, 2H, C2-H), 6.17 (br s, 2H, NH_2); **^{13}C NMR** (126 MHz, DMSO-d_6) δ 166.0 (C2'), 156.4 (C3'a), 153.4 (C1), 145.7 (C5'), 142.3 (C7'a), 129.6 (C3), 119.3 (C6'), 117.8 (C7'), 113.5 (C2), 111.7 (C4); ***m/z*** (ES^+) 212.0 ($[M+H]^+$, 100%); **HRMS** (ES^+) Calcd for $C_{12}H_{10}ON_3$ $[M+H]^+$: 212.0818, found 212.0818. Spectroscopic data are in accordance with the literature.[110]

2-Fluoro-5-(oxazolo[4,5-b]pyridin-2-yl)aniline (35f)

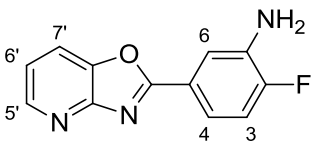

Prepared from 2-amino-3-hydroxypyridine **34** (75 mg, 0.68 mmol, 1.0 eq.) and 3-amino-4-fluorobenzoic acid (105 mg, 0.68 mmol, 1.0 eq.) using general method A. **35f** was obtained as an off-

white solid (65 mg, 50%). **mp** 214-216 °C; **IR** (solid) ν $_{max}$: 3464 (NH), 3318 (NH), 3194, 3039, 1613, 1497, 1404, 1173 (C-F); **^{1}H NMR** (400 MHz, DMSO-d_6) δ 8.52 (dd, *J* = 4.9, 1.4 Hz, 1H, C5'-H), 8.21 (dd, *J* = 8.2, 1.4 Hz, 1H, C7'-H), 7.69 (dd, *J* = 8.6, 2.2 Hz, 1H, C6-H), 7.51 – 7.35 (m, 2H, C6'-H, C4-H), 7.25 (dd, *J* = 11.3, 8.4 Hz, 1H, C3-H), 5.65 (br s, 2H, NH$_2$); **^{13}C NMR** (101 MHz, DMSO-d_6) δ 164.8 (C2'), 155.6 (C3'a), 153.1 (d, *J* = 245.3 Hz, C2), 146.4 (C5'), 142.7 (C7'a), 137.5 (d, *J* = 13.8 Hz, C1), 122.4 (d, *J* = 2.7 Hz, C5), 120.53 (C6'), 118.9 (C7'), 116.0 (d, *J* = 19.8 Hz, C3), 115.8 (d, *J* = 7.4 Hz, C4), 115.0 (d, *J* = 6.3 Hz, C6); ***m/z*** (ES$^+$) 230.07 ([M+H]$^+$, 100 %); **HRMS** (ES$^+$) Calcd for $C_{12}H_9ON_3F$ [M+H]$^+$: 230.0724, found 230.0725.

2-Methyl-5-(oxazolo[4,5-b]pyridin-2-yl)aniline (35g)

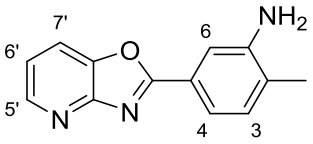

Prepared from 2-amino-3-hydroxypyridine **34** (500 mg, 4.54 mmol, 1.0 eq.) and 3-amino-4-methylbenzoic acid (686 mg, 4.54 mmol, 1.0 eq.) using general method A. **35g** was obtained as a pale brown solid (716 mg, 71%). **mp** 171-173 °C; **IR** (solid) ν $_{max}$: 3426 (NH), 3325 (NH), 3055, 1736, 1620, 1551, 1497, 1404, 1234, 779; **^{1}H NMR** (500 MHz, DMSO-d_6) δ 8.51 (dd, *J* = 4.9, 1.4 Hz, 1H, C5'-H), 8.19 (dd, *J* = 8.1, 1.4 Hz, 1H, C7'-H), 7.53 (d, *J* = 1.8 Hz, 1H, C6-H), 7.42 (dd, *J* = 8.1, 4.9 Hz, 1H, C6'-H), 7.36 (dd, *J* = 7.6, 1.8 Hz, 1H, C4-H), 7.17 (d, *J* = 7.6 Hz, 1H, C3-H), 5.33 (br s, 2H, NH$_2$), 2.15 (s, 3H, CH$_3$); **^{13}C NMR** (126 MHz, DMSO-d_6) δ 165.8 (C2'), 155.8 (C3'a), 147.5 (C1), 146.3 (C5'), 142.5 (C7'a), 130.8 (C3), 126.6 (C2), 124.0 (C5), 120.3 (C6'), 118.7 (C7'), 115.3 (C4), 112.3 (C6), 17.7 (CH$_3$); ***m/z*** (ES$^+$) 226.09 ([M+H]$^+$, 100 %); **HRMS** (ES$^+$) Calcd for $C_{12}H_{12}ON_3$ [M+H]$^+$: 226.0975, found 226.0974. ^{1}H & ^{13}C NMR data not in accordance with literature.[109]

4-Amino-2-(oxazolo[4,5-b]pyridin-2-yl)phenol (35h)[111]

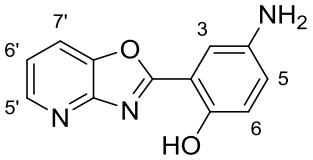

Prepared from 2-amino-3-hydroxypyridine **34** (600 mg, 5.45 mmol, 1.0 eq.) and 5-aminosalicylic acid (835 mg, 5.45 mmol, 1.0 eq.) using general method A. **35h** was obtained as a dark yellow solid (690 mg, 49%). **mp** 191-193 °C (lit. 181-183 °C[111]); **IR** (solid) ν $_{max}$: 3426 (NH), 3310 (NH), 3202 (OH), 1620, 1535, 1497, 1404, 779; **^{1}H NMR** (500 MHz, DMSO-d_6) δ 10.19 (br s, 1H, OH), 8.55 (dd, *J* = 4.9, 1.4 Hz, 1H, C5'-H), 8.27 (dd, *J* = 8.1, 1.4 Hz, 1H, C7'-H), 7.48 (dd, *J* = 8.1, 4.9 Hz, 1H, C6'-H), 7.27 (d, *J* = 2.3 Hz, 1H, C3-H), 6.89 – 6.86 (m, 2H, C5-H, C6-H), 5.02 (br s, 2H, NH$_2$); **^{13}C NMR** (126 MHz, DMSO-d_6) δ

165.2 (C2'), 153.9 (C3'a), 149.7 (C1), 146.6 (C5'), 141.8 (C4), 141.4 (C7'a), 122.3 (C5), 120.8 (C6'), 119.0 (C7'), 117.9 (C6), 110.4 (C3), 109.5 (C2); ***m/z*** (ES^+) 228.07 ($[M+H]^+$, 100%); **HRMS** (ES^+) Calcd for $C_{12}H_{10}O_2N_3$ $[M+H]^+$: 228.0768, found 228.0768.

3-(Oxazolo[4,5-b]pyridin-2-yl)phenol (35i)[112]

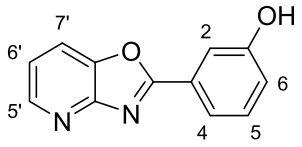

Prepared from 2-amino-3-hydroxypyridine **34** (55 mg, 0.5 mmol, 1.0 eq.) and 3-hydroxybenzoic acid (69 mg, 0.5 mmol, 1.0 eq.) using general method A. **35i** was obtained as a white solid (75 mg, 71%). **mp** 198-201 °C (lit. 203-204 °C[112]); **IR** (solid) ν $_{max}$: 3030 (OH), 2922 (OH), 2603, 1601, 1551, 1449, 1294, 887, 781; **^{1}H NMR** (500 MHz, DMSO-d_6) δ 10.06 (br s, 1H, O<u>H</u>), 8.54 (dd, *J* = 4.9, 1.4 Hz, 1H, C5'-<u>H</u>), 8.24 (dd, *J* = 8.1, 1.4 Hz, 1H, C7'-<u>H</u>), 7.69 (d, *J* = 7.9 Hz, 1H, C4-<u>H</u>), 7.72 – 7.66 (m, 1H, C2-<u>H</u>), 7.50 – 7.40 (m, 2H, C6'-<u>H</u>, C5-<u>H</u>), 7.07 (ddd, *J* = 8.2, 2.5, 1.0 Hz, 1H, C6-<u>H</u>); **^{13}C NMR** (126 MHz, DMSO-d_6) δ 164.9 (C2'), 158.0 (C1), 155.5 (C3'a), 146.6 (C5'), 142.8 (C7'a), 130.7 (C5), 127.0 (C3), 120.8 (C6'), 120.0 (C6), 119.1 (C7'), 118.5 (C4), 114.0 (C2); ***m/z*** (ES^+) 213.06 ($[M+H]^+$, 100 %); **HRMS** (ES^+) Calcd for $C_{12}H_9O_2N_2$ $[M+H]^+$: 213.0659, found 213.0659. Spectroscopic data are in accordance with the literature.[112]

5-(Benzo[d]oxazol-2-yl)-2-bromoaniline (35j)

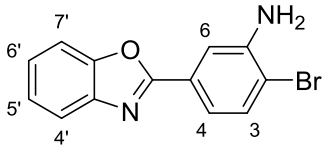

Prepared from 2-aminophenol (545 mg, 5.00 mmol, 1.0 eq.) and 3-amino-4-bromobenzoic acid (1.08 g, 5.00 mmol, 1.0 eq.) using general method A. **35j** was obtained as an off-white solid (653 mg, 45%). **mp** 198-200 °C; **IR** (solid) ν $_{max}$: 3449 (NH), 3310 (NH), 3179, 1612, 1543, 1435, 1242, 1065, 741; **^{1}H NMR** (500 MHz, DMSO-d_6) δ 7.81 – 7.75 (m, 2H, C4'-<u>H</u>, C7'-<u>H</u>), 7.66 (d, *J* = 2.1 Hz, 1H, C6-<u>H</u>), 7.57 (d, *J* = 8.2 Hz, 1H, C3-<u>H</u>), 7.46 – 7.37 (m, 2H, C5'-<u>H</u>, C6'-<u>H</u>), 7.27 (dd, *J* = 8.2, 2.1 Hz, 1H, C4-<u>H</u>), 5.75 (br s, 2H, N<u>H$_2$</u>); **^{13}C NMR** (126 MHz, DMSO-d_6) δ 162.2 (C2'), 150.1 (C3'a), 146.6 (C1), 141.5 (C7'a), 133.2 (C3), 126.3 (C5), 125.5 (C5'), 124.9 (C6'), 119.8 (C4'), 115.7 (C4), 113.3 (C6), 111.0 (C2), 110.9 (C7'); ***m/z*** (ES^+) 288.99 ($[^{79}BrM+H]^+$, 100 %), 290.99 ($[^{81}BrM+H]^+$, 100%); **HRMS** (ES^+) Calcd for $C_{13}H_{10}ON_2Br$ $[M+H]^+$: 288.9971, found 288.9975.

***N*-(2-Chloro-5-(oxazolo[4,5-b]pyridin-2-yl)phenyl)-[1,1'-biphenyl]-4-carboxamide (17)**

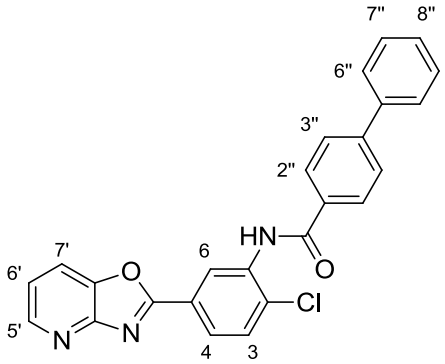

Prepared from **35a** (300 mg, 1.42 mmol, 1.0 eq.) and biphenyl-4-carbonyl chloride (769 mg, 3.55 mmol, 2.5 eq.) using general method B. **17** was obtained after recrystallisation as a white solid (346 mg, 57%). **mp** 254-256 °C; **IR** (KBr) ν $_{max}$: 3416 (NH), 3275, 3059, 3033, 1653 (C=O); **^{1}H NMR** (400 MHz, DMSO-d_6) δ 10.39 (br s, 1H, NH), 8.61 – 8.53 (m, 2H, C5'-H, C6-H), 8.29 (dd, *J* = 8.2, 1.5 Hz, 1H, C7'-H), 8.19 – 8.11 (m, 3H, C4-H, 2 × C2''-H), 7.93 – 7.83 (m, 3H, C3-H, 2 × C3''-H), 7.82 – 7.75 (m, 2H, 2 × C6''-H), 7.57 – 7.46 (m, 3H, C6'-H, 2 × C7''-H), 7.49 – 7.39 (m, 1H, C8''-H); **^{13}C NMR** (101 MHz, DMSO-d_6) δ 165.3 (CO), 163.7 (C2'), 155.4 (C3'a), 146.8 (C5'), 143.6 (C4''), 143.0 (C7'a), 139.0 (C5''), 136.2 (C1), 133.4 (C2), 132.5 (C1''), 131.0 (C3), 129.1 (2 × C7''), 128.6 (2 × C2''), 128.3 (C8''), 127.0 (2 × C6''), 126.8 (2 × C3''), 126.6 (C6), 126.1 (C4), 125.2 (C5), 121.1 (C6'), 119.3 (C7'); ***m/z*** (ES$^-$) 423.82 ([M-H]$^-$, 100 %); **HRMS** (ES$^-$) Calcd for $C_{25}H_{15}ClN_3O_2$ [M-H]$^-$: 424.0839, found 424.0853.

***N*-(2-Bromo-5-(oxazolo[4,5-b]pyridin-2-yl)phenyl)benzamide (42)**

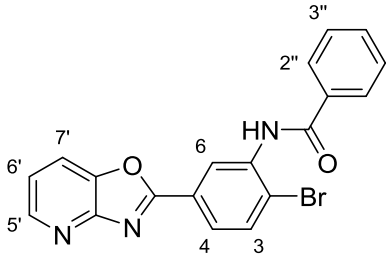

Prepared from **35b** (80 mg, 0.28 mmol, 1.0 eq.) and benzoyl chloride (98 mg, 0.70 mmol, 2.5 eq.) using general method B. **42** was obtained after recrystallisation as a white solid (74 mg, 67%). **mp** 249-251 °C; **IR** (solid) ν $_{max}$: 3271 (NH), 3055, 1651 (C=O), 1520, 1404, 1257, 779, 709, 640 (C-Br); **^{1}H NMR** (400 MHz, DMSO-d_6) δ 10.29 (br s, 1H, NH), 8.58 (dd, *J* = 4.9, 1.4 Hz, 1H, C5'-H), 8.47 (d, *J* = 2.0 Hz, 1H, C6-H), 8.28 (dd, *J* = 8.3, 1.4 Hz, 1H, C7'-H), 8.10 – 7.98 (m, 4H, C3-H, C4-H, 2 × C2''-H), 7.69 – 7.62 (m, 1H, C4''-H), 7.58 (dd, *J* = 8.3, 6.5 Hz, 2H, 2 × C3''-H), 7.50 (dd, *J* = 8.3, 4.9 Hz, 1H, C6'-H); **^{13}C NMR** (101 MHz, DMSO-d_6) δ 165.6 (CO), 163.7 (C2'), 155.3 (C3'a), 146.8 (C5'), 142.9 (C7'a), 137.6 (C1), 134.1 (C3), 133.8 (C1''), 132.1 (C4''), 128.6 (2 × C2''), 127.8 (2 × C3''), 126.8 (C6), 126.4 (C4),

125.8 (C5), 124.9 (C2), 121.1 (C6'), 119.3 (C7'); ***m/z*** (ES^+) 394.02 ($[^{79}BrM+H]^+$, 100 %), 396.02 ($[^{81}BrM+H]^+$, 100%); **HRMS** (ES^+) Calcd for $C_{19}H_{13}O_2N_3Br$ $[M+H]^+$: 394.0186, found 394.0188.

***N*-(2-Bromo-5-(oxazolo[4,5-b]pyridin-2-yl)phenyl)-2-(3-methoxyphenyl)acetamide (43)**

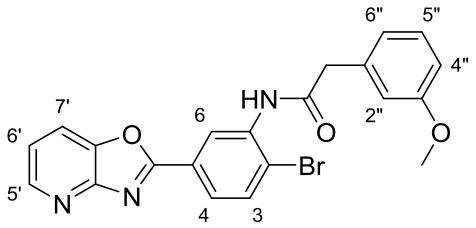

Prepared from **35b** (80 mg, 0.28 mmol, 1.0 eq.) and 3-methoxyphenylacetyl chloride (129 mg, 0.70 mmol, 2.5 eq.) using general method B. **43** was obtained after recrystallisation as a white solid (92 mg, 75%). **mp** 211-213 °C; **IR** (solid) ν_{max}: 3271 (NH), 1667 (C=O), 1551, 1404, 1265, 1157, 802; **^{1}H NMR** (400 MHz, DMSO-d_6) δ 9.87 (br s, 1H, NH), 8.56 (dd, *J* = 4.8, 1.4 Hz, 1H, C5'-H), 8.52 (s, 1H, C6-H), 8.27 (dd, *J* = 8.3, 1.4 Hz, 1H, C7'-H), 7.94 (br s, 2H, C3-H, C4-H), 7.48 (dd, *J* = 8.3, 4.8 Hz, 1H, C6'-H), 7.27 (t, *J* = 7.8 Hz, 1H, C5''-H), 7.02 – 6.95 (m, 2H, C2''-H, C6''-H), 6.85 (dd, *J* = 7.8, 2.3 Hz, 1H, C4''-H), 3.78 (s, 2H, CH_2), 3.76 (s, 3H, OCH_3); **^{13}C NMR** (101 MHz, DMSO-d_6) δ 169.7 (CO), 163.8 (C2'), 159.3 (C3''), 155.3 (C3'a), 146.8 (C5'), 142.9 (C7'a), 137.2 (C), 137.0 (C), 134.1 (C3), 129.4 (C5''), 125.6 (C5), 125.4 (C4), 124.7 (C6), 121.6 (C2), 121.5 (C6''), 121.1 (C6'), 119.3 (C7'), 115.0 (C2''), 112.2 (C4''), 55.0 (OCH_3), 42.6 (CH_2); ***m/z*** (ES^+) 438.04 ($[^{79}BrM+H]^+$, 100 %), 440.04 ($[^{81}BrM+H]^+$, 100%); **HRMS** (ES^+) Calcd for $C_{21}H_{17}O_3N_3Br$ $[M+H]^+$: 438.0448, found 438.0449.

***N*-(5-Chloro-2-(oxazolo[4,5-b]pyridin-2-yl)phenyl)-[1,1'-biphenyl]-4-carboxamide (44)**

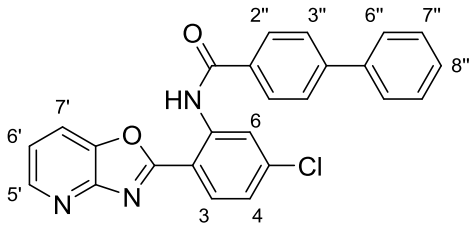

Prepared from **35c** (550 mg, 2.60 mmol, 1.0 eq.) and biphenyl-4-carbonyl chloride (1.41 g, 6.50 mmol, 2.5 eq.) using general method B. **44** was obtained after recrystallisation as a pale yellow solid (185 mg, 17%). **mp** 254-256 °C **IR** (KBr) ν_{max}: 3408 (NH), 3072, 3032, 1684 (C=O), 1590; **^{1}H NMR** (500 MHz, Chloroform-*d*) δ 12.64 (br s, 1H, NH), 9.21 (d, *J* = 2.0 Hz, 1H, C6-H), 8.63 (dd, *J* = 4.9, 1.4 Hz, 1H, C5'-H), 8.36 (d, *J* = 8.3 Hz, 2H, 2 × C2''-H), 8.20 (d, *J* = 8.5 Hz, 1H, C3-H), 7.92 (dd, *J* = 8.1, 1.4 Hz, 1H, C7'-H), 7.86 (d, *J* = 8.3 Hz, 2H, 2 × C3''-H), 7.73 – 7.66 (m, 2H, 2 × C6''-H), 7.49 (dd, *J* = 8.3, 6.8 Hz, 2H, 2 × C7''-H), 7.44 – 7.39 (m, 1H, C8''-H), 7.38 (dd, *J* = 8.1, 4.9 Hz, 1H, C6'-H), 7.23 (dd, *J* = 8.5, 2.0 Hz, 1H, C4-H); **^{13}C NMR** (126 MHz, Chloroform-*d*) δ 166.1 (CO), 164.0 (C2'), 154.9 (C3'a), 147.3 (C5'),

145.2 (C4''), 141.8 (C7'a), 141.0 (C5), 140.6 (C1), 140.1 (C5''), 133.0 (C1''), 129.4 (C3), 129.0 (2 × C7''), 128.5 (2 × C2''), 128.2 (C8''), 127.8 (2 × C3''), 127.4 (2 × C6''), 123.6 (C4), 121.0 (C6'), 120.9 (C6), 118.6 (C7'), 110.8 (C2); ***m/z*** (ES^+) 447.86 $[M+Na]^+$; **HRMS** (ES^+) Calcd for $C_{25}H_{16}ClN_3O_2Na$ $[M+Na]^+$: 448.0829, found 448.0826.

***N*-(3-(Oxazolo[4,5-b]pyridin-2-yl)phenyl)-[1,1'-biphenyl]-4-carboxamide (45)**

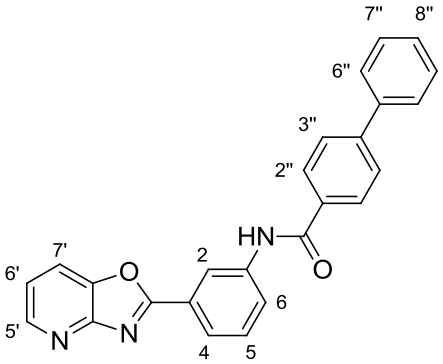

Prepared from **35d** (150 mg, 0.71 mmol, 1.0 eq.) and biphenyl-4-carbonyl chloride (385 mg, 1.78 mmol, 2.5 eq.) using general method B. **45** was obtained after recrystallisation as a white solid (33 mg, 12%). **mp** 261-264 °C; **IR** (KBr) ν $_{max}$: 3440 (NH), 2962, 2924, 1649 (C=O), 1527; **^{1}H NMR** (300 MHz, DMSO-d_6) δ 10.63 (br s, 1H, NH), 8.87 (t, *J* = 1.9 Hz, 1H, C2-H), 8.56 (dd, *J* = 4.9, 1.4 Hz, 1H, C5'-H), 8.27 (dd, *J* = 8.2, 1.4 Hz, 1H, C7'-H), 8.19 – 8.06 (m, 3H, C6-H, 2 × C2''-H), 8.04 – 7.93 (m, 1H, C4-H), 7.92 – 7.82 (m, 2H, 2 × C3''-H), 7.82 – 7.72 (m, 2H, 2 × C6''-H), 7.64 (t, *J* = 8.0 Hz, 1H, C5-H), 7.57 – 7.36 (m, 4H, C6'-H, C8''-H, 2 × C7''-H); **^{13}C NMR** (75 MHz, DMSO-d_6) δ 165.5 (CO), 164.8 (C2'), 155.5 (C3'a), 146.6 (C5'), 143.4 (C4''), 142.8 (C7'a), 140.2 (C1), 139.1 (C5''), 133.3 (C1''), 129.9 (C5), 129.1 (2 × C7''), 128.5 (2 × C2''), 128.2 (C8''), 127.0 (2 × C6''), 126.7 (2 × C3''), 126.3 (C3), 124.1 (C6), 122.8 (C4), 120.9 (C6'), 119.1 (CH), 119.0 (CH); ***m/z*** (ES^-) 389.84 ($[M-H]^-$, 100 %); **HRMS** (ES^-) Calcd for $C_{25}H_{16}N_3O_2$ $[M-H]^-$: 390.1245, found 390.1243.

***N*-(4-(Oxazolo[4,5-b]pyridin-2-yl)phenyl)-[1,1'-biphenyl]-4-carboxamide (46)**

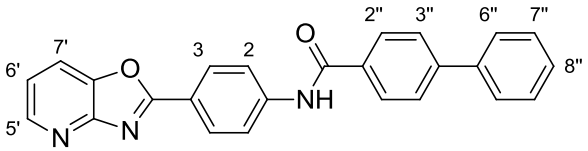

Prepared from **35e** (300 mg, 1.42 mmol, 1.0 eq.) and biphenyl-4-carbonyl chloride (769 mg, 3.55 mmol, 2.5 eq.) using general method B. **46** was obtained after recrystallisation as an off-white solid (202 mg, 36%). **mp** 322-325 °C; **IR** (KBr) ν $_{max}$: 3358 (NH), 3067, 3056, 1672 (C=O), 1599; **^{1}H NMR** (400 MHz, DMSO-d_6) δ 10.70 (br s, 1H, NH), 8.54 (dd, *J* = 4.9, 1.4 Hz, 1H, C5'-H), 8.27 (d, *J* = 8.8 Hz, 2H, 2 × C3-H), 8.23 (dd, *J* = 8.1, 1.4 Hz, 1H, C7'-H), 8.17 – 8.06 (m, 4H, 2 × C2-H, 2 × C2''-H) 7.91 – 7.84 (m,

2H, 2 × C3''-H), 7.83 – 7.72 (m, 2H, 2 × C6''-H), 7.57 – 7.49 (m, 2H, 2 × C7''-H), 7.48 – 7.38 (m, 2H, C6'-H, C8''-H); **^{13}C NMR** (101 MHz, DMSO-d_6) δ 165.7 (CO), 164.8 (C2'), 155.8 (C3'a), 146.4 (C5'), 143.5 (C), 143.4 (C), 142.7 (C7'a), 139.0 (C5''), 133.3 (C1''), 129.1 (2 × C7''), 128.6 (2 × CH), 128.6 (2 × CH), 128.3 (C8''), 127.0 (2 × C6''), 126.7 (2 × C3''), 120.6 (C4), 120.5 (C6'), 120.3 (2 × C2), 118.8 (C7'); ***m/z*** (ES^-) 389.91 ($[M-H]^-$, 100 %); **HRMS** (ES^-) Calcd for $C_{25}H_{16}N_3O_2$ $[M-H]^-$: 390.1234, found 390.1243.

***N*-(2-Fluoro-5-(oxazolo[4,5-b]pyridin-2-yl)phenyl)-[1,1'-biphenyl]-4-carboxamide (47)**

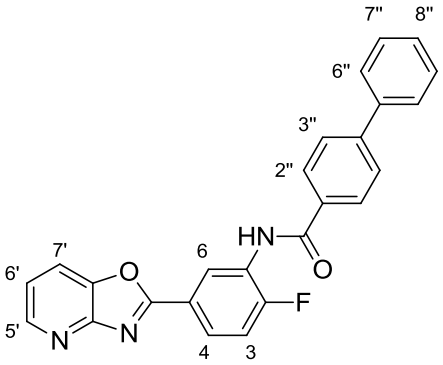

Prepared from **35f** (51 mg, 0.22 mmol, 1.0 eq.) and biphenyl-4-carbonyl chloride (119 mg, 0.55 mmol, 2.5 eq.) using general method B. **47** was obtained after recrystallisation as a white solid (75 mg, 83%). **mp** 230-232 °C; **IR** (solid) ν_{max}: 3441 (NH), 3040, 1674 (C=O), 1520, 1404, 1250 (C-F); **^{1}H NMR** (400 MHz, DMSO-d_6) δ 10.47 (br s, 1H, NH), 8.65 (dd, *J* = 7.3, 2.3 Hz, 1H, C6-H), 8.57 (dd, *J* = 4.9, 1.4 Hz, 1H, C5'-H), 8.28 (dd, *J* = 8.2, 1.4 Hz, 1H, C7'-H), 8.20 – 8.15 (m, 1H, C4-H), 8.13 (d, *J* = 8.4 Hz, 2H, 2 × C2''-H), 7.94 – 7.83 (m, 2H, 2 × C3''-H), 7.83 – 7.74 (m, 2H, 2 × C6''-H), 7.62 (dd, *J* = 10.2, 8.7 Hz, 1H, C3-H), 7.58 – 7.37 (m, 4H, C6'-H, 2 × C7''-H, C8''-H); **^{13}C NMR** (101 MHz, DMSO-d_6) δ 165.3 (CO), 163.9 (C2'), 157.8 (d, *J* = 254.7 Hz, C2), 155.5 (C3'a), 146.67 (C5'), 143.6 (C4''), 142.9 (C7'a), 139.0 (C5''), 132.4 (C1''), 129.1 (2 × C7''), 128.7 (2 × C2''), 128.3 (C8''), 127.1 (d, *J* = 12.6 Hz, C1), 127.0 (2 × C6''), 126.7 (2 × C3''), 126.3 (d, *J* = 9.1 Hz, C4), 125.7 (C6), 122.4 (d, *J* = 3.0 Hz, C5), 120.9 (C6'), 119.2 (C7'), 117.4 (d, *J* = 21.6 Hz, C3); ***m/z*** (ES^+) 410.12 ($[M+H]^+$, 100 %); **HRMS** (ES^+) Calcd for $C_{25}H_{17}FN_3O_2$ $[M+H]^+$: 410.1299, found 410.1299.

***N*-(2-Bromo-5-(oxazolo[4,5-b]pyridin-2-yl)phenyl)-[1,1'-biphenyl]-4-carboxamide (48; Liddean)**

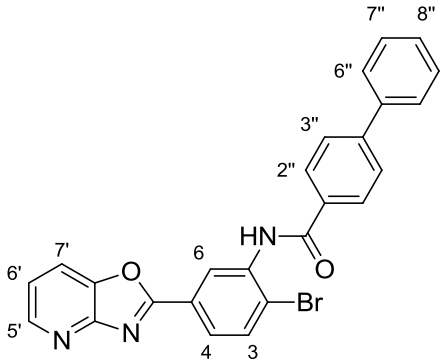

Prepared from **35b** (300 mg, 1.04 mmol, 1.0 eq.) and biphenyl-4-carbonyl chloride (563 mg, 2.60 mmol, 2.5 eq.) using general method B. **Liddean (48)** was obtained after recrystallisation as a white solid (200 mg, 41%). **mp** 237-240 °C; **IR** (KBr) ν $_{max}$: 3460 (NH), 3271, 2666, 1653 (C=O), 1521; **^{1}H NMR** (500 MHz, DMSO-d_6) δ 10.34 (br s, 1H, NH), 8.58 (dd, *J* = 4.8, 1.4 Hz, 1H, C5'-H), 8.49 (d, *J* = 2.1 Hz, 1H, C6-H), 8.29 (dd, *J* = 8.1, 1.4 Hz, 1H, C7'-H), 8.18 – 8.11 (m, 2H, 2 × C2''-H), 8.07 (dd, *J* = 8.4, 2.1 Hz, 1H, C4-H), 8.03 (d, *J* = 8.4 Hz, 1H, C3-H), 7.93 – 7.86 (m, 2H, 2 × C3''-H), 7.79 (m, 2H, 2 × C6''-H), 7.56 – 7.47 (m, 3H, C6'-H, 2 × C7''-H), 7.47 – 7.40 (m, 1H, C8''-H); **^{13}C NMR** (126 MHz, DMSO-d_6) δ 165.2 (CO), 163.8 (C2'), 155.4 (C3'a), 146.9 (C5'), 143.7 (C4''), 143.0 (C7'a), 139.1 (C5''), 137.6 (C1), 134.2 (C3), 132.5 (C1''), 129.1 (2 × C7''), 128.5 (2 × C2''), 128.3 (C8''), 127.0 (2 × C6''), 126.9 (C6), 126.9 (2 × C3''), 126.4 (C4), 125.8 (C5), 124.9 (C2), 121.2 (C6'), 119.4 (C7'); ***m/z*** (ES$^-$) 467.81 ([^{79}BrM-H]$^+$, 100 %), 469.81 ([^{81}BrM-H]$^-$, 100%); **HRMS** (ES$^-$) Calcd for $C_{25}H_{15}O_2N_3Br$ [M-H]$^-$: 468.0348, found 468.0351.

***N*-(2-Methyl-5-(oxazolo[4,5-b]pyridin-2-yl)phenyl)-[1,1'-biphenyl]-4-carboxamide (49)**

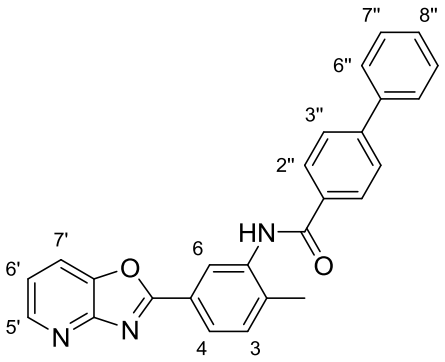

Prepared from **35g** (600 mg, 2.66 mmol, 1.0 eq.) and biphenyl-4-carbonyl chloride (1.44 g, 6.65 mmol, 2.5 eq.) using general method B. **49** was obtained after recrystallization as a white solid (360 mg, 33%). **mp** 275-277 °C; **IR** (solid) ν $_{max}$: 3264 (NH), 1670 (C=O), 1520, 1404, 1258, 741; **^{1}H NMR** (400 MHz, DMSO-d_6) δ 10.17 (br s, 1H, NH), 8.55 (dd, *J* = 4.8, 1.4 Hz, 1H, C5'-H), 8.36 (d, *J* = 1.9 Hz, 1H, C6-H), 8.26 (dd, *J* = 8.2, 1.4 Hz, 1H, C7'-H), 8.14 (d, *J* = 8.3 Hz, 2H, 2 × C2''-H), 8.06 (dd, *J* = 8.0, 1.9

Hz, 1H, C4-H), 7.88 (d, *J* = 8.3 Hz, 2H, 2 × C3''-H), 7.81 – 7.73 (m, 2H, 2 × C6''-H), 7.58 (d, *J* = 8.0 Hz, 1H, C3-H), 7.53 (t, *J* = 7.5 Hz, 2H, 2 × C7''-H), 7.49 – 7.46 (m, 1H, C6'-H), 7.48 – 7.39 (m, 1H, C8''-H), 2.41 (s, 3H, CH_3); **^{13}C NMR** (101 MHz, DMSO-d_6) δ 165.3 (CO), 164.7 (C2'), 155.6 (C3'a), 146.6 (C5'), 143.3 (C4''), 142.8 (C7'a), 139.1 (C5''), 138.8 (C2), 137.4 (C1), 133.0 (C1''), 131.6 (C3), 129.1 (2 × C7''), 128.5 (2 × C2''), 128.2 (C8''), 127.0 (2 × C6''), 126.7 (2 × C3''), 125.2 (C6), 124.9 (C4), 123.9 (C5), 120.8 (C6'), 119.0 (C7'), 18.3 (CH_3); ***m/z*** (ES$^+$) 406.15 ([M+H]$^+$, 100 %); **HRMS** (ES$^+$) Calcd for $C_{26}H_{20}N_3O_2$ [M+H]$^+$: 406.1550, found 406.1548.

_N_-(4-Hydroxy-3-(oxazolo[4,5-b]pyridin-2-yl)phenyl)-[1,1'-biphenyl]-4-carboxamide (50)

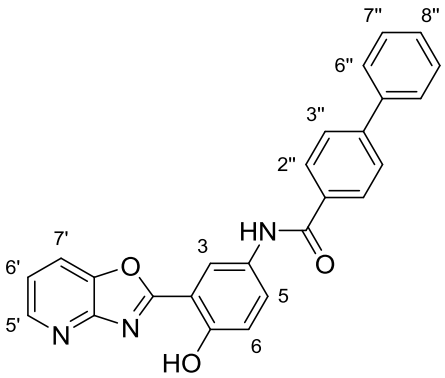

Prepared from **35h** (300 mg, 1.32 mmol, 1.0 eq.) and biphenyl-4-carbonyl chloride (715 mg, 3.30 mmol, 2.5 eq.) the general method B. **50** was obtained after recrystallisation as an off-white solid (346 mg, 64%). **mp** 330-332 °C; **IR** (KBr) ν $_{max}$: 3425 (NH), 3257, 3094, 3044, 1636 (C=O), 1534; **^{1}H NMR** (500 MHz, DMSO-d_6) δ 10.85 (br s, 1H, OH), 10.44 (br s, 1H, NH), 8.72 (d, *J* = 2.7 Hz, 1H, C3-H), 8.59 (dd, *J* = 4.7, 1.4 Hz, 1H, C5'-H), 8.35 (dd, *J* = 7.9, 1.4 Hz, 1H, C7'-H), 8.11 (d, *J* = 8.0 Hz, 2H, 2 × C2''-H), 7.92 (dd, *J* = 8.9, 2.7 Hz, 1H, C5-H), 7.86 (d, *J* = 8.0 Hz, 2H, 2 × C3''-H), 7.77 (d, *J* = 7.3 Hz, 2H, 2 × C6''-H), 7.58 – 7.48 (m, 3H, C6'-H, 2 × C7''-H), 7.43 (t, *J* = 7.3 Hz, 1H, C8''-H), 7.18 (d, *J* = 8.9 Hz, 1H, C6-H); **^{13}C NMR** (126 MHz, DMSO-d_6) δ 165.0 (CO), 164.6 (C2'), 154.4 (C1), 153.9 (C3'a), 146.8 (C5'), 143.2 (C4''), 141.7 (C7'a), 139.1 (C5''), 133.4 (C1''), 131.8 (C4), 129.1 (2 × C7''), 128.3 (2 × C2''), 128.2 (C8''), 127.5 (C5), 127.0 (2 × C6''), 126.7 (2 × C3''), 121.1 (C6'), 119.3 (C7'), 119.1 (C3), 117.6 (C6), 109.8 (C2); ***m/z*** (ES$^-$) 405.88 ([M-H]$^-$, 100 %); **HRMS** (ES$^-$) Calcd for $C_{25}H_{16}N_3O_3$ [M-H]$^-$: 406.1185, found 406.1192.

3-(Oxazolo[4,5-b]pyridin-2-yl)phenyl [1,1'-biphenyl]-4-carboxylate (51)

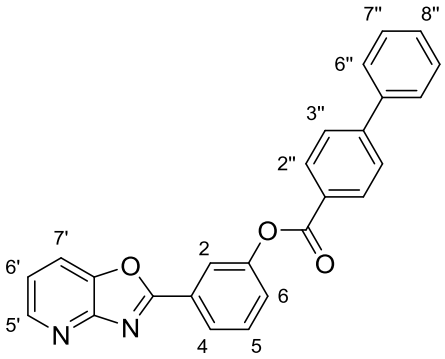

Prepared from **35i** (85 mg, 0.40 mmol, 1.0 eq.) and biphenyl-4-carbonyl chloride (212 mg, 1.00 mmol, 2.5 eq.) using general method B. **51** was obtained after recrystallisation as a white solid (95 mg, 61%). **mp** 185-187 °C; **IR** (solid) ν $_{max}$: 3063, 1728 (C=O), 1605, 1551, 1481, 1404; **^{1}H NMR** (500 MHz, Chloroform-*d*) δ 8.61 (dd, *J* = 4.8, 1.5 Hz, 1H, C5'-H), 8.30 (dd, *J* = 8.4, 1.8 Hz, 2H, 2 × C2''-H), 8.27 (dt, *J* = 7.9, 1.3 Hz, 1H, C4-H), 8.22 (t, *J* = 1.9 Hz, 1H, C2-H), 7.88 (dd, *J* = 8.2, 1.5 Hz, 1H, C7'-H), 7.77 (dd, *J* = 8.4, 1.8 Hz, 2H, 2 × C3''-H), 7.68 (dt, *J* = 6.0, 1.4 Hz, 2H, 2 × C6''-H), 7.64 (t, *J* = 7.9 Hz, 1H, C5-H), 7.54 – 7.47 (m, 3H, C6-H, 2 × C7''-H), 7.47 – 7.40 (m, 1H, C8''-H), 7.32 (dd, *J* = 8.2, 4.8 Hz, 1H, C6'-H); **^{13}C NMR** (126 MHz, Chloroform-*d*) δ 164.9 (C), 164.8 (C), 156.3 (C3'a), 151.5 (C1), 147.1 (C5'), 146.8 (C4''), 143.3 (C7'a), 139.9 (C5''), 130.9 (2 × C2''), 130.4 (C5), 129.2 (2 × C7''), 128.5 (C8''), 128.1 (C3), 127.9 (C1''), 127.5 (2 × C6'', 2 × C3''), 126.1 (C6), 125.8 (C4), 121.6 (C2), 120.5 (C6'), 118.5 (C7'); ***m/z*** (ES^{+}) 393.12 ([M+H]$^{+}$, 100 %); **HRMS** (ES^{+}) Calcd for $C_{25}H_{17}O_3N_2$ [M+H]$^{+}$: 393.1234, found 393.1233.

***N*-(3-(Oxazolo[4,5-b]pyridin-2-yl)phenyl)-[1,1'-biphenyl]-4-sulfonamide (52)**

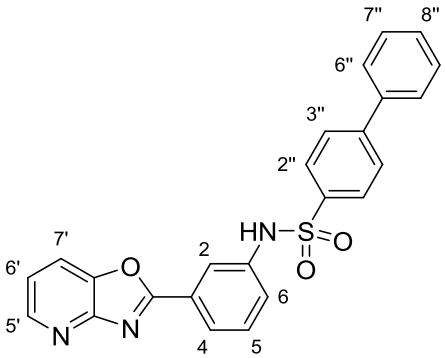

Prepared from **35d** (85 mg, 0.40 mmol, 1.0 eq.) and biphenyl-4-sulfonyl chloride (253 mg, 1.00 mmol, 2.5 eq.) using general method B. **52** was obtained after recrystallisation as a white solid (120 mg, 70%). **mp** 193-195 °C; **IR** (KBr) ν $_{max}$: 3067 (NH), 2893, 1551, 1404, 1337 (S=O), 1157 (S=O), 945, 777, 762; **^{1}H NMR** (500 MHz, DMSO-d_6) δ 10.82 (br s, 1H, NH), 8.55 (dd, *J* = 4.8, 1.4 Hz, 1H, C5'-H), 8.26 (dd, *J* = 8.2, 1.4 Hz, 1H, C7'-H), 8.07 (t, *J* = 1.9 Hz, 1H, C2-H), 7.94 – 7.83 (m, 5H, C4-H, 2 × C2''-H,

2 × C3''-H), 7.71 – 7.64 (m, 2H, 2 × C6''-H), 7.54 (t, *J* = 8.0 Hz, 1H, C5-H), 7.49 – 7.43 (m, 4H, C6'-H, C6-H, 2 × C7''-H), 7.43 – 7.36 (m, 1H, C8''-H); **^{13}C NMR** (126 MHz, DMSO-d_6) δ 164.2 (C2'), 155.3 (C7'a), 146.7 (C5'), 144.6 (C4''), 142.8 (C3'a), 138.8 (C1), 138.1 (C), 138.0 (C), 130.6 (C5), 129.1 (2 × C7''), 128.7 (C8''), 127.6 (2 × CH), 127.4 (2 × CH), 127.1 (2 × C6''), 126.9 (C3), 123.5 (C6), 123.2 (C4), 121.0 (C6'), 119.3 (C7'), 118.2 (C2); ***m/z*** (ES$^+$) 428.10 ([M+H]$^+$, 100 %); **HRMS** (ES$^+$) Calcd for $C_{24}H_{18}O_3N_3S$ [M+H]$^+$: 428.1063, found 428.1063.

***N*-(2-Bromo-5-(oxazolo[4,5-b]pyridin-2-yl)phenyl)-[1,1'-biphenyl]-4-sulfonamide (53)**

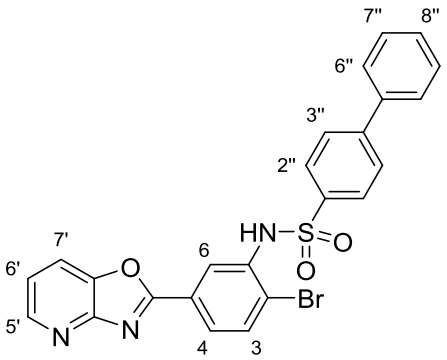

Prepared from **35b** (80 mg, 0.28 mmol, 1.0 eq.) and biphenyl-4-sulfonyl chloride (177 mg, 0.70 mmol, 2.5 eq.) using the general method B. **53** was obtained after recrystallisation as a white solid (75 mg, 53%). **mp** 240-242 °C; **IR** (solid) ν_{max}: 3233 (NH), 1605, 1543, 1474, 1396 (S=O), 1342, 1258, 1157 (S=O); **^{1}H NMR** (500 MHz, Chloroform-*d*) δ 8.66 – 8.60 (m, 2H, C5'-H, C6-H), 7.98 (dd, *J* = 8.4, 2.0 Hz, 1H, C4-H), 7.96 – 7.88 (m, 3H, C7'-H, 2 × C2''-H), 7.66 (d, *J* = 8.4 Hz, 2H, 2 × C3''-H), 7.63 (d, *J* = 8.4 Hz, 1H, C3-H), 7.60 – 7.54 (m, 2H, 2 × C6''-H), 7.44 (t, *J* = 7.6 Hz, 2H, 2 × C7''-H), 7.42 – 7.37 (m, 1H, C8''-H), 7.36 (dd, *J* = 8.1, 4.9 Hz, 1H, C6'-H), 7.17 (br s, 1H, NH); **^{13}C NMR** (126 MHz, Chloroform-*d*) δ 164.1 (C2'), 156.2 (C3'a), 147.3 (C5'), 146.6 (C4''), 143.4 (C7'a), 139.0 (C5''), 137.1 (C1''), 135.7 (C1), 133.7 (C3), 129.2 (2 × C7''), 128.8 (C8''), 128.1 (2 × C2''), 127.9 (2 × C3''), 127.4 (2 × C6''), 127.3 (C5), 125.8 (C4), 121.0 (C6), 120.8 (C6'), 120.0 (C2), 118.7 (C7'); ***m/z*** (ES$^+$) 506.02 ([^{79}BrM+H]$^+$, 100 %), 508.02 ([^{81}BrM+H]$^+$, 100%); **HRMS** (ES$^+$) Calcd for $C_{24}H_{17}O_3N_3BrS$ [M+H]$^+$: 506.0169, found 506.0160.

***N*-(5-(Benzo[d]oxazol-2-yl)-2-bromophenyl)-[1,1'-biphenyl]-4-carboxamide (54)**

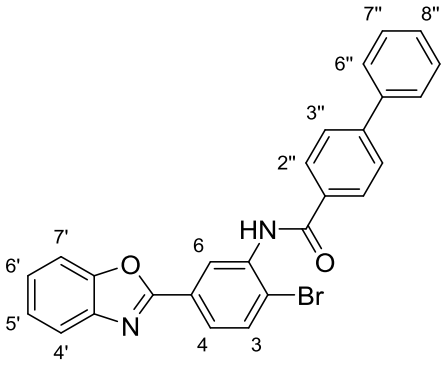

Prepared from **35j** (289 mg, 1.00 mmol, 1.0 eq.) and biphenyl-4-carbonyl chloride (542 mg, 2.50 mmol, 2.5 eq.) using general method B. **54** was obtained after recrystallisation as a white solid (250 mg, 53%). **mp** 260-262 °C; **IR** (KBr) ν $_{max}$: 3269 (NH), 1653 (C=O), 1558, 1508, 1240; **^{1}H NMR** (500 MHz, Chloroform-*d*) δ 9.48 (d, *J* = 2.1 Hz, 1H, C6-H), 8.61 (br s, 1H, NH), 8.10 – 8.03 (m, 2H, 2 × C2''-H), 7.96 (dd, *J* = 8.4, 2.1 Hz, 1H, C4-H), 7.82 – 7.73 (m, 4H, C3-H, C4'-H, 2 × C3''-H), 7.70 – 7.64 (m, 2H, 2 × C6''-H), 7.64 – 7.60 (m, 1H, C7'-H), 7.52 – 7.46 (m, 2H, 2 × C7''-H), 7.45 – 7.40 (m, 1H, C8''-H), 7.39 – 7.36 (m, 2H, C5'-H, C6'-H); **^{13}C NMR** (126 MHz, Chloroform-*d*) δ 165.1 (CO), 162.1 (C2'), 151.0 (C7'a), 145.5 (C4''), 142.2 (C3'a), 139.9 (C5''), 136.6 (C1), 133.1 (C3), 132.9 (C1''), 129.2 (2 × C7''), 128.4 (C8''), 127.9 (2 × C2'', 2 × C3''), 127.4 (2 × C6''), 125.6 (CH), 124.9 (CH), 124.9 (C5), 124.3 (C4), 120.5 (C6), 120.3 (C4'), 117.0 (C2), 111.0 (C7'); ***m/z*** (ES^{+}) 469.05 ([^{79}BrM+H]$^{+}$, 100 %), 471.05 ([^{81}BrM+H]$^{+}$, 100%); **HRMS** (ES^{+}) Calcd for $C_{26}H_{18}O_2N_2Br$ [M+H]$^{+}$: 469.0546, found 469.0544.

***N*-(2-Chlorophenyl)-[1,1'-biphenyl]-4-carboxamide (55)**

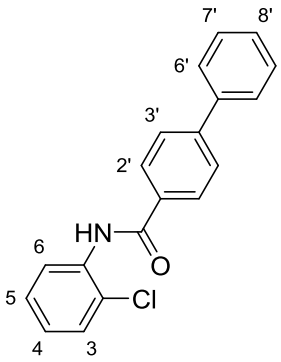

Prepared from 2-chloroaniline (128 mg, 1.00 mmol, 1.0 eq.) and biphenyl-4-carbonyl chloride (542 mg, 2.50 mmol, 2.5 eq.) using general method B. **55** was obtained after recrystallisation as a white solid (250 mg, 81%). **mp** 144-146 °C; **IR** (solid) ν $_{max}$: 3279 (NH), 1643 (C=O), 1520, 1435, 1312, 741; **^{1}H NMR** (500 MHz, DMSO-d_6) δ 10.13 (br s, 1H, NH), 8.10 (d, *J* = 8.4 Hz, 2H, 2 × C2'-H), 7.85 (d, *J* = 8.4 Hz, 2H, 2 × C3'-H), 7.80 – 7.73 (m, 2H, 2 × C6'-H), 7.62 (dd, *J* = 7.7, 1.6 Hz, 1H, C6-H), 7.57 (dd, *J* = 8.1, 1.6 Hz, 1H, C3-H), 7.55 – 7.49 (m, 2H, 2 × C7'-H), 7.47 – 7.40 (m, 1H, C8'-H), 7.40 (dd, *J* = 7.7, 1.6 Hz,

1H, C5-H), 7.31 (td, *J* = 7.7, 1.6 Hz, 1H, C4-H); **^{13}C NMR** (126 MHz, DMSO-d_6) δ 165.0 (CO), 143.4 (C4'), 139.1 (C5'), 135.1 (C1), 132.7 (C1'), 129.6 (C3), 129.1 (C2, 2 × C7'), 128.6 (C6), 128.4 (2 × C2'), 128.2 (C8'), 127.5 (C4, C5), 127.0 (2 × C6'), 126.7 (2 × C3'); ***m/z*** (ES$^+$) 308.08 ([M+H]$^+$, 100 %); **HRMS** (ES$^+$) Calcd for $C_{19}H_{15}ClNO$ [M+H]$^+$: 308.0837, found 308.0839.

_N_-(2-Bromo-5-nitrophenyl)-[1,1'-biphenyl]-4-carboxamide (59)

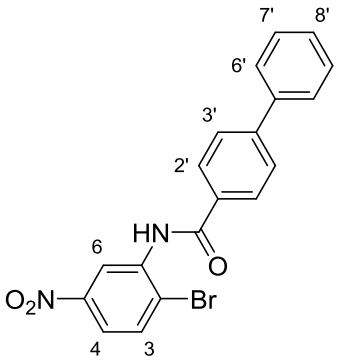

Biphenyl-4-carbonyl chloride (461 mg, 2.13 mmol, 1.0 eq.) was added to 2-bromo-5-nitroaniline **58** (308 mg, 1.42 mmol, 1.5 eq.) in DCM (15 mL), followed by pyridine (0.17 mL, 2.13 mmol, 1.5 eq.). The reaction was stirred at room temperature for 18 hours. **59** was obtained after recrystallisation (DCM) as a white solid (300 mg, 53%). **mp** 203-205 °C; **IR** (solid) ν $_{max}$: 3379 (NH), 1690 (C=O), 1528 (N-O), 1412, 1312, 741, 602 (C-Br); **^{1}H NMR** (500 MHz, DMSO-d_6) δ 10.38 (s, 1H, NH), 8.51 (d, *J* = 1.8 Hz, 1H, C6-H), 8.12 (d, *J* = 8.1 Hz, 2H, 2 × C2'-H), 8.06 (br s, 2H, C3-H, C4-H), 7.89 (d, *J* = 8.1 Hz, 2H, 2 × C3'-H), 7.81 – 7.75 (m, 2H, 2 × C6'-H), 7.52 (t, *J* = 7.5 Hz, 2H, 2 × C7'-H), 7.44 (t, *J* = 7.5 Hz, 1H, C8'-H); **^{13}C NMR** (126 MHz, DMSO-d_6) δ 165.2 (CO), 146.9 (C5), 143.8 (C4'), 139.0 (C5'), 137.8 (C1), 134.0 (C3), 132.2 (C1'), 129.1 (2 × C7'), 128.6 (2 × C2'), 128.3 (C8'), 127.5 (C2), 127.0 (2 × C6'), 126.8 (2 × C3'), 122.3 (C6), 121.9 (C4); ***m/z*** (ES$^+$) 497.02 ([^{79}BrM+Na]$^+$, 100 %), 399.02 ([^{81}BrM+H]$^+$, 100%); **HRMS** (ES$^+$) Calcd for $C_{19}H_{14}N_2O_3Br$ [M+H]$^+$: 397.0182, found 397.0184.

_N_-(5-Amino-2-bromophenyl)-[1,1'-biphenyl]-4-carboxamide (60)

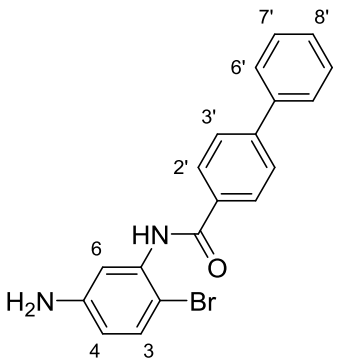

To **59** (100 mg, 0.25 mmol, 1.0 eq.) and NH_4Cl (67 mg, 1.25 mmol, 5.0 eq.) in MeOH (2 mL) and H_2O (1 mL) at 100 °C was added iron powder (70 mg, 1.25 mmol, 5.0 eq.) portionwise. After 3 hours the reaction was cooled to room temperature, filtered through Celite and concentrated *in vacuo*. The residue was dissolved in EtOAc (10 mL) and washed with H_2O (2 × 5 mL), brine (5 mL), dried over $MgSO_4$, filtered and concentrated to yield the desired product **60** as a white solid (83 mg, 90%). **60** was used in the next step without further purification. **^{1}H NMR** (500 MHz, DMSO-d_6) δ 9.77 (br s, 1H, NH), 8.11 – 7.99 (m, 2H, 2 × C2'-H), 7.89 – 7.79 (m, 2H, 2 × C3'-H), 7.79 – 7.73 (m, 2H, 2 × C6'-H), 7.55 – 7.46 (m, 2H, 2 × C7'-H), 7.46 – 7.39 (m, 1H, C8'-H), 7.27 (d, *J* = 8.6 Hz, 1H, C3-H), 6.85 (d, *J* = 2.7 Hz, 1H, C6-H), 6.44 (dd, *J* = 8.6, 2.7 Hz, 1H, C4-H), 5.39 (br s, 2H, NH_2); **^{13}C NMR** (126 MHz, DMSO-d_6) δ 164.7 (CO), 148.8 (C5), 143.2 (C4'), 139.1 (C5'), 136.4 (C1), 133.1 (C1'), 132.3 (C3), 129.1 (2 × C7'), 128.3 (2 × C2'), 128.2 (C8'), 127.0 (2 × C6'), 126.7 (2 × C3'), 113.6 (C4, C6), 104.5 (C2).

***N*-(3-([1,1'-Biphenyl]-4-carboxamido)-4-bromophenyl)thiophene-2-carboxamide (56)**

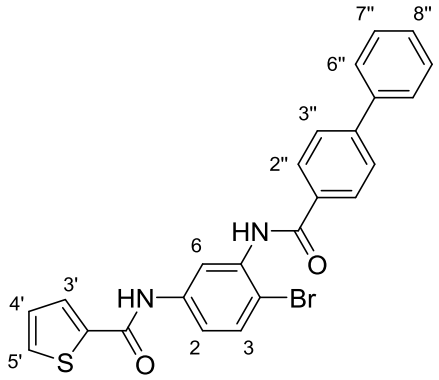

2-Thiophene carbonyl chloride (36 mg, 0.25 mmol, 3.0 eq.) was added to **60** (30 mg, 0.08 mmol, 1.0 eq.) in DCM (1.0 mL), followed by pyridine (20 µL, 0.25 mmol, 3.0 eq.). The reaction was stirred at room temperature for 18 hours. The reaction was concentrated *in vacuo* and purified *via* the Biotage SP4 (silica-packed SNAP column 4 g; 0-40% EtOAc/hexanes) to give the title product **56** as a white solid (30 mg, 85%). **mp** 189-191 °C; **IR** (solid) ν_{max}: 3410 (NH), 3279 (NH), 1643 (C=O), 1589, 1515, 1420, 1258, 1018, 802, 741, 694; **^{1}H NMR** (500 MHz, Chloroform-*d*) δ 8.58 – 8.47 (m, 2H, C6-H, NH), 8.11 (br s, 1H, NH), 8.02 – 7.95 (m, 2H, 2 × C2''-H), 7.91 (dd, *J* = 8.8, 2.6 Hz, 1H, C2-H), 7.77 – 7.69 (m, 2H, 2 × C3''-H), 7.68 – 7.60 (m, 3H, C5'-H, 2 × C6''-H), 7.56 (d, *J* = 8.8 Hz, 1H, C3-H), 7.54 (dd, *J* = 5.0, 1.2 Hz, 1H, C3'-H), 7.52 – 7.46 (m, 2H, 2 × C7''-H), 7.45 – 7.39 (m, 1H, C8''-H), 7.11 (dd, *J* = 5.0, 3.7 Hz, 1H, C4'-H); **^{13}C NMR** (126 MHz, Chloroform-*d*) δ 165.4 (CO), 160.2 (CO), 145.4 (C4''), 139.8 (C5''), 139.1 (C2'), 138.3 (C5), 136.0 (C1), 133.0 (C1''), 132.8 (C3), 131.3 (C3'), 129.2 (2 × C7''), 128.8 (C5'), 128.4 (C8''), 128.1 (C4'), 127.8 (2 × C2'', 2 × C3''), 127.4 (2 × C6''), 117.5 (C2), 112.7 (C6), 108.2 (C4); ***m/z*** (ES^+) 499.01 ($[^{79}BrM+Na]^+$, 100 %), 501.01 ($[^{81}BrM+H]^+$, 100%); **HRMS** (ES^+) Calcd for $C_{24}H_{17}N_2O_2BrSNa$ $[M+Na]^+$: 499.0086, found 499.0080.

_N_-(3-([1,1'-Biphenyl]-4-carboxamido)-4-bromophenyl)furan-2-carboxamide (57)

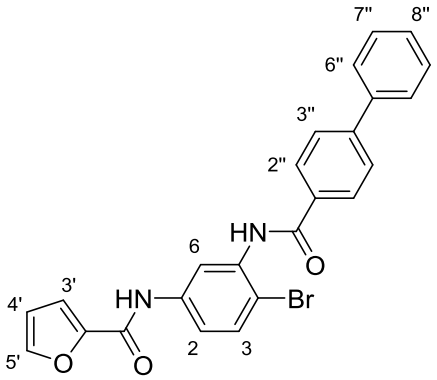

2-Furoyl chloride (47 mg, 0.36 mmol, 3.0 eq.) was added to **60** (44 mg, 0.12 mmol, 1.0 eq.) in DCM (1.2 mL), followed by pyridine (29 µL, 0.36 mmol, 3.0 eq.). The reaction was stirred at room temperature for 18 hours. The reaction was concentrated *in vacuo* and purified *via* the Biotage SP4 (silica-packed SNAP column 4 g; 0-4% MeOH/DCM) to give the title product **57** as a white solid (40 mg, 72%). **mp** 210-212 °C; **IR** (solid) ν_{max}: 3410 (NH), 3317 (NH), 1674 (C=O), 1647 (C=O), 1508, 1260, 750; **^{1}H NMR** (500 MHz, Chloroform-*d*) δ 8.58 (d, *J* = 2.6 Hz, 1H, C6-H), 8.57 (br s, 1H, NH), 8.24 (br s, 1H, NH), 8.04 – 8.00 (m, 2H, 2 × C2''-H), 7.94 (dd, *J* = 8.8, 2.6 Hz, 1H, C2-H), 7.79 – 7.74 (m, 2H, 2 × C3''-H), 7.69 – 7.63 (m, 2H, 2 × C6''-H), 7.58 (d, *J* = 8.8 Hz, 1H, C3-H), 7.54 (dd, *J* = 1.7, 0.9 Hz, 1H, C5'-H), 7.53 – 7.46 (m, 2H, 2 × C7''-H), 7.45 – 7.38 (m, 1H, C8''-H), 7.27 (dd, *J* = 3.5, 0.9 Hz, 1H, C3'-H), 6.58 (dd, *J* = 3.5, 1.7 Hz, 1H, C4'-H); **^{13}C NMR** (126 MHz, Chloroform-*d*) δ 165.2 (CO), 156.2 (CO), 147.6 (C2'), 145.4 (C4''), 144.6 (C5'), 139.9 (C5''), 137.9 (C5), 136.2 (C1), 133.1 (C1''), 132.9 (C3), 129.2 (2 × C7''), 128.4 (C8''), 127.8 (2 × C2'', 2 × C3''), 127.4 (2 × C6'), 117.0 (C2), 115.8 (C3'), 112.9 (C4'), 112.3 (C6), 108.0 (C4); ***m/z*** (ES^+) 461.05 ($[^{79}BrM+Na]^+$, 100 %), 463.05 ($[^{81}BrM+H]^+$, 100%); **HRMS** (ES^+) Calcd for $C_{24}H_{18}BrN_2O_3$ $[M+H]^+$: 461.0495, found 461.0493.

1-(Benzo[d][1,3]dioxol-5-yl)-4,4,4-trifluorobutane-1,3-dione (68)

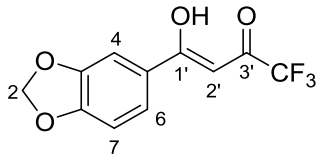

To 3',4'-(methylenedioxy)acetophenone **67** (500 mg, 3.04 mmol, 1.0 eq.) in anhydrous THF (15 mL) at 0 °C was added LiHMDS (6.08 mL, 2 eq., 1M in THF) dropwise. Ethyl trifluoroacetate (864 mg, 6.08 mmol, 2.0 eq.) was added after 10 minutes and the reaction was stirred for a further 1 hour at 0 °C followed by 2 hours at room temperature. The reaction was quenched by addition of a saturated aqueous solution of NH_4Cl (10 mL) and extracted with EtOAc (3 × 10 mL). The organic extracts were combined, washed with NH_4Cl (10 mL), brine (10 mL), dried over Na_2SO_4, filtered and concentrated

in vacuo to give the title product **68** as a pale yellow solid (790 mg, 100%). **IR** (solid) ν_{max}: 2911 (OH), 1584 (C=O), 1489, 1437, 1260, 1126 (CF_3), 887, 797; **^{1}H NMR** (500 MHz, Chloroform-*d*) δ 7.58 (dd, *J* = 8.3, 1.8 Hz, 1H, C6-H), 7.41 (d, *J* = 1.8 Hz, 1H, C4-H), 6.91 (d, *J* = 8.3 Hz, 1H, C7-H), 6.47 (s, 1H, C2'-H), 6.10 (s, 2H, C2-H_2); **^{13}C NMR** (126 MHz, Chloroform-*d*) δ 186.3 (C1'), 175.4 (C3'), 153.1 (C7a), 148.7 (C3a), 127.5 (C5), 124.4 (C6), 117.7 (br, CF_3) 108.7 (C7), 107.5 (C4), 102.4 (C2), 92.1 (C2'). ***m/z*** (ES^-) 259.02 ($[M-H]^-$, 100 %); **HRMS** (ES^-) Calcd for $C_{11}H_6O_4F_3$ $[M-H]^-$: 259.0218, found 259.0223.

5-(Benzo[d][1,3]dioxol-5-yl)-7-(trifluoromethyl)pyrazolo[1,5-a]pyrimidine-3-carboxylic acid (70)

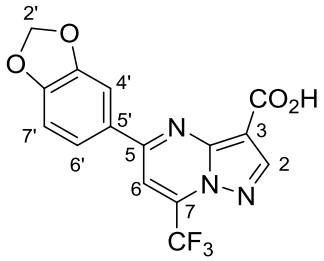

A solution of ethyl 3-amino-1*H*-pyrazole-4-carboxylate **64** (194 mg, 1.25 mmol, 1.0 eq.) and **68** (325 mg, 1.25 mmol, 1.0 eq.) in acetic acid (0.7 mL) was heated at reflux for 5 hours. After cooling to room temperature, the reaction mixture was poured onto ice (1.5 g). The resulting precipitate was filtered off, washed with water (2 × 5 mL), and dried to yield ethyl 5-(benzo[d][1,3]dioxol-5-yl)-7-(trifluoromethyl)pyrazolo[1,5-a]pyrimidine-3-carboxylate **69** (420 mg, 90%). **^{1}H NMR** (500 MHz, DMSO-d_6) δ 8.72 (s, 1H, C2-H), 8.30 (s, 1H, C6-H), 8.06 (dd, *J* = 8.3, 1.8 Hz, 1H, C6'-H), 7.96 (d, *J* = 1.8 Hz, 1H, C4'-H), 7.14 (d, *J* = 8.3 Hz, 1H, C7'-H), 6.18 (s, 2H, C2'-H_2), 4.34 (q, *J* = 7.1 Hz, 2H, $CO_2CH_2CH_3$), 1.37 (t, *J* = 7.1 Hz, 3H, $CO_2CH_2CH_3$); **^{13}C NMR** (126 MHz, DMSO-d_6) δ 161.5 (CO_2Et), 157.7 (C5), 150.9 (C7'a), 148.4 (C3'a), 147.9 (C2), 147.8 (C3a), 133.8 (d, *J* = 36.9 Hz, C7), 129.4 (C5'), 123.8 (C6'), 119.4 (d, *J* = 275.0, CF_3), 108.8 (C7'), 107.3 (C4'), 106.0 (C6), 102.8 (C3), 102.1 (C2'), 59.9 ($CO_2CH_2CH_3$), 14.4 ($CO_2CH_2CH_3$). **69** was added to a mixture of NaOH (30 mg, 0.75 mmol) in EtOH/ water (1:3) (0.7 mL), and the reaction mixture was heated at 65 °C for 4 hours. The mixture was cooled to room temperature and acidified with concentrated HCl until pH 1 was reached. The formed precipitate was filtered off, washed with water, and dried to yield a 4:1 mixture of **70** and **69** (260 mg). This mixture was used in the next step without further purification.

5-(Benzo[d][1,3]dioxol-5-yl)-*N*-((tetrahydrofuran-2-yl)methyl)-7-(trifluoromethyl)pyrazolo[1,5-a]pyrimidine-3-carboxamide (13)

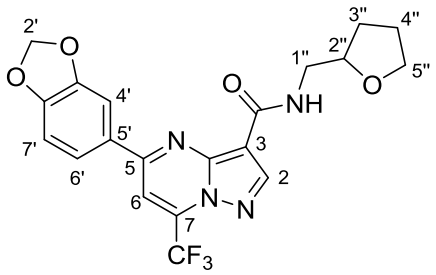

To a solution of oxalyl chloride (53 µL, 0.62 mmol, 2.0 eq.) and **70** (110 mg, 0.31 mmol, 1.0 eq., containing **69** (~25%)) in DCM (4 mL) at 0 °C was added 2 drops of DMF. The reaction was stirred at room temperature for 2 hours before being concentrated *in vacuo*. To the resulting acid chloride in MeCN (6 mL) was added tetrahydrofurfurylamine (70 µL, 0.62 mmol, 2.0 eq.) and the reaction was stirred at room temperature for 2 hours. The reaction was concentrated *in vacuo* and purified *via* the Biotage SP4 (silica-packed SNAP column 10 g; 0-80% EtOAc/hexanes) followed by recrystallisation from hot EtOH provided the title product **13** as a yellow solid (97 mg, 72%). **mp** 253-255 °C; **IR** (solid) ν_{max}: 2918 (NH), 1663 (C=O), 1551, 1503, 1443, 1396, 1319, 1233, 1159 (CF_3), 1032, 799; **^{1}H NMR** (500 MHz, Chloroform-*d*) δ 8.74 (s, 1H, C2-H), 8.54 (br s, 1H, NH), 7.96 (d, *J* = 1.9 Hz, 1H, C4'-H), 7.70 (dd, *J* = 8.2, 1.9 Hz, 1H, C6'-H), 7.67 (s, 1H, C6-H), 6.97 (d, *J* = 8.2 Hz, 1H, C7'-H), 6.12 (s, 2H, C2'-H_2), 4.15 (qd, *J* = 7.3, 3.3 Hz, 1H, C2''-H), 4.09 – 4.00 (m, 1H, C5''-H_2), 3.98 – 3.92 (m, 1H, C1''-H_2), 3.94 – 3.86 (m, 1H, C5''-H_2), 3.41 (ddd, *J* = 13.6, 7.7, 4.2 Hz, 1H, C1''-H_2), 2.11 – 2.00 (m, 1H, C3''-H_2), 2.01 – 1.91 (m, 2H, C4''-H_2), 1.74 – 1.62 (m, 1H, C3''-H_2); **^{13}C NMR** (126 MHz, Chloroform-*d*) δ 161.6 (CO), 156.7 (C5), 151.6 (C7'a), 149.4 (C3'a), 147.9 (C2), 146.7 (C3a), 135.3 (d, *J* = 37.3 Hz, C7), 129.4 (C5'), 123.2 (C6'), 119.3 (d, *J* = 274.6 Hz, CF_3), 108.8 (C7'), 107.7 (C4'), 107.0 (C3), 104.0 (d, *J* = 3.9 Hz, C6), 102.3 (C2'), 78.1 (C2''), 68.3 (C5''), 42.8 (C1''), 28.8 (C3''), 26.3 (C4''); **^{19}F NMR** (471 MHz, Chloroform-*d*) δ -68.4; ***m/z*** (ES^+) 457.11 ($[M+Na]^+$, 100 %); **HRMS** (ES^+) Calcd for $C_{20}H_{17}O_4N_4F_3Na$ $[M+Na]^+$: 457.1100, found 457.1094.

3 Total Synthesis of JBIR-22, a Natural Product PPI Inhibitor of PAC3 Homodimerisation

3.1 Introduction

3.1.1 Natural products

Natural products have played a major role in the development of the pharmaceutical industry, providing a tremendously rich and profitable source of drug molecules.[113,114] The boom in the pharmaceutical industry after World War II led to wide-spread screening of natural extracts in the hunt for pharmaceutically active agents. By the 1990s, approximately 80% of drugs were either natural products or related analogues, including antibiotics (e.g., penicillin, erythromycin), lipid control agents (e.g., lovastatin), antimalarials (e.g., quinine, artemisinin) and anticancer drugs (e.g., taxol, doxorubicin).[115] Despite the rich source of drug leads supplied by nature, interest in natural product drug development waned during the past two decades as a result of the expansion in synthetic medicinal chemistry and combinatorial chemistry. As a result of the technical difficulties associated with screening natural product extracts, the often unsustainable supply from natural sources and the chemical complexity of natural products which frequently prohibited chemical synthesis of sufficient quantities for advanced biological evaluation, the proportion of new drugs based on natural products shrank to ~50%.[115] Nevertheless, natural products will continue to provide a rich source of drug molecules due to their biological activity, unrivalled structural complexity and the diversity of chemical space which they occupy.

The technological advances in high-throughput screening (HTS)[116] and the development in natural-product-derived fragment libraries[117] have renewed interest in natural products.[118,115] This renewed interest has spurred research towards the identification of chemical or genetic methods of providing easy access to sufficient quantities of biologically active natural products and diverse analogue libraries of these. This has fostered a range of new techniques including semisynthesis (chemical modification of an advanced intermediate from nature), mutagenesis (reprogramming of a biosynthetic pathway or engineering an artificial cellular synthetic system to assemble natural products in a host organism) and biology-oriented synthesis (generation of a focused library of structurally diverse compounds based around validated scaffolds which predominate in drug molecules and natural products).[1] In spite of these technological advances, the total synthesis of a complex natural product is frequently essential for the confirmation of its predicted structure and as

a method to provide sufficient material for initial biological evaluation. Furthermore, a successful synthetic route provides access to structural analogues for structure-activity relationship (SAR) studies, the opportunity for diverted total synthesis of chemical probes and the development of alternative semisynthetic routes.

3.1.2 Natural product inspired PPI modulators

The increasing interest in PPI modulators and the changing perception regarding the druggability of PPI interfaces has resulted in increased screening of natural extracts in the hunt for drug leads, particularly in the field of anticancer drug discovery.[15] Although research into PPI modulators from nature is still in its infancy, there have been several promising drug leads identified such as thymoquinone (**1**), chlorofusin (**2**) and CGP049090 (**3**) (Figure 3.1).[15,1]

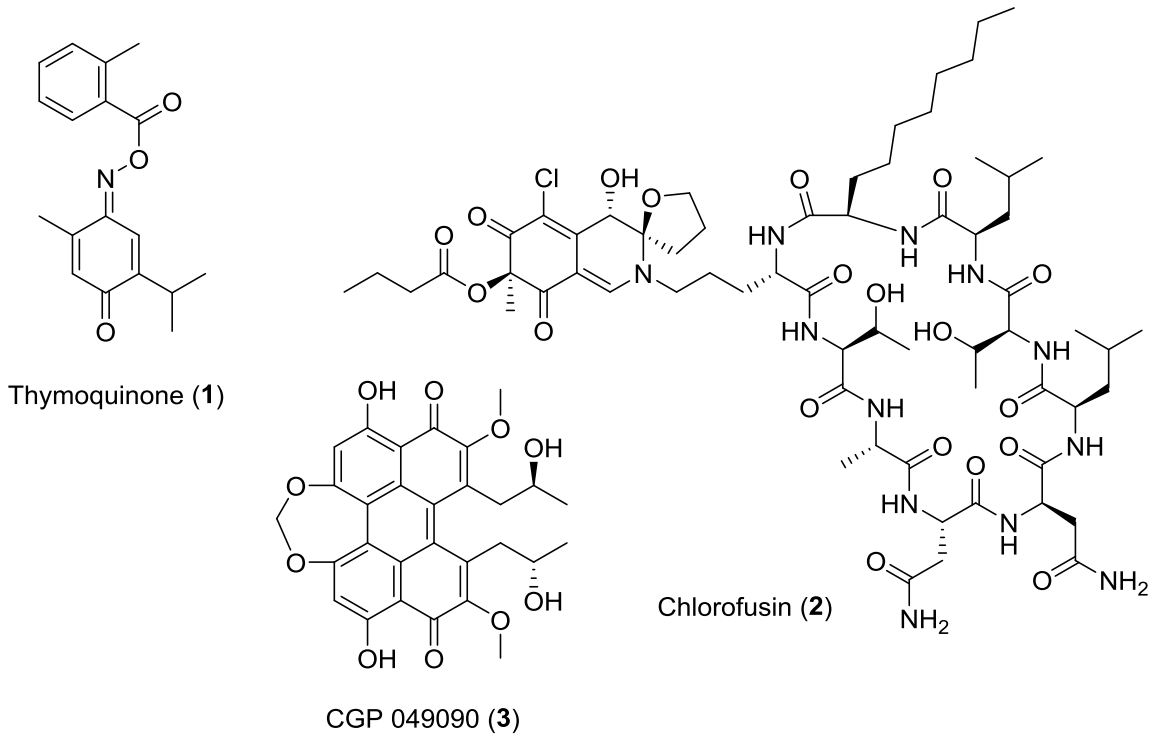

Figure 3.1. PPI modulators isolated from nature.

Thymoquinone (**1**), the bioactive constituent of the volatile oil of black seed (*Nigella sativa*) was recently reported as the first nonpeptidic inhibitor (IC_{50} = 1.14 μM) of the polo-box domain (PBD) of Polo-like kinase 1 (Plk1) binding to phosphoserine/phosphothreonine-containing peptides.[119] Inhibition of the PPI formed between the PBD and target phosphorylated peptide motifs disrupts the intracellular anchoring of Plk1 resulting in mitotic arrest and apoptosis in HeLa cancer cells. Chlorofusin (**2**) was isolated from a microfungus of the genus *Fusarium* and was shown to inhibit the MDM2/p53 interaction with an IC_{50} value of 4.6 μM.[120] MDM2 is an ubiquitin ligase involved in the

proteasomal degradation of the tumour suppressor protein p53. Inhibition of the MDM2/p53 PPI induces growth arrest and apoptosis in cancer cells (see Section 5.1.3 for further discussion). CGP049090 (**3**) was identified from a high-throughput ELISA assay of 7,000 natural compounds as an inhibitor of the T-cell factor 4 (Tcf4)/β-catenin PPI with an IC_{50} value of <10 μM.[121] Further studies confirmed that this fungal metabolite disrupted the Tcf4/β-catenin complex and also demonstrated that it inhibited proliferation of several cancer cell lines.

3.1.3 JBIR-22

An additional example which highlights the capacity to identify PPI modulators from nature was provided by Hashimoto *et al.*[122] The development of a high-throughput *in vitro* protein fragment complementation assay (PCA) facilitated the screening of a 123,599-member natural product library containing microbial metabolites, plant extracts, and marine natural products (Figure 3.2A). The HTS system identified JBIR-22 (**4**) as a potent inhibitor of proteasome assembling chaperone 3 (PAC3) homodimerisation (IC_{50} = 0.2 μM). JBIR-22 (**4**) was subsequently identified by extensive NMR and MS analyses to be a novel tetramic acid based fungal metabolite from *Verticillus sp* (Figure 3.2B).[123]

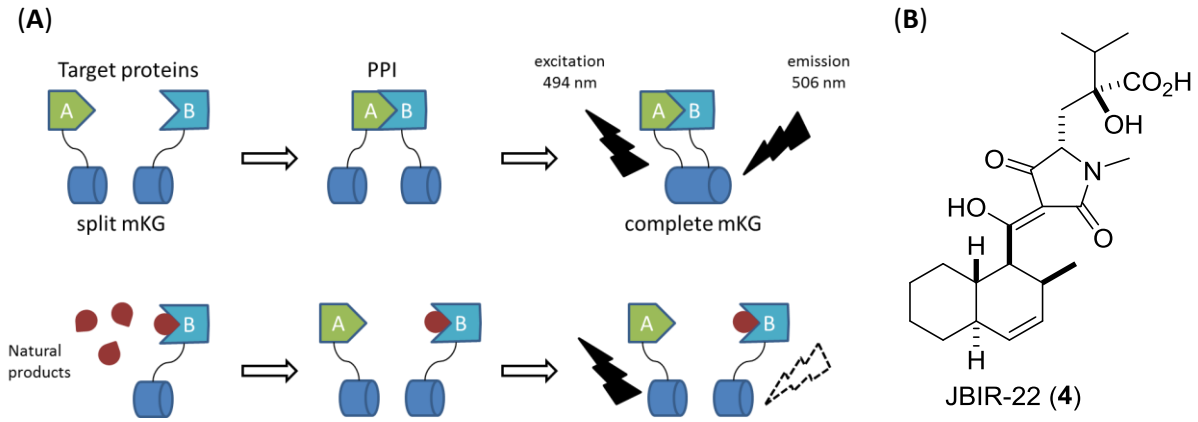

Figure 3.2. Identification of novel PPI inhibitor JBIR-22 (4). (**A**) Schematic representation of the protein fragment complementation assay (PCA).[122] (*Top*) The target proteins fused with split monomeric Kusabira-Green protein (mKG) are mixed. The local effective concentration of split mKG fragments increases by the formation of a PPI between the target proteins A and B. The PPI can be detected by the fluorescence emitted by the reformed mKG reporter chromophore. (*Bottom*) High-throughput *in vitro* PPI inhibitor assay. One of the split mKG-fused target proteins (B) is incubated with the natural product sample. The second split mKG-fused target protein (A) is then added. No mKG fluorescence is detected if the natural product sample has bound to protein B and inhibited the formation of the PPI. (**B**) Structure of novel tetramic acid JBIR-22 (**4**) showing the assigned relative stereochemical configuration.[123]

JBIR-22 (**4**) showed a specific inhibition of PAC3 homodimerisation (IC_{50} = 6 μM against both the TCF7/β-catenin and the PAC1/PAC2 PPIs)[122], an essential chaperone involved in the assembly of the 20S proteasome. The 20S proteasome is the catalytic core of the 26S proteasome, an enzyme involved in the regulation of protein expression and function by the degradation of ubiquitin-conjugated proteins.[124] The proteasomal degradation pathway is involved in many cellular processes,

including cell cycle control, the regulation of gene expression, and oxidative stress response, through the degradation of short-lived signalling proteins, and abnormal or misfolded proteins.[125] The importance of the proteasomal degradation pathway in many essential regulatory systems and its higher activity in rapidly proliferating cancer cells highlighted it as a promising anticancer target. This approach was validated by the approval of bortezomib (**5**)[126] as the first therapeutic proteasome inhibitor, which is currently in clinical use as a chemotherapeutic agent for the treatment of relapsed multiple myeloma and mantle-cell lymphoma. Inhibition of the proteasomal machinery by bortezomib (**5**) or the chemical tool lactacystin (**6**)[127] (a non-peptidic natural product from *Streptomyces* bacteria) results in the effective inhibition of tumour cell growth and the induction of apoptosis by disruption of the controlled degradation of pro-growth cell cycle proteins (Figure 3.3).[128]

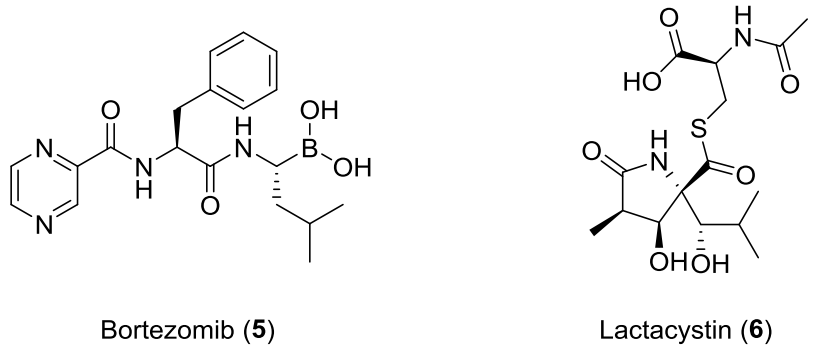

Figure 3.3. Current proteasome inhibitors.

To further understand JBIR-22's inhibition of PAC3's homodimerisation, Izumikawa *et al*. undertook a docking study using the previously reported crystal structure of the PAC3 homodimer, which identified a potential binding site on the PPI interaction surface of the PAC3 homodimer.[123] In the same study, JBIR-22 (**4**) was evaluated for its long-term cytotoxicity against the human cancer cervical carcinoma (HeLa) cell line due to the long half-life of the 20S proteasome in mammalian cells. Inhibition of PAC3's role in the assembly of the 20S proteasome would be expected to inhibit proteasome generation and thereby induce a gradual decrease in proteasome activities. JBIR-22 (**4**) was shown to have an IC_{50} value of 68 μM after 120 hours but had no cytotoxic effect at the same concentration after 48 hours. The time-dependent cytotoxicity of JBIR-22 (**4**) is believed to support the *in vivo* inhibition of the generation of the proteasome machinery.

Extensive NMR and MS analysis revealed that JBIR-22 (**4**) consists of a 4,4-disubstituted glutamic acid containing tetramic acid core, coupled to a decalin ring at its 3'-position (Figure 3.4). Izumikawa *et al*.[123] were able to infer a relative configuration for both the glutamic acid side chain and the decalin ring of JBIR-22 (**4**) through the use of a range of NMR experiments (NOESY, *J*-resolved HMBC, DQF-

COSY, (CT)-HMBC). NOEs and coupling constant analysis revealed that the decalin protons H6 and H11 were diaxial, indicating a *trans*-decalin ring (Figure 3.4). The NOEs between H2, H3 and H6 proved that these protons were cofacial. The relative configuration of the glutamic acid side chain was determined by the *J*-based method[129] to be either (*S*,*S*) or (*R*,*R*). These studies concluded that JBIR-22 (**4**) was one of four possible stereoisomers (Figure 3.4, **4**(**a**-**d**)). Based on analysis of the absolute configuration of structurally related tetramic acids (e.g. harzianic acid (**19**), Section 3.1.7), the most likely diastereomer of JBIR-22 (**4**) contains a glutamic acid side chain with a (5'*S*,7'*S*) stereochemical configuration (Figure 3.4, **4a** or **4b**).

(**A**)

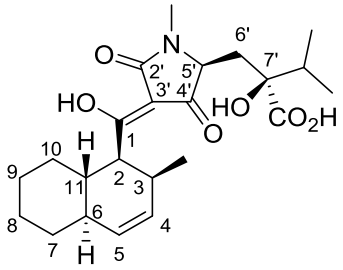

JBIR-22 (**4a**)

(**B**)

Compound	Glutamic acid side chain	Decalin ring
4a	5'*S*,7'*S*	2*S*, 3*S*, 6*R*, 11*S*
4b	5'*S*,7'*S*	2*R*, 3*R*, 6*S*, 11*R*
4c	5'*R*,7'*R*	2*S*, 3*S*, 6*R*, 11*S*
4d	5'*R*,7'*R*	2*R*, 3*R*, 6*S*, 11*R*

Figure 3.4. (A) Structure and numbering of JBIR-22 diastereomer 4a. (B) Stereochemical configuration of the four possible stereoisomers of JBIR-22 (4).

The assignment of the absolute configuration of JBIR-22 (**4**) is further complicated by the presence of a doubling of the majority of the ^{13}C signals in the reported NMR spectrum (Figure 3.5).[123] Although not discussed in the isolation paper, this might suggest that the natural sample contains a minor diastereomer, epimer or closely related compound.

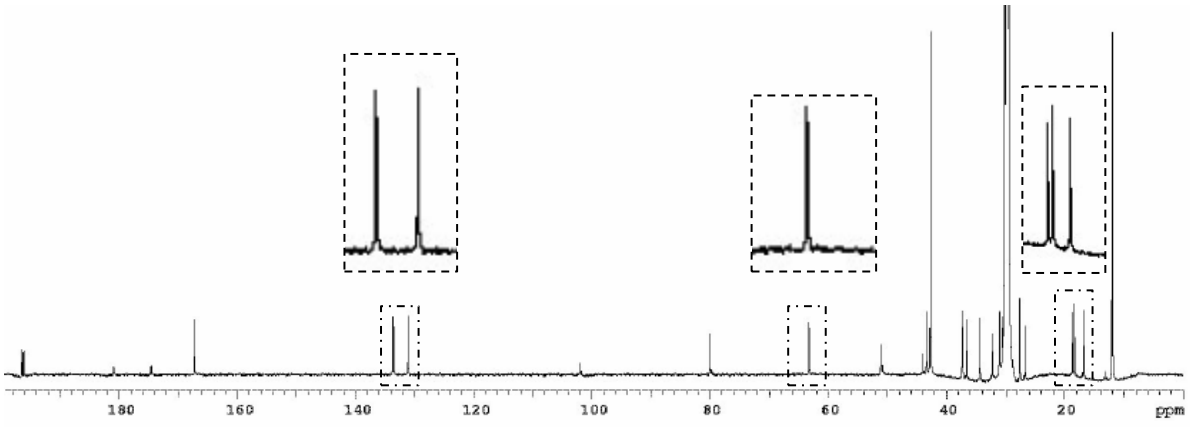

Figure 3.5. Reported ^{13}C NMR spectrum of isolated tetramic acid JBIR-22 (4).[123]

3.1.4 Tetramic acids: Structure and function

JBIR-22 (**4**) is part of a diverse family of biosynthetically related natural products which contain a tetramic acid (pyrrolidine-2,4-dione) ring system. The tetramic acid structural motif serves as one of the key building blocks present in biologically active molecules isolated from natural sources ranging from marine organisms to fungi and terrestrial bacteria.[130] Pyrrolidine-2,4-diones bearing an acyl substituent at the C3' position (Figure 3.6) are the most commonly occurring tetramic acid derivatives in nature and have been extensively studied due to their remarkably varied and potent biological activities, spanning from antibiotic (reutericyclin (**7**), streptolydigin (**8**)) and antiviral (tenuazonic acid (**9**)) to anti-HIV (equisetin (**10**)) and anti-cancer activities (penicillenol A_1 (**11**), melophlin B (**12**)).[131]

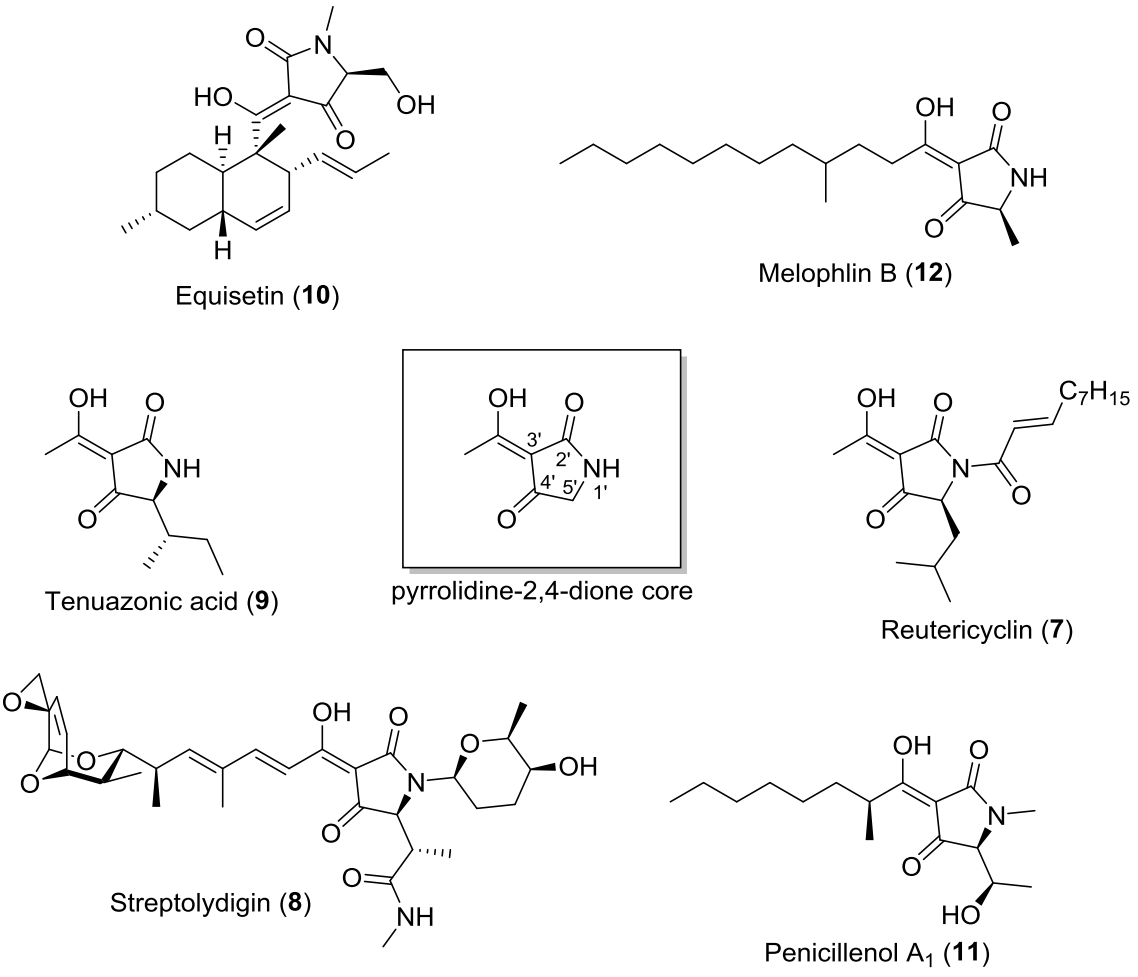

Figure 3.6. Representative bioactive natural products containing the 3-acyltetramic acid structural motif.

The diverse physiological properties of the 3-acyltetramic acids have been linked with their ability to strongly chelate biochemically indispensible metal ions.[132] The strongly acidic 3-acyltetramic acids (pKa in the range 3.0-3.5[130]) predominately exist as the 2,4-diketo tautomer which is stabilised by an intramolecular hydrogen bond between the C2'-ketone and the C3'-enolic hydroxyl.[133]

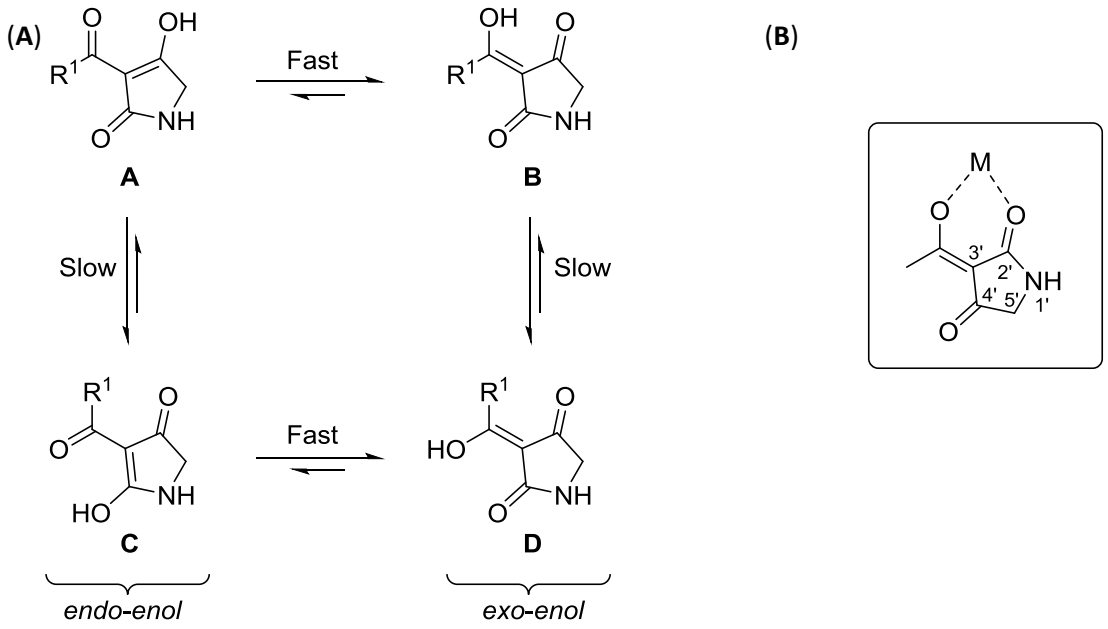

Figure 3.7. (A) Tautomeric forms of 3-acyltetramic acids. 3-Acyltetramic acids predominantly exist in solution as a slowly interconverting mixture of the *exo-enol* tautomers **B** and **D**, with the **D**-tautomer prevailing. **(B) 3-Acyltetramic acids form strong chelate complexes containing a metal ion sandwiched between the enolic oxygen of the C3'-acyl group and the C2'-carbonyl oxygen.** M = metal; R^1 = alkyl.

3-Acyltetramic acids can exist as mixture of four possible tautomers (Figure 3.7A, **A**-**D**).[132,131] The slowly interconverting *exo-enol* pair (**B** & **D**) are typically the predominant tautomeric forms in solution, with the **D**-tautomer being the prevailing form in both solution and crystalline state (Figure 3.7A).[134,135] As a consequence, 3-acyltetramic acids form strong chelate complexes containing a metal ion sandwiched between the enolic oxygen of the C3'-acyl group and the C2'-carbonyl oxygen (Figure 3.7B).[132] Metal chelation by 3-acyltetramic acids of a wide range of divalent metal ions including Ca(II), Mg(II) and heavier metals such as Cu(II), Ni(II) and Fe(II) seems to be crucial for their stability and transport through biological tissues and across membranes.[136]

The high polarity, acidity and metal-chelating ability of 3-acyltetramic acids in addition to the existence of multiple tautomeric forms render them difficult to handle and characterise, thus providing a significant synthetic challenge.[137]

3.1.5 Biosynthesis of 3-acyltetramic acids

In general, 3-acyltetramic acids are assembled from polyketide and α-amino acid precursors by the concerted actions of a polyketide synthase (PKS) - nonribosomal synthetase (NRPS) hybrid.[132,138,139] The highly reducing iterative PKS generates the polyketide which is then linked to the amino acid by peptide synthetases before an intramolecular cyclisation to form the pyrrolidine-2,4-dione ring system (Scheme 3.1). Fungal secondary metabolites containing a decalin ring at the C3'-acyl position

such as equisetin (**10**) and trichosetin (**13**), are products of a fungal polyketide synthase type-I (type-I PKS).[140,141] The proposed biosynthetic pathway for the structurally related JBIR-22 (**4**) analogues, equisetin (**10**) and trichosetin (**13**), involves an asymmetric intramolecular Diels-Alder (IMDA) cycloaddition of heptaketide **14** before incorporation of the amino acid serine and formation of the tetramic acid ring (Scheme 3.1).[138,140] Type I PKS can produce linear *E*,*E*-conjugated polyene and *E*-enone systems which are reactive substrates for intramolecular [4+2] cycloadditions (Scheme 3.1). The biosynthetic Diels-Alder (DA) cycloaddition usually affords a *trans*-decalin adduct as a single diastereomer from an *endo*-transition state.[142] The numerous examples of polyketide natural products containing structures which likely originated from highly diastereo- and enantioselective [4+2] cycloadditions supports the argument that their construction involves an enzymatically controlled DA reaction.[143] The stereochemical outcome of asymmetric Diels-Alder reaction in the biosynthesis of equisetin (**10**) and trichosetin (**13**) is believed to be controlled by the polyketide synthetase enzyme EqiS.[141]

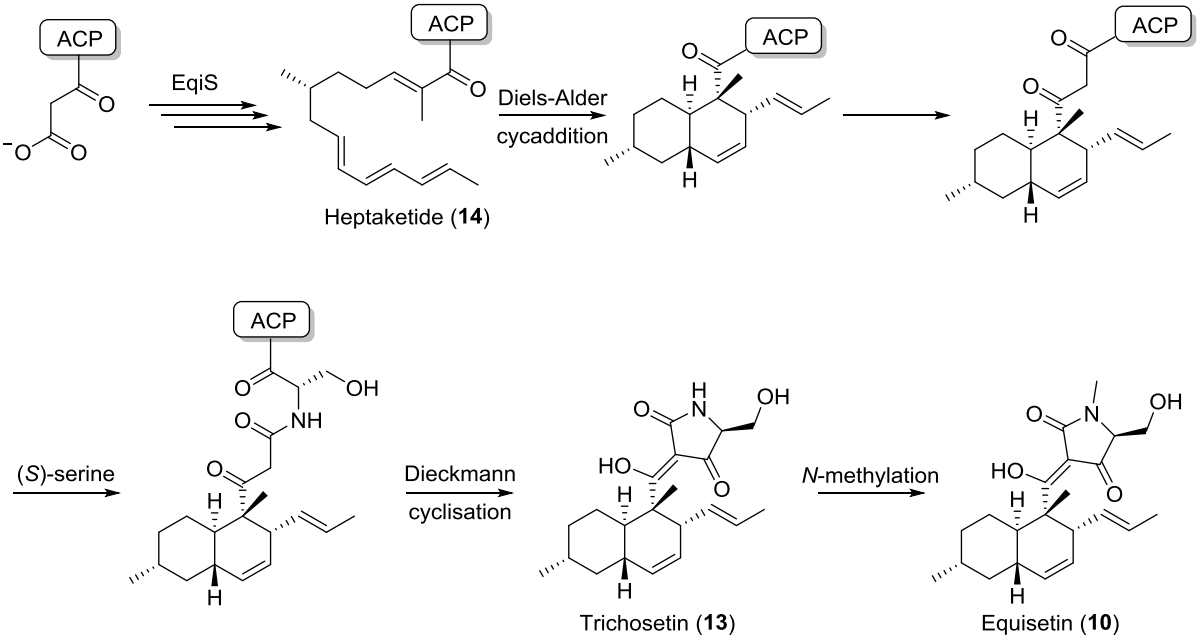

Scheme 3.1. Proposed hybrid PKS-NRPS biosynthesis of trichosetin (13) and equisetin (10).[138,141] Iterative PKS type-1 synthetase EqiS generates heptaketide **14** which undergoes a [4+2] cycloaddition. NRPS mediated incorporation of (*S*)-serine followed by EqiS R-domain promoted Dieckmann cyclisation releases trichosetin (**13**). *N*-methylation of trichosetin (**13**) by EqiD produces equisetin (**10**). Acyl-carrier protein (ACP).

The Diels-Alder reaction has been proposed as a key transformation in the biosynthesis of numerous cyclohexene-containing secondary metabolites.[142–144] However, the identification and validation of the enzymes implicated in this biotransformation has proven challenging. Examples of enzymatic systems which have demonstrated experimental evidence consistent with an enzyme catalysed DA reaction include solanapyrone synthase (SPS), lovastatin nonaketide synthase (LovB) and SpnF which

construct the core framework of the phytotoxin solanapyrone A (**15**), the cholesterol-lowering agent lovastatin (**16**) and the insecticide spinosyn A respectively (Figure 3.8).[142–145] In addition to facilitating the DA reaction, these enzymes often catalyse other biosynthetic reactions, such as oxidation (solanapyrone synthase) and polyketide chain formation (lovastatin nonaketide synthase).[142] Despite the extensive research undertaken in the quest to prove the existence of a Diels-Alderase, rigorous proof for an enzyme catalysed DA cycloaddition, mediated by transition state stabilisation has yet to be obtained.[143] This challenge is particularly highlighted by mechanistic studies which revealed that the proposed natural Diels-Alderase macrophomate synthase (MPS) likely catalyses a stepwise Michael-aldol reaction in contrast to the predicted concerted Diels-Alders reaction.[146–149] The concerns surrounding product inhibition of a transition state stabilised enzymatic model and the observation that the known putative Diels-Alderases have secondary functions have resulted in the widely held theory that these enzymes function as an entropy trap for the [4+2] cycloaddition. The enzymes convert their substrates into reactive DA precursors, which then readily undergo a stereoselective cycloaddition in the enzyme active site before being released.[142]

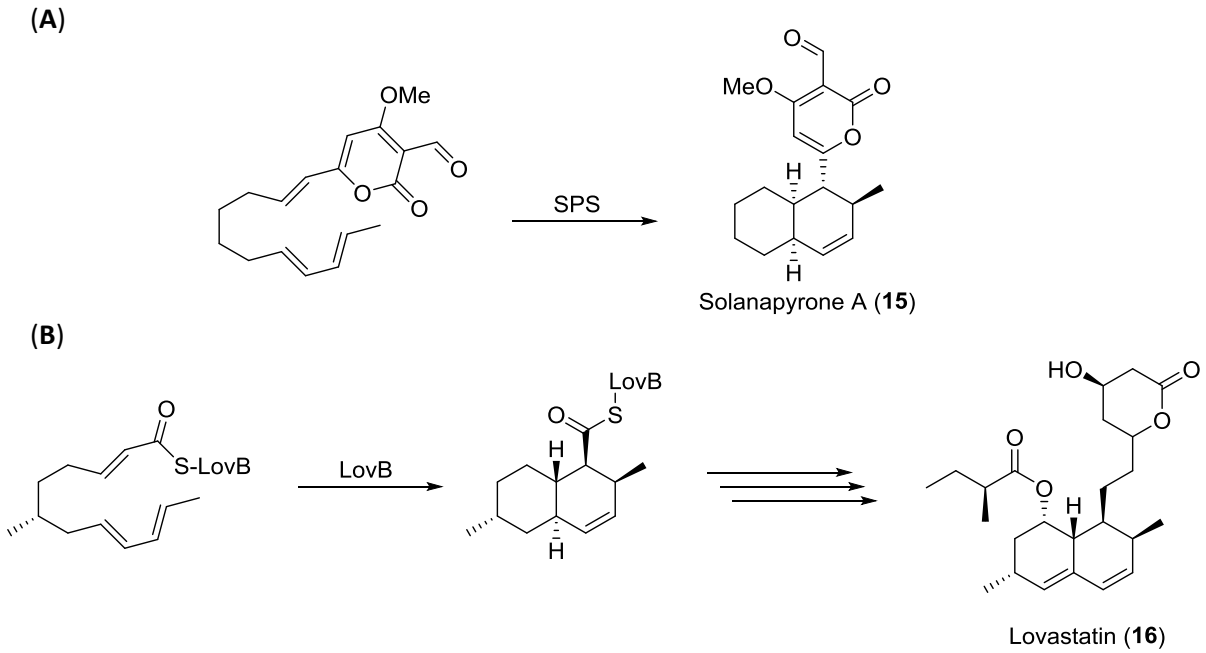

Figure 3.8. Proposed "Diels-Alderase" catalysed [4+2]-cycloaddition in the biosynthesis of (A) solanapyrone A (15) and (B) lovastatin (16).

The discovery by Janda *et al*.[150] of an alternative non-enzymatic biosynthetic route to 3-acyltetramic acids from *N*-acylhomoserine lactones (AHLs) resulted in a renewed interest in their antibiotic activity.[151] AHLs are a class of quorum sensing molecules produced by certain gram-negative bacteria (e.g. *Pseudomonas aeruginosa*) to control and initiate cell density dependent processes such as biofilm formation.[152] The AHL **17** was shown to convert spontaneously into 3-acyltetramic acid **18** under physiological conditions *via* an intramolecular Claisen alkylation (Scheme 3.2).[150,137] This

appears to provide a competitive advantage to the AHL producing species as a result of the antimicrobial and siderophoric (iron-chelating) properties of the ensuing 3-acyltetramic acids.[132] Although the antimicrobial mode of action of these 3-acyltetramic acids remains to be established, it is believed to be linked to their ability to sequester the scarce quantities of iron in the environment.[153]

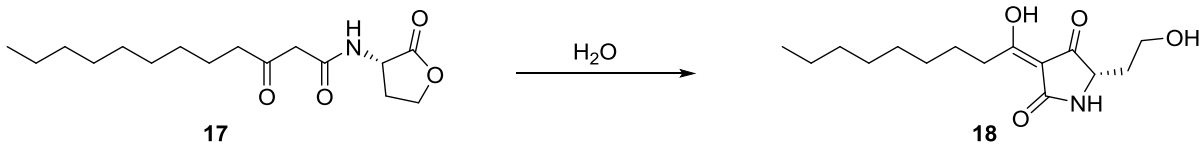

Scheme 3.2. Spontaneous non-enzymatic intramolecular Claisen alkylation of 3-oxo-AHL 17 to generate tetramic acid 18.[150]

3.1.6 Synthesis of 3-acyltetramic acids

The total synthesis of tetramic acid based natural products has experienced a renaissance in the past 20 years due to their desirable biological activity and challenging structural complexity.[132] This has resulted in a steadily increasing number of reports dealing with their isolation, biosynthesis, medicinal potential and the development and refinement of synthetic approaches to these natural products. Despite the extensive research in this area, the development of a comprehensive and general protocol for the synthesis of 3-acyltetramic acids is substantially less advanced due to the intrinsic difficulty in accessing this structural system.[154] Conventional synthetic strategies have generally followed two main routes (Figure 3.9).[130,137,154,155]

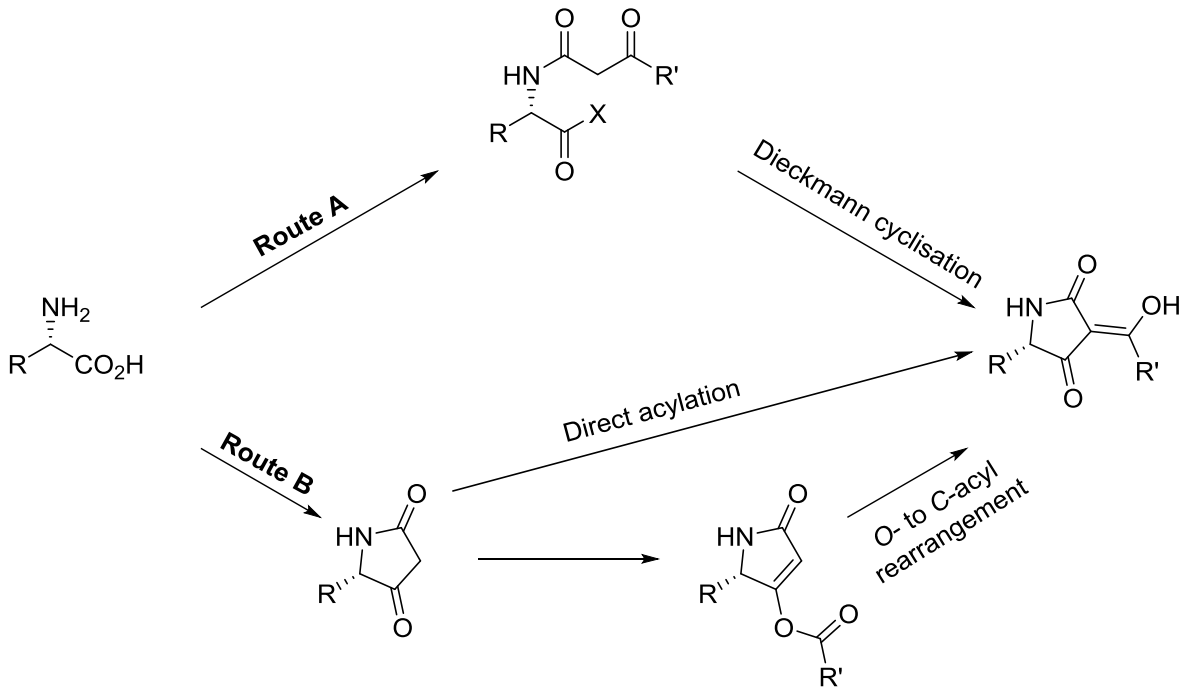

Figure 3.9. Conventional synthetic approaches to 3-acyltetramic acids.[154]

The first route involves the incorporation of the C3'-acyl group prior to the construction of the tetramic acid core (Figure 3.9, Route A). This is most commonly achieved *via* a Lacey-Dieckmann cyclisation[156] of the appropriate β-ketoamide under basic conditions. However, partial racemisation of the C5' stereogenic center is often observed using this protocol.[157] The alternative route relies on the incorporation of the C3'-acyl group after the construction of the tetramic acid core. Common synthetic strategies to achieve this include direct C3'-acylation using an acid chloride or an *O*4'- to *C*3'-acyl rearrangement. Both of these methods have limited functional group tolerance due to the harsh conditions required in the case of the direct C3'-acylation or the poor migratory ability of α-branched or unsaturated side chains in the *O*- to *C*-acyl rearrangement methodology. In general, both of these routes make use of commercially available amino acids as the source of chirality in the product.[136]

The first route described is the most common strategy used for the assembly of tetramic acids containing more advanced C3'-acyl substituents such as a decalin ring. This synthetic strategy is exemplified by Ley *et al*.'s biomimetic synthesis of Equisetin (**10**) (Scheme 3.3).[158,159] Their protocol involved an early IMDA cycloaddition of a β-ketoamide functionalised polyene chain (Scheme 3.3, step a) to form the decalin ring followed by incorporation of (*S*)-serine (Scheme 3.3, step b) and a Lacey-Dieckmann cyclisation (Scheme 3.3, step c) to furnish Equisetin (**10**).

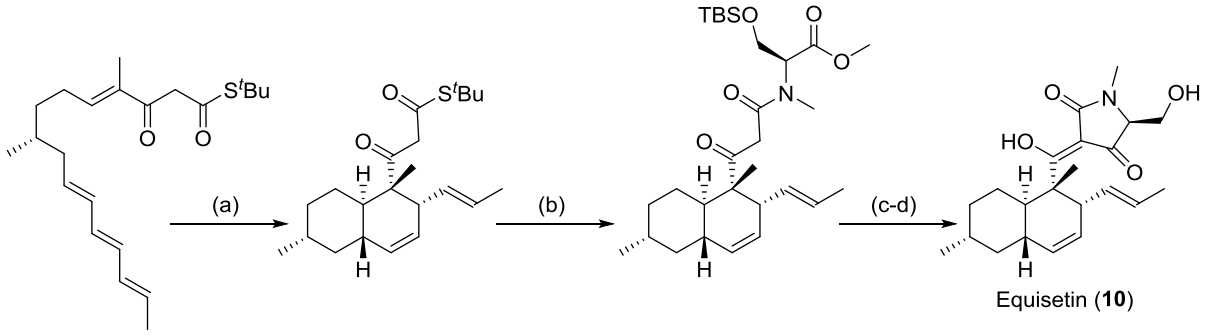

Scheme 3.3. Ley's synthesis of Equisetin.[158,159] *Reagents and conditions*: (**a**) $BF_3.Et_2O$, DCM, -78 °C → 0 °C, 71%. (**b**) (*S*)-*N*-methyl-*O*-*tert*-butyldimethylsilyl serine methyl ester, CF_3CO_2Ag, THF, Et_3N, 0 °C, 97%. (**c**) HF, CH_3CN, r.t., 85% (**d**) MeONa, MeOH, r.t., quantitative.

Although Ley's synthetic strategy proved to be an excellent method to access Equisetin (**10**), it does not address the challenges associated with the synthesis of JBIR-22 (**4**), a member of a small sub-family of tetramic acids containing an unnatural amino acid.

3.1.7 Tetramic acids containing an unnatural amino acid

An apparent unmet challenge in the tetramic acid field appears to be the total synthesis of the members of a small sub-family of 3-acyltetramic acids containing an unnatural 4,4-disubstituted glutamic acid derivative. To date 4 members of this subfamily have been reported, although no synthesis has been described (Figure 3.10). Members of this sub-family display diverse biological activities with potential as novel therapeutic agents for the treatment of cancer (JBIR-22 (**4**),[123] harzianic acid (**19**)),[160,161] HIV (Sch210972 (**20**))[162,163] and as plant growth promoting agents (harzianic acid (**19**))[164,165] and antimicrobials (zopfiellamide A (**21**)).[166]

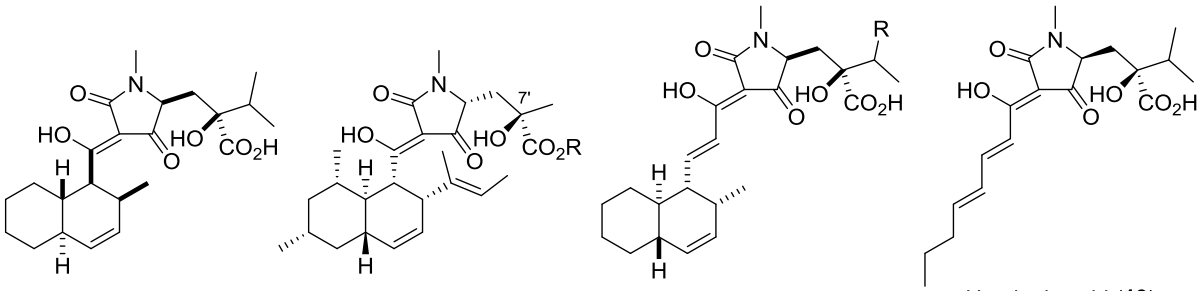

Figure 3.10. Sub-family of tetramic acids containing an unnatural 4,4-disubstituted glutamic acid. Absolute stereochemistry shown for Sch210972 (**20**)[162] and harzianic acid (**19**)[164]; relative stereochemistry shown for JBIR-22 (**4**)[123] and zopfiellamide A (**21**).[166]

The CCR-5 receptor is a member of the super family of seven-*trans*-membrane G-protein coupled receptors (GPCRs), which in conjugation with the CD4 glycoprotein is implicated in viral attachment and infection of macrophages, monocytes and T-cells in the initial stages of HIV-1 infection.[167,168] The validation of the CCR-5 receptor as an attractive therapeutic target for the treatment of HIV triggered extensive research focused on the identification of selective, potent CCR-5 antagonists as novel anti-HIV-1 agents.[169–171] A high-throughput screening campaign of a collection of extracts derived from bacteria, fungi and actinomycetes led to the discovery of the novel fungal secondary metabolite, Sch210972 (**20**) (Figure 3.10), produced by *Chaetomium globosum*, as a selective and potent inhibitor of the chemokine receptor, CCR-5 with an IC_{50} value of 79 nM.[162] Interestingly, two highly related isolated secondary metabolites, Sch213766 (**22**), the methyl ester of Sch210972 (**20**) and Sch210971 (**23**), the 7'-epimer of Sch210972 (**20**) were significantly less potent with IC_{50} values of 8.6 μM[162] and 1.2 μM[163] respectively (Figure 3.10). This decrease in potency strongly suggests that the 4,4-disubstituted glutamic acid side chain is essential for the biological activity of Sch21092 (**20**).[163]

Zopfiellamide A (**21**) (Figure 3.10) is a secondary metabolite isolated from fermentations of the facultative marine fungus *Zopfiella latipes*.[166] Zopfiellamide A (**21**) displayed moderate antibacterial activity with minimal inhibitory concentrations between 2 and 10 μg/mL against Gram-positive *Arthrobacter citreus*, *Bacillus brevis*, *B. subtilis*, *B. licheniformis*, *Corynebacterium insidiosum*, *Micrococcus luteus*, *Mycobacterium phlei*, *Streptomyces* sp. and Gram-negative *Acinetobacter calcoaceticus*. Promisingly, it proved to be selectively antimicrobial, exhibiting no cytotoxic effects against several mammalian cell lines at concentrations up to 100 μg/mL.[166] The isolation of a second highly related metabolite, Zopfiellamide B (**24**) (Figure 3.10) which is 5-fold less potent than Zopfiellamide A (**21**), further supports the importance of the glutamic acid side chain in the biological activity of this family of tetramic acids.

The final member of this sub-family, harzianic acid (**19**) (Figure 3.10), contains a polyene chain at the C3'-acyl position in contrast to the decalin ring moiety present in the other members (Figure 3.10). Harzianic acid (**19**) is a fungal secondary metabolite isolated from *Trichoderma harzianum*,[172] a filamentous fungus which is widely used as a biopesticide and biofertiliser due to its growth promoting and antifungal properties.[173,174] The isolated secondary metabolite harzianic acid (**19**) also demonstrates antimicrobial activity, completely inhibiting the growth of phytopathogenic agents *P.irregulare* and *S.sclerotiorum* in plate antifungal assays at 10 μg and *R.solani* at 100 μg.[164,165] Furthermore, harzianic acid (**19**) was identified as a plant growth promoting agent, which significantly increased seed germination and shoot and root growth in tomato seedlings.[164,165] The plant growth promoting activity of harzianic acid (**19**) is believed to be linked to its potent siderophoric properties (binding affinity of 1.79×10^{-25} M for Fe(III)[165]). Microbial siderophores are iron-chelating agents involved in iron solubilisation which is a crucial mechanism in plant nutrient regulation.[175–177] Harzianic acid (**19**) improved seedling growth even under iron-deficient conditions and increased the iron concentration in the plants. The antifungal and plant growth promoting activities of harzianic acid (**19**) has highlighted it as a promising bioactive compound which could be used as an alternative to living antagonists.[165]

In addition, harzianic acid (**19**) was also identified from two fungal metabolite screens as a promising anticancer agent.[160,161] Kawada and coworkers identified harzianic acid (**19**) as a selective serine/threonine phosphatase type 2A (PP2A) inhibitor with an IC_{50} value of 10 μg/mL.[160] Inhibition of the intracellular protein phosphatase PP2A augments natural killer cells *in vivo* and inhibits tumour metastasis. Interestingly, harzianic acid (**19**) was only active against PP2A when chelated to zinc (harzianic acid:zinc – 2:1 complex).[165] This chelation dependent biological activity has been

observed previously for members of the tetramic acid family.[132,178] Harzianic acid (**19**) was also identified in a screen of fungal metabolites as possessing low micromolar activity against three different cancer cell lines.[161]

3.2 Aim of this work

The absence of a reported synthetic route to JBIR-22 (**4**), the ambiguity surrounding its relative and absolute stereochemical configuration, the potential involvement of a "Diels-Alderase" in its biosynthesis and its potent activity against the promising anti-cancer PPI target PAC3, highlighted it as a rewarding and challenging target for total synthesis. The development of a concise and versatile route which could be adapted to access the other members of the sub-family of tetramic acids would be highly desirable. Therefore an elegant synthetic strategy would ideally fulfil the following requirements:

- Enable a short and efficient route to furnish JBIR-22 (**4**)
- Allow easy access to the stereoisomers of JBIR-22 (**4**) for relative and absolute stereochemical assignment
- Facilitate a synthetic investigation of the possible role of a "Diels-Alderase" in the biosynthesis of JBIR-22 (**4**)
- Provide a versatile route which could be utilised to access the other therapeutically promising members of this sub-family of tetramic acids

3.3 Synthetic strategy

3.3.1 Retrosynthetic analysis

To achieve the main goals of our synthesis, our approach should ideally form the tetramic acid core of JBIR-22 (**4**) with the attached glutamic acid side chain early in the synthesis, as this is common to all members of the tetramic acid sub-family. This would be followed by incorporation of the divergent C3'-acyl moiety. This is in contrast to the synthetic approach most commonly used to access related tetramic acids such as equisetin (**10**), which generally form the decalin ring prior to formation of the tetramic acid core (Section 3.1.6). Therefore, to develop an efficient and practical route to this family of tetramic acids our synthetic strategy needed to address three main challenges:

1.) Access to the different members of this family containing a decalin ring at the C3' position would require a late-stage Diels-Alder reaction of the appropriate polyene chain or the incorporation of a pre-formed decalin moiety.

2.) Identification of a stable masked tetramic acid core onto which the polyene chain could be attached, thereby reducing the significant synthetic challenges associated with tetramic acids (Section 3.1.4).

3.) Development of a novel, asymmetric synthesis of the required 4,4-disubstituted glutamic acids.

The key step in our initial retrosynthetic strategy (Scheme 3.4) of JBIR-22 (**4**) was a late stage Diels-Alder cyclisation of the appropriate polyene derivative **25**. By altering the polyene side chain, a range of different analogues with diverse ring systems such as zopfiellamide A (**21**) and Sch210972 (**20**) could be accessed (Figure 3.10). A range of tetramic acids with an uncyclised polyene side chain such as harzianic acid (**19**) could also be prepared (Figure 3.10).

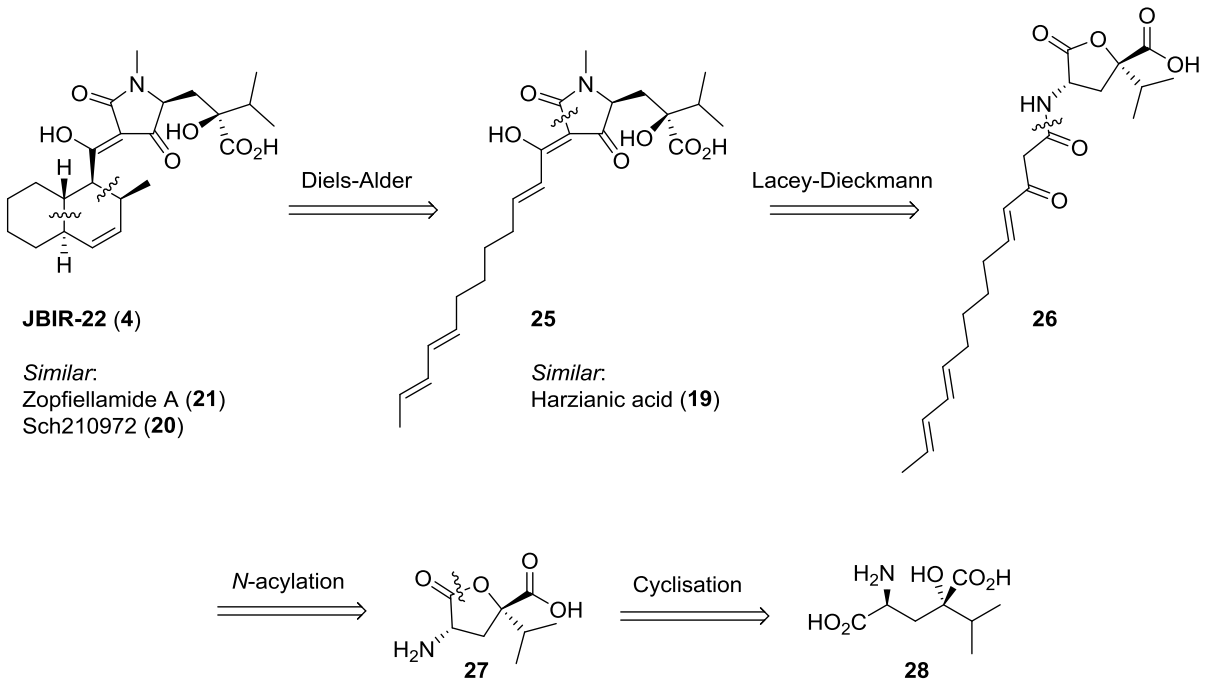

Scheme 3.4. Retrosynthetic analysis of JBIR-22 (4).

This strategy required the identification of an advanced masked tetramic acid intermediate due to the considerable synthetic challenges associated with handling compounds containing the tetramic acid motif (Section 3.1.4). Inspiration for an appropriate masked tetramic acid came from Janda *et al*.'s non-enzymatic biosynthetic route to 3-acyltetramic acids from *N*-acylhomoserine lactones (AHL) (Section 3.1.5).[179] Based on this transformation it was proposed that a biomimetic synthesis using 3-oxo-AHL derivative **26** which could undergo a late stage Lacey-Dieckmann cyclisation to reveal the desired tetramic acid **25** could be achieved (Scheme 3.4). It was envisioned that **26** could be

obtained by an *N*-acylation of lactone **27** with the desired polyene side chain. Intramolecular cyclisation of the 4,4-disubstitued glutamic acid **28** (Scheme 3.4) would furnish **27**, a key intermediate from which a divergent approach could lead to a large and diverse collection of tetramic acids (Scheme 3.4).

Harzianic acid (**19**) was identified as a being structurally related to **25**, a precursor of JBIR-22 (**4**) in our retrosynthetic strategy. It was decided that it would therefore be a good initial target for development of this synthetic route (Scheme 3.4). The identification of a synthetic approach to harzianic acid (**19**) which could be readily adapted to access JBIR-22 (**4**) would provide the ideal validation of this approach as a general protocol for accessing the members of this tetramic acid sub-family. Furthermore, harzianic acid (**19**)'s anticancer and potent siderophoric properties make it an attractive and rewarding synthetic target in its own right (see Section 3.1.7).

3.3.2 A novel approach to 4,4-disubstituted amino acids

The first aim in our synthetic strategy was a concise and stereoselective synthesis of the 4,4-disubstituted glutamic acid **28**. Although, there is no reported synthesis of the required 4-hydroxy-4-*iso*propylglutamic acid (**28**), a chemical[180] and an enzymatic route[181,182] to the related 4-hydroxy-4-methylglutamic acid (**29**) have been described. Baldwin and Long[180] devised a 5-step route to 4-hydroxy-4-methylglutamic acid (**29**) from Seebach's *tert* butyl-substituted imidazolidinone **30**[183] *via* cycloadduct **32** (Scheme 3.5). Whilst this approach did provide **29** in good yield and stereoselectivity, it was not ideal for our synthesis due to the length of the route and the cost of reagent **30**. In addition, it would only provide access to the (*S*,*S*) and (*R*,*R*) diastereomers of **29** as it proceeds *via* cycloadduct **32**.

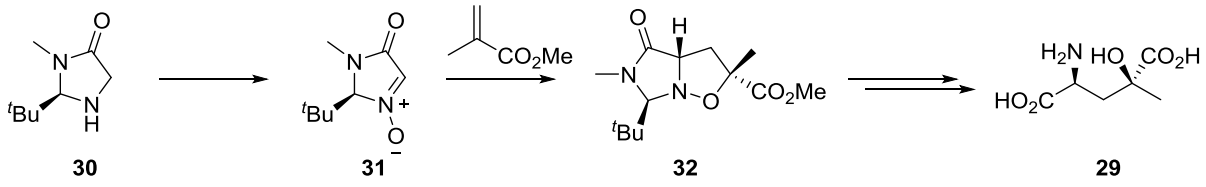

Scheme 3.5. Baldwin and Long's synthesis of 4-hydroxy-4-methylglutamic acid (29).[180] The cycloaddition reaction between the homochiral-derived nitrone **31** and the appropriate alkene afforded cycloadduct **32** which after subsequent elaboration provided 4-hydroxy-4-methylglutamic acid (**29**).

Instead, we focused on developing a novel synthesis of these 4,4-disubstituted amino acids. The simplicity and efficiency often obtained by an elegant biomimetic synthesis attracted our attention to a potentially biomimetic approach to these amino acids. Although the isolation of 4-hydroxy-4-*iso*propylglutamic acid (**28**) has to the best of our knowledge not been reported, the (2*S*,4*S*) and

(2*S*,4*R*) isomers of 4-hydroxy-4-methylglutamic acid (**29**) have been isolated from *Pandanus veitchii*[184] and *Ledenbergia roseo-aena*[185] respectively, with both diastereomers occurring in *Phyllitis scolopendrium*[186]. It is proposed that 4-hydroxy-4-methylglutamic acid (**29**) derives from a homo-aldol condensation of pyruvic acid (**33**), followed by transamination of the resulting 4-hydroxy-4-methyl-2-oxoglutaric acid (**34**) (Scheme 3.6).[187]

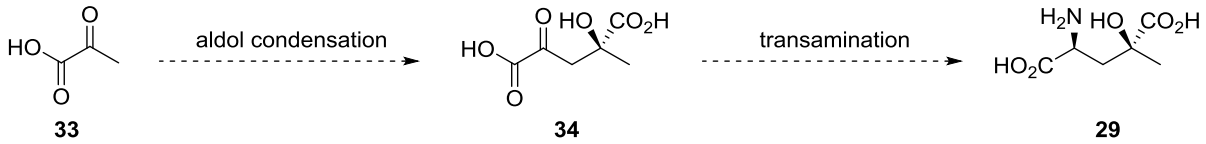

33 **34** **29**

Scheme 3.6. Proposed biosynthesis of (2*S*,4*R*)-4-hydroxy-4-methylglutamic acid 29 from pyruvic acid 33 *via* an aldol condensation followed by a transamination.[187]

Based on this biosynthetic pathway our proposed synthetic strategy to access the protected 4-hydroxy-4-*iso*propylglutamic ethyl ester (**35**) would involve an asymmetric aldol reaction of ethyl pyruvate (**36**) and ethyl dimethylpyruvate (**37**) followed by a diastereoselective transamination (Scheme 3.7).

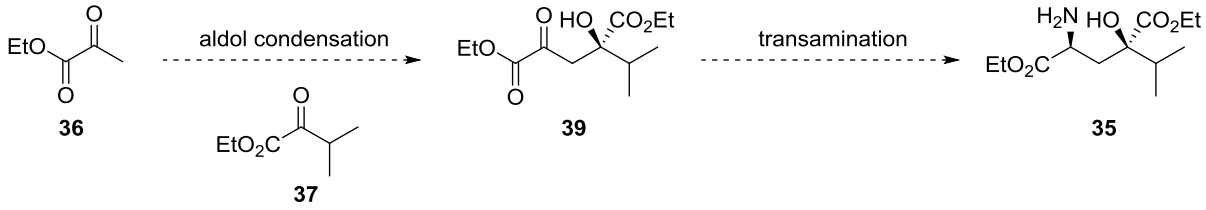

36 **37** **39** **35**

Scheme 3.7. Proposed biomimetic synthesis of protected 4-hydroxy-4-*iso*propylglutamic ethyl ester (35).

We believed that the transamination could be achieved with high selectivity using Ellman's *tert*-butanesulfinamide **38**. Since its introduction by Ellman in 1997 as a chiral ammonia equivalent,[188] *tert*-butanesulfinamide **38** has proven to be a versatile chiral auxiliary which has found extensive use both in industry and academia.[189] The condensation of *tert*-butanesulfinamide **38** with aldehydes and ketones yields the corresponding *N*-*tert*-butanesulfinyl aldimines and ketimines in good yield (Scheme 3.8). The *tert*-butanesulfinyl group activates these imines towards the addition of a range of nucleophiles and serves as a powerful chiral directing group to provide products with generally high diastereoselectivity.[189] Subsequent removal of the *tert*-butanesulfinyl group under mild conditions cleanly provides the corresponding amines (Scheme 3.8).[190]

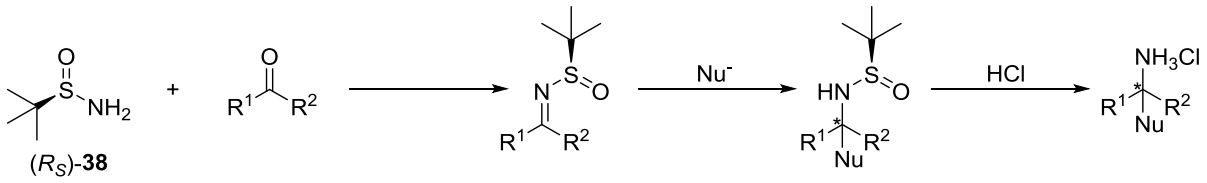

Scheme 3.8. General sequence for the asymmetric synthesis of amines using *tert*-butanesulfinamide 38.[189]

In particular this method has become one of the most extensively used approaches for the asymmetric synthesis of amines in the development and production of drug candidates. We have successfully applied this methodology in the asymmetric synthesis of both enantiomers of the chiral amine MJ05 (see Chapter 5). Using this method, selective reduction of the imine formed by condensation of glutaric acid **39** and *tert*-butanesulfinamide **38** could provide both the (2*S*) or the (2*R*) diastereomers of **35** depending on the nature of the reducing agent used (Scheme 3.9).

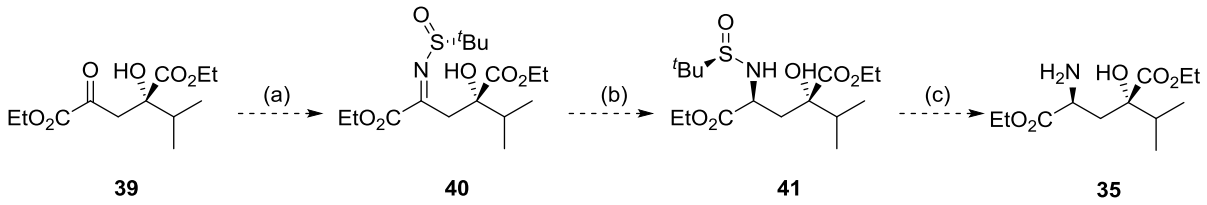

Scheme 3.9. Proposed diastereoselective reductive amination of 39 *via* the *N-tert*-butanesulfinyl ketimine 40. (a) Condensation of **39** with (R_S)-**38**. (b) Diastereoselective reduction of the *N-tert*-butanesulfinyl ketimine **40**. (c) Acidic deprotection of the *tert*-butanesulfinyl group.

Access to the required glutaric acid **39** would require an asymmetric aldol reaction of ethyl pyruvate (**36**) and ethyl dimethylpyruvate (**37**). Due to the prominence of the aldol structural motif in numerous important natural and synthetic molecules, extensive research has been carried out to identify and optimise asymmetric conditions for the aldol reaction.[191] This has resulted in the identification of numerous methods including the utilisation of chiral auxiliaries (e.g. Evan's oxazolidinone[192]), organocatalysts (e.g. proline[193]) or transition metal-based catalysts such as chiral bisoxazoline copper(II) complexes which were used successfully by Gathergood *et al*.[194] to catalyse a homo-aldol reaction of ethyl pyruvate.

Unfortunately, there has been limited development of a comprehensive and general methodology for the asymmetric cross aldol reaction involving the use of a chiral catalyst, due to the added complication of a competing homo-aldol condensation and the propensity of the product to participate in subsequent condensation reactions. These concerns limit the options for this reaction, resulting in the selection of a chiral auxiliary approach. Drawbacks to this approach include the need for a stoichiometric quantity of an expensive chiral reagent and the added steps required for its

incorporation and removal. In an attempt to overcome these issues, we proposed using Ellman's *tert*-butanesulfinamide **38** as a chiral directing group for the aldol reaction. This would then be followed by a diastereoselective reduction to form the desired 4,4-disubstituted amino acid **35** (Scheme 3.10) in an analogous manner to that previously reported for the synthesis of simple 1,3-amino alcohols.[195,196] The coupling of these two steps would improve the cost and efficiency of accessing the required amino acid **35**.

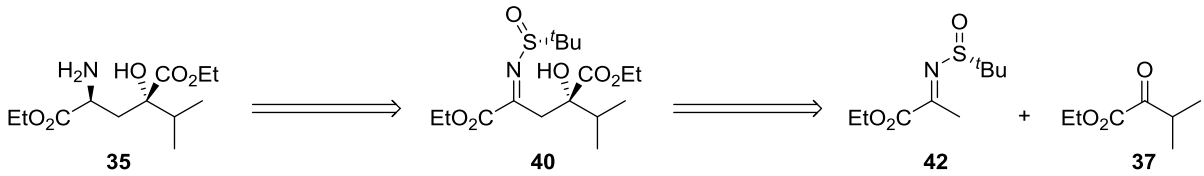

Scheme 3.10. Retrosynthetic analysis of (2*S*,4*S*)-4-hydroxy-4-isopropylglutamic acid 35. Synthetic strategy would involve a (R_S)-**38** mediated asymmetric aldol condensation of **42** and **37** to furnish **40** which could then undergo a diastereoselective reduction to provide the desired amino acid **35**.

In summary, our synthetic route to **35** would involve condensing (R_S)-*tert*-butanesulfinamide **38** with ethyl pyruvate (**36**) to provide ketimine **42** (Scheme 3.10). An asymmetric aldol reaction between **42** and ethyl dimethylpyruvate (**37**) would provide the glutarate **40** which could be reduced selectively to form the desired 4-hydroxy-4-isopropylglutamate ethyl ester (**35**) after removal of the *tert*-butanesulfinyl group (Scheme 3.10).

3.4 Total Synthesis of Harzianic Acid

3.4.1 Synthesis of the masked tetramic acid

The synthetic route began with the condensation of (R_S)-*tert*-butanesulfinamide **38** and ethyl pyruvate (**36**) in the presence of $Ti(OEt)_4$ in THF at reflux for 6 hours as previously reported for this reaction.[197] However, under these conditions only 30% of the desired *tert*-butanesulfinyl imine **42** was obtained (Table 3.1). With the aid of 2D NMR and mass spectrometry the major side product was identified as lactone **43** which was formed in a 5:3 ratio to the desired imine **42**. It was proposed that the formation of **43** occured *via* an *in situ* aldol reaction between initially formed imine **42** and remaining ethyl pyruvate (**36**) catalysed by $Ti(OEt)_4$, followed by an intramolecular cyclisation and tautomerisation (Table 3.1). Promisingly **43** was isolated as a single diastereomer (dr >98%), indicating that the *tert*-butanesulfinyl group had a directing effect on the aldol reaction. **43** is tentatively assigned as the (R_S,*R*)-diastereomer based on the later X-ray crystal structure analysis of related compound **46** (Scheme 3.11).

Table 3.1. A selection of the key results obtained from a screen of reaction conditions for the condensation of ethyl pyruvate (36) and (R_S)-*tert*-butanesulfinamide 38. *Reagents and conditions*: (**a**) (R_S)-*tert*-butanesulfinamide **38**, THF. Ratio of **42**:**43** was determined by ^{1}H NMR analysis of the crude reaction mixture. The proposed mechanism for synthesis of **43** from **42** is shown, involving an asymmetric aldol reaction of **42** and ethyl pyruvate (**36**) to provide **44**, followed by an intramolecular cyclisation to form **43**.

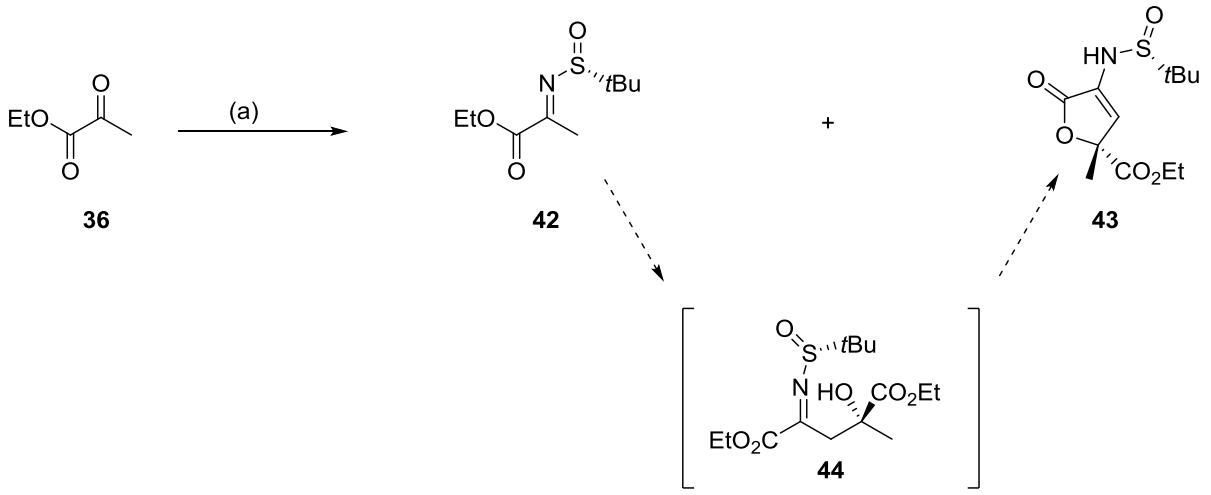

Entry	Lewis acid	Temperature (°C)	Time (hours)	42 (isolated yield)	42:43 (% by NMR)
1	$Ti(OEt)_4$	65	6	36	3:5
2	$Ti(OEt)_4$	r.t.	6	23	8:1
3	$MgSO_4$	65	6	-	-
4	$ZnBr_2$	65	6	-	-
5	$Ti(O\textit{i}Pr)_4$	65	6	22	2:5
6	$TiCl_4$	0 → r.t.	3	-	-
7	$Ti(OEt)_4$	40	6	29	4:1
8	$Ti(OEt)_4$	60	6	60	3:1

Although **43** is not a synthetically useful intermediate for the synthesis of harzianic acid (**19**), the one-pot, highly diastereoselective synthesis of **43** could be used as a highly efficient first step in the synthesis of Sch210972 (**20**) (Figure 3.10). A screen of reaction conditions (a selection of which are shown in Table 3.1) was undertaken to improve the ratio of the desired *tert*-butanesulfinyl imine **42** to the undesired lactone **43**. This led to the following observations. At room temperature the aldol reaction to give **42** was favoured, which resulted in a higher ratio of **42**:**43** but in a lower overall yield due to a competing homo-aldol condensation of ethyl pyruvate resulting in polymerisation (entry 2). Changing the Lewis acid to $MgSO_4$ or $ZnBr_2$ resulted in no reaction whereas $Ti(O\textit{i}Pr)_4$ provided a mixture of **42** and **43** but in a lower overall yield than $Ti(OEt)_4$ (entries 3-5). It was found that using $TiCl_4$ (entry 6) or carrying out the reaction at temperatures below 60 °C with $Ti(OEt)_4$ (entries 2 and 7), favoured the homo-aldol reaction, promoting polymerisation of ethyl pyruvate (**36**) resulting in a significantly reduced yield of **42**. Based on these observations it was proposed that in order to obtain both a good ratio of **42**:**43** and a good overall yield, ethyl pyruvate **36** would need to be added to the (R_S)-**38** and $Ti(OEt)_4$ in THF at 60 °C. This should limit the competing aldol condensation during the

heating of the reaction to 60 °C and allow the ethyl pyruvate (**36**) to react quickly with **38** on addition. These optimised conditions resulted in the isolation of **42** in a 3:1 ratio to **43** with an isolated yield of **42** of 60% (entry 8).

The next step involved a LDA-mediated aldol reaction between **42** and ethyl dimethylpyruvate (**37**) (Scheme 3.11). This provided the desired aldol product **45** which similarly to **44** cyclised *in situ* to form lactone **46** in a very good yield and diastereoselectivity (dr >98%). Although the source of diastereocontrol is unclear, Ellman and coworkers have previously proposed a Zimmerman-Traxler-type transition state[198] guided by the formation of M-O and M-N interactions for the related condensation of *N*-sulfinyl imines to simple aldehydes.[196] Invoking a similar stereochemical model, in which the bulky *iso*propyl substituent of **42** is placed in the pseudo-equatorial position to reduce 1,3-diaxial interactions would predict the formation of the (*R*s,*S*) diastereomer of **46** (Scheme 3.11). Subsequently a small molecule X-ray crystal structure was obtained which confirmed that **46** was the expected (*R*s,*S*) diastereomer (Scheme 3.11).

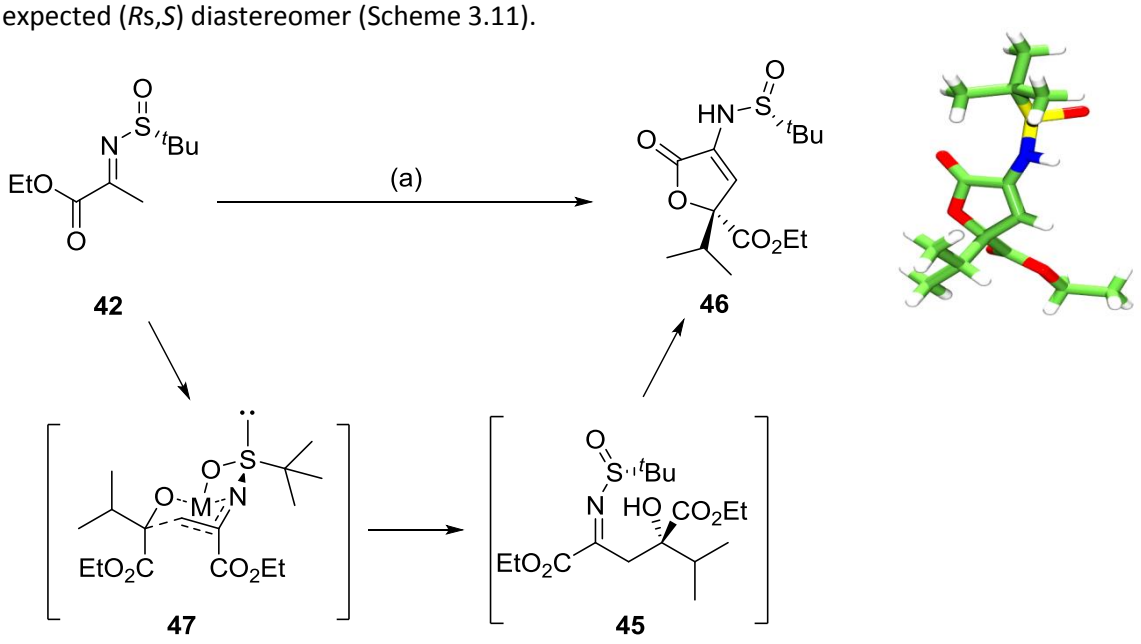

Scheme 3.11. Synthesis and small molecule X-ray crystal structure of 46. The observed stereoselectivity is consistent with a Zimmerman-Traxler-type transition state **47** in which the bulky *iso*propyl group is in a pseudo-equatorial position. *Reagents and conditions*: (**a**) (i) *i*-Pr_2NH, *n*-BuLi (2.2M in hexanes), THF, 0 °C. (ii) Ethyl dimethylpyruvate (**37**), $ZnBr_2$, -78 °C, 88%. X-ray crystallographic data provided by Prof. Alexandra Slawin.

Although the one-pot domino aldol-cyclisation reaction removed an additional cyclisation step to form key intermediate **46**, it introduced some significant concerns regarding the selective reduction of **46** to the corresponding amine **51** (Scheme 3.13). In Ellman's proposed stereochemical model for the diastereoselective reduction of the β-hydroxy-*N*-sulfinyl imine **48** to the corresponding 1,3-amino alcohol, the hydroxyl group plays a key role in the transition state (Scheme 3.12).[196] The

reduction of **48** with $LiBHEt_3$ and catecholborane has been shown to give the *anti*-**49** and *syn*-**50** 1,3-amino alcohols respectively, with high diastereoselectivity (Scheme 3.12).

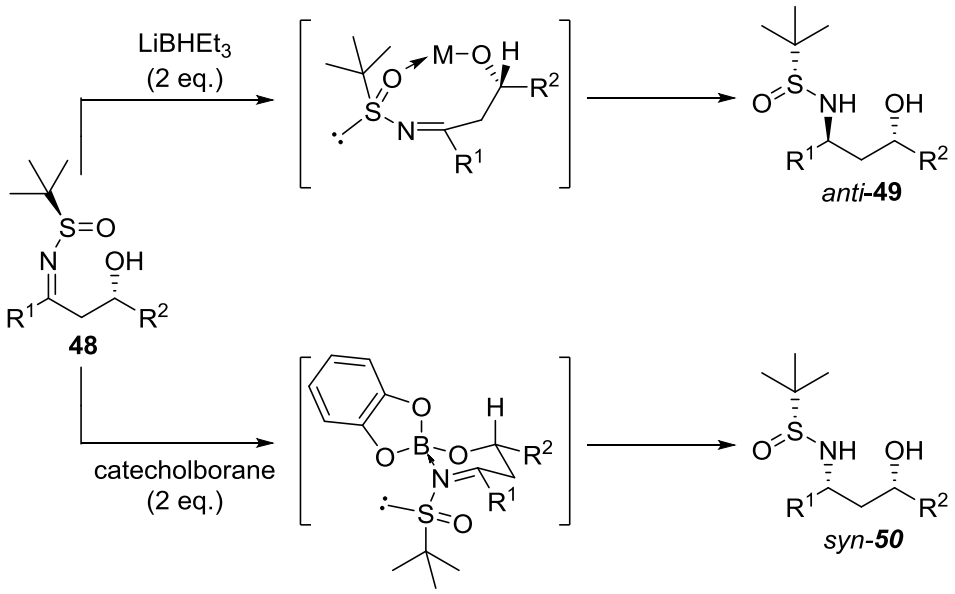

Scheme 3.12. Proposed stereochemical model for the diastereoselective reduction of β-hydroxy-*N*-sulfinyl imine 48 to the corresponding *syn* or *anti* 1,3-amino alcohols.

It is proposed that the observed reversal in diastereofacial selectivity can be rationalised by considering the geometry of the *N*-sulfinyl imine **48** during the reduction step. Numerous X-ray crystal structures and NMR studies have demonstrated that the *N*-sulfinyl imines preferentially exist in the *E*-geometry.[199,196,200] The addition of $LiBHEt_3$ is unlikely to alter the imine geometry, resulting in the attack of the hydride from the opposite face to the *tert*-butyl substituent of (R_S)-**38**, which would furnish *anti*-**49** (Scheme 3.12). In contrast, it is believed that catecholborane can form a stable six-membered intermediate which would promote isomerisation of **48** from the *E*- to *Z*-imine, resulting in the formation of *syn*-**50** (Scheme 3.12). Due to the lactonisation step, the hydroxyl group of **46** is not free to chelate the metal and thus aid the formation of the transition state required for the selective hydride attack. In addition, **46** exists predominantly as the enamine tautomer in solution (the imine tautomer is not observed by ^1H NMR analysis) due to the greater stability provided to the enamine tautomer as a result of conjugation with the lactone carbonyl. As a result of the enamine stability, **46** is considerably more resistant to reduction than the corresponding imine tautomer.

An added complication arises due the presence of the reactive lactone and ester moieties in **46**. Therefore, only mild reducing conditions could be utilised to prevent any unwanted reduction of these groups. A screen of hydride reducing agents ($NaBH_4$, L-Selectride, $NaBH_3CN$), transfer hydrogenation conditions (NH_4HCO_2 and Pd/C) and hydrogenation conditions (H_2 and 10% Pd/C or

PtO_2) confirmed that as predicted the enamine was stable to reduction, with either no reaction occurring or unselective reduction in the case of L-Selectride. Due to the added stability conferred by the enamine tautomer, it was decided to attempt the reduction under acidic conditions with the aim of forming the corresponding iminium ion, which given its increased electrophilicity would be easier to reduce. Initial attempts using $NaBH_3CN$/TFA,[201] $NaBH_4$/AcOH[202] and $NaBH_3CN$/HCl (1.25N in MeOH)[203] proved unsuccessful. A common method to cleave the *N-tert*-butanesulfinyl group is under acidic conditions (HCl, 4N in dioxane) which is proposed to protonate the sulfinamide nitrogen, activating it towards attack of Cl^- at the sulfinyl group.[204] With the knowledge that these conditions will protonate the amine, it was therefore decided to try to reduce **46** using $NaBH_3CN$/HCl (4N in dioxane). Gratifyingly these conditions furnished the desired amine **51** in good yield and very good diastereoselectivity (dr > 95%) with concomitant deprotection of the *tert*-butanesulfinyl group (Scheme 3.13).

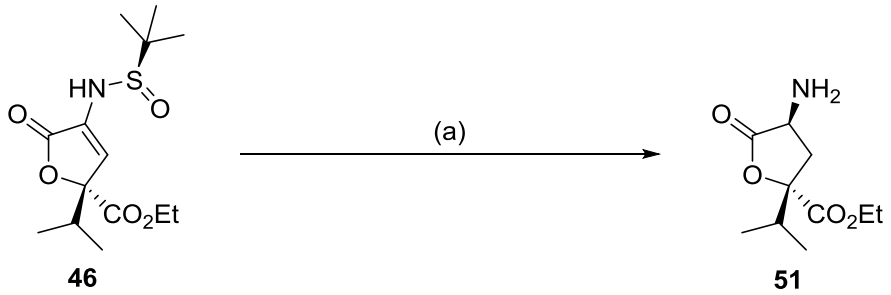

46 **51**

Scheme 3.13. Diastereoselective reduction. *Reagents and conditions*: (**a**) (i) HCl (4N in dioxane), THF, 0 °C, 10 minutes. (ii) $NaBH_3CN$, MeOH, 1.5 hours, 0 °C, 76%, dr >95%.

This reaction development was undertaken using **46** which contains a free NH. However, as harzianic acid (**19**) contains a methylated amino-group, it was decided that **46** was the optimal intermediate to methylate. This was achieved in very high yield using iodomethane to provide **52**. The tandem deprotection-reduction was then carried out using **52** which provided **53** with improved yield and diastereoselectivity (dr >98%) when compared to **51** (Scheme 3.14).

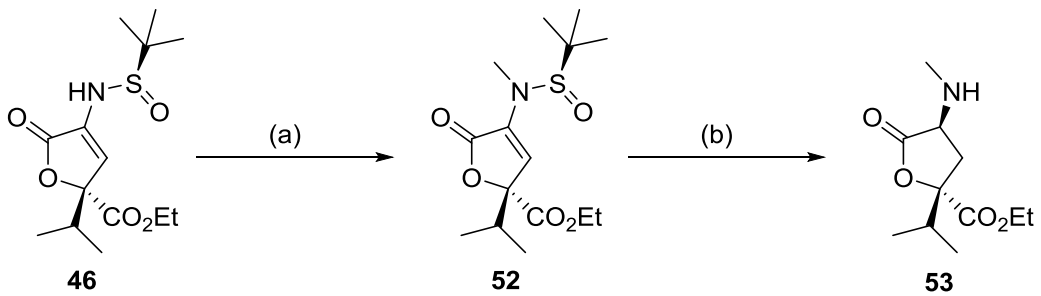

46 **52** **53**

Scheme 3.14. Synthesis of 53. *Reagents and conditions*: (**a**) LiHMDS, iodomethane (2 eq.), DMF, -15 °C → r.t., 95%. (**b**) (i) HCl (4N in dioxane), THF, 0 °C, 10 minutes. (ii) $NaBH_3CN$, MeOH, 1.5 hours, 0 °C, 85%, dr > 98%.

Initial NOE studies on crude **53** indicated that the amine and *iso*propyl substituents were cofacial, suggesting the formation of the desired (*S*,*S*)-diastereomer, which was subsequently confirmed by NOE analysis of the more advanced harzianic acid intermediate **55** (Section 3.4.3, Figure 3.11). Some further mechanistic studies were carried out to elucidate the reaction sequence in the tandem deprotection-reduction. The experimental procedure involved the addition of HCl (4N in dioxane) to **52** in THF at 0 °C followed by addition of $NaBH_3CN$ in methanol after 10 minutes. Work-up of the reaction prior to the addition of the reducing agent revealed the deprotected enamine was formed (Scheme 3.15). Subsequent $NaBH_3CN$-mediated reduction of the iminium ion **54** in the presence of HCl (4N in dioxane) provided the desired product **53** with similar diastereoselectivity but diminished yield when compared to the one-pot process. As the chiral auxiliary had been cleaved prior to the addition of the reducing agent, the observed diastereoselectivity appears to be purely substrate controlled with the hydride attacking from the same side as the ester substituent (Scheme 3.15). The high level of diastereocontrol would suggest that it may not be purely sterically induced and could be a result of chelation of the reducing agent by the ester, directing the facial attack of the hydride.

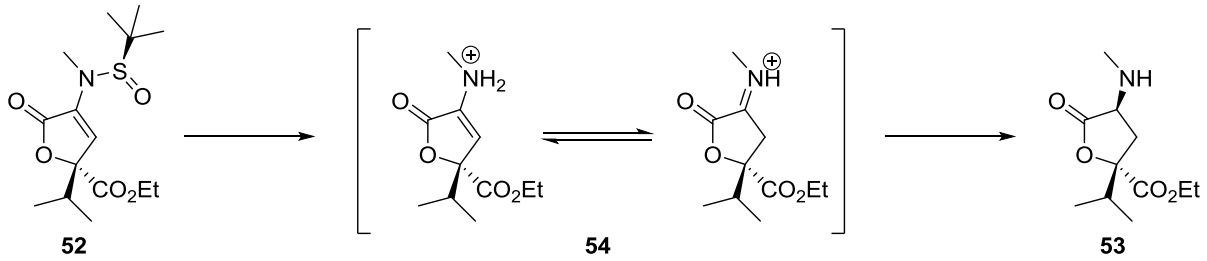

Scheme 3.15. Mechanistic studies of the deprotection-reduction reaction sequence revealed that it occurs *via* acid-mediated removal of the *tert*-butanesulfinyl group followed by a substrate controlled diastereoselective reduction of the resulting iminium to provide 53.

Due to the relatively high purity of the crude amine **53** isolated from the one-pot process and the difficulties generally associated with the purification of amines, it was decided to trap directly the crude amine **53** with the desired harzianic acid polyene side chain.

3.4.2 Synthesis of the polyene side chain

In the previously outlined convergent synthetic strategy, the polyene chain was introduced through an *N*-acylation of the masked tetramic acid (Scheme 3.4). A β-ketothioester was selected as the acylating reagent as it is often used as a biomimetic of acetyl-CoA, the acyl-transfer unit used in the polyketide synthase (PKS) pathway.[205] Direct aminolysis of the *tert*-butyl thioester moiety in **56** by **53** *via* a silver trifluoroacetate mediated protocol developed by the Ley group[206,159] would provide the desired β-keto amide **55** (Scheme 3.16). As a main aim of this synthesis was the development of a versatile and convergent route, the β-ketothioester **56** was disconnected to provide a core fragment

which could be easily modified to access a range of different polyene chains. To this end, the γ,δ-unsaturated bond of **56** was disconnected. In the forward sense this bond could ultimately be formed *via* a Horner-Wadsworth-Emmons (HWE) olefination of phosphonate **57** and aldehyde **58** (Scheme 3.16). By utilising the phosphonate **57** as a core fragment, a range of saturated and unsaturated aldehydes could be incorporated to access a diverse selection of β-ketothioesters.

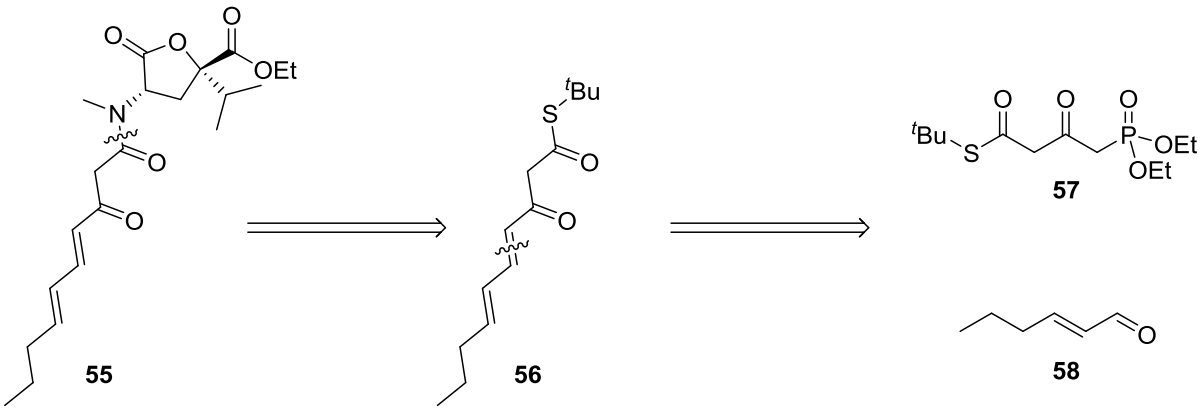

Scheme 3.16. Retrosynthetic analysis of the polyene chain of harzianic acid (19).

Assembly of the polyene side chain began with a PCC oxidation of commercially available *trans*-2-hexen-1-ol (**59**) to the corresponding aldehyde **58**. Whilst these conditions promoted complete conversion of **59** to the desired aldehyde **58**, the chromium side products proved difficult to remove. Upon completion, the reaction was concentrated *in vacuo*, the residue dissolved in Et_2O, filtered through Celite and concentrated again. For complete removal of the remaining chromium, this work-up procedure often had to be repeated, resulting in a reduced yield of volatile **58**. As a result, alternative oxidation protocols were explored. Manganese(IV) oxide was initially selected due to the simple filtration required at the end of the reaction. However, whilst this method did provide the desired product **58** in excellent yield, it required regular addition of manganese(IV) oxide over a 48 hour period to push it to completion which was not optimal. We therefore tried a DDQ-mediated oxidation, which provided the desired aldehyde **58** quantitatively after a simple aqueous work-up (Scheme 3.17).

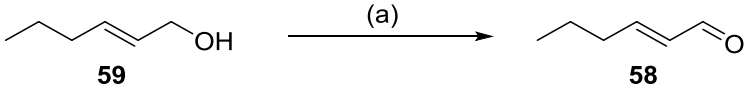

Scheme 3.17. Oxidation of 59 to 58. *Reagents and conditions*: DDQ, DCM, r.t., 16 h, quantitative.

With aldehyde **58** in hand we turned our attention to the synthesis of phosphonate **57**. Although **57** is a highly versatile reagent often used in the synthesis of 3-oxomacrolides,[207–209] tetronic[210,211] and

tetramic acids,[212,213] its synthesis has not been optimised since it was first reported by Woodward and Ley in 1987.[214] Their synthetic route involved the acylation of Meldrum's acid **60** (2,2-dimethyl-1,3-dioxane-4,6-dione) with bromoacetyl bromide to provide **61**. A thermally induced pericyclic reaction of **61**, released acetone, carbon dioxide and a highly reactive substituted ketene,[215] which was trapped *in situ* by *t*-butylthiol to afford the 1,3-dicarbonyl containing compound **62**. Treatment of the monosodium salt of **62** with sodium diethylphosphite afforded the desired phosphonate **57** (Scheme 3.18, Route A). Here we report an alternative route to **57** *via* a direct acylation of Meldrum's acid **60** with commercially available phosphonoacetic acid. Formation of phosphonoacetyl chloride followed by addition to Meldrum's acid provided **63**, which without purification was treated with *t*-butylthiol to give the desired phosphonate **57** in excellent yield (Scheme 3.18, Route B).

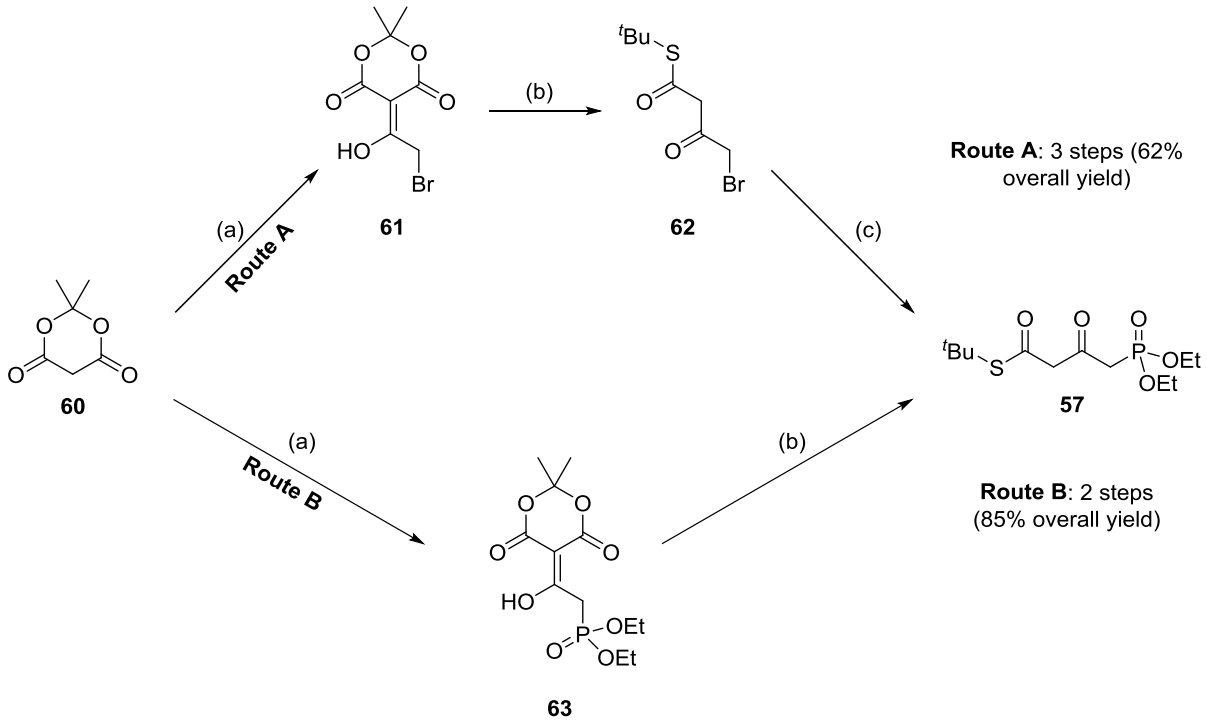

Scheme 3.18. Synthesis of 57. Route A – Woodward and Ley synthesis.[214] *Reagents and conditions*: (**a**) Bromoacetyl bromide, pyridine, DCM, 0 °C → r.t. (**b**) *t*-Butylthiol, benzene, reflux, 73% over 2 steps. (**c**) (i) Na, THF, reflux. (ii) NaH, THF, -10 °C → r.t., 85% **Route B – Novel synthesis.** *Reagents and conditions*: (**a**) (i) Phosphonoacetic acid, $SOCl_2$. (ii) Pyridine, DCM, 0 °C → r.t., quantitative. (**b**) *t*-Butylthiol, MeCN, reflux, 85%.

In addition to being a simpler and more efficient route it also provides access to a highly synthetically useful intermediate **63** (Scheme 3.18). Acyl derivatives of Meldrum's acid are widely used as synthetic equivalents for the introduction of 1,3-dicarbonyl motifs in the synthesis of natural products.[216] Using this methodology, **63** could be used to incorporate a 1,3-dicarbonyl motif into polyketide based-natural products bearing an attached phosphonate handle. This would facilitate the incorporation of a range of side chains *via* a HWE olefination (see Section 5.5.6 for utilisation of

this approach). Finally, a HWE olefination of aldehyde **58** and the dilithio-anion of **57** furnished the required β-ketothioester **56** (Scheme 3.19).

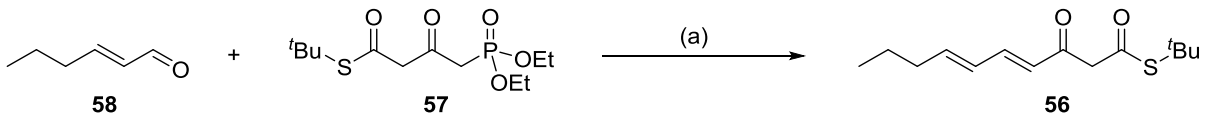

58 **57** **56**

Scheme 3.19. Synthesis of 56. *Reagents and conditions*: LiHMDS (2 eq.), THF, -78 °C → 0 °C, 87%.

3.4.3 End-game strategy: total synthesis of harzianic acid

The end-game strategy for the synthesis of harzianic acid (**19**) involved coupling of the polyene side chain **56** to the masked tetramic acid intermediate **52**, followed by cyclisation and ester hydrolysis. The crude amine **53** obtained from the deprotection-reduction sequence was redissolved in THF before the addition of CF_3CO_2Ag, Et_3N and **56** according to Ley's protocol (Scheme 3.20).[159] This afforded the desired β-ketoamide **55** in good yield.

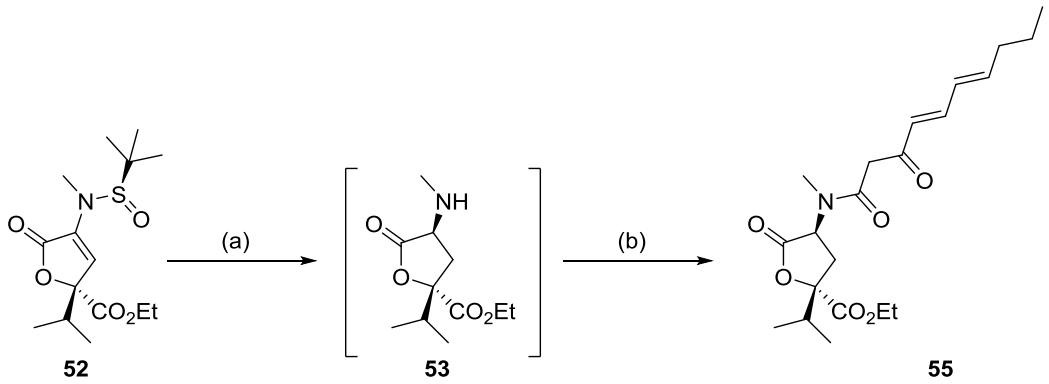

52 **53** **55**

Scheme 3.20. Synthesis of harzianic acid ethyl ester 55. *Reagents and conditions*: (**a**) (i) HCl (4N in dioxane), THF, 0 °C, 10 minutes. (ii) $NaBH_3CN$, MeOH, 1.5 hours, 0 °C. (**b**) **56**, CF_3CO_2Ag, Et_3N, THF, 0 °C → r.t., 63% over 2 steps.

With the desired β-ketoamide **55** in hand an NOE study was undertaken to confirm the expected relative stereochemistry of the product. The NOE analysis confirmed that **55** exists as a mixture of *keto* and *enol* tautomers due to an observed chemical exchange (EXSY) between H1 in the two tautomers. In addition, it revealed that the amine and *iso*propyl functional groups were on the same face of the lactone ring (Figure 3.11). The previous assignment of the *iso*propyl group stereogenic centre as (*S*) by analysis of the small molecule X-ray crystal structure **46** (Scheme 3.11) enabled the assignment of the amine stereogenic centre as (*S*) also.

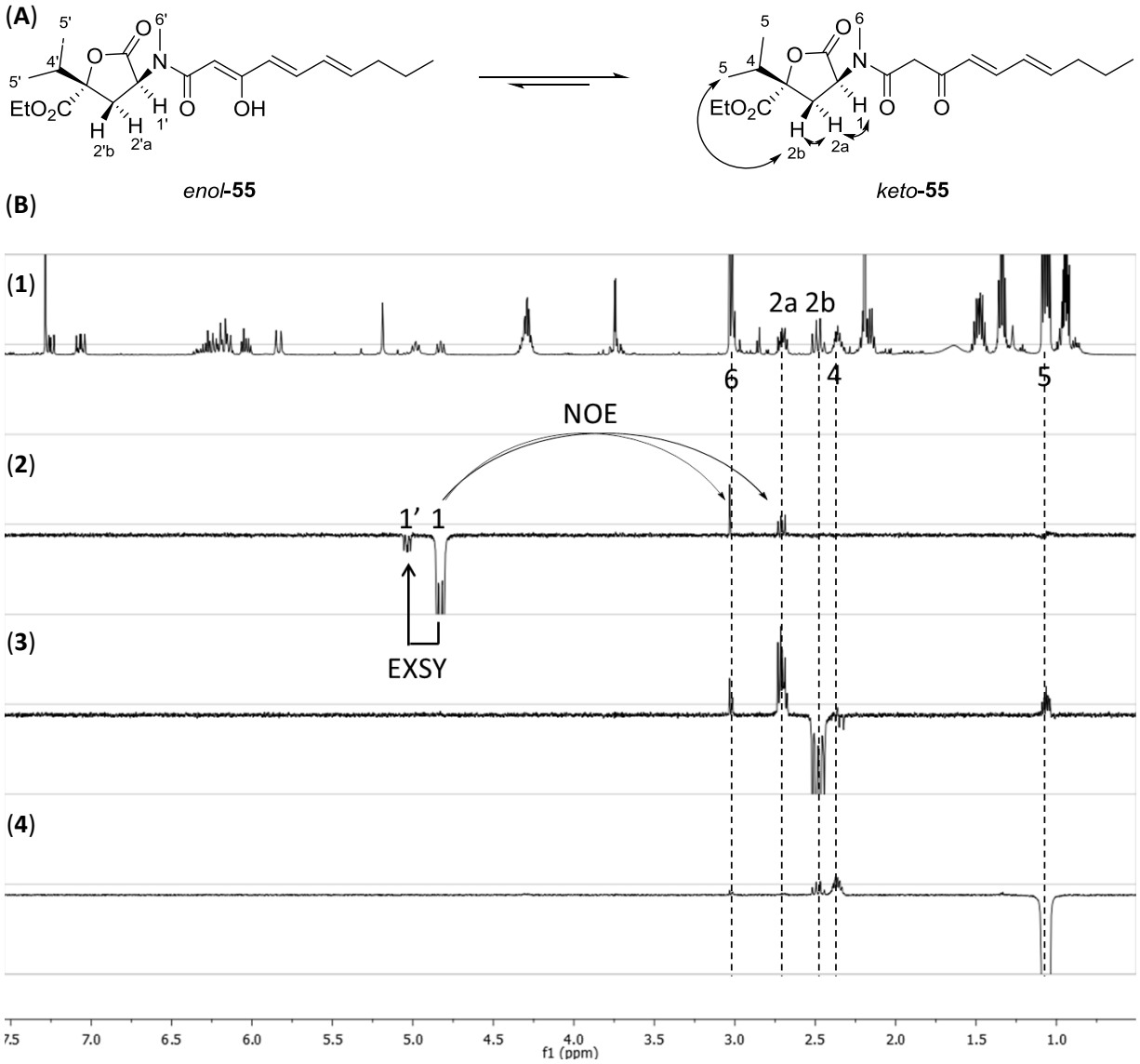

Figure 3.11. NOE analysis of 55. (**a**) Structure of the *enol* and *keto* tautomers of **55**. Observed NOEs are highlighted. (**b**) (1) – ^{1}H NMR spectra of **55** showing a (5:4) *enol*:*keto* mix of tautomers. (2) – Irradiation of H-1 (*keto*) reveals an EXSY with H-1' (*enol*), which confirmed they are chemically exchangeable and thus that **55** is present as a mixture of *enol*:*keto* tautomers. An NOE was also observed between H-1 and H-6 and H-2a. This demonstrated that H-1 and H-2a are cofacial. COSY and HSQC experiments showed that H-2b is on the same carbon as H-2a (data not shown). (3) – Irradiation of H-2b revealed an NOE of H-2a as expected and H-6 and H-5. This demonstrated that H-2b and H-5 were cofacial and therefore on the opposite face to H-1 and H-2a. (4) – Irradiation of H-5 revealed an NOE with H-4 as expected and confirmed the NOE with H-2b.

Having established the formation of the (*S*,*S*) diastereomer of **55**, cyclisation of the β-ketoamide was then investigated. Initial attempts to cyclise the β-ketoamide **55** using ^{t}BuOK (3 eq.) in THF were unsuccessful, yielding a small quantity of the desired harzianic acid ethyl ester (**64**) with significant formation of unassigned side products. Optimisation of this reaction identified ^{t}BuOK (1 eq.) in THF as the optimal conditions, resulting in the clean conversion of **55** to **64** in 1 hour (Scheme 3.21). Further optimisation of this reaction focused on the observation that a small quantity (<10%) of the cyclised harzianic acid ethyl ester (**64**) formed during the silver-mediated *N*-acylation reaction. It was found that changing the solvent of this reaction from THF to MeCN resulted in the isolation of the

desired cyclised product **64** in very good yield (75% from lactone **52**). This highly efficient tandem deprotection-reduction-*N*-acylation-cyclisation reaction sequence produced the highly advanced harzianic acid ethyl ester (**64**) in just one day from **52** (Scheme 3.21).

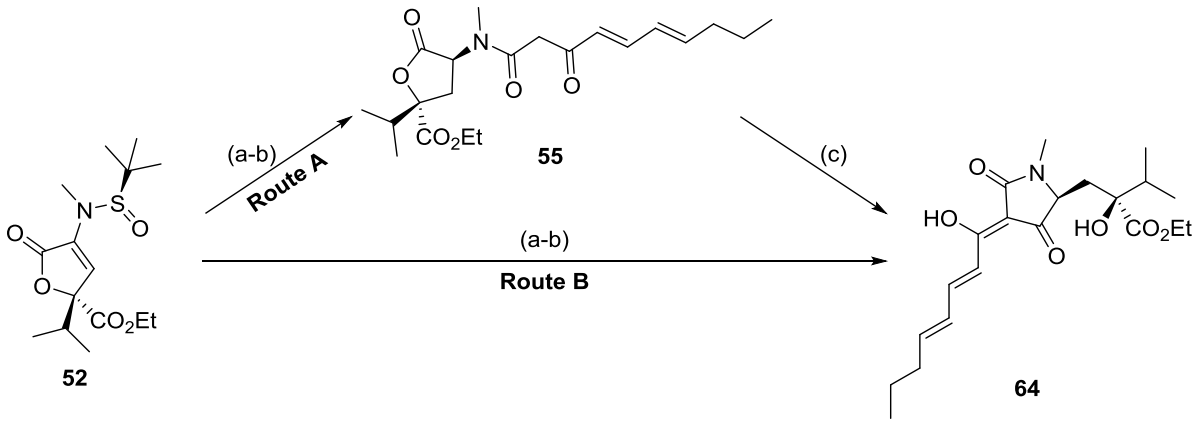

Scheme 3.21. Tandem deprotection-reduction-*N*-acylation-cyclisation synthesis of 64. *Reagents and conditions*: **Route A**: (**a**) (i) HCl (4N in dioxane), THF, 0 °C, 10 minutes. (ii) $NaBH_3CN$, MeOH, 1.5 hours, 0 °C. (**b**) **56**, CF_3CO_2Ag, Et_3N, THF, 0 °C → r.t., 2 h, 65% over 2 steps. (**c**) ^{t}BuOK (1 eq.), THF, 0 °C → r.t., 93%. **Route B**: (**a**) (i) HCl (4N in dioxane), THF, 0 °C, 10 minutes. (ii) $NaBH_3CN$, MeOH, 1.5 hours, 0 °C. (**b**) **56**, CF_3CO_2Ag, Et_3N, MeCN, 0 °C → r.t., 2 h, 75% over 2 steps.

A preliminary investigation of ester hydrolysis conditions was undertaken, which included refluxing **64** in EtOH under acidic conditions (1N HCl) or basic conditions (2N NaOH). The acid hydrolysis conditions resulted in the recovery of the starting material **64** after 14 hours. The reaction carried out under basic hydrolysis conditions yielded a mixture of starting material **64**, (*S*,*S*)-harzianic acid (**19**) and (*R*,*S*)-5'-*epi*harzianic acid (**19b**) after 3 hours (Scheme 3.22). The partial epimerisation at the C5' stereogenic centre is a common issue observed with tetramic acids.[157] While extending the reaction time did increase the conversion of **64** to **19**, it also resulted in an increased epimerisation at the C5' position, resulting in an approximate 1:1 mixture of the two diastereomers **19** and **19b** (Scheme 3.22). Based on the observed correlation between reaction time and epimerisation, the focus turned towards microwave irradiation conditions which could greatly reduce the reaction time and hence potentially epimerisation. A screen of bases (LiOH, NaOH, KOH, $Ba(OH)_2$), temperatures (80 → 150 °C) and time revealed that the optimal conditions were NaOH (2N) in EtOH for 20 minutes at 110 °C, providing complete conversion of **64** to **19** in an approximate 3:1 ratio to the (*R*,*S*)-diastereomer **19b** (Scheme 3.22). Harsher conditions such as the use of a stronger base (e.g., 5N KOH) or higher temperatures (>110 °C) did reduce the reaction time, however this resulted in a concomitant increase in unassigned side products with no reduction in the degree of epimerisation.

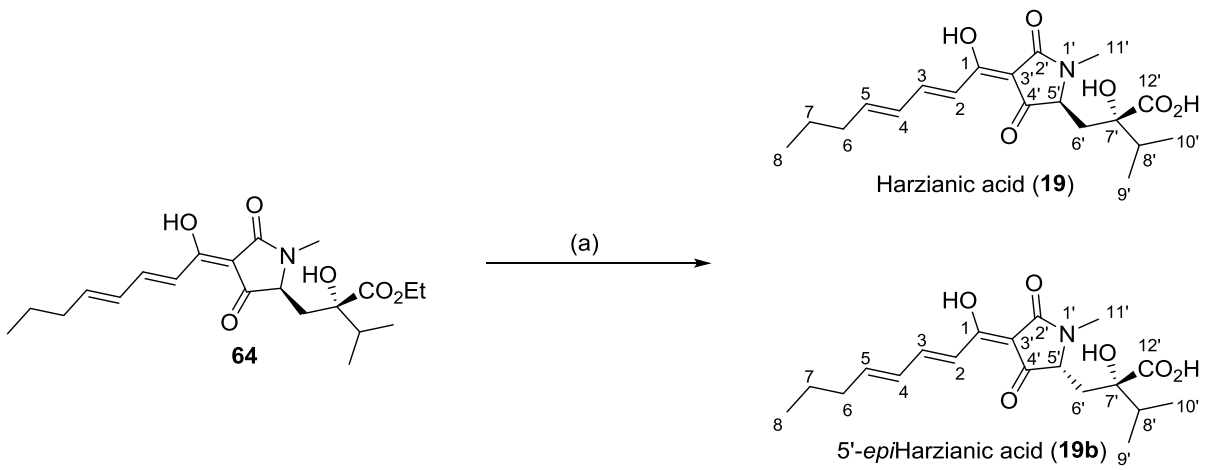

Scheme 3.22. Microwave irradiation assisted ester hydrolysis of 64. *Reagents and conditions*: (**a**) NaOH (2N), EtOH, 110 °C, 20 minutes, **19** - 52%; **19b** – 19%.

Harzianic acid (**19**) and 5'-*epi*harzianic acid (**19b**, see Table 3.2 for spectroscopic data and Appendix D) were readily separable by reverse phase chromatography. An additional purification step to remove any chelating metals was utilised, which involved passing the samples through a plug of tosic acid functionalised silica. The ^{1}H NMR, ^{13}C NMR, HRMS, IR and the specific rotation obtained for the synthetic harzianic acid (**19**) were in excellent agreement with the data provided for the natural sample (Table 3.2).[160,164,172]

Table 3.2. Comparison of the physico-chemical and spectroscopic properties of isolated harzianic acid (19)[172] and synthetic harzianic acid diastereomers (19) and (19b).

(*S*,*S*)-Harzianic acid (19)[172] (reported for isolated sample)			**(*S*,*S*)-Harzianic acid (19) (synthesised)**		**(*R*,*S*)-5'*epi*Harzianic acid (19b) (synthesised)**	
$[\alpha]_D^{20}$	+19.6° (*c* 1.06, MeOH)		+18.6° (*c* 1.06, MeOH)		+118.0° (*c* 0.5, MeOH)	
HRMS	366.1922 $[M+H]^+$		366.1911 $[M+H]^+$		364.1757 $[M-H]^-$	
Position	**^{1}H NMR** (ppm)	**^{13}C NMR** (ppm)	**^{1}H NMR** (ppm)	**^{13}C NMR** (ppm)	**^{1}H NMR** (ppm)	**^{13}C NMR** (ppm)
	(CD_3OD, 400 MHz)		(CD_3OD, 500 MHz)		(CD_3OD, 500 MHz)	
1	-	175.9		175.8		173.4
2	7.09	120.4	7.09	120.3	7.11	120.6
3	7.53	147.2	7.53	147.3	7.44	145.6
4	6.39	131.0	6.39	131.0	6.34	131.0
5	6.39	149.7	6.39	149.8	6.34	148.2
6	2.23	36.4	2.24	36.4	2.23	36.3
7	1.50	22.9	1.51	23.0	1.50	23.0
8	0.95	14.0	0.96	14.1	0.96	14.0
2'	-	173.9	-	173.9	-	176.4
3'	-	100.9	-	100.9	-	102.3
4'	-	198.9	-	198.9	-	196.3
5'	3.80	65.5	3.80	65.5	3.77	66.0
6'	1.99	36.4	1.99	36.4	2.40	37.0
	2.33		2.34		2.47	
7'	-	79.8	-	79.8	-	78.8
8'	2.02	37.4	2.02	37.4	1.89	37.5
9'	0.97	17.5	0.98	17.9	0.95	17.6
10'	0.94	16.5	0.95	16.5	0.87	16.6
11'	2.94	27.1	2.94	27.1	2.92	28.3
12'	-	178.6	-	178.6	-	178.2

The absolute configuration of harzianic acid (**19**) was determined by Vinale *et al.* through X-ray diffraction studies.[164] In addition, this study also revealed that in the solid state harzianic acid (**19**) is stabilised by intramolecular hydrogen bonds between O1 and O2' and between O7' and O4' (Figure 3.12A). ^{13}C NMR analysis of **19** in MeOD (see Appendix C) revealed that the quaternary carbons (C2'-C4') of the tetramic acid were poorly resolved, which is in agreement with the isolation paper which assigned them as broad. It was found that recording the NMR spectra using deuterated chloroform provided very clear and well resolved signals both in ^{1}H (Figure 3.12B) and ^{13}C spectra (see Appendix C). This is presumably due to the inability of $CDCl_3$ to participate or disrupt possible intramolecular and intermolecular hydrogen bonding networks in solution, thus resulting in **19** appearing as a single tautomer. Further analysis of the ^{1}H NMR spectrum of **19** in $CDCl_3$ identified the tertiary alcohol (O7') at 7.25 ppm (Figure 3.12B). This is a significant downfield shift in comparison with the typically

observed chemical shift for alcohols between 2.0 – 5.5 ppm. The observed downfield shift is consistent with the deshielding of the O7'-proton *via* an intramolecular hydrogen bond, in agreement with the previously determined X-ray crystal structure.[164]

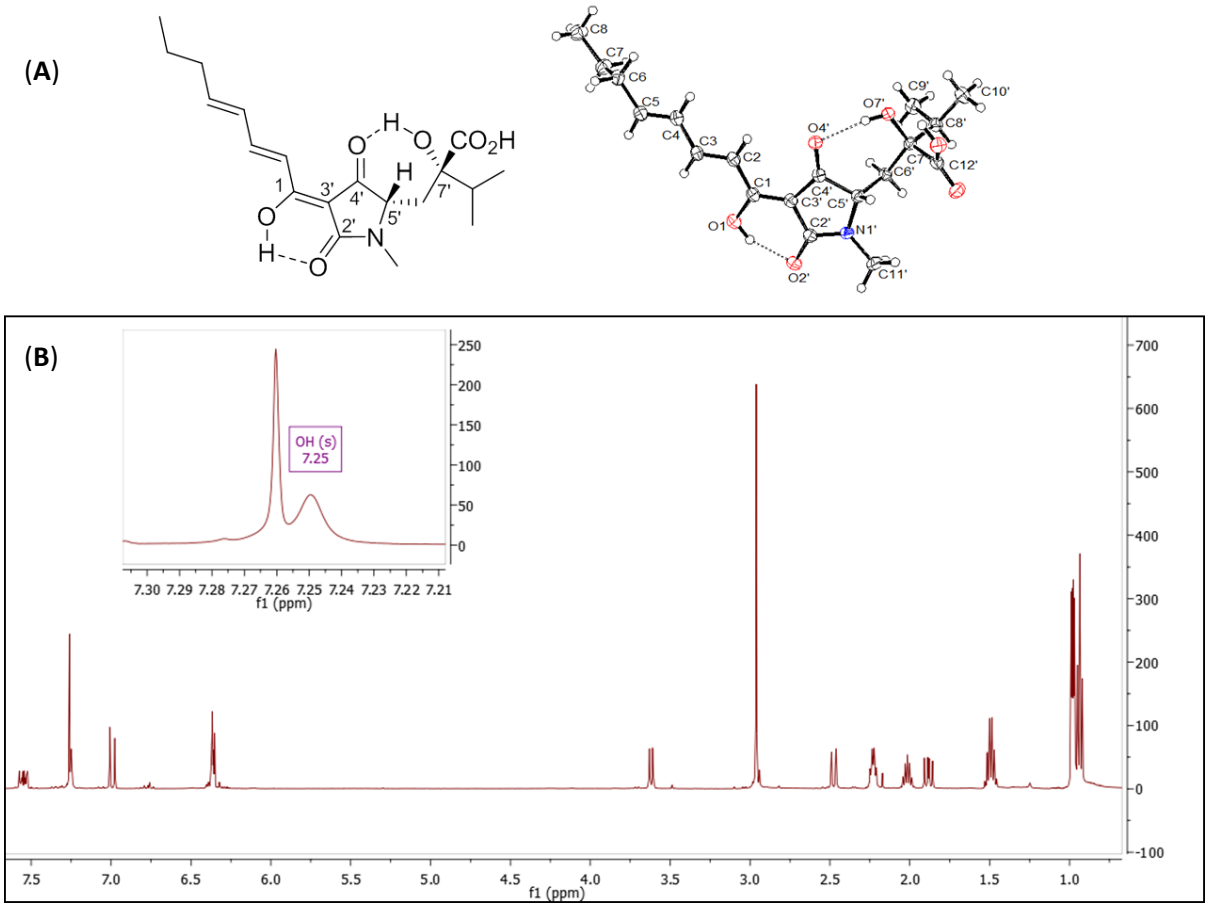

Figure 3.12. (A) Small molecule X-ray crystal structure of (*S*,*S*)-harzianic acid (19) reported by Vinale *et al*. showing intramolecular hydrogen bonding.[164] (B) ^{1}H NMR spectrum of synthesised (*S*,*S*)-harzianic acid (19) in $CDCl_3$ (500 MHz).

In summary, a biomimetic, convergent and efficient synthesis of (*S*,*S*)-harzianic acid (**19**) has been developed. This route could be adapted for the synthesis of a range of similar tetramic acid natural products and analogues. The synthesis of harzianic acid (**19**) was achieved with a longest linear sequence (LLS) of 6 steps and an overall yield of 22%. Using this route we were also able to isolate 5'-*epi*harzianic acid (**19b**) and by utilising the (*S*)-enantiomer of *tert*-butanesulfinamide **38,** (*R*,*R*)-harzianic acid (**19c**) and its 5'-epimer (*S*,*R*)-harzianic acid (**19d**) were also prepared (Table 3.3).

Table 3.3. Quantities and optical rotation of all four synthesised harzianic acid diastereomers.

Compound		Quantity Synthesised (mg)	Optical Rotation ($[\alpha]_D^{20}$; MeOH)
(*S*,*S*)-Harzianic acid	**19**	92	+18.6°
(*R*,*S*)-5'*epi*Harzianic acid	**19b**	33	+118.0°
(*R*,*R*)-Harzianic acid	**19c**	81	-16.9°
(*S*,*R*)-5'*epi*Harzianic acid	**19d**	24	-121.2°

3.5 Total Synthesis of JBIR-22

3.5.1 Retrosynthetic analysis

The development of a synthetic route to harzianic acid (**19**) provided a highly synthetically useful common intermediate **52** (Scheme 3.14) which could be elaborated to access JBIR-22 (**4**). The original retrosynthetic analysis of JBIR-22 (**4**) involved a late-stage intramolecular Diels-Alder cyclisation of the appropriate polyene intermediate **65** (Scheme 3.23, Route A). Incorporation of the polyene chain **66** could be achieved by *N*-acylation of the masked tetramic core **52** in an analogous manner to the synthesis of harzianic acid (**19**).

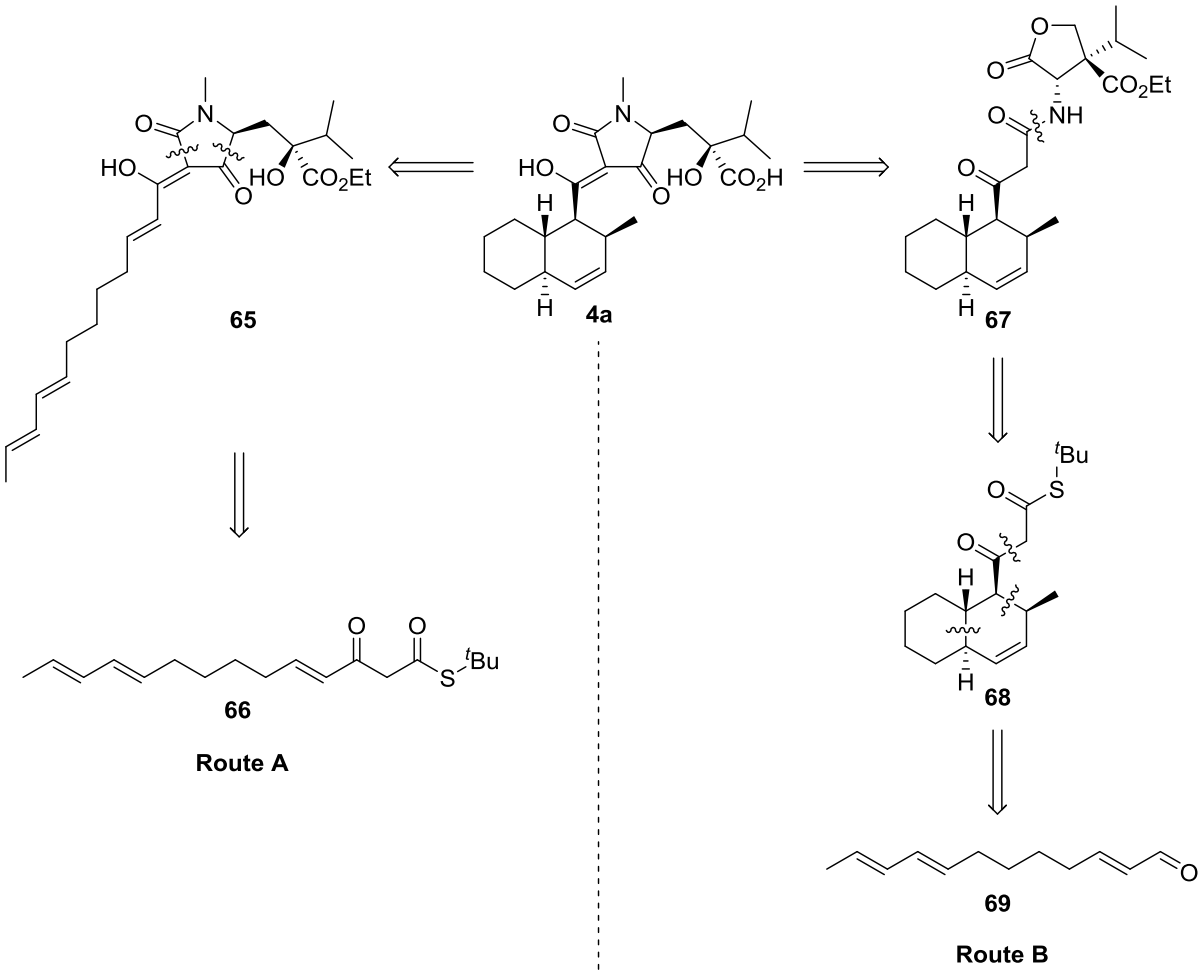

Scheme 3.23. Retrosynthetic analysis of JBIR-22 (diastereomer-4a represented). Route A – Entails a late-stage IMDA of intermediate 65 which derives from polyene chain 66. Route B – Highlights include the incorporation of decalin moiety 68 *via* an *N*-acylation reaction. Synthesis of 68 involves a key enantioselective Diels-Alder cyclisation of polyene 69.

A key challenge in this route is the identification of a diastereoselective IMDA cyclisation of the complex intermediate **65**. This could potentially be achieved under substrate control using an achiral catalyst, or through the development of a chiral catalyst-based methodology. Insight into the biosynthesis of JBIR-22 (**4**) could be provided by investigation of a possible substrate-controlled non-

enzymatic asymmetric DA cycloaddition versus an enzymatic "Diels-Alderase" mediated reaction. However, a major challenge associated with this strategy is the assignment of the absolute configuration of the Diels-Alder product **4** in the absence of a small molecule X-ray crystal structure. To aid the stereochemical assignment of JBIR-22 (**4**), an alternative route was proposed which would entail an enantioselective Diels-Alder cyclisation of the trienal **69** to provide a single enantiomer of the decalin ring **68** prior to attaching it to **52** (Scheme 3.23, Route B). This route could provide access to all four predicted stereoisomers of JBIR-22 (Scheme 3.4, **4**(**a**-**d**)), thus facilitating the absolute stereochemical assignment of JBIR-22 (**4**). In addition, this would also provide authentic samples of the diastereomers as standards for the development of a late-stage diastereoselective Diels-Alder cyclisation (Scheme 3.23, Route A).

3.5.2 Synthesis of polyene 66

Due to the high probability of the glutamic acid side chain existing as the (*S*) configuration (see Section 3.1.3), a large-scale synthesis of the (*S*)-diastereomer of the masked tetramic acid intermediate **52** (>5 g) was carried out. This provided a common intermediate onto which the appropriate polyene chain or decalin ring could be attached. With **52** in hand, the next focus was on the synthesis of the β-ketothioester **66**, a key intermediate in Route A (Scheme 3.23).

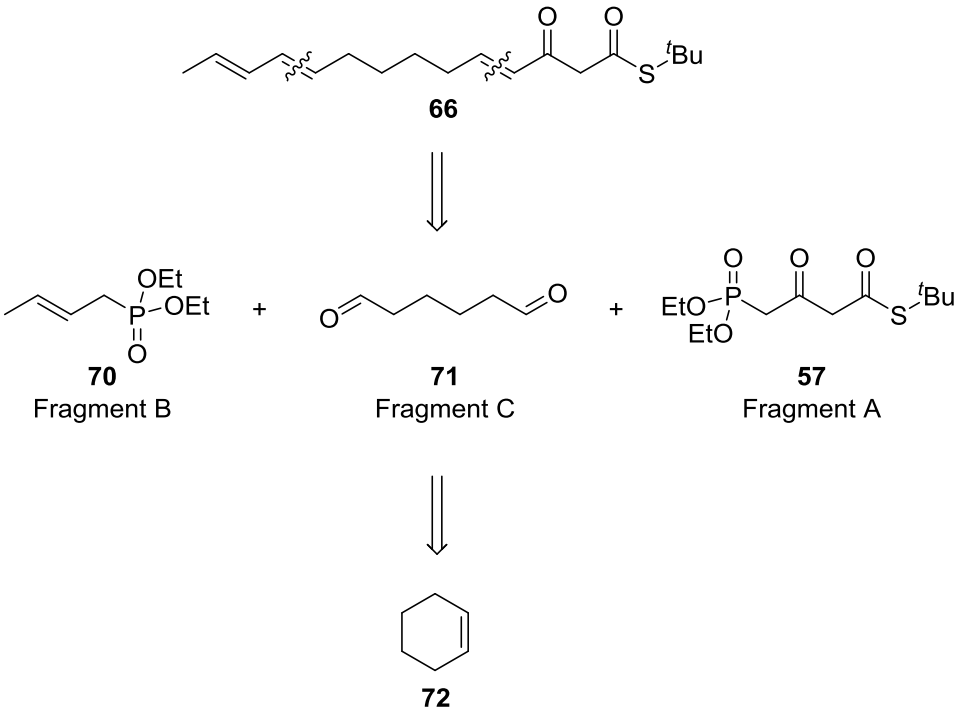

Scheme 3.24. Retrosynthetic analysis of 66.

It was proposed that **66** could be formed from three different fragments (Scheme 3.24). Fragment A) phosphonate **57** could be used to introduce the β-ketothioester functionality in an analogous manner to its utilisation in the synthesis of harzianic acid (**19**). Fragment B) the terminal diene could be introduced *via* phosphonate **70**. Employing a range of different phosphonates would facilitate the modification of the terminal end of the chain providing access to analogues of JBIR-22 (**4**). Fragment C) the remaining core 6-carbon di-aldehyde fragment **71** could be accessed through an atom-economical ozonolysis of cheap and readily available cyclohexene (**72**).

Assembly of **66** began with a Schreiber ozonolysis[217] of cyclohexene (**72**) which incorporates an *in situ* protection of one of the terminal aldehydes as an acetal to give **73**, thereby differentiating between the terminal aldehydes (Scheme 3.25). The next step involved a HWE olefination between phosphonate **70** and the mono-protected aldehyde **73**. Synthesis of the diene **74** from the mono-protected aldehyde has been reported previously by Uchida *et al*.[218] in the total synthesis of (+)-UCS1025A (Scheme 3.25). However in contrast to our proposed synthesis, the chain elongation step was achieved *via* a Wittig reaction with 2-butenyl triphenylphosphonium bromide (**76**). This provided **74** as a mixture of isomers at the C4-C5 double bond (*E*/*Z* – 1:1) which required an additional isomerisation step to improve the ratio of the desired *E*-isomer to the unwanted *Z*-isomer (1:1 → 5:1). The utilisation of a HWE reaction in place of a Wittig reaction could eliminate this drawback, potentially providing the diene **74** in a good ratio of (*E*:*Z*) isomers (Scheme 3.25).

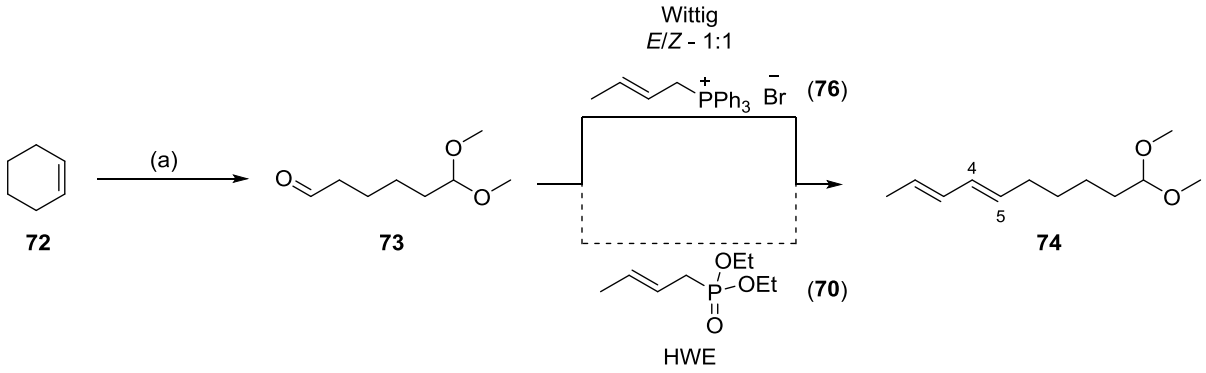

Scheme 3.25. Synthesis of 73. Schreiber ozonolysis of cyclohexene (72) provides 73. *Reagents and conditions*: (**a**) (i) O_3, DCM, MeOH, -78 °C, (ii) PTSA, $NaHCO_3$, DMS, r.t., 82%. Chain elongation of **73** to provide diene **74** has been reported previously *via* a Wittig reaction with **76.**[218] We proposed an alternative route *via* a HWE reaction with **70**.

An initial HWE test reaction using LiHMDS in THF did not yield any of the desired product **74**. Further literature scrutiny revealed that although phosphonate **70** has been reported as a reactant/reagent in 53 reactions in Scifinder, its utilisation in a HWE olefination has not been reported. The most

common reactions of phosphonate **70** involve addition across the double bond or substitution of the α-position, indicating that the development of a HWE using phosphonate **70** could be difficult.

An investigation of common HWE reaction conditions was conducted to identify if this transformation was viable (Table 3.4). This study revealed that none of the desired product **74** was formed when common lithium bases such as LiHMDS or *n*BuLi were used (entries 1 & 2), with several side reactions occurring. KHMDS was selected as an alternative base to investigate if the resulting more reactive phosphonate-stabilised carbanion would promote the desired HWE olefination. These conditions did promote the desired transformation, resulting in the isolation of **74** in good yield and moderate (*E*:*Z*) selectivity (entry 3). The higher reactivity of the phosphonate-carbanion is due to the comparably lower coordination ability of potassium cations compared to lithium cations.[219] However, a drawback to the lower coordination ability of potassium is a reduction in the *E*:*Z* selectivity of the HWE reaction. To partially overcome this issue, the solvent was changed from THF to DME which has been reported to improve the *E*-selectivity.[219] This modification resulted in an improved *E*-selectivity with an *E*:*Z* ratio of 8:1 compared to 4:1 in the presence of THF, although with a small drop in yield (entry 4). The reaction was repeated with LiHMDS in DME which confirmed that the potassium base was essential as none of the desired product **74** was isolated (entry 5).

Table 3.4. Optimisation of HWE reaction conditions for the formation of 74.

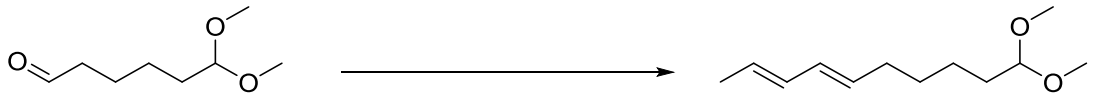

73 **74**

Entry	Base	Solvent	**74** (isolated yield, %)	***E*:*Z***
1	LiHMDS	THF	-	-
2	*n*BuLi	THF	-	-
3	KHMDS	THF	73	~4:1
4	KHMDS	DME	69	~8:1
5	LiHMDS	DME	-	-

Acid-deprotection of the acetal group of diene **74** yielded dienal **75**, which after a further HWE olefination with **57** furnished the desired β-ketothioester polyene chain **66**. Separation of the undesired *Z*-isomer was achieved by chromatographic purification to provide isomerically pure polyene **66**.

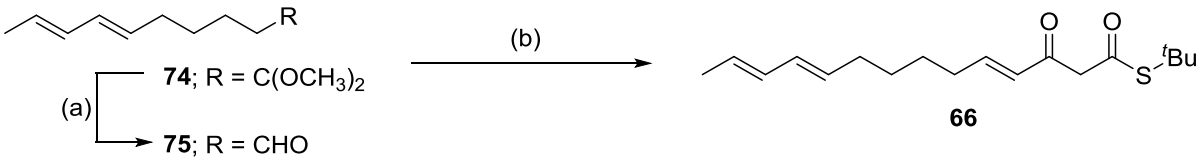

Scheme 3.26. Synthesis of 66. *Reagents and conditions*: (**a**) Aq. HCl, THF, r.t., 12 h, 94%. (**b**) LiHMDS, **57**, THF, -78 °C → 0 °C, 3 h, 72%.

A BF_3-mediated Diels-Alder cyclisation of **66** was investigated as a possible route to access a racemic mixture of the *endo*-diastereomer of the decalin ring **(±)-68**, which could in turn be elaborated to provide a mixture of JBIR-22 diastereomers **4a** and **4b** (Scheme 3.23, Route B). This would facilitate the preliminary structural validation of JBIR-22 (**4**) and in addition, provide a useful standard for the development of the asymmetric synthesis. Highly diastereoselective IMDA cyclisations have been reported previously in the synthesis of decalin ring containing natural products (e.g., equisetin (**10**), see Section 3.1.6). Reaction of polyene **66** with $BF_3.Et_2O$ smoothly effected the desired IMDA cyclisation in very good yield and excellent selectivity for the racemic *endo* diastereomer **(±)-68** (>20:1 *endo*:*exo*). The formation of the expected *endo* diastereomer was confirmed by NOE analysis (see Appendix E).

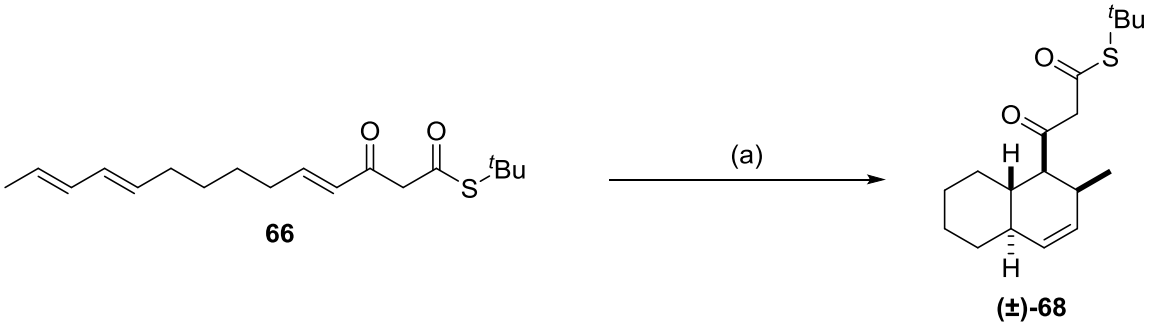

Scheme 3.27. IMDA cycloaddition of 66. *Reagents and conditions*: (**a**) $BF_3.Et_2O$, DCM, -78 °C → 0 °C, 73%. Relative stereochemistry of **(±)-68** is shown.

Conversion of decalin **(±)-68** to **4a**/**b** proceeded smoothly *via* a silver-mediated *N*-acylation of **53**, followed by an intramolecular Lacey-Dieckmann cyclisation to provide a mixture of JBIR-22 ethyl ester diastereomers **77a**/**b**. Subsequent ester hydrolysis provided an inseparable mixture of JBIR-22 diastereomers **4a** and **4b** (Scheme 3.28). Surprisingly, no epimerisation of the C5' position was detected during the final hydrolysis step.

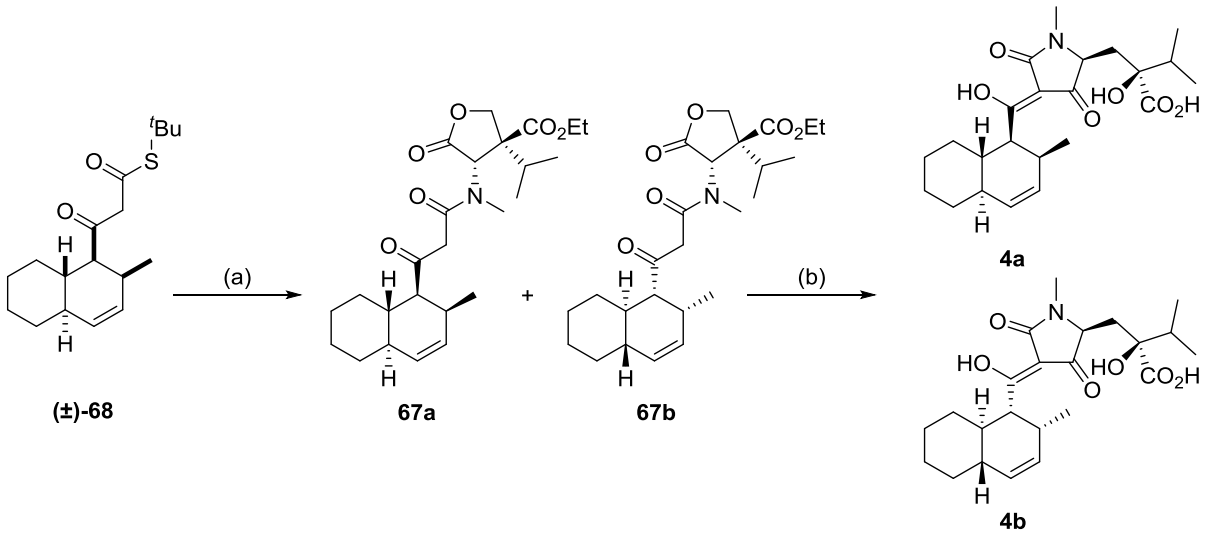

Scheme 3.28. End game strategy: synthesis of a diastereomeric mixture JBIR-22 diastereomers 4a and 4b. *Reagents and conditions*: (**a**) **53**, $AgCF_3CO_2$, Et_3N, THF, 0 °C → r.t., 2 h, 64% over 2 steps. (**b**) (i) ^{t}BuOK, THF, 0 °C → r.t., 2 h. (ii) Aq. NaOH, EtOH, 110 °C (MW), 20 mins, 87% over 2 steps. Relative stereochemistry of **(±)-68** is shown.

Comparison of the ^{1}H and ^{13}C NMR spectra of **4a**/**b** with that reported for isolated JBIR-22 (**4**) showed significant discrepancies. Further investigation revealed that the final eluting step in the HPLC purification of the isolated JBIR-22 (**4**) was carried out in the presence of diethylamine.[123] Due to the highly acidic nature of the JBIR-22 (**4**) carboxylic acid, the reported NMR is most likely to be that of the diethylamine salt of JBIR-22 (**4**) and not of the free acid. The NMR of the synthesised mixture **4a**/**b** was repeated in the presence of diethylamine. The resulting NMR spectra were in high agreement with the reported NMR of JBIR-22 (**4**), however, with the added complication of the presence of more complex splitting patterns in the ^{1}H NMR spectra and the appearance of doubling of the ^{13}C NMR signals as a result of the mixture of diastereomers **4a** and **4b** (Figure 3.13).

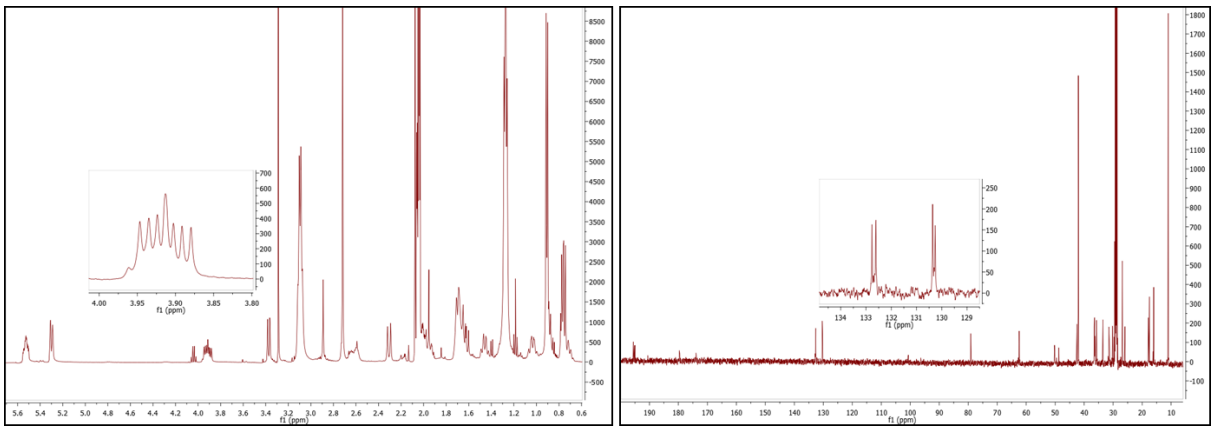

Figure 3.13. ^{1}H and ^{13}C NMR spectra of the diethylamine salt of JBIR-22 mixture 4a/b [Acetone-d_6, 500 MHz]. Representative examples of the increased splitting pattern complexity (^{1}H NMR) and doubling of signals (^{13}C NMR) observed as a result of the diastereomeric mixture are magnified. See Appendix F for full spectra.

3.5.3 Development of an enantioselective IMDA route to JBIR-22 (4)

As **4a** and **4b** could not be separated from this mixture, access to pure samples of the predicted stereoisomers of JBIR-22 (**4a**-**d**) would require an asymmetric synthesis of **68**. The critical step in the synthetic strategy involved an enantioselective IMDA cyclisation of trienal **69** to provide either enantiomer of aldehyde **78**, [(2*S*,3*S*, 6*R*, 7*S*)-**78a** or (2*R*,3*R*, 6*S*, 7*R*)-**78b**] which could be elaborated to furnish a single enantiomer of the desired intermediate **68** (Scheme 3.23, Route B). The trienal **69** could be accessed *via* chain elongation of our previously synthesised dienal **75** (Scheme 3.29).

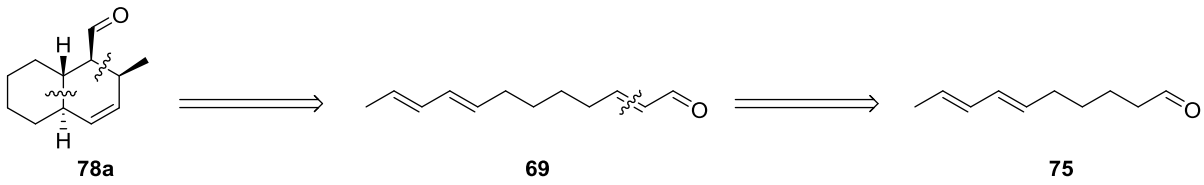

Scheme 3.29. Retrosynthetic analysis of 78a. 78a could be accessed by an enantioselective IMDA cycloaddition of 69 which would arise from a chain elongation of dienal 75.

Extensive research has been carried out into the development of enantioselective IMDA routes to **78** due to its occurrence in natural products with potent biological activities such as the antiproliferative agent (+)-UCS1025A (**79**)[220] and the phytotoxic polyketide solanapyrone D (**80**).[221] Studies towards these and related natural products have centred around the use of either an organocatalytic IMDA developed by MacMillan[222] or a chiral auxiliary mediated IMDA pioneered by Evans.[223]

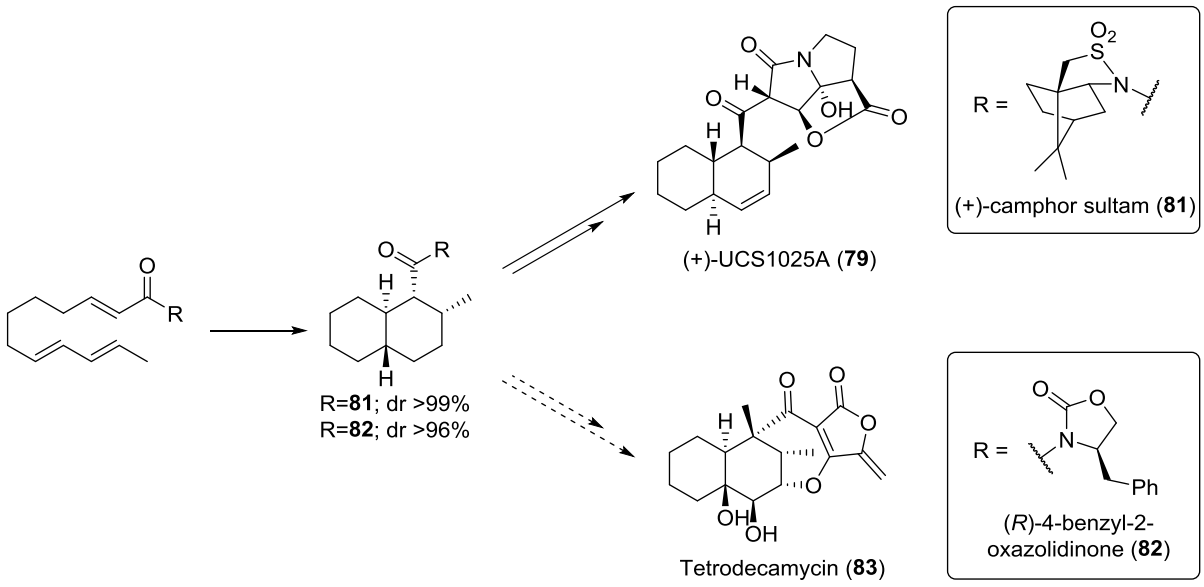

Scheme 3.30. Examples of the utilisation of the chiral auxiliary approach in the synthesis of (+)-UCS1025A (79)[218] and tetrodecamycin (83).[224]

Examples using the chiral auxiliary methodology include the use of (+)-camphor sultam (**81**) in the synthesis of (+)-UCS1025A (**79**)[218] and (*R*)-4-benzyl-2-oxazolidinone (**82**) in the synthesis of the

decalin ring of tetrodecamycin (**83**) (Scheme 3.30).[224] MacMillan and co-workers are pioneers in the field of organocatalytic IMDA reactions with the development of a range of chiral imidazolidinone organocatalysts which displayed excellent enantio- and diastereocontrol with good yields and substrate scope.[225] This methodology has been used in the total synthesis of (+)-UCS1025A (**79**),[220] solanapyrone D (**80**)[221] and related natural products such as amaminol A (**84**)[226] and B[227] (Scheme 3.31).

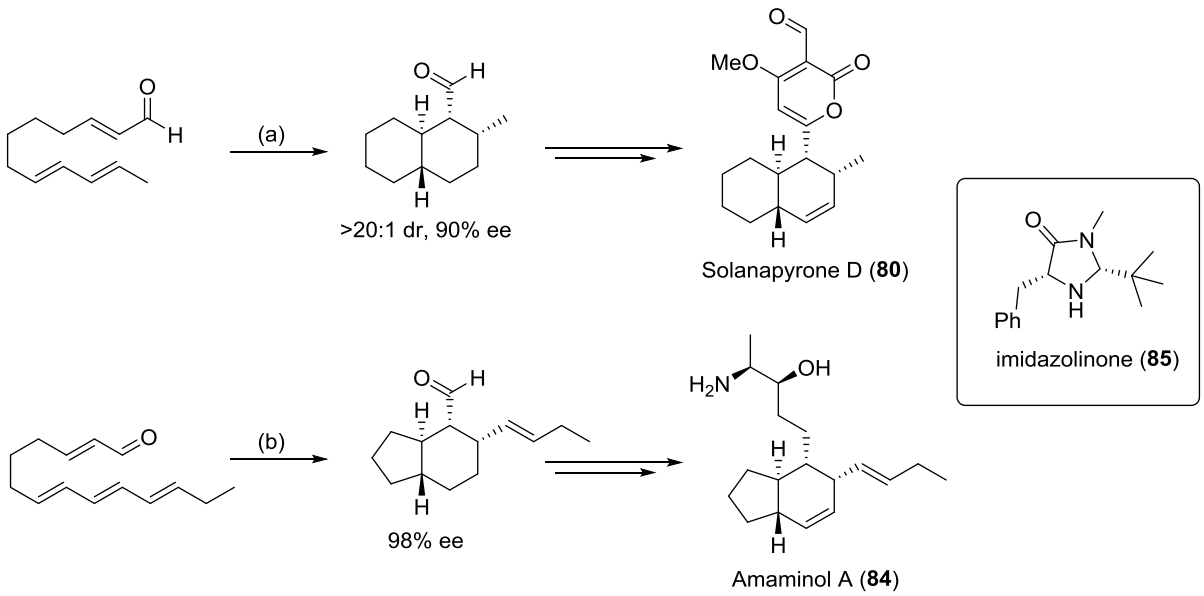

Scheme 3.31. Utilisation of imidazoline organocatalyst (*R*,*R*)-85 in the total synthesis of solananpyrone D (80)[221] and amaminol A (84).[226] *Reagents and conditions*: (**a**) 20 mol% **85**.TfOH, CH_3CN (2% H_2O), 5 °C, 48 hours, 71%. (b) 20 mol% **85**.TFA, CH_3CN (2% H_2O), -20 °C.

Based on literature precedent, an organocatalytic IMDA methodology was selected for the conversion of **69** to **78** (Scheme 3.29), due to the high levels of diastereo- (>20:1) and enantiocontrol (90% ee) reported for this transformation without the extra synthetic steps required to introduce and remove a chiral auxiliary.[221]

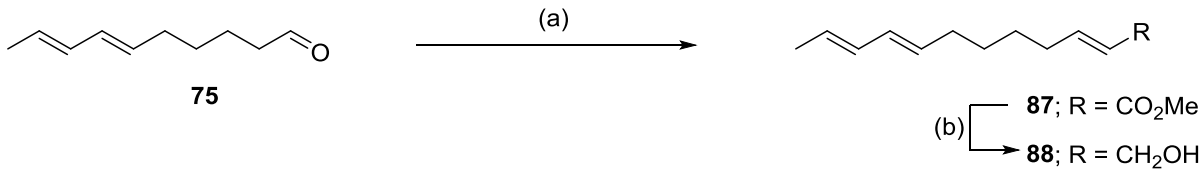

Scheme 3.32. Chain elongation of 75 to 87. *Reagents and conditions*: (**a**) Di*iso*propyl(ethoxycarbonylmethyl) phosphonate (**86**), LiHMDS, THF, -78 C → r.t., 4 h, 88%. (**b**) DIBAL-H, DCM, -78 °C, 30 mins, 97%.

Trienal **69** was prepared using a route adapted from MacMillan's approach in the synthesis of solanapyrone D (**80**).[221] This involved an olefination of dienal **75** to furnish **87** which was subsequently reduced by DIBAL-H to provide alcohol **88** in excellent yield (Scheme 3.32). The final step in MacMillan's route involved a catalytic tetrapropylammonium perruthenate (TPAP) oxidation

of alcohol **88** to the corresponding aldehyde **69** in a 59% yield. In an attempt to improve on this yield, a screen of oxidation conditions was carried out (Table 3.5). Conditions that removed the need for purification facilitating the direct use of the trienal **69** in the next step were considered highly valuable due to the instability of **69**.

Table 3.5. Optimisation of the oxidation of 88 to 78.

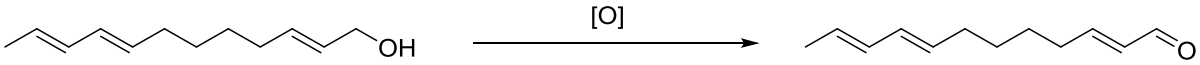

88 **69**

Entry	Oxidant	Solvent	Time	**69** (isolated yield, %)
1	cat. TPAP/NMO	DCM	50 mins	59[221]
2	DDQ	DCM	12 h	-
3	PCC	DCM	12 h	63
4	PCC	DCM	3 h	78
5	Dess-Martin	DCM	30 mins	100

Dess-Martin periodinane was identified from the screen as the optimal oxidant for this transformation providing quantitative conversion to **69** in 30 minutes. In addition, a simple aqueous work-up furnished pure trienal **69** which could be directly used in the IMDA reaction without further chromatographic purification. Although this optimised route provides **69** in excellent yield (85% over 3 steps; Scheme 3.33, Route A) from **75**, it was not an ideal approach as it contained two concession steps.[228] In an "ideal synthesis",[228–232] nonstrategic redox manipulations such as the reduction of ester **87** to the alcohol **88**, followed by subsequent oxidation to the aldehyde **69** are regarded as concession steps. A strategic redox manipulation is defined as a reaction which establishes the correct functionality found in the target product.[228] As our desired polyene **69** is in the aldehyde oxidation state, an ideal synthesis would transform **75** to the desired aldehyde **69** in one-step, without any nonstrategic redox manipulations. This was achieved by reacting **75** with the commercially available Wittig reagent **89**, which after a simple acidic deprotection of the acetal provided the desired aldehyde **69** in good yield (64%) and in just one-step (Scheme 3.33, Route B).

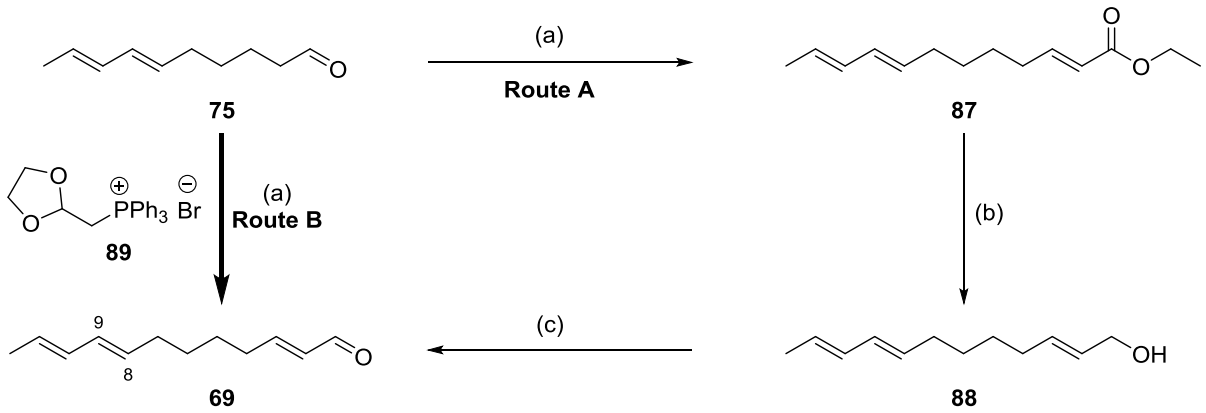

Scheme 3.33. Optimised chain elongation strategy. *Reagents and conditions*: **Route A**: (**a**) LiHMDS, THF, di*iso*propyl(ethoxycarbonylmethyl) phosphonate (**86**), -78 C → r.t., 4 h, 88%. (**b**) DIBAL-H, DCM, -78 °C, 30 mins, 97%. (**c**) Dess-Martin periodinane, DCM, H_2O, r.t., 1 h, quantitative. **Route B**: (**a**) (i) (1,3-dioxolan-2-ylmethyl)triphenylphosphonium bromide (**89**), ^{t}BuOK, THF, 0 °C, 3.5 h. (ii) 10% aq. oxalic acid, r.t., 1 h, 64%.

In contrast with our previously synthesised triene **66** (Scheme 3.26), it was not possible to remove the undesired minor *Z*-isomer of trienal **69** (C8-C9 double bond). However, this was not an issue as it has been shown that *Z*,*E*-dienes are uniformly inert to this catalytic IMDA, resulting in a kinetic purification.[221,226] Trienal **69** was subjected to the catalytic IMDA conditions (20 mol% imidazolidinone (*S*,*S*)-**85**/(*R*,*R*)-**85**.TfOH) which afforded the desired decalins **78a** and **78b** respectively, in good yields (**78a**, 65%; **78b**, 68%; based on consumed *E*,*E*,*E*-trienal) and moderate diastereoselectivity (*dr* 4:1) (Scheme 3.34). This moderate diastereoselectivity was surprising when compared to the selectivity reported by MacMillan and co-workers (*dr* >20:1). However, it was in agreement with the findings of Christmann *et al*.[233] for the same transformation. This reduction in diastereoselectivity may be due to epimerisation of the C2 position which was also observed by MacMillan for similar substrates.[221] The removal of the minor diastereomer was not possible until the final step of the synthesis. A portion of the aldehydes **78a** and **78b** were converted to the corresponding alcohols **90a** and **90b** *via* $NaBH_4$ mediated reduction for determination of their enantiomeric purity (Scheme 3.34). A racemic standard was obtained by a $BF_3.OEt_2$ catalysed cycloaddition of **69** to provide (±)-**78** as a single diastereomer, which was subsequently reduced to the corresponding alcohol (±)-**90** (Scheme 3.34A). Enantiomeric excesses were obtained by chiral GC analysis using an Agilent Cyclosil-B (isotherm, 140 °C, Scheme 3.34B). The determined enantiomeric purity of **78a** (87% ee) and **78b** (84% ee) are in agreement with the reported values for this reaction (~80-90% ee).[221,233,234] The enantiomeric purity could be improved if required by recrystallisation at the alcohol oxidation state.[235]

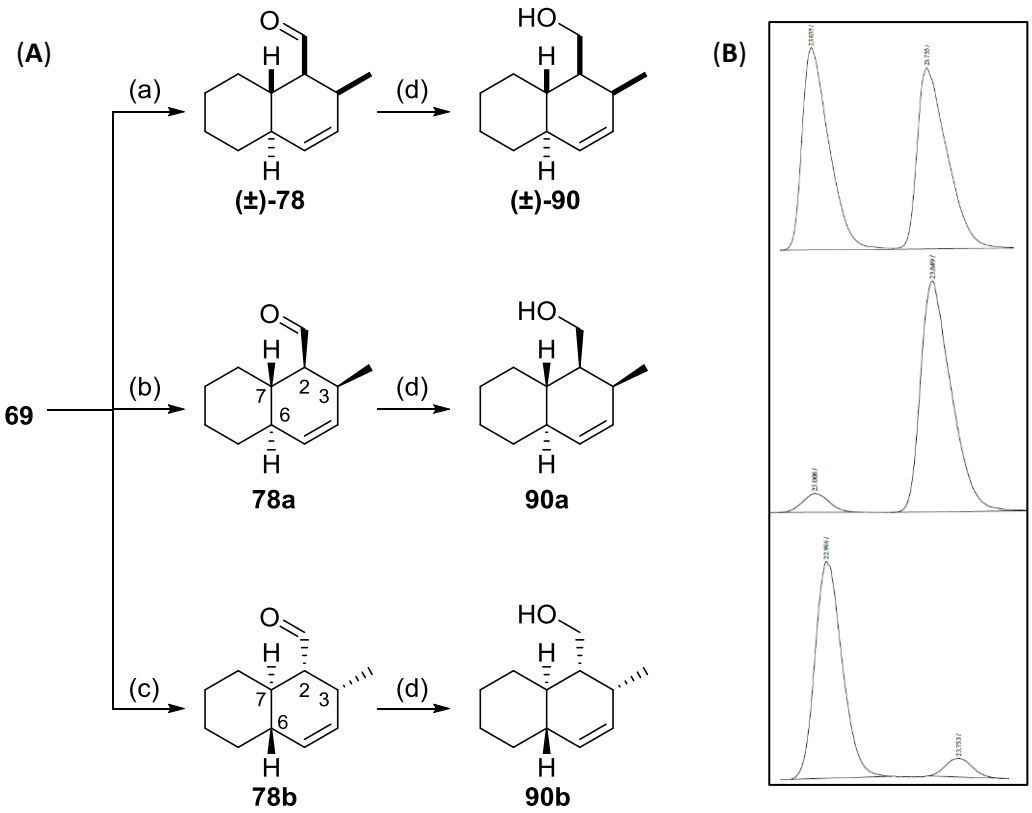

Scheme 3.34. (A) Synthesis of racemic decalin (±)-78 and enantiomerically enriched decalins (2*S*,3*S*, 6*R*, 7*S*)-78a and (2*R*,3*R*, 6*S*, 7*R*)-78b. *Reagents and conditions*: (**a**) $BF_3.Et_2O$, DCM, -78 °C → 0 °C, 3 h, 74%. (**b**) 20 mol% imidazolidinone (*S*,*S*)-**85**.TfOH, MeCN (2% H_2O), -5 °C, 48 h, 65%, *dr* 4:1, 87% ee. (**c**) 20 mol% imidazolidinone (*R*,*R*)-**85**.TfOH, MeCN (2% H_2O), -5 °C, 48 h, 68%, *dr* 4:1, 84% ee. (**d**) $NaBH_4$, EtOH, 0 °C, 1 h, **(±)-90** - 86%; **90a** – 88%; **90b** – 91%. **(B) Determination of the enantiomeric purity of decalins 90a (*middle*) and 90b (*bottom*) *via* chiral GC analysis.** Only section corresponding to the major diastereomer of **90a** and **90b** is shown, see Appendix G for full chromatograms.

The expected relative and absolute configuration of **78a** and **78b** were confirmed by analysis of the X-ray crystallographic structures of the corresponding carboxylic acid derivatives **91a** and **91b** (Scheme 3.35). The crystalline acids **91a** and **91b** were obtained by rapid air oxidation (at 4 °C) of aldehydes **78a** and **78b** respectively.

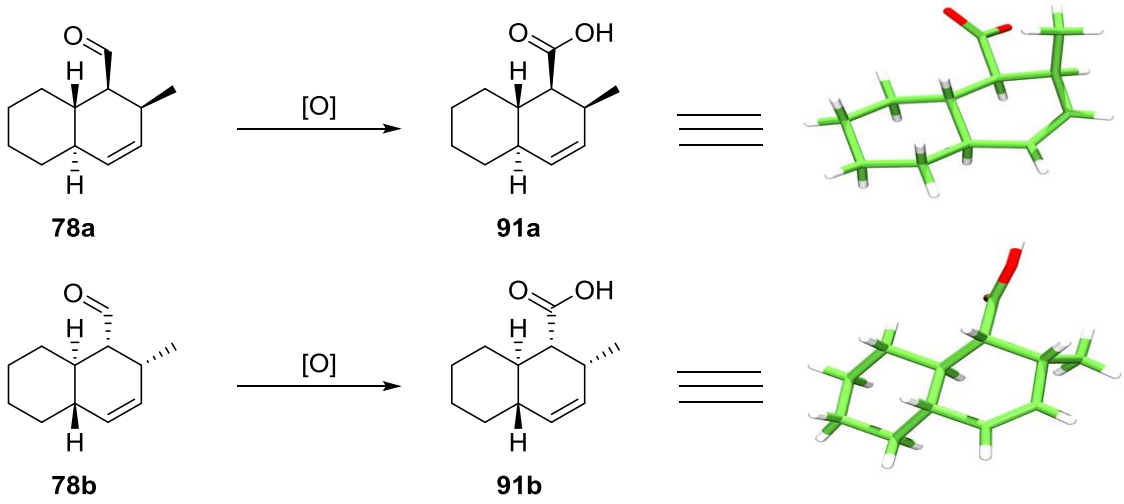

Scheme 3.35. Confirmation of the expected absolute configuration of 78a and 78b by analysis of the small molecule X-ray crystal structures of the corresponding carboxylic acids 91a and 91b. X-ray crystallographic data provided by Dr David Cordes.

3.5.4 Synthesis of pure samples of JBIR-22 diastereomers 4a and 4b

Conversion of enantiomerically enriched **78a** and **78b** to the corresponding β-ketothioesters **68a** and **68b** was required for completion of the two diastereomers of JBIR-22, **4a** and **4b**. This was achieved *via* a LDA-promoted aldol condensation of *S*-*tert*-butyl thioacetate (**92**) and the aldehydes **78a** and **78b** to furnish the β-hydroxythioesters **93a** and **93b** respectively (Scheme 3.36). Dess-Martin periodinane oxidation of **93a** and **93b** proceeded smoothly to provide the desired β-ketothioesters **68a** and **68b** respectively (Scheme 3.36).

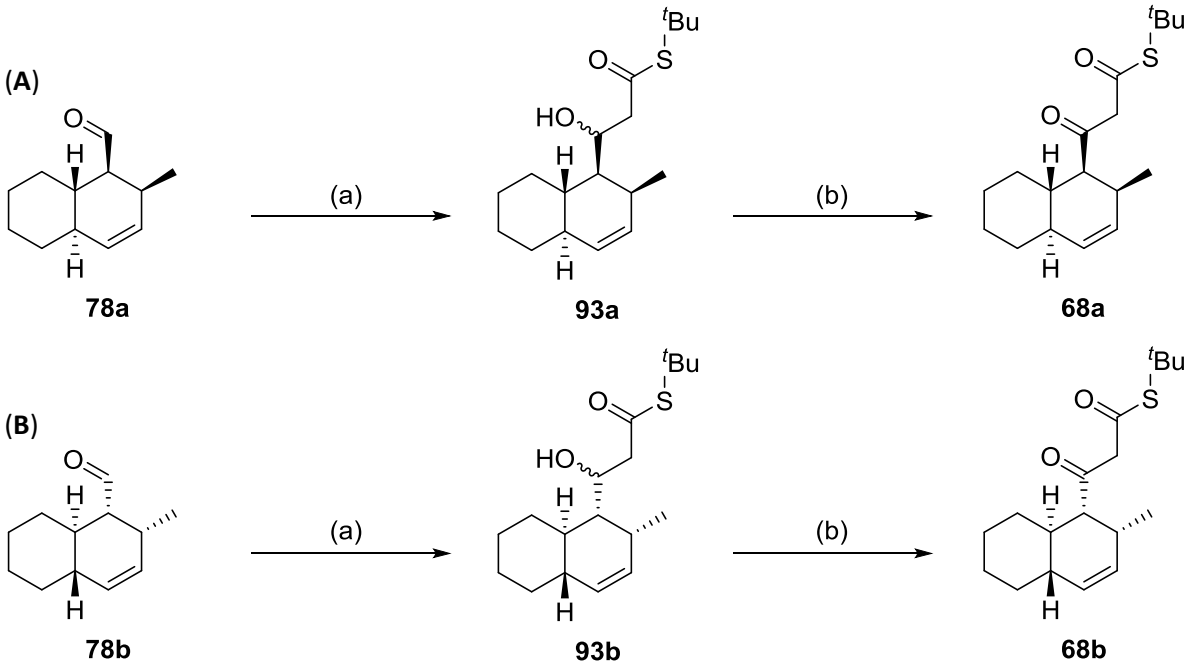

Scheme 3.36. Synthesis of β-ketothioesters (A) 68a and (B) 68b. *Reagents and conditions*: (**a**) (i) *i*-Pr_2NH, *n*-BuLi (2.3M in hexanes), THF, 0 °C, 30 mins. (ii) *S*-*tert*-butyl-thioacetate (**92**), THF, -78 °C, 2.5 h, **93a** – 66%; **93b** – 69%. (**b**) Dess-Martin periodinane, DCM, r.t., 2 h, **68a** – 79%; **68b** – 82%.

The NMR spectroscopic data obtained for **68a** and **68b** were in agreement with the data previously obtained for (±)-**68**, the relative stereochemistry of which had been assigned by NOE experiments (see Appendix E). Conversion of the β-ketothioesters **68a** and **68b** to the corresponding JBIR-22 diastereomers **4a** and **4b** was accomplished *via* a silver-mediated *N*-acylation of **53**, followed by an intramolecular Lacey-Dieckmann cyclisation and ester hydrolysis, as described previously in the synthesis of the diastereomeric mixture **4a**/**b** (Scheme 3.37). **4a** and **4b** were purified by reverse phase column chromatography and a portion of each was converted to the corresponding diethylamine salt for spectroscopic comparison with the reported JBIR-22 (**4**) data and the previously synthesised mixture of **4a**/**b**.

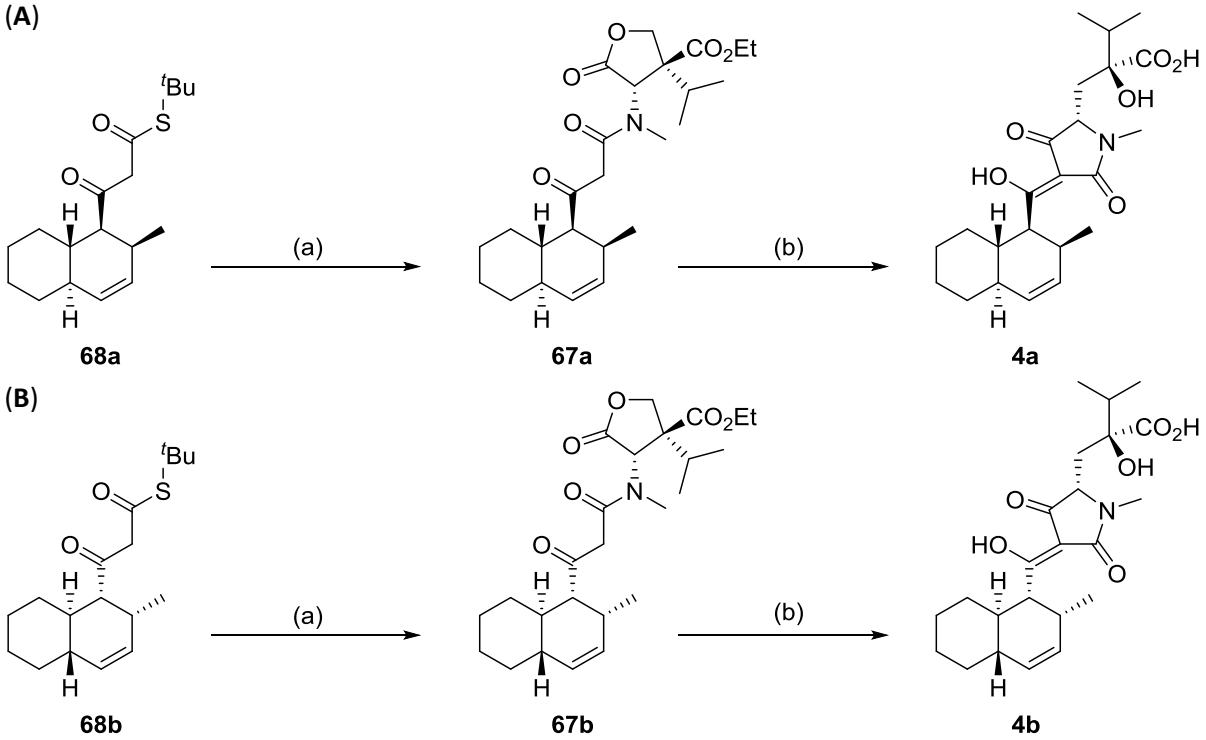

Scheme 3.37. Synthesis of JBIR-22 diastereomers (A) 4a and (B) 4b. *Reagents and conditions*: (**a**) **53**, $AgCF_3CO_2$, Et_3N, THF, 0 °C → r.t., 2 h, **67a** – 76%; **67b** – 71% over 2 steps. (**b**) (i) ^{t}BuOK, THF, 0 °C → r.t., 2 h. (ii) Aq. NaOH, EtOH, 110 °C (MW), 20 mins, **4a** – 71%; **4b** – 74% over 2 steps.

3.5.5 Synthesis-guided configurational determination

With pure samples of the two proposed diastereomers of JBIR-22 (**4**) in hand, a comparison with the authentic mixture of the two diastereomers **4a**/**b** prepared previously was carried out. Both diastereomers have very similar ^{1}H and ^{13}C NMR spectra. However, comparison of the ^{1}H NMR and ^{13}C NMR spectra of the two diastereomers with the **4a**/**b** spectra, confirmed that pure samples of the single diastereomers had been successfully prepared and highlighted three protons (H2, H3,

H12), which had a noticeable chemical shift difference between **4a** and **4b** (Figure 3.14, see Appendix H for full spectra).

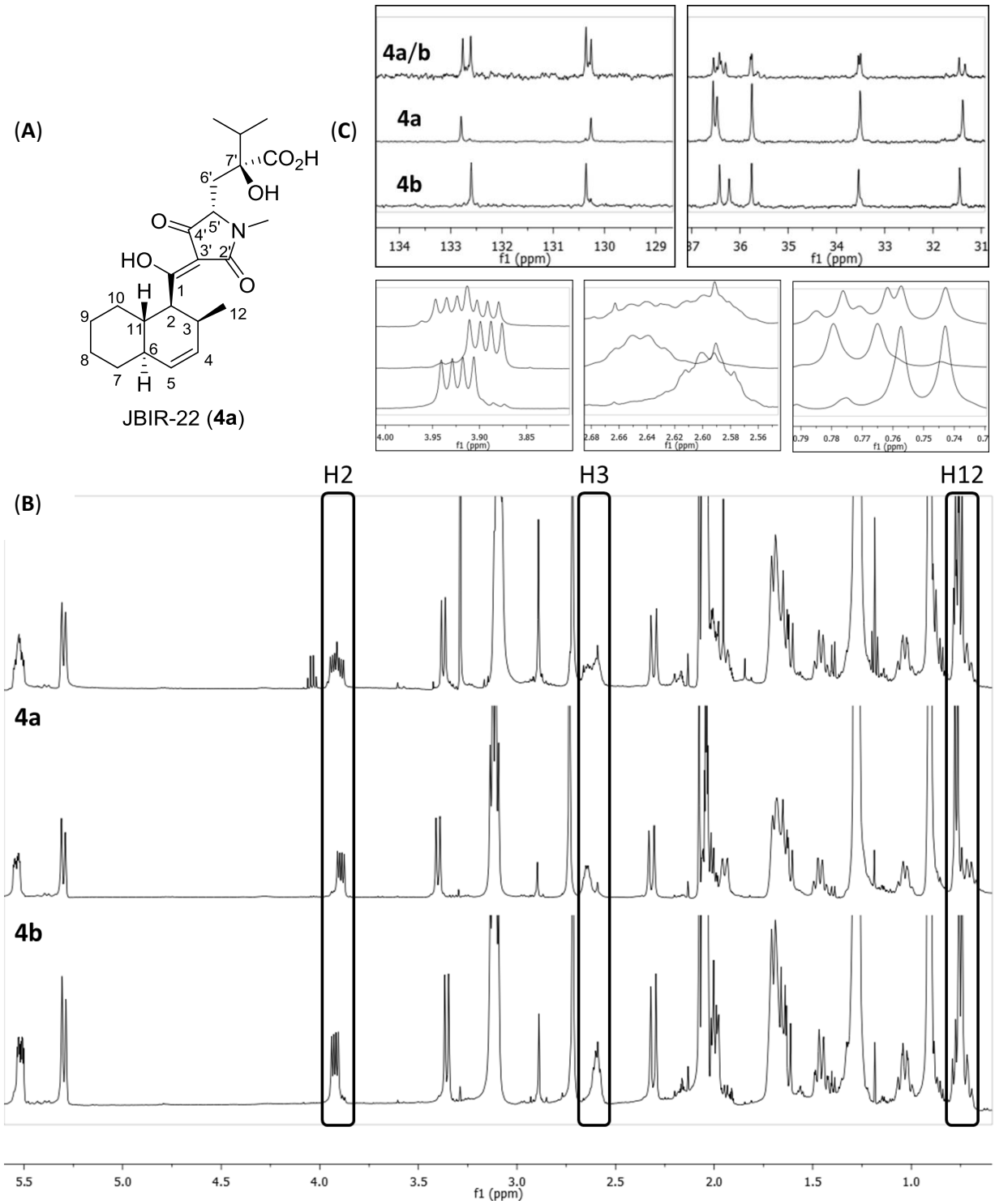

Figure 3.14. ^{1}H NMR analysis of synthesised JBIR-22 diastereomers 4a and 4b. (**A**) Structure and numbering of **4a**. (**B**) Stacked spectra of the diastereomeric mixture **4a**/**b** and the single diastereomers **4a** and **4b**. Characteristic proton signals H2, H3 and H12 are highlighted. (**C**) Magnification of the H2, H3 and H12 regions of the ^{1}H NMR spectra of **4a**/**b**, **4a** and **4b** and magnification of sections of the ^{13}C NMR spectra of **4a**/**b**, **4a** and **4b**. See Appendix H for the full ^{1}H spectra of **4a** and **4b**.

Comparison of the chemical shift of protons (H2, H3, H12) with that reported for the isolated sample of JBIR-22 (**4**) revealed that the relative configuration of diastereomer **4a** (Figure 3.14A) was the most likely structure of **4** (Table 3.6A). A detailed comparison of the ^{13}C NMR of both diastereomers **4a** and **4b** with that reported for the isolated JBIR-22 **4** was undertaken to further validate the stereochemical assignment. This comparative study revealed that ^{13}C chemical shifts of **4a** were in very high agreement with that reported for **4**, while **4b** had some significant permutations (Δ ppm > 0.1) (Table 3.6B).

Table 3.6. (A) Comparison of the reported ^{1}H NMR signals of H2, H3 and H12 of isolated JBIR-22 (4) and synthesised JBIR-22 diastereomers 4a and 4b. (B) Comparison of the reported ^{13}C NMR signals of isolated JBIR-22 (4) and synthesised JBIR-22 diastereomers 4a and 4b. JBIR-22 (**4**) – ^{13}C (150 MHz) in Acetone-d_6. **4a** and **4b** – ^{13}C (126 MHz) in Acetone-d_6. See Appendix H for the full ^{13}C spectra of **4a** and **4b**.

(**A**)

	JBIR-22 (4) [ppm]	**JBIR-22 (4a)** [ppm]	**JBIR-22 (4b)** [ppm]
H2	3.90	3.90	3.92
H3	2.64	2.64	2.60
H12	0.76	0.77	0.75

(**B**)

Compound number	**JBIR-22 (4)**[123]	**4a**		**4b**	
	δc (ppm)	δc (ppm)	Δ (ppm)	δc (ppm)	Δ (ppm)
1	196.4	196.3	-0.1	196.4	0
2	51.0	51.0	0	51.0	0
3	32.2	32.2	0	32.3	0.1
4	133.6	133.6	0	133.4	-0.2
5	131.1	131.1	0	131.2	0.1
6	43.4	43.4	0	43.3	-0.1
7	34.3	34.4	0.1	34.4	0.1
8	27.6	27.6	0	27.7	0.1
9	27.7	27.7	0	27.7	0
10	31.0	31.1	0.1	31.0	0
11	37.4	37.4	0	37.3	-0.1
12	18.3	18.4	0.1	18.3	0
2'	174.6	174.7	0.1	174.8	0.2
3'	101.9	101.9	0	101.5	-0.4
4'	196.1	196.1	0	195.7	-0.4
5'	63.3	63.3	0	63.2	-0.1
6'	37.3	37.3	0	37.1	-0.2
7'	80	80.0	0	79.9	-0.1
8'	36.6	36.6	0	36.6	0
9'	18.7	18.8	0.1	18.6	-0.1
10'	26.8	26.9	0.1	26.8	0
11'	180.9	180.9	0	180.1	-0.8
12'	16.8	16.9	0.1	16.8	0

With the relative stereochemical configuration of JBIR-22 (**4**) being assigned as that of diastereomer **4a**, the final investigation involved identifying which enantiomeric series the natural product

belonged in, *i.e*. diastereomer **4a** or its enantiomer **4d**. However comparison of the optical rotation (α_D) of **4a** [$[\alpha]_D^{20}$ **=** +71.4° (*c* 0.7, MeOH)] and that reported for **4** [$[\alpha]_D^{25}$ **=** -330.0° (*c* 0.7, MeOH)] revealed a very high discrepancy, which would not be corrected by the enantiomer **4d** which should have an optical rotation of approximately [$[\alpha]_D^{20}$ **=** -71.4° (*c* 0.7, MeOH)]. Similarly it is significantly different from diastereomer **4b** which has an optical rotation of [$[\alpha]_D^{20}$ **=** -20.5° (*c* 0.7, MeOH)]. This discrepancy could be due to many factors, including the significant differences in optical rotation resulting from small changes in concentration, particularly when working with small quantities of material isolated from natural sources. Furthermore, as previously mentioned (Figure 3.5, Section 3.1.3), the published ^{13}C NMR spectrum of JBIR-22 (**4**) contains a doubling of many signals, likely indicating the presence of a stereoisomer which could have a significant effect on the optical rotation of the sample.

In an attempt to clarify this issue and provide an absolute stereochemical assignment for the isolated JBIR-22 (**4**), an authentic sample (~0.9 mg) was obtained from Dr Kazuo Shin-ya.[122,123] Unfortunately, the original sample had degraded significantly (see Appendix I) and work is on-going to develop a suitable HPLC purification method to isolate a pure sample. This authentic sample would facilitate NMR doping experiments to validate **4a** as having the correct relative configuration and comparison of the CD spectra or chiral HPLC chromatogram of the samples should provide a method for assigning the absolute configuration of JBIR-22 (**4**).

In summary, the first total synthesis of JBIR-22 diastereomers **4a** and **4b** has been completed. This was achieved *via* a stereoselective and convergent approach, involving a longest linear sequence (LLS) of 10 steps and an overall yield of 6%. This synthetic approach incorporates biomimetic and tandem one-pot processes and has limited nonstrategic redox reactions and protecting group manipulations. Utilisation of this versatile approach to access **4a** and **4b** facilitated the validation of the predicted structure of isolated JBIR-22 (**4**) and identification that **4a** contains the correct relative configuration. Assignment of the absolute configuration requires further comparative studies with an authentic isolated sample of JBIR-22 (**4**).

Our initial synthetic strategy provided a short and stereoselective route to the desired JBIR-22 diastereomers **4a** and **4b**. However, we believed an alternative synthetic strategy (Scheme 3.23, Route A) involving a late stage stereocontrolled IMDA cycloaddition could further optimise this sequence, making it more step-efficient and providing access to a diverse set of potential analogues.

Furthermore, exploring this route would allow additional speculation on the possible role of a "Diels-Alderase" in the biosynthesis of JBIR-22 (**4**).

3.5.6 Synthesis of the IMDA precursor

The required IMDA precursor **65** was accessed by cyclisation of β-ketoamide **94**, which in turn was generated *via* *N*-acylation of (*S,S*)-**53** with the previously synthesised β-ketothioester polyene chain **66** (Scheme 3.38).

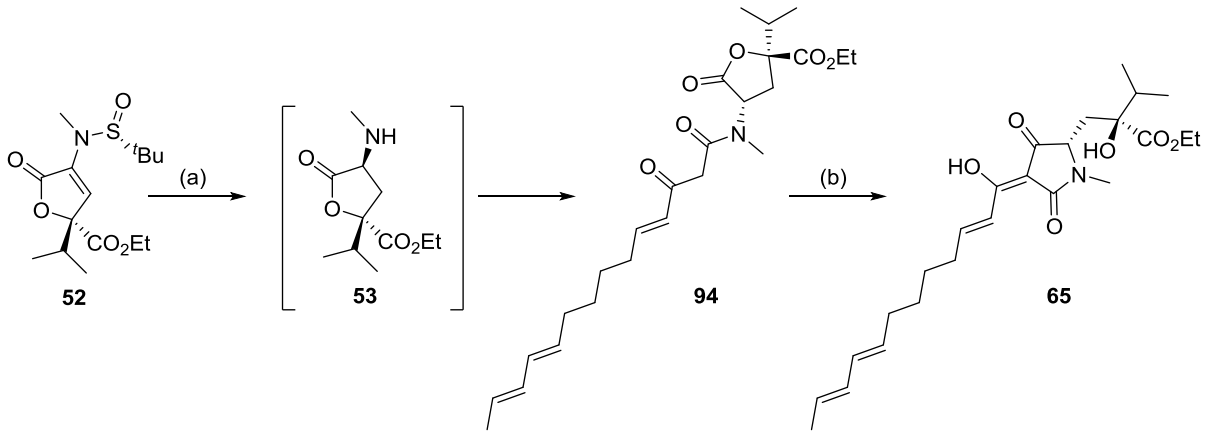

Scheme 3.38. Synthesis of IMDA precursor 65 *via* a tandem deprotection-reduction-*N*-acylation process followed by cyclisation. *Reagents and conditions*: (**a**) (i) HCl (4N in dioxane), THF, 0 °C, 10 minutes. (ii) $NaBH_3CN$, MeOH, 1.5 hours, 0 °C. (**b**) **66**, CF_3CO_2Ag, Et_3N, THF, 0 °C → r.t., 2 h, 67% over 2 steps. (**b**) ^{t}BuOK, THF, 0 °C → r.t., 2 h, 94%.

The final optimisation of the synthetic route explored the possibility of circumventing the silver-mediated *N*-acylation reaction. Drawbacks to this method include the often difficult purification of the strongly chelating tetramic acids, the disposal of the toxic silver salt by-products and the challenges associated with handling the highly pungent *tert*-butylthiol (odour threshold of <0.33 ppb[236]). An alternative retrosynthetic strategy was devised which involved a HWE olefination of phosphonate **95** and aldehyde **75** (Scheme 3.39), an approach which has been used successfully in the synthesis of the tirandamycins.[237–239] Phosphonate **95** would arise from a base-mediated cyclisation of β-ketoamide **96**. As the cyclisation of **96** to **95** and subsequent HWE olefination are both base-catalysed processes, this potentially could be carried out in a one-pot reaction. The β-ketoamide **96** could be readily formed by a thermally induced *N*-acylation reaction using the novel Meldrum's acid derivative **63** (Scheme 3.39), without the need for the silver-mediated coupling or the added steps to form the β-ketothioester **66** (Scheme 3.26).

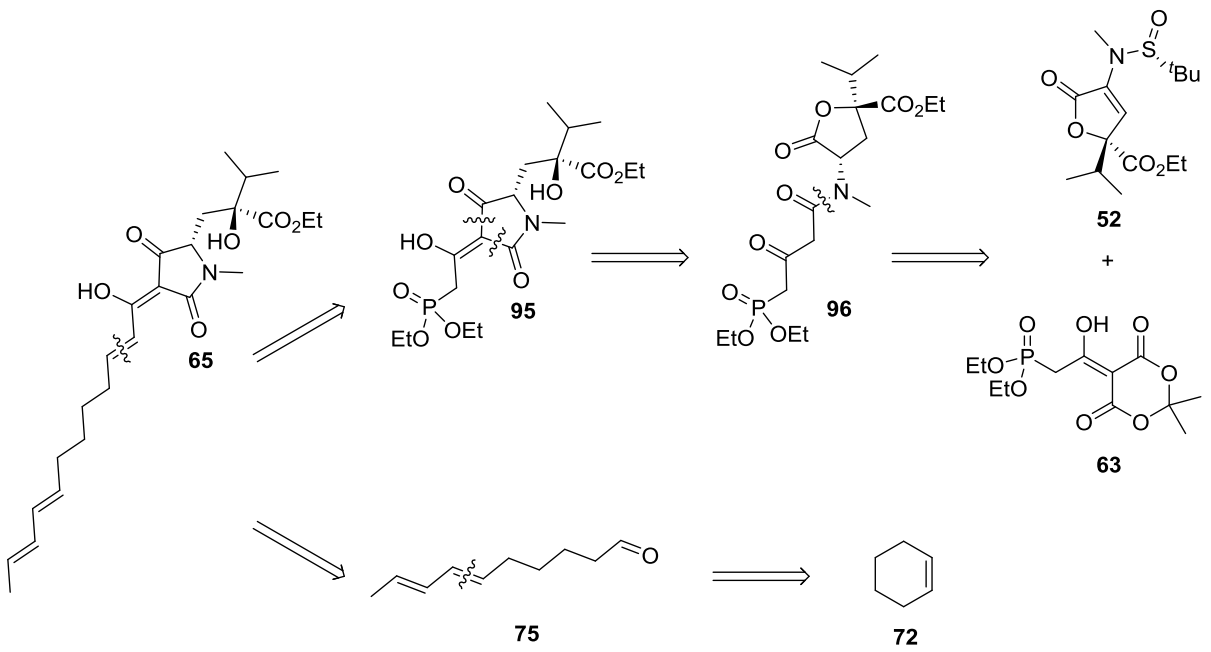

Scheme 3.39. Alternative retrosynthetic analysis of 65.

The tandem deprotection-reduction of **52** followed by *N*-acylation with **63**, quickly and cleanly provided the desired β-ketoamide **96** (Scheme 3.40). Initial test reaction conditions for the one-pot domino cyclisation-HWE reaction involved the treatment of **96** with ^{t}BuOK (3 equiv.) in THF, as had been reported for a related process in the synthesis of streptolydigin (**8**).[240] This method provided the desired product **65** in good yield (71%, Scheme 3.40).

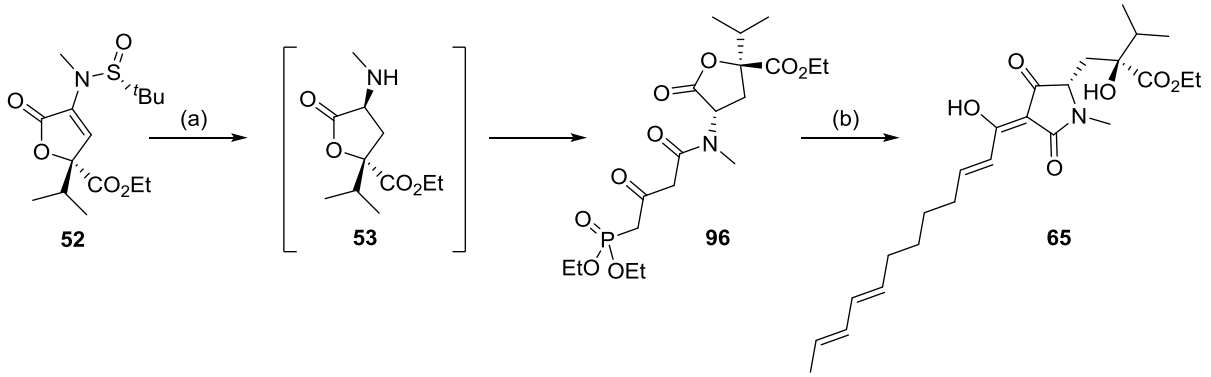

Scheme 3.40. Alternative synthesis of IMDA precursor 65 *via* a tandem deprotection-reduction-*N*-acylation followed by a one-pot cyclisation-HWE olefination. *Reagents and conditions*: (**a**) (i) HCl (4N in dioxane), THF, 0 °C, 10 minutes. (ii) $NaBH_3CN$, MeOH, 1.5 hours, 0 °C. (**b**) (i) ^{t}BuOK (3 eq.), THF, 0 °C, 40 min. (ii) **75**, THF, 0 °C → r.t., 16 h, 71%.

This one-pot process entails several consecutive steps, including initial cyclisation of the β-ketoamide **96** to form **95a**, the anion of **95** (which was verified by quenching of the reaction and isolation of **95**), before addition of aldehyde **75** (Scheme 3.41).

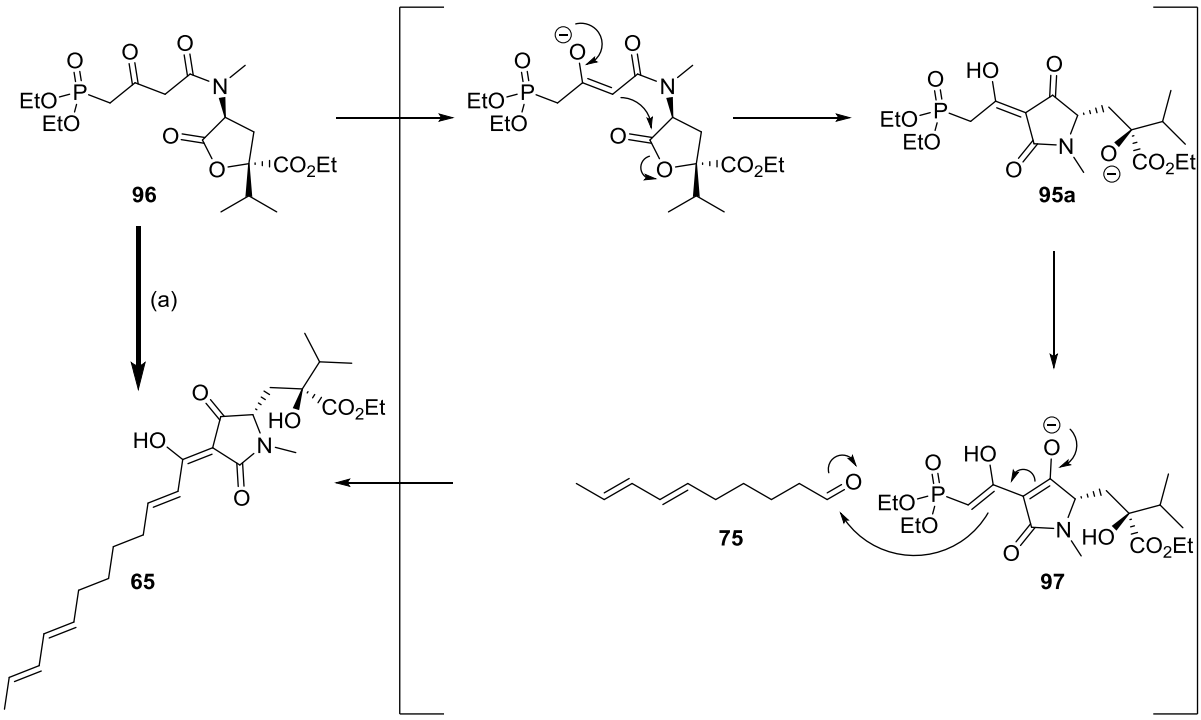

Scheme 3.41. One-pot domino cyclisation-HWE olefination. *Reagents and conditions*: (**a**) (i) ^{t}BuOK (1.1 eq.), THF, 0 °C, 40 min. (ii) **75**, THF, 0 °C → r.t., 16 h, 85%.

Excess ^{t}BuOK has been used previously in related reactions to form the required enolate to undergo the HWE reaction. However in this case, the tertiary alkoxide **95a** formed from the cyclisation step should abstract a proton from the methylene, α to the phosphonate, thus forming the extended enolate **97** required for the HWE reaction. Further optimisation of this reaction guided by these mechanistic insights revealed that, as predicted, only 1.1 equivalents of ^{t}BuOK was required to promote this one-pot process (Scheme 3.41). The desired product **65** was isolated in excellent yield (85%). This efficient and convergent route provided the IMDA precursor **65** in only 6 steps (LLS) from ethyl pyruvate (**36**). In addition, a simple hydrolysis of **65** could provide a novel harzianic acid (**19**) analogue.

3.5.7 Investigation of the biosynthetic Diels-Alder cycloaddition

The isolation of the natural product JBIR-22 (**4**) as an apparent single diastereomer[123] would suggest that the *trans*-decalin ring was formed in a stereocontrolled manner, either in a non-enzymatic substrate-directed process or by the chiral binding site of a "Diels-Alderase". As JBIR-22 (**4**) does not contain a stereogenic center on its polyketide chain, a non-enzyme directed biosynthetic pathway (Scheme 3.42, Route A) would require the incorporation of the chiral glutamic acid prior to a substrate-controlled IMDA cycloaddition.

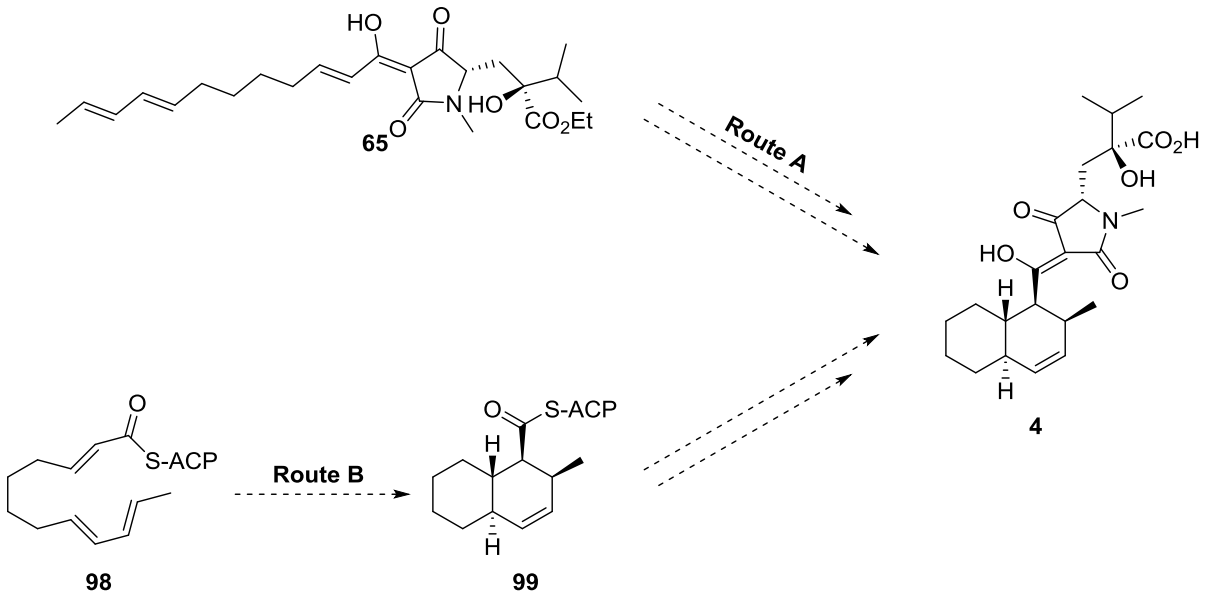

Scheme 3.42. Proposed JBIR-22 (4) biosynthetic pathways. Route A: Substrate-controlled diastereoselective IMDA of **65**. **Route B**: "Diels-Alderase" mediated asymmetric IMDA of hexaketide **98** to generate the decalin ring **99**; (ACP = Acyl Carrier Protein).

An alternative "Diels-Alderase" mediated pathway (Scheme 3.42, Route B) would involve an enzyme-influenced asymmetric IMDA of the JBIR-22 hexaketide **98** prior to incorporation of the glutamic acid in an analogous manner to that proposed for the biosynthesis of lovastatin (**16**) and equisetin (**10**) (see Section 3.1.5).

The synthesis of the IMDA precursor **65** provided a useful tool to investigate the viability of a substrate-controlled DA reaction in the biosynthesis of JBIR-22 (**4**). The experiment involved investigating, if **65** in the presence of an achiral Lewis acid ($BF_3.OEt_2$) could 1.) form the decalin ring of JBIR-22 (**4**) and 2.) if the glutamic acid side chain had a directing effect on the IMDA, promoting the formation of a single diastereomer of JBIR-22 (**4**). This DA reaction proceeded smoothly to form the *trans*-decalin ring; however analysis of the ^{1}H and ^{13}C NMR spectra of the product in comparison with those of the JBIR-22 ethyl ester mixture **77a**/**b** and the single diastereomers of JBIR-22 ethyl ester, **77a** and **77b** revealed that there was no significant asymmetric induction, resulting in a ~1:1 mixture of the two diastereomers, **77a** and **77b** (Scheme 3.43 and Appendix J for spectra). The lack of stereocontrol observed in this reaction would suggest that a substrate controlled biosynthetic pathway is unlikely. Based on this, it is likely that JBIR-22 (**4**) is biosynthesised in an analogous manner to that proposed for lovastatin (**16**) and equisetin (**10**), *i.e*. it involves an asymmetric IMDA early in the biosynthesis where the stereochemical outcome is influenced by an enzyme involved in the biosynthetic pathway.

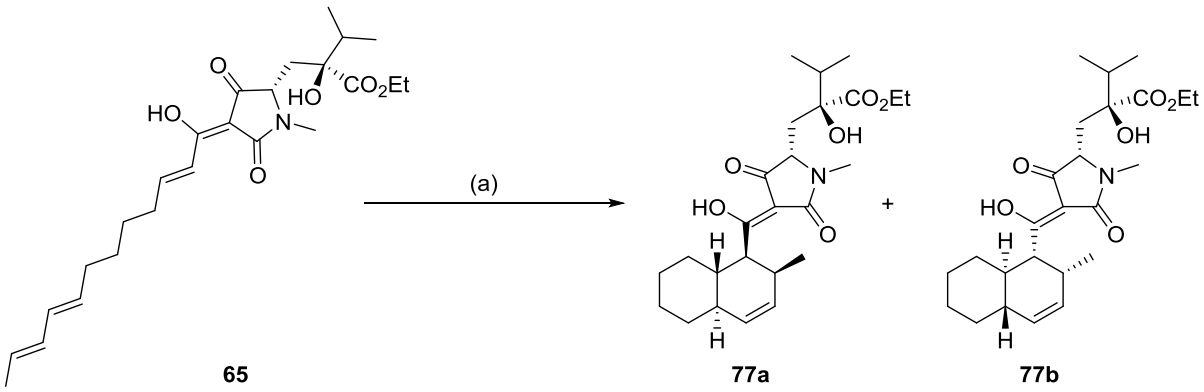

Scheme 3.43. Achiral Lewis acid catalysed IMDA cycloaddition of 65. *Reagents and condtions*: (a) $BF_3.Et_2O$, DCM, -78 °C → 0 °C, 6 h; **77a**:**77b** (~1:1).

As no stereoinduction was observed during the formation of the decalin ring in the presence of the achiral Lewis acid, $BF_3.OEt_2$, the identification of a chiral catalyst which would catalyse the formation of a single diastereomer of JBIR-22 (**4**) was required.

3.5.8 Development of a late-stage diastereoselective IMDA on 65

Extensive research has resulted in the development of numerous catalytic, asymmetric intermolecular DA reactions.[225,241,242] However, this is in stark contrast to its intramolecular counterpart of which there are relative few examples in the literature. In particular, the abundance of substrate-controlled diastereoselective IMDAs in total synthesis[243] has resulted in a dearth of IMDA reactions for which a chiral catalyst is used to control the stereochemical outcome of the cycloaddition of advanced natural product intermediates. Previous research has focused nearly exclusively on the identification of catalytic, asymmetric conditions for the selective intramolecular cycloaddition of simple trienal substrates which could be elaborated to access natural products. This approach is epitomised by the successful application of MacMillan's organocatalyst in the asymmetric synthesis of the key precursors in the total synthesis of (+)-UCS1025A (**79**),[220] solanapyrone D (**80**),[221] amaminol A (**84**)[226] and B[227] and our 1st total synthesis of JBIR-22 (**4a**). Yamamoto and coworkers reported one of the first successful applications of a chiral Lewis acid to catalyse an asymmetric IMDA reaction.[244] Treatment of trienal **100** with a single-point binding chiral acyloxyborane (CAB) catalyst **101** produced the [4.3.0]-bicyclic IMDA product **102** in good yields and high diastereo- and enantiocontrol (Scheme 3.44). However, this system was not applicable to trienal substrates lacking an α-substituent, resulting in significantly reduced enantiocontrol.

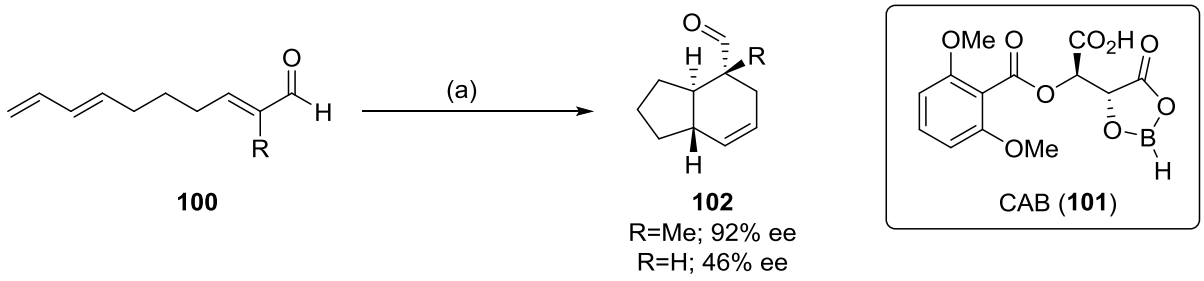

Scheme 3.44. Single-point binding acyloxyborane 101 catalysed asymmetric IMDA cycloaddition. *Reagents and conditions*: 10 mol% **101**, DCM, -40 °C, 84%, dr 99:1.

An alternative strategy is the use of two-point catalysts which bind to bidentate dienophiles. The bidentate nature of the coordinating dienophile facilitates a stronger complexation with the Lewis acid and increased activation of the dienophile. This chelation assists the formation of a stable pre-transition-state complex which creates a steric environment surrounding the dienophile, thus controlling the facial approach of the diene.

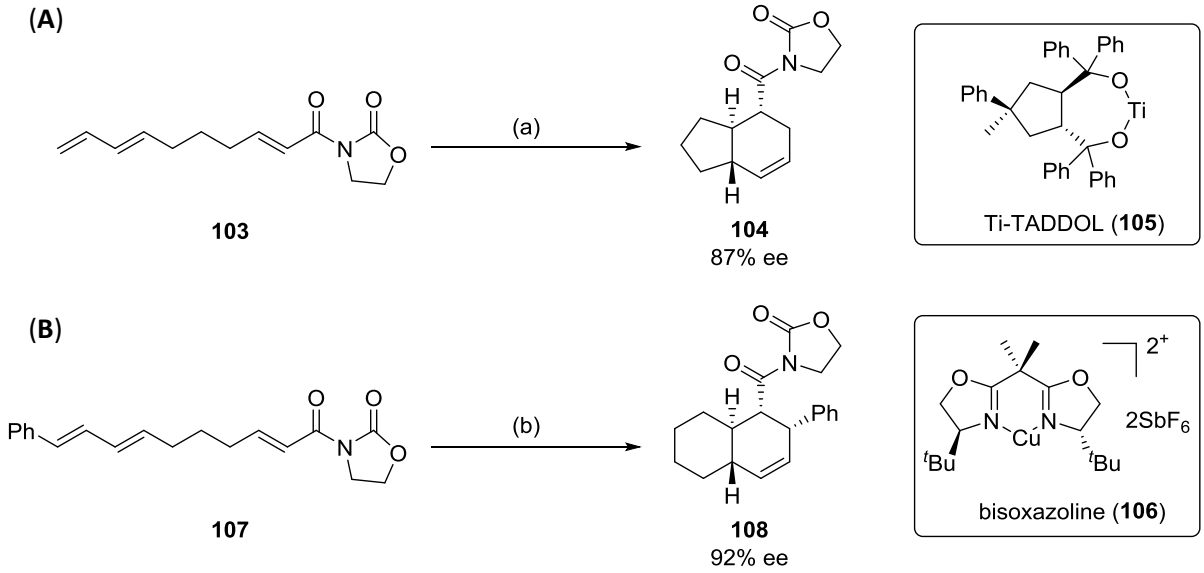

Scheme 3.45. Asymmetric IMDA cycloadditions catalysed by two-point binding Lewis acid catalysts (A) 105 and (B) 106. *Reagents and conditions*: (**a**) 30 mol% **105**, 4Å molecular sieves, DCM, 25 °C, 10 days, 87%, dr >99:1. (**b**) 10 mol% **106**, DCM, 25 °C, 14 hours, 97%, dr >99:1.

Narasaka *et al*. reported the asymmetric IMDA cycloaddition of acyl oxazolidinone **103** in the presence of a Ti-TADDOL catalyst **105**, although high catalyst loadings and extended reaction times were necessary (Scheme 3.45).[245] Evans reported the successful application of the widely used intermolecular DA cationic C_2-symmetric Cu(II)-*tert*-butyl-bis(oxazoline) catalyst **106** in the asymmetric IMDA cycloaddition of trienal **107** to furnish the [4.4.0]-bicyclic IMDA product **108** (Scheme 3.45).[246,247] This was subsequently applied to form a key precursor *en route* to the natural product (-)-isopulo'upone.[247]

The main and significant disadvantage of this method is the required incorporation and cleavage of the oxazolidinone auxiliary. However, when designing this synthetic approach we proposed that the 1,3-dicarbonyl functionality present in the tetramic acid core of the IMDA precursor **65** could potentially act as a bidentate dienophile (Figure 3.15A). The inherent chelating effect of this moiety (Section 3.1.4) provides a synthetic advantage, potentially forming a strong coordination complex with the chiral catalyst. To test this hypothesis we carried out a preliminary screen of three chiral Lewis acid catalysts; 1.) single-point binding chiral oxazaborolidine **109**, 2.) two-point binding chiral bisoxazoline **110**, and 3.) two-point binding bis(sulfinyl)imidoamidine (siam) catalyst **111** (Figure 3.15B).

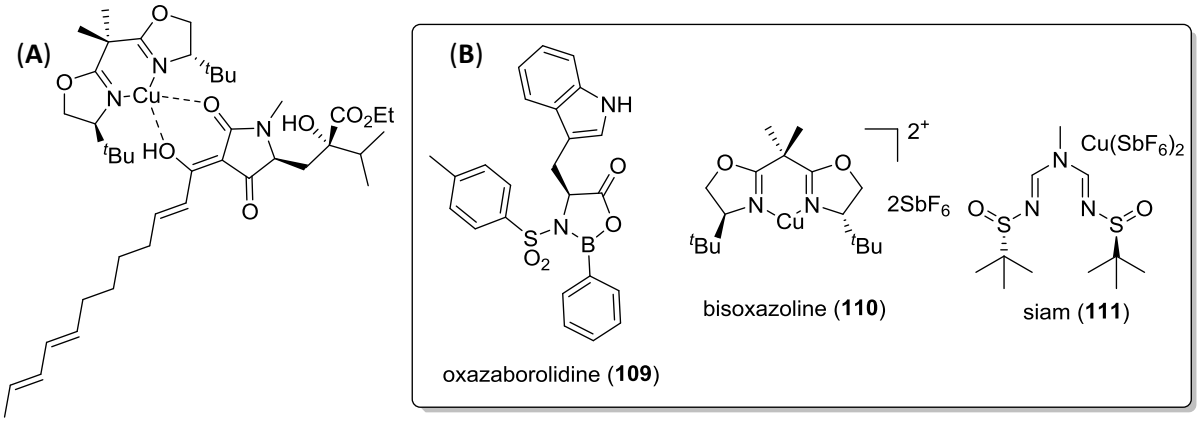

Figure 3.15. (A) Proposed bidentate coordination of IMDA precursor 65 to the two-point binding Lewis acid catalyst 110. (B) Structures of the three selected chiral Lewis acid catalysts.

Corey and coworkers reported the first examples of (*S*)-tryptophan-derived chiral oxazaborolidine catalysed enantioselective intermolecular Diels-Alder reactions.[248] The pre-transition-state assembly is proposed to be formed by one-point coordination of an enal with the boron atom in **109**, orientating the dienophile to form a π-π interaction with the π-electron-donating tryptophan indole ring, which in turn sterically shields one face of the dienophile from attack by the diene.[242] Chiral oxazaborolidine **109** was synthesised from *L*-tryptophan **112** as described by Simsek *et al*. (Scheme 3.46).[249]

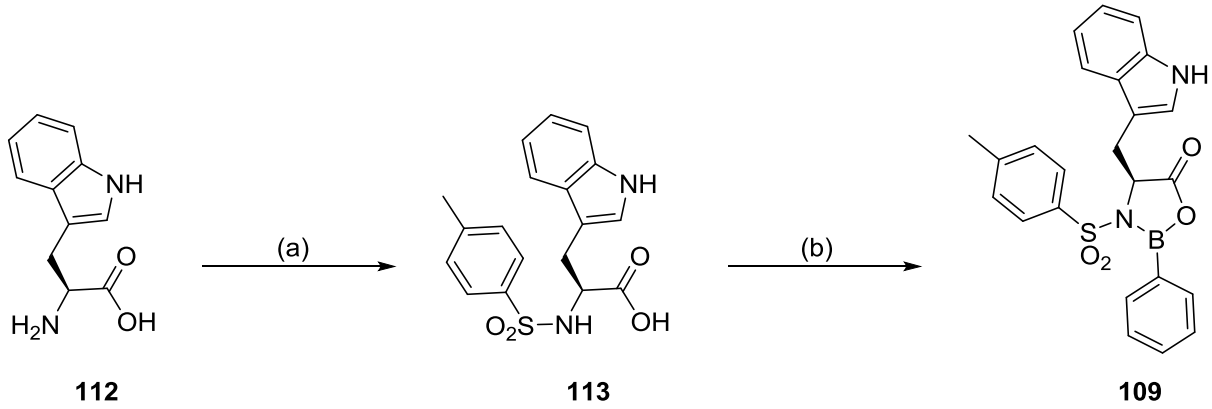

112 **113** **109**

Scheme 3.46. Synthesis of chiral oxazaborolidine 109.[249] *Reagents and conditions*: (**a**) *p*-Toluenesulfonyl chloride, H_2O/THF (9:1), Et_3N, 0 °C → r.t., 2.5 h, 87%. (b) Dichlorophenylborane, DCM, r.t., 1 h.

Evans and coworkers pioneered the use of chiral C_2-symmetric bisoxazoline-copper(II) complexes to catalyse enantioselective DA reactions.[246,250,251] This chiral copper(II) complex has been used extensively to catalyse highly diastereoselective and enantioselective DA reactions, including the IMDA cycloaddition of **107** (Scheme 3.45), *via* a rigid square-planar transition state.[252] Commercially available 2,2'-*iso*propylidenebis-[(4*S*)-4-*tert*-butyl-2-oxazoline] was stirred with $CuCl_2$ and $AgSbF_6$ in DCM for 12 hours to provide a dark blue solution of bis(oxazoline)-copper(II) catalyst **110**.[247] The C_2-symmetric bis(sulfinyl)imidoamidine (siam) ligands were developed by Ellman and coworkers as novel catalysts for enantioselective Diels-Alder reactions.[253,254] It was envisioned that the sulfinyl nitrogens of the siam ligand **111** would coordinate to copper(II) in accordance with the mechanism proposed by the Evans group for the that Cu(II)-bisoxazoline complex **110** (Figure 3.15). However, although the pre-transition-state assembly has not been fully deduced, it appears the Cu(II) predominantly coordinates the sulfinyl oxygens of **111** in solution. The siam ligand **111** was synthesised by a modular route which was adapted from Ellman's original reported synthesis (Scheme 3.47).[253,254]

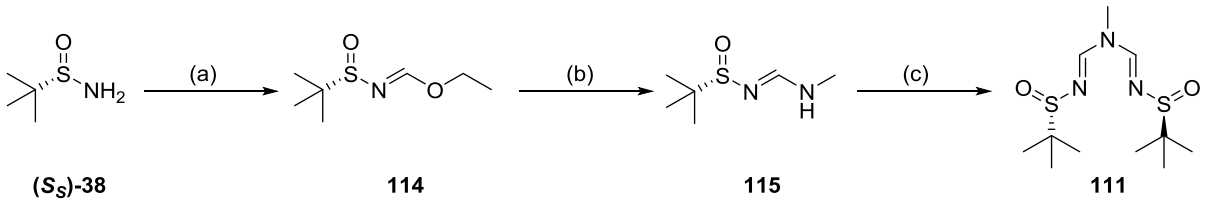

(S_S)-38 **114** **115** **111**

Scheme 3.47. Synthesis of siam ligand 111. *Reagents and conditions*: (a) Triethyl orthoformate, *p*-toluenesulfonic acid, 120 °C, 3 h, 97%. (b) $MeNH_2$ (8.0M in EtOH), r.t., 16 h, 82%. (c) KHMDS, **114**, THF, 0 °C → r.t., 16 h, 71%.

A preliminary screen of the 3 chiral catalysts involved stirring with IMDA precursor **65** in DCM at -78 °C followed by slowly warming to room temperature over 16 hours (Figure 3.16A). The reaction

diastereoselectivity was monitored by analysis of the chemical shift of one of the H6' diastereotopic protons of the JBIR-22 ethyl ester **77** which appears as overlapping doublet of doublets in **77a**/**b** (1:1 mixture of **77a** & **77b**) compared to a single doublet of doublets in the single JBIR-22 ethyl ester diastereomers **77a** and **77b** (Figure 3.16B). As expected, the one-point binding oxazaborolidine **109** resulted in poor conversion to the desired cycloadduct with no significant diastereoselectivity observed by ^{1}H NMR (data not shown). However, both of the bidentate catalysts **110** and **111** catalysed the IMDA cycloaddition, forming the decalin ring with excellent diastereoselectivity (*endo*) and moderate enantioselectivity, to yield a mixture which was diastereomerically enriched in **77a** (Figure 3.16B). Furthermore, similarly to the organocatalytic cycloaddition of **69** (section 3.5.3), the minor *E*,*Z*,*E*-isomer of **65** was inert to this catalytic IMDA, resulting in kinetic purification of the IMDA precursor.

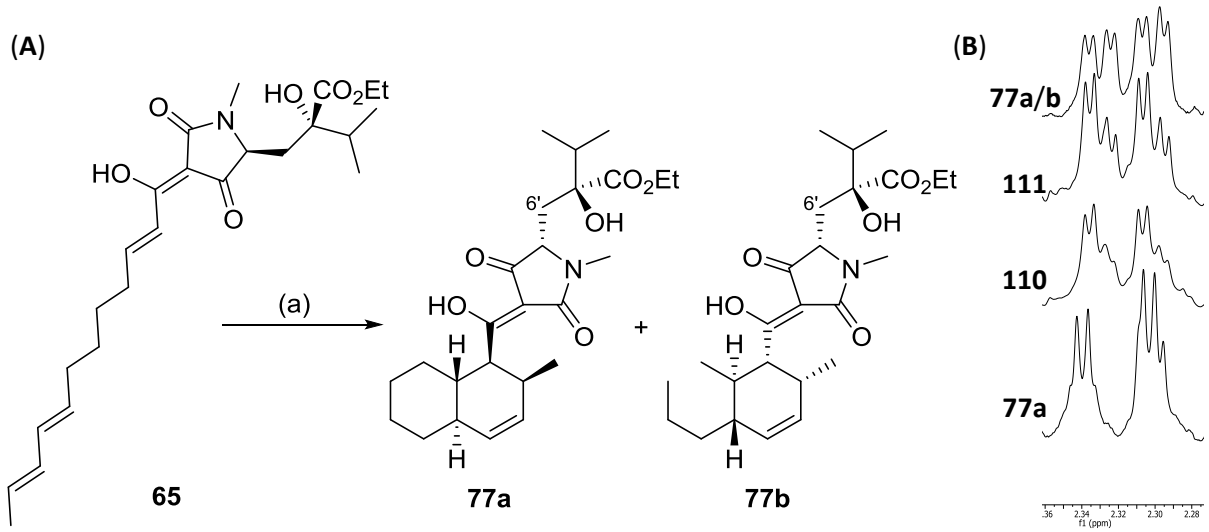

Figure 3.16. (A) Initial test conditions for the chiral Lewis acid catalysed IMDA. *Reagents and conditions*: (**a**) Appropriate chiral catalyst (**110**/**111**), DCM, -78 °C → r.t., 16 h. **(B) Stacked magnification of the H6' peak region in the ^{1}H spectra of 77a/b (*top*), the product of the siam 111 catalysed IMDA, the product of the bisoxazoline 110 catalysed IMDA and 77a (*bottom*).**

The siam ligand **111** catalysed the preferred formation of a the decalin ring containing the (2*S*, 3*S*, 6*R*, 11*S*) stereochemistry, to afford diastereomer **77a** as the main stereoisomer, which is in agreement with the expected stereochemical outcome of a DA reaction using a (S_S)-*tert*butanesulfinamide **38** derived siam ligand based on the current literature.[253,254] As the reaction had gone to completion under the initial test conditions, identification of the optimal temperature for this reaction could improve the observed diastereoselectivity. The reaction was repeated, maintaining the temperature at -78 °C for 12 hours before warming the reaction to room temperature over 12 hours. No further significant enrichment of diastereomer **77a** was observed (data not shown), suggesting either this is not a temperature sensitive process, or the reaction is

only occurring on warming to room temperature, therefore requiring further experiments at fixed temperatures between -78 °C and room temperature to identify the optimal conditions.

Analysis of the bisoxazoline-copper(II) **110** catalysed IMDA reaction highlighted two striking observations. It was observed that the cycloaddition had not gone to completion within the reaction time, indicating that this is a slower reaction and likely only occurs at temperatures higher than -78 °C. Therefore, identifying the optimal temperature for this reaction could be essential to optimising the diastereoselectivity. To assess this, the reaction was allowed to warm slowly from -78 °C to -5 °C over 5 hours, followed by stirring at this temperature for 16 hours. Full conversion to the desired cycloadduct was observed under these conditions with an apparent moderate enhancement in stereocontrol of the reaction as observed by ^{1}H NMR analysis of the crude product when compared to the initial conditions (data not shown). However, it was difficult to quantify the level of improvement due to the overlapping and sloping nature of the observed signals for the H6' proton. Therefore, monitoring the stereoselectivity of this IMDA reaction by ^{1}H NMR is not optimal for conditions which give apparent high levels of diastereoselectivity. As a result, a chiral HPLC method (as no separation was achieved using standard reverse-phase HPLC methods) is currently being developed which will be used to analyse this IMDA reaction. As the reaction went to completion at -5 °C, a screen of temperatures between -78 °C and -5 °C should identify the conditions which result in the optimal conversion and stereoselectivity.

The second and most significant observation was the isolation of diastereomer **77a** as the major product. Based on the existing literature, the (2*R*, 3*R*, 6*S*, 11*R*)-decalin ring is the predicted stereochemical outcome of a (*S*)- bisoxazoline **110** catalysed IMDA reaction as observed in the cycloaddition of **107** to **108** (Scheme 3.45),[255] which would result in diastereomer **77b** as the major product. The observed switch in stereoinduction could provide key insights into the pre-transition-state assembly of the IMDA precursor **65**-catalyst **110** complex. The expected stereochemical outcome (2*R*, 3*R*, 6*S*, 11*R*) is based on a model involving bidentate coordination of the dienophile to form a distorted square planar copper center, resulting in the diene approaching from the α-*Re* face (Figure 3.17A).[250] This model is supported by mechanistic investigations and X-ray and computational structures of the relevant models.[246,255] However, the opposite sense of stereoinduction can be achieved by using Mg(II)- or Zn(II)- bisoxazoline complexes through the preferential formation of a tetrahedral pre-transition-state assembly which directs the diene to approach from the α-*Si* face (Figure 3.17B).[256,251] This model would predict the formation of the (2*S*, 3*S*, 6*R*, 11*S*)-isomer of the decalin ring, providing diastereomer **77a** as the major product, which is in agreement with the

experimental observation. This possible switch from a distorted square planar to a tetrahedral pre-transition-state complex[257] could be due to a steric clash between the glutamic acid side chain of **65** and the bisoxazoline ligand **110**. Although C3'-acyltetramic acids are known to coordinate preferentially metals between the C3'-acyl group and the C2'-amide oxygen (Section 3.1.4), this complex could potentially be in equilibrium in solution with a minor coordination complex involving the C3'-acyl group and the C4'-ketone oxygen. This alternative coordination complex would be particularly sterically encumbered (Figure 3.17A).

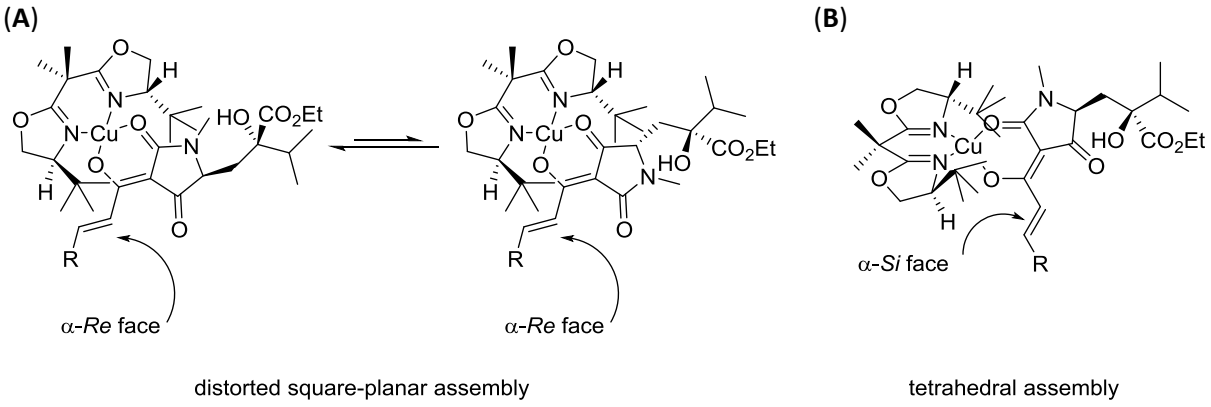

Figure 3.17. (A) Distorted square-planar pre-transition-state assembly formed using a bis(oxazoline)-Cu(II) catalyst. This assembly favours attack of the diene from the α-*Re* face to preferentially form diastereomer **77b**. Two possible coordination modes of IMDA precursor **65** to the bisoxazoline-Cu(II) catalyst **110**. **(B) Alternative tetrahedral pre-transition-state assembly.** This assembly may be favoured due to reduced steric interference between IMDA precursor **65** and the bisoxazoline-Cu(II) catalyst **110**. Attack of the diene would occur from the α-*Si* face to preferentially form diastereomer **77a**. R = C_9H_{15}.

This bisoxazoline-catalysed reaction could potentially be optimised by two alternative approaches. Switching from the (*S*)-bisoxazoline ligand **110** to its (*R*)-enantiomer may result in no steric interference, facilitating the formation of the distorted square-planer pre-transition-state, which would be predicted to provide the diastereomer **77a** as the major product. However, an alternative and potentially more beneficial approach would involve optimising the reaction conditions to promote a tetrahedral pre-transition-state, which should improve the enantioselectivity of the cycloaddition by reducing any competing formation of the opposite enantiomer *via* the square-planar assembly. This could be potentially achieved by changing the Lewis acid to Mg(II)[242,256] or Zn(II)[251] and/or utilising a phenyl-substituted bisoxazoline[246,251] in place of the *tert*-butyl-substituted bisoxazoline **110**.

3.6 Conclusions & Future Work

Over the past century nature has provided a rich source of novel bioactive agents which have been developed into efficacious drugs for a multitude of disease indications. Innovative technological advances have provided biochemical techniques by which to screen nature's tremendous supply of bioactive agents in the hunt for novel PPI modulators. Although still in its infancy, this approach has identified several promising therapeutic candidates, particularly in the area of cancer research.

This approach is exemplified by the discovery of JBIR-22 (**4**), a 0.2 μM inhibitor of PAC3 homodimerisation identified from a screen of 123,599 natural product extracts *via* a high-throughput *in vitro* protein fragment complementation assay (PCA). JBIR-22 (**4**) is a novel member of the tetramic acid family of natural products, a ubiquitous collection of bioactive agents containing a pyrrolidine-2,4-dione core motif. In particular, JBIR-22 (**4**) forms part of a small sub-family of tetramic acids defined by a tetramic acid core containing an unnatural 4,4-disubstituted glutamic acid. The absence of a reported total synthesis targeting members of this sub-family is in sharp contrast to their potent activity against therapeutically relevant targets involved in HIV, cancer and microbial pathogenesis.

3.6.1 Harzianic acid – a novel siderophoric plant growth promoting agent

We proposed a general synthetic approach to access the members of this tetramic acid sub-family centred on the development of a masked tetramic acid core which could be modified by the attachment of the broad range of substituents to optimise diversity. A late stage manipulation would then reveal the synthetically challenging tetramic acid moiety. Central to this concept was the design of a short and stereoselective synthesis of 4,4-disubstituted glutamic acids which on cyclisation would provide our AHL biomimetic masked tetramic acid. This was achieved in a three step process involving a diastereoselective *tert*-butanesulfinamide **38** directed aldol cyclisation followed by an *in situ* cyclisation to furnish lactone **46**. *N*-methylation of **46** followed by a highly diastereoselective substrate controlled reduction provided the free amine **53** which could be trapped by the appropriate β-ketothioester side chain. To validate this approach as a comprehensive and general protocol to access these tetramic acids we initially focused on the total synthesis of plant growth promoting siderophore harzianic acid (**19**).

The polyene side chain of harzianic acid (**19**) was assembled from commerically available *trans*-hexan-2-ol (**59**) *via* oxidation to the corresponding aldehyde **58** and subsequent incorporation of the β-ketothioester functionality by means of a HWE olefination. Optimisation of the silver mediated *N*-

acylation protocol developed by Woodward and Ley facilitated the one-pot coupling of **53** and β-ketothioester **56** followed by subsequent cyclisation to afford harzianic acid ethyl ester **64**. Microwave assisted hydrolysis of **64** furnished (*S*,*S*)-harzianic acid (**19**) in a separable 3:1 ratio to (*R*,*S*)-5'-*epi*harzianic acid (**19b**). This stereoselective and convergent route facilitated the first total synthesis of harzianic acid (**19**) with a LLS of 6 steps and an overall yield of 22% (Scheme 3.48).

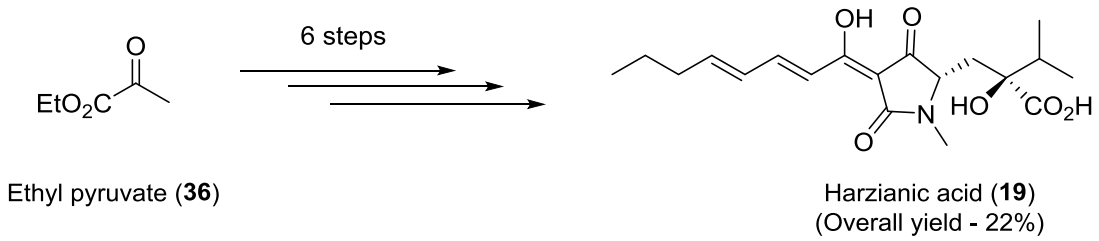

Scheme 3.48. First total synthesis of harzianic acid (19).

The efficacy of this synthetic approach is illustrated by the isolation of all four possible diastereomers of harzianic acid (**19**). These compounds could prove to be highly valuable tools for the investigation of harzianic acid's anticancer and plant growth promoting activities. In particular, exploration of harzianic acid's potent siderophoric properties could be vital to unravelling its mode of action. Comparison of the iron binding affinity of (*R*,*S*)-5'-*epi*harzianic acid (**19b**) and its biological activities, could provide a mechanism by which to explore the proposed correlation between harzianic acid's iron binding properties and its antifungal and growth promoting functions. Analysis of the biological activity of the harzianic acid enantiomer (**19c**) could reveal the possibility of a chirally discriminating uptake mechanism or an alternative biological target by which harzianic acid (**19**) affects its physiological response.

3.6.2 Identification of JBIR-22's PAC3 binding site

Synthesis of PPI inhibitor JBIR-22 (**4**) was investigated through two approaches, which were distinguished by the method and stage at which the IMDA cycloaddition to form the decalin ring of JBIR-22 (**4**) occurred. The first approach involved formation of the tetramic acid core with the attached polyene chain, prior to the IMDA cycloaddition. The second route involved an IMDA cycloaddition of trienal **69** to furnish the decalin ring, prior to its attachment to the masked tetramic acid core. As the absolute configuration of JBIR-22 (**4**) had not been elucidated, the second route was initially prioritised so the stereochemical configuration of the products could be unambiguously assigned.

Schreiber ozonolysis of cyclohexene (**72**), followed by a HWE olefination and acetal deprotection furnished trienal **75**. A subsequent chiral imidazolidinone **85** catalysed IMDA cycloaddition afforded the enantiomerically enriched decalins **78a** and **78b**. Incorporation of *S*-*tert*-butyl-thioacetate provided the desired β-ketothioesters **68a** and **68b** which were coupled to **53** *via* the end-game strategy utilised in the synthesis of harzianic acid (**19**). Comparison of spectroscopic data of the pure JBIR-22 diastereomers **4a** and **4b** with that reported for the isolated JBIR-22 (**4**) revealed that **4a** contains the correct relative stereochemical configuration. Significant discrepancies between the reported optical rotation value for JBIR-22 (**4**) and the synthesised sample **4a** prevented absolute stereochemical assignment of the natural product. Chiral HPLC or CD analysis of a sample of natural JBIR-22 (**4**) sample in comparison with that of **4a** should enable absolute stereochemical assignment. In summary, this expedient approach facilitated the first total synthesis of JBIR-22 diastereomers **4a** and **4b** with a LLS of 10 steps and of overall yield for **4a** of 6% (Scheme 3.49).

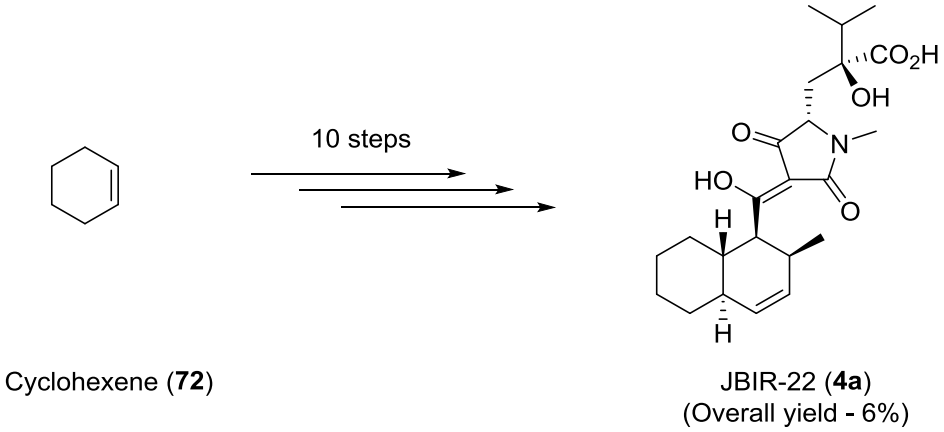

Scheme 3.49. First total synthesis of JBIR-22 (4a).

The succinct and adaptable nature of the JBIR-22 (**4a**) synthetic route provides ample opportunity to explore and optimise the activity of this potent PAC3 PPI inhibitor. A particular area of interest is the proposed JBIR-22 binding site. A docking study reported by Izumikawa *et al*. identified a potential binding site for (2*R*, 3*R*, 6*S*, 11*R*, 5'*R*, 7'*R*)-JBIR-22 diastereomer **4d** on the PAC3 homodimerisation interface (Figure 3.18).[123] We have identified an alternative binding site on the PAC3 homodimerisation interface using the docking software GOLD (data not shown). Analysis of the biological activity of the JBIR-22 diastereomers in comparison to their proposed binding site may reveal which site is most likely, and facilitate the optimisation of these compounds through a SAR study. Furthermore, it would provide a novel drug binding site for the development of future inhibitors of the proteasomal machinery, a validated anticancer target.

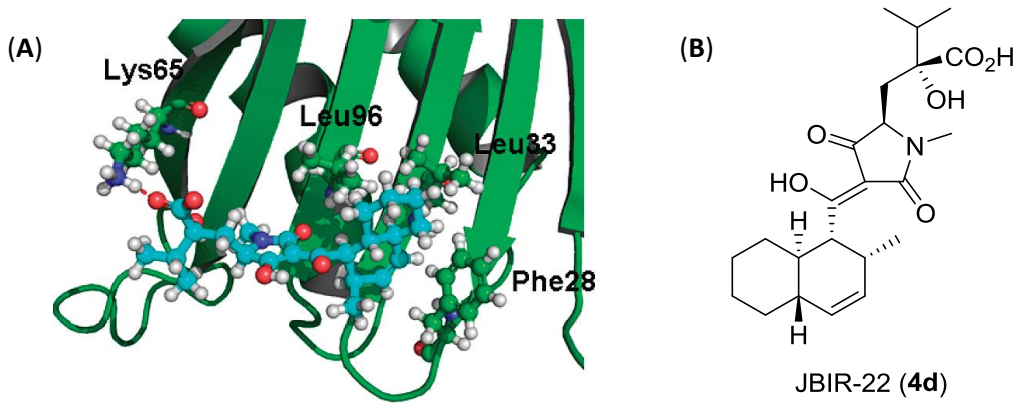

Figure 3.18. (A) The proposed JBIR-22 binding site on the PAC3 homodimerisation interface.[123] PAC3 is shown as cartoon surface model with key residues shown in ball and stick model. Carbon atoms are in green. **4d** is shown as ball and stick and carbon atoms are in cyan. In all cases, oxygen atoms are in red and nitrogen atoms in blue. **(B) Structure of bound JBIR-22 diastereomer 4d.**

3.6.3 Probing JBIR-22's biosynthetic pathway and the role of a "Diels-Alderase"

The synthesis of the JBIR-22 diastereomers **4a** and **4b** provided pure standards for the development of the late-stage asymmetric IMDA approach. The IMDA precursor **65** was assembled by means of two alternative routes. The initial approach proceeded *via* a coupling of **53** and the appropriate β-ketothioester **66**, followed by subsequent cyclisation to afford **65**. In contrast, the alternative approach aimed to circumvent the silver mediated *N*-acylation by incorporating the polyene side chain *via* a HWE olefination. This was achieved by *N*-acylation of amine **53** by the novel Meldrum's acid derivative **63** to afford the phosphonate substituted masked tetramic acid **96**. A tandem one-pot cyclisation-HWE olefination furnished the desired IMDA precursor **65**.

IMDA precursor **65** proved to be a very synthetically useful chemical tool, both for the development of an asymmetric IMDA methodology but also as a mechanism to probe the biosynthesis of JBIR-22 (**4**). JBIR-22 (**4**) contains a chiral decalin ring similar to that observed in lovastatin (**16**), equisetin (**10**) and solanapyrone A (**15**), which are proposed to be formed by a controversial enzyme-mediated enantioselective [4+2]-cycloaddition. An alternative biosynthesis of the decalin ring of JBIR-22 (**4**) could involve a non-enzymatic substrate controlled IMDA. To probe this hypothesis, an achiral Lewis acid catalysed cycloaddition of **65** was investigated. This resulted in the formation of the decalin ring as a single diastereomer but as a racemic mixture, thus forming an approximately 1:1 mixture of JBIR-22 ethyl ester diastereomers **77a** and **77b**. This would suggest that JBIR-22 (**4**) is formed by a similar biosynthetic pathway to that reported for equisetin (**10**), involving a "Diels-Alderase" mediated enantioselective IMDA.

3.6.4 Development of a catalytic asymmetric IMDA protocol

Preliminary investigation of a chiral Lewis acid catalysed IMDA cycloaddition of **65**, focused on exploiting the inherent chelating properties of the tetramic acid core. It was proposed that the 1,3-dicarbonyl motif present in the tetramic acid core of **65** could potentially function as a bidentate dienophile. An initial screen identified that two-point binding Cu(II) complexes involving a bisoxazoline **110** or siam ligand **111** catalysed the cycloaddition in high diastereoselectivity and moderate enantioselectivity, affording the diastereomerically enriched **77a** cycloadduct (Scheme 3.50). Further insight into the pre-transition state assembly of the catalyst-**65** complex may prove to be essential for optimising the diastereoselectivity. Information regarding the effect of the steric environment surrounding the bidentate dienophile on the stereoselectivity of the cycloaddition is limited due to the scarcity of reported IMDA cycloadditions of advanced natural product intermediates. This is compounded by the widespread use of simple oxazolidinone precursors as bidentate dienophiles for the development of catalytic asymmetric IMDA procedures. Therefore, the future optimisation of the catalytic asymmetric IMDA cycloaddition of **65**, in addition to providing a concise and highly versatile route to JBIR-22 (**4a**) and related analogues, would also assist the development of a more general and comprehensive method for the utilisation of catalytic IMDA cycloadditions in the later stages of total synthesis projects.

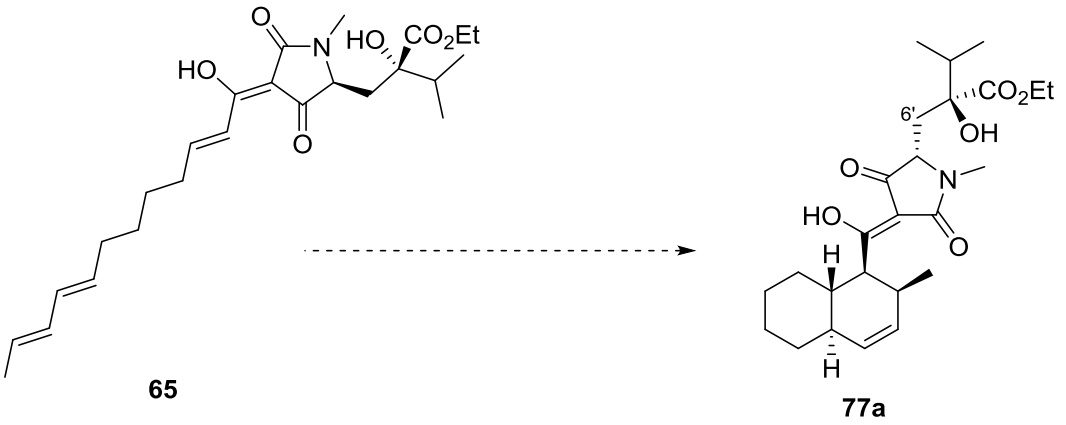

Scheme 3.50. Proposed late stage catalytic asymmetric IMDA cycloaddition.

3.7 Experimental section

3.7.1 General considerations

See Section 2.8.1 for general considerations.

GC analyses were obtained on a Shimadzu GC consisting of a Shimadzu AOC-20i auto injector and a Shimadzu GC-2025 gas chromatograph. Analysis was performed using Shimadzu GCsolution v2.41 software and separation was achieved using an Agilent Cyclosil-B column.

3.7.2 Experimental procedures

Ethyl (*R*,*E*)-2-((*tert*-butylsulfinyl)imino)propanoate (42)[197]

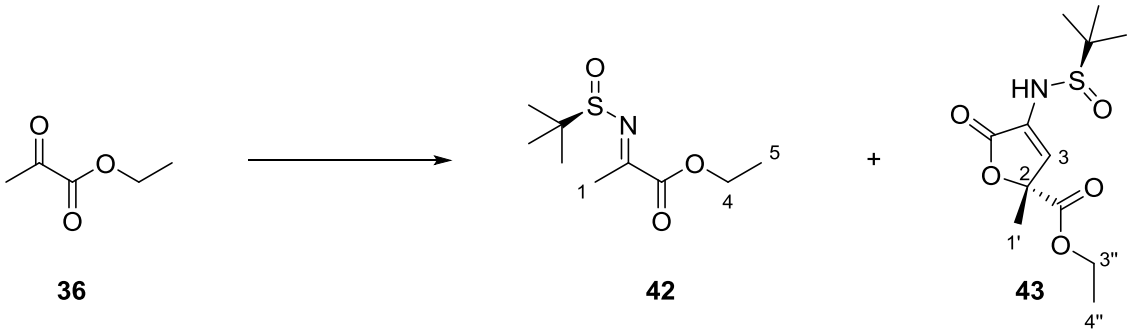

36 **42** **43**

Ethyl pyruvate **36** (4.3 g, 37.1 mmol, 1.5 eq.) was added to a stirred solution of (*R*)-(+)-2-methyl-2-propanesulfinamide **38** (3.0 g, 24.8 mmol, 1.0 eq.) and $Ti(OEt)_4$ (8.5 g, 37.1 mmol, 1.5 eq.) in THF (100 mL) at reflux. The reaction was stirred at the same temperature for 3 hours before cooling to room temperature. The crude reaction mixture was poured into brine (100 mL) whilst being vigorously stirred. The resulting suspension was filtered through Celite, and the filter cake was washed with EtOAc (2 × 30 mL). The filtrate was washed with brine (30 mL), and the brine layer was back extracted with EtOAc (3 × 30 mL). The combined organic extracts were dried over $MgSO_4$, filtered, concentrated *in vacuo* and purified *via* the Biotage SP4 (silica-packed SNAP column 180 g; 10-50% EtOAc/hexanes) to give the title product **42** as a pale yellow oil (2.5 g, 45%) and the enamine tautomer as a pale yellow oil (0.8 g, 15%). **42** was isolated in a 3:1 ratio (by analysis of the crude NMR spectrum) to lactone **43** (1.1 g). The NMR analysis of the imine tautomer of **42** was complicated by the existence of rotamers. **^{1}H NMR** (500 MHz, Chloroform-*d*) δ(*major imine-form*) 4.50 – 3.96 (m, 2H, C4-$\underline{H}_2$), 2.46 (d, *J* = 120.8 Hz, 3H, C1-$\underline{H}_3$), 1.37 – 1.32 (m, 3H, C5-$\underline{H}_3$), 1.27 (d, *J* = 27.6 Hz, 9H, $(C\underline{H}_3)_3$); **^{13}C NMR** (126 MHz, Chloroform-*d*) δ(*major imine-form*) 167.8 (C3), 163.6 (C2), 62.4 (d, *J* =

42.6 Hz, C4), 59.4 (C(CH$_3$)$_3$), 25.4 (C1), 22.8 (d, *J* = 37.8 Hz, (CH$_3$)$_3$), 18.5 (C1), 14.1 (d, *J* = 14.9 Hz, C5); **^{1}H NMR** (500 MHz, Chloroform-*d*) δ(*minor enamine-form*) 5.95 (s, 1H, NH), 5.50 (t, *J* = 1.6 Hz, 1H, C1-H$_2$), 5.23 (d, *J* = 1.6 Hz, 1H, C1-H$_2$), 4.28 (q, *J* = 7.1, 2H, C4-H$_2$), 1.33 (t, *J* = 7.1 Hz, 3H, C5-H$_3$), 1.28 (s, 9H, (CH$_3$)$_3$); **^{13}C NMR** (126 MHz, Chloroform-*d*) δ(*minor enamine-form*) 164.0 (C3), 136.2 (C2), 100.7 (C1), 62.4 (C4), 56.7 (C(CH$_3$)$_3$), 22.4 (CH$_3$)$_3$), 14.3 (C5); ***m/z*** (ES$^+$) 220.10 ([M+H]$^+$, 100 %); **HRMS** (ES$^+$) Calcd for $C_9H_{18}NO_3S$ [M+H]$^+$: 220.1002, found 220.0999; **$[\alpha]_D^{20}$** = -121.8 (*c* 1.15, $CHCl_3$). (lit. -125.8).[197] Spectroscopic data are in accordance with the literature.[197]

Ethyl (*R*)-4-(((*R*)-*tert*-butylsulfinyl)amino)-2-methyl-5-oxo-2,5-dihydrofuran-2-carboxylate (43)

In $CDCl_3$ at room temperature the title compound **43** exists as a mixture of rotamers. **IR** (KBr) ν $_{max}$: 2978 (NH), 1769 (C=O), 1748 (C=O), 1651, 1458, 1248, 1126, 1063; **^{1}H NMR** (500 MHz, Chloroform-*d*) δ 6.42 (d, *J* = 2.1 Hz, 1H, C3-H), 5.74 (d, *J* = 4.6 Hz, 1H, NH), 4.22 (qt, *J* = 7.1, 1.8 Hz, 2H, C3''-H$_2$), 1.72 (d, *J* = 7.3 Hz, 3H, C1'-H$_3$), 1.29 (s, 9H, (CH$_3$)$_3$), 1.30 – 1.26 (m, 3H, C4''-H$_3$); **^{13}C NMR** (126 MHz, Chloroform-*d*) δ 168.5 (d, *J* = 15.8 Hz, CO), 168.0 (C5), 131.1 (d, *J* = 4.1 Hz, C4), 120.3 (d, *J* = 11.9 Hz, C3), 84.7 (d, *J* = 7.0 Hz, C2), 62.6 (d, *J* = 15.4 Hz, C3''), 57.6 (d, *J* = 13.0 Hz, C(CH$_3$)$_3$), 22.9 (d, *J* = 6.6 Hz, C1'), 22.1 ((CH$_3$)$_3$), 14.0 (C4''); ***m/z*** (ES$^+$) 312.09 ([M+Na]$^+$, 100 %); **HRMS** (ES$^+$) Calcd for $C_{12}H_{19}NO_5SNa$ [M+Na]$^+$: 312.0876, found 312.0869. **$[\alpha]_D^{20}$** = -52.9 (*c* 1.0, MeOH).

Ethyl (*R*)-4-(((*R*)-*tert*-butylsulfinyl)amino)-2-isopropyl-5-oxo-2,5-dihydrofuran-2-carboxylate (46)

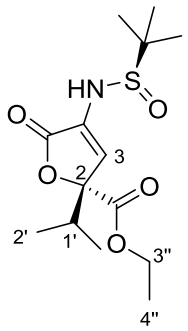

To a solution of *i*-Pr$_2$NH (1.68 mL, 12.0 mmol, 1.2 eq.) in THF (50 mL) was added *n*-BuLi (5.1 mL, 2.2 M in hexanes, 1.1 eq.) at 0 °C and the mixture was stirred for 30 minutes. The solution was then cooled to -78 °C and **42** (2.20 g, 10.0 mmol, 1.0 eq.) was added. The reaction was stirred for a further 30 minutes at this temperature before the addition of $ZnBr_2$ (4.50 g, 20.0 mmol, 2.0 eq.), followed by ethyl dimethylpyruvate **37** (1.87 g, 13.0 mmol, 1.3 eq.). The reaction was then stirred for 3 hours at -78 °C before the addition of a saturated solution of NH_4Cl (30 mL). The reaction was allowed to slowly warm to room temperature. The mixture was extracted with EtOAc (3 × 30 mL) and the organic layers combined and washed with brine (30 mL), dried over $MgSO_4$, filtered, concentrated *in vacuo* and purified *via* the Biotage SP4 (silica-packed SNAP column 120 g; 20-60% EtOAc/hexanes) to

give the title product **46** as a white solid (2.80 g, 88%). **mp** 77-79 °C; **IR** (KBr) ν $_{max}$: 2965 (NH), 1775 (C=O), 1714 (C=O), 1647, 1366, 1236, 1103, 1051, 1018; **^{1}H NMR** (500 MHz, Chloroform-*d*) δ 6.37 (s, 1H, C3-H), 5.71 (s, 1H, NH), 4.24 (q, *J* = 7.1 Hz, 2H, C3''-H_2), 2.46 (hept, *J* = 6.9 Hz, 1H, C1'-H), 1.34 – 1.21 (m, 12H, (CH_3)$_3$, C4''-H_3), 1.04 (d, *J* = 6.9 Hz, 3H, C2'-H_3), 0.89 (d, *J* = 6.9 Hz, 3H, C2'-H_3); **^{13}C NMR** (126 MHz, Chloroform-*d*) δ 168.5 (CO), 168.3 (C5), 131.3 (C4), 119.2 (C3), 90.7 (C2), 62.5 (C3''), 57.6 ($C(CH_3)_3$), 34.2 (C1'), 22.2 ((CH_3)$_3$), 17.4 (C2'), 15.8 (C2'), 14.3 (C4''); ***m/z*** (ES$^+$) 318.14 ([M+H]$^+$, 100 %); **HRMS** (ES$^+$) Calcd for $C_{14}H_{24}NO_5S$ [M+H]$^+$: 318.1370, found 318.1366; **$[\alpha]_D^{20}$** = +24.1 (*c* 1.0, MeOH).

Ethyl (*R*)-4-(((*R*)-*tert*-butylsulfinyl)(methyl)amino)-2-isopropyl-5-oxo-2,5-dihydrofuran-2-carboxylate (52)

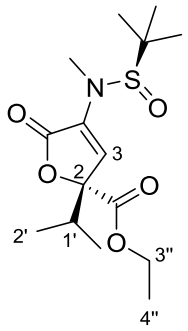

To a solution of **46** (0.98 g, 3.09 mmol, 1.0 eq.) in DMF (12 mL) at -15 °C was added LiHMDS (3.09 mL, 1 M in THF, 1.0 eq.) dropwise and the reaction was stirred for 40 minutes. Iodomethane (0.38 mL, 6.18 mmol, 2.0 eq.) was then added and the reaction was allowed to slowly warm to room temperature before stirring at this temperature for 2 hours. The reaction was diluted with H_2O (15 mL) before being extracted with EtOAc (3 × 20 mL). The organic layers were combined and washed with $Na_2S_2O_3$ (20 mL), brine (20 mL), dried over $MgSO_4$, filtered, concentrated *in vacuo* and purified *via* the Biotage SP4 (silica-packed SNAP column 40 g; 0-30% EtOAc/hexanes) to give the title product **52** as a white solid (0.97 g, 95%). **mp** 70-72 °C; **IR** (KBr) ν $_{max}$: 2970, 1763 (C=O), 1738 (C=O), 1622, 1248, 1198, 1092, 1038, 1005; **^{1}H NMR** (500 MHz, Chloroform-*d*) δ 6.21 (s, 1H, C3-H), 4.31 – 4.10 (m, 2H, C3''-H_2), 2.94 (s, 3H, NCH_3), 2.45 (hept, *J* = 6.9 Hz, 1H, C1'-H), 1.29 (t, *J* = 7.1 Hz, 3H, C4''-H_3), 1.25 (s, 9H, (CH_3)$_3$), 1.03 (d, *J* = 6.9 Hz, 3H, C2'-H_3), 0.86 (d, *J* = 6.9 Hz, 3H, C2'-H_3); **^{13}C NMR** (126 MHz, Chloroform-*d*) δ 168.7 (CO), 166.9 (C5), 137.0 (C4), 122.7 (C3), 89.3 (C2), 62.5 (C3''), 60.8 ($C(CH_3)_3$), 34.2 (C1'), 29.3 (NCH_3), 23.4 ((CH_3)$_3$), 17.3 (C2'), 15.7 (C2'), 14.3 (C4''); ***m/z*** (ES$^+$) 332.15 ([M+H]$^+$, 100 %); **HRMS** (ES$^+$) Calcd for $C_{15}H_{26}NO_5S$ [M+H]$^+$: 332.1526, found 332.1521; **$[\alpha]_D^{20}$** = +229.5 (*c* 1.0, MeOH).

(*E*)-Hex-2-enal (58)[258]

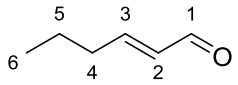

trans-2-Hexen-1-ol **59** (1.0 g, 9.98 mmol, 1.0 eq.) was added to a suspension of DDQ (2.72 g, 12.0 mmol, 1.2 eq.) in DCM (50 mL) and the reaction was stirred at room temperature for 16 h. The reaction was diluted with DCM (20 mL) and washed with $NaHCO_3$ (3 × 30 mL), $Na_2S_2O_4$ (3 × 30 mL) and brine (30 mL). The organic layer was separated and filtered through a plug of Celite. The filtrate was concentrated *in vacuo* to yield the title product **58** as a pale yellow liquid (0.97 g, 99%) which was used in the next step without further purification. **^{1}H NMR** (500 MHz, Chloroform-*d*) δ 9.50 (d, *J* = 7.9 Hz, 1H, C1-H), 6.85 (dt, *J* = 15.6, 6.8 Hz, 1H, C3-H), 6.11 (ddt, *J* = 15.6, 7.9, 1.5 Hz, 1H, C2-H), 2.37 – 2.26 (m, 2H, C4-H_2), 1.54 (h, *J* = 7.4 Hz, 2H, C5-H_2), 0.96 (t, *J* = 7.4 Hz, 3H, C5-H_3); **^{13}C NMR** (126 MHz, Chloroform-*d*) δ 194.3 (C1), 159.0 (C3), 133.2 (C2), 34.8 (C4), 21.3 (C5), 13.8 (C6); ***m/z*** (ES^+) 99.08 ($[M+H]^+$, 100 %); **HRMS** (ES^+) Calcd for $C_6H_{11}O_1$ $[M+H]^+$: 99.0804, found 99.0802. Spectroscopic data are in accordance with the literature.[258]

Diethyl (2-(2,2-dimethyl-4,6-dioxo-1,3-dioxan-5-ylidene)-2-hydroxyethyl)phosphonate (63)

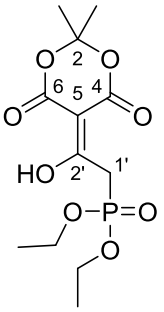

Thionyl chloride (1.11 mL, 15.3 mmol, 3.0 eq.) was added dropwise to diethylphosphoacetic acid (1.0 g, 5.1 mmol, 1.0 eq.) and the reaction was stirred at room temperature for 3 hours. The resulting red solution (diethylphosphoacetyl chloride) was added dropwise to a solution of 2,2-dimethyl-1,3-dioxane-4,6-dione **60** (0.59 g, 4.08 mmol, 0.8 eq.) and pyridine (0.82 mL, 10.2 mmol, 2 eq.) in DCM (25 mL) at 0 °C. The reaction was stirred for 1 hour at 0 °C followed by 1 hour at room temperature. The reaction was washed with an aqueous solution of HCl (3 × 10 mL), brine (10 mL), dried over Na_2SO_4, filtered and concentrated *in vacuo* to yield the title product **63** as a red oil which solidified at ~4 °C to yield a red amorphous solid (1.26 g, 96%). **63** was used in the next step without further purification. **IR** (KBr) ν_{max}: 2995 (OH), 2928 (OH), 1736 (C=O), 1668 (C=O), 1578, 1396, 1248, 1196, 1146, 1013, 920; **^{1}H NMR** (500 MHz, Chloroform-*d*) δ 4.18 (dq, *J* = 8.1, 7.1 Hz, 4H, OCH_2CH$_3$), 3.93 (d, *J* = 23.9 Hz, 2H, C1'-H_2), 1.76 (s, 6H, (CH_3)$_2$), 1.33 (td, *J* = 7.1, 0.6 Hz, 6H, OCH$_2$CH_3); **^{13}C NMR** (126 MHz, Chloroform-*d*) δ 187.6 (C2'), 170.3 (C6), 160.6 (C4), 105.4 (C2), 93.4 (C5), 63.2 (d, *J* = 6.2 Hz, OCH_2CH$_3$), 34.5 (d, *J* = 126.9 Hz, C1'), 27.0 ((CH_3)$_2$), 16.5 (OCH$_2$CH_3); **^{31}P NMR** (202 MHz, Chloroform-

d) δ 19.0; ***m/z*** (ES^+) 323.09 ($[M+H]^+$, 100 %); **HRMS** (ES^+) Calcd for $C_{12}H_{20}O_8P$ $[M+H]^+$: 323.0890, found 323.0893.

_S_-(_tert_-Butyl) 4-(diethoxyphosphoryl)-3-oxobutanethioate (57)[207]

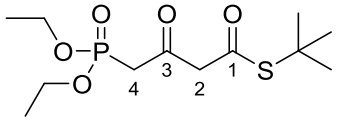

2-Methyl-2-propanethiol (4.46 mL, 39.5, 2.0 eq.) was added to a solution of **63** (6.37 g, 19.8, 1.0 eq.) in MeCN (120 mL) and the reaction was heated at reflux for 3 hours. The reaction was cooled to room temperature, concentrated *in vacuo* and purified *via* the Biotage SP4 (silica-packed SNAP column 200 g; 0-5% MeOH/DCM) to give the title product **57** as an orange oil (5.20 g, 85%). **^{1}H NMR** (500 MHz, Chloroform-*d*) δ 4.15 (dq, *J* = 8.1, 7.1 Hz, 4H, $OC\underline{H}_2CH_3$), 3.80 (s, 2H, C2-$\underline{H}_2$), 3.24 (d, *J* = 22.7 Hz, 2H, C4-$\underline{H}_2$), 1.47 (s, 9H, $(C\underline{H}_3)_3$), 1.34 (td, *J* = 7.1, 2.4 Hz, 6H, $OCH_2C\underline{H}_3$); **^{13}C NMR** (126 MHz, Chloroform-*d*) δ 194.3 (d, *J* = 6.4 Hz, C3), 192.4 (C1), 62.9 (d, *J* = 6.4 Hz, $O\underline{C}H_2CH_3$), 58.7 (C2), 49.4 ($\underline{C}(CH_3)_3$), 42.8 (d, *J* = 126.6 Hz, C4), 29.8 ($(\underline{C}H_3)_2$), 16.5 (d, *J* = 6.1 Hz, $OCH_2\underline{C}H_3$); ***m/z*** (ES^+) 333.09 ($[M+Na]^+$, 100 %); **HRMS** (ES^+) Calcd for $C_{12}H_{24}O_5PS$ $[M+H]^+$: 311.1077, found 311.1083. Spectroscopic data are in accordance with the literature.[207]

_S_-(_tert_-Butyl) (4_E_,6_E_)-3-oxodeca-4,6-dienethioate (56)[212]

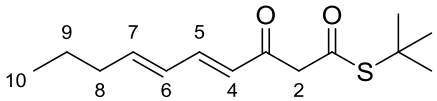

LiHMDS (7.14 mL, 1 M in THF, 2.1 eq.) was added dropwise to a solution of **57** (1.05 g, 3.40 mmol, 1.0 eq.) in THF (34 mL) at -78 °C. The reaction was stirred for 30 minutes at -78 °C before the addition of a solution of **58** (0.40 g, 4.08 mmol, 1.2 eq.) in THF (17 mL). The reaction was stirred at -78 °C for 30 minutes before slowly warming to 0 °C over 1 hour. The reaction was maintained at 0 °C for 1 hour before quenching by addition of a saturated aqueous solution of NH_4Cl (20 mL). The resulting mixture was extracted with EtOAc (3 × 20 mL). The organic extracts were combined, washed with brine (20 mL), dried over Na_2SO_4, filtered, concentrated *in vacuo* and purified *via* the Biotage SP4 (silica-packed SNAP column 25 g; 0-5% EtOAc/hexanes) to give the title product **56** as a pale yellow oil (0.75 g, 87%). In $CDCl_3$ at room temperature the title compound exists as a (4 : 3) *enol* : *keto* mixture. **^{1}H NMR** (500 MHz, Chloroform-*d*) δ(*major enol-form*) 12.58 (d, *J* = 1.5 Hz, 1H, O$\underline{H}$), 7.07 (dd, *J* = 15.2, 10.8 Hz, 1H, C5-$\underline{H}$), 6.19 – 6.10 (m, 1H, C6-$\underline{H}$), 6.03 (dt, *J* = 14.6, 6.9 Hz, 1H, C7-$\underline{H}$), 5.68 (d, *J* = 15.2 Hz, 1H, C4-$\underline{H}$), 5.35 (s, 1H, C2-$\underline{H}$), 2.22 – 2.15 (m, 2H, C8-$\underline{H}_2$), 1.52 (s, 9H, $(C\underline{H}_3)_3$), 1.51 – 1.41 (m, 2H, C9-$\underline{H}_2$), 0.92 (td, *J* = 7.4, 5.7 Hz, 3H, C10-$\underline{H}_3$); **^{13}C NMR** (126 MHz, Chloroform-*d*)

δ(*major enol-form*) 196.2 (C1), 167.1 (C3), 142.6 (C7), 139.1 (C5), 129.5 (C6), 123.0 (C4), 101.3 (C2), 48.5 (C($\underline{C}H_3)_3$), 35.3 (C8), 30.3 (($\underline{C}H_3)_3$), 22.2 (C9), 13.9 (C10); **^{1}H NMR** (500 MHz, Chloroform-*d*) δ(*minor keto-form*) 7.20 (dd, *J* = 15.2, 9.9 Hz, 1H, C5-$\underline{H}$), 6.31 – 6.19 (m, 2H, C6-$\underline{H}$, C7-$\underline{H}$), 6.15 (dd, *J* = 15.2, 10.3 Hz, 1H, C4-$\underline{H}$), 3.71 (s, 2H, C2-$\underline{H}_2$), 2.17 – 2.09 (m, 2H, C8-$\underline{H}_2$), 1.47 (s, 9H, ($C\underline{H}_3)_3$), 1.54 – 1.38 (m, 2H, C9-$\underline{H}_2$), 0.92 (td, *J* = 7.4, 5.7 Hz, 3H, C10-$\underline{H}_3$); **^{13}C NMR** (126 MHz, Chloroform-*d*) δ(*minor keto-form*) 193.0 (C1), 192.0 (C3), 147.4 (C7), 145.8 (C5), 129.0 (C6), 127.0 (C4), 56.7 (C2), 49.1 (C($\underline{C}H_3)_3$), 35.4 (C8), 29.8 (($\underline{C}H_3)_3$), 22.0 (C9), 13.9 (C10); ***m/z*** (ES$^+$) 255.14 ([M+H]$^+$, 100 %); **HRMS** (ES$^+$) Calcd for $C_{14}H_{23}O_2S$ [M+H]$^+$: 255.1413, found 255.1413. Spectroscopic data are in accordance with the literature.[212]

Ethyl (2*S*,4*S*)-2-isopropyl-5-oxo-4-((4*E*,6*E*)-3-oxodeca-4,6-dienamido)tetrahydrofuran-2-carboxylate (55)

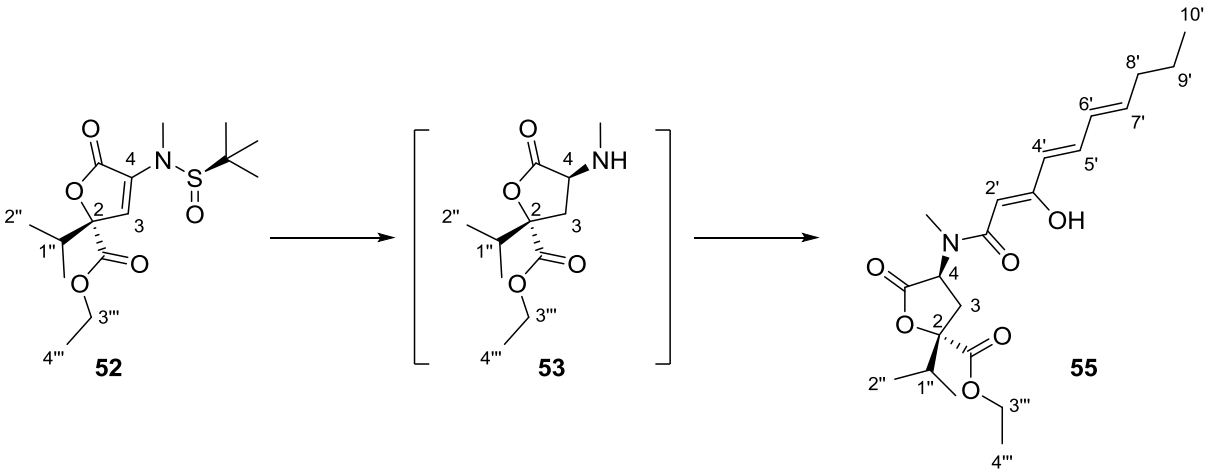

To a solution of **52** (186 mg, 0.56 mmol, 1.0 eq.) in THF (1.5 mL) at 0 °C was added HCl (0.56 mL, 4 N in dioxane, 4.0 eq.). The reaction was stirred for 10 minutes at this temperature before the addition of a solution of $NaBH_3CN$ (106 mg, 1.69 mmol, 3.0 eq.) in MeOH (3 mL). The reaction was stirred for a further 1 hour at 0 °C before being concentrated *in vacuo*. The residue was partitioned between $NaHCO_3$ (5 mL) and EtOAc (5 mL). The aqueous layer was extracted with EtOAc (3 × 10 mL) and the combined organic extracts were washed with brine (10 mL), dried over $MgSO_4$, filtered, concentrated *in vacuo* to yield the crude free amine **53**. **^{1}H NMR** (500 MHz, Chloroform-*d*) δ 4.26 (q, *J* = 7.1 Hz, 2H, C3'''-$\underline{H}_2$), 3.56 (dd, *J* = 11.5, 8.4 Hz, 1H, C4-$\underline{H}$), 2.75 (dd, *J* = 12.8, 8.4 Hz, 1H, C3-$\underline{H}_2$), 2.47 (s, 3H, NC$\underline{H}_3$), 2.29 – 2.21 (m, 1H, C1''-$\underline{H}$), 2.06 (dd, *J* = 12.8, 11.5 Hz, 1H, C3-$\underline{H}_2$), 1.31 (t, *J* = 7.1 Hz, 3H, C4'''-$\underline{H}_3$), 1.03 (d, *J* = 6.9 Hz, 3H, C2''-$\underline{H}_3$), 0.99 (d, *J* = 6.9 Hz, 3H, C2''-$\underline{H}_3$). To a solution of **53** in anhydrous THF (7 mL) at 0 °C was added **56** (158 mg, 0.62 mmol, 1.1 eq.) followed by Et_3N (0.31 mL, 2.26 mmol, 4.0 eq.) and CF_3CO_2Ag (250 mg, 1.13 mmol, 2.0 eq.). The reaction was then stirred for 1 hour at 0 °C followed by 1 hour at room temperature. The reaction was concentrated *in vacuo* and purified *via* the Biotage SP4 (silica-packed SNAP column 12 g; 0-40% EtOAc/hexanes) to give the title

product **55** as a pale yellow oil (143 mg, 65%). In $CDCl_3$ at room temperature the title compound exists as a (5 : 4) *enol* : *keto* mixture. **IR** (thin film) ν_{max}: 2963 (OH), 2934 (OH), 1786 (C=O), 1736 (C=O), 1634, 1578, 1489, 1180, 997; **^{1}H NMR** (400 MHz, Chloroform-*d*) δ(*major enol-form*) 7.04 (dd, *J* = 15.2, 10.7 Hz, 1H, C5'-H), 6.21 – 6.08 (m, 1H, C6'-H), 6.06 – 5.96 (m, 1H, C7'-H), 5.81 (d, *J* = 15.2 Hz, 1H, C4'-H), 5.16 (s, 1H, C2'-H), 4.96 (dd, *J* = 11.5, 9.0 Hz, 1H, C4-H), 4.38 – 4.14 (m, 2H, C3'''-H_2), 2.99 (s, 3H, NCH_3), 2.74 – 2.62 (m, 1H, C3-H_2), 2.53 – 2.39 (m, 1H, C3-H_2), 2.39 – 2.24 (m, 1H, C1''-H), 2.16 – 2.10 (m, 2H, C8'-H_2), 1.52 – 1.39 (m, 2H, C9'-H_2), 1.36 – 1.27 (m, 3H, C4'''-H_3), 1.11 – 0.98 (m, 6H, (C2''-H_3)$_2$), 0.98 – 0.86 (m, 3H, C10'-H_3); **^{13}C NMR** (101 MHz, Chloroform-*d*) δ(*major enol-form*) 172.3 (C1'), 172.1 (C5), 170.9 (C1'''), 170.5 (C3'), 141.9 (C7'), 137.4 (C5'), 129.3 (C6'), 123.9 (C4'), 88.3 (C2'), 86.9 (C2), 62.3 (C3'''), 55.7 (C4), 35.1 (C8'), 34.1 (C1'', NCH_3), 31.4 (C3), 22.1 (C9'), 16.8 (C2''), 16.3 (C2''), 14.2 (C4'''), 13.7 (C10'); **^{1}H NMR** (400 MHz, Chloroform-*d*) δ(*minor keto-form*) 7.23 (dd, *J* = 15.4, 10.0 Hz, 1H, C5'-H), 6.36 – 6.18 (m, 2H, C6'-H, C7'-H), 6.16 (d, *J* = 15.4 Hz, 1H, C4'-H), 4.80 (dd, *J* = 11.5, 9.0 Hz, 1H, C4-H), 4.37 – 4.16 (m, 2H, C3'''-H_2), 3.73 (d, *J* = 1.7 Hz, 2H, C2'-H_2), 3.01 (s, 3H, NCH_3), 2.74 – 2.62 (m, 1H, C3-H_2), 2.53 – 2.39 (m, 1H, C3-H_2), 2.39 – 2.24 (m, 1H, C1''-H), 2.23 – 2.15 (m, 2H, C8'-H_2), 1.52 – 1.39 (m, 2H, C9'-H_2), 1.36 – 1.27 (m, 3H, C4'''-H_3), 1.11 – 0.98 (m, 6H, (C2''-H_3)$_2$), 0.98 – 0.86 (m, 3H, C10'-H_3); **^{13}C NMR** (101 MHz, Chloroform-*d*) δ(*minor keto-form*) 193.0 (C3'), 172.1 (C5), 170.9 (C1'''), 167.8 (C1'), 147.7 (C7'), 145.8 (C5'), 128.8 (C4'), 126.5 (C6'), 87.1 (C2), 62.3 (C3'''), 56.6 (C4), 47.4 (C2'), 35.1 (C8'), 34.1 (C1'', NCH_3), 31.8 (C3), 21.8 (C9'), 16.8 (C2''), 16.3 (C2''), 14.2 (C4'''), 13.7 (C10'); ***m/z*** (ES^+) 416.20 ($[M+Na]^+$, 100 %); **HRMS** (ES^+) Calcd for $C_{21}H_{31}NO_6Na$ $[M+Na]^+$: 416.2044, found 416.2037; **$[\alpha]_D^{20}$** = -22.0 (*c* 0.5, $CHCl_3$).

Harzianic acid ethyl ester (64)

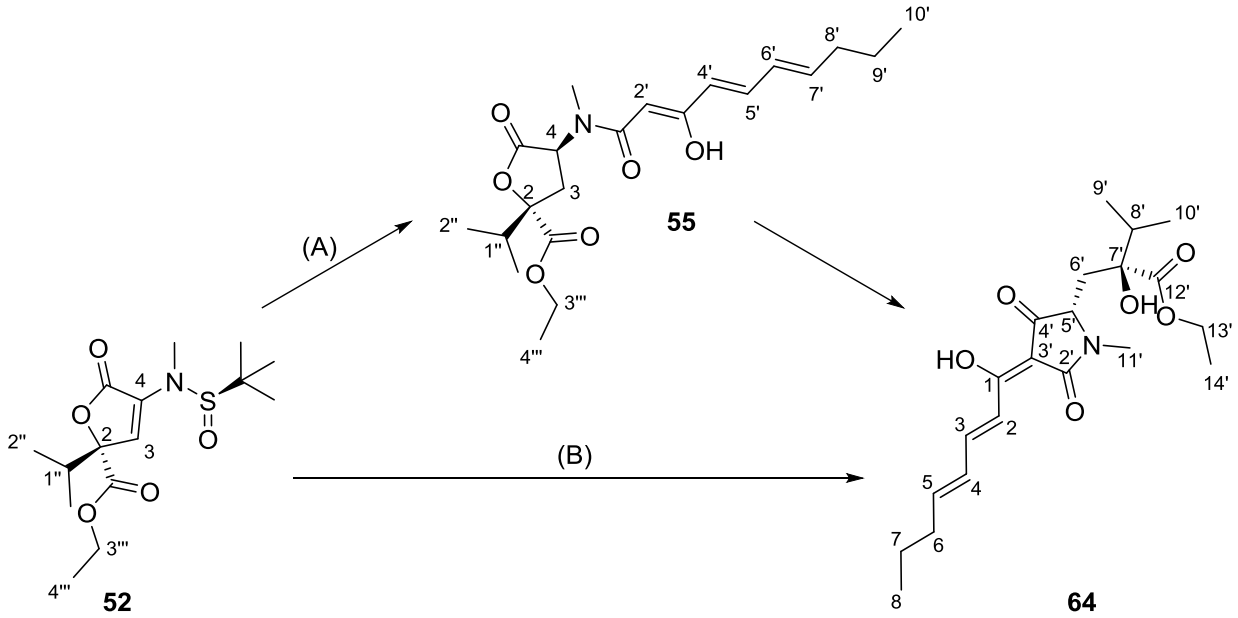

Route A: To a solution of **55** (115 mg, 0.29 mmol, 1.0 eq.) in THF (6 mL) at 0 °C was added ^{t}BuOK (36 mg, 0.32 mmol, 1.1 eq.) and the reaction was stirred for 30 minutes. The reaction was slowly warmed to room temperature and stirred at this temperature for 1 hour. The reaction was concentrated *in vacuo* and the residue partitioned between DCM (10 mL) and an aqueous solution of HCl (10 mL, 1 N). The aqueous layer was separated and extracted with DCM (3 × 10 mL). The organic extracts were combined, washed with an aqueous solution of HCl (5 mL, 1 N), brine (5 mL), dried over Na_2SO_4, filtered, concentrated *in vacuo* and purified *via* the Biotage SP4 (silica-packed SNAP column 12 g; 0-60% EtOAc/hexanes) to give the title product **64** as an pale yellow oil (107 mg, 93%).

Route B: To a solution of **52** (400 mg, 1.20 mmol, 1.0 eq.) in THF (3 mL) at 0 °C was added HCl (1.20 mL, 4 N in dioxane, 4.0 eq.). The reaction was stirred for 10 minutes at this temperature before the addition of a solution of $NaBH_3CN$ (228 mg, 3.62 mmol, 3.0 eq.) in MeOH (6 mL). The reaction was stirred for a further 1 hour at 0 °C before being concentrated *in vacuo*. The residue was partitioned between a saturated aqueous solution of $NaHCO_3$ (10 mL) and EtOAc (10 mL). The aqueous layer was extracted with EtOAc (3 × 15 mL) and the combined organic extracts were washed with brine (15 mL), dried over $MgSO_4$, filtered, concentrated *in vacuo* to yield the crude free amine **53**. To a solution of **53** in anhydrous MeCN (24 mL) at 0 °C was added **56** (305 mg, 1.20 mmol, 1.0 eq.) followed by Et_3N (0.67 mL, 4.80 mmol, 4.0 eq.) and CF_3CO_2Ag (530 mg, 2.40 mmol, 2.0 eq.). The reaction was then stirred for 1 hour at 0 °C followed by 1 hour at room temperature. The reaction was concentrated *in vacuo* and purified *via* the Biotage SP4 (silica-packed SNAP column 12 g; 0-40% EtOAc/hexanes) to give the title product **64** as a pale yellow oil (354 mg, 75%). **IR** (KBr) ν_{max}: 2965 (OH), 2934 (OH), 1724 (C=O), 1682 (C=O), 1614, 1568, 1447, 1238, 1188, 999; **^{1}H NMR** (500 MHz, Chloroform-*d*) δ 7.49 (dd, *J* = 15.3, 9.9 Hz, 1H, C3-H), 7.05 (d, *J* = 15.3 Hz, 1H, C2-H), 6.45 – 6.17 (m, 2H, C4-H, C5-H), 5.30 (s, 1H, OH), 4.25 (q, *J* = 7.1, 2H, C13'-H_2), 3.68 (dd, *J* = 9.8, 2.2 Hz, 1H, C5'-H), 2.98 (s, 3H, C11'-H_3), 2.32 (dd, *J* = 14.4, 2.2 Hz, 1H, C6'-H_2), 2.24 – 2.18 (m, 2H, C6-H_2), 2.06 (hept, *J* = 6.9 Hz, 1H, C8'-H), 1.90 (dd, *J* = 14.4, 9.8 Hz, 1H, C6'-H_2), 1.54 – 1.43 (m, 2H, C7-H_2), 1.32 (t, *J* = 7.1 Hz, 3H, C14'-H_3), 1.00 – 0.88 (m, 9H, C9'-H_3, C10'-H_3, C8-H_3); **^{13}C NMR** (126 MHz, Chloroform-*d*) δ 196.3 (C4'), 175.5 (C12'), 175.5 (C1), 173.4 (C2'), 148.8 (C5), 146.5 (C3), 129.9 (C4), 119.5 (C2), 99.3 (C3'), 78.9 (C7'), 64.5 (C5'), 61.6 (C13'), 36.8 (C8'), 35.6 (C6), 34.9 (C6'), 26.8 (C11'), 22.0 (C7), 17.5 (C9'), 16.4 (C10'), 14.5 (C14'), 13.8 (C8); ***m/z*** (ES^+) 394.22 ($[M+H]^+$, 100 %); **HRMS** (ES^+) Calcd for $C_{21}H_{32}NO_6$ $[M+H]^+$: 394.2224, found 394.2223.

Harzianic acid (19)[172]

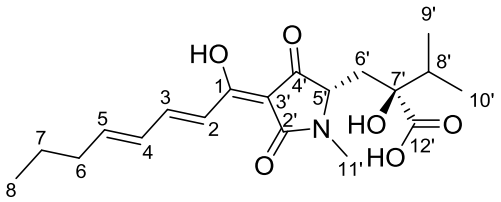

To a solution of **64** (190 mg, 0.48 mmol, 1.0 eq.) in EtOH (1 mL) was added an aqueous solution of NaOH (1 mL, 2 N) and the reaction was heated to 110 °C under microwave irradiation for 20 minutes. The reaction was diluted with an aqueous solution of HCl (5 mL, 1N) and extracted with DCM (3 × 5 mL). The organic layers were combined, washed with brine (10 mL), dried over Na_2SO_4, filtered, concentrated *in vacuo* and purified *via* the Biotage SP4 (Reverse-phase silica-packed SNAP column 4 g; 20-100% H_2O/(MeOH:MeCN)) to give the title product **19** (92 mg, 52%) and the 5'-epimer **19b** (33 mg, 19%) as orange solids. **IR** (thin film) ν_{max}: 2963, 2934, 1717 (br), 1613, 1560, 1449, 1408, 1261, 1042, 1003, 885; **^{1}H NMR** (500 MHz, Chloroform-*d*) δ 7.58 – 7.50 (m, 1H, C3-H), 7.25 (br s, 1H, OH), 6.99 (d, *J* = 15.2 Hz, 1H, C2-H), 6.39 – 6.34 (m, 2H, C4-H, C5-H), 3.62 (dd, *J* = 10.6, 1.3 Hz, 1H, C5'-H), 2.96 (s, 3H, C11'-H_3), 2.48 (dd, *J* = 14.7, 1.3 Hz, 1H, C6'-H_2), 2.23 (dtd, *J* = 7.4, 5.4, 2.8 Hz, 1H, C6-H_2), 2.01 (hept, *J* = 6.8 Hz, 1H, C8'-H), 1.88 (dd, *J* = 14.7, 10.6 Hz, 1H, C6'-H_2), 1.49 (app. hept, *J* = 7.4, 2H, C7-H_2), 0.98 (d, *J* = 6.8 Hz, 3H, C9'-H_3), 0.98 (d, *J* = 6.8 Hz, 3H, C10'-H_3), 0.94 (t, *J* = 7.4 Hz, 3H, C8-H_3); **^{13}C NMR** (126 MHz, Chloroform-*d*) δ 197.4 (C4'), 176.8 (C1), 176.2 (C12'), 173.3 (C2'), 150.1 (C5), 147.7 (C3), 129.8 (C4), 119.2 (C2), 98.8 (C3'), 80.0 (C7'), 64.2 (C5'), 36.1 (C8'), 35.6 (C6), 33.9 (C6'), 26.7 (C11'), 21.9 (C7), 17.6 (C9'), 16.4 (C10'), 13.9 (C8); **^{1}H NMR** (500 MHz, Methanol-d_4) δ 7.53 (m, 1H, C3-H), 7.09 (d, *J* = 15.3 Hz, 1H, C2-H), 6.39 (m, 2H, C4-H, C5-H), 3.80 (dd, *J* = 9.1, 2.5 Hz, 1H, C5'-H), 2.94 (s, 3H, C11'-H_3), 2.34 (dd, *J* = 14.7, 2.5 Hz, 1H, C6'-H_2), 2.24 (m, 2H, C6-H_2), 2.02 (m, 1H, C8'-H), 2.00 (dd, *J* = 14.7, 9.1 Hz, 1H, C6'-H_2), 1.51 (m, 2H, C7-H_2), 0.98 (d, *J* = 6.9 Hz, 3H, C9'-H_3), 0.96 (t, *J* = 7.2 Hz, 3H, C8-H_3), 0.95 (d, *J* = 6.9 Hz, 3H, C10'-H_3); **^{13}C NMR** (126 MHz, Methanol-d_4) δ 198.9 (C4'), 178.6 (C12'), 175.8 (C1), 173.9 (C2') 149.8 (C5), 147.3 (C3), 131.0 (C4), 120.3 (C2), 100.9 (C3'), 79.8 (C7'), 65.5 (C5'), 37.4 (C8'), 36.4 (C6'), 27.1 (C11'), 23.0 (C7), 17.9 (C9'), 16.5 (C10'), 14.1 (C8); ***m/z*** (ES^+) 366.19 ($[M+H]^+$, 100 %); **HRMS** (ES^+) Calcd for $C_{19}H_{28}NO_6$ $[M+H]^+$: 366.1911, found 366.1905; $[\alpha]_D^{20}$ = +18.6 (*c* 1.06, MeOH). (lit. +19.6).[172] Spectroscopic data are in accordance with the literature.[172]

5'-*epi*Harzianic acid (19b)

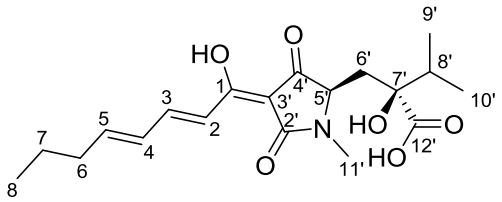

IR (thin film) ν $_{max}$: 2963, 2926, 1717 (br), 1636 (br), 1616, 1456, 1260, 1036, 804; **^{1}H NMR** (500 MHz, Chloroform-*d*) δ 7.56 – 7.48 (m, 1H, C3-H), 7.07 (d, *J* = 15.3 Hz, 1H, C2-H), 6.38 – 6.32 (m, 2H, C4-H, C5-H), 3.87 (dd, *J* = 8.2, 2.8 Hz, 1H, C5'-H), 3.02 (s, 3H, C11'-H_3), 2.57 (dd, *J* = 15.2, 2.8 Hz, 1H, C6'-H_2), 2.29 – 2.21 (m, 2H, C6-H_2), 2.16 (dd, *J* = 15.2, 8.2 Hz, 1H, C6'-H_2), 2.13 – 1.99 (m, 1H, C8'-H), 1.57 – 1.44 (m, 2H, C7-H_2), 1.05 (d, *J* = 6.9 Hz, 3H, C9'-H_3), 1.04 (d, *J* = 6.9 Hz, 3H, C10'-H_3), 0.96 (t, *J* = 7.4 Hz, 3H, C8-H_3); **^{13}C NMR** (126 MHz, Chloroform-*d*) δ 196.1 (C4'), 175.6 (C12'), 175.3 (C1), 174.0 (C2'), 149.0 (C5), 146.7 (C3), 129.9 (C4), 119.4 (C2), 99.6 (C3'), 78.3 (C7'), 63.6 (C5'), 36.0 (C8'), 35.6 (C6), 34.7 (C6'), 27.4 (C11'), 22.0 (C7), 17.4 (C9'), 16.7 (C10'), 13.9 (C8); **^{1}H NMR** (500 MHz, Methanol-d_4) δ 7.44 (dd, *J* = 15.3, 10.0 Hz, 1H, C3-H), 7.11 (d, *J* = 15.3 Hz, 1H, C2-H), 6.41 – 6.27 (m, 2H, C4-H, C5-H), 3.77 (br s, 1H, C5'-H), 2.92 (s, 3H, C11'-H_3), 2.47 (dd, *J* = 15.1, 5.2 Hz, 1H, C6'-H_2), 2.40 (dd, *J* = 15.1, 3.2 Hz, 1H, C6'-H_2), 2.23 (app. q, *J* = 7.0 Hz, 2H, C6-H_2), 1.89 (hept, *J* = 6.8 Hz, 1H, C8'-H), 1.57 – 1.43 (m, 2H, C7-H_2), 0.96 (t, *J* = 7.3 Hz, 3H, C8-H_3), 0.95 (d, *J* = 6.8 Hz, 3H, C9'-H_3), 0.87 (d, *J* = 6.8 Hz, 3H, C10'-H_3); **^{13}C NMR** (126 MHz, Methanol-d_4) δ 196.3 (C4'), 178.2 (C12'), 176.4 (C2'), 173.4 (C1), 148.2 (C5), 145.6 (C3), 131.0 (C4), 120.6 (C2), 102.3 (C3'), 78.8 (C7'), 66.0 (C5'), 37.5 (C8'), 37.0 (C6'), 36.3 (C6), 28.3 (C11'), 23.0 (C7), 17.6 (C9'), 16.6 (C10'), 14.0 (C8); ***m/z*** (ES$^+$) 364.18 ([M-H]$^-$, 100 %); **HRMS** (ES$^+$) Calcd for $C_{19}H_{26}NO_6$ [M-H]$^-$: 364.1766, found 364.1757; **$[\alpha]_D^{20}$** = +118.0 (*c* 0.5, MeOH).

6,6-Dimethoxyhexanal (73)[217]

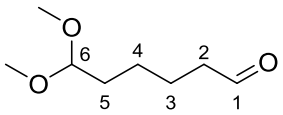

A solution of cyclohexene **72** (5.06 mL, 50.0 mmol, 1.0 eq.) in dry DCM (150 mL)/MeOH (50 mL) at -78 °C was purged with O_2. O_3 was bubbled through the solution until it became a blue colour. The reaction was purged with N_2 until the blue colour disappeared. PTSA (951 mg, 5.00 mmol, 0.1 eq.) was added and the reaction was stirred at room temperature for 1.5 hours before the addition of anhydrous $NaHCO_3$ (16.8 g, 200 mmol, 4.0 eq.). Dimethyl sulfide (6.21 g, 100 mmol, 2.0 eq.) was added after a further 15 minutes and the reaction was stirred at room temperature for 12 hours. The reaction was concentrated *in vacuo* to approximately 40 mL. The resulting mixture was diluted with DCM (40 mL) and washed with H_2O (3 × 30 mL). The aqueous extracts were combined and extracted with DCM (2 × 20 mL). The organic extracts were combined, washed with brine (30 mL),

dried over $MgSO_4$, filtered, concentrated *in vacuo* and purified *via* the Biotage SP4 (silica-packed SNAP column 100 g; 0-40% EtOAc/hexanes) to give the title product **73** as a colourless oil (6.54 g, 82%). **^{1}H NMR** (500 MHz, Chloroform-*d*) δ 9.76 (t, *J* = 1.7 Hz, 1H, C1-H), 4.35 (t, *J* = 5.7 Hz, 1H, C6-H), 3.31 (d, *J* = 2.1 Hz, 6H, $(OCH_3)_2$), 2.44 (td, *J* = 7.3, 1.7 Hz, 2H, C2-H_2), 1.80 – 1.45 (m, 4H, C3-H_2, C5-H_2), 1.48 – 1.26 (m, 2H, C4-H_2); **^{13}C NMR** (126 MHz, Chloroform-*d*) δ 202.7 (C1), 104.4 (C6), 52.9 ($(CH_3)_3$), 44.0 (C2), 32.4 (C5), 24.3 (C4), 22.0 (C3). Spectroscopic data are in accordance with the literature.[217]

(2*E*,4*E*)-10,10-Dimethoxydeca-2,4-diene (74)[218]

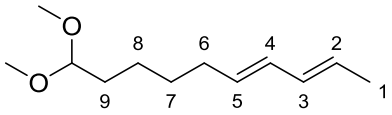

To a solution of diethyl 2-butenylphosphonate **70** (2.96 mL, 15.6 mmol, 1.0 eq.) in DME (60 mL) at -78 °C was added KHMDS (17.2 mmol, 1.1 eq., 1 M in THF) and the reaction was stirred for 30 minutes. A solution of **73** in DME (30 mL) was then added and the reaction was stirred for a further 30 minutes before stirring at 0 °C for 2 hours followed by 2 hours at room temperature. The reaction was diluted with Et_2O (30 mL)/saturated aqueous solution of NH_4Cl (30 mL). The aqueous layer was extracted with Et_2O (3 × 20 mL). The organic extracts were combined, washed with brine (30 mL), dried over $MgSO_4$, filtered, concentrated *in vacuo* and purified *via* the Biotage SP4 (silica-packed SNAP column 80 g; 0-20% EtOAc/hexanes) to give the title product **74** as a colourless oil (1.76 g, 57%, ~8:1 *E*:*Z*). **^{1}H NMR** (500 MHz, Chloroform-*d*) δ 6.05 – 5.93 (m, 2H, C3-H, C4-H), 5.63 – 5.48 (m, 2H, C2-H, C5-H), 4.35 (t, *J* = 5.7 Hz, 1H, C10-H), 3.31 (s, 6H, $(OCH_3)_2$), 2.06 (app. q, *J* = 7.0 Hz, 2H, C6-H_2), 1.72 (d, *J* = 6.1 Hz, 3H, C1-H_3), 1.63 – 1.54 (m, 2H, C9-H_2), 1.46 – 1.29 (m, 4H, C7-H_2, C8-H_2); **^{13}C NMR** (126 MHz, Chloroform-*d*) δ 131.9 (C5), 131.8 (C3), 130.6 (C4), 127.0 (C2), 104.6 (C10), 52.7 ($(OCH_3)_2$), 32.6 (C6), 32.5 (C9), 29.4 (C7), 24.3 (C8), 18.2 (C1); ***m/z*** (ES^+) 216.20 ($[M+NH_4]^+$, 100 %); **HRMS** (ES^+) Calcd for $C_{12}H_{26}NO_2$ $[M+NH_4]^+$: 216.1958, found 216.1954. Spectroscopic data are in accordance with the literature.[218]

(6*E*,8*E*)-Deca-6,8-dienal (75)[259]

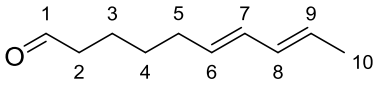

To **74** (1.74 g, 8.77 mmol, 1.0 eq.) in THF (35 mL) was added an aqueous solution of HCl (9.65 mL, 1 N, 1.1 eq.) and the reaction was stirred at room temperature for 12 hours. The reaction was quenched by the addition of a saturated aqueous solution of $NaHCO_3$ (30 mL). The mixture was extracted with Et_2O (3 × 30 mL) and the organic layers were combined, washed with brine (30 mL), dried over $MgSO_4$, filtered and concentrated *in vacuo*. Title product **75** was isolated as a pale yellow

liquid (1.26 g, 94%) which was used in the next step without further purification. **^{1}H NMR** (500 MHz, Chloroform-*d*) δ 9.76 (t, *J* = 1.8 Hz, 1H, C1-H), 6.04 – 5.92 (m, 2H, C7-H, C8-H), 5.64 – 5.45 (m, 2H, C6-H, C9-H), 2.42 (td, *J* = 7.4, 1.8 Hz, 2H, C2-H_2), 2.08 (app. q, *J* = 7.2 Hz, 2H, C5-H_2), 1.72 (d, *J* = 6.6 Hz, 3H, C10-H_3), 1.68 – 1.55 (m, 2H, C3-H_2), 1.47 – 1.37 (m, 2H, C4-H_2); **^{13}C NMR** (126 MHz, Chloroform-*d*) δ 202.7 (C1), 131.5 (C8), 131.0 (C6), 130.8 (C7), 127.2 (C9), 43.8 (C2), 32.2 (C5), 28.9 (C4), 21.6 (C3), 18.0 (C10); ***m/z*** (ES^+) 153.12 ($[M+H]^+$, 100 %); **HRMS** (ES^+) Calcd for $C_{10}H_{17}O$ $[M+H]^+$: 153.1274, found 153.1270. Spectroscopic data are in accordance with the literature.[259]

***S*-(*tert*-Butyl) (4*E*,10*E*,12*E*)-3-oxotetradeca-4,10,12-trienethioate (66)**

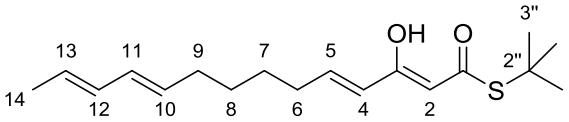

To a solution of **57** (2.81 g, 9.05 mmol, 1.0 eq.) in THF (70 mL) at -78 °C was added LiHMDS (18.1 mL, 1 M in THF, 2.0 eq.) and the reaction was stirred for 30 minutes before the addition of a solution of **75** (1.24 g, 8.15 mmol, 0.9 eq.) in THF (35 mL). The reaction was stirred for a further 30 minutes at -78 °C before slowly warming to 0 °C over 2 hours. The reaction was quenched by the addition of a saturated aqueous solution of NH_4Cl (30 mL) and extracted with EtOAc (3 × 30 mL). The organic extracts were combined, washed with brine (30 mL), dried over $MgSO_4$, filtered and concentrated *in vacuo* and purified *via* the Biotage SP4 (silica-packed SNAP column 80 g; 0-10% EtOAc/hexanes) to give the title product **66** as a colourless oil (1.82 g, 72%). In $CDCl_3$ at room temperature the title compound exists as a (2 : 3) *keto* : *enol* mixture. **IR** (thin film) ν_{max}: 2924, 2859, 1653 (C=O), 1582, 1074; **^{1}H NMR** (500 MHz, Chloroform-*d*) δ(*major enol-form*) 12.61 (br s, OH), 6.76 – 6.54 (m, 1H, C5-H), 6.05 – 5.90 (m, 2H, C11-H, C12-H), 5.74 – 5.61 (m, 1H, C4-H), 5.61 – 5.43 (m, 2H, C10-H, C13-H), 5.30 (s, 1H, C2-H), 2.21 – 2.14 (m, 2H, C6-H_2), 2.10 – 2.01 (m, 2H, C9-H_2), 1.76 – 1.68 (m, 3H, C14-H_3), 1.51 (s, 9H, (C3''-H_3)$_3$), 1.46 – 1.36 (m, 4H, C7-H_2, C8-H_2); **^{13}C NMR** (126 MHz, Chloroform-*d*) δ(*major enol-form*) 196.5 (C1), 166.8 (C3), 142.6 (C5), 131.6 (C10, C12), 130.7 (C11), 127.2 (C13), 124.4 (C4), 100.5 (C2), 48.42 (C2''), 32.7 (C6), 32.4 (C9), 30.3 ((C3'')$_3$), 29.0 (CH_2), 28.1 (CH_2), 18.2 (C14); **^{1}H NMR** (500 MHz, Chloroform-*d*) δ(*minor keto-form*) 6.98 – 6.79 (m, 1H, C5-H), 6.21 – 6.08 (m, 1H, C4-H), 6.07 – 5.93 (m, 2H, C11-H, C12-H), 5.63 – 5.46 (m, 2H, C10-H, C13-H), 3.70 (d, *J* = 1.0 Hz, 2H, C2-H_2), 2.29 – 2.20 (m, 2H, C6-H_2), 2.10 – 2.01 (m, 2H, C9-H_2), 1.76 – 1.68 (m, 3H, C14-H_3), 1.46 (s, 9H, (C3''-H_3)$_3$), 1.47 – 1.39 (m, 4H, C7-H_2, C8-H_2); **^{13}C NMR** (126 MHz, Chloroform-*d*) δ(*minor keto-form*) 192.9 (C1), 192.0 (C3), 150.6 (C5), 131.7 (C10), 131.4 (C12), 130.9 (C11), 129.8 (C4), 127.3 (C13), 56.3 (C2), 49.1 (C2''), 32.6 (C6), 32.4 (C9), 29.8 ((C3''-H_3)$_3$), 29.0 (CH_2), 28.1 (CH_2), 18.2 (C14); ***m/z*** (ES^+) 309.19 ($[M+H]^+$, 100 %); **HRMS** (ES^+) Calcd for $C_{18}H_{29}O_2S$ $[M+H]^+$: 309.1883, found 309.1883.

***S*-(*tert*-Butyl) 3-(2-methyl-1,2,4a,5,6,7,8,8a-octahydronaphthalen-1-yl)-3-oxopropanethioate ((±)-68)**

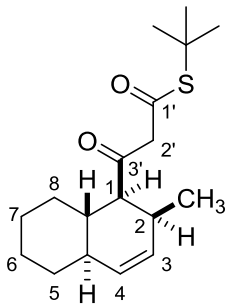

To a solution of **66** (815 mg, 2.64 mmol, 1.0 eq.) in DCM (80 mL) at -78 °C was added $BF_3.Et_2O$ (750 mg, 5.28 mmol, 2.0 eq.) and the reaction was stirred for 1 hour before slowly warming to 0 °C over 5 hours. The reaction was diluted with H_2O (40 mL) and extracted with DCM (3 × 40 mL).The organic layers were combined, washed with brine (40 mL), dried over $MgSO_4$, filtered and concentrated *in vacuo* and purified *via* the Biotage SP4 (silica-packed SNAP column 25 g; 0-2% EtOAc/hexanes) to give the title product (±)-**68** as a colourless oil (636 mg, 78%). In $CDCl_3$ at room temperature the title compound exists as a (3 : 1) *keto* : *enol* mixture. **IR** (thin film) ν_{max}: 2920, 2851, 1717, 1670 (C=O), 1609, 1071; **^{1}H NMR** (500 MHz, Chloroform-*d*) δ(*major keto-form*) 5.54 (ddd, *J* = 10.0, 4.6, 2.6 Hz, 1H, C3-H), 5.39 (dd, *J* = 10.0, 1.8 Hz, 1H, C4-H), 3.63 – 3.42 (m, 2H, C2'-H_2), 2.92 (dd, *J* = 11.3, 5.8 Hz, 1H, C1-H), 2.63 – 2.51 (m, 1H, C2-H), 1.93 – 1.83 (m, 1H, C8-H_2), 1.78 – 1.69 (m, 3H, C5-H_2, C6-H_2, C7-H_2), 1.69 – 1.64 (m, 1H, C4a-H), 1.47 (s, 9H, (CH_3)$_3$), 1.47 – 1.44 (m, 1H, C8a-H), 1.36 – 1.21 (m, 2H, C5-H_2, C6-H_2), 1.12 – 1.01 (m, 1H, C7-H_2), 0.82 (d, *J* = 7.1 Hz, 2H, CH_3), 0.81 – 0.69 (m, 1H, C8-H_2); **^{13}C NMR** (126 MHz, Chloroform-*d*) δ(*major keto-form*) 203.6 (C3'), 192.3 (C1'), 131.4 (C4), 130.6 (C3), 59.4 (C2'), 56.0 (C1), 49.2 (C), 42.2 (C4a), 36.3 (C8a), 33.2 (C5), 31.6 (C2), 29.8 ((CH_3)$_3$), 29.7 (C8), 26.8 (C6), 26.6 (C7), 17.8 (CH_3); **^{1}H NMR** (500 MHz, Chloroform-*d*) δ(*minor enol-form*) 12.96 (d, *J* = 1.3 Hz, 1H, OH), 5.57 – 5.49 (m, 1H, C3-H), 5.39 – 5.35 (m, 1H, C4-H), 5.32 (s, 1H, C2'-H), 2.40 – 2.32 (m, 1H, C2-H), 2.20 (ddd, *J* = 11.0, 5.6, 1.0 Hz, 1H, C1-H), 1.93 – 1.83 (m, 1H, C8-H_2), 1.77 – 1.68 (m, 3H, C5-H_2, C6-H_2, C7-H_2), 1.69 – 1.64 (m, 1H, C4a-H), 1.51 (s, 9H, (CH_3)$_3$), 1.46 – 1.43 (m, 1H, C8a-H), 1.36 – 1.21 (m, 2H, C5-H_2, C6-H_2), 1.13 – 1.01 (m, 1H, C7-H_2), 0.99 (d, *J* = 7.1 Hz, 3H, CH_3), 0.81 – 0.69 (m, 1H, C8-H_2); **^{13}C NMR** (126 MHz, Chloroform-*d*) δ(*minor enol-form*) 196.10 (C1'), 178.15 (C3'), 131.62 (C4), 130.85 (C3), 101.60 (C2'), 49.84 (C1), 48.29 (C), 43.01 (C4a), 36.40 (C8a), 35.05 (C2), 33.29 (C5), 30.36 ((CH_3)$_3$), 30.19 (C8), 26.82 (C6), 26.70 (C7), 18.03 (CH_3); ***m/z*** (ES^+) 331.17 ([M+Na]$^+$, 100 %); **HRMS** (ES^+) Calcd for $C_{18}H_{28}O_2SNa$ [M+Na]$^+$: 331.1708, found 331.1698.

Ethyl (3*S*,4*S*)-3-*iso*propyl-4-(3-(2-methyl-1,2,4a,5,6,7,8,8a-octahydronaphthalen-1-yl)-3-oxopropanamido)-5-oxotetrahydrofuran-3-carboxylate (67a/b)

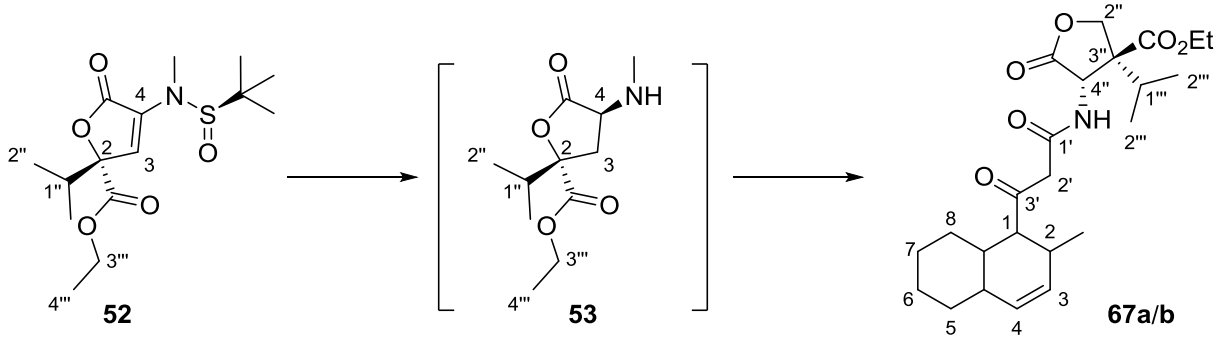

To a solution of **52** (140 mg, 0.42 mmol, 1.0 eq.) in THF (1 mL) at 0 °C was added HCl (0.42 mL, 4 N in dioxane, 4.0 eq.). The reaction was stirred for 10 minutes at this temperature before the addition of a solution of $NaBH_3CN$ (80 mg, 1.27 mmol, 3.0 eq.) in MeOH (2 mL). The reaction was stirred for a further 1 hour at 0 °C before being concentrated *in vacuo*. The residue was partitioned between a saturated aqueous solution of $NaHCO_3$ (5 mL) and EtOAc (5 mL). The aqueous layer was extracted with EtOAc (3 × 10 mL) and the combined organic extracts were washed with brine (10 mL), dried over $MgSO_4$, filtered and concentrated *in vacuo* to yield the crude free amine **53**. To a solution of **53** in anhydrous THF (5 mL) at 0 °C was added (±)-**68** (96 mg, 0.42 mmol, 1.0 eq.) followed by Et_3N (0.23 mL, 1.68 mmol, 4.0 eq.) and CF_3CO_2Ag (186 mg, 0.84 mmol, 2.0 eq.). The reaction was then stirred for 1 hour at 0 °C followed by 1 hour at room temperature. The reaction was concentrated *in vacuo* and purified *via* the Biotage SP4 (silica-packed SNAP column 12 g; 0-40% EtOAc/hexanes) to give the title product **67a**/**b** as a colourless oil (120 mg, 64%). NMR analysis is complicated by the presence of 2 diastereomers (**67a** and **67b**) and *keto*/*enol* tautomers of both. See **67a** and **67b** for the spectroscopic data of each diastereomer.

(2*S*)-2-Hydroxy-2-(((2*S*,*E*)-4-(hydroxy(2-methyl-1,2,4a,5,6,7,8,8a-octahydronaphthalen-1-yl)methylene)-1-methyl-3,5-dioxopyrrolidin-2-yl)methyl)-3-methylbutanoic acid (4a/b)

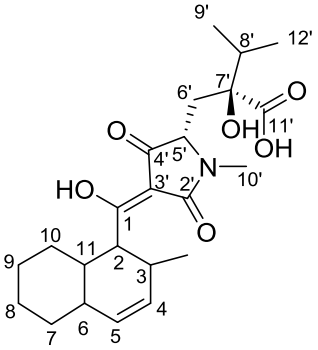

To a solution of **67a**/**b** (100 mg, 0.22 mmol, 1.0 eq.) in THF (5 mL) at 0 °C was added ^{t}BuOK (28 mg, 0.25 mmol, 1.1 eq.) and the reaction was stirred for 1 hour. The reaction was slowly warmed to room temperature and stirred at this temperature for 1 hour. The reaction was concentrated *in vacuo* and the residue partitioned between DCM (5 mL) and an aqueous solution of HCl (5 mL, 1N). The organic layer was separated and washed with an aqueous solution of HCl (5 mL, 1N), brine (5 mL), dried over Na_2SO_4, filtered and concentrated *in vacuo* to give JBIR-22 ethyl ester **77a**/**b** as a colourless oil (100 mg, 100%), which was used in the next step without further purification.

To a solution of **77a**/**b** (90 mg, 0.20 mmol, 1.0 eq.) in EtOH (2 mL) was added an aqueous solution of NaOH (1 mL, 2N) and the reaction was heated to 110 °C under microwave irradiation for 20 minutes. The reaction was diluted with an aqueous solution of HCl (5 mL, 1N) and extracted with DCM (3 × 5 mL). The organic layers were combined, washed with brine (10 mL), dried over Na_2SO_4, filtered, concentrated *in vacuo* and purified *via* the Biotage SP4 (Reverse-phase silica-packed SNAP column 4 g; 20-100% H_2O/(MeOH:MeCN)) to give the title product **77a**/**b** as an amorphous white solid (73 mg, 87%). See **4a** and **4b** for the spectroscopic data of each diastereomer.

Ethyl (2*E*,8*E*,10*E*)-dodeca-2,8,10-trienoate (87)[260]

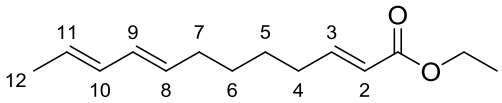

To a solution of di*iso*propyl(ethoxycarbonylmethyl) phosphonate **86** (5.86 mL, 24.6 mmol, 1.0 eq.) in THF (250 mL) at -78 °C was added LiHMDS (25.9 mmol, 1.05 eq., 1 M in THF) and the reaction was stirred for 30 minutes. A solution of **75** (3.75 g, 24.6 mmol, 1.0 eq.) in THF (40 mL) was then added and the reaction was stirred for a further 1.5 hours at -78 °C before stirring at 0 °C for 1.5 hours followed by 30 minutes at room temperature. The reaction was quenched by addition of a saturated aqueous solution of NH_4Cl (100 mL). The reaction was extracted with EtOAc (3 × 100 mL). The organic extracts were combined, washed with brine (50 mL), dried over Na_2SO_4, filtered, concentrated *in vacuo* and purified *via* the Biotage SP4 (silica-packed SNAP column 300 g; 0-10% EtOAc/hexanes) to give the title product **87** as a colourless oil (4.83 g, 88%). **^{1}H NMR** (500 MHz, Chloroform-*d*) δ 6.95 (dt, *J* = 15.6, 7.0 Hz, 1H, C3-H), 6.08 – 5.90 (m, 2H, C9-H, C10-H), 5.80 (dt, *J* = 15.6, 1.6 Hz, 1H, C2-H), 5.63 – 5.46 (m, 2H, C8-H, C11-H), 4.18 (q, *J* = 7.1 Hz, 2H, OCH_2CH_3), 2.26 – 2.14 (m, 2H, C4-H_2), 2.06 (dt, *J* = 7.0, 7.0 Hz, 2H, C7-H_2), 1.72 (d, *J* = 6.3 Hz, 3H, C12-H_3), 1.54 – 1.36 (m, 4H, C5-H_2, C6-H_2), 1.28 (t, *J* = 7.1 Hz, 3H, OCH_2CH_3); **^{13}C NMR** (126 MHz, Chloroform-*d*) δ 166.9 (C1), 149.3 (C3), 131.7 (C8), 131.5 (C10), 130.8 (C9), 127.2 (C11), 121.5 (C2), 60.3 (OCH_2CH_3), 32.4 (C7), 32.2 (C4), 29.0 (C6), 27.6 (C5), 18.2 (C12), 14.4 (OCH_2CH_3); ***m/z*** (ES^+) 245.13 ($[M+Na]^+$, 100 %). Spectroscopic data are in accordance with the literature.[260]

(2*E*,8*E*,10*E*)-Dodeca-2,8,10-trien-1-ol (88)[221]

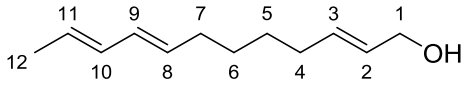

To a solution of **87** (4.83 g, 21.7 mmol, 1.0 eq.) in DCM (210 mL) at -78 °C was added DIBAL-H (54.3 mmol, 2.5 eq., 1.1 M in cyclohexane) and the reaction was stirred for 30 minutes before being quenched by addition of MeOH (24 mL). Upon warming to room temperature, a saturated solution of sodium potassium tartrate (200 mL) was added and the mixture was stirred vigorously for 12 hours. The mixture was extracted with DCM (3 × 100 mL). The organic extracts were combined, washed with brine (100 mL), dried over Na_2SO_4, filtered, concentrated *in vacuo* and purified *via* the Biotage SP4 (silica-packed SNAP column 300 g; 0-20% EtOAc/hexanes) to give the title product **88** as a colourless oil (3.80 g, 97%). **^{1}H NMR** (500 MHz, Chloroform-*d*) δ 6.07 – 5.93 (m, 2H, C9-H, C10-H), 5.70 – 5.63 (m, 2H, C2-H, C3-H), 5.63 – 5.48 (m, 2H, C8-H, C11-H), 4.08 (d, *J* = 5.4 Hz, 2H, C1-H_2), 2.13 – 1.96 (m, 4H, C4-H_2, C7-H_2), 1.72 (d, *J* = 6.3 Hz, 3H, C12-H_3), 1.46 – 1.33 (m, 4H, C5-H_2, C6-H_2); **^{13}C NMR** (126 MHz, Chloroform-*d*) δ 133.5 (C3), 132.0 (C8), 131.8 (C10), 130.5 (C9), 129.1 (C2), 127.0 (C11), 64.0 (C1), 32.5 (C7), 32.2 (C4), 29.1 (C6), 28.8 (C5), 18.2 (C12). Spectroscopic data are in accordance with the literature.[221]

(2*E*,8*E*,10*E*)-Dodeca-2,8,10-trienal (69)[221]

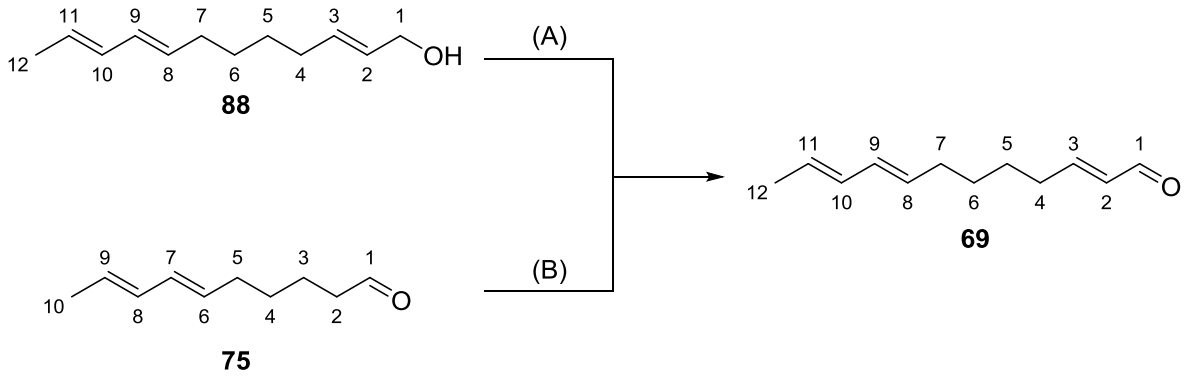

Route A: To a solution of **88** (1.19 g, 6.57 mmol, 1.0 eq.) in DCM (40 mL) at room temperature was added Dess-Martin Periodinane (4.18 g, 9.86 mmol, 1.5 eq.). After stirring for 30 minutes, H_2O (0.18 mL, 9.86 mmol, 1.5 eq.) was added and the reaction stirred for a further 30 minutes. The reaction was concentrated *in vacuo*, diluted with EtOAc (80 mL) and a 1:1 (v:v) 10% sodium thiosulfate: saturated sodium bicarbonate solution (40 mL). After stirring for 30 minutes, the organic layer was separated and the aqueous layer was extracted with EtOAc (3 × 40 mL). The organic layers were combined, washed with a saturated aqueous solution of $NaHCO_3$ (3 × 40 mL), brine (40 mL), dried over Na_2SO_4, filtered and concentrated *in vacuo* to give the title product **69** as a colourless oil which was used directly in the next step without further purification (1.17 g, 100%).

Route B: To a solution of (1,3-dioxolan-2-ylmethyl)triphenylphosphonium bromide **89** (368 mg, 0.85 mmol, 1.3 eq.), in anhydrous THF (2 mL) at 0 °C was added ^{t}BuOK (1.05 mL, 1.6 eq., 1 M in THF) dropwise. The mixture was stirred for 30 minutes before the addition of a solution of **75** (100 mg, 0.66 mmol, 1.0 eq.) in anhydrous THF (2.5 mL). The reaction was stirred at 0 °C for 3 hours. A 10% aqueous solution of oxalic acid (5 mL) was added and the reaction was stirred at room temperature for a further 1 hour. The mixture was extracted with Et_2O (4 × 10 mL) and the combined organic layers were washed with a saturated aqueous solution of $NaHCO_3$ (10 mL), brine (10 mL), dried over Na_2SO_4, filtered, concentrated *in vacuo* and purified *via* the Biotage SP4 (silica-packed SNAP column 4 g; 0-2% EtOAc/hexanes) to give the title product **69** as a colourless oil (75 mg, 64%). **^{1}H NMR** (500 MHz, Chloroform-*d*) δ 9.50 (d, *J* = 7.9 Hz, 1H, C1-H), 6.84 (dt, *J* = 15.5, 6.8 Hz, 1H, C3-H), 6.11 (ddt, *J* = 15.5, 7.9, 1.5 Hz, 1H, C2-H), 6.04 – 5.95 (m, 2H, C9-H, C10-H), 5.63 – 5.55 (m, 1H, C11-H), 5.56 – 5.47 (m, 1H, C8-H), 2.39 – 2.29 (m, 2H, C4-H_2), 2.08 (td, *J* = 7.1, 7.1 Hz, 2H, C7-H_2), 1.73 (d, *J* = 6.2 Hz, 3H, C12-H_3), 1.58 – 1.47 (m, 2H, C5-H_2), 1.49 – 1.39 (m, 2H, C6-H_2); **^{13}C NMR** (126 MHz, Chloroform-*d*) δ 194.3 (C1), 158.9 (C3), 133.2 (C2), 131.6 (C8), 131.2 (C10), 130.9 (C9), 127.4 (C11), 32.7 (C7), 32.3 (C4), 29.0 (C6), 27.4 (C5), 18.2 (C12). Spectroscopic data are in accordance with the literature.[221]

2-Methyl-1,2,4a,5,6,7,8,8a-octahydronaphthalene-1-carbaldehyde (78)[221,233]

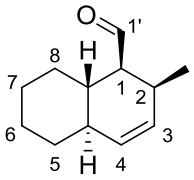

78a
(1*S*, 2*S*, 4a*R*, 8a*S*)

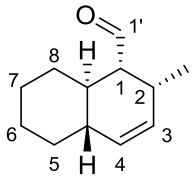

78b
(1*R*, 2*R*, 4a*S*, 8a*R*)

To **69** (**78a**, 1.25 g, 7.01 mmol, 1.0 eq.; **78b**, 1.45 g, 8.13 mmol, 1.0 eq.; 85% *E*,*E*-diene geometry) in a 2% v/v solution of H_2O/MeCN (3.3 mL/mmol) at -5 °C was added a solution of (2*S*,5*S*)-5-benzyl-2-*tert*butyl-3-methylimidazolidin-4-one trifluoromethanesulfonic acid salt (1.4 mL, 0.2 eq., 1M in MeCN) for **78a**, or (2*R*,5*R*)-5-benzyl-2-*tert*butyl-3-methylimidazolidin-4-one trifluoromethanesulfonic acid salt (1.63 mL, 0.2 eq., 1M in MeCN) for **78b**. The reaction was stirred at -5 °C for 48 hours before being concentrated *in vacuo* and purified *via* the Biotage SP4 (silica-packed SNAP column 4 g; 0-2% EtOAc/hexanes) to give **78a** (0.69 g, 65%,[1] *dr* 4:1,[2] 87% ee[3]) and **78b** (0.84 g, 68%,[1] *dr* 4:1,[2] 84% ee[3]) as colourless oils. [1]Yields reported based on the conversion of the *E*,*E*-diene substrate to IMDA product. [2]Diastereomeric ratios were determined by ^{1}H NMR analysis. [3]Enantiomeric purity was determined by chiral GC analysis of the corresponding alcohols (**90a** & **90b**). **^{1}H NMR** (500 MHz, Chloroform-*d*) δ 9.75 (d, *J* = 4.3 Hz, 1H, C1'-H), 5.54 (ddd, *J* = 9.9, 4.5, 2.6 Hz, 1H, C3-H), 5.42 (d, *J* = 9.9 Hz, 1H, C4-H), 2.66 – 2.51 (m, 1H, C2-H), 2.38 (ddd, *J* = 11.4, 6.0, 4.3 Hz, 1H, C1-H), 1.85 – 1.71 (m,

4H, C5-H$_2$, C6-H$_2$, C7-H$_2$, C8-H$_2$), 1.74 – 1.64 (m, 1H, C4a-H), 1.67 – 1.58 (m, 1H, C8a-H), 1.39 – 1.29 (m, 2H, C6-H$_2$, C7-H$_2$), 1.17 – 1.07 (m, 1H, C5-H$_2$), 1.04 (d, *J* = 7.1 Hz, 3H, CH$_3$), 1.02 – 0.93 (m, 1H, C8-H$_2$); **^{13}C NMR** (126 MHz, Chloroform-*d*) δ 207.2 (C1'), 131.4 (C4), 131.1 (C3), 55.6 (C1), 42.2 (C4a), 35.7 (C8a), 33.1 (C5), 31.9 (C2), 30.3 (C8), 26.7 (CH$_2$), 26.6 (CH$_2$), 17.1 (CH$_3$). Spectroscopic data are in accordance with the literature.[221,233]

2-Methyl-1,2,4a,5,6,7,8,8a-octahydronaphthalen-1-yl)methanol (90)[233]

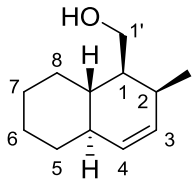

90a
(1*S*, 2*S*, 4a*R*, 8a*S*)

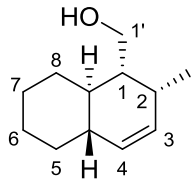

90b
(1*R*, 2*R*, 4a*S*, 8a*R*)

$NaBH_4$ (1.5 eq.) was added slowly to a solution of **78a** (40 mg, 0.22 mmol, 1.0 eq.) or **78b** (83 mg, 0.47 mmol, 1.0 eq.) in EtOH (5 mL/mmol) at 0 °C, and the reaction was stirred for 1 hour. The reaction was quenched by addition of a saturated aqueous solution of NH_4Cl and extracted with Et_2O. The organic layers were combined, washed with H_2O, brine, dried over Na_2SO_4, filtered, concentrated *in vacuo* and purified *via* the Biotage SP4 (silica-packed SNAP column; 0-10% EtOAc/hexanes) to give **90a** (35 mg, 88%, dr 4:1) and **90b** (77 mg, 91%, dr 4:1) as white solids. **90a** - Chiral GC analysis Agilent Cyclosil-B (length: 30 m, thickness: 0.250 mm, film thickness: 0.25 µm), carrier gas: He, linear velocity: 40 cm/sec, temperature: 140 °C, tR minor (1*R,* 2*R*, 4a*S*, 8a*R*) 23.0 min, tR major (1*S,* 2*S*, 4a*R*, 8a*S*) 23.6 min, 87% ee; **90b** - Chiral GC analysis Agilent Cyclosil-B (length: 30 m, thickness: 0.250 mm, film thickness: 0.25 µm), carrier gas: He, linear velocity: 40 cm/sec, temperature: 140 °C, tR major (1*R,* 2*R*, 4a*S*, 8a*R*) 23.0 min, tR minor (1*S,* 2*S*, 4a*R*, 8a*S*) 23.8 min, 84% ee; **^{1}H NMR** (400 MHz, Chloroform-*d*) δ 5.59 (ddd, *J* = 9.9, 4.8, 2.6 Hz, 1H, C3-H), 5.36 (d, *J* = 9.9 Hz, 1H, C4-H), 3.83 (dd, *J* = 10.7, 5.4 Hz, 1H, C1'-H$_2$), 3.53 (dd, *J* = 10.7, 9.3 Hz, 1H, C1'-H$_2$), 2.49 – 2.33 (m, 1H, C2-H), 1.81 – 1.64 (m, 6H, C1-H, C4a-H, C5-H$_2$, C6-H$_2$, C7-H$_2$, C8-H$_2$), 1.36 – 1.18 (m, 2H, C6-H$_2$, C7-H$_2$), 1.16 – 1.06 (m, 1H, C8a-H), 1.06 – 0.95 (m, 2H, C5-H$_2$, C8-H$_2$), 0.92 (d, *J* = 7.0 Hz, 3H, CH$_3$); **^{13}C NMR** (101 MHz, Chloroform-*d*) δ 132.4 (C3), 131.4 (C4), 63.2 (C1'), 44.3 (C1), 43.7 (C4a), 37.8 (C8a), 33.4 (C5), 31.6 (C2), 29.4 (C8), 26.9 (CH$_2$), 26.7 (CH$_2$), 15.6 (CH$_3$). Spectroscopic data is in accordance with the literature.[233]

***S*-(*tert*-Butyl) 3-hydroxy-3-(2-methyl-1,2,4a,5,6,7,8,8a-octahydronaphthalen-1-yl)propanethioate (93)**

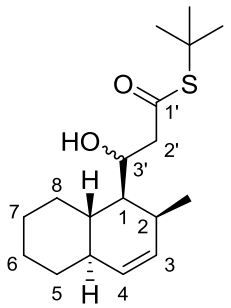

93a
(1*S*, 2*S*, 4a*R*, 8a*S*)

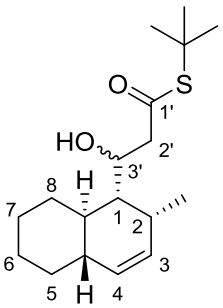

93b
(1*R*, 2*R*, 4a*S*, 8a*R*)

To a solution of *i*-Pr_2NH (1.3 eq.) in anhydrous THF (4 mL/mmol) was added *n*-BuLi (1.2 eq., 2.3 M in hexanes) at 0 °C and the mixture was stirred for 30 minutes. The solution was then cooled to -78 °C and a solution of *S-tert*-butyl-thioacetate **92** (1.5 eq.) in anhydrous THF (2 mL/mmol) was added. After a further 30 minutes at -78 °C, a solution of **78a** (0.34 g, 1.9 mmol, 1.0 eq.) or **78b** (0.5 g, 2.8 mmol, 1.0 eq.) in anhydrous THF (2 mL/mmol) was added, and the reaction was stirred for 2 hours. The reaction was quenched by the addition of a saturated aqueous solution of NH_4Cl, warmed to room temperature and extracted with EtOAc. The organic layers were combined, washed with H_2O, brine, dried over Na_2SO_4, filtered, concentrated *in vacuo* and purified *via* the Biotage SP4 (silica-packed SNAP column; 0-5% EtOAc/hexanes) to give **93a** (0.38 g, 66%) and **93b** (0.60 g, 69%) as colourless oils. **93a** and **93b** were obtained as an inconsequential 7:3 mixture of diastereomers. **IR** (thin film) ν_{max}: 2920, 2851, 1680, 1670, 1456, 1364, 1030; **^{1}H NMR** (400 MHz, Chloroform-*d*) δ(*major diastereomer*) 5.53 (ddd, *J* = 9.9, 4.9, 2.5 Hz, 1H, C3-H), 5.33 (d, *J* = 9.9 Hz, 1H, C4-H), 4.25 – 4.11 (m, 1H, C3'-H), 2.79 (dd, *J* = 15.8, 9.3 Hz, 1H, C2'-H_2), 2.70 (dd, *J* = 15.8, 2.9 Hz, 1H, C2'-H_2), 2.52 (d, *J* = 3.8 Hz, 1H, OH), 2.33 – 2.22 (m, 1H, C2-H), 2.08 – 1.97 (m, 1H, C8-H_2), 1.85 – 1.67 (m, 4H, C4a-H, C5-H_2, C6-H_2, C7-H_2), 1.66 – 1.58 (m, 1H, C1-H), 1.47 (s, 9H, (CH_3)$_3$), 1.34 – 1.23 (m, 3H, C8a-H, C6-H_2, C7-H_2), 1.18 – 1.03 (m, 2H, C5-H_2, C8-H_2), 0.99 (d, *J* = 7.0 Hz, 3H, CH_3); **^{13}C NMR** (101 MHz, Chloroform-*d*) δ(*major diastereomer*) 201.1 (C1'), 132.4 (C3), 131.5 (C4), 70.7 (C3'), 50.4 (C2'), 46.9 (C1), 44.5 (C4a), 38.4 (C8a), 33.9 (C2), 33.7 (C5), 31.3 (C8), 29.9 ((CH_3)$_3$), 27.2 (CH_2), 26.7 (CH_2), 17.0 (CH_3); **^{1}H NMR** (400 MHz, Chloroform-*d*) δ(*minor diastereomer*) 5.51 (ddd, *J* = 9.9, 5.0, 2.6 Hz, 1H, C3-H), 5.32 (d, *J* = 9.9 Hz, 1H, C4-H), 4.46 – 4.33 (m, 1H, C3'-H), 2.81 (dd, *J* = 15.7, 10.0 Hz, 1H, C2'-H_2), 2.59 (dd, *J* = 15.7, 2.5 Hz, 1H, C2'-H_2), 2.39 (d, *J* = 3.2 Hz, 1H, OH), 2.36 – 2.25 (m, 1H, C2-H), 2.09 – 1.99 (m, 1H, C8-H_2), 1.87 – 1.64 (m, 4H, C4a-H, C5-H_2, C6-H_2, C7-H_2), 1.47 (s, 9H, (CH_3)$_3$), 1.45 – 1.41 (m, 1H, C1-H), 1.42 – 1.34 (m, 1H, C8a-H), 1.34 – 1.21 (m, 2H, C6-H_2, C7-H_2), 1.14 – 1.02 (m, 1H, C5-H_2), 1.07 (d, *J* = 7.0 Hz, 3H, CH_3), 1.04 – 0.94 (m, 1H, C8-H_2); **^{13}C NMR** (101 MHz, Chloroform-*d*) δ(*minor diastereomer*) 201.2 (C1'), 132.8 (C3), 130.9 (C4), 68.1 (C3'), 49.3 (C2'), 46.4 (C1), 44.6 (C4a),

36.9 (C8a), 33.5 (C5), 31.6 (C2), 29.9 (($\underline{C}H_3)_3$), 29.3 (C8), 26.9 ($\underline{C}H_2$), 26.8 ($\underline{C}H_2$), 18.3 ($\underline{C}H_3$); ***m/z*** (ES^+) 333.19 ($[M+Na]^+$, 100 %); **HRMS** (ES^+) Calcd for $C_{18}H_{30}O_2SNa$ $[M+Na]^+$: 333.1864, found 333.1855.

***S*-(*tert*-Butyl) 3-(2-methyl-1,2,4a,5,6,7,8,8a-octahydronaphthalen-1-yl)-3-oxopropanethioate (68)**

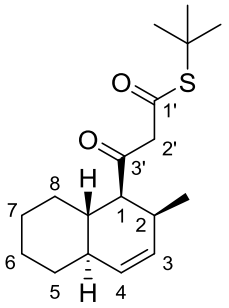

68a
(1*S*, 2*S*, 4a*R*, 8a*S*)

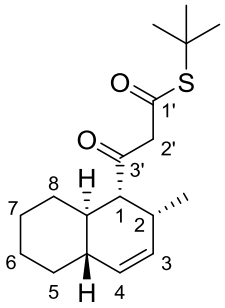

68b
(1*R*, 2*R*, 4a*S*, 8a*R*)

To a solution of **93a** (0.29 g, 0.93 mmol, 1.0 eq.) or **93b** (0.58 g, 1.88 mmol, 1.0 eq.) in DCM (10 mL/mmol) at room temperature was added Dess-Martin Periodinane (1.2 eq.). The reaction was stirred for 2 hours before being quenched by addition of a 1:1 (v:v) saturated sodium thiosulfate: saturated sodium bicarbonate solution (10 mL/mmol). The mixture was extracted with DCM. The organic extracts were combined, washed with brine, dried over Na_2SO_4, filtered, concentrated *in vacuo* and purified *via* the Biotage SP4 (silica-packed SNAP column; 0-1% EtOAc/hexanes) to give **68a** (0.23 g, 79%, dr 4:1) and **68b** (0.48 g, 82%, dr 4:1). Spectroscopic data for the major diastereomer was in accordance with that obtained for **68a**/**b**.

Ethyl (2*S*,4*S*)-2-*iso*propyl-4-(*N*-methyl-3-((1*S*,2*S*,4a*R*,8a*S*)-2-methyl-1,2,4a,5,6,7,8,8a-octahydronaphthalen-1-yl)-3-oxopropanamido)-5-oxotetrahydrofuran-2-carboxylate (67a)

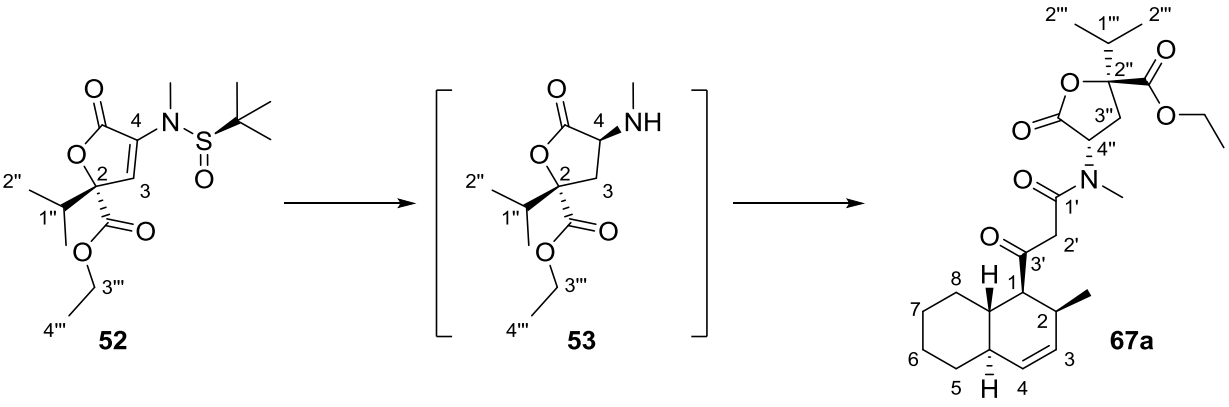

52 **53** **67a**

To a solution of **52** (0.32 g, 0.97 mmol, 1.0 eq.) in THF (2.5 mL) at 0 °C was added HCl (0.97 mL, 4 eq., 4 N in dioxane). The reaction was stirred for 10 minutes at this temperature before the addition of a solution of $NaBH_3CN$ (0.18 g, 2.92 mmol, 3.0 eq.) in MeOH (5 mL). The reaction was stirred for a further 1 hour at 0 °C before being concentrated *in vacuo*. The residue was partitioned between a

saturated aqueous solution of $NaHCO_3$ (5 mL) and EtOAc (5 mL). The aqueous layer was extracted with EtOAc (3 × 5 mL) and the combined organic extracts were washed with brine (10 mL), dried over Na_2SO_4, filtered and concentrated *in vacuo* to yield the crude free amine **53**. To a solution of **53** in anhydrous THF (12 mL) at 0 °C was added **68a** (0.27 g, 0.88 mmol, 0.9 eq.) followed by Et_3N (0.54 mL, 3.89 mmol, 4.0 eq.) and CF_3CO_2Ag (0.43 g, 1.95 mmol, 2.0 eq.). The reaction was then stirred for 1 hour at 0 °C followed by 1 hour at room temperature. The reaction was concentrated *in vacuo* and purified *via* the Biotage SP4 (silica-packed SNAP column 12 g; 0-40% EtOAc/hexanes) to give **67a** as a pale yellow oil (0.30 g, 76%). **IR** (thin film) ν_{max}: 2963, 2922, 2853, 1786, 1734 (C=O), 1717, 1647 (C=O), 1260, 1022; **^{1}H NMR** (500 MHz, Chloroform-*d*) δ 5.55 (ddd, *J* = 9.9, 4.7, 2.6 Hz, 1H, C3-H), 5.39 (d, *J* = 9.9 Hz, 1H, C4-H), 4.76 (dd, *J* = 11.5, 9.1 Hz, 1H, C4''-H), 4.33 – 4.19 (m, 2H, $CO_2CH_2CH_3$), 3.60 (d, *J* = 15.1 Hz, 1H, C2'-H_2), 3.53 (d, *J* = 15.1 Hz, 1H, C2'-H_2), 3.02 (s, 3H, NCH_3), 3.00 – 2.93 (m, 1H, C1-H), 2.68 (dd, *J* = 12.8, 9.1 Hz, 1H, C3''-H_2), 2.65 – 2.57 (m, 1H, C2-H), 2.48 (dd, *J* = 12.8, 11.5 Hz, 1H, C3''-H_2), 2.39 – 2.30 (m, 1H, C1'''-H), 1.93 – 1.82 (m, 1H, C8-H_2), 1.79 – 1.66 (m, 4H, C4a-H, C5-H_2, C6-H_2, C7-H_2), 1.52 – 1.42 (m, 1H, C8a-H), 1.37 – 1.27 (m, 2H, C6-H_2, C7-H_2), 1.32 (t, *J* = 7.2 Hz, 3H, $CO_2CH_2CH_3$), 1.31 – 1.22 (m, 1H, C8-H_2), 1.09 – 0.99 (m, 1H, C5-H_2), 1.05 (d, *J* = 7.1 Hz, 3H, C2'''-H_3), 1.03 (d, *J* = 6.8 Hz, 3H, C2'''-H_3), 0.83 (d, *J* = 7.1 Hz, 3H, CH_3); **^{13}C NMR** (126 MHz, Chloroform-*d*) δ 205.7 (C3'), 172.1 (C1''), 171.0 (CO_2Et), 167.2 (C1'), 131.4 (C4), 130.5 (C3), 87.2 (C2''), 62.4 ($CO_2CH_2CH_3$), 56.8 (C4''), 55.8 (C1), 50.3 (C2'), 42.1 (C4a), 36.3 (C8a), 35.6 (NCH_3), 34.2 (C1'''), 33.2 (C5), 31.7 (C2), 31.4 (C3''), 29.6 (C8), 26.7 (CH_2), 26.6 (CH_2), 17.8 (CH_3), 17.0 (C2'''), 16.5 (C2'''), 14.3 ($CO_2CH_2CH_3$); ***m/z*** (ES$^+$) 470.25 ([M+Na]$^+$, 100 %); **HRMS** (ES$^+$) Calcd for $C_{25}H_{37}O_6NNa$ [M+Na]$^+$: 470.2513, found 470.2507.

Ethyl (2*S*,4*S*)-2-*iso*propyl-4-(*N*-methyl-3-((1*R*,2*R*,4a*S*,8a*R*)-2-methyl-1,2,4a,5,6,7,8,8a-octahydronaphthalen-1-yl)-3-oxopropanamido)-5-oxotetrahydrofuran-2-carboxylate (67b)

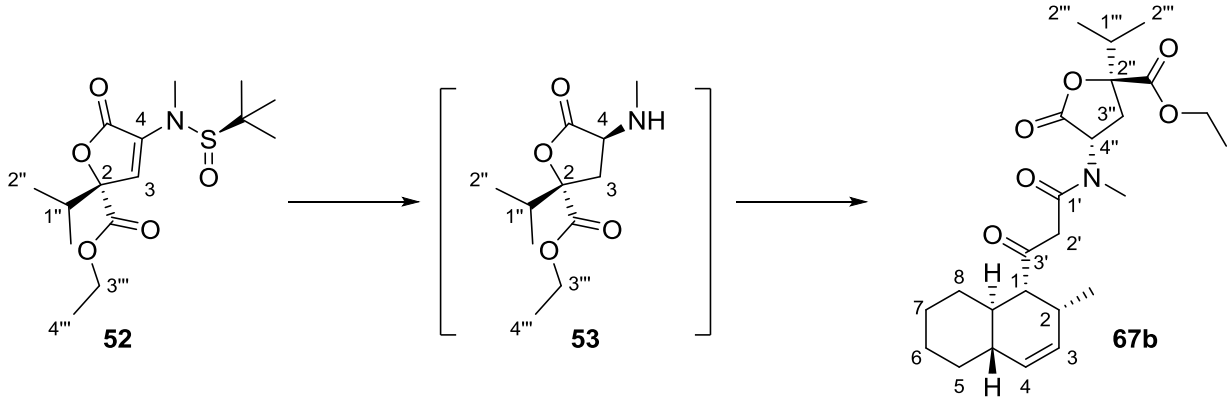

To a solution of **52** (0.31 g, 0.95 mmol, 1.0 eq.) in THF (2.5 mL) at 0 °C was added HCl (0.95 mL, 4 eq., 4 N in dioxane). The reaction was stirred for 10 minutes at this temperature before the addition of a solution of $NaBH_3CN$ (0.18 g, 2.85 mmol, 3.0 eq.) in MeOH (5 mL). The reaction was stirred for a

further 1 hour at 0 °C before being concentrated *in vacuo*. The residue was partitioned between a saturated aqueous solution of $NaHCO_3$ (5 mL) and EtOAc (5 mL). The aqueous layer was extracted with EtOAc (3 × 5 mL) and the combined organic extracts were washed with brine (10 mL), dried over Na_2SO_4, filtered and concentrated *in vacuo* to yield the crude free amine **53**. To a solution of **53** in anhydrous THF (12 mL) at 0 °C was added **68b** (0.26 g, 0.86 mmol, 0.9 eq.) followed by Et_3N (0.53 mL, 3.82 mmol, 4.0 eq.) and CF_3CO_2Ag (0.42 g, 1.91 mmol, 2.0 eq.). The reaction was then stirred for 1 hour at 0 °C followed by 1 hour at room temperature. The reaction was concentrated *in vacuo* and purified *via* the Biotage SP4 (silica-packed SNAP column 12 g; 0-40% EtOAc/hexanes) to give **77b** as a pale yellow oil (0.27 g, 71%). **IR** (thin film) ν_{max}: 2924, 2853, 1790, 1734 (C=O), 1717, 1647 (C=O), 1624, 1261, 1022; **^{1}H NMR** (500 MHz, Chloroform-*d*) δ 5.55 (ddd, *J* = 9.9, 4.7, 2.6 Hz, 1H, C3-H), 5.39 (d, *J* = 9.9 Hz, 1H, C4-H), 5.01 (dd, *J* = 11.6, 9.1 Hz, 1H, C4''-H), 4.33 – 4.20 (m, 2H, $CO_2CH_2CH_3$), 3.59 (s, 2H, C2'-H_2), 2.99 (s, 3H, NCH_3), 2.97 – 2.91 (m, 1H, C1-H), 2.71 (dd, *J* = 12.9, 9.1 Hz, 1H, C3''-H_2), 2.66 – 2.57 (m, 1H, C2-H), 2.42 (dd, *J* = 12.9, 11.6 Hz, 1H, C3''-H_2), 2.38 – 2.30 (m, 1H, C1'''-H), 1.90 – 1.81 (m, 1H, C8-H_2), 1.79 – 1.65 (m, 4H, C4a-H, C5-H_2, C6-H_2, C7-H_2), 1.53 – 1.42 (m, 1H, C8a-H), 1.32 (t, *J* = 7.1 Hz, 3H, $CO_2CH_2CH_3$), 1.37 – 1.27 (m, 3H, C6-H_2, C7-H_2, C8-H_2), 1.05 (d, *J* = 6.9 Hz, 3H, C2'''-H_3), 1.09 – 0.99 (m, 1H, C5-H_2), 1.03 (d, *J* = 6.8 Hz, 3H, C2'''-H_3), 0.84 (d, *J* = 7.1 Hz, 3H, CH_3); **^{13}C NMR** (126 MHz, Chloroform-*d*) δ 205.7 (C3'), 172.3 (C1''), 170.9 (CO_2Et), 167.4 (C1'), 131.4 (C4), 130.5 (C3), 87.1 (C2''), 62.4 ($CO_2CH_2CH_3$), 55.9 (C4'', C1), 50.4 (C2'), 42.2 (C4a), 36.4 (C8a), 34.7 (NCH_3), 34.3 (C1'''), 33.2 (C5), 31.7 (C2), 31.5 (C3''), 29.7 (C8), 26.8 (CH_2), 26.6 (CH_2), 17.8 (CH_3), 17.0 (C2'''), 16.4 (C2'''), 14.3 ($CO_2CH_2CH_3$); ***m/z*** (ES$^+$) 470.25 ([M+Na]$^+$, 100 %); **HRMS** (ES$^+$) Calcd for $C_{25}H_{37}O_6NNa$ [M+Na]$^+$: 470.2513, found 470.2506.

(1*S*,2*S*,4a*R*,8a*S*,5'*S*,7'*S*) – JBIR-22 (4a)

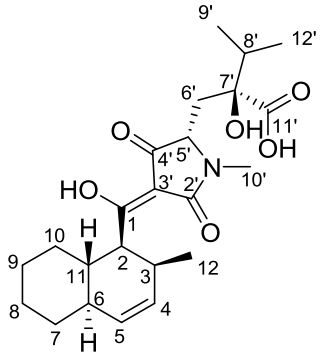

To a solution of **67a** (226 mg, 0.50 mmol, 1.0 eq.) in THF (10 mL) at 0 °C was added ^{t}BuOK (62 mg, 0.56 mmol, 1.1 eq.) and the reaction was stirred for 1 hour. The reaction was slowly warmed to room temperature and stirred at this temperature for 1 hour. The reaction was concentrated *in vacuo* and the residue partitioned between DCM (10 mL) and an aqueous solution of HCl (10 mL,

1N). The aqueous layer was separated and extracted with DCM (3 × 10 mL). The organic extracts were combined, washed with an aqueous solution of HCl (5 mL, 1 N), brine (5 mL), dried over Na_2SO_4, filtered and concentrated *in vacuo* to give JBIR-22 ethyl ester **77a** as a colourless oil (226 mg, 100%), which was used in the next step without further purification. To a solution of **77a** (215 mg, 0.48 mmol, 1.0 eq.) in EtOH (4 mL) was added an aqueous solution of NaOH (3 mL, 2N) and the reaction was heated to 110 °C under microwave irradiation for 20 minutes. The reaction was diluted with an aqueous solution of HCl (5 mL, 1N) and extracted with DCM (3 × 5 mL). The organic extracts were combined, washed with brine (10 mL), dried over Na_2SO_4, filtered, concentrated *in vacuo* and purified *via* the Biotage SP4 (Reverse-phase silica-packed SNAP column 4 g; 20-100% H_2O/(MeOH:MeCN)) to give the title product **4a** as an orange solid (143 mg, 71%). A portion of **4a** was treated with Et_2N to form the salt. Spectroscopic data was obtained for the JBIR-22 **4a**-Et_2N salt. $[\alpha]_D^{20}$= +71.4 (*c* 0.7, MeOH); **IR** (thin film) ν_{max}: 2920, 2849, 1645, 1616, 1570, 1447, 1387, 1233, 1032, 999, 891, 779; **^{1}H NMR** (500 MHz, Acetone-d_6) δ 5.54 (ddd, *J* = 9.8, 4.5, 2.5 Hz, 1H, C4-H), 5.30 (d, *J* = 9.8 Hz, 1H, C5-H), 3.90 (dd, *J* = 11.5, 5.8 Hz, 1H, C2-H), 3.41 (dd, *J* = 10.0, 1.3 Hz, 1H, C5'-H), 2.73 (s, 3H, C10'-H_3), 2.70 – 2.59 (m, 1H, C3-H), 2.31 (dd, *J* = 13.7, 1.3 Hz, 1H, C6'-H_2), 2.04 – 1.97 (m, 1H, C8'-H), 2.00 – 1.91 (m, 1H, C10-H_2), 1.73 – 1.70 (m, 1H, C7-H_2), 1.70 – 1.67 (m, 1H, C6-H), 1.67 – 1.65 (m, 2H, C8-H_2, C9-H_2), 1.62 (dd, *J* = 13.7, 10.0 Hz, 1H, C6'-H_2), 1.52 – 1.38 (m, 1H, C11-H), 1.30 – 1.28 (m, 2H, C8-H_2, C9-H_2), 1.09 – 0.97 (m, 1H, C7-H_2), 0.91 (d, *J* = 6.6 Hz, 3H, C9'-H_3), 0.90 (d, *J* = 6.6 Hz, 3H, C12'-H_3), 0.77 (d, *J* = 7.2 Hz, 3H, C12-H_3), 0.75 – 0.63 (m, 1H, C10-H_2); **^{13}C NMR** (126 MHz, Acetone-d_6) δ 196.3 (C1), 196.1 (C4'), 180.9 (C11'), 174.7 (C2'), 133.6 (C4), 131.1 (C5), 101.9 (C3'), 80.0 (C7'), 63.3 (C5'), 51.0 (C2), 43.4 (C6), 37.4 (C11), 37.3 (C6'), 36.6 (C8'), 34.4 (C7), 32.2 (C3), 31.1 (C10), 27.7 (C9), 27.6 (C8), 26.9 (C10'), 18.8 (C9'), 18.4 (C12), 16.9 (C12'). ***m/z*** (ES^-) 418.22 ($[M-H]^-$, 100 %); **HRMS** (ES^-) Calcd for $C_{23}H_{32}O_6N$ $[M-H]^-$: 418.2235, found 418.2226.

(1*R*,2*R*,4a*S*,8a*R*,5'*S*,7'*S*) – JBIR-22 (4b)

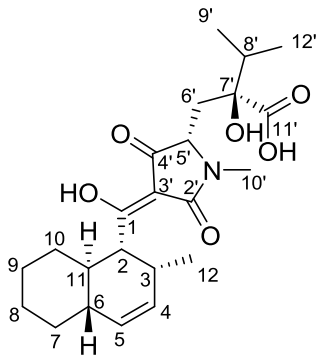

To a solution of **67b** (121 mg, 0.27 mmol, 1.0 eq.) in THF (5 mL) at 0 °C was added ^{t}BuOK (34 mg, 0.30 mmol, 1.1 eq.) and the reaction was stirred for 1 hour. The reaction was slowly warmed to

room temperature and stirred at this temperature for 1 hour. The reaction was concentrated and the residue partitioned between DCM (5 mL) and an aqueous solution of HCl (5 mL, 1N). The aqueous layer was separated and extracted with DCM (3 × 10 mL). The organic extracts were combined, washed with HCl (5 mL, 1 N), brine (5 mL), dried over Na_2SO_4, filtered and concentrated *in vacuo* to give JBIR-22 ethyl ester **77b** as a colourless oil (121 mg, 100%), which was used in the next step without further purification. To a solution of **77b** (110 mg, 0.25 mmol, 1.0 eq.) in EtOH (3 mL) was added an aqueous solution of NaOH (2 mL, 2N) and the reaction was heated to 110 °C under microwave irradiation for 20 minutes. The reaction was diluted with an aqueous solution of HCl (5 mL, 1N) and extracted with DCM (3 × 5 mL). The organic layers were combined, washed with brine (10 mL), dried over Na_2SO_4, filtered, concentrated *in vacuo* and purified *via* the Biotage SP4 (Reverse-phase silica-packed SNAP column 4 g; 20-100% H_2O/(MeOH:MeCN)) to give the title product **4b** as an orange solid (78 mg, 74%). A portion of **4b** was treated with Et_2N to form the salt. Spectroscopic data was obtained for the JBIR-22 **4b**-Et_2N salt. $\mathbf{[\alpha]_D^{20}}$= -20.5 (*c* 0.7, MeOH); **IR** (thin film) ν_{max}: 2916, 2849, 1647, 1560, 1437, 1387, 1234, 1065, 1032, 997, 891, 781; **^{1}H NMR** (500 MHz, Acetone-d_6) δ 5.52 (ddd, *J* = 9.8, 4.5, 2.5 Hz, 1H, C4-H), 5.30 (d, *J* = 9.8 Hz, 1H, C5-H), 3.92 (dd, *J* = 11.5, 5.8 Hz, 1H, C2-H), 3.36 (dd, *J* = 10.0, 1.2 Hz, 1H, C5'-H), 2.72 (s, 3H, C10'-H_3), 2.65 – 2.55 (m, 1H, C3-H), 2.31 (dd, *J* = 13.7, 1.2 Hz, 1H, C6'-H), 2.02 – 1.97 (m, 2H, C8'-H, C10-H_2), 1.74 – 1.70 (m, 1H, C7-H_2), 1.70 – 1.68 (m, 3H, C6-H, C8-H_2, C9-H_2), 1.64 (dd, *J* = 13.7, 10.0 Hz, 1H, C6'-H_2), 1.51 – 1.40 (m, 1H, C11-H), 1.29 – 1.27 (m, 2H, C8-H_2, C9-H_2), 1.09 – 0.98 (m, 1H, C7-H_2), 0.91 (d, *J* = 6.6 Hz, 3H, C9'-H_3), 0.91 (d, *J* = 6.6 Hz, 3H, C12'-H_3), 0.75 (d, *J* = 7.3 Hz, 3H, C12-H_3), 0.73 – 0.68 (m, 1H, C10-H_2); **^{13}C NMR** (126 MHz, Acetone-d_6) δ 196.4 (C1), 195.7 (C4'), 180.1 (C11'), 174.8 (C2'), 133.4 (C4), 131.2 (C5), 101.5 (C3'), 79.9 (C7'), 63.2 (C5'), 51.0 (C2), 43.3 (C6), 37.3 (C11), 37.1 (C6'), 36.6 (C8'), 34.4 (C7), 32.3 (C3), 31.0 (C10), 27.7 (C9, C8), 26.8 (C10'), 18.6 (C9'), 18.3 (C12), 16.8 (C12'); ***m/z*** (ES^-) 418.22 ($[M-H]^-$, 100 %); **HRMS** (ES^-) Calcd for $C_{23}H_{32}O_6N$ $[M-H]^-$: 418.2235, found 418.2226.

Isopropyl (2*S*,4*S*)-4-(4-(diethoxyphosphoryl)-*N*-methyl-3-oxobutanamido)-2-isopropyl-5-oxotetrahydrofuran-2-carboxylate (96)

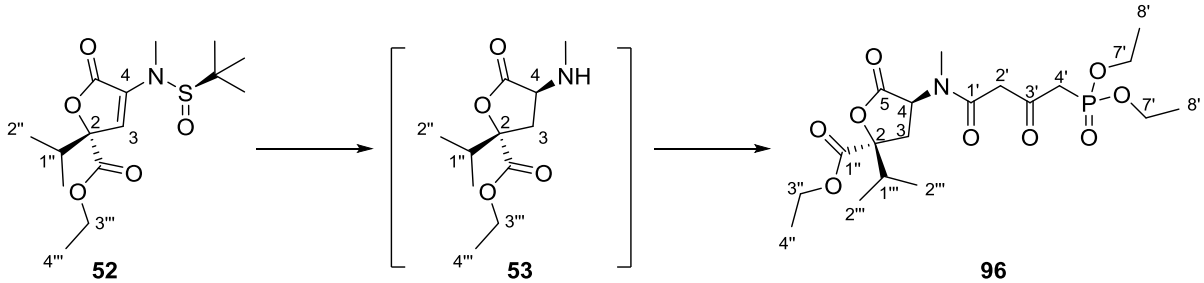

To a solution of **52** (205 mg, 0.62 mmol, 1.0 eq.) in THF (1.5 mL) at 0 °C was added HCl (0.62 mL, 4 eq., 4 N in dioxane). The reaction was stirred for 10 minutes at this temperature before the addition

of a solution of $NaBH_3CN$ (117 mg, 1.86 mmol, 3.0 eq.) in MeOH (3 mL). The reaction was stirred for a further 1 hour at 0 °C before being concentrated *in vacuo*. The residue was partitioned between a saturated aqueous solution of $NaHCO_3$ (5 mL) and EtOAc (5 mL). The aqueous layer was extracted with EtOAc (3 × 5 mL) and the combined organic extracts were washed with brine (10 mL), dried over Na_2SO_4, filtered and concentrated *in vacuo* to yield the crude free amine **53**. To a solution of **53** in anhydrous MeCN (6 mL) was added a solution of **63** in anhydrous MeCN (3 mL), and the reaction was heated at reflux for 2.5 hours. The reaction was concentrated *in vacuo* and purified *via* the Biotage SP4 (silica-packed SNAP column 12 g; 0-8% MeOH/DCM) to give the title product **96** as an orange oil (220 mg, 79%). In $CDCl_3$ at room temperature the title compound **96** exists as a (7 : 3) *enol* : *keto* mixture. The NMR signals are reported for the major *keto* tautomer. ^{1}H and ^{13}C spectra are complicated by ^{31}P splitting. **IR** (thin film) ν_{max}: 2978, 2936, 1784, 1734 (C=O), 1636 (C=O), 1236, 1184, 1022; **^{1}H NMR** (500 MHz, Chloroform-*d*) δ 4.83 – 4.71 (m, 1H, C4-H), 4.33 – 4.21 (m, 2H, C3''-H_2), 4.21 – 4.07 (m, 4H, (C7'-H_2)$_2$), 3.81 (s, 2H, C2'-H_2), 3.25 (dd, *J* = 22.6, 4.4 Hz, 2H, C4'-H_2), 3.01 (s, 3H, NCH_3), 2.68 (dd, *J* = 12.8, 9.1 Hz, 1H, C3-H_2), 2.47 (dd, *J* = 12.8, 11.4 Hz, 1H, C3-H_2), 2.38 – 2.29 (m, 1H, C1'''-H), 1.37 – 1.28 (m, 9H, C4''-H_3, (C8'-H_3)$_2$), 1.05 (d, *J* = 6.9 Hz, 3H, C2'''-H_3), 1.02 (d, *J* = 6.9 Hz, 3H, C2'''-H_3); **^{13}C NMR** (126 MHz, Chloroform-*d*) δ 195.7 (C3'), 172.1 (C5), 171.0 (C1''), 167.3 (C1'), 87.2 (C2), 63.0 (d, *J* = 6.5 Hz, C7'), 62.4 (C3''), 56.7 (C4), 49.7 (C2'), 42.5 (d, *J* = 125.9 Hz, C4'), 35.3 (NCH_3), 34.2 (C1'''), 31.5 (C3), 17.0 (C2'''), 16.5 (C2'''), 16.4 (C8'), 14.3 (C4''). **^{31}P NMR** (202 MHz, Chloroform-*d*) δ 19.2. ***m/z*** (ES^+) 472.17 ($[M+Na]^+$, 100 %); **HRMS** (ES^+) Calcd for $C_{19}H_{32}O_9NPNa$ $[M+Na]^+$: 472.1707, found 472.1696; $\mathbf{[\alpha]_D^{20}}$ = -9.2 (*c* 1.0, MeOH).

Ethyl (2*S*,4*S*)-2-*iso*propyl-4-((4*E*,10*E*,12*E*)-*N*-methyl-3-oxotetradeca-4,10,12-trienamido)-5-oxotetrahydrofuran-2-carboxylate (94)

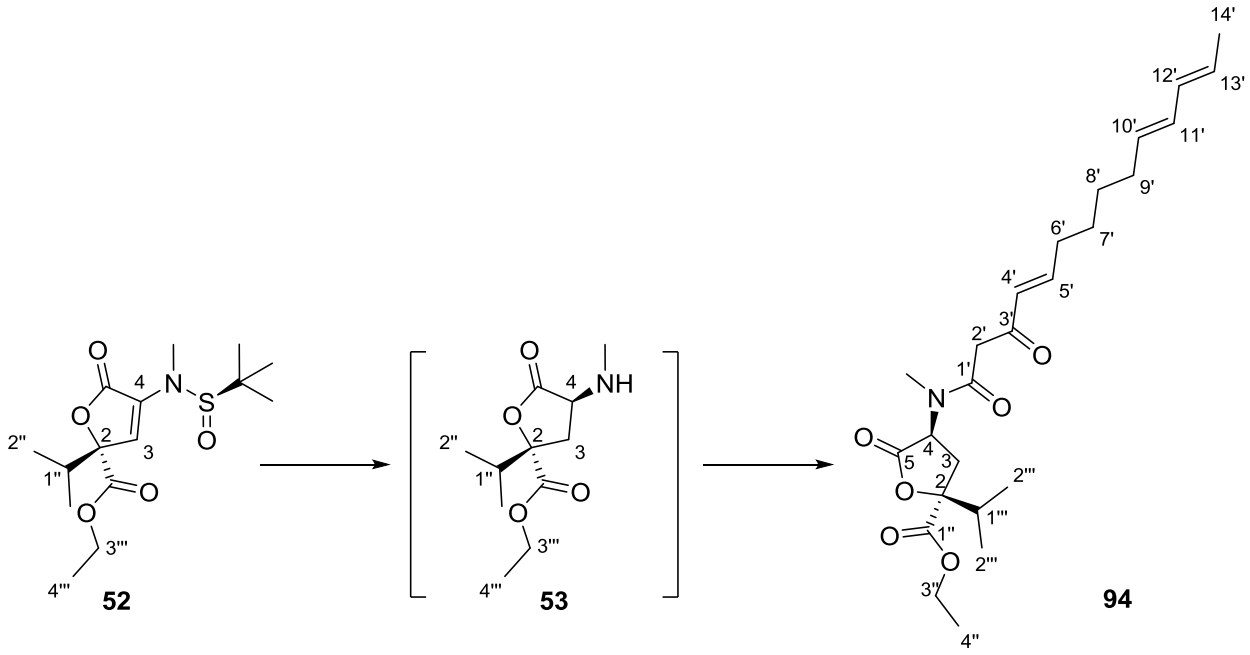

To a solution of **52** (0.53 g, 1.59 mmol, 1.0 eq.) in THF (4 mL) at 0 °C was added HCl (1.59 mL, 4 eq., 4 N in dioxane). The reaction was stirred for 10 minutes at this temperature before the addition of a solution $NaBH_3CN$ (0.30 g, 4.77 mmol, 3.0 eq.) in MeOH (8 mL). The reaction was stirred for a further 1 hour at 0 °C before being concentrated *in vacuo*. The residue was partitioned between a saturated aqueous solution of $NaHCO_3$ (10 mL) and EtOAc (10 mL). The aqueous layer was extracted with EtOAc (3 × 10 mL) and the combined organic extracts were washed with brine (10 mL), dried over Na_2SO_4, filtered and concentrated *in vacuo* to yield the crude free amine **53**. To a solution of **53** in anhydrous THF (19 mL) at 0 °C was added a solution of **66** (0.39 g, 1.27 mmol, 0.8 eq.) in anhydrous THF (13 mL), followed by Et_3N (0.89 mL, 6.36 mmol, 4.0 eq.) and CF_3CO_2Ag (0.70 g, 3.18 mmol, 2.0 eq.). The reaction was then stirred for 1 hour at 0 °C followed by 1 hour at room temperature. The reaction was concentrated *in vacuo* and purified *via* the Biotage SP4 (silica-packed SNAP column 12 g; 0-40% EtOAc/hexanes) to give **94** as a pale yellow oil (0.38 g, 67%). In $CDCl_3$ at room temperature the title compound **94** exists as a (5 : 4) *enol* : *keto* mixture. **IR** (thin film) ν_{max}: 2970, 2936, 1790, 1734 (C=O), 1647 (C=O), 1184; **^{1}H NMR** (500 MHz, Chloroform-*d*) δ(*major enol-form*) 6.65 (ddd, *J* = 15.0, 8.9, 5.3 Hz, 1H, C5'-H), 6.05 – 5.93 (m, 2H, C11'-H, C12'-H), 5.85 – 5.75 (m, 1H, C4'-H), 5.63 – 5.46 (m, 2H, C10'-H, C13'-H), 5.12 (s, 1H, C2'-H), 4.99 – 4.92 (m, 1H, C4-H), 4.33 – 4.21 (m, 2H, C3''-H_2), 2.99 (s, 3H, NCH_3), 2.74 – 2.61 (m, 1H, C3-H_2), 2.52 – 2.39 (m, 1H, C3-H_2), 2.38 – 2.28 (m, 1H, C1'''-H), 2.22 – 2.14 (m, 2H, C6'-H_2), 2.10 – 2.02 (m, 2H, C9'-H_2), 1.72 (d, *J* = 6.7 Hz, 3H, C14'-H_3), 1.54 – 1.37 (m, 4H, C7'-H_2, C8'-H_2), 1.36 – 1.26 (m, 3H, C4''-H_3), 1.09 – 0.99 (m, 6H, (C2'''-H_3)$_2$); **^{13}C NMR**

(126 MHz, Chloroform-*d*) δ(*major enol-form*) 172.6 (C1'), 172.2 (C5), 171.0 (C1''), 170.4 (C3'), 140.8 (C5'), 131.7 (C10'), 131.6 (C12'), 130.7 (C11'), 127.1 (C13'), 125.3 (C4'), 87.6 (C2'), 87.2 (C2), 62.4 (C3''), 55.8 (C4), 34.3 (C1'''), 34.2 (N$\underline{C}H_3$), 32.6 ($\underline{C}H_2$), 32.3 ($\underline{C}H_2$), 31.5 (C3), 29.1 ($\underline{C}H_2$), 28.1 ($\underline{C}H_2$), 18.2 (C14'), 17.0 (C2'''), 16.5 (C2'''), 14.3 (C4''); **^{1}H NMR** (500 MHz, Chloroform-*d*) δ(*minor keto-form*) 7.00 – 6.89 (m, 1H, C5'-$\underline{H}$), 6.17 (d, *J* = 16.3 Hz, 1H, C4'-$\underline{H}$), 6.08 – 5.88 (m, 2H, C11'-$\underline{H}$, C12'-$\underline{H}$), 5.64 – 5.49 (m, 2H, C10'-$\underline{H}$, C13'-$\underline{H}$), 4.79 (dd, *J* = 11.5, 9.0 Hz, 1H, C4-$\underline{H}$), 4.36 – 4.18 (m, 2H, C3''-$\underline{H}_2$), 3.71 (d, *J* = 2.9 Hz, 2H, C2'-$\underline{H}_2$), 3.00 (s, 3H, NC$\underline{H}_3$), 2.73 – 2.62 (m, 1H, C3-$\underline{H}_2$), 2.52 – 2.39 (m, 1H, C3-$\underline{H}_2$), 2.40 – 2.29 (m, 1H, C1'''-$\underline{H}$), 2.30 – 2.20 (m, 2H, C6'-$\underline{H}_2$), 2.10 – 2.02 (m, 2H, C9'-$\underline{H}_2$), 1.72 (d, *J* = 6.7 Hz, 3H, C14'-$\underline{H}_3$), 1.54 – 1.44 (m, 4H, C7'-$\underline{H}_2$, C8'-$\underline{H}_2$), 1.36 – 1.28 (m, 3H, C4''-$\underline{H}_3$), 1.09 – 0.99 (m, 6H, (C2'''-$\underline{H}_3$)$_2$); **^{13}C NMR** (126 MHz, Chloroform-*d*) δ(*minor keto-form*) 193.1 (C3'), 172.2 (C5), 171.0 (C1''), 167.7 (C1'), 150.8 (C5'), 131.7 (C10'), 131.4 (C12'), 130.9 (C11'), 129.5 (C4'), 127.3 (C13'), 87.1 (C2), 62.4 (C3''), 56.7 (C4), 47.2 (C2'), 34.3 (C1'''), 35.4 (N$\underline{C}H_3$), 32.6 ($\underline{C}H_2$), 32.5 ($\underline{C}H_2$), 32.0 (C3), 29.1 ($\underline{C}H_2$), 27.5 ($\underline{C}H_2$), 18.2 (C14'), 17.0 (C2'''), 16.5 (C2'''), 14.3 (C4''); ***m/z*** (ES$^+$) 448.27 ([M+H]$^+$, 100 %); **HRMS** (ES$^+$) Calcd for $C_{25}H_{38}O_6N$ [M+H]$^+$: 448.2694, found 448.2691; **$[\alpha]_D^{20}$** = +16.5 (*c* 1.0, MeOH).

Ethyl (*S*)-2-hydroxy-2-(((*S*,*E*)-4-((2*E*,8*E*,10*E*)-1-hydroxydodeca-2,8,10-trien-1-ylidene)-1-methyl-3,5-dioxopyrrolidin-2-yl)methyl)-3-methylbutanoate (65)

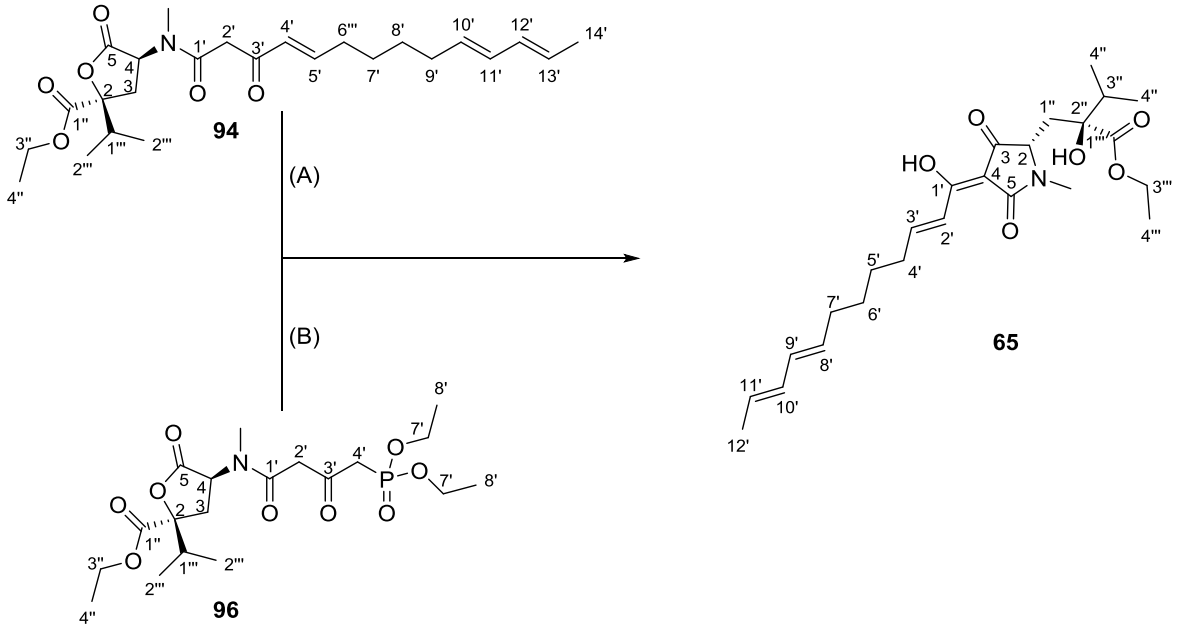

Route A: To a solution of **94** (170 mg, 0.38 mmol, 1.0 eq.) in THF (8 mL) at 0 °C was added ^{t}BuOK (47 mg, 0.42 mmol, 1.1 eq.) and the reaction was stirred for 1 hour. The reaction was slowly warmed to room temperature and stirred for a further 1 hour. The reaction was concentrated and the residue partitioned between DCM (10 mL) and an aqueous solution of HCl (10 mL, 1N). The aqueous layer was separated and extracted with DCM (3 × 10 mL). The organic extracts were combined, washed

with an aqueous solution of HCl (5 mL), brine (5 mL), dried over Na_2SO_4, filtered, concentrated *in vacuo* and purified *via* the Biotage SP4 (Reverse-phase silica-packed SNAP column 4 g; 20-100% H_2O/(MeOH:MeCN)) to give the title product **65** as an yellow oil (159 mg, 94%).

Route B: To a solution of **96** (100, 0.22 mmol, 1.0 eq.) in THF (2.5 mL) at 0 °C was added ^{t}BuOK (0.24 mL, 1.1 eq., 1M in THF) and the reaction was stirred for 40 minutes. To the mixture was added a solution of **75** (102 mg, 0.67 mmol, 3.0 eq.) in THF (1 mL) and the reaction was stirred for a further 15 minutes before being warmed to room temperature and stirred for 16 hours. The reaction was quenched by the addition of an aqueous solution of HCl (3 mL, 1N) and extracted with DCM (3 × 10 mL). The organic extracts were combined, washed with brine (10 mL), dried over Na_2SO_4, filtered, concentrated *in vacuo* and purified *via* the Biotage SP4 (Reverse-phase silica-packed SNAP column 4 g; 20-100% H_2O/(MeOH:MeCN)) to give the title product **65** as an yellow oil (83 mg, 85%). **IR** (thin film) ν_{max}: 2964, 2931, 1717 (C=O), 1690 (C=O), 1645 (C=O), 1586, 1449, 1242, 989; **^{1}H NMR** (500 MHz, Chloroform-*d*) δ 7.24 – 7.13 (m, 1H, C3'-H), 7.08 – 7.03 (m, 1H, C2'-H), 6.04 – 5.90 (m, 2H, C9'-H, C10'-H), 5.62 – 5.45 (m, 2H, C8'-H, C11'-H), 4.24 (q, *J* = 7.1 Hz, 2H, C3'''-H_2), 3.67 (dd, *J* = 9.6, 2.2 Hz, 1H, C2-H), 2.97 (s, 3H, NCH_3), 2.37 – 2.29 (m, 2H, C4'-H_2), 2.30 – 2.28 (m, 1H, C1''-H_2), 2.10 – 2.00 (m, 3H, C3''-H, C7'-H_2), 1.90 (dd, *J* = 14.5, 9.6 Hz, 1H, C1''-H_2), 1.71 (d, *J* = 6.4 Hz, 3H, C12'-H_3), 1.57 – 1.45 (m, 2H, C5'-H_2), 1.46 – 1.37 (m, 2H, C6'-H_2), 1.31 (t, *J* = 7.1 Hz, 3H, C4'''-H_3), 0.94 (d, *J* = 7.3 Hz, 3H, C4''-H_3), 0.93 (d, 7.3 Hz, 3H, C4''-H_3); **^{13}C NMR** (126 MHz, Chloroform-*d*) δ 196.3 (C3), 175.5 (C1'''), 175.1 (C1'), 173.4 (C5), 151.8 (C3'), 131.6 (C10'), 131.4 (C8'), 130.8 (C9'), 127.2 (C11'), 121.6 (C2'), 98.9 (C4), 78.8 (C2''), 64.5 (C2), 61.6 (C3'''), 36.8 (C3''), 34.9 (C1''), 33.3 (C4'), 32.4 (C7'), 29.1 (C6'), 27.7 (C5'), 26.8 (NCH_3), 18.1 (C12'), 17.5 (C4''), 16.4 (C4''), 14.5 (C4'''); ***m/z*** (ES^-) 446.25 ($[M-H]^-$, 100 %); **HRMS** (ES^-) Calcd for $C_{25}H_{36}O_6N$ $[M-H]^-$: 446.2548, found 446.2549.

4 Design and Development of Peptidomimetic Inhibitors of PICK1 PDZ mediated PPIs

4.1 Introduction

4.1.1 Peptidomimetics

The direct application of native proteins/peptides as pharmacologically active compounds is a widely exploited starting point in the development of PPI modulators.[261] However, the low bioavailability, poor proteolytic stability and off-target effects of the conformationally flexible polypeptides has limited the clinical application of peptide-based drug discovery (PBDD).[262] One way to overcome the drawbacks associated with native peptides is the development of peptidomimetics.[261,263,264] These are small molecules which are designed to mimic the biological activity of peptides but with improved pharmacodynamic and pharmacokinetic profiles. Numerous examples of three-dimensional X-ray crystallographic or NMR spectroscopic structures of proteins complexed with their biological partners have facilitated the rational structure-based design of peptidomimetic PPI inhibitors through modification of novel scaffolds or the optimisation of native peptide ligands.[261,264,1]

Peptidomimetics are classified as structural mimetics (Type-I), functional mimetics (Type-II) or topographical mimetics (Type-III).[262,263] Type-I peptidomimetics or pseudopeptides typically contain a structurally similar peptide backbone bearing the required functionalities to mimic the side-chains of the native amino acids. Several successful examples of type-I peptidomimetics have been reported, including the recently developed inhibitors of the MLL1-WDR5 PPI (Figure 4.1).[265] Mixed lineage leukemia 1 (MLL1) is a histone-lysine-methyltransferase (HMT) responsible for the methylation of histones. Disruption of the MLL1-WDR5 PPI through point mutations at WDR5 caused dissociation of the protein complex and loss of MLL1 HMT activity.[266] This makes small molecule inhibition of the MLL1-WDR5 PPI a highly promising strategy for the treatment of certain forms of leukemia. Previous studies had identified tripeptide Ac-ARA-NH_2 **1**, the minimum binding epitope of MLL1, to be a potent binder of WDR5 (K_i = 120 nM). Systematic evaluation of the binding of **1** to WDR5 through the incorporation of natural and unnatural amino acids resulted in MM-101 **2**, which had a 100-fold increase in binding affinity (K_i = <1 nM) (Figure 4.1). Most importantly, **2** was effective at inhibiting cell growth and inducing apoptosis in MLL1 mediated leukemia without general toxicity to normal bone marrow cells or non-MLL cells.[267]

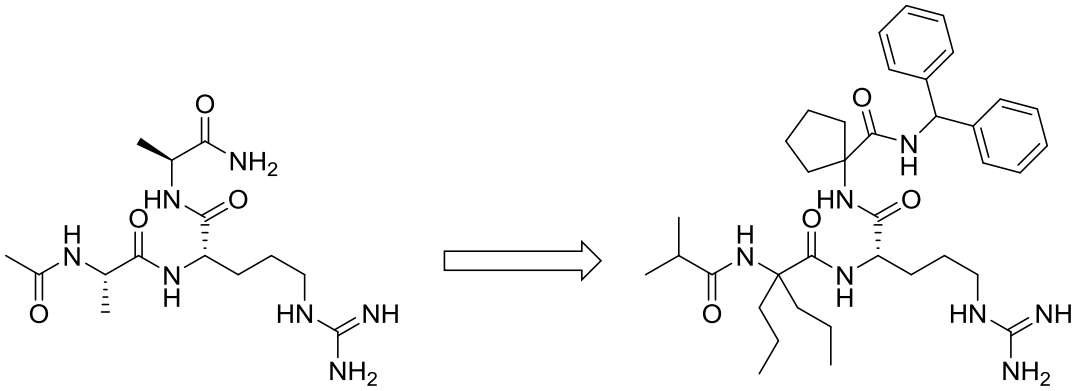

Figure 4.1. Development of a novel MLL1-WDR5 PPI inhibitor 2 from tripeptide 1.[1]

Type-II peptidomimetics are small non-peptide molecules which do not mimic the structure of the parent peptide but can bind to the peptide receptor and modulate the associated PPI. Initially, type II mimetics were considered to be direct structural analogues of the natural peptide, but further studies indicate that a large number of these antagonists bind to receptor subsites different than those used by the parent peptide. Despite this uncertainty, the approach has been successful in producing a number of potential drug lead structures; in particular the identification of several G-protein coupled receptor (GPCR) antagonists.[263]

Type-III peptidomimetics represent the ideal concept for mimetics and are characterised by novel non-peptide scaffolds, containing the required functional groups in a well-defined spatial orientation to form a strong interaction with the biological target.[262,263] Structure-based design coupled with structure-activity relationship studies are first used to define the minimum binding epitope and the main pharmacophoric elements involved in binding. A novel scaffold is then designed which aligns the critical structural features, in a 3D arrangement, to facilitate strong binding to the biological target. The resulting peptidomimetic is expected to produce a similar physiological response to that observed with the native peptide, but with enhanced properties such as higher proteolytic stability, increased bioavailability and improved potency and selectivity.[261] Type-III peptidomimetics have been used successfully to target a range of PPIs involved in cancer progression. By combining chemical synthesis with X-ray crystallography and conformational analysis, Rew *et al*. discovered novel inhibitors of the p53-MDM2 PPI,[268] an important negative regulator of the tumour suppressor protein p53[269] (see Chapter 5 for further discussion on the biological significance of the p53-MDM2 PPI). This structure-based design approach identified AM-8553 (**3**), a highly potent (IC_{50} = 2.2 nM), selective and orally bioavailable inhibitor of the p53-MDM2 PPI.[268] In addition, type-III

peptidomimetics have proven to be a rich source of potent, cell permeable inhibitors of PDZ domain mediated PPIs.[270–275]

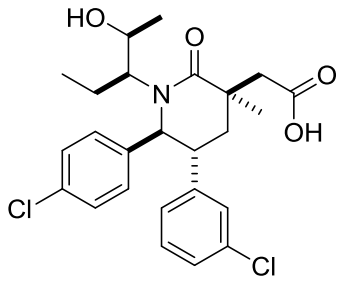

AM-8553 (**3**)

Figure 4.2. The structure of p53-MDM2 PPI inhibitor AM-8553 (3).[268]

4.1.2 PDZ Domains

PSD-95/Discs-large/ZO-1 homology (PDZ) domains are among the most common protein domains in the human genome, playing important roles in several therapeutically relevant protein–protein interactions, like those involved in protein trafficking and the formation of multiprotein signalling complexes.[276] The role of PDZ domains in the clustering and localisation of proteins at the plasma membrane has important biological implications, e.g. in signalling, mediating the adhesive properties of specific cells, ion transport and formation of the paracellular barriers (tight junctions).[276,277]

Of all canonical PPIs, PDZ domains are the most similar to traditional ligand–receptor interactions, as the interaction interface is comprised of a groove on the PDZ domain, binding to the terminal (3–5) amino-acid residues of the C-terminus of its interacting partner (Figure 4.3).[278] The structure of the PDZ domain comprises of six β-strands (βA-βF) and two α-helices (αA and αB), which fold into a six-stranded β-sandwich domain (Figure 4.3). Peptide ligands bind in an extended groove between strand βB and helix αB, thus serving as an additional antiparallel β-strand within the PDZ domain. As only three residues of the PDZ binding motif contribute to the majority of the energetics of the interaction with the PDZ domain (the 'hotspot'), the development of a predictive pharmacophore model leading to the identification of a nonpeptide small-molecule inhibitor is thought possible.[279]

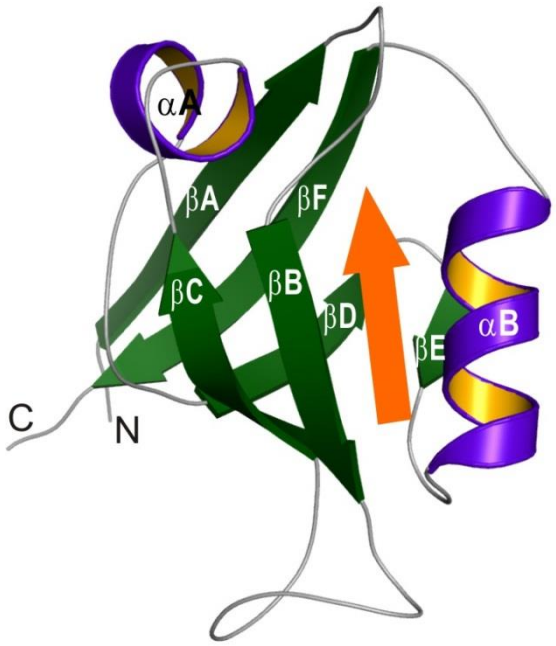

Figure 4.3. A ribbon representation of the structure of PSD-95 PDZ2. The canonical fold contains six β-sheets and two α-helices. A peptide ligand (orange) is shown bound to the PDZ between the βB strand and αB helix.[280]

Recent evidence has supported the idea that PDZ domains might be valuable drug targets. Membrane-permeable peptides that block the PDZ interaction between PSD-95 and the NMDA glutamate receptor result in the selective inhibition of neuronal nitric oxide synthase (nNOS) activation.[281] This effect is believed to reduce ischemic brain injury during stroke. Other recent findings suggest that blocking the PDZ domains of the NHERF-1,[274] AF-6,[282] or dishevelled[283] proteins which are involved in cell signalling and cell differentiation might provide potential therapeutic approaches towards the treatment of cancer.[284] Furthermore, the PDZ domain of the PICK1 protein, which binds to the C-terminus of ionotropic glutamate receptors, has recently been recognised as a valid therapeutic target for the treatment of brain ischemia, pain and cocaine addiction.[285]

4.1.3 Protein Interacting with C Kinase (PICK1)

Protein interacting with C kinase (PICK1) is a scaffolding protein containing a single *N*-terminal PDZ domain that interacts with the PDZ motifs of several proteins, which have roles in neuronal cell morphology, mitochondrial-dependent apoptosis and synaptic plasticity.[286] PICK1 regulates the synaptic clustering, trafficking and recycling of its interacting partners, by facilitating their PKC (protein kinase C)-mediated phosphorylation.[287,276]

4.1.4 PICK1 in the brain

PICK1 has been studied extensively due to its role in regulating several important neuronal proteins and its interactions with a number of disease-associated proteins implicated in cancer,[288] schizophrenia[289] and pain.[278] At the synapse, PICK1 has been shown to have an important role in neurotransmission, plasticity, neurotransmitter vesicle docking and receptor cycling.[290] PICK1 interacts with the C-terminal tail of AMPAR subunits GluR2 and GluR3.[291] It was reported to change the subcellular localisation of GluR2, regulating the removal and insertion of AMPARs from the plasma membrane, a process that plays an important role in regulating long-term depression (LTD) and long-term potentiation (LTP).[290] These processes have recently received a lot of attention due to their proposed role in learning and memory.[290] Hence, specific small-molecule inhibitors of the PICK1 PDZ domain could facilitate the exploration of a variety of physiological processes and provide leads for potential novel therapeutics targeted towards a number of neurological disorders, including stroke, neurodegeneration, pain, depression, anxiety, epilepsy and schizophrenia.

4.1.5 PICK1 and cancer

PICK1 also interacts with proteins that are involved in governing processes such as cellular morphology, cellular polarity and migration. For instance, PICK1 interacts with the ephrin family of receptor tyrosine kinases (RTKs) and the neuregulin (NRG) ErbB receptor tyrosine kinases.[278] The ErbB-Rs are overexpressed in a number of breast, lung and kidney cancers.[292] These receptors consist of four members named epidermal growth factor (EGF), ErbB2/HER2, ErbB3/HER3 and ErbB4/HER4. The C-terminus located PDZ motif of ErbB2/HER2 binds the PDZ domain of PICK1, which regulates its surface expression, clustering and activation.[279] The ErbB2/HER2 receptor is overexpressed in about 30% of human breast cancers and is also frequently altered in carcinoma of lungs and kidneys.[292] The important role of the ErB2/HER2 in human breast cancer development has being highlighted by its utilisation as a novel target for the monoclonal antibody Herceptin in breast cancer therapy.[293] Furthermore, PICK1 has been shown to be overexpressed in a range of human cancers, including, breast, lung, gastric, colorectal and ovarian. Zhang *et al.* demonstrated that siRNA mediated silencing of PICK1 expression in breast cancer cells led to significant inhibition of cell proliferation and cell cycle arrest in the S phase *in vitro* and inhibited xenograft tumour growth in nude mice.[288]

In the same study, high levels of PICK1 in cancer were found to correlate with ErbB2/HER2 protein expression, suggesting this specific protein-protein interaction as a potential novel therapeutic target for the treatment of breast cancer. A small molecule inhibitor of the PICK1 PDZ domain would

allow further investigation of PICK1's greatly understudied role in cancer and potentially provide new leads for targeted breast cancer therapies.

4.1.6 Small molecule PICK1 Inhibitors

Thorsen *et al*. reported the first small-molecule inhibitor (FSC231 **4**) of the PICK1 PDZ domain, identified from a screen of ~44,000 compounds in a fluorescent polarisation assay (Figure 4.4).[285] The inhibitor bound the PICK1 PDZ domain with a K_i value of 9.6 μM, which is comparable to that observed for the endogenous C-terminal peptide ligands. FSC231 (**4**) was shown to inhibit the role of PICK1 in GluR2 trafficking and block both LTD and LTP expression in hippocampal CA1 neurons.[285] However, further SAR studies revealed that modifications of this core structure decreased activity in all cases, except for compound **5** which showed a marginal increase in activity with a K_i value of 7.2 μM (Figure 4.4).[294] The inability to modify successfully this structure has prevented its use as a lead compound for the identification of a nanomolar inhibitor of the PICK1 PDZ domain. In addition, poor solubility and cell permeability has limited its use as a biological tool to study these important physiological processes.

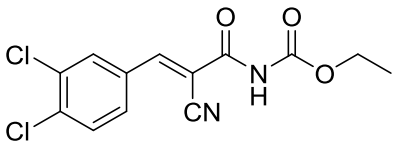

FSC231 (**4**)
K_i = 9.6 μM

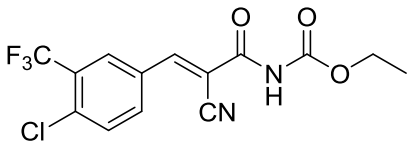

5
K_i = 7.2 μM

Figure 4.4. Structures of known PICK1 PDZ domain inhibitors FSC231 (4) and 5.

4.1.7 Small molecule PDZ Inhibitors

In 2003, Fujii *et al.* developed the first cell permeable small molecule PDZ inhibitor (Figure 4.5, compound **6**), which targeted MAGI3, an important regulator of tissue organisation and differentiation.[295] This selective peptidomimetic inhibitor was rationally designed to bind the second PDZ domain of MAGI3 and docking studies revealed that the indole overlaps with the C-terminal tetrapeptide of the known MAGI3 PDZ ligand PTEN. This designed indole scaffold has since been modified by Fujii and others to target a range of PDZ domains such as that of dishevelled,[270,273] NHERF1[274,296] and PSD-95.[297,271] This scaffold therefore provides the opportunity for the design and development of a small focused library of cell permeable small molecules to target the PICK1 PDZ domain.

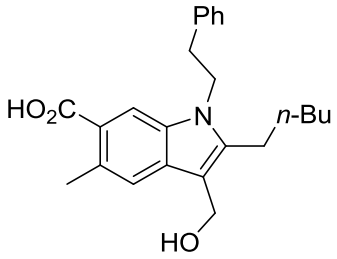

6

Figure 4.5. Structure of the first small molecule inhibitor of the MAGI3 PDZ domain.

4.2 Aims of this work

Our interest in PICK1 arose from its significant role in excitatory neurotransmission and synaptic function *via* its interaction with the GluR2 subunit of the glutamate receptor family and its interaction with ErbB2 which is involved in governing processes such as cellular morphology, cellular polarity and migration. The PICK1 PDZ domain binds the C-terminal 3-5 amino acids of its binding partner, resulting in a more traditional ligand–receptor interaction. This small, well-defined binding pocket should facilitate the design of small molecule inhibitors of PICK1's PPIs providing a useful biological tool for the study of the important physiological processes in which PICK1 plays a key role. It could also potentially provide a lead compound for the development of a novel therapeutic agent.

The design of PICK1 PDZ inhibitors is greatly aided by the identification of a core indole scaffold which has been used successfully to target a wide range of PDZ domains (Section 4.1.7). Extensive PICK1 PDZ domain mapping and the availability of crystal structures of the PDZ domain and co-crystal structures with bound ligand should facilitate the design of a series of PICK1 inhibitors.

The main aims of this project were to:

1. Utilise the modelling software GOLD to design a series of small molecule PICK1 inhibitors based on an indole scaffold.
2. Develop a high-yielding and versatile route to the desired compounds.
3. Synthesise all designed compounds for biological testing.

4.3 Analysis of the PICK1 PDZ Domain

An important step in the rational design of small molecules that occlude crucial binding sites ("hotspots") on protein-protein interaction interfaces is the use of site-directed mutagenesis and in-depth molecular modelling to map the interaction site. The therapeutic interest in PICK1's PDZ interactions and the availability of X-ray crystal structures of the PICK1 PDZ domain and co-crystal structures with bound peptide partners has resulted in comprehensive domain-mapping studies of the PICK1 PDZ domain.[286,298,299] These studies have helped to refine the binding site more precisely, which should facilitate the design of selective small molecule inhibitors.[279]

PDZ domains bind three different C-terminal consensus sequences, which are referred to as class I, class II and class III interactions. These motifs are identified by the consensus sequence of the terminal three amino acids of the interacting ligand; type I terminates with (S/T)XΦ, type II with ΦXΦ, and type III with (D/E) XΦ, where X is any amino acid and Φ is any hydrophobic amino acid.[276] The PDZ domain of PICK1 does not fully conform to this classification, since it binds both type I ligands (e.g. PKCα) and type II ligands (e.g. GluR2). However, it has been shown to bind a prototypical class II sequence (-WLKV) with 10-fold greater affinity that the class I sequence of PKCα (-QSAV).[299]

To aid our design of small molecules targeting the PICK1 PDZ domain we focused on PICK1's interaction with class II ligands, since these include the two protein interactions of interest (GluR2 and ErbB2). Furthermore, PICK1's interaction with class II ligands has been shown to be more biologically relevant due to their stronger binding affinity and the much greater number of class II than class I interactions.[286]

The binding between the PICK1 PDZ domain and the GluR2 peptide (VKI) has been extensively studied using site-directed mutagenesis and analysis of the available X-ray crystal (PDB code: 3HPK[300]) and solution NMR (PDB code: 2PK2[277]) structures. This has resulted in the identification of binding pockets for P-2 to P0 residues of the GluR2 peptide (where P0 corresponds to the terminal amino acid). In the GluR2 peptide (-VKI), the residues P-2 (Val) and P0 (Ile) made the major binding contributions, while the side chain of P-1 (Lys) makes minimal contact with the PDZ domain (Figure 4.6). The role of the P-1 residue in binding is thought to be insignificant due to the highly diverse selection of amino acid residues present at this position in PICK1 PDZ-binding peptides.[277,301] However, a key cation-π interaction between the lysine residue and the Phe[53] of the PICK1 PDZ domain may have been overlooked (Figure 4.6). A cation-π interaction is the electrostatic attraction between a cation and an negative electrostatic potential associated with the face of a simple π

system.[302] Studies have shown that this specific interaction is energetically comparable or stronger than a typical hydrogen bond. Cation-π interactions make a significant contribution to the overall stability of most proteins;[303] with on average one such interaction occurring per 77 amino acid residues.[304] They also contribute significantly to intermolecular contacts and interactions at protein-protein interfaces[305] as well as between proteins and endogenous ligands and drug molecules.[306] The existence of a cation-π interaction in this case is strongly supported by the localisation of the P-1 lysine directly above Phe[53] (4.3 Å) within the 6.0 Å distance required for the interaction to occur.[307] This interaction may be important for the strength of the binding interaction and selectivity.

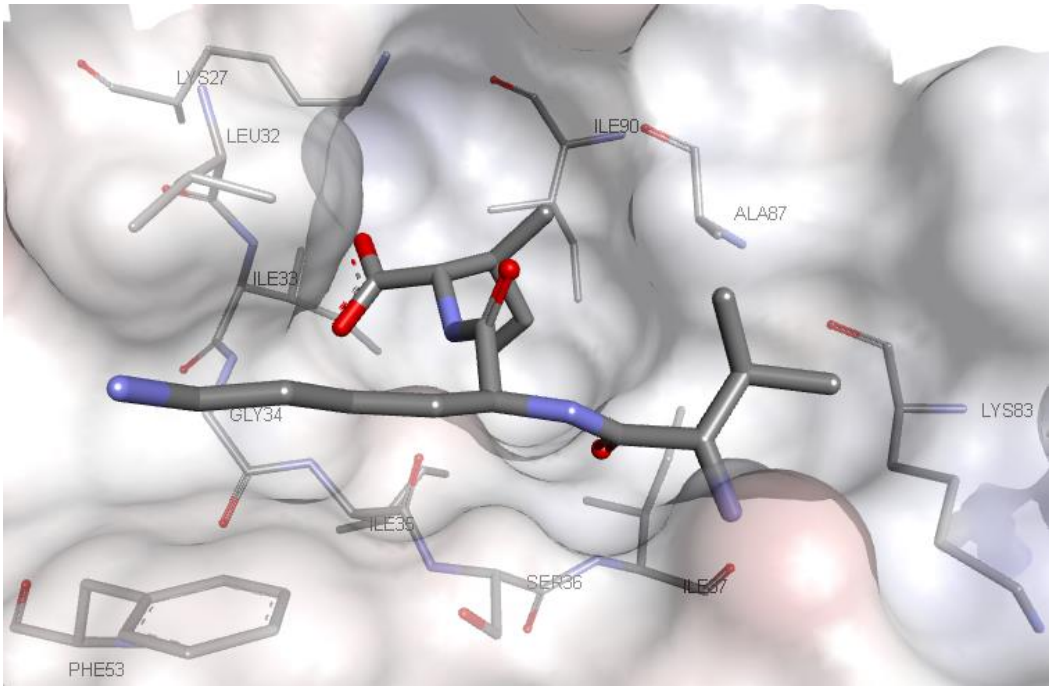

Figure 4.6. Representation of the crystal structure of the GluR2 peptide VKI bound into the PICK1 PDZ domain (PDB: 3HPK). Important residues are highlighted. The PDZ domain is shown as a transparent surface (electrostatic). Carbons are shown in grey, nitrogens in blue and oxygens in red. Figure created using Accelrys Discovery Studio Visualiser 4.1.

The P0 pocket consists of a small hydrophobic pocket that accommodates the Ile(0) side chain and a carboxylate binding domain (CBD), which binds the carboxyl-terminus of the peptide. The pocket is formed by the residues Lys[27] and Asp[28] (KD motif), Ile[37] and Ile[90] which make important hydrophobic interactions with the P0 and P-2 residues and the CBD which contains the PDZ domain GLGF motif, which in PICK1 consists of the residues Leu[32]-Ile[33]-Gly[34]-Ile[35] (LIGI motif) (Figure 4.6).[286] The size of the P-2 pocket is influenced by the conformation of the Ile[37] residue, which is set by the amino acid side chain of the P0 residue.[298] The Lys[83] residue in the P-2 pocket creates a hydrophobic interaction with the Val(-2) residue which is essential for the class II binding motif. The side chain of the P-2 residue is sandwiched between the Lys[83] and Ala[87] residues on the αβ helix (Figure 4.6).[277]

The extensive domain mapping undertaken for the PICK1 PDZ domain has identified key hydrophobic interactions in the P0 and P-2 pockets and hydrogen bonding interactions with the CBD required by peptides and hence small molecules to bind strongly to the PDZ domain. The variability at the P-1 position should facilitate the incorporation of a range of side chains to potentially identify substituents with added bonding interactions, improved selectivity between class II PDZ domains and improved pharmokinetic properties.

4.4 Series 1 Inhibitors

4.4.1 Design of series 1 inhibitors

The first aim of this project was to use an indole scaffold based on Fujii's MAGI3 PDZ inhibitor **6**[295] (Figure 4.5) to design a PICK1 PDZ domain inhibitor. To achieve this aim, it was necessary to compare the binding of Fujii's indole **6** with that of an endogenous PICK1 ligand to identify the regions of the indole scaffold that could be utilised to mimic the peptide binding (Figure 4.7). This revealed that substitution at the 1- and 3-positions of the indole ring could be used to mimic the P-1 and P-2 amino acid side chains respectively. Further modelling showed that the incorporation of an amide group at the 3-position of the indole could potentially mimic the 2nd amide group of the GluR2 peptide backbone. This analysis resulted in the indole scaffold **7** being designed to target the PICK1 PDZ domain, where substituents R^1, R^2 and R^3 should bind in the P0, P-1 and P-2 pockets respectively (Figure 4.7).

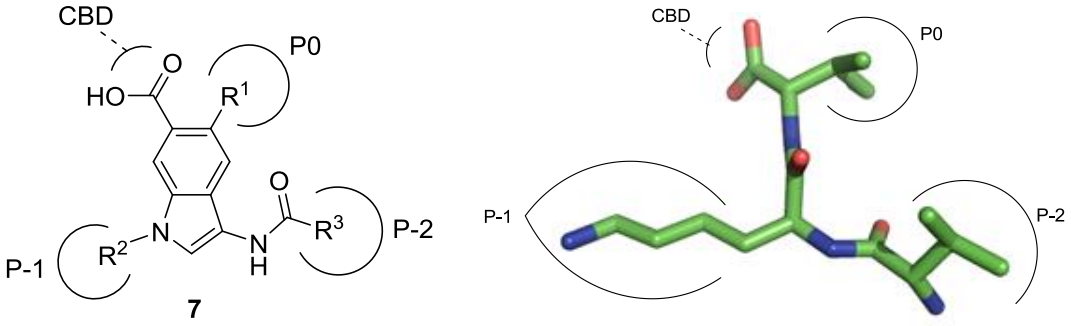

Figure 4.7. Comparison of binding of indole scaffold 7 with GluRu peptide (VKI).

Analysis of the size, shape and possible interactions in the binding pockets led to the identification of a series of substituents which were predicted to bind well in these pockets. Further analysis of the

amino acid side chains of known PICK1 peptide ligands, especially those with high binding affinities,[286] provided a second set of potential substituents for our lead compound. These two sets of potential substituents were combined in all possible permutations and docked in both available crystal structures using the modelling software GOLD.[308] These results were then analysed to identify analogues that adopted a similar binding pose to the GluR2 peptide (VKI) and ranked using the GoldScore algorithm (see Appendix K for selection of the docking results).[309]

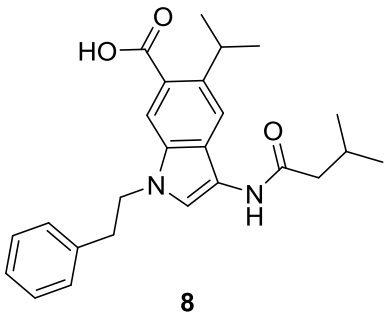

8

Figure 4.8. A designed indole based inhibitor of the PICK1 PDZ domain.

The two substituents selected for the R^1 position to bind in the P0 pocket were a methyl and an *iso*propyl group (Figure 4.10). Valine is the most common P0 residue of all PICK1 ligands and has been shown to be accommodated by the P0 hydrophobic pocket with little effect on the size and shape of the P-2 pocket.[299,298] The methyl group was selected since all previously reported PDZ inhibitors based on Fujii's indole scaffold contain a methyl group at this position, and the modelling study predicted that it should also fit in the P0 pocket.

Three hydrophobic substituents were selected for the R^3 substituent (Figure 4.10). A benzyl group was chosen as three of the four peptides with the strongest binding affinities for PICK1 contain a residue with an aromatic based side chain at the P-2 position (e.g., Ephrin B1 (Tyr), Parkin (Phe)).[286] Analysis of a series of different length and branched aliphatic chains identified an ethyl and an *iso*butyl (leucine mimic) group at the R^3 position as forming the strongest hydrophobic interactions with the P-2 pocket.

The final step was the identification of substituents for the highly variable P-1 position. Due to this variability, the selection of substituents based on known PICK1 ligands was not feasible. Our focus instead concentrated on substituents that may be able to provide additional interactions not exploited by the endogenous ligands, thus, potentially increasing the binding affinity of these designed ligands. Analysis of the crystal structure of PICK1 revealed that the base of the P-1 pocket is

formed by the aromatic side chain of Phe[53] (Figure 4.6). This highlighted several potential interactions that could be targeted such as π-π stacking, hydrophobic and cation-π interactions.[307]

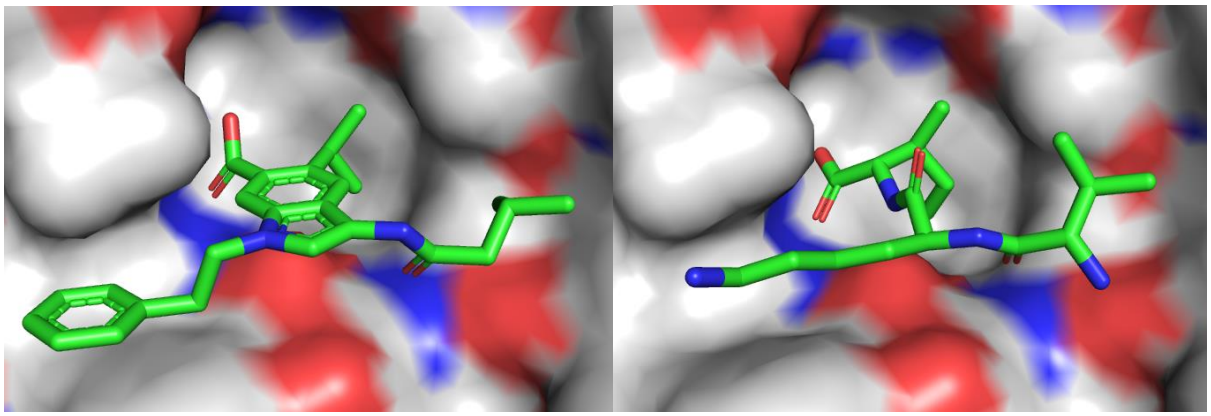

Figure 4.9. Comparison of the GOLD binding mode of a designed indole ligand 8 (Figure 4.8) (*left*) versus the crystal structure (PDB: 3HPK) of the PICK1 PDZ domain with the GluR2 peptide (VKI) bound (*right*). The solvent accessible surface of the protein is shown, with positively charged regions in blue and negatively charged regions in red. Ligands are shown as sticks with carbon atoms in green, nitrogen atoms in blue and oxygen atoms in red. Figure created using Pymol.

Docking studies showed that an ethylbenzene substituent at the R^2 position would place the aromatic ring above the Phe[53] within the 3.4-3.6 Å distance required for a π-π interaction (Figure 4.9).[307] This also resulted in a high predicted GoldScore (see Appendix K). PICK1 ligands contain a range of short aliphatic side chains at this particular position; docking studies predicted that an *iso*pentane group in the R^2 position would form the strongest hydrophobic interactions in the P-1 pocket.

The cation-π interaction was the final interaction selected as a possible target binding interaction in the P-1 pocket. A di-alkylated amine was selected as the desired cation source based on a recent study conducted by the Diederich group on factor Xa inhibitors, which demonstrated that stepwise methylation of an ammonium substituent binding in an aromatic pocket increased the binding affinity by 3 orders of magnitude.[310] Dennis Dougherty proposed that the correlation between increasing activity and increasing amine methylation resulted from the dispersion of the cationic charge onto the methyl groups due to the inherent electronegativity of the nitrogen atom, which ultimately resulted in a larger interaction area. The reduction of the desolvation cost of the hydrogens in the ammonium NH groups with stepwise methylation was also implicated in the observed increase in affinity.[311] Modelling studies identified that an *N*-dimethylethanamine substituent in the R^2 position would place the di-alkylated amine directly over Phe[53].

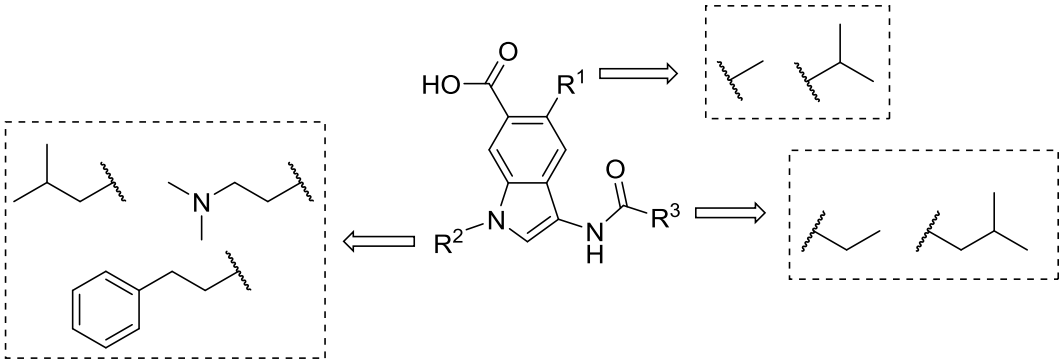

Figure 4.10. Selected R^1, R^2 & R^3 substituents for the core indole scaffold.

Further analysis of this substituted indole scaffold as a good peptidomimetic of the GluR2 peptide was carried out using Accelrys Discovery Studio. Overlay of the designed inhibitor **8** (Figure 4.8) and the GluR2 peptide (VKI) revealed that the R^1, R^2 and R^3 substituents were placed in the same proximity as the desired peptide residue side-chains (Figure 4.11A).The carboxylic acid group and the amide also aligned well with the analogous groups on the peptide. Analysis of the bonding interactions of **8** with the PICK1 PDZ domain demonstrated that the inhibitor could be forming all the key interactions required for binding of a class II peptide to the PICK1 PDZ domain (Figure 4.11B). **8** was predicted to form hydrogen bonds to Ile^{33}, Gly^{34} and Ile^{35} within the LIGI motif of the carboxylic acid binding domain (CBD), hydrophobic interactions with Ile^{90} and Lys^{83} and the added π-π interaction with Phe^{53}.

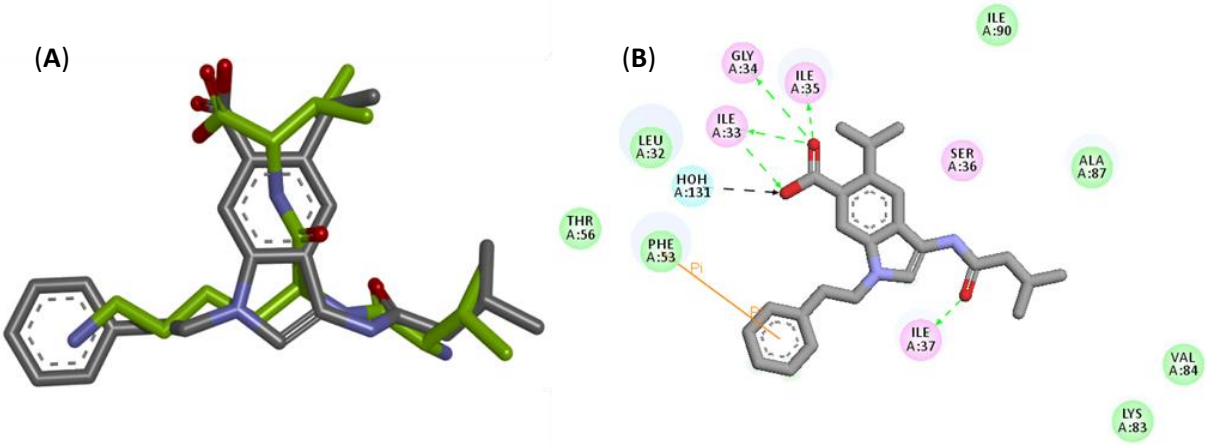

Figure 4.11. (A) Overlay of the GluR2 peptide ligand for the PICK1 PDZ and the designed small molecule inhibitor 8. Carbons are shown as grey (**8**) or green (VKI), nitrogen as blue and oxygen as red. **(B) Predicted binding interactions of 8 with the PICK1 PDZ domain.** Hydrophobic interactions are highlighted by green disks, electrostatic interactions by pink disks and dotted lines show specific hydrogen bonds and π-π interactions.

4.4.2 Synthesis of series 1 inhibitors

The designed indole-3-amide scaffold would allow generation of a small, focused chemical library with varying substituents at the R^1, R^2 and R^3 positions (Figure 4.10). A synthetic route was developed that would set the R^1 position at the beginning of the synthesis and provide an opportunity to modify the R^2 and R^3 positions towards the end of the process, thus facilitating simpler analogue synthesis (Scheme 4.1).

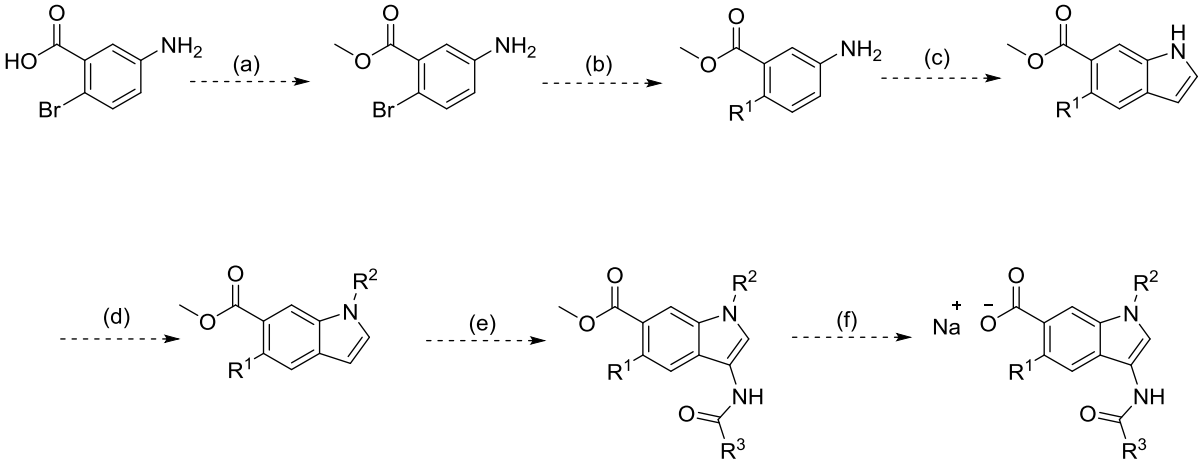

Scheme 4.1. Proposed synthetic route to the series 1 inhibitors. (**a**) Esterification. (**b**) Cross-coupling. (**c**) Indole formation. (**d**) *N*-alkylation. (**e**) Nitration and reductive acylation. (**f**) Saponifaction.

It was decided to first synthesise the series of analogues containing a methyl group at the R^1 position as the required starting material **9** (Scheme 4.2) was commercially available. This eliminated the potentially difficult cross-coupling step needed to incorporate the *iso*propyl group in place of the methyl group.

The preparation of the key indole intermediate **13** proceeded smoothly from commercially available **9** (Scheme 4.2). Esterification of **9** and *ortho*-iodination using iodine monochloride gave **11**. Sonogashira cross-coupling of **11** with ethynyltrimethylsilane provided alkynylaniline **12**, which afforded in turn the desired indole **13** *via* a CuI-mediated heteroannulation (Scheme 4.2).[312] The use of CuI in the heteroannulation step instead of palladium resulted in the simultaneous removal of the trimethylsilyl group, consequently removing the need for a further synthetic step to cleave it.

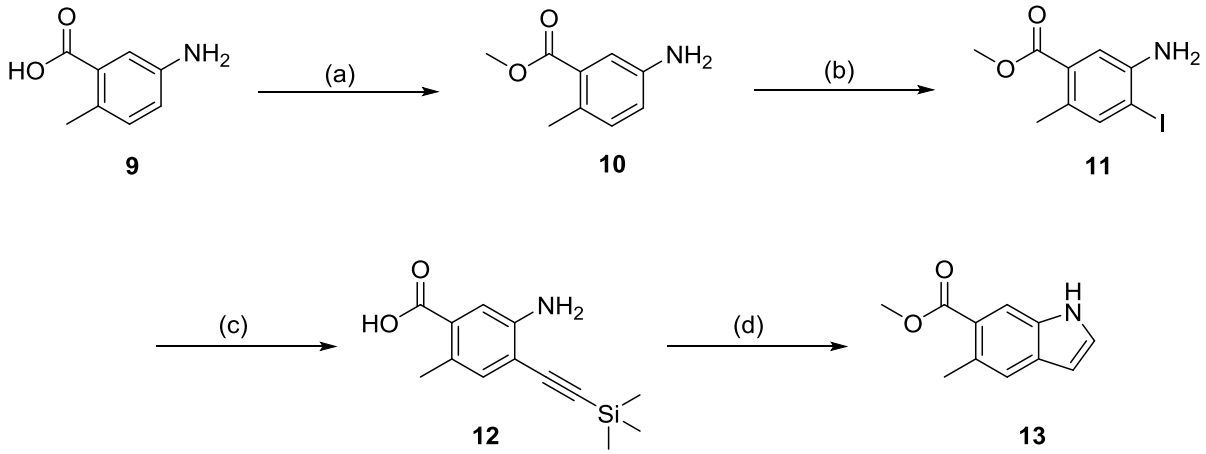

Scheme 4.2. Synthetic route to key indole intermediate 13. *Reagents & conditions*: (**a**) $SOCl_2$, MeOH, 12 h, r.t., 94%. (**b**) ICl, MeOH, H_2O, $CaCO_3$, 0 °C, 4 h, 56%. (**c**) Ethynyltrimethylsilane, $Pd(PPh_3)_2Cl_2$, CuI, Et_3N, r.t., 87%. (**d**) CuI, DMF, 100 °C, 74%.

The relatively low yield obtained for the *ortho*-iodination step resulted from the formation of the competing *ortho*-iodinated regioisomer. Fujii *et al*.[295] reported a 34% yield when using iodine monochloride at room temperature. However, dropwise addition of ICl at 0 °C, improved the yield of **11** to 56% (Scheme 4.2, step b). Starting material **10** can be recovered by hydrogenation of the carbon-iodine bond of the unwanted isomer using H_2 and Pd/C if required.

The alkylation of **13** with a range of alkyl halides provided the desired *N*-substituted indoles (**14a**-**c**), which could be readily nitrated under mild conditions using *in situ* formed acetyl nitrate to furnish the corresponding 3-nitroindoles (**15a**-**c**, Scheme 4.3).[313] The nitro group provided a useful synthetic handle for the incorporation of the selected R^3 side chains through a one-pot reductive acylation (Scheme 4.4).

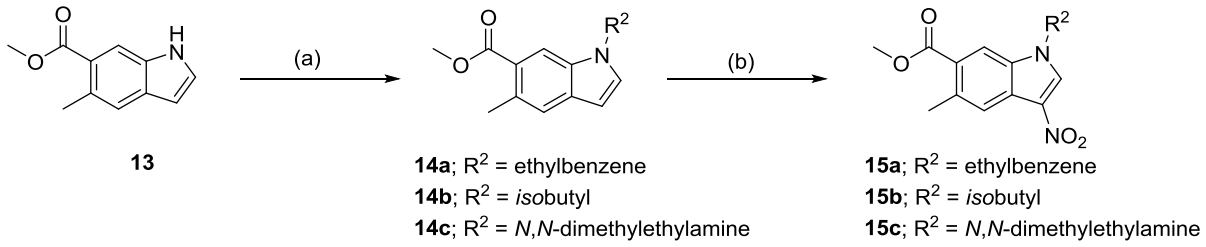

Scheme 4.3. *N*-alkylation and nitration. *Reagents & conditions*: (**a**) **14a** - (Bromoethyl)benzene, NaH, DMF, r.t., 8 h, 46%, **14b** - 1-bromo-2-methylpropane, NaH, DMF, r.t., 8 h, 63%, **14c** - 2-chloro-*N*,*N*-dimethylethylamine hydrochloride, NaH, DMF, r.t., 8 h, 68% (**b**) HNO_3, Ac_2O, 0 °C, 2 h, **15a** - 70%, **15b** - 44%, **15c** - 42%.

The reductive acylation was achieved *via* a Pd/C catalysed hydrogenation of the 3-nitroindole **15** to the corresponding amine, followed by *in situ* trapping of the reactive amine by an anhydride (Scheme 4.4).[314] In addition to the benefit of reducing a two-step process to a one-pot procedure,

this method also bypassed possible difficulties associated with purifying and handling reactive 3-aminoindoles. Ester hydrolysis gave the desired final compounds **16**(**a**-**f**), which were isolated as the sodium salts, to improve their water solubility for biological testing.

15(**a**-**c**) **16**(**a**-**f**)

Compound	R^2	R^3	Yield (%, over 2 steps)
16a	ethylbenzene	ethyl	61
16b	ethylbenzene	*iso*butyl	47
16c	*iso*butyl	ethyl	76
16d	*iso*butyl	*iso*butyl	82
16e	*iso*butyl	ethylbenzene	39
16f	*N*,*N*-dimethylethane	ethyl	42

Scheme 4.4. *Reagents & conditions*: (**a**) (i) Propionic anhydride, isovaleric anhydride or 2-phenylacetic anhydride, MeOH, 10% Pd/C, H_2, 40 °C, 1 h. (ii) MeOH, NaOH, reflux, 4 h. See table for yields.

4.4.3 Development of an alkyl-aryl cross coupling reaction

With a synthetic route developed to the series of compounds containing a methyl group at the R^1 position, an additional step was required to enable the incorporation of an *iso*propyl group at the same position. The initial strategy involved the use of a Suzuki cross-coupling.

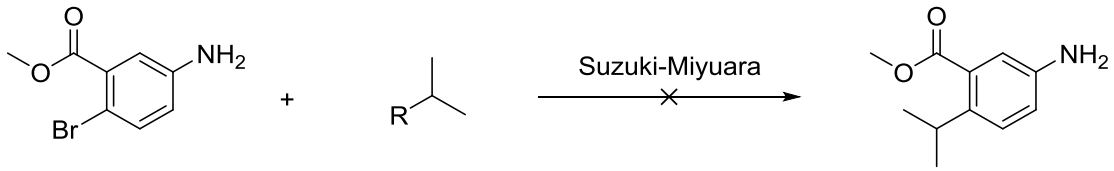

17 **19a**; R = $B(OH)_2$ **18**
19b; R = $B(O_2C_6H_{12})$

Scheme 4.5. Attempted Suzuki-Miyuara cross-coupling. Selected examples of the conditions screened – (**1**) **19a**, $Pd(PPh_3)_4$, Na_2CO_3 (H_2O), Toluene, Ethanol, reflux. (**2**) **19a**, $Pd(PPh_3)_4$, K_3PO_4, dioxane, 90 °C. (**3**) **19b**, $Pd(PPh_3)_4$, Cs_2CO_3, dimethoxyethane, H_2O, 125 °C, MW. (**4**) **19b**, $Pd(PPh_3)_4$, K_2CO_3, Toluene, Ethanol, H_2O, reflux. (**5**) **19a**, $Pd(dppf)Cl_2$, Na_2CO_3 (H_2O), DMF, 70 °C.

This was attempted by reacting methyl 5-amino-2-bromobenzoate (**17**) with both *iso*propylboronic acid (**19a**) or its pinacol ester **19b** under a wide variety of base, solvent and temperature conditions

(Scheme 4.5). However, this route proved to be unsuccessful under the reaction conditions investigated.

Further literature research revealed, that although transition metal-catalysed cross-coupling has seen significant advances in the coupling of sp^2-hybridised carbon nucleophiles with aryl or vinyl halides, only a handful of studies have been published concerning the analogous cross-coupling of secondary sp^3-hybridised carbon nucleophiles with aryl halides.[315] The major difficulties with this transformation are associated with two key steps in the mechanistic cycle: the transmetalation step, which is more difficult for secondary alkyl groups than other organic moieties, and the reductive elimination process, which competes with facile β-hydride elimination leading to isomerised coupling products (Figure 4.12).[316] The development of a successful catalytic method requires the identification of ligands that enhance the rate of reductive elimination relative to β-hydride elimination, thus suppressing product isomerisation.

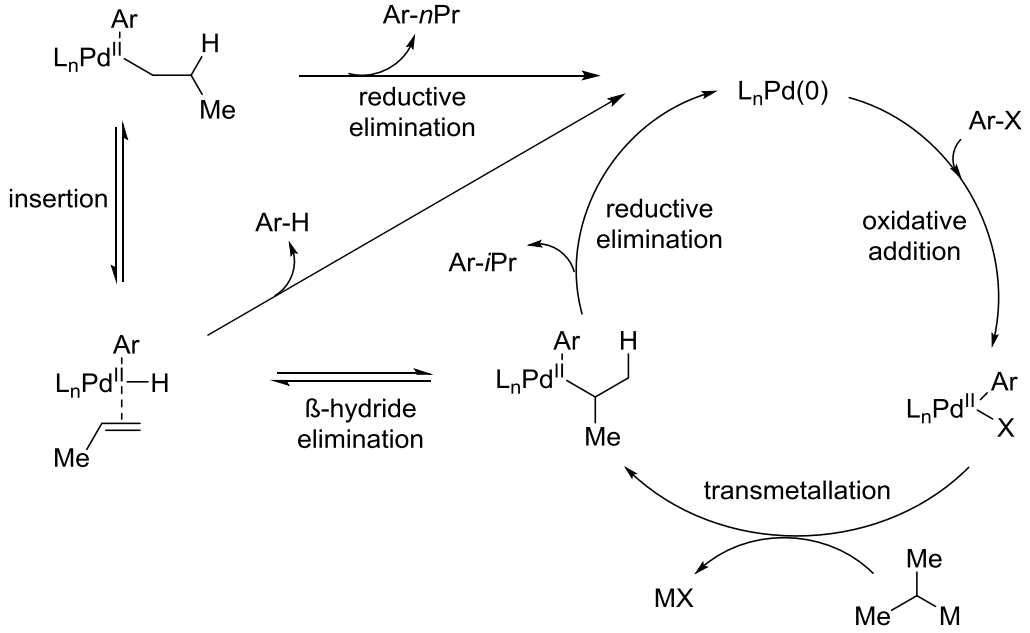

Figure 4.12. Proposed catalytic cycle for the cross-coupling of *i*-PrM and an aryl halide.[316]

Pioneering work carried out by Kumada/Tamao (1972)[317] and Hayashi (1984)[318] demonstrated that secondary alkyl Grignard reagents could be coupled with a limited range of aryl and vinyl halides using dichloro[1,3-bis(diphenylphosphino)-propane] nickel(II) ($NiCl_2$(dppp)) and dichloro[1,1'-bis(diphenylphosphino) ferrocene] palladium(II) ($PdCl_2$(dppf)). A test reaction using $PdCl_2$(dppf) and *iso*propyl zinc bromide resulted in the isolation of only the *n*-propyl product **20** that results from β-

hydride elimination (Figure 4.12), thus indicating that this catalytic method was not suitable for our substrate (Scheme 4.6).

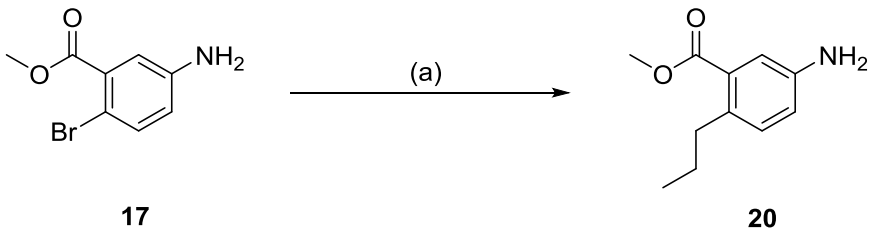

17 **20**

Scheme 4.6. Attempted cross-coupling using $PdCl_2$(dppf) and *iso*propyl zinc bromide yielded the undesired isomerised product 20. *Reagents & conditions*: (**a**) *Iso*propylzinc bromide, Pd(dppf)Cl_2, THF, 70 °C, 4 h.

Additional research in this area includes Molander's comprehensive study of the Pd-catalysed Suzuki-Miyaura coupling of secondary alkyltrifluoroborates with aryl halides in the presence of *n*BuPAd_2.[319] They reported the formation of the desired secondary product in a good ratio to the isomerised primary alkyl coupling product in a number of examples. However, poor product ratios and yields were obtained when electron-deficient and/or *ortho*-substituted aryl halide substrates were used, and limited functional group tolerance was observed. In other work Joshi-Pangu *et al*. reported a general Ni-catalysed Negishi process for the cross-coupling of secondary alkylzinc halides and aryl iodides.[320] They postulated that a Ni-based catalytic system could overcome the inherent problems associated with the Pd-catalysed systems based upon the success of nickel catalysis in cross-couplings involving an alkyl moiety. This process solved the β-hydride elimination problem, with selectivity up to 300:1 in favour of the secondary alkyl product over the primary product. However, the authors reported that this method did not work well with *ortho*-substituted aryl halides, in accordance with previous reports. This would limit the use of this method for our substrate **17** as it contains an *ortho* electron-withdrawing ester group. Hence unsurprisingly, no reaction occurred with our substrate under their reported conditions at 40 °C, or at higher temperatures of 60 °C, reflux or microwave irradiation at 120 °C, with starting material **17** being recovered in all cases.

A more recent investigation for a general Pd-catalysed procedure which facilitates the coupling of secondary nucleophiles and aryl halides was carried out by Han and Buchwald.[316] The published report detailed the Pd-catalysed coupling of secondary alkylzinc halides with aryl bromides using sterically-bulky phosphine ligands (Figure 4.13). They carried out a screen of phosphine ligands, which resulted in the identification of a new ligand CPhos (**21a**), which gave a high ratio of branched (*i*-Pr) to linear (*n*-Pr) products in excellent yields. Furthermore, they demonstrated that this method

was compatible with electron-deficient and/or *ortho*-substituted aryl halide substrates with only a small decrease in selectivity and yield reported in these particular cases.

CPhos (21a) **RuPhos (21b)**

Figure 4.13. The structures of the CPhos (21a) and RuPhos ligands (21b).

As CPhos (**21a**) was not commercially available, a test reaction using this method with the commercially available phosphine ligand RuPhos (**21b**) was attempted. Buchwald obtained a 3:1 ratio of the branched (*i*-Pr)-**24** to linear (*n*-Pr)-**25** product with an overall yield of 78% when **21b** was used in the presence of an *ortho*-ether substituted aryl bromide **22**. In contrast, a 27:1 ratio of products with an overall yield of 97% was obtained when CPhos (**21a**) was used with the same substrate **22** (Scheme 4.7).[316]

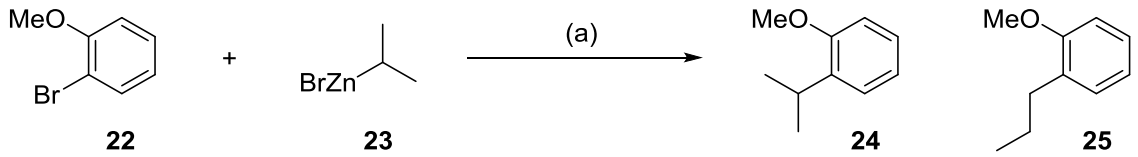

22 **23** **24** **25**

Scheme 4.7. Ligand effects in the coupling of 22 and 23. (a) $Pd(OAc)_2$ (1 mol%), ligand (**21a**/**21b**) (2 mol%), THF, 0 °C → r.t., 30 minutes. **21a – 24**:**25** (27:1), 97%; **21b – 24**:**25** (3:1), 78%.[316]

We therefore postulated that if a similar selectivity and yield could be achieved with our substrate using RuPhos (**21b**), this would validate this approach and CPhos (**21a**) would be synthesised for testing with our substrate.

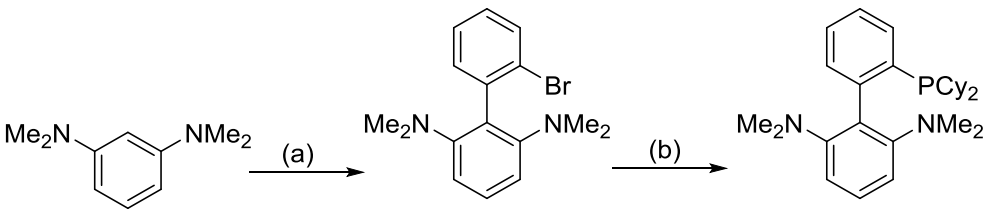

26 **27** CPhos (**21a**)

Scheme 4.8. Synthesis of the CPhos (21a) ligand. *Reagents & conditions*: (**a**) (i) *n*-BuLi, hexane, reflux. (ii) 2-Bromochlorobenzene, hexane, reflux, 84% (**b**) (i) *n*-BuLi, THF, -78 °C. (ii) $ClPCy_2$, -78 °C ⟶ r.t., 72%.

The utilisation of Buchwald's Pd-catalysis system and the RuPhos ligand provided an inseparable 6:1 mixture of the desired branched (*i*-Pr) product **18** to the unwanted linear (*n*-Pr) product **20**, with an overall yield of 85% (Figure 4.14). The increase in selectivity and yield when compared to Buchwald's system presumably resulted from the electron-donating effect of the amine reducing the electron-deficiency of the aryl bromide. Encouraged by this very promising result, the synthesis of the CPhos ligand (**21a**) was carried out *via* a 3-step process starting from commercially available N^1,N^1,N^3,N^3-tetramethylbenzene-1,3-diamine **26** (Scheme 4.8).[316] *Ortho*-lithiation of **26** and subsequent reaction with 2-bromochlorobenzene yielded **27**. Lithium-halogen exchange of the aryl bromide of **27** followed by reaction with chlorodicyclohexylphosphine furnished the desired CPhos (**21a**) ligand (Scheme 4.8).

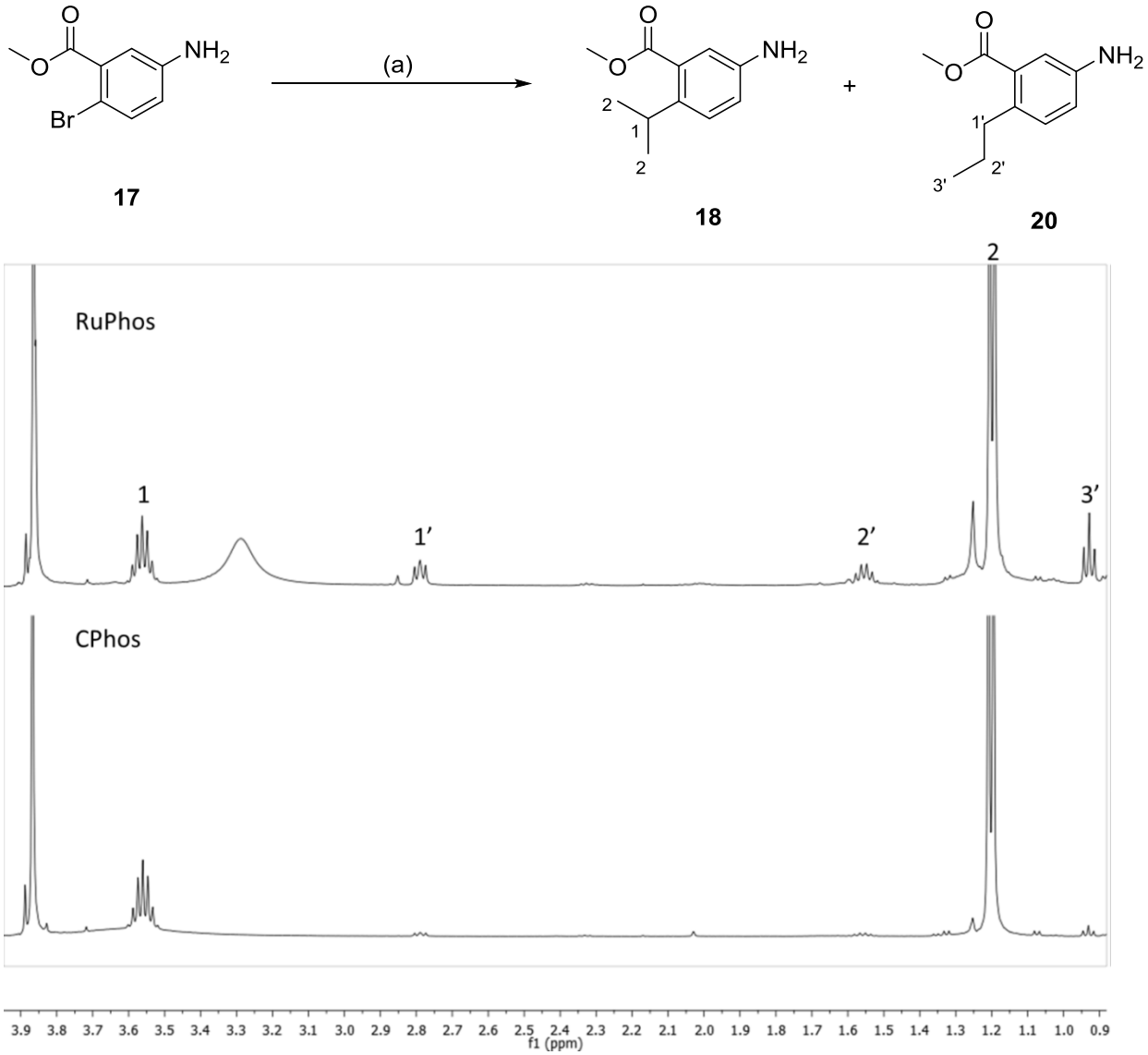

Figure 4.14. Aryl-alkyl cross-coupling reaction in the presence of the RuPhos (21b) or CPhos (21a) ligand. *Reagents & conditions*: (**a**) $Pd(OAc)_2$, *Iso*propylzinc bromide (0.5 M in THF), toluene, r.t., 30 minutes. ^{1}H NMR spectra – magnification of the alkyl region. (*Top*) RuPhos – 85%, **18**:**20** (6:1). (*Bottom*) CPhos – 93%, **18**:**20** (>30:1).

With the CPhos ligand **21a** in hand, the cross-coupling reaction between aryl halide **17** and *iso*propyl zinc bromide (**23**) was repeated. In the presence of **21a**, the cross-coupling reaction occurred with very high selectivity (>30:1) for the branched (*i*-Pr) product **18** to the linear (*n*-Pr) product **20** with an excellent overall yield of 93% (Figure 4.14). Han and Buchwald provided evidence in their report that the improved ratio of branched to linear products in the presence of the CPhos ligand was due to the slow relative rates of β-hydride elimination-reinsertion versus reductive elimination (Figure 4.12).[316]

This mild and highly selective cross-coupling reaction provides an easy, high-yielding route to the required starting material **18**. This methodology will facilitate the future synthesis of a range of analogues with an *iso*propyl group at the R^1 position. The future selection of substituents for the R^2 and R^3 positions will be guided by biological data acquired for analogues **16**(**a**-**f**), which contain a methyl group at the R^1 position.

4.5 Series 2 Inhibitors

4.5.1 Design of series 2 inhibitors

While carrying out the docking studies on the first series of potential PICK1 PDZ inhibitors, it was observed that in certain cases, the compound docked in the pocket in a flipped orientation placing the indole 2'-position pointing into the pocket instead of out of it. As a result, it was decided to modify the indole scaffold to exploit this potential new binding mode and ultimately identify a second series of PICK1 PDZ inhibitors. This led to the design of indole scaffold **28** (Figure 4.15).

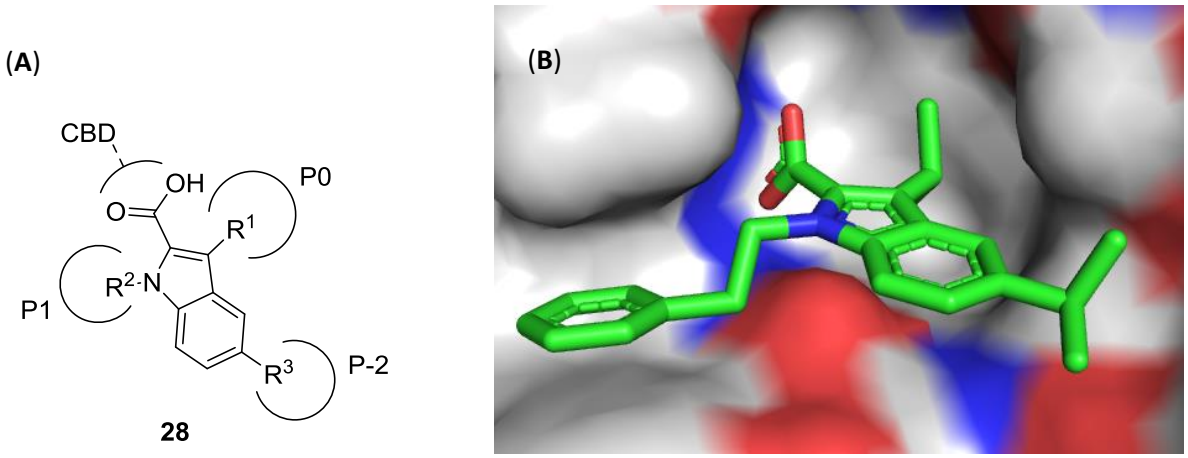

Figure 4.15. (A) Core indole scaffold 28 of the series 2 inhibitors with the predicted binding mode highlighted. (B) Predicted GOLD binding mode of a designed series 2 inhibitor in the PICK1 PDZ domain. The solvent accessible surface of the protein is shown, with positively charged regions in blue and negatively charged regions in red. Ligand is shown as sticks, carbons in green, nitrogens in blue and oxygens in red.

This alternative binding mode has since be identified by Ducki and co-workers for a related indole peptidomimetic designed to competitively inhibit the interaction between the C-terminal domain of the 5-HT_{2A} serotonin receptor and the PDZ1 domain of PSD-95.[271] The design, synthesis and biological evaluation of a series of substituted indoles identified compound **29** which inhibited the 5-HT_{2A}/PSD-95 PPI with an IC_{50} value of 190 µM. Subsequent determination of the three-dimensional structure of the protein/ligand complex through $^{1}H–^{15}N$ HSQC NMR analysis of the PSD-95 PDZ domain in the absence or presence of **29** coupled with intermolecular nuclear Overhauser effect (NOE) restraints and high ambiguity driven protein-protein DOCKing (HADDOCK) provided an insight into the binding mode of **29**. The NMR solution structure revealed that the indole-2'-COOH of **29** interacted with the backbone of the carboxyl binding domain (GLGF), in agreement with the predicted binding of both **29** and in our case **28**.

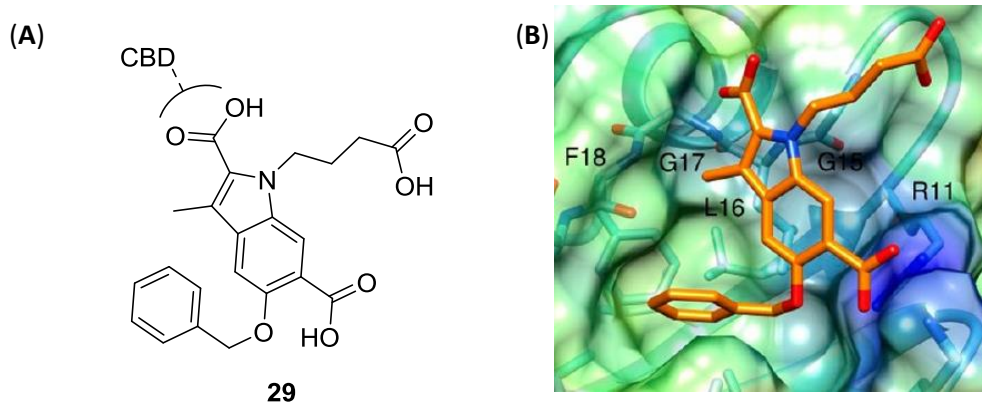

Figure 4.16. (A) The structure of 5-HT_{2A}/PSD-95 PPI inhibitor 29. (B) NMR solution structure of the PSD-95 PDZ1/ligand 29 complex.[271] Protein is shown as a surface representation (Coulombic charges). Ligand **29** is shown in sticks with carbon atoms in orange, oxygen atoms in red, and nitrogen atoms in blue.

Similarly to the series 1 inhibitors, the analysis of known PICK1 peptide ligands and an extensive modelling study led to the selection of a range of substituents on the indole scaffold **29**, which should facilitate strong binding to the PICK1 PDZ domain (Figure 4.17). The predicted binding score (GoldScore) for series 2 was shown to be comparable with the first series. Furthermore, it was proposed that access to the desired analogues in this series should be less challenging synthetically than series 1.

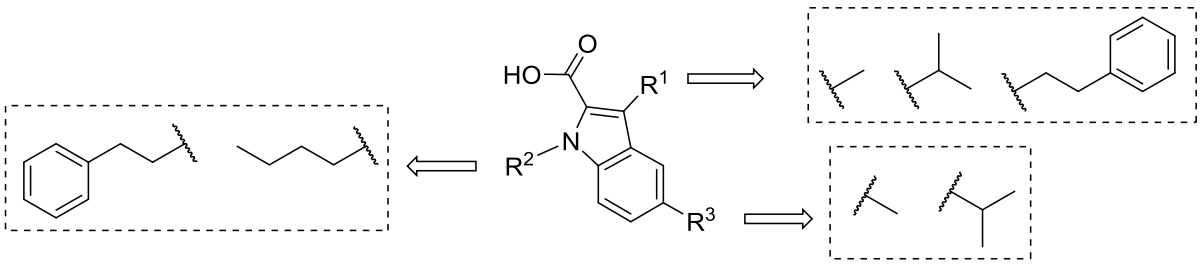

Figure 4.17. Selected R^1, R^2 & R^3 substituents for series 2 small molecule inhibitors.

4.5.2 Synthesis of series 2 inhibitors

The route to the second series of peptidomimetics was greatly simplified by the removal of the carboxylic acid at the 6-position of the indole ring. This resulted in a symmetrical starting material which did not require pre-functionalisation in order to control the indole formation, as only one isomer was possible. To take advantage of this, a modified version of the robust Fischer indole synthesis was chosen as the key step in this route.[321] Furthermore, given the large number of commercially available hydrazine compounds, it was possible to introduce the *iso*propyl substituent at the 5-position without the need for the troublesome cross-coupling reaction required for the previous series of compounds.

The proposed synthesis of the desired compounds involved a 3-step procedure starting with a Fischer indole synthesis, followed by *N*-alkylation and ester hydrolysis to give the free acid. The route began with condensation of the substituted hydrazine hydrochloride with an α-ketoacid ester in an acetic acid catalysed Fischer indole cyclisation.[321] The α-ketoacid esters **30b** and **30c** required for the Fischer indole step were prepared from their corresponding α-ketoacid (Scheme 4.9B) or by a Grignard reaction in the case of methyl 2-oxo-5-phenylpentanoate **30a** (Scheme 4.9A).

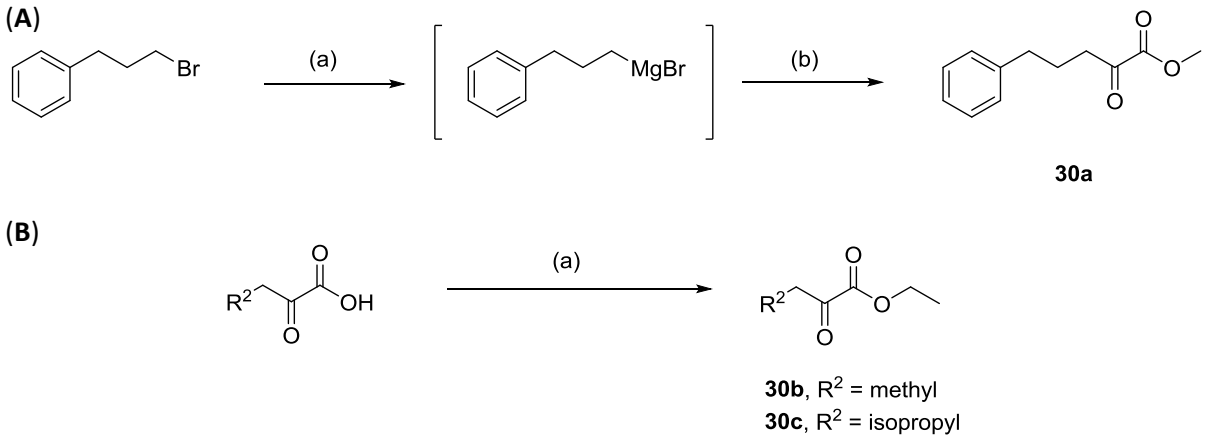

Scheme 4.9. Synthesis of the α-ketoacid esters 30(a-c). *Reagents & conditions*: **Route A** (**a**) Mg, THF, reflux, 1 h. (**b**) Dimethyl oxalate, Et_2O, -78 °C → 0 °C, 69%. **Route B** (**a**) H_2SO_4, EtOH, reflux, 6 h, quantitative.

The condensation of substituted hydrazine hydrochlorides **31a** and **31b** with α-ketoacid ester **30a** provided the desired indole esters **32a** and **32b** as an inseparable mixture of the methyl and ethyl esters, resulting from a transesterfication reaction between the ethanol solvent that was used and the α-ketoacid methyl ester **30a** (Scheme 4.10). This transesterification reaction did not prove to be too troublesome as the ester group was hydrolysed in the final step to give the corresponding acid.

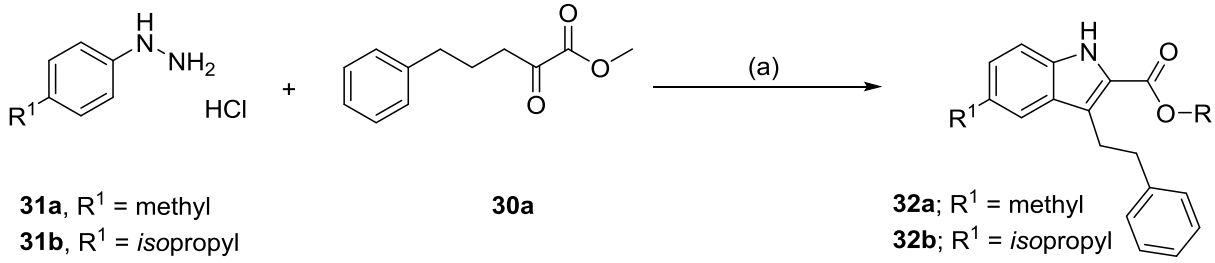

31a, R^1 = methyl
31b, R^1 = *iso*propyl

30a

32a; R^1 = methyl
32b; R^1 = *iso*propyl

Scheme 4.10. Synthesis of compounds 32(a-b). (a) AcOH, EtOH, reflux, 4-6 h. R = methyl/ethyl.

In the case of **32**(**c**-**f**), the required α-ketoacid was protected as the α-ketoacid ethyl ester **30**(**b**-**c**) to avoid the formation of the mixture of methyl and ethyl esters observed with **32a** and **32b** (Scheme 4.9). A significantly reduced yield was obtained for the Fisher indole reaction when γ-branched α-ketoacid esters were used, as demonstrated by **32d** and **32f** (Scheme 4.11).

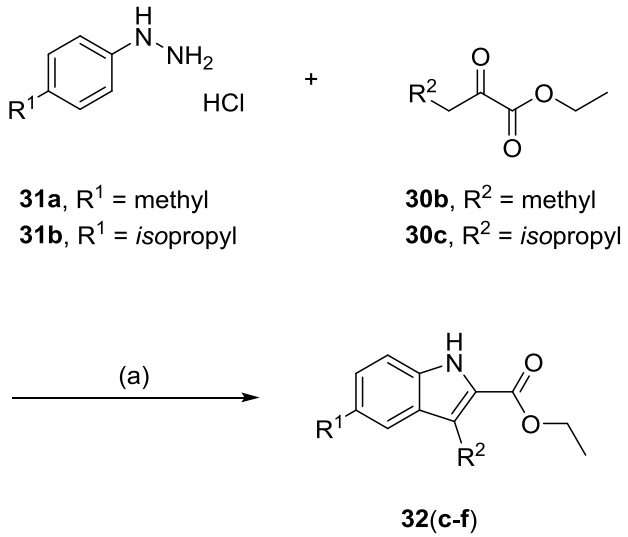

31a, R^1 = methyl
31b, R^1 = *iso*propyl

30b, R^2 = methyl
30c, R^2 = *iso*propyl

32(**c-f**)

Compound	R^1	R^2	Yield (%)
32c	*Iso*propyl	Methyl	67
32d	*Iso*propyl	*Iso*propyl	38
32e	Methyl	Methyl	67
32f	Methyl	*Iso*propyl	28

Scheme 4.11. Synthesis of compounds 32(c-f). (a) AcOH, EtOH, reflux, 4-6 h. For yield see table.

The final steps to convert the indoles **32** to the desired compounds **33** involved *N*-alkylation of the indole nitrogen followed by ester hydrolysis. This was achieved using sodium hydride in DMF in the presence of the appropriate alkyl bromide, followed by sodium hydroxide mediated ester hydrolysis. This method was used successfully to synthesise **33b** and **33c** (Scheme 4.12).

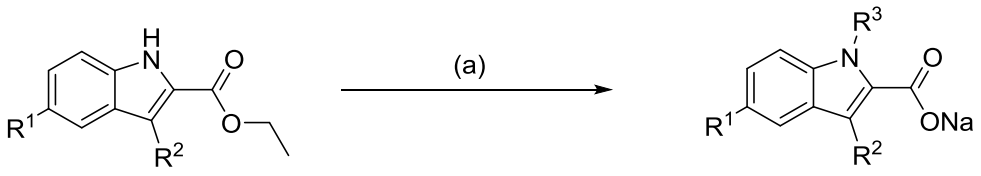

32(**a-j**) **33**(**a-j**)

Compound	R^1	R^2	R^3	Yield (%)
33a	Methyl	Ethylbenzene	Ethylbenzene	50
[a]**33b**	*Iso*propyl	Ethylbenzene	*n*-butyl	68
[a]**33c**	*Iso*propyl	Methyl	*n*-butyl	57
33d	*Iso*propyl	Methyl	Ethylbenzene	38
33e	*Iso*propyl	*Iso*propyl	Ethylbenzene	41
33f	*Iso*propyl	Ethylbenzene	Ethylbenzene	53
33g	*Iso*propyl	*Iso*propyl	*n*-butyl	81
33h	Methyl	Methyl	Ethylbenzene	56
33i	Methyl	*Iso*propyl	*n*-butyl	73
33j	Methyl	*Iso*propyl	Ethylbenzene	41

Scheme 4.12. Synthesis of final compounds 33(a-j). *Reagents & conditions*: (**a**) Appropriate alkyl bromide, NaH (4 eq.), DMF, 100 °C, 5 h. [a] **Final compounds 33b & 33c were synthesised *via* an alternative two-step procedure.** *Reagents & conditions*: (**a**)(i) Appropriate alkyl bromide, NaH (2 eq.), DMF, 100 °C, 4 h. (ii) NaOH (2N), EtOH, reflux, 4 h.

The *N*-alkylation of the indole ring did not go to completion when attempting to *N*-alkylate **32a** with (bromoethyl)benzene. In an attempt to push the reaction to completion, a further 2 equivalents of sodium hydride were added to the reaction mixture. This resulted in complete *N*-alkylation of **32a** with concurrent hydrolysis of the ester to provide the desired acid product **33a** in one step. This was thought to have occurred due to the reaction of NaH with H_2O during the addition of the extra equivalents of NaH, to form NaOH. The NaOH would have subsequently hydrolysed the ester. This method was observed to be reproducible with the other intermediates and proceeded in reasonable yields in all cases. This route was therefore chosen as a one-pot procedure for the synthesis of the desired compounds (Scheme 4.12).

4.6 Biological Assessment

The series 1 and series 2 compounds were investigated for their ability to bind the PICK1 PDZ domain in a fluorescence polarisation (FP) assay by the Gether group (University of Copenhagen, Denmark). In this FP competition binding experiment, fixed concentrations of PICK1 protein and a fluorescently labelled peptide were titrated with an increasing amount of ligand. Competitive binding of the ligand results in a decrease in FP signal. An Oregon Green-fluorescently labelled peptide (OG-DATC13) corresponding to the 13C-terminal residues of the dopamine transporter (DAT), a potent PICK1 PDZ domain ligand was used in the assay. This assay identified 5 compounds with promising PICK1 PDZ binding activity, series 1 compound **16a**, and series 2 compounds **33c**, **33e**, **33g** and **33j**.

The series 2 compounds could be grouped into two pairs based on their relative binding affinities and chemical structure. The first pair **33e** and **33j**, displayed moderate binding affinities with K_i values of 63.9 and 23.8 µM respectively (Figure 4.18). Analysis of the predicted binding modes of these compounds in comparison with their binding affinities revealed insights into important factors for binding.

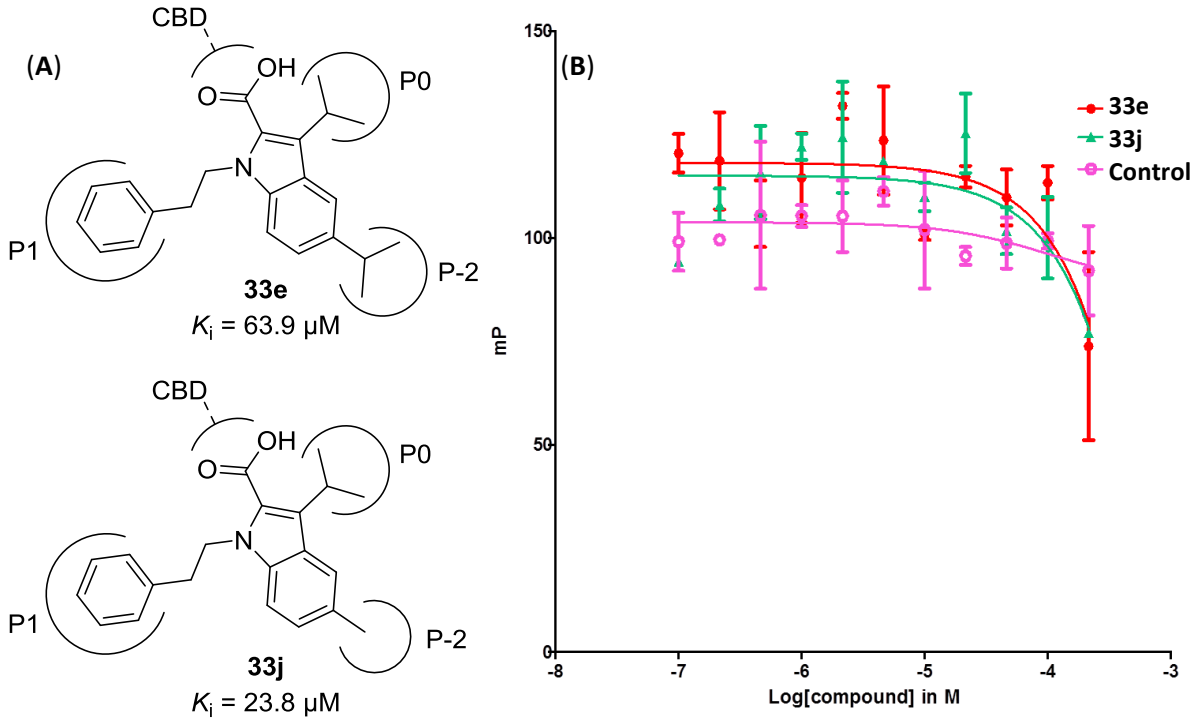

Figure 4.18. 33e and 33j dose-dependently inhibit peptide binding to the PICK1 PDZ domain (**A**) Chemical structure of **33e** and **33j**. (**B**) FP competition curves for **33e** and **33j** using a fixed concentration of Oregon Green-labelled DAT peptide (OG-DAT C13,~30 nM) and incubation (1 hour) together with purified PICK1 and indicated compounds before FP measurements. The control is a 5% DMSO/buffer solution. Data are shown as bound relative to maximum bound OG-DAT C13 (means of triplicates ± SE) and representative of n = 2. Data provided by the Gether group.

Both compounds contain an *iso*propyl group which is predicted to reside in the P0 pocket of the PICK1 PDZ domain. This is in agreement with the preference for a valine in this position of the endogenous peptides. Similarly, both compounds contain an ethylbenzene substituent which is predicted to bind in the variable P-1 pocket. This would suggest that the phenyl group is positioned correctly to form the proposed π-π stacking interaction with the Phe[53] present in the PICK1 PDZ domain. Finally, an approximate 3-fold increase in binding affinity was observed for **33j**, which contains a methyl group in the P-2 position in contrast to the *iso*propyl group present at the same position on **33e**. Previous studies undertaken with the endogenous peptides revealed that the size of the P-2 pocket is influenced by the conformation of the Ile[37] residue, which is set by the amino acid side chain of the P0 residue. It was observed that the presence of a bulky residue (i.e. valine) in the P0 pocket induced a conformational change which reduced the size of the P-2 pocket, thereby increasing the preference for smaller substituents at this position. This is in agreement with the increased binding affinity observed on replacing the *iso*propyl of **33e** for the smaller methyl of **33j** (Figure 4.18).

The second pair of series 2 inhibitors displayed an order of magnitude increase in binding affinity for the PICK1 PDZ domain with low μM affinities [K_i = 5.8 μM (**33g**), 2.0 μM (**33c**)]. The large increase in binding affinity appears to be largely due to the presence of an *n*-butyl group in the P-1 position of **33g** and **33c**, in place of the ethylbenzene present in **33e** and **33j** (Figure 4.19).

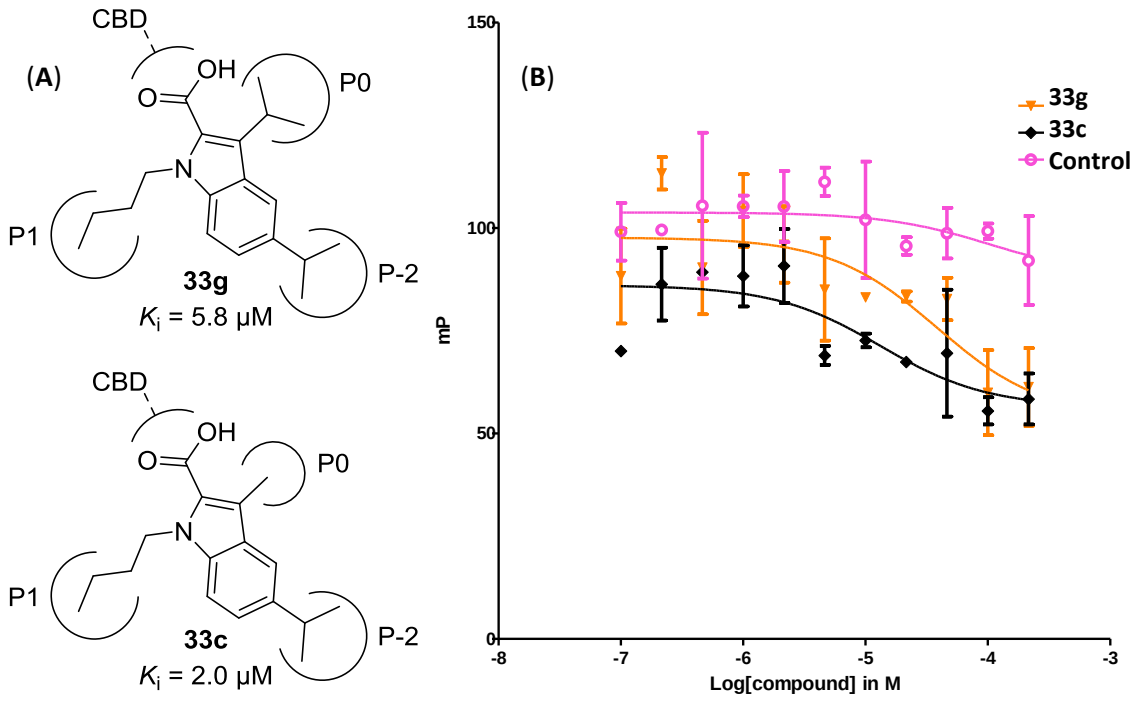

Figure 4.19. 33g and 33c dose-dependently inhibit peptide binding to the PICK1 PDZ domain (**A**) Chemical structure of **33g** and **33c**. (**B**) FP competition curves for **33g** and **33c**. Data provided by the Gether group.

The *n*-butyl substituent was selected as a mimic for the hydrophobic backbone of the lysine residue of the GluR2 peptide (VKI). This suggests that optimal binding is achieved with substituents which attempt to mimic the residues present on the endogenous peptides. The *n*-butyl substituent appears to result in a preference for a bulkier *iso*propyl group in the P-2 position. However, the placement of a bulkier group in the P-2 pocket results in a conformational change of Ile[37], thereby reducing the size of the P0 pocket. This is in agreement by the approximate 3-fold increase in affinity observed for **33c** which contains a smaller methyl group in the P0 pocket when compared to **33g** which contains an *iso*propyl.

One compound, **16a** from the series 1 inhibitors displayed a promising binding affinity with a K_i value of 8.7 μM. Similarly, to **33e** and **33j**, **16a** contains an ethylbenzene substituent which is predicted to form a π-π interaction in the P-1 pocket. All of the series 1 inhibitors contain a methyl group in the P0 position, and it appears this induces a preference for an ethyl substituent at the P-2 position.

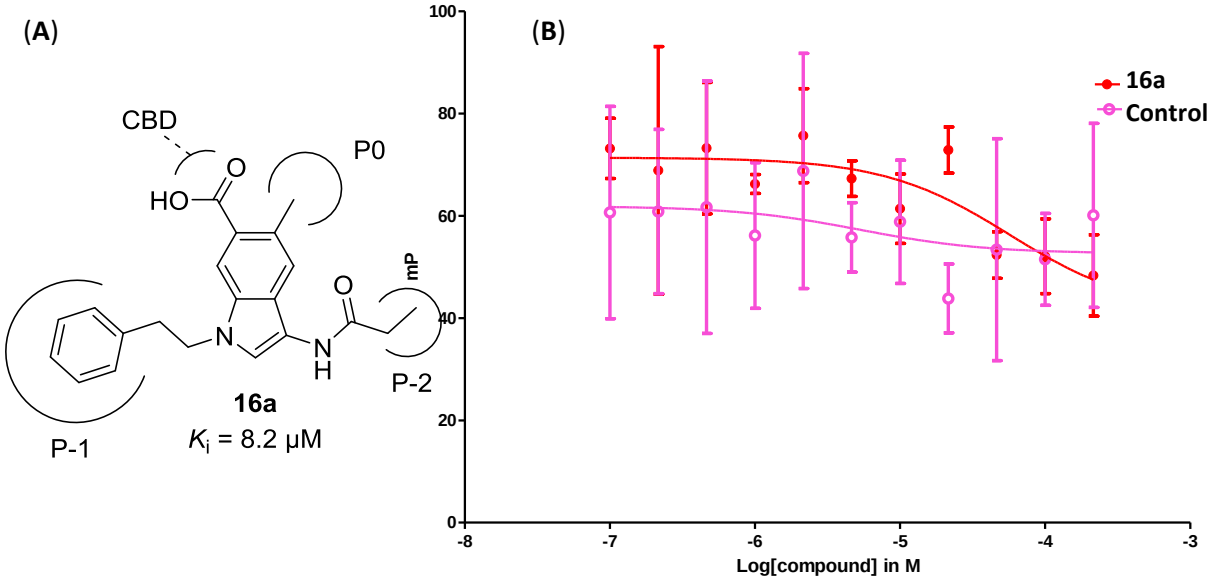

Figure 4.20. 16a dose-dependently inhibits peptide binding to the PICK1 PDZ domain (**A**) Chemical structure of **16a**. (**B**) FP competition curves for **16a**. Data provided by the Gether group.

In the above cases the error on the data points is higher than normally observed for peptides screened in this FP assay. This is believed to be due to the kinetics of binding of these molecules which appear to have slower binding rates than peptides. Further control experiments are currently being carried out to rule out other possibilities such as compound precipitation.

4.7 Conclusions & Future Work

PICK1 contains a single *N*-terminal PDZ domain that interacts with the PDZ motifs of several proteins, which have roles in neuronal cell morphology, mitochondrial-dependent apoptosis and synaptic plasticity. Herein we reported the design and synthesis of two series of small molecule peptidomimetic inhibitors of the PICK1 PDZ domain. A docking study based on Fujii's previously reported PDZ domain inhibitor **6** led to the identification of two indole scaffolds **7** and **29**, which were subsequently used as core fragments for two series of compounds designed to inhibit PICK1 PDZ domain mediated PPIs. Molecular modelling and analysis of known endogenous PICK1 peptide ligands guided the selection of a range of substituents for the indole scaffolds, with the aim of identifying selective high affinity binders.

The development of an 8-step synthetic route to the series 1 inhibitors involving late stage functionalisation of indole intermediate **13** provided access to 6 diverse analogues. These analogues contain a methyl group in the R^1 position originating from the indole intermediate **13**, however, the design process had identified an *iso*propyl group as the optimum R^1-substituent for binding in the P0 pocket. The lack of a general and comprehensive method to introduce diversity at this position is presumably a contributing factor to the exclusive use of a methyl group at this position in the previously reported indole-based peptidomimetic PDZ inhibitors.[271,273,274,295–297]

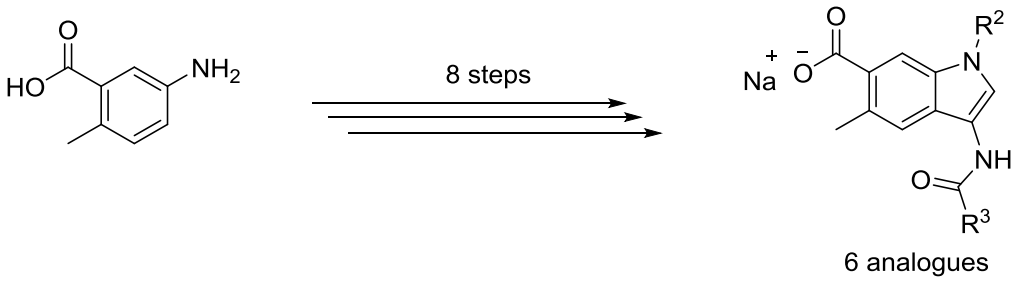

Scheme 4.13. Summary of the synthetic route utilised to access the series 1 inhibitors.

The most efficient method for the introduction of diversity at the R^1 position is a cross coupling reaction. However, few studies have been reported which address the issues associated with the challenging cross-coupling reaction of secondary sp^3-hybridised carbon nucleophiles with aryl halides. Further investigation led to the identification of a recent method reported by the Buchwald group,[316] which utilised a Pd(II)-CPhos (**21a**) catalyst system to promote the sp^3-sp^2 cross coupling reaction. This method was subsequently employed to access the required *iso*propyl starting material **18** in high yield and selectivity for the desired product over the linear (*n*-Pr) product **20**. This method

not only addressed the issues we encountered but also could provide a general method by which to incorporate an *iso*propyl or similar branched alkyl substituent at this position of related indole peptidomimetics.

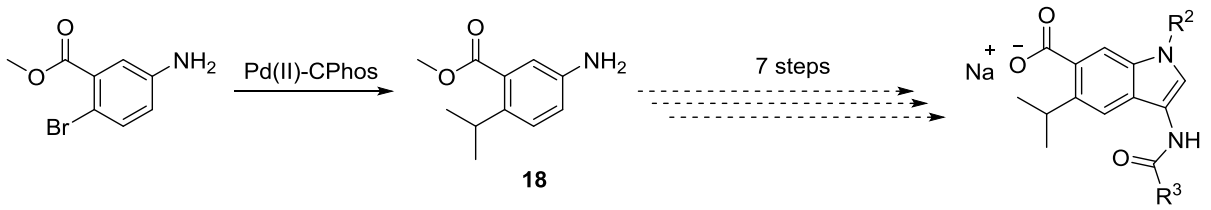

Scheme 4.14. A Pd(II)-CPos (21a) catalysed sp^3-sp^2 cross coupling reaction provided *iso*propyl derivative 18 which could be utilised to provide series 1 inhibitors with an *iso*propyl substituent at the R^1 position.

Biological assessment of these analogues in a FP binding assay revealed that **16a** displayed high affinity for the PICK1 PDZ domain with a K_i value of 8.2 μM. Optimisation of this promising lead compound will explore the modification of the R^1 and R^2 positions. In particular, the development of the Pd(II)-CPhos (**21a**) cross coupling reaction to access to the *iso*propyl reagent **18** will facilitate the synthesis of the *iso*propyl derivative **34**. The second optimisation approach will be guided by the observed order of magnitude increase in binding affinity observed in the series 2 inhibitors on exchanging the ethylbenzene substituent binding in the P-1 pocket for an *n*-butyl substituent. A similar modification of **16a** could greatly improve its binding affinity. Biological assessments of these analogues **34** and **35** will guide additional optimisation studies.

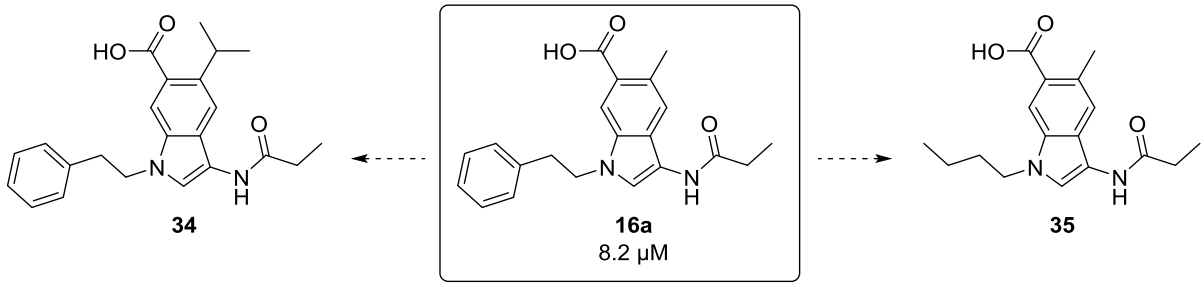

Scheme 4.15. Proposed optimised series 1 analogues.

An expedient and versatile 2-step synthesis was developed to access the novel series 2 inhibitors. A Fischer indole synthesis was utilised to provide the indole ring containing the desired substituents at the R^1 and R^2 positions. A subsequent one-pot domino alkylation-hydrolysis incorporated the R^3 substituents and hydrolysed the ester to form the desired acid products. This concise route was used to synthesis 10 analogues which were assessed in a FP binding assay. Two of the analogues **33g** and **33c** displayed potent binding affinity for the PICK1 PDZ domain with K_i values of 5.8 and 2.0 μM

respectively. Noteworthy observations from the preliminary SAR study revealed that an alkyl substituent is optimal at the R^3 position, and that cross-talk between the P0 and P-2 pockets of the PICK1 PDZ domain is an important regulator of ligand binding affinity. Future optimisation studies will attempt to identify the optimal alkyl substituent at the R^3 position and the best combination of substituents at the R^1 and R^2 positions for high affinity binding.

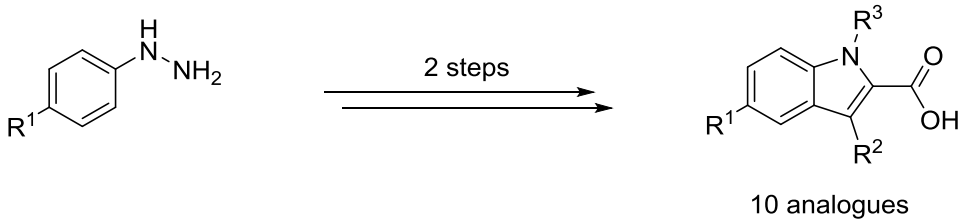

Scheme 4.16. Summary of the synthetic route utilised to access the series 1 inhibitors.

In conclusion, two series of novel peptidomimetic PICK1 PDZ domain inhibitors were developed. Three of these compounds displayed <10 μM binding affinity for the PICK1 PDZ domain, which are among the most active inhibitors of a PDZ domain reported to date. Interestingly, the series 2 inhibitors which were designed to exploit a potentially novel binding mode resulted in a higher percentage of active binders with higher binding affinities for the PICK1 PDZ domain than the series 1 inhibitors. The high affinity binders from both series will be utilised as chemical tools for the investigation of PICK1's role in disease states such as schizophrenia, depression and particularly to investigate its role in activation and surface expression of the dominant breast cancer drug target HER2. Future optimisation of these compounds will aim to identify a nanomolar inhibitor of a PDZ domain as a part of a PICK1 PPI inhibition drug discovery programme.

4.8 Experimental

4.8.1 General Considerations

See Section 2.8.1 for general considerations.

4.8.2 General Methods

General Method A: Indole *N*-alkylation

To a stirred suspension of sodium hydride (2.0 eq., 60% in mineral oil) in anhydrous DMF (3 mL/mmol) at 0 °C was added a solution of the appropriate indole (1.0 eq.) in anhydrous DMF (2 mL/mmol) dropwise. The mixture was stirred at 0 °C for 30 minutes followed by the slow addition of the appropriate alkyl bromide (1.5 – 3.0 eq.). The mixture was stirred at room temperature for 8 hours. The mixture was poured onto crushed ice (10 g/mmol) and extracted with ether (×3). The combined organics were washed with water, brine, dried over $MgSO_4$, filtered and concentrated *in vacuo*. The crude product was purified *via* the Biotage SP4 (silica-packed SNAP column).

General Method B: Nitration

Preformed acetyl nitrate was generated by the dropwise addition of neat 70% HNO_3 (3.0 eq.) to acetic anhydride (2 mL/mmol) at 0 °C, followed by standing at room temperature for 10 minutes. To a stirred solution of the appropriate indole (1.0 eq.) in acetic anhydride (5 mL/mmol) at -78 °C was added dropwise the solution of freshly prepared acetyl nitrate. The mixture was allowed to warm to 0 °C and maintained at this temperature for 2 hours. The mixture was poured into ice (10 g/mmol) and stirred for 1 hour. The aqueous solution was extracted with EtOAc (×3). The combined organic extracts were washed with brine, dried over $MgSO_4$, filtered and concentrated *in vacuo*. The crude product was purified *via* the Biotage SP4 (silica-packed SNAP column).

General Method C: Reductive acylation

To a solution of the nitro indole (1.0 eq.) and the appropriate anhydride (3.0-8.0 eq.) in anhydrous methanol (14 mL/mmol) was added 10% palladium on carbon (0.4 eq.). The reaction mixture was heated at 40 °C under a hydrogen atmosphere (hydrogen filled balloon) for 1 hour. The catalyst was removed by filtration through Celite and the mixture was concentrated in *vacuo*.

General Method D: Ester hydrolysis

The crude ester was treated with an aqueous sodium hydroxide solution (2N, 0.1 mL) in methanol (1 mL) and heated at reflux for 16 hours. The reaction was concentrated *in vacuo* and the crude product was purified *via* the Biotage SP4 (Reverse-phase silica-packed SNAP column 4 g; 0-8% MeOH/H_2O).

General Method E: Fischer Indole Synthesis

A mixture of the appropriate hydrazine monochloride (1.0 eq.), corresponding α-ketoacid ester (1.6 eq.) and glacial acetic acid (0.2 eq.) in anhydrous ethanol (2 mL/mmol) was heated at reflux for 4-6 hours, cooled to room temperature and concentrated *in vacuo*. The crude product was purified *via* the Biotage SP4 (silica-packed SNAP column; EtOAc/hexanes).

General Method F: One-pot indole *N*-alkylation and ester hydrolysis

Anhydrous DMF (3 mL/mmol) was added to sodium hydride (2.0 eq., 60% in mineral oil) in an oven-dried round bottom flask. The solution was cooled to 0 °C and the appropriate indole (1.0 eq.) in anhydrous DMF (1 mL/mmol) was added. The mixture was stirred at room temperature for 30 minutes followed by the addition of the alkyl bromide (1.5 eq.). The reaction was heated at 100 °C for 4 hours. A second portion of sodium hydride (2.0 eq., 60% in mineral oil) was added and the reaction stirred at 100 °C for 1 hour. The reaction was then cooled to room temperature, poured into ice water and extracted with Et_2O (x3). The combined organic extracts were washed with brine, dried over $MgSO_4$, filtered and concentrated *in vacuo*. The crude product was purified *via* the Biotage SP4 (silica-packed SNAP column; EtOAc/hexanes).

4.8.3 Experimental procedures (Series 1)

Methyl 5-amino-2-methylbenzoate (10)

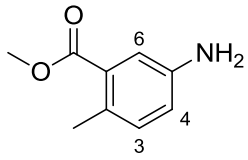

Thionyl chloride (2.4 mL, 33.0 mmol, 10.0 eq.) was added to a solution of 5-amino-2-methylbenzoic acid **9** (0.5 g, 3.3 mmol, 1.0 eq.) in anhydrous methanol (10 mL/mmol) at 0 °C. The reaction was then stirred at room temperature for 12 hours. The solvent was removed under reduced pressure and the resulting white solid was dissolved by the slow addition of a saturated aqueous solution of $NaHCO_3$ (20 mL). The mixture was extracted with EtOAc (3 × 20 mL) and the combined organic extracts were washed with brine (20 mL), dried over $MgSO_4$, filtered and concentrated. The title product **10** was obtained as a colourless oil (0.51 g, 94%), which did not require further purification. **^{1}H NMR** (400 MHz, Chloroform-*d*) δ 7.25 (d, *J* = 2.7 Hz, 1H, C6-H), 7.02 (d, *J* = 8.1 Hz, 1H, C3-H), 6.75 (dd, *J* = 8.1, 2.7 Hz, 1H, C4-H), 3.87 (s, 3H, OCH_3), 2.46 (s, 3H, $ArCH_3$); **^{13}C NMR** (101 MHz, Chloroform-*d*) δ 168.3 (CO_2Me), 144.1 (C), 132.6 (C3), 130.2 (C), 130.1 (C), 119.1 (C4), 117.1 (C6), 51.9 (OCH_3), 20.9 ($ArCH_3$); ***m/z*** (ES^+) 166.07 ($[M+H]^+$, 100 %). Spectroscopic data are in accordance with the literature.[322]

Methyl 5-amino-4-iodo-2-methylbenzoate (11)

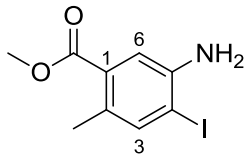

A solution of iodine monochloride dichloromethane(53.4 mL, 1M, 1.5 eq.) was added dropwise to a mixture of methyl 5-amino-2-methylbenzoate **10** (5.87 g, 35.6 mmol, 1.0 eq.), methanol (75 mL), water (7.5 mL), and calcium carbonate (10.7 g, 107 mmol, 3.0 eq.) at 0 °C and stirred for 4 hours. A solution of sodium sulfite (5.3 g) in water (20 mL) was added to the reaction and the resulting mixture was stirred at room temperature for 1 hour, filtered and concentrated *in vacuo*. The residue was diluted with EtOAc (30 mL) and washed with water (2 × 30 mL) followed by brine (30 mL), dried over $MgSO_4$, filtered and concentrated *in vacuo*. The crude product was purified *via* the Biotage SP4 (silica-packed SNAP column 100 g; 0-3% EtOAc/hexanes) to give the title product **11** as a pale yellow solid (5.83 g, 56%). **mp** 73-75 °C (lit. 77 °C[295]); **^{1}H NMR** (400 MHz, Chloroform-*d*) δ 7.55 (s, 1H, C3-H), 7.29 (s, 1H, C6-H), 3.86 (s, 3H, OCH_3), 2.42 (s, 3H, $ArCH_3$); **^{13}C NMR** (101 MHz, Chloroform-*d*) δ 167.8 (CO_2Me), 144.9 (C4), 141.8 (C3), 131.1 (C1), 130.5 (C2), 116.3 (C6), 89.3 (C5), 52.0 (OCH_3), 20.4

(Ar<u>C</u>H$_3$); ***m/z*** (ES$^+$) 291.91 ([M+H]$^+$, 100 %). Spectroscopic data are in accordance with the literature.[295]

Methyl 5-amino-2-methyl-4-((trimethylsilyl)ethynyl)benzoate (12)

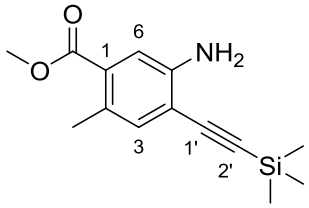

Methyl 5-amino-4-iodo-2-methylbenzoate **11** (4.79 g, 16.5 mmol, 1.0 eq.), Pd(PPh$_3$)$_2$Cl$_2$ (0.58 g, 0.83 mmol, 0.05 eq.), and CuI (0.16 g, 0.83 mmol, 0.05 eq.) were added to an oven-dried flask under a N_2 atmosphere. Dry Et$_3$N (5 mL/mmol) was added, and the resulting suspension was cooled to 0 °C. Ethynyltrimethylsilane (2.6 mL, 18.2 mmol, 1.1 eq.) was added dropwise, followed by stirring at room temperature for 3 hours. The Et$_3$N was removed *in vacuo*, and ether (20 mL) was added to the resulting residue. After filtration through Celite, the organic extract was washed with brine (20 mL), dried over MgSO$_4$, filtered and concentrated *in vacuo*. The crude product was purified *via* the Biotage SP4 (silica-packed SNAP column 100 g; 0-30% EtOAc/hexanes) to give the title product **12** as a pale yellow solid (3.71 g, 87%). **mp** 61-63 °C; **IR** (KBr) ν $_{max}$: 3469 (NH$_2$), 3371 (NH$_2$), 2947, 2144 (-C≡C-), 1694 (C=O), 1625 (C=C), 1248 (C-O); **^{1}H NMR** (300 MHz, Chloroform-*d*) δ 7.28 (s, 1H, C6-<u>H</u>), 7.17 (s, 1H, C3-<u>H</u>), 3.86 (s, 3H, OC<u>H</u>$_3$), 2.42 (s, 3H, ArC<u>H</u>$_3$), 0.26 (s, 9H, Si(C<u>H</u>$_3$)$_3$); **^{13}C NMR** (126 MHz, Chloroform-*d*) δ 167.8 (<u>C</u>O$_2$Me), 145.8 (C4), 135.1 (C3), 130.4 (C1), 129.0 (C2), 116.4 (C6), 111.8 (C5), 102.2 (C2'), 101.0 (C1'), 52.0 (O<u>C</u>H$_3$), 20.7 (Ar<u>C</u>H$_3$), 0.17 (Si(<u>C</u>H$_3$)$_3$); ***m/z*** (ES$^+$) 262.10 ([M+H]$^+$, 100 %). **HRMS** (ES$^-$) Calcd for $C_{14}H_{19}NO_2SiNa$ [M+Na]$^+$: 284.1083, found 284.1073.

Methyl 5-methyl-1*H*-indole-6-carboxylate (13)

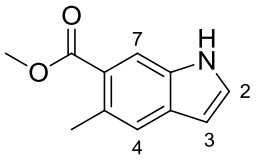

To methyl 5-amino-2-methyl-4-((trimethylsilyl)ethynyl)benzoate **12** (1.8 g, 6.9 mmol, 1.0 eq.) and CuI (2.63 g, 13.8 mmol, 2.0 eq.) was added DMF (4 mL/mmol). The mixture was heated at 100 °C for 2 hours before being cooled to room temperature. The reaction was diluted with Et$_2$O (60 mL), filtered over Celite, washed with brine (30 mL), dried over MgSO$_4$, filtered and concentrated *in vacuo*. The crude product was purified *via* the Biotage SP4 (silica-packed SNAP column 50 g; 0-20% EtOAc/hexanes) to give the title product **13** as a pale yellow solid (0.95 g, 74%). **mp** 63-65 °C; **IR** (KBr) ν $_{max}$: 3322 (NH), 2926, 1695 (C=O), 1444 (C=C), 1314, 1262 (C-O); **^{1}H NMR** (500 MHz, Chloroform-*d*) δ

8.30 (br s, 1H, NH), 8.09 (s, H, C7-H), 7.48 (s, 1H, C4-H), 7.33 (d, *J* = 2.6 Hz, 1H, C3-H), 6.50 (d, *J* = 2.6 Hz, 1H, C2-H), 3.91 (s, 3H, OCH_3), 2.69 (s, 3H, $ArCH_3$); **^{13}C NMR** (126 MHz, Chloroform-*d*) δ 169.0 (CO_2Me), 133.8 (C3a), 131.2 (C), 131.2 (C), 127.7 (C3), 123.5 (C6), 122.8 (C4), 114.5 (C7), 102.4 (C2), 51.8 (OCH_3), 22.4 ($ArCH_3$); ***m/z*** (ES^-) 187.90 ($[M-H]^-$, 100 %); **HRMS** (ES^-) Calcd for $C_{11}H_{10}NO_2$ $[M-H]^-$: 188.0712, found 188.0710.

Methyl 5-methyl-1-phenethyl-1*H*-indole-6-carboxylate (14a)

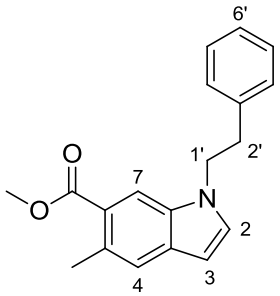

14a was prepared from methyl 5-methyl-1*H*-indole-6-carboxylate **13** (0.20 g, 1.06 mmol, 1.0 eq.) and (bromoethyl)benzene (0.22 mL, 1.59 mmol, 1.5 eq.) using general method A. The crude product was purified *via* the Biotage SP4 (silica-packed SNAP column 10 g; 0-20% EtOAc/hexanes) to give a mixture of the starting material methyl 5-methyl-1*H*-indole-6-carboxylate **13** (80 mg), and the title product **14a** as a yellow oil (0.14 g, 46%, 76% based on recovered **13**). **IR** (KBr) ν_{max}: 2951, 1710 (C=O), 1442 (C=C), 1240 (C-O), 1649 (C=O); **^{1}H NMR** (500 MHz, Chloroform-*d*) δ 8.01 (s, 1H, C7-H), 7.44 (s, 1H, C4-H), 7.32 – 7.18 (m, 3H, 3 × ArH), 7.08 – 7.04 (m, 2H, 2 × ArH), 6.97 (d, *J* = 3.0, 1H, C2-H), 6.35 (d, *J* = 3.0, 1H, C3-H), 4.38 (t, *J* = 7.2 Hz, 2H, C1'-H_2), 3.93 (s, 3H, OCH_3), 3.12 (t, *J* = 7.2 Hz, 2H, C2'-H_2), 2.69 (s, 1H, $ArCH_3$); **^{13}C NMR** (126 MHz, Chloroform-*d*) δ 169.1 (CO_2Me), 138.5 (C3'), 133.8 (C7a), 132.0 (C3a), 131.5 (C2), 130.7 (C5), 128.9 (2 × ArCH), 128.8 (2 × ArCH), 126.9 (C6'), 123.1 (C4), 122.9 (C6), 112.8 (C7), 100.6 (C3), 51.8 (OCH_3), 48.4 (C1'), 36.9 (C2'), 22.5 ($ArCH_3$); ***m/z*** (ES^+) 315.94 ($[M+Na]^+$, 100 %); **HRMS** (ES^+) Calcd for $C_{19}H_{19}NO_2Na$ $[M+Na]^+$: 316.1313, found 316.1320.

Methyl 1-*iso*butyl-5-methyl-1*H*-indole-6-carboxylate (14b)

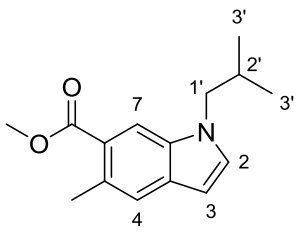

14b was prepared from methyl 5-methyl-1*H*-indole-6-carboxylate **13** (0.35 g, 1.85 mmol, 1.0 eq.) and 1-bromo-2-methylpropane (0.40 mL, 3.70 mmol, 2.0 eq.) using general method A. The crude product was purified *via* the Biotage SP4 (silica-packed SNAP column 10 g; 0-20% EtOAc/hexanes) to give the

title product **14b** as a pale yellow oil (0.29 g, 63%). **IR** (thin film) ν $_{max}$: 2957, 2361, 1717 (C=O), 1437, 1236 (C-O); **^{1}H NMR** (500 MHz, Chloroform-*d*) δ 8.00 (s, 1H, C7-H), 7.45 (s, 1H, C4-H), 7.18 (d, *J* = 3.0 Hz, 1H, C2-H), 6.41 (d, *J* = 3.0, 1H, C3-H), 3.93 (m, 5H, OCH_3, C1'-H_2), 2.68 (s, 3H, ArCH_3), 2.31 – 2.09 (m, 1H, C2'-H), 0.92 (d, *J* = 6.7 Hz, 6H, 2 × C3'-H_3); **^{13}C NMR** (126 MHz, Chloroform-*d*) δ 169.1 (CO_2Me), 134.4 (C7a), 131.9 (C2), 131.8 (C3a), 130.5 (C5), 123.0 (C4), 122.8 (C6), 113.1 (C7), 100.4 (C3), 54.4 (C1'), 51.8 (OCH_3), 29.7 (C2'), 22.5 (ArCH_3), 20.4 (C3'); ***m/z*** (ES$^+$) 246.15 ([M+H]$^+$, 100 %); **HRMS** (ES$^+$) Calcd for $C_{15}H_{19}NO_2Na$ [M+Na]$^+$: 268.1313, found 268.1302.

Methyl 1-(2-(dimethylamino)ethyl)-5-methyl-1*H*-indole-6-carboxylate (14c)

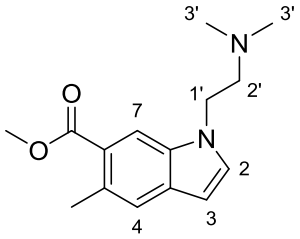

14c was prepared from methyl 5-methyl-1*H*-indole-6-carboxylate **13** (0.20 g, 1.06 mmol, 1.0 eq.) and 2-chloro-*N*,*N*-dimethylethylamine hydrochloride (0.46 g, 3.18 mmol, 3.0 eq.) using general method A. The crude product was purified *via* the Biotage SP4 (silica-packed SNAP column 10 g; 0-5% MeOH/DCM) to give the title product **14c** as a yellow oil (0.19 g, 68%). **IR** (thin film) ν $_{max}$: 2947, 2361, 1713 (C=O), 1694, 1437, 1234 (C-O), 1045; **^{1}H NMR** (400 MHz, Chloroform-*d*) δ 8.03 (s, 1H, C7-H), 7.44 (s, 1H, C4-H), 7.27 (d, *J* = 3.1 Hz, 1H, C2-H), 6.42 (d, *J* = 3.1, 1H, C3-H), 4.26 (t, *J* = 7.0 Hz, 2H, C1'-H_2), 3.92 (s, 3H, OCH_3), 2.71 (t, *J* = 7.0 Hz, 2H, C2'-H_2), 2.68 (s, 3H, ArCH_3), 2.30 (s, 6H, 2 × C3'-H_3); **^{13}C NMR** (101 MHz, Chloroform-*d*) δ 169.0 (CO_2Me), 134.1 (C7a), 131.8 (C3a), 131.6 (C2), 130.7 (C5), 123.1 (C4), 122.9 (C6), 112.7 (C7), 101.0 (C3), 59.2 (C2'), 51.8 (OCH_3), 45.9 (C3'), 44.9 (C1'), 22.4 (ArCH_3); ***m/z*** (ES$^+$) 261.16 ([M+H]$^+$, 100 %); **HRMS** (ES$^+$) Calcd for $C_{15}H_{21}N_2O_2$ [M+H]$^+$: 261.1603, found 261.1594.

Methyl 5-methyl-3-nitro-1-phenethyl-1*H*-indole-6-carboxylate (15a)

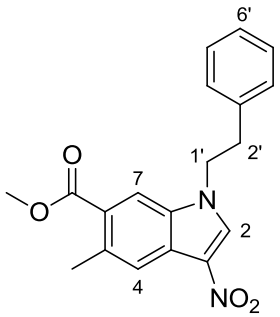

15a was prepared from methyl 5-methyl-1-phenethyl-1*H*-indole-6-carboxylate **14a** (0.28 g, 0.95 mmol, 1.0 eq.) using general method B. The crude product was purified *via* the Biotage SP4 (silica-packed SNAP column 10 g; 0-20% EtOAc/hexanes) to give the title product **15a** as a yellow solid (0.22 g, 70%). **mp** 119-121 °C; **IR** (KBr) ν $_{max}$: 1708 (C=O), 1516 (N-O), 1380 (N-O) 1243 (C-O); **^{1}H NMR** (500 MHz, Chloroform-*d*) δ 8.14 (s, 1H, C4-H), 8.00 (s, 1H, C7-H), 7.83 (s, 1H, C2-H), 7.32 – 7.19 (m, 3H, 3 × ArH), 7.06 – 6.98 (m, 2H, 2 × ArH), 4.45 (t, *J* = 6.9 Hz, 2H, C1'-H_2), 3.95 (s, 3H, OCH_3), 3.18 (t, *J* = 6.9 Hz, 2H, C2'-H_2), 2.74 (s, 3H, ArCH_3); **^{13}C NMR** (126 MHz, Chloroform-*d*) δ 168.0 (CO_2Me), 136.8 (C3'), 136.1 (C5), 133.0 (C7a), 132.8 (C2), 129.2 (2 × ArCH), 128.7 (2 × ArCH), 128.1 (C3), 127.6 (C6'), 126.2 (C6), 123.7 (C3a), 123.2 (C4), 113.8 (C7), 52.2 (OCH_3), 49.5 (C1'), 36.3 (C2'), 22.5 (ArCH_3); ***m/z*** (ES^+) 339.13 ([M+H]$^+$, 100 %); **HRMS** (ES^+) Calcd for $C_{19}H_{19}N_2O_4$ [M+H]$^+$: 339.1339, found 339.1345.

Methyl 1-*iso*butyl-5-methyl-3-nitro-1*H*-indole-6-carboxylate (15b)

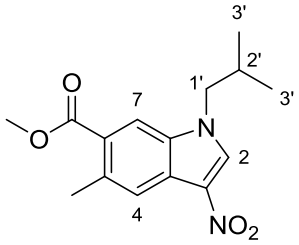

15b was prepared from methyl 1-*iso*butyl-5-methyl-1*H*-indole-6-carboxylate **14b** (0.29 g, 1.17 mmol, 1.0 eq.) using general method B. The crude product was purified *via* the Biotage SP4 (silica-packed SNAP column 10 g; 0-10% EtOAc/hexanes) to give the title product **15b** as a yellow amorphous solid (0.15 g, 44%). **IR** (neat) ν $_{max}$: 3125, 2959, 1703 (C=O), 1522 (N-O), 1373 (N-O), 1236 (C-O), 1076, 781; **^{1}H NMR** (400 MHz, Chloroform-*d*) δ 8.16 (s, 1H, C4-H), 8.14 (s, 1H, C2-H), 8.02 (s, 1H, C7-H), 4.01 (d, *J* = 7.5 Hz, 2H, C1'-H_2), 3.95 (s, 3H, OCH_3), 2.74 (s, 3H, ArCH_3), 2.34 – 2.19 (m, 1H, C2'-H), 0.98 (d, *J* = 6.7 Hz, 6H, 2 × C3'-H_3); **^{13}C NMR** (101 MHz, Chloroform-*d*) δ 168.1 (CO_2Me), 136.0 (C5), 133.5 (C7a), 133.1 (C2), 128.2 (C3), 126.3 (C6), 123.6 (C3a), 123.1 (C4), 114.0 (C7), 55.4 (C1'), 52.3 (OCH_3), 29.3 (C2'), 22.5 (ArCH_3), 20.2 (C3'); ***m/z*** (ES^+) 313.12 ([M+Na]$^+$, 100 %); **HRMS** (ES^+) Calcd for $C_{15}H_{18}N_2O_4Na$ [M+Na]$^+$: 313.1164, found 313.1151.

Methyl 1-(2-(dimethylamino)ethyl)-5-methyl-3-nitro-1*H*-indole-6-carboxylate (15c)

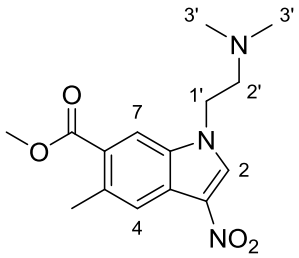

15c was prepared from methyl 1-(2-(dimethylamino)ethyl)-5-methyl-1*H*-indole-6-carboxylate **14c** (0.28 g, 1.08 mmol, 1.0 eq.) using general method B. The crude product was purified *via* the Biotage SP4 (silica-packed SNAP column 10 g; 0-5% MeOH/DCM) to give the title product **15c** as a yellow solid (0.14 g, 42%). **mp** 138-140 °C; **IR** (neat) ν_{max}: 3113, 2951, 2771, 1703 (C=O), 1520 (N-O), 1454, 1369 (N-O) 1240 (C-O), 1078; **^{1}H NMR** (400 MHz, Chloroform-*d*) δ 8.30 (s, 1H, C2-H), 8.12 (s, 1H, C4-H), 8.03 (s, 1H, C7-H), 4.27 (t, *J* = 6.3 Hz, 2H, C1'-H_2), 3.94 (s, 3H, OCH_3), 2.77 (t, *J* = 6.3 Hz, 2H, C2'-H_2), 2.72 (s, 3H, ArCH_3), 2.30 (s, 6H, 2 × C3'-H_3); **^{13}C NMR** (101 MHz, Chloroform-*d*) δ 168.0 (CO_2Me), 136.0 (C5), 133.6 (C2), 133.3 (C7a), 128.3 (C3), 126.1 (C6), 123.6 (C3a), 123.1 (C4), 113.6 (C7), 58.2 (C2'), 52.2 (OCH_3), 45.5 (C3'), 45.2 (C1'), 22.4 (ArCH_3); ***m/z*** (ES$^+$) 306.14 ([M+H]$^+$, 100 %); **HRMS** (ES$^+$) Calcd for $C_{15}H_{20}N_3O_4$ [M+H]$^+$: 306.1454, found 306.1441.

Sodium 5-methyl-1-phenethyl-3-propionamido-1*H*-indole-6-carboxylate (16a)

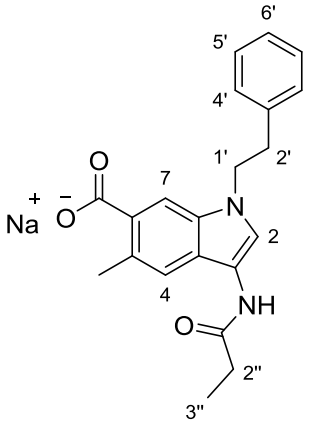

Methyl 5-methyl-1-phenethyl-3-propionamido-1*H*-indole-6-carboxylate was prepared from methyl 5-methyl-3-nitro-1-phenethyl-1*H*-indole-6-carboxylate **15a** (40 mg, 0.12 mmol, 1.0 eq.) and propionic anhydride (50 μL, 0.36 mmol, 3.0 eq.) using general method C. The crude product was used in the next step without further purification. **^{1}H NMR** (400 MHz, Chloroform-*d*) δ 7.91 (s, 1H, C7-H), 7.82 (s, 1H, C2-H), 7.31 – 7.24 (m, 3H, 2 × ArCH, C4-H), 7.24 – 7.19 (m, 1H, C6'-H), 7.16 – 7.08 (m, 2H, 2 × ArCH), 4.32 (t, *J* = 7.6 Hz, 2H, C1'-H_2), 3.92 (s, 3H, OCH_3), 3.13 – 3.08 (m, 2H, C2'-H_2), 2.68 (s, 3H, ArCH_3), 2.47 (q, *J* = 7.6 Hz, 2H, C2''-H_2), 1.30 (t, *J* = 7.6 Hz, 3H, C3''-H_3); **^{13}C NMR** (101 MHz, Chloroform-*d*) δ 171.3 (C1''), 168.8 (CO_2Me), 138.3 (C3'), 131.7 (C7a), 130.3 (C5), 128.8 (4 × ArCH), 126.9 (C6'), 123.5 (C3a), 123.4 (C6), 122.6 (C2), 118.7 (C4), 113.6 (C3), 113.2 (C7), 51.9 (OCH_3), 48.3 (C1'), 37.1 (C2'), 30.2 (C2''), 22.5 (ArCH_3), 10.1 (C3''). The crude methyl 5-methyl-1-phenethyl-3-propionamido-1*H*-indole-6-carboxylate was hydrolysed according to general method D. The crude product was purified *via* the Biotage SP4 (Reverse-phase silica-packed SNAP column 4 g; 0-20% MeOH/DCM) to give the title product **16a** as a white solid (27 mg, 61% over 2 steps). **IR** (neat) ν_{max}: 3262 (NH), 2922, 1684 (C=O), 1645, 1558, 1281, 1246, 1072, 880; **^{1}H NMR** (500 MHz, Methanol-d_4) δ

7.92 (s, 1H, C7-H), 7.65 (s, 1H, C2-H), 7.51 (s, 1H, C4-H), 7.23 – 7.18 (m, 2H, C5'-H), 7.17 – 7.12 (m, 1H, C6'-H), 7.11 – 7.06 (m, 2H, C4'-H), 4.38 (t, *J* = 7.1 Hz, 2H, C1'-H_2), 3.09 (t, *J* = 7.1 Hz, 2H, C2'-H_2), 2.64 (s, 3H, ArCH_3), 2.46 (q, *J* = 7.6 Hz, 2H, C2''-H_2), 1.24 (t, *J* = 7.6 Hz, 3H, C3''-H_3); **^{13}C NMR** (126 MHz, Methanol-d_4) δ 174.7 (C1''), 172.7* (CO_2Na), 139.9 (C3'), 133.1 (C7a), 130.7 (C5), 129.8 (C4'), 129.5 (C5'), 127.5 (C6'), 125.3 (C3a, C6), 124.1 (C2), 120.8 (C4), 115.0 (C3), 113.9 (C7), 48.8* (C1'), 37.9 (C2'), 30.1 (C2''), 22.5 (ArCH_3), 10.7 (C3''); ***m/z*** (ES$^+$) 349.15 ([M-H]$^-$, 100 %); **HRMS** (ES$^-$) Calcd for $C_{21}H_{21}N_2O_3$ [M-H]$^-$: 349.1558, found 349.1549. *denotes that the carbon was identified *via* HMBC.

Sodium 5-methyl-3-(3-methylbutanamido)-1-phenethyl-1*H*-indole-6-carboxylate (16b)

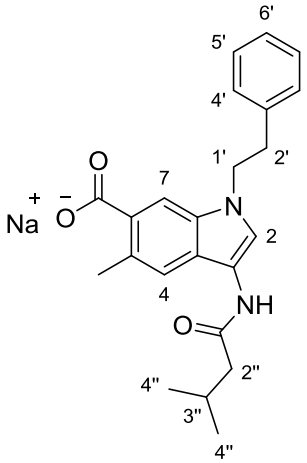

Methyl 5-methyl-3-(3-methylbutanamido)-1-phenethyl-1*H*-indole-6-carboxylate was prepared from methyl 5-methyl-3-nitro-1-phenethyl-1*H*-indole-6-carboxylate **15a** (40 mg, 0.12 mmol, 1.0 eq.) and *iso*valeric anhydride (72 μL, 0.36 mmol, 3.0 eq.) using general method C. The crude product was used in the next step without further purification. **^{1}H NMR** (500 MHz, Chloroform-*d*) δ 7.92 (s, 1H, C7-H), 7.82 (s, 1H, C2-H), 7.30 – 7.26 (m, 3H, 2 × ArCH, C4-H), 7.24 – 7.20 (m, 1H, C6'-H), 7.13 (dd, *J* = 6.9, 1.7 Hz, 2H, 2 × ArCH), 4.32 (dd, *J* = 8.4, 6.8 Hz, 2H, C1'-H_2), 3.92 (s, 3H, OCH_3), 3.15 – 3.06 (m, 2H, C2'-H_2), 2.69 (s, 3H, ArCH_3), 2.34 – 2.21 (m, 3H, C2''-H_2, C3''-H), 1.05 (d, *J* = 6.3 Hz, 6H, 2 × C4''-H_3); **^{13}C NMR** (126 MHz, Chloroform-*d*) δ 170.1 (C1''), 168.8 (CO_2Me), 138.3 (C3'), 131.6 (C7a), 130.4 (C5), 128.8 (4 × ArCH), 126.9 (C6'), 123.5 (C3a), 123.5 (C6), 122.7 (C2), 118.7 (C4), 113.5 (C3), 113.2 (C7), 51.9 (OCH_3), 48.3 (C1'), 46.5 (C2''), 37.1 (C2'), 26.6 (C3''), 22.7 (C4''), 22.6 (ArCH_3). The crude methyl 5-methyl-3-(3-methylbutanamido)-1-phenethyl-1*H*-indole-6-carboxylate was hydrolysed according to general method D. The crude product was purified *via* the Biotage SP4 (Reverse-phase silica-packed SNAP column 4 g; 0-20% MeOH/DCM) to give the title product **16b** as a white solid (23 mg, 47% over 2 steps). **mp** 233-235 °C; **IR** (neat) ν_{max}: 3281 (NH), 2953, 1681 (C=O), 1641, 1558, 1406, 1283, 1248, 881; **^{1}H NMR** (500 MHz, Methanol-d_4) δ 7.93 (s, 1H, C7-H), 7.64 (s, 1H, C2-H), 7.51 (s, 1H, C4-H), 7.23 – 7.18 (m, 2H, C5'-H), 7.18 – 7.10 (m, 1H, C6'-H), 7.10 – 7.07 (m, 2H, C4'-H), 4.38 (t, *J* =

7.1 Hz, 2H, C1'-$\underline{H}_2$), 3.09 (t, *J* = 7.1 Hz, 2H, C2'-$\underline{H}_2$), 2.65 (s, 3H, ArC$\underline{H}_3$), 2.31 (d, *J* = 7.3 Hz, 2H, C2''-$\underline{H}_2$), 2.24 – 2.12 (m, 1H, C3''-$\underline{H}$), 1.03 (d, *J* = 6.6 Hz, 6H, 2 × C4''-$\underline{H}_3$); **^{13}C NMR** (126 MHz, Methanol-d_4) δ 173.4 (C1''), 172.3* ($\underline{C}O_2Na$), 139.9 (C3'), 133.1 (C7a), 130.8 (C5), 129.8 (C4'), 129.5 (C5'), 127.5 (C6'), 125.5 (C3a, C6), 124.4 (C2), 120.8 (C4), 114.8 (C3), 114.0 (C7), 49.1* (C1'), 46.2 (C2''), 37.9 (C2'), 27.7 (C3''), 22.8 (C4''), 22.6 (Ar$\underline{C}H_3$); ***m/z*** (ES$^+$) 401.18 ([M+H]$^+$, 100 %); **HRMS** (ES$^+$) Calcd for $C_{23}H_{26}N_2O_3Na$ [M+H]$^+$: 401.1833, found 401.1836. *denotes that the carbon was identified *via* HMBC.

Sodium 1-*iso*butyl-5-methyl-3-propionamido-1*H*-indole-6-carboxylate (16c)

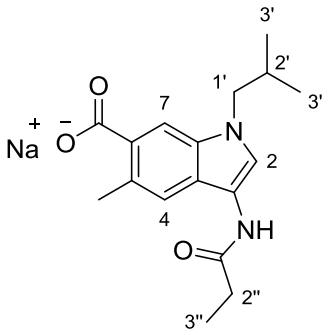

Methyl 1-*iso*butyl-5-methyl-3-propionamido-1*H*-indole-6-carboxylate was prepared from methyl 1-*iso*butyl-5-methyl-3-nitro-1*H*-indole-6-carboxylate **15b** (45 mg, 0.16 mmol, 1.0 eq.) and propionic anhydride (0.1 mL, 0.8 mmol, 5.0 eq.) using general method C. The crude product was used in the next step without further purification. **^{1}H NMR** (400 MHz, Chloroform-*d*) δ 7.97 (s, 1H, C7-$\underline{H}$), 7.87 (s, 1H, C2-$\underline{H}$), 7.86 (br s, 1H, N$\underline{H}$), 7.30 (s, 1H, C4-$\underline{H}$), 3.92 (s, 3H, OC$\underline{H}_3$), 3.88 (d, *J* = 7.4 Hz, 2H, C1'-$\underline{H}_2$), 2.67 (s, 3H, ArC$\underline{H}_3$), 2.48 (q, *J* = 7.6 Hz, 2H, C2''-$\underline{H}_2$), 2.25 – 2.10 (m, 1H, C2'-$\underline{H}$), 1.30 (t, *J* = 7.6 Hz, 3H, C3''-$\underline{H}_3$), 0.90 (d, *J* = 6.7 Hz, 6H, 2 × C3'-$\underline{H}_3$); **^{13}C NMR** (101 MHz, Chloroform-*d*) δ 171.3 (C1''), 168.9 ($\underline{C}O_2Me$), 132.0 (C7a), 130.1 (C5), 123.4 (C), 123.3 (C), 123.2 (C2), 118.7 (C4), 113.4 (C7), 113.3 (C3), 54.2 (C1'), 51.9 (O$\underline{C}H_3$), 30.1 (C2''), 29.8 (C2'), 22.5 (Ar$\underline{C}H_3$), 20.4 (C3'), 10.1 (C3''). The crude methyl 1-*iso*butyl-5-methyl-3-propionamido-1*H*-indole-6-carboxylate was hydrolysed according to general method D. The crude product was purified *via* the Biotage SP4 (Reverse-phase silica-packed SNAP column 4 g; 0-10% MeOH/DCM) to give the title product **16c** as a white solid (39 mg, 76% over 2 steps). **mp** 243-245 °C; **IR** (neat) ν_{max}: 3260, 2961, 1676, 1650, 1560, 1406, 1381, 1275, 1240, 880; **^{1}H NMR** (500 MHz, Methanol-d_4) δ 8.00 (s, 1H, C7-$\underline{H}$), 7.77 (s, 1H, C2-$\underline{H}$), 7.54 (s, 1H, C4-$\underline{H}$), 3.96 (d, *J* = 7.4 Hz, 2H, C1'-$\underline{H}_2$), 2.66 (s, 3H, ArC$\underline{H}_3$), 2.48 (q, *J* = 7.6 Hz, 2H, C2''-$\underline{H}_2$), 2.18 (dt, *J* = 12.9, 6.4 Hz, 1H, C2'-$\underline{H}$), 1.25 (t, *J* = 7.6 Hz, 3H, C3''-$\underline{H}_3$), 0.92 (d, *J* = 6.6 Hz, 6H, 2 × C3'-$\underline{H}_3$); **^{13}C NMR** (126 MHz, Methanol-d_4) δ 174.7 (C1''), 172.5* ($\underline{C}O_2Na$), 133.5 (C7a), 130.7 (C5), 125.2 (C3a, C6), 124.5 (C2), 120.8 (C4), 114.9 (C3), 114.1 (C7), 54.8 (C1'), 31.0 (C2'), 30.1 (C2''), 22.6 (Ar$\underline{C}H_3$), 20.5 (C3'), 10.7 (C3''); ***m/z*** (ES$^+$) 325.15 ([M+H]$^+$, 100 %); **HRMS** (ES$^+$) Calcd for $C_{17}H_{22}N_2O_3Na$ [M+H]$^+$: 325.1523, found 325.1522. *denotes that the carbon was identified *via* HMBC.

Sodium 1-*iso*butyl-5-methyl-3-(3-methylbutanamido)-1*H*-indole-6-carboxylate (16d)

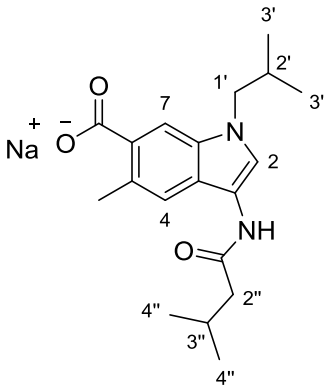

Methyl 1-*iso*butyl-5-methyl-3-(3-methylbutanamido)-1*H*-indole-6-carboxylate was prepared from methyl 1-*iso*butyl-5-methyl-3-nitro-1*H*-indole-6-carboxylate **15b** (50 mg, 0.17 mmol, 1.0 eq.) and *iso*valeric anhydride (0.27 mL, 1.36 mmol, 8.0 eq.) using general method C. The crude product was used in the next step without further purification. **^{1}H NMR** (400 MHz, Chloroform-*d*) δ 7.97 (s, 1H, C7-H), 7.87 (s, 1H, C2-H), 7.29 (s, 1H, C4-H), 3.92 (s, 3H, OCH_3), 3.88 (d, *J* = 7.4 Hz, 2H, C1'-H_2), 2.68 (s, 3H, ArCH_3), 2.34 – 2.13 (m, 4H, C2'-H, C2''-H_2, C3''-H), 1.04 (d, *J* = 6.3 Hz, 6H, 2 × C4''-H_3), 0.91 (d, *J* = 6.6 Hz, 6H, 2 × C3'-H_3); **^{13}C NMR** (101 MHz, Chloroform-*d*) δ 170.1 (C1''), 168.9 (CO_2Me), 132.0 (C7a), 130.1 (C5), 123.4 (C3a, C6), 123.3 (C2), 118.7 (C4), 113.4 (C7), 113.3 (C3), 54.2 (C1'), 51.9 (OCH_3), 46.5 (C2''), 29.8 (C2'), 26.5 (C3''), 22.7 (C4''), 22.6 (ArCH_3), 20.4 (C3'). The crude methyl 1-*iso*butyl-5-methyl-3-(3-methylbutanamido)-1*H*-indole-6-carboxylate was hydrolysed according to general method D. The crude product was purified *via* the Biotage SP4 (Reverse-phase silica-packed SNAP column 4 g; 0-15% MeOH/DCM) to give the title product **16d** as a white solid (49 mg, 82% over 2 steps). **mp** 244-246 °C; **IR** (neat) ν_{max}: 3281 (NH), 2953, 2932, 1682 (C=O), 1651, 1558, 1279, 1246, 883; **^{1}H NMR** (400 MHz, Methanol-d_4) δ 7.92 (s, 1H, C7-H), 7.74 (s, 1H, C2-H), 7.53 (s, 1H, C4-H), 3.94 (d, *J* = 7.3 Hz, 2H, C1'-H_2), 2.64 (s, ArCH_3), 2.38 – 2.28 (m, 2H, C2''-H_2), 2.25 – 2.14 (m, 2H, C2'-H, C3''-H), 1.04 (d, *J* = 6.6 Hz, 6H, 2 × C4''-H_3), 0.92 (d, *J* = 6.6 Hz, 6H, 2 × C3'-H_3); **^{13}C NMR** (101 MHz, Methanol-d_4) δ 173.8 (CO_2Na), 173.4 (C1''), 133.5 (C7a), 130.0 (C5), 127.5 (C6), 124.8 (C3a), 124.2 (C2), 120.6 (C4), 114.7 (C3), 113.3 (C7), 54.8 (C1'), 46.2 (C2''), 31.0 (C2'), 27.7 (C3''), 22.8 (C4''), 22.3 (ArCH_3), 20.5 (C3'); ***m/z*** (ES$^+$) 353.18 ([M+H]$^+$, 100 %); **HRMS** (ES$^+$) Calcd for $C_{19}H_{26}N_2O_3Na$ [M+H]$^+$: 353.1836, found 353.1840.

Sodium 1-*iso*butyl-5-methyl-3-(2-phenylacetamido)-1*H*-indole-6-carboxylate (16e)

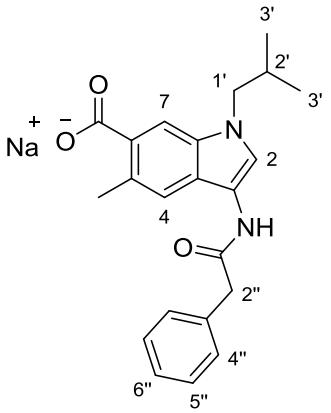

Methyl 1-*iso*butyl-5-methyl-3-(2-phenylacetamido)-1*H*-indole-6-carboxylate was prepared from methyl 1-*iso*butyl-5-methyl-3-nitro-1*H*-indole-6-carboxylate **15b** (35 mg, 0.12 mmol, 1.0 eq.) and 2-phenylacetic anhydride (0.18 g, 0.72 mmol, 6.0 eq.) using general method C. The crude product was used in the next step without further purification. **^{1}H NMR** (400 MHz, Chloroform-*d*) δ 7.95 (s, 1H, C7-H), 7.82 (d, *J* = 0.5 Hz, 1H, C2-H), 7.48 – 7.38 (m, 5H, C4''-H, C5''-H, C6''-H), 6.95 (s, 1H, C4-H), 3.91 (s, 3H, OCH_3), 3.87 (d, *J* = 7.4 Hz, 2H, C1'-H_2), 3.82 (s, 2H, C2''-H_2), 2.62 (s, 3H, ArCH_3), 2.25 – 2.10 (m, 1H, C2'-H), 0.90 (d, *J* = 6.7 Hz, 6H, 2 × C3'-H_3); **^{13}C NMR** (126 MHz, Chloroform-*d*) δ 168.8 (CO_2Me), 168.4 (C1''), 134.8 (C3''), 132.0 (C7a), 130.2 (C5), 129.8 (2 × ArCH), 129.4 (2 × ArCH), 127.9 (C6''), 123.5 (C), 123.2 (C), 123.1 (C2), 118.4 (C4), 113.4 (C7), 113.0 (C3), 54.2 (C1'), 51.9 (OCH_3), 44.2 (C2''), 29.8 (C2'), 22.6 (ArCH_3), 20.4 (C3'). The crude methyl 1-*iso*butyl-5-methyl-3-(2-phenylacetamido)-1*H*-indole-6-carboxylate was hydrolysed according to general method D. The crude product was purified *via* the Biotage SP4 (Reverse-phase silica-packed SNAP column 4 g; 0-10% MeOH/DCM) to give the title product **16e** as a white solid (18 mg, 39% over 2 steps). **mp** 236 -238 °C; **IR** (neat) ν_{max}: 3279, 2957, 1672 (C=O), 1647, 1557, 1389, 1277, 1244, 878; **^{1}H NMR** (500 MHz, Methanol-d_4) δ 7.79 (s, 1H, C7-H), 7.69 (s, 1H, C2-H), 7.50 (s, 1H, C4-H), 7.42 – 7.37 (m, 2H, C4''-H), 7.33 (dd, *J* = 8.5, 6.8 Hz, 2H, C5''-H), 7.27 – 7.23 (m, 1H, C6''-H), 3.92 (d, *J* = 7.4 Hz, 2H, C1'-H_2), 3.77 (s, 2H, C2''-H_2), 2.62 (s, 3H, ArCH_3), 2.24 – 2.05 (m, 1H, C2'-H), 0.90 (d, *J* = 6.7 Hz, 6H, 2 × C3'-H_3); **^{13}C NMR** (126 MHz, Methanol-d_4) δ 175.7 (CO_2Na), 171.5 (C1''), 137.2 (C3''), 133.6 (C7a), 130.1 (C6, C4''), 129.6 (C5''), 129.2 (C5), 127.9 (C6''), 124.1 (C3a), 123.5 (C2), 120.2 (C4), 114.6 (C3), 112.3 (C7), 54.8 (C1'), 43.7 (C2''), 30.9 (C2'), 22.0 (ArCH_3), 20.4 (C3'); ***m/z*** (ES^+) 387.17 ($[M+H]^+$, 100 %); **HRMS** (ES^+) Calcd for $C_{22}H_{24}N_2O_3Na$ $[M+H]^+$: 387.1679, found 387.1678.

Sodium 1-(2-(dimethylamino)ethyl)-5-methyl-3-propionamido-1*H*-indole-6-carboxylate (16f)

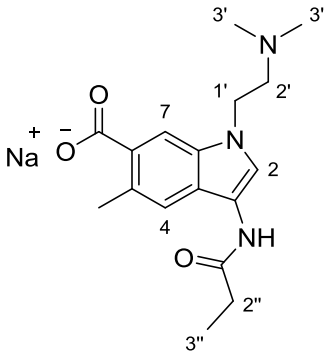

Methyl 1-(2-(dimethylamino)ethyl)-5-methyl-3-propionamido-1*H*-indole-6-carboxylate was prepared from methyl 1-(2-(dimethylamino)ethyl)-5-methyl-3-nitro-1*H*-indole-6-carboxylate **15c** (35 mg, 0.11 mmol, 1.0 eq.) and propionic anhydride (73 µL, 0.57 mmol, 5.0 eq.) using general method C. The crude product was used in the next step without further purification. **^{1}H NMR** (400 MHz, Chloroform-*d*) δ 8.00 (s, 1H, C7-H), 7.89 (s, 1H, C2-H), 7.36 (br s, 1H, N*H*), 7.29 (s, 1H, C4-H), 4.21 (t, *J* = 7.1 Hz, 2H, C1'-H_2), 3.91 (s, 3H, OCH_3), 2.70 (t, *J* = 7.1 Hz, 2H, C2'-H_2), 2.67 (s, 3H, ArCH_3), 2.47 (q, *J* = 7.6 Hz, 2H, C2''-H_2), 2.29 (s, 6H, 2 × C3'-H_3), 1.29 (t, *J* = 7.6 Hz, 3H, C3''-H_3); **^{13}C NMR** (101 MHz, Chloroform-*d*) δ 171.4 (C1''), 168.8 (CO_2Me), 131.8 (C7a), 130.4 (C5), 123.5 (C3a, C6), 122.9 (C2), 118.8 (C4), 113.7 (C3), 113.0 (C7), 59.1 (C2'), 51.9 (OCH$_3$), 45.8 (C3'), 44.7 (C1'), 30.1 (C2''), 22.5 (ArCH$_3$), 10.1 (C3''). The crude methyl 1-(2-(dimethylamino)ethyl)-5-methyl-3-propionamido-1*H*-indole-6-carboxylate was hydrolysed according to general method D. The crude product was purified *via* the Biotage SP4 (Reverse-phase silica-packed SNAP column 4 g; 0-20% H_2O/MeOH) to give the title product **16f** as an amorphous yellow solid (16 mg, 42% over 2 steps). **^{1}H NMR** (500 MHz, Methanol-d_4) δ 7.69 (s, 1H, C2-H), 7.62 (s, 1H, C7-H), 7.47 (s, 1H, C4-H), 4.31 (t, *J* = 7.1 Hz, 2H, C1'-H_2), 2.89 (t, *J* = 7.1 Hz, 2H, C2'-H_2), 2.58 (s, 3H, ArCH_3), 2.47 (q, *J* = 7.6 Hz, 2H, C2''-H_2), 2.39 (s, 6H, 2 × C3'-H_3), 1.24 (t, *J* = 7.6 Hz, 3H, C3''-H_3); **^{13}C NMR** (126 MHz, Methanol-d_4) δ 178.5* (CO_2Na), 174.7 (C1''), 135.3* (C6), 133.3 (C7a), 128.2* (C5), 123.3 (C3a), 121.9 (C2), 119.8 (C4), 115.3 (C3), 110.1 (C7), 59.3 (C2'), 45.4 (C3'), 44.7 (C1'), 30.1 (C2''), 21.3 (ArCH$_3$), 10.7 (C3''); ***m/z*** (ES$^+$) 340.16 ([M+H]$^+$, 100 %); **HRMS** (ES$^+$) Calcd for $C_{17}H_{23}N_2O_3Na$ [M+H]$^+$: 340.1632, found 340.1632. *denotes that the carbon was identified *via* HMBC.

2'-Bromo-N_2,N_2,N_6,N_6-tetramethylbiphenyl-2,6-diamine (27)

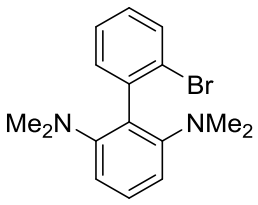

To *N*,*N*,*N*,*N*-tetramethylbenzene-1,3-diamine **26** (0.2 g, 1.22 mmol, 1.0 eq.) in anhydrous hexanes (2.5 mL) under a N_2 atmosphere was added *n*-butyllithium (0.6 mL, 1.2 eq., 2.5M in THF). The reaction mixture was heated at reflux for 1 hour before cooling to room temperature. 2-Bromochlorobenzene (0.16 mL, 1.34 mmol, 1.1 eq.) was then added dropwise over 15 minutes with vigorous stirring. The reaction mixture was heated at reflux for a further 2 hours. The reaction was quenched at room temperature by the slow addition of water (2.5 mL). The aqueous layer was extracted with ether (3 × 2.5 mL). The combined organic layers were dried over $MgSO_4$, filtered, concentrated *in vacuo* and purified *via* the Biotage SP4 (silica-packed SNAP column 10 g; 0-5% EtOAc/hexanes) to give the title product **27** as a white solid (0.33 g, 84%). **^{1}H NMR** (400 MHz, Chloroform-*d*) δ 7.65 (ddd, *J* = 8.0, 1.2, 0.5 Hz, 1H), 7.38 – 7.28 (m, 3H), 7.14 (ddd, *J* = 8.0, 6.6, 2.5 Hz, 1H), 6.88 (d, *J* = 8.0 Hz, 2H), 2.44 (s, 12H, 2 × $NC\underline{H}_3$); **^{13}C NMR** (101 MHz, Chloroform-*d*) δ 153.4 (C), 140.3 (C), 133.4 (Ar$\underline{C}$H), 132.8 (Ar$\underline{C}$H), 130.4 (C), 129.0 (Ar$\underline{C}$H), 127.7 (Ar$\underline{C}$H), 127.0 (Ar$\underline{C}$H), 126.4 (C), 114.0 (2 × Ar$\underline{C}$H), 44.1 ($N\underline{C}H_3)_2$). ***m/z*** (ES^+) 319.05 ($[M+H]^+$, 100 %); Spectroscopic data are in accordance with the literature.[316]

2'-(Dicyclohexylphosphino)-*N*$_2$,*N*$_2$,*N*$_6$,*N*$_6$-tetramethylbiphenyl-2,6-diamine (CPhos (21a))

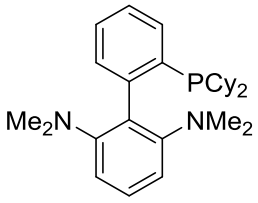

n-Butylithium (0.38 mL, 1.2 eq., 2.5M in THF) was added dropwise to a solution of **27** (0.25 g, 0.78 mmol, 1.0 eq.) in THF (3.2 mL) at -78 °C and the resulting mixture was maintained at this temperature for 30 minutes. Chlorodicyclohexylphosphine (0.20 mL, 0.94 mmol, 1.2 eq.) was then added dropwise *via* syringe over 15 min. The reaction mixture was stirred at -78 °C for 1 hour and then allowed to slowly warm to room temperature. The reaction mixture was quenched by the slow addition of MeOH (5 mL) and filtered through a plug of silica gel topped with Celite, eluting with EtOAc (12 mL). The filtrate was concentrated *in vacuo* and purified using preparative TLC (10% EtOAc/hexanes) to give the title product **CPhos** (**21a**) as a white solid (0.26 g, 72%). **^{1}H NMR** (500 MHz, Chloroform-*d*) δ 7.69 (d, *J* = 7.4 Hz, 1H), 7.43 – 7.30 (m, 4H), 6.91 (d, *J* = 8.0 Hz, 2H), 2.48 (s, 12H, 2 × $NC\underline{H}_3$), 2.01 – 1.54 (m, 12H), 1.36 – 1.01 (m, 10H); **^{13}C NMR** (126 MHz, Chloroform-*d*) δ 153.5, 146.3 (d, *J* = 31.2 Hz), 136.9 (d, *J* = 17.0 Hz), 133.2 (d, *J* = 6.5 Hz), 132.7 (d, *J* = 3.2 Hz), 132.2, 128.6, 127.5, 125.8, 114.0, 44.9, 35.2 (d, *J* = 15.2 Hz), 31.3 (d, *J* = 16.4 Hz), 29.6 (d, *J* = 12.2 Hz), 28.0 (d, *J* = 11.3 Hz), 27.7 (d, *J* = 8.6 Hz), 26.7 (observed complexity due to P-C splitting); **^{31}P NMR** (202

MHz, Chloroform-*d*) δ -9.01. ***m/z*** (ES^+) 437.25 ($[M+H]^+$, 100 %); Spectroscopic data are in accordance with the literature.[316]

Methyl 5-amino-2-*iso*propylbenzoate (18)

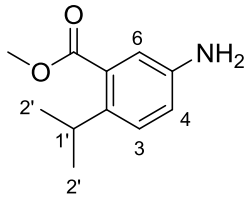

To an oven-dried microwave vial charged with CPhos (**21a**) (61 mg, 0.14, 0.04 eq.) and $Pd(OAc)_2$ (16 mg, 0.07 mmol, 0.02 eq.) was added a solution of methyl 5-amino-2-bromobenzoate **17** (0.80 g, 3.48 mmol, 1.0 eq.) in toluene (5.6 mL). The reaction mixture was cooled to 0 °C before the slow addition of *iso*propylzinc bromide (8.4 mL, 1.2 eq., 0.5M in THF). The reaction was allowed to warm to room temperature and stirred for 30 minutes. The reaction mixture was then quenched by the addition of aqueous hydrochloric acid (10 mL, 1N) and extracted with ethyl acetate (3 × 10 mL).The organic layers were combined, dried over $MgSO_4$, filtered, concentrated *in vacuo* and purified *via* the Biotage SP4 (silica-packed SNAP column 25 g; 0-10% EtOAc/hexanes) to give the title product **18** as a yellow oil (0.63 g, 93%). **IR** (thin film) ν_{max}: 3372 (NH), 2957, 1713 (C=O), 1624, 1503, 1443, 1315; **^{1}H NMR** (500 MHz, Chloroform-*d*) δ 7.19 (d, *J* = 8.4 Hz, 1H, C3-H), 7.04 (d, *J* = 2.7 Hz, 1H, C6-H), 6.79 (dd, *J* = 8.4, 2.7 Hz, 1H, C4-H), 3.87 (s, 3H, OCH_3), 3.56 (hept, *J* = 6.9 Hz, 1H, C1'-H), 1.20 (d, *J* = 6.9 Hz, 6H, 2 × C2'-H_3); **^{13}C NMR** (126 MHz, Chloroform-*d*) δ 169.1 (CO), 143.8 (C5), 139.7 (C2), 130.5 (C1), 127.3 (C3), 118.9 (C4), 116.0 (C6), 52.1 (OCH_3), 29.0 (C1'), 24.3 (C2'); ***m/z*** (ES^+) 194.12 ($[M+H]^+$, 100 %); **HRMS** (ES^+) Calcd for $C_{11}H_{16}NO_2$ $[M+H]^+$: 194.1103, found 194.1174.

4.8.4 Experimental procedures (Series 2)

Methyl 2-oxo-5-phenylpentanoate (30a)[274]

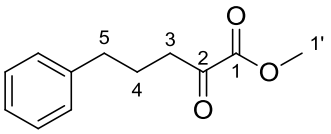

Magnesium turnings (0.32 g, 13.1 mmol, 1.3 eq.) were activated by vigorous stirring overnight under a nitrogen atmosphere and then suspended in anhydrous THF (20 mL). 1-Bromo-3-phenylpropane (1.53 mL, 10.1 mmol, 1.0 eq.) was added dropwise under a gentle reflux. The stirring was continued for 30 minutes to give a solution of (3-phenylpropyl)magnesium bromide. In a separate flask, dimethyl oxalate (3.56 g, 30.3 mmol, 3.0 eq.) in dry Et_2O (20 mL) was cooled to -78 °C before

dropwise addition of the (3-phenylpropyl)magnesium bromide solution. The mixture was stirred at 0 °C for 3 hours, diluted with aqueous 1M hydrochloric acid (20 mL), and extracted with EtOAc (3 × 20 mL). The combined organic extracts were washed with a saturated aqueous solution of $NaHCO_3$ (30 mL), brine (30 mL), dried over $MgSO_4$, filtered and concentrated *in vacuo*. The crude product was purified *via* the Biotage SP4 (silica-packed SNAP column 10 g; 0-20% EtOAc/hexanes) to give the title product **30a** as a colourless liquid (1.42 g, 69%). **^{1}H NMR** (300 MHz, Chloroform-*d*) δ 7.34 – 7.25 (m, 2H, 2 × Ar<u>H</u>), 7.24 – 7.14 (m, 3H, 3 × Ar<u>H</u>), 3.85 (s, 3H, C1'-<u>H</u>), 2.86 (t, *J* = 7.3 Hz, 2H, C3-<u>H_2</u>), 2.67 (t, *J* = 7.6 Hz, 2H, C5-<u>H_2</u>), 2.10 – 1.88 (m, 2H, C4-<u>H_2</u>); **^{13}C NMR** (75 MHz, Chloroform-*d*) δ 194.0 (C2), 161.5 (C1), 141.1 (C6), 128.5 (4 × Ar<u>C</u>H), 126.2 (C9), 52.9 (C1'), 38.6 (C3), 34.8 (C5), 24.5 (C4); ***m/z*** (ES^+) 206.09 ($[M+Na]^+$, 100 %). Spectroscopic data are in agreement with the literature.[274]

Ethyl 2-oxobutanoate (30b)[323]

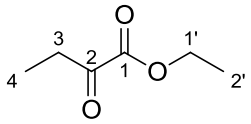

To solution of 2-ketobutyric acid (0.75 g, 7.4 mmol, 1.0 eq.) in EtOH (7 mL) was added H_2SO_4 (0.08 mL, 1.5 mmol, 0.2 eq.) dropwise. The mixture was heated at reflux for 6 hours. The mixture was cooled to room temperature and concentrated *in vacuo*. The residue was diluted with EtOAc (20 mL), washed with a saturated aqueous solution of $NaHCO_3$ (10 mL), water (10 mL), brine (10 mL), dried over $MgSO_4$, filtered and concentrated *in vacuo*. The title product **30b** was obtained as a colourless liquid (0.95 g, quant.), which did not require further purification. **^{1}H NMR** (400 MHz, Chloroform-*d*) δ 4.31 (q, *J* = 7.1 Hz, 2H, C1'-<u>H_2</u>), 2.87 (q, *J* = 7.2 Hz, 1H, C3-<u>H_2</u>), 1.36 (t, *J* = 7.1 Hz, 3H, C2'-<u>H_3</u>), 1.13 (t, *J* = 7.2 Hz, 3H, C4-<u>H_3</u>). Spectroscopic data are in agreement with the literature.[323]

Ethyl 4-methyl-2-oxopentanoate (30c)[324]

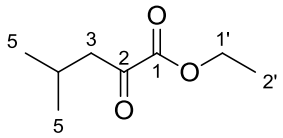

To solution of 2-ketobutyric acid (0.5 g, 3.8 mmol, 1 eq.) in EtOH (4 mL) was added H_2SO_4 (0.04 mL, 0.8 mmol, 0.2 eq.) dropwise. The mixture was heated at reflux for 6 hours. The mixture was cooled to room temperature and concentrated *in vacuo*. The residue was diluted with EtOAc (20 mL), washed with a saturated aqueous solution of $NaHCO_3$ (10 mL), water (10 mL), brine (10 mL), dried over $MgSO_4$, filtered and concentrated *in vacuo*. The title product **30c** was obtained as a colourless liquid (0.60 g, quantitative), which did not require further purification. **^{1}H NMR** (300 MHz, Chloroform-*d*) δ 4.31 (q, *J* = 7.1 Hz, 2H, C1'-<u>H_2</u>), 2.71 (d, *J* = 6.8 Hz, 2H, C3-<u>H_2</u>), 2.19 (m, 1H, C4-<u>H</u>),

1.36 (t, *J* = 7.1 Hz, 3H, C2'-$\underline{H}_3$), 0.96 (d, *J* = 6.7 Hz, 6H, 2 × C5-$\underline{H}_3$); **^{13}C NMR** (75 MHz, Chloroform-*d*) δ 194.6 (C2), 161.6 (C1), 62.5 (C1'), 48.0 (C3), 24.3 (C4), 22.6 (2 × C5), 14.2 (C2'); ***m/z*** (ES^+) 144.98 ($[M+H]^+$, 100 %). Spectroscopic data are in agreement with the literature.[324]

Methyl/ethyl 5-methyl-3-phenethyl-1*H*-indole-2-carboxylate (32a)

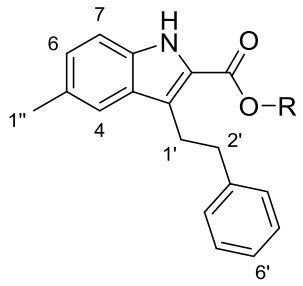

R= methyl/ethyl

32a was prepared from *p*-tolylhydrazine hydrochloride **31a** (200 mg, 1.26 mmol) and methyl 2-oxo-5-phenylpentanoate **30a** (417 mg, 2.02 mmol) using general method A. The crude mixture was purified *via* the Biotage SP4 (silica-packed SNAP column 10 g; 0-8% EtOAc/hexanes) to give the title product **32a** as an inseparable mixture of the methyl and ethyl ester (10:1). The mixture was isolated as a pale yellow solid (322 mg). The ratio of products was determined by analysis of the integration of the methyl-CH_3 (major product) compared to the ethyl-CH_3 (minor product). All other signals are as they appear in the spectra and represent the mixture of esters. **^{1}H NMR** (400 MHz, Chloroform-*d*) δ 8.63 (br s, 1.1H, N$\underline{H}$), 7.40 (s, 1.1H, C4-$\underline{H}$), 7.34 – 7.07 (m, 7.7H, 7 × Ar$\underline{H}$), 4.41 (q, *J* = 7.1 Hz, 0.2H, $CO_2C\underline{H}_2CH_3$) 3.91 (s, 3H, $CO_2C\underline{H}_3$), 3.41 – 3.32 (m, 2.2H, C1'-$\underline{H}_2$), 2.98 – 2.89 (m, 2.2H, C2'-$\underline{H}_2$), 2.46 (s, 3.3H, C1''-$\underline{H}_3$), 1.42 (t, *J* = 7.1 Hz, 0.3H, $CO_2CH_2C\underline{H}_3$); **^{13}C NMR** (101 MHz, Chloroform-*d*) δ 162.8 ($\underline{C}O_2R$), 142.3 (C3'), 134.3 (C7a), 129.4 (C5), 128.6 (2 × Ar$\underline{C}$H), 128.3 (2 × Ar$\underline{C}$H), 128.0 (C3a), 127.6 (C6), 125.9 (C6'), 123.8 (C3), 123.1 (C2), 120.0 (C4), 111.5 (C7), 60.8 ($CO_2\underline{C}H_2CH_3$), 51.7 ($CO_2\underline{C}H_3$), 37.4 (C2'), 27.2 (C1'), 21.5 (C1''), 13.4 ($CO_2CH_2\underline{C}H_3$).

Methyl/ethyl 5-*iso*propyl-3-phenethyl-1*H*-indole-2-carboxylate (32b)

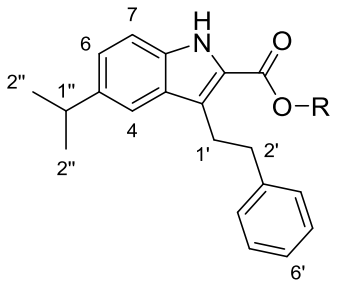

R= methyl/ethyl

32b was prepared from 4-*iso*propylphenylhydrazine hydrochloride **31b** (200 mg, 1.07 mmol) and methyl 2-oxo-5-phenylpentanoate **30a** (353 mg, 1.71 mmol) using general method A. The crude mixture was purified *via* the Biotage SP4 (silica-packed SNAP column 10 g; 0-8% EtOAc/hexanes) to

give the title product **32b** as an inseparable mixture of the methyl and ethyl esters (3:1.2). The mixture was isolated as a pale yellow solid (255 mg). The ratio of products was determined by analysis of the integration of the methyl-CH_3 (major product) compared to the ethyl-CH_3 (minor product). All other signals are as they appear in the spectra and represent the mixture of esters. **^{1}H NMR** (400 MHz, Chloroform-*d*) δ 8.64 (br s, 1.4H, N<u>H</u>), 7.38 (s, 1.4H, C4-<u>H</u>), 7.35 – 7.15 (m, 9.8H, 7 × Ar<u>H</u>), 4.40 (q, *J* = 7.1 Hz, 0.8H, $CO_2C\underline{H}_2CH_3$), 3.92 (s, 3H, $CO_2C\underline{H}_3$), 3.40 – 3.36 (m, 2.8H, C1'-<u>H_2</u>), 3.07 – 2.91 (m, 4.2H, C2'-<u>H_2</u>, C1''-<u>H</u>), 1.43 (t, *J* = 7.1 Hz, 1.2H, $CO_2CH_2C\underline{H}_3$), 1.30 (d, *J* = 6.9 Hz, 8.4H, 2 × C2''-<u>H_3</u>); **^{13}C NMR** (101 MHz, Chloroform-*d*) δ 162.9 ($\underline{C}O_2R$), 142.4 (C3'), 140.9 (C5), 134.7 (C7a), 128.7 (2 × Ar<u>C</u>H), 128.4 (2 ×Ar<u>C</u>H), 128.0 (C3a), 126.0 (C6), 125.4 (C6'), 124.3 (C2), 123.2 (C3), 117.4 (C4), 111.7 (C7), 60.8 ($CO_2\underline{C}H_2CH_3$), 51.8 ($CO_2\underline{C}H_3$), 37.5 (C2'), 34.4 (C1''), 27.2 (C1'), 24.6 (2 × <u>C</u>2''), 13.4 ($CO_2CH_2\underline{C}H_3$).

Ethyl 5-*iso*propyl-3-methyl-1*H*-indole-2-carboxylate (32c)

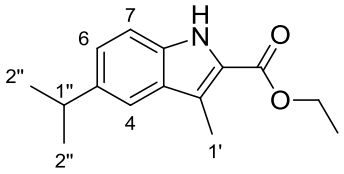

32c was prepared from 4-*iso*propylphenylhydrazine hydrochloride **31b** (250 mg, 1.34 mmol) and ethyl 2-oxobutanoate **30b** (450 mg, 5.0 mmol) using general method E. The crude product was purified *via* the Biotage SP4 (silica-packed SNAP column 10 g; 0-10% EtOAc/hexanes) to give the title product **32c** as a crystalline white solid (222 mg, 67%). **mp** 129-131 °C; **IR** (KBr) ν $_{max}$: 3330 (NH), 2927, 1674 (C=O), 1463 (C=C), 1264 (C-O); **^{1}H NMR** (500 MHz, $CDCl_3$) δ 8.61 (br s, 1H, N<u>H</u>), 7.47 (d, *J* = 1.6 Hz, 1H, C4-<u>H</u>), 7.30 (d, *J* = 8.5 Hz, 1H, C7-<u>H</u>), 7.23 (dd, *J* = 8.5, 1.6 Hz, 1H, C6-<u>H</u>), 4.41 (q, *J* = 7.1 Hz, 2H, $CO_2C\underline{H}_2CH_3$), 3.03 (hept, *J* = 6.8 Hz, 1H, C1''-<u>H</u>), 2.61 (s, 3H, C1'-<u>H_3</u>), 1.43 (t, *J* = 7.1 Hz, 3H, $CO_2CH_2\underline{C}H_3$), 1.32 (d, *J* = 6.8 Hz, 6H, 2 × C2''-<u>H_3</u>); **^{13}C NMR** (126 MHz, $CDCl_3$) δ 162.8 ($\underline{C}O_2CH_2CH_3$), 140.7 (C5), 134.6 (C7a), 128.7 (C3a), 125.4 (C6), 123.7 (C2), 120.1 (C3), 117.4 (C4), 111.6 (C7), 60.7 ($CO_2\underline{C}H_2CH_3$), 34.4 (C1''), 24.7 (2 × C2''), 14.6 ($CO_2CH_2\underline{C}H_3$), 10.1 (C1'); ***m/z*** (ES^+) 246.13 ($[M+H]^+$, 100 %); **HRMS** (ES^+) Calcd for $C_{15}H_{20}NO_2$ $[M+H]^+$: 246.1494, found 246.1487.

Ethyl 3,5-di*iso*propyl-1*H*-indole-2-carboxylate (32d)

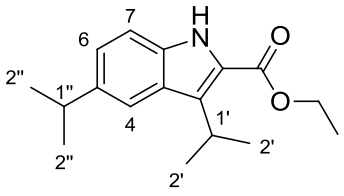

32d was prepared from 4-*iso*propylphenylhydrazine hydrochloride **31b** (222 mg, 1.19 mmol) and ethyl 4-methyl-2-oxopentanoate **30c** (300 mg, 1.9 mmol) using general method E. The crude product was purified *via* the Biotage SP4 (silica-packed SNAP column 10 g; 0-10% EtOAc/hexanes) to give the title product **32d** as a yellow solid (122 mg, 38%). **mp** 64-66 °C; **IR** (KBr) ν $_{max}$: 3320 (NH), 2961, 1688 (C=O), 1467 (C=C), 1255 (C-O); **^{1}H NMR** (400 MHz, $CDCl_3$) δ 8.58 (br s, 1H, NH), 7.68 (dd, *J* = 1.7, 0.7 Hz, 1H, C4-H), 7.31 (dd, *J* = 8.5, 0.7 Hz, 1H, C7-H), 7.21 (ddd, *J* = 8.5, 1.7, 0.7 Hz, 1H, C6-H), 4.40 (q, *J* = 7.1 Hz, 2H, $CO_2CH_2CH_3$), 4.08 (hept, *J* = 7.1 Hz, 1H, C1'-H), 3.01 (hept, *J* = 6.9 Hz, 1H, C1''-H), 1.48 (d, *J* = 7.1 Hz, 6H, 2 × C2'-H_3), 1.42 (t, *J* = 7.1 Hz, 3H, $CO_2CH_2CH_3$), 1.32 (d, *J* = 6.9 Hz, 6H, 2 × C2''-H_3); **^{13}C NMR** (101 MHz, $CDCl_3$) δ 162.5 ($CO_2CH_2CH_3$), 140.3 (C5), 135.0 (C7a), 131.0 (C3), 126.7 (C3a), 124.8 (C6), 122.1 (C2), 119.4 (C4), 111.9 (C7), 60.7 ($CO_2CH_2CH_3$), 34.4 (C1''), 25.8 (C1'), 24.7 (2 × C2''), 22.9 (2 × C2'), 14.6 ($CO_2CH_2CH_3$); ***m/z*** (ES^+) 296.01 ($[M+Na]^+$, 100 %); **HRMS** (ES^-) Calcd for $C_{17}H_{22}NO_2$ $[M-H]^-$: 272.1651, found 272.1657.

Ethyl 3,5-dimethyl-1*H*-indole-2-carboxylate (32e)

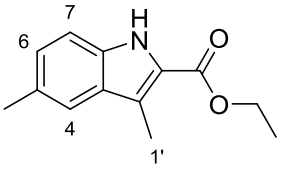

32e was prepared from *p*-tolylhydrazine hydrochloride **31a** (444 mg, 2.8 mmol) and ethyl 2-oxobutanoate **30b** (650 mg, 5.0 mmol) using general method E. The crude product was purified *via* the Biotage SP4 (silica-packed SNAP column 10 g; 0-10% EtOAc/hexanes) to give the title product **32e** as a white solid (409 mg, 67%). **mp** 133-135 °C; **IR** (KBr) ν $_{max}$: 3307 (NH), 2931, 1680 (C=O), 1473 (C=C), 1264 (C-O); **^{1}H NMR** (500 MHz, $CDCl_3$) δ 8.60 (br s, 1H, NH), 7.46-7.42 (m, 1H, C4-H), 7.26 (d, *J* = 8.4 Hz, 1H, C7-H), 7.15 (dd, *J* = 8.4, 1.6 Hz, 1H, C6-H), 4.41 (q, *J* = 7.1 Hz, 2H, $CO_2CH_2CH_3$), 2.59 (s, 3H, C1'-H_3), 2.46 (s, 3H, ArCH_3), 1.43 (t, *J* = 7.1 Hz, 3H, $CO_2CH_2CH_3$); **^{13}C NMR** (126 MHz, $CDCl_3$) δ 162.8 ($CO_2CH_2CH_3$), 134.4 (C7a), 129.3 (C5), 128.9 (C3a), 127.6 (C6), 123.6 (C2), 120.2 (C4), 119.8 (C3), 111.4 (C7), 60.7 ($CO_2CH_2CH_3$), 21.6 (ArCH_3), 14.6 ($CO_2CH_2CH_3$), 10.1 (C1'); ***m/z*** (ES^+) 240.04 ($[M+Na]^+$, 100 %); **HRMS** (ES^+) Calcd for $C_{13}H_{15}NO_2Na$ $[M+Na]^+$: 240.1000, found 240.0992.

Ethyl 3-*iso*propyl-5-methyl-1*H*-indole-2-carboxylate (32f)

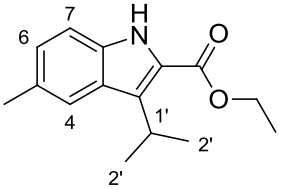

32f was prepared from *p*-tolylhydrazine hydrochloride **31a** (189 mg, 1.19 mmol) and ethyl 4-methyl-2-oxopentanoate **30c** (300 mg, 1.9 mmol) using general method E. The crude product was purified *via* the Biotage SP4 (silica-packed SNAP column 10 g; 0-8% EtOAc/hexanes) to give the title product **32f** as a yellow solid (82 mg, 28%). **mp** 103-105 °C; **IR** (KBr) ν_{max}: 3347 (NH), 2975, 1675 (C=O), 1433 (C=C), 1253 (C-O); **^{1}H NMR** (300 MHz, $CDCl_3$) δ 8.66 (br s, 1H, NH), 7.68 – 7.64 (m, 1H, C4-H), 7.27 (d, *J* = 8.4 Hz, 1H, C7-H) 7.13 (dd, *J* = 8.4, 1.6 Hz, 1H, C6-H), 4.41 (q, *J* = 7.1 Hz, 2H, $CO_2CH_2CH_3$), 4.11 (hept, *J* = 7.1 Hz, 1H, C1'-H), 2.46 (s, 3H, $ArCH_3$), 1.48 (d, *J* = 7.1 Hz, 6H, 2 × C2'-H_3), 1.43 (t, *J* = 7.1 Hz, 3H, $CO_2CH_2CH_3$); **^{13}C NMR** (75 MHz, $CDCl_3$) δ 162.5 ($CO_2CH_2CH_3$), 134.7 (C7a), 130.7 (C3), 128.8 (C5), 127.2 (C6), 126.8 (C3a), 122.1 (C4), 122.1 (C2), 111.7 (C7), 60.7 ($CO_2CH_2CH_3$), 25.8 (C1'), 22.9 (2 × C2'), 21.8 ($ArCH_3$), 14.6 ($CO_2CH_2CH_3$); ***m/z*** (ES^-) 268.00 ([M+Na]$^+$, 100 %); **HRMS** (ES^+) Calcd for $C_{15}H_{20}NO_2$ [M+H]$^+$: 246.1494, found 246.1482.

5-Methyl-1,3-diphenethyl-1*H*-indole-2-carboxylic acid (33a)

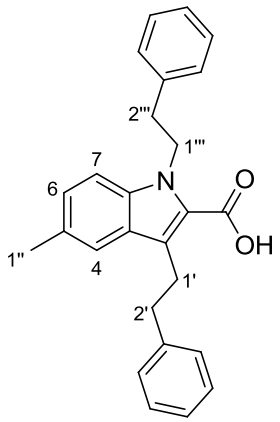

33a was prepared from **32a** (100 mg, 0.34 mmol) and (bromoethyl)benzene (0.09 mL, 0.68 mmol) using general method F. The crude product was purified *via* the Biotage SP4 (silica-packed SNAP column 10 g; 0-10% EtOAc/hexanes) to give the title product **33a** as a white solid (65 mg, 50%). **mp** 202-204 °C; **IR** (KBr) ν_{max}: 3436 (OH), 2925, 1666 (C=O), 1456 (C=C), 1287 (C-O); **^{1}H NMR** (500 MHz, $CDCl_3$) δ 7.46 (s, 1H, C4-H), 7.37 – 7.20 (m, 12H, 12 × ArH), 4.81 – 4.73 (m, 2H, C1'''-H_2), 3.50 – 3.43 (m, 2H, C1'-H_2), 3.15 – 3.07 (m, 2H, C2'''-H_2), 3.04 – 2.97 (m, 2H, C2'-H_2), 2.49 (s, 3H, C1''-H_3); **^{13}C NMR** (126 MHz, $CDCl_3$) δ 167.8 (CO_2H), 142.6 (C3'), 138.9 (C3'''), 137.3 (C7a), 129.7 (C5), 129.1 (2 × ArCH), 128.7 (2 × ArCH), 128.7 (2 × ArCH), 128.5 (2 × ArCH), 128.3 (C6), 127.5 (C3), 126.9 (C3a), 126.7 (ArCH), 126.0 (ArCH), 122.9 (C2), 120.3 (C4), 110.2 (C7), 47.0 (C1'''), 37.7 (C2'), 37.3 (C2'''), 28.2 (C1'), 21.6 (C1''); ***m/z*** (ES^-) 381.91 ([M-H]$^-$, 100 %); **HRMS** (ES^-) Calcd for $C_{26}H_{24}NO_2$ [M-H]$^-$: 382.1807, found 382.1803.

1-Butyl-5-*iso*propyl-3-phenethyl-1*H*-indole-2-carboxylic acid (33b)

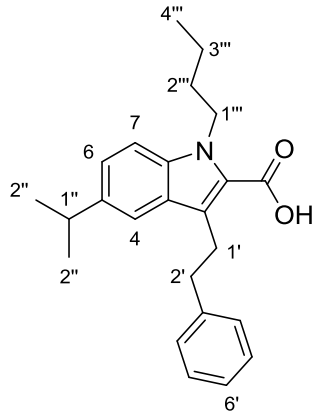

To a suspension of sodium hydride (22 mg, 0.54 mmol, 2.0 eq., 60% in mineral oil) in anhydrous DMF (1.0 mL) at 0 °C was added **32b** (88 mg, 0.27 mmol, 1.0 eq.) in anhydrous DMF (0.3 mL). The mixture was stirred at room temperature for 30 minutes before the addition of 1-bromobutane (0.09 mL, 0.81 mmol, 3.0 eq.). The reaction was then heated at 100 °C for 4 hours before being cooled to room temperature and poured into ice water (10 mL). The mixture was extracted with Et_2O (3 × 10 mL) and the organic layers were combined, washed with brine (10 mL), dried over $MgSO_4$, filtered and concentrated *in vacuo*. To a solution of the crude ester in ethanol (5 mL) was added an aqueous solution of NaOH (1.5 mL, 2N) and the resulting mixture was heated at reflux for 4 hours. The reaction was then cooled to room temperature, diluted with brine (10 mL), acidified to pH 6 with HCl (1 N) and extracted with Et_2O (3 × 10 mL). The combined organic extracts were washed with a saturated solution of $NaHCO_3$ (10 mL), brine (10 mL), dried over $MgSO_4$, filtered and concentrated *in vacuo*. The crude product was purified *via* the Biotage SP4 (silica-packed SNAP column 4 g; 0-8% EtOAc/hexanes) to give the title product **33b** as a crystalline white solid (65 mg, 68% over 2 steps). **mp** 122-124 °C; **IR** (KBr) ν_{max}: 3445 (OH), 2957, 1666 (C=O), 1454 (C=C), 1265 (C-O); **^{1}H NMR** (500 MHz, $CDCl_3$) δ 7.42 (s, 1H, C4-H), 7.34 (d, *J* = 8.6 Hz, 1H, C7-H), 7.29 (m, 5H, C6-H, 2 × C4'-H, 2 × C5'H), 7.23 – 7.19 (m, 1H, C6'-H), 4.56 (t, *J* = 7.4 Hz, 2H, C1'''-H_2), 3.49 – 3.42 (m, 2H, C1'-H_2), 3.01 (m, 3H, C1''-H, C2'-H_2), 1.81 (p, *J* = 7.4 Hz, 2H, C2'''-H_2), 1.41 (h, *J* = 7.4 Hz, 2H, C3'''-H_2), 1.31 (d, *J* = 6.9 Hz, 6H, 2 × C2''-H_3), 0.98 (t, *J* = 7.4 Hz, 3H, C4'''-H_3); **^{13}C NMR** (126 MHz, $CDCl_3$) δ 167.6 (CO_2H), 142.6 (C3'), 140.8 (C5), 137.8 (C7a), 128.7 (2 × ArCH), 128.4 (2 × ArCH), 127.6 (C3), 126.6 (C3a), 126.0 (C6'), 125.7 (C6), 123.0 (C2), 117.4 (C4), 110.6 (C7), 45.1 (C1'''), 37.7 (C2'), 34.3 (C1''), 33.0 (C2'''), 28.1 (C1'), 24.6 (2 × C2''), 20.4 (C3'''), 14.1 (C4'''); ***m/z*** (ES^-) 361.93 ([M-H]$^-$, 100 %); **HRMS** (ES^-) Calcd for $C_{24}H_{28}NO_2$ [M-H]$^-$: 362.2120, found 362.2123.

1-Butyl-5-*iso*propyl-3-methyl-1*H*-indole-2-carboxylic acid (33c)

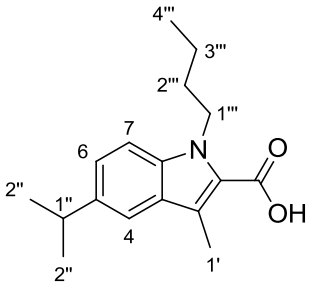

To a suspension of sodium hydride (25 mg, 0.62 mmol, 2.0 eq., 60% in mineral oil) in anhydrous DMF (1.0 mL) at 0 °C was added a solution of **32c** (71 mg, 0.31 mmol, 1.0 eq.) in anhydrous DMF (0.3 mL). The mixture was stirred at room temperature for 30 minutes before the addition of 1-bromobutane (0.05 mL, 0.43 mmol, 1.4 eq.). The reaction was then heated at 100 °C for 4 hours before being cooled to room temperature and poured into ice water (10 mL). The mixture was extracted with Et_2O (3 × 10 mL) and the organic layers were combined, washed with brine (10 mL), dried over $MgSO_4$, filtered and concentrated *in vacuo*. To a solution of the crude ester in ethanol (5 mL) was added an aqueous solution of NaOH (1.5 mL, 2N) and the resulting mixture was heated at reflux for 4 hours. The reaction was then cooled to room temperature, diluted with brine (10 mL), acidified to pH 6 with HCl (1 N) and extracted with Et_2O (3 × 10 mL). The combined organic extracts were washed with a saturated solution of $NaHCO_3$ (10 mL), brine (10 mL), dried over $MgSO_4$, filtered and concentrated *in vacuo*. The crude product was purified *via* the Biotage SP4 (silica-packed SNAP column 4 g; 0-8% EtOAc/hexanes) to give the title product **33c** as a white solid (67 mg, 57% over 2 steps). **mp** 152-154 °C; **IR** (KBr) ν_{max}: 3444 (OH), 2959, 1666 (C=O), 1455 (C=C), 1269 (C-O); **^{1}H NMR** (500 MHz, $CDCl_3$) δ 7.51 (s, 1H, C4-H), 7.30 (m, 2H, C6-H, C7-H), 4.53 (t, *J* = 7.5 Hz, 2H, C1'''-H_2), 3.04 (hept, *J* = 6.9 Hz, 1H, C1''-H), 2.67 (s, 3H, C1'-H_3), 1.77 (p, *J* = 7.5 Hz, 2H, C2'''-H_2), 1.38 (h, *J* = 7.5 Hz, 2H, C3'''-H_2), 1.33 (d, *J* = 6.9 Hz, 6H, 2 × C2''-H_3), 0.95 (t, *J* = 7.5 Hz, 3H, C4'''-H_3); **^{13}C NMR** (126 MHz, $CDCl_3$) δ 168.0 (CO_2H), 140.6 (C5), 137.8 (C7a), 127.2 (C3a), 125.7 (C6), 123.7 (C3), 123.3 (C2), 117.6 (C4), 110.5 (C7), 45.0 (C1'''), 34.3 (C1''), 33.1 (C2'''), 24.6 (2 × C2''), 20.4 (C3'''), 14.0 (c4'''), 11.3 (C1'); ***m/z*** (ES^-) 272.11 ($[M-H]^-$, 100 %); **HRMS** (ES^-) Calcd for $C_{17}H_{22}NO_2$ $[M-H]^-$: 272.1651, found 272.1652.

5-*Iso*propyl-3-methyl-1-phenethyl-1*H*-indole-2-carboxylic acid (33d)

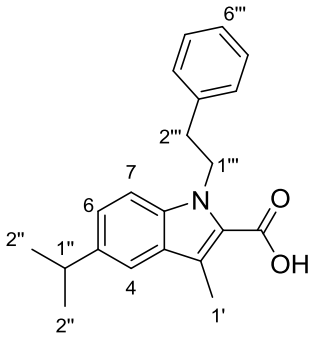

33d was prepared from **32c** (100 mg, 0.41 mmol) and (bromoethyl)benzene (0.29 mL, 1.64 mmol) using general method F. The crude product was purified *via* the Biotage SP4 (silica-packed SNAP column 10 g; 0-10% EtOAc/hexanes) to give the title product **33d** as a white solid (50 mg, 38%). **mp** 177-179 °C; **IR** (KBr) ν $_{max}$: 3445 (OH), 2956, 1666 (C=O), 1455 (C=C), 1268 (C-O); **^{1}H NMR** (500 MHz, $CDCl_3$) δ 7.53 (s, 1H, C4-H), 7.27 (m, 7H, 7 × ArH), 4.76 – 4.72 (m, C1'''-H_2), 3.07 (m, 3H, C1''-H, C2'''-H_2), 2.71 (s, 3H, C1'-H_3), 1.34 (d, *J* = 6.8 Hz, 6H, 2 × C2''-H_3); **^{13}C NMR** (126 MHz, $CDCl_3$) δ 167.9 (CO_2H), 140.8 (C5), 139.0 (C3'''), 137.6 (C7a), 129.1 (2 × ArCH), 128.7 (2 × ArCH), 127.3 (C3a), 126.6 (C6'''), 126.0 (C6), 124.0 (C3), 123.1 (C2), 117.7 (C4), 110.2 (C7), 47.0 (C1'''), 37.4 (C2'''), 34.3 (C1''), 24.6 (2 × C2''), 11.3 (C1'); ***m/z*** (ES^-) 320.16 ($[M-H]^-$, 100 %); **HRMS** (ES^-) Calcd for $C_{21}H_{22}NO_2$ $[M-H]^-$: 320.1656, found 320.1653.

3,5-Di*iso*propyl-1-phenethyl-1*H*-indole-2-carboxylic acid (33e)

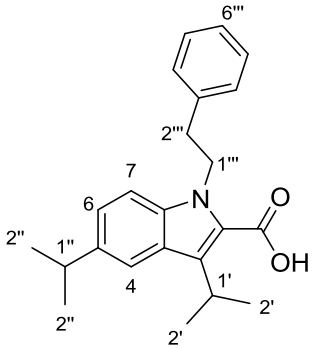

33e was prepared from **32d** (40 mg, 0.18 mmol) and (bromoethyl)benzene (0.07 mL, 0.54 mmol) using general method F. The crude product was purified *via* the Biotage SP4 (silica-packed SNAP column 4 g; 0-10% EtOAc/hexanes) to give the title product **33e** as a white solid (26 mg, 41%). **mp** 152-154 °C; **IR** (KBr) ν $_{max}$: 3429 (OH), 2959, 1658 (C=O), 1459 (C=C), 1262 (C-O); **^{1}H NMR** (300 MHz, $CDCl_3$) δ 7.68 (s, 1H, C4-H), 7.32 – 7.09 (m, 7H, 7 × ArH), 4.67 – 4.55 (m, 2H, C1'''-H_2), 4.10 (hept, *J* = 7.1 Hz, 1H, C1'-H), 3.08 – 2.89 (m, 3H, C1''-H, C2'''-H_2), 1.46 (d, *J* = 7.1 Hz, 6H, 2 × C2'-H_3), 1.27 (d, *J* = 6.9 Hz, 6H, 2 × C2''-H_3); **^{13}C NMR** (126 MHz, $CDCl_3$) δ 167.8 (CO_2H), 140.3 (C5), 139.0 (C3'''), 137.9 (C7a), 133.6 (C3), 129.0 (2 × ArCH), 128.7 (2 × ArCH), 126.7 (C6'''), 125.4 (C3a), 125.1 (C6), 122.3

(C2), 120.0 (C4), 110.6 (C7), 47.0 (C1'''), 37.2 (C2'''), 34.4 (C1''), 26.4 (C1'), 24.7 (2 × C2''), 23.2 (2 × C2'); ***m/z*** (ES^-) 347.93 ($[M-H]^-$, 100 %); **HRMS** (ES^-) Calcd for $C_{23}H_{26}NO_2$ $[M-H]^-$: 348.1964, found 348.1970.

5-*Iso*propyl-1,3-diphenethyl-1*H*-indole-2-carboxylic acid (33f)

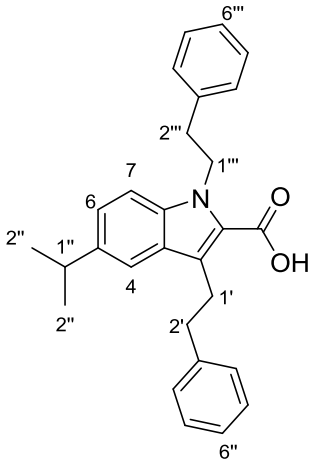

33f was prepared from **32b** (50 mg, 0.16 mmol) and (bromoethyl)benzene (0.04 mL, 0.32 mmol) using general method F. The crude product was purified *via* the Biotage SP4 (silica-packed SNAP column 4 g; 0-10% EtOAc/hexanes) to give the title product **33f** as a white solid (35 mg, 53%). **mp** 175-177 °C; **IR** (KBr) ν_{max}: 3424 (OH), 2958, 1663 (C=O), 1456 (C=C), 1261; **^{1}H NMR** (400 MHz, $CDCl_3$) δ 7.42 (s, 1H, C4-H), 7.36 – 7.19 (m, 12H, ArH), 4.81 – 4.72 (m, 2H, C1'''-H_2), 3.53 – 3.44 (m, 2H, C1'-H_2), 3.15 – 3.08 (m, 2H, C2'''-H_2), 3.08 – 2.96 (m, 3H, C1''-H, C2'-H_2), 1.32 (d, *J* = 6.9 Hz, 6H, 2 × C2''-H_3); **^{13}C NMR** (101 MHz, $CDCl_3$) δ 167.5 (CO_2H), 142.6 (C3'), 141.0 (C5), 139.0 (C3'''), 137.6 (C7a), 129.1 (2 × ArCH), 128.8 (2 × ArCH), 128.7 (2 × ArCH), 128.5 (2 × ArCH), 127.9 (C3), 126.8 (C3a), 126.7 (C6'''), 126.0 (C6'), 125.9 (C6), 122.9 (C2), 117.6 (C4), 110.3 (C7), 47.0 (C1'''), 37.7 (C2'), 37.4 (C2'''), 34.3 (C1''), 28.1 (C1'), 24.6 (2 × C2''); ***m/z*** (ES^-) 409.91 ($[M-H]^-$, 100 %); **HRMS** (ES^-) Calcd for $C_{28}H_{28}NO_2$ $[M-H]^-$: 410.2120, found 410.2115.

1-Butyl-3,5-di*iso*propyl-1*H*-indole-2-carboxylic acid (33g)

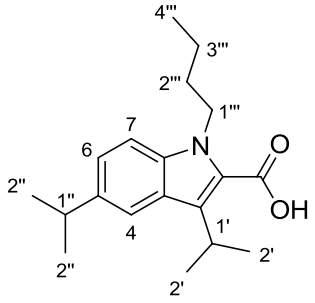

33g was prepared from **32d** (62 mg, 0.23 mmol) and 1-bromobutane (0.08 mL, 0.69 mmol) using general method F. The crude product was purified *via* the Biotage SP4 (silica-packed SNAP column 4 g; 0-10% EtOAc/hexanes) to give the title product **33g** as a white solid (56 mg, 81%). **mp** 155-157 °C; **IR** (KBr) ν $_{max}$: 3438 (OH), 2961, 1666 (C=O), 1457 (C=C), 1259 (C-O); **^{1}H NMR** (500 MHz, $CDCl_3$) δ 7.73 (d, *J* = 1.5 Hz, 1H, C4-H), 7.33 (d, *J* = 8.7 Hz, 1H, C7-H), 7.26 (dd, *J* = 8.7, 1.5 Hz, 1H, C6-H), 4.46 (t, *J* = 7.4 Hz, 2H, C1'''-H_2), 4.16 (hept, *J* = 7.3 Hz, 1H, C1'-H), 3.02 (hept, *J* = 7.0 Hz, 1H, C1''-H), 1.77 (p, *J* = 7.4 Hz, 2H, C2'''-H_2), 1.51 (d, *J* = 7.3 Hz, 6H, 2 × C2'-H_3), 1.39 (h, *J* = 7.4 Hz, 2H, C3'''-CH_2), 1.33 (d, *J* = 7.0 Hz, 6H, 2 × C2''-H_3), 0.96 (t, *J* = 7.4 Hz, 3H, C4'''-H_3); **^{13}C NMR** (126 MHz, $CDCl_3$) δ 168.1 (CO_2H), 140.0 (C5), 138.1 (C7a), 133.3 (C3), 125.2 (C3a), 124.9 (C6), 122.4 (C2), 119.8 (C4), 110.8 (C7), 45.1 (C1'''), 34.4 (C1''), 32.9 (C2'''), 26.4 (C1'), 24.6 (2 × C2''), 23.2 (2 × C2'), 20.4 (C3'''), 14.0 (C4'''); ***m/z*** (ES^-) 389.84 ($[M-H]^-$, 100 %); **HRMS** (ES^-) Calcd for $C_{25}H_{16}N_3O_2$ $[M-H]^-$: 390.1245, found 390.1243.

3,5-Dimethyl-1-phenethyl-1*H*-indole-2-carboxylic acid (33h)

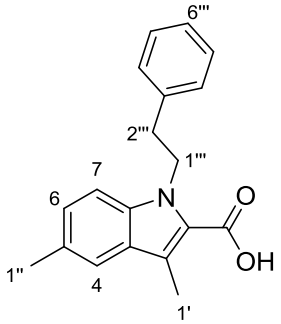

33h was prepared from **32e** (100 mg, 0.46 mmol) and (bromoethyl)benzene (0.25 mL, 1.84 mmol) using general method F. The crude product was purified *via* the Biotage SP4 (silica-packed SNAP column 10 g; 0-10% EtOAc/hexanes) to give the title product **33h** as a white solid (75 mg, 56%). **mp** 201-203 °C; **IR** (KBr) ν $_{max}$: 3442 (OH), 2929, 1666 (C=O), 1454 (C=C), 1267 (C-O); **^{1}H NMR** (500 MHz, $CDCl_3$) δ 7.49 (s, 1H, C4-H), 7.33 – 7.18 (m, 7H, 7 × ArH), 4.76 – 7.42 (m, 2H, C1'''-H_2), 3.10 – 3.06 (m, 2H, C2'''-H_2), 2.69 (s, 3H, C1'-H_3), 2.48 (s, 3H, C1''-H_3); **^{13}C NMR** (126 MHz, $CDCl_3$) δ 168.0 (CO_2H), 139.0 (C3'''), 137.3 (C7a), 129.4 (C5), 129.1 (2 × ArCH), 128.7 (2 × ArCH), 128.2 (C6), 127.5 (C3a), 126.6 (C6'''), 123.7 (C3), 123.1 (C2), 120.5 (C4), 110.1 (C7), 46.9 (C1'''), 37.3 (C2'''), 21.6 (C1''), 11.3 (C1'); ***m/z*** (ES^-) 292.07 ($[M-H]^-$, 100 %); **HRMS** (ES^-) Calcd for $C_{19}H_{18}NO_2$ $[M-H]^-$: 292.1338, found 292.1328.

1-Butyl-3-*iso*propyl-5-methyl-1*H*-indole-2-carboxylic acid (33i)

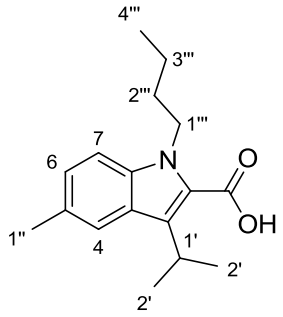

33i was prepared from **32f** (40 mg, 0.16 mmol) and 1-bromopropane (0.05 mL, 0.48 mmol) using general method F. The crude product was purified *via* the Biotage SP4 (silica-packed SNAP column 4 g; 0-10% EtOAc/hexanes) to give the title product **33i** as a white solid (32 mg, 73%). **mp** 162-164 °C; **IR** (KBr) ν $_{max}$: 3424 (OH), 2932, 1663 (C=O), 1440 (C=C), 1269 (C-O); **^{1}H NMR** (500 MHz, $CDCl_3$) δ 7.70 (s, 1H, C4-H), 7.29 (d, *J* = 8.6 Hz, 1H, C7-H), 7.18 (d, *J* = 8.6 Hz, 1H, C6-H), 4.47 (t, *J* = 7.5 Hz, 2H, C1'''-H_2), 4.15 (hept, *J* = 7.4 Hz, 1H, C1'-H), 2.47 (s, 3H, C1''-H_3), 1.76 (p, *J* = 7.5 Hz, 2H, C2'''-H_2), 1.50 (d, *J* = 7.4 Hz, 6H, 2 × C2'-H_3), 1.36 (h, *J* = 7.5 Hz, 2H, C3'''-H_2), 0.95 (t, *J* = 7.5 Hz, 3H, C4'''-H_3); **^{13}C NMR** (126 MHz, $CDCl_3$) δ 168.1 (CO_2H), 137.9 (C7a), 133.1 (C3), 128.7 (C5), 127.3 (C6), 125.4 (C3a), 122.5 (C4), 122.4 (C2), 110.7 (C7), 45.1 (C1'''), 32.8 (C2'''), 26.4 (C1'), 23.2 (2 × C2'), 21.7 (C1''), 20.4 (C3'''), 14.0 (C4'''); ***m/z*** (ES^+) 274.18 ($[M+H]^+$, 100 %); **HRMS** (ES^+) Calcd for $C_{17}H_{24}NO_2$ $[M+H]^+$: 274.1802, found 274.1804.

3-*Iso*propyl-5-methyl-1-phenethyl-1*H*-indole-2-carboxylic acid (33j)

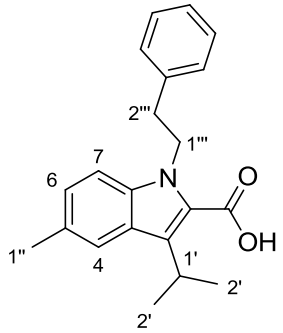

33j was prepared from **32f** (40 mg, 0.16 mmol) and (bromoethyl)benzene (0.07 mL, 0.48 mmol) using general method F. The crude product was purified *via* the Biotage SP4 (silica-packed SNAP column 4 g; 0-10% EtOAc/hexanes) to give the title product **33j** as a white solid (21 mg, 41%). **mp** 170-172 °C; **IR** (KBr) ν $_{max}$: 3443 (OH), 2961, 1661 (C=O), 1460 (C=C), 1263 (C-O); **^{1}H NMR** (500 MHz, $CDCl_3$) δ 7.72 (s, 1H, C4-H), 7.32 – 7.17 (m, 7H, 7 × ArH), 4.69 (t, *J* = 7.9 Hz, 2H, C1'''-H_2), 4.16 (hept, *J* = 7.3 Hz, 1H, C1'-H), 3.08 (t, *J* = 7.9 Hz, 2H, C2'''-H_2), 2.48 (s, 3H, C1''-H_3), 1.52 (d, *J* = 7.3 Hz, 6H, 2 × C2'-H_3); **^{13}C NMR** (126 MHz, $CDCl_3$) δ 168.0 (CO_2H), 138.9 (C3'''), 137.7 (C7a), 133.3 (C3), 129.0 (2 ×

Ar<u>C</u>H), 128.9 (C5), 128.7 (2 × Ar<u>C</u>H), 127.6 (C6), 126.7 (C6'''), 125.5 (C3a), 122.6 (C4), 122.4 (C2), 110.5 (C7), 46.9 (C1'''), 37.1 (C2'''), 26.4 (C1'), 23.1 (2 × C2'), 21.8 (C1''); ***m/z*** (ES^+) 322.18 ($[M+H]^+$, 100 %); **HRMS** (ES^+) Calcd for $C_{21}H_{24}NO_2$ $[M+H]^+$: 322.1802, found 322.1808.

5 High-Throughput Screening as a Method for the Discovery of p53 Activators

5.1 Introduction

5.1.1 High-throughput screening

High-throughput Screening (HTS) is a well-established drug discovery process that has been used for several decades both in academia and the pharmaceutical industry to assess quickly the biological or biochemical activity of a library of drug-like compounds.[325,326] Technological advances in robotic automation, data handling and miniaturisation of assay methods has facilitated the rapid, efficient and increasingly cost effective screening of large libraries of small molecules in order to identify modulators of a target protein's activity.[327] HTS of large compound libraries can be a highly effective method to discover novel PPI modulators.[328,329] In particular, it can provide the opportunity to serendipitously discover modulators with novel modes of action, such as modulation of a PPI through binding to unknown hot spots or clefts, or through novel mechanisms such as alteration of a protein partner's oligomeric or conformational status. For new or less well-defined PPIs, which lack structural information, or endogenous lead compounds, HTS is arguably the only reliable method to discover modulators.[1]

However, despite many impressive success stories in classical drug discovery, HTS has had mixed results in identifying new PPI modulators, partly owing to the difficulties associated with developing reliable *in vitro* high-throughput PPI assays.[11] This issue often occurs as a result of the inability to recreate the target PPI in an *in vitro* setting, rather than the availability of a suitable assay method, as numerous robust examples have been developed which primarily monitor a change in fluorescence or absorption on formation of the PPI, *i.e.*, fluorescence resonance energy transfer (FRET), enzyme-linked immunosorbent assay (ELISA) and fluorescence polarisation (FP). The development of an appropriate *in vitro* HTS assay is usually hampered by the difficulties associated with the isolation of the pure, functional protein partners due to complexities such as the requirement for membrane stabilisation, essential cofactors or additional adapter proteins to form a multiprotein complex. Often, a peptide or domain fragment is used in place of one or both of the protein partners, and inhibition of this PPI *in vitro* may not be transferable to the corresponding PPI between the full-length proteins.[11]

The dynamic, transient and heterogeneous behaviour of many therapeutically interesting PPIs makes them significantly more challenging drug targets, particularly in an *in vitro* setting.[1] Forward chemical genetic screens provide a solution to many of these issues by monitoring changes in phenotype on a cellular level as a result of modulation of a protein's signalling pathway or interactome.[330] This approach can provide a mechanism by which to identify PPI modulators of intractable transient or multiprotein interactions.

5.1.2 Non-genotoxic p53 activators

The forward chemical genetic (FCG) approach (Figure 5.1) utilises cell-based assays to search for small molecules that promote a specific phenotype.[330–332] This approach to drug discovery has many advantages over the more classical methods based on biochemical screens but also provides a significant challenge in elucidating a hit compound's precise mechanism of action in cells. Although the FCG approach can result in the identification of modulators of complex PPIs, this is purely serendipitous as it monitors primarily a particular phenotypic change without any preconception of the molecular target. Therefore the observed phenotypic response could be as a result of numerous pathways including modulation of a PPI, or a classical enzyme target. Identification of the biological target is often the most significant challenge associated with this approach.[333,334]

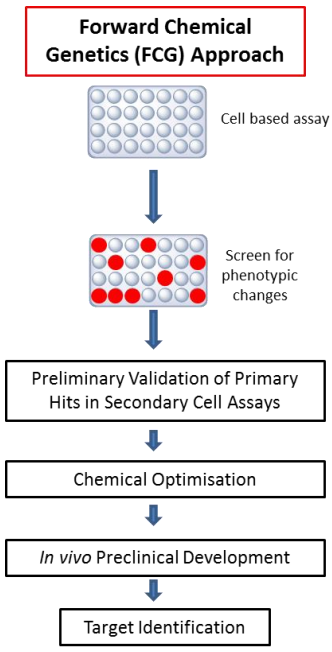

Figure 5.1. The forward chemical genetic (FCG) approach to drug discovery.[335]

In the case of high-throughput screens carried out using a mammalian cell based assay, one clear advantage is that hit compounds show activity in cells at a concentration required for further

preclinical development. In addition, cell-based assays that require the expression of a reporter protein, select for compounds that are not general cytotoxics due to the fact that a synthetic event must occur in their presence.[335] Therefore this approach can be particularly valuable for the identification of selective, non-toxic anticancer drug leads. In particular, the FCG approach is increasingly being applied to the discovery of compounds that activate the tumour suppressor protein p53.[335–337]

5.1.3 p53 & cancer

Carcinogenesis is a multistep process involving dynamic changes in the genome. The transformation of a normal cell to a cancer cell generally involves the activation of oncogenes and the inactivation of tumour suppressor genes and pro-apoptotic genes.[5] A major advance in this area was the discovery of the tumour suppressor gene p53 in 1979.[338,339] This gene encodes for a homotetrameric transcription factor that regulates the expression of a variety of genes involved in cell cycle progression, apoptosis, DNA repair, cell-cycle arrest, nitric oxide production and angiogenesis.[340] p53 accumulates in the nucleus in response to genotoxic and nongenotoxic cellular stresses, including DNA damage and oncogene activation. This triggers transcriptional activation of p53 target genes such as those involved in DNA repair, cell cycle arrest, senescence and/or apoptosis.[341,342]

In the absence of a genotoxic stress, p53 undergoes a rapid turnover which keeps it at a low level. The levels of p53 are mainly regulated by ubiquitin ligases, such as MDM2, MDM4, Pirh2 and Cop1. MDM2 and MDM4 (or MDMX) are key regulators of p53 whose amplification or overexpression are frequently observed in human tumours.[343] MDM2 is an E3 ubiquitin ligase that catalyses ubiquitination of p53, an event that results in subsequent degradation of p53 by the proteasome.[344,345] MDM4 also contributes to the E3 ligase activity of MDM2 and MDM2/MDM4 heterodimers have greater E3 ligase activity towards p53 than MDM2 alone. There are now a variety of known small molecules that impair the interaction of p53 with MDM2[346–349] including Nutlin-3 (**2**, Figure 5.2).[350]

The central role played by p53 in preventing tumour development is clear. More than 50% of adult human cancers are characterised by inactivating mutations or deletions in the p53 gene.[351,352] In addition to these, there are several other tumour types in which p53 is wild-type but errors in the control mechanisms that lead to p53 activation occur.[353] Therefore, it is widely accepted that new non-genotoxic small molecule activators of wild-type p53 may play a crucial role in providing novel therapeutic treatments for cancer.[336] The challenge resides in the activation of p53 transcription

without the DNA damaging mutagenic effects of classical chemotherapeutic and radiotherapy treatments.

5.1.4 Identification of a new p53 activator (±)-MJ05

In collaboration with the Lain group at the Karolinski Institute in Sweden, a FCG screen of 20,000 drug-like molecules was carried out using an ARN8 human cancer cell line. This cell line derives from A375 human melanoma cells which bear wild type p53, and contain a reporter gene (β-galactosidase) placed under the control of a p53-dependent promoter. This initial screen identified 77 compounds, which activated p53 transcription greater than 2-fold. These hits were then rescreened in a secondary MTT assay, to determine their cytotoxicity on ARN8 cells. 11 compounds were found to reduce cell viability at less than 10 μM, thus identifying them as potential lead compounds.

The second focus of this screening process was the identification of lead compounds which displayed promising therapeutic windows (therapeutic index). The therapeutic window is the concentration range between the ED_{50} (effective dose for 50% of the population) and TD_{50} (toxic dose for 50% of the population).[354] The greater the concentration range of this therapeutic window, the less toxicity is observed at the concentration of drug required for its therapeutic effect. For many drugs, the optimum dose required for effective and safe therapy varies significantly from patient to patient.[355] A wide therapeutic window allows for the alteration of an individual's drug dose to better fulfil their requirements without adverse effects, and also to reduce the risk of serious toxicity from poor patient compliance. The majority of current cancer chemotherapies are plagued by very narrow therapeutic windows, which results in significant adverse side effects and the inability to increase drug concentration for resistant cases due to a potentially severe toxic response. This highlights the need to identify new potent anti-cancer agents with wide therapeutic windows.

In the case of this screening program, all hit compounds were analysed based on their effect on cell viability of the ARN8 cancer cell line and on human normal dermal fibroblasts (HNDFs). Their therapeutic window was determined by the difference in IC_{50} values across the two cell lines. The larger the concentration range between the two IC_{50} values the less risk of toxic side effects due to unselective targeting of normal cells. The 11 compounds were rescreened in the MTT assay against the HNDF cell line. This identified one compound, named (±)-MJ05 (**1**), which was shown to have minimal effect on the cell viability or proliferation of HNDFs, whilst displaying significant activity against ARN8 cells with an IC_{50} value <10 μM (Figure 5.2). (±)-MJ05 (**1**) was also shown to have an

IC_{50} value against the HNDF cells, which was greater than 5-fold the IC_{50} value observed against the cancer cell line. This was a very promising therapeutic window when compared to Nutlin-3 (**2**),[350] a Roche PPI inhibitor of MDM2 mediated degradation of p53 which is currently in clinical trials (Figure 5.2). Nutlin-3 (**2**) was shown to have a similar IC_{50} against both the HNDF and the ARN8 cell lines, which could potentially lead to significant toxicity and selectivity issues in clinical use.

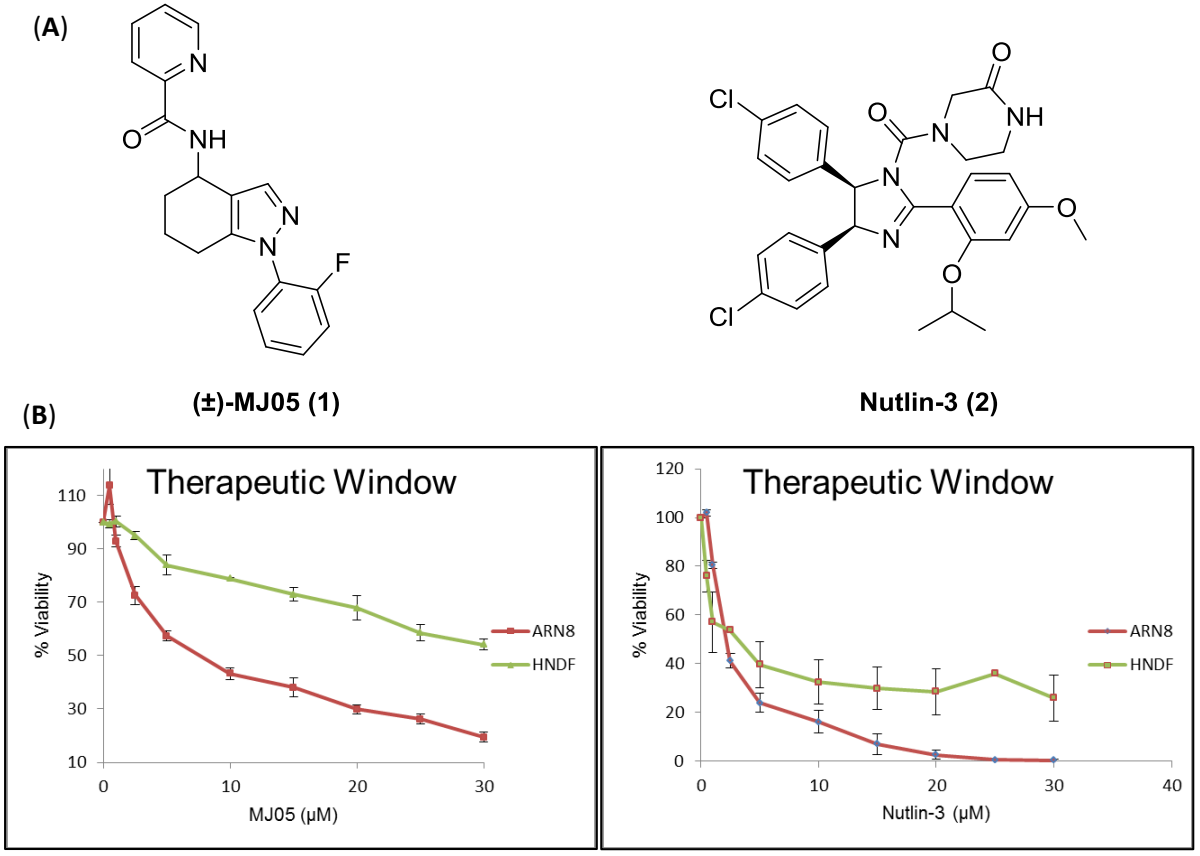

Figure 5.2. (A) Structures of (±)-MJ05 (1) and Nutlin-3 (2). (B) Therapeutic window of (±)-MJ05 (1) and Nutlin-3 (2). Data provided by the Lain group.

Having identified (±)-MJ05 (**1**) as an interesting compound, the challenging process of target identification was considered. A chemoinformatic search revealed that (±)-MJ05 (**1**) had been previously shown to inhibit the MDM2/MDM4 interaction in a cell based screen (NCBI database; deposited by the Sanford-Burnham Centre for Chemical Genomics), an event that according to the current literature could lead to the activation of p53.[346,348] According to the Sandord-Burnham screen, (±)-MJ05 (**1**) inhibited the MDM2/MDM4 interaction by 72% at a concentration of 8 μM.

5.2 Aims of this work

In collaboration with the Lain group at the Karolinski Institute in Sweden, a forward chemical genetics approach was used to screen 20,000 drug-like molecules using an ARN8 human tumour cell line. This led to the identification of (±)-MJ05 (**1**), which was shown to be a p53 activator with cytotoxicity against ARN8s cells. Further analysis revealed that (±)-MJ05 (**1**) had a very promising therapeutic window, with an IC_{50} value >30 μM against human normal dermal fibroblasts (HNDFs). Literature research revealed that (±)-MJ05 (**1**) had been previously identified as an MDM2/MDM4 protein-protein interaction inhibitor, suggesting a novel route to modulate p53 activity. (±)-MJ05 (**1**) was selected as a promising lead compound for further biological and chemical development as a novel non-genotoxic small molecule p53 activator based on its biological activity, promising therapeutic window but most relevant in the context of this thesis, its potential mechanism of p53 activation.

The first aim of this project was to devise an efficient method to synthesise an authentic sample of (±)-MJ05 (**1**) to validate its previously observed biological activity. The synthetic route should allow for easy modification of (±)-MJ05 (**1**) for structure-activity relationships (SAR) studies and facilitate a large scale synthesis of (±)-MJ05 (**1**) for further exploration of its biological effects, for example, xenograft experiments in mice.

The second aim of this work was the development of an asymmetric synthesis to access enantiomerically pure samples of (+)- and (-)-MJ05 (**1**). Thus providing a mechanism by which to determine if MJ05 (**1**)'s activity is as a result of modulation of a chirally discriminating biological target (*i.e*. only one enantiomer would be expected to produce the observed activity), in contrast to unselective cytotoxicity. This could potentially facilitate a reduction in dosage, provide a valuable control molecule (the inactive enantiomer) and decrease off-target toxic effects.

5.3 Synthesis and Biological Assessment of (±)-MJ05

5.3.1 Synthesis of target compound (±)-MJ05

A 4-step synthesis of (±)-MJ05 (**1**) was developed, starting from commercially available 1,3-cyclohexanedione (**3**) (Scheme 5.1). 1,3-Cyclohexanedione (**3**) was treated with dimethylformamide-dimethylacetal (DMF-DMA) to provide the enamine-substituted cyclohexanedione **4**,[356] which was subjected to AcOH-catalysed cyclocondensation with 4-fluorophenylhydrazine hydrochloride to afford pyrazole **5**.[357] Subsequent reductive amination of **5** gave the 4-aminotetrahydroindazole **6**. Finally, the target compound (±)-MJ05 (**1**) was readily prepared by an *N*-acylation of crude **6** with 2-picolinic acid

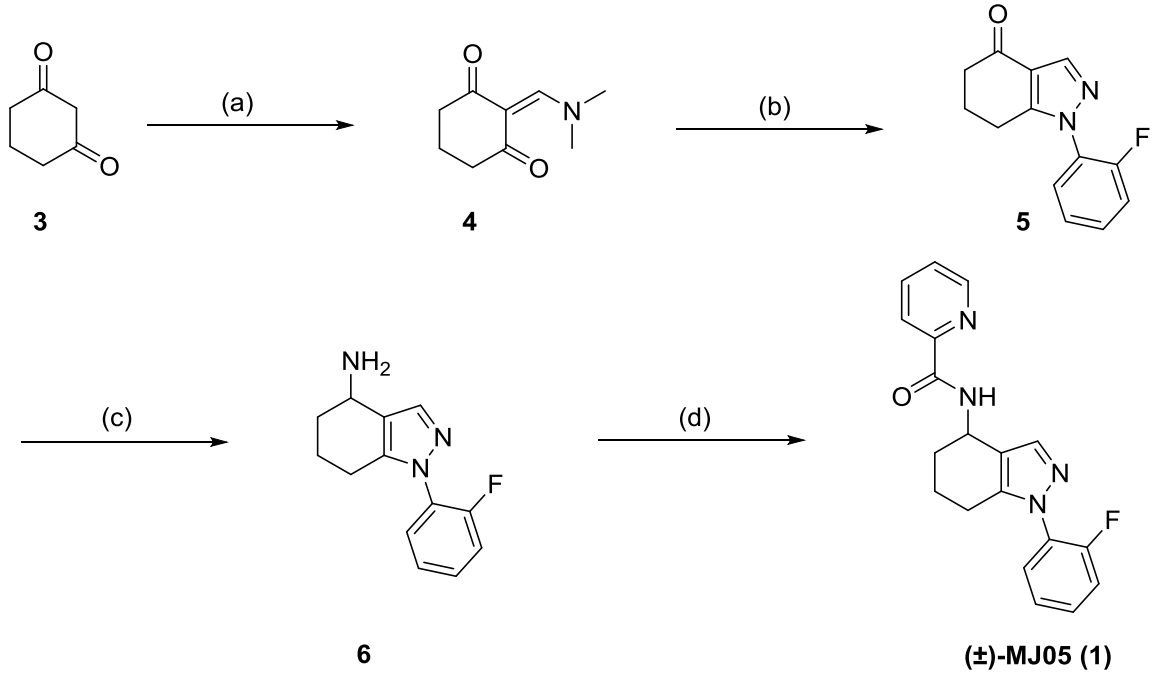

Scheme 5.1. Synthetic route to target compound (±)-MJ05 (1). *Reagents & conditions*: (**a**) DMF-DMA, reflux, 2 h, 71%. (**b**) (i) 4-Fluorophenylhydrazine hydrochloride, MeOH, H_2O, NaOH, reflux, 2 h. (ii) AcOH, H_2O, 110 ℃, 1.5 h, 77%. (**c**) NH_4Ac, $NaBH_3CN$, 2-propanol, 4 Å molecular sieves, 70 ℃, 12 h. (**d**) 2-Picolinic acid, EDC.HCl, Et_3N, HOBt, DMAP, DCM, r.t., overnight, 65% over 2 steps.

This synthetic route provided a short, high-yielding approach to the desired compound (±)-MJ05 (**1**). Furthermore, the incorporation of a range of hydrazines in the cyclocondensation step (Scheme 5.1, step b) and carboxylic acids in the *N*-acylation step (Scheme 5.1, step d) would enable a relatively simple and thorough future exploration of the SAR of (±)-MJ05 (**1**). The structure of (±)-MJ05 (**1**) was validated and characterised by ^{1}H NMR, ^{13}C NMR, 2D NMR and ESI-MS and a sample was sent to the Lain group at the Karolinski Institute in Sweden for testing in the previously described p53 activation and cell death assays (Figure 5.3).

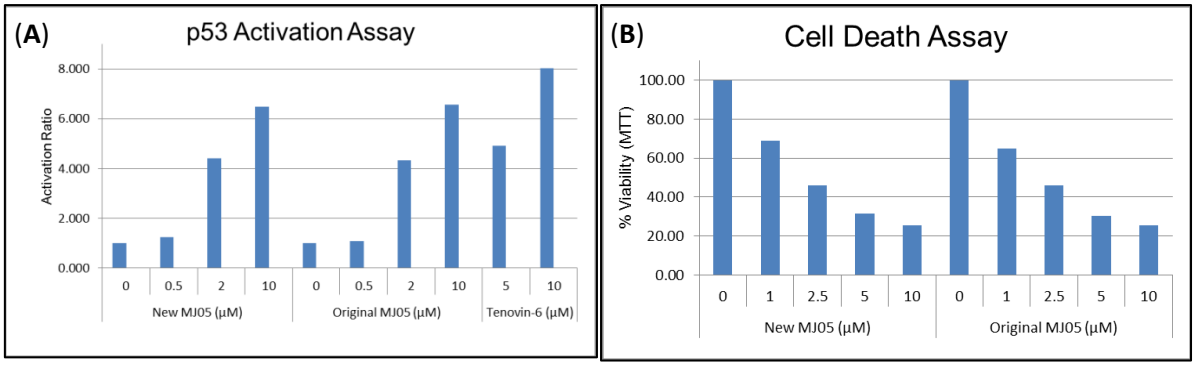

Figure 5.3. Comparison of the biological activity of the "original" (±)-MJ05 (1) sample with the "new" synthesised sample. (**A**) p53 transcriptional activation in the β-galactosidase assay as a result of increasing concentrations of "original" or "new" (±)-MJ05 (**1**) sample and known p53 activator Tenovin-6. (**B**) Percentage cell viability as measured in the MTT assay in the presence of increasing concentrations of "original" and "new" (±)-MJ05 (**1**) sample. Data provided by the Lain group.

The authentic synthesised sample of (±)-MJ05 (**1**) elicited a similar p53 transcriptional activation response and cytotoxicity as the original sample obtained from the commercial supplier for the HTS (Figure 5.3). This confirmed the authenticity of the "original" sample and highlighted **1** as a promising compound for future development.

5.3.2 Mouse xenograft studies

The previously described synthesis (Scheme 5.1) was repeated to provide a greater quantity of (±)-MJ05 (**1**) (~2 g) for mouse xenograft studies. In this study, mice were implanted with ARN8 (melanoma cell line) derived tumours onto their backs, and the tumour size/volume was monitored over 15 days. The increase in tumour size was then compared between mice which were treated with (±)-MJ05 (**1**) (150 mg/Kg) and the control mice which were treated with the vector (DMSO) control (Figure 5.4).

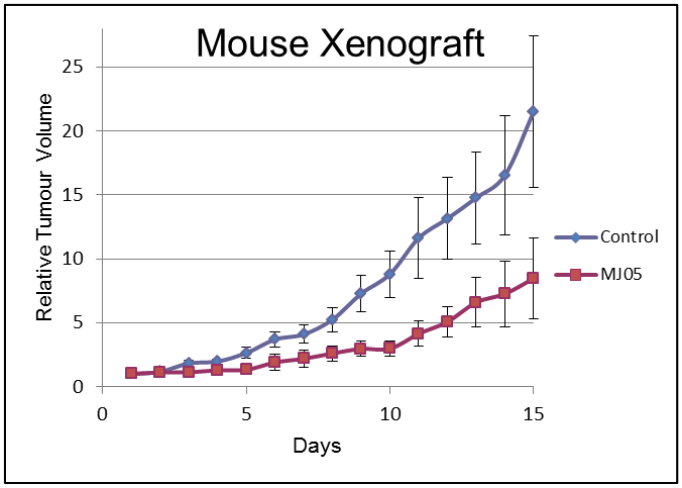

Figure 5.4. Effect of (±)-MJ05 (1) (150 mg/Kg) on tumour volume over 15 days. Each data point represents the average of 10 mice. Data provided by the Lain group.

The mouse xenograft study showed a significant difference in tumour size between the mice treated with (±)-MJ05 (**1**) compared with the untreated mice after 15 days. (±)-MJ05 (**1**) impaired tumour growth over this time period resulting in significantly smaller tumours compared with the control mice (Figure 5.4). It should be noted, however that tumour growth was not stopped and the tumour was not cleared at this dose of (±)-MJ05 (**1**). Promisingly, (±)-MJ05 (**1**) did not appear to have any toxic effect on the mice at concentrations up to 150 mg/Kg. Encouraged by this result, it was decided to synthesise both enantiomers of (±)-MJ05 (**1**) and assess whether there was a difference in activity between the two enantiomers.

5.4 Synthesis and Biological Assessment of (+)-MJ05 and (-)-MJ05

5.4.1 Synthesis of MJ05 enantiomers

To achieve this aim, an asymmetric variant of the reductive amination step described in the previous synthesis (Scheme 5.1, step c) would be required to access either enantiomer of 4-amino-tetrahydroindazole **6**. Methods based upon the chiral amine reagent *tert*-butanesulfinamide **7** (Scheme 5.2) have become some of the most extensively used synthetic approaches for asymmetric amine synthesis for both the discovery and production of drug candidates.[190,204] From a practical standpoint, either enantiomer of **7** was commercially available and also relatively inexpensive to synthesise on a large scale if required in the future.[358] More importantly, the synthetic steps used to prepare amines from **7** are typically robust and broad in scope, providing a straightforward route to both enantiomers of (±)-MJ05 (**1**).

A previous study by the Ellman group identified that $NaBH_4$ reduction of *tert*-butanesulfinyl imines occurred with high levels of diastereofacial control (Scheme 5.2).[359] (R_S)-*tert*-Butanesulfinamide **7** was condensed with a variety of ketones prior to *in situ* $NaBH_4$ mediated reduction, to yield predominantly the (R_S,*R*) diastereomer **8** of the sulfinamide product.

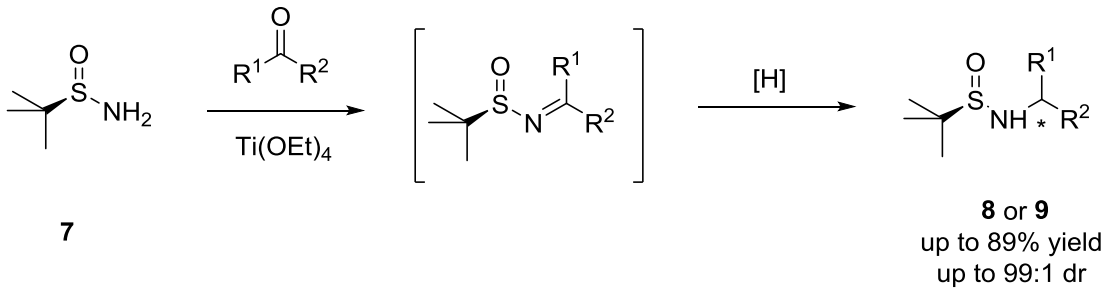

Scheme 5.2. Condensation of (R_S)-*tert*-butanesulfinamide 7 with a variety of ketones followed by *in situ* reduction with $NaBH_4$ or L-Selectride to yield the (R_S,*R*)-8 and (R_S,*S*)-9 diastereomers respectively.[358]

In subsequent research it was observed that the alternative reducing agent L-Selectride gave the opposite sense of asymmetric induction to provide predominantly the (R_S,*S*) diastereomer **9**.[358] The complementary sense of induction provided by these two reducing reagents would allow for the preparation of both amine stereoisomeric precursors of (±)-MJ05 (**1**) from a single enantiomer of **7**. Coyler *et al*.[199] proposed a cyclic *versus* acyclic transition state model to explain the origin of the reversal in diastereofacial selectivity observed upon switching the reducing agent. ^{1}H NMR analysis revealed that the sulfinyl imines formed during the condensation step existed solely as the (*E*)-isomers. They proposed that in the case of $NaBH_4$ reduction, the (R_S,*E*)-sulfinyl imine was reduced *via* a closed transition state, wherein the sulfinyl oxygen participates in the delivery of the hydride which would result in the observed (R_S,*R*)-sulfinamide product **10** (Scheme 5.3A).

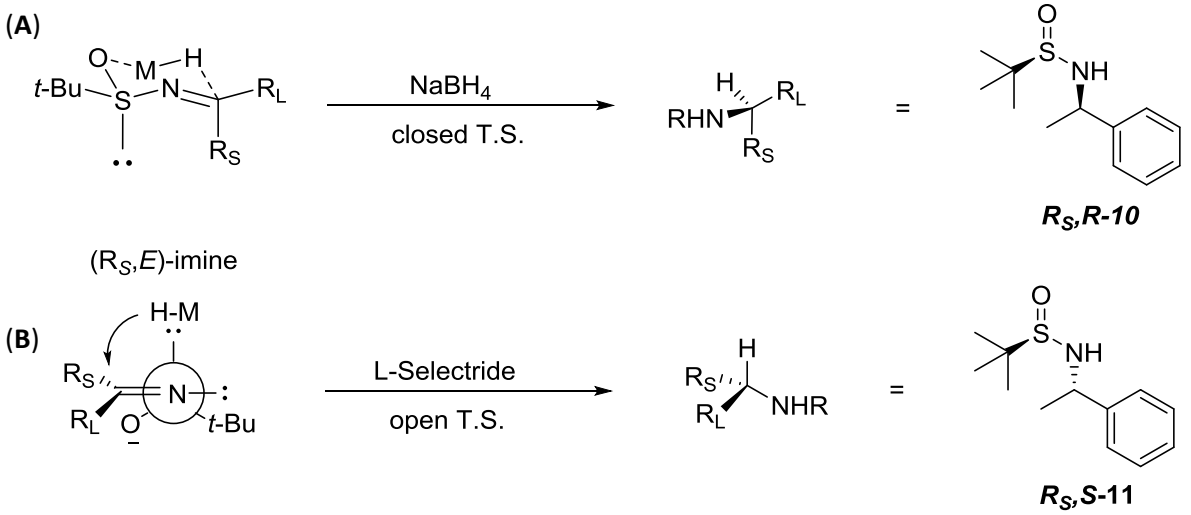

Scheme 5.3. Coyler *et al*.'s mechanistic proposal to rationalise the stereoselectivity of the sulfinyl imine reduction.[17]

However, in the case of poorly coordinating metal hydrides such as L-Selectride (due to its bulky *sec*-butyl groups), the hydride would attack the electrophilic imine carbon atom in a sterically controlled fashion *via* an open transition state. As a result, hydride delivery would occur from the same face as the sulfur lone pair to furnish the observed (R_S,*S*)-sulfinamide product **11** as predicted by the Felkin-Ahn model (Scheme 5.3B).

Sulfinyl imine **12** was prepared by condensation of ketone **5** and (R_S)-**7** in the presence of $Ti(OEt)_4$, which acted both as a desiccant and as a Lewis acid. *In situ* reduction of the sulfinyl imine **12** with either L-Selectride or $NaBH_4$ in THF at -48 ℃ yielded two diastereomers, which were predicted to be the (R_S,*S*)-**13** and (R_S,*R*)-**14** diastereomers (Scheme 5.4) of the sulfinamide product respectively based on the previously discussed transition state models (Scheme 5.3).

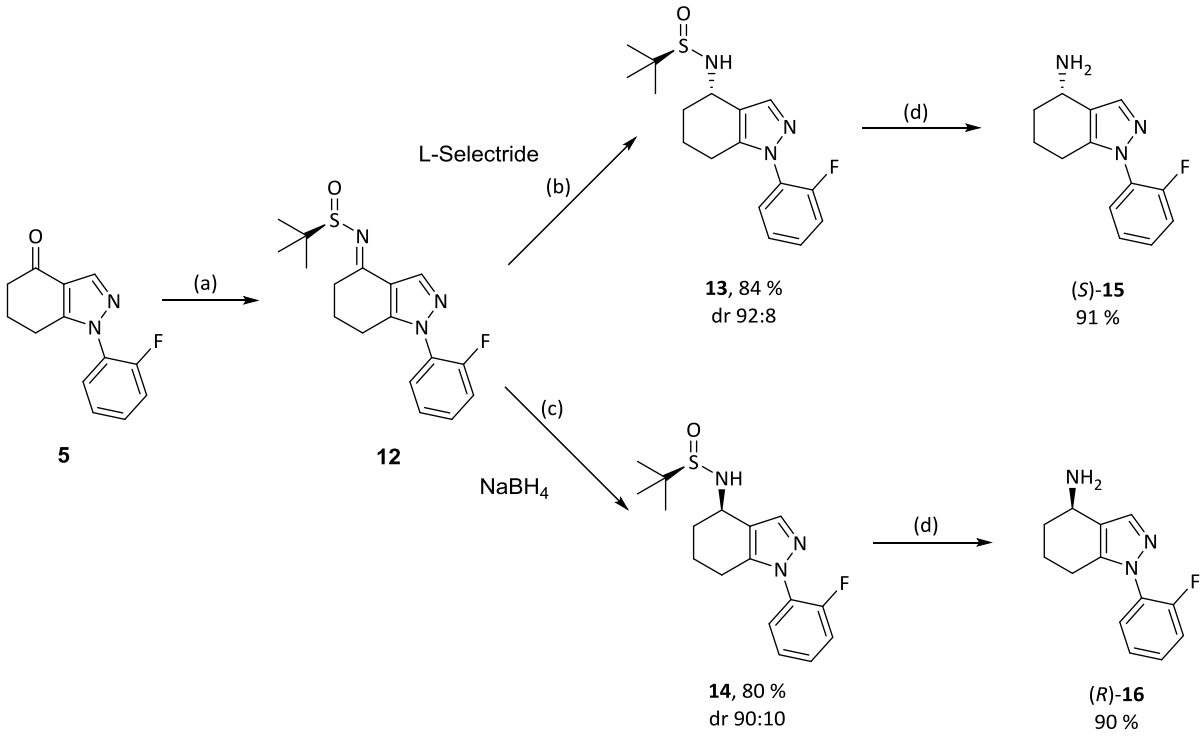

Scheme 5.4. Diastereoselective reductive amination. *Reagents & conditions*: (**a**) (R_S)-**7**, $Ti(OEt)_4$, THF, 75 °C. (**b**) L-Selectride, THF, -48 °C, 2 h (**c**) $NaBH_4$, THF, -48 °C → 0 °C, 16 h. (**d**) HCl, MeOH, r.t.

Purification by flash chromatography resulted in both diastereomers (**13** and **14**) being isolated in high yield and purity.

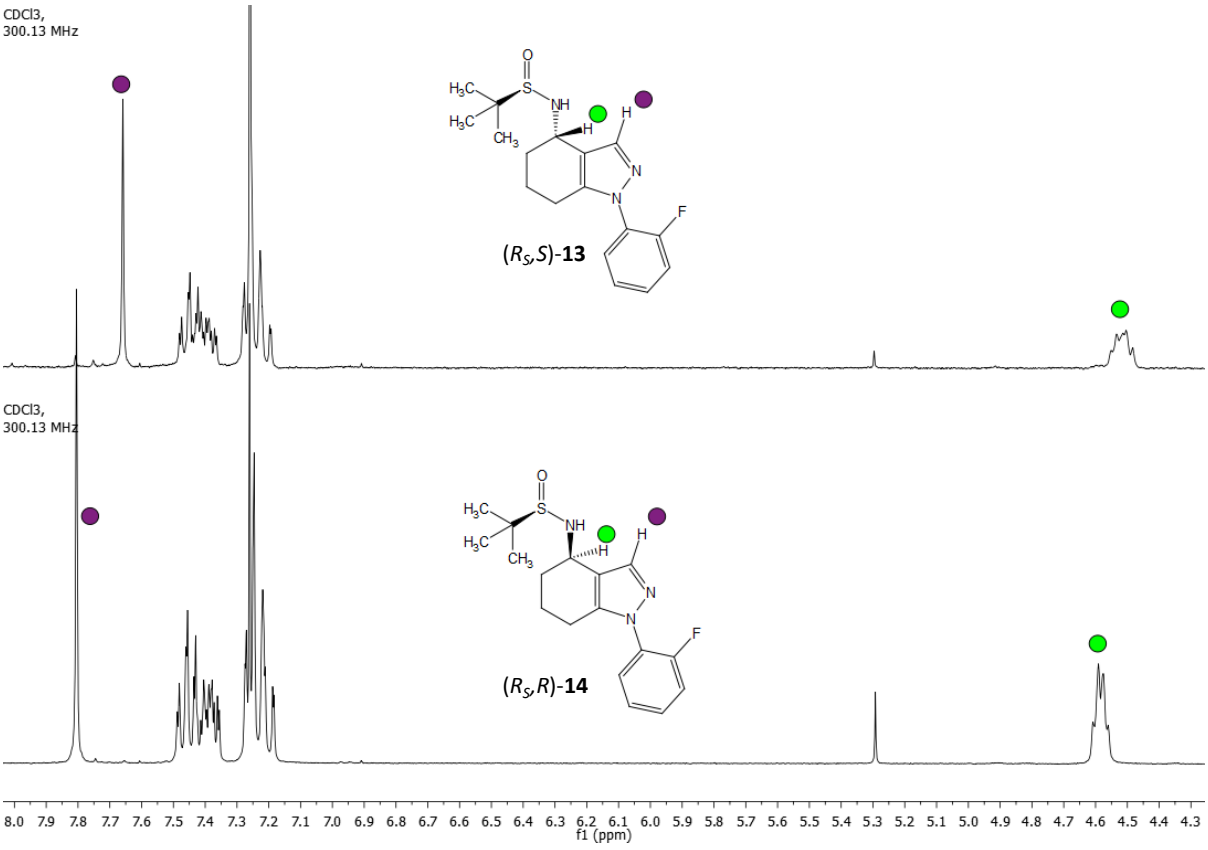

Figure 5.5. ^{1}H NMR analysis of the diastereomers (R_S,*S*)-13 and (R_S,*R*)-14.

The ^{1}H NMR spectra of **13** and **14** showed two diagnostic peaks that were used to distinguish between the two diastereomers (Figure 5.5). The proton at the stereogenic centre has a small chemical shift and splitting pattern difference between the two diastereomers, and the pyrazole protons are also distinguishable by a significant change in chemical shift (from 7.65 ppm in **13** to 7.80 ppm in **14**).

The *tert*-butanesulfinyl group of **13** and **14** was cleaved under acidic conditions to obtain both the *S*-(**15**) and *R*-(**16**) amine stereoisomers respectively (Scheme 5.4). **15** and **16** were subsequently subjected to the previously described *N*-acylation step with 2-picolinic acid to provide enantiomerically pure (-)-MJ05 (**1**) and (+)-MJ05 (**1**) (Scheme 5.5). Based on the predicted diastereofacial control in the reduction, these enantiomers were assigned as the (*S*)-**1** and (*R*)-**1** enantiomers of MJ05.

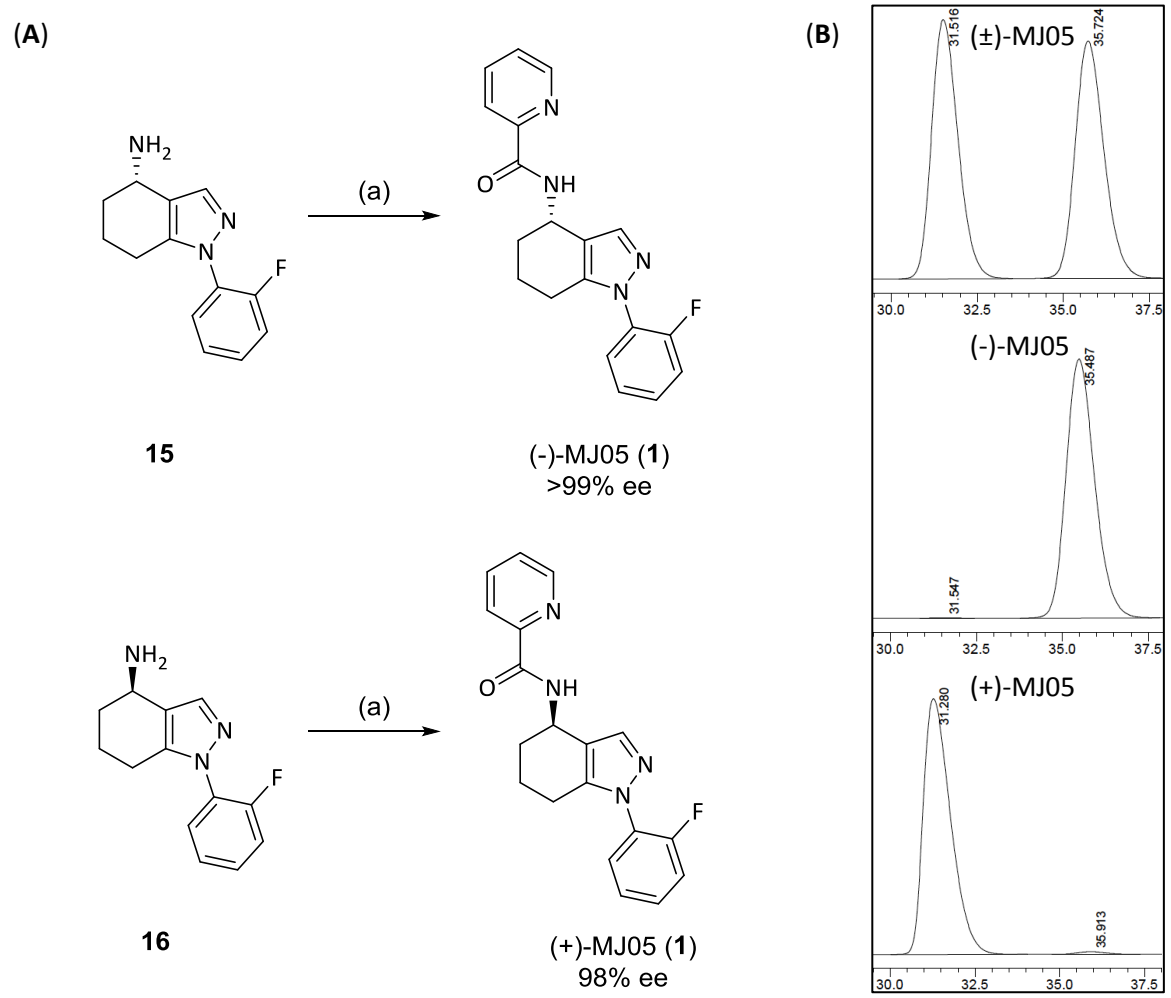

Scheme 5.5. (A) *N*-acylation of amines 15 and 16 with 2-picolinic acid to form (-)-MJ05 (1) and (+)-MJ05 (1). *Reagents &* conditions: (**a**) 2-Picolinic acid, EDC.HCl, Et_3N, HOBt, DMAP, DCM, r.t., overnight; (-)-MJ05 (**1**) – 88%, >99% ee, $[\alpha]_D^{20}$= -71.8° (*c* 0.1, $CHCl_3$); (+)-MJ05 (**1**) – 93%, 98% ee, $[\alpha]_D^{20}$= +72.4° (*c* 0.1, $CHCl_3$). **(B) Chiral HPLC analysis of (±)-MJ05, (-)-MJ05 and (+)-MJ05.** Chiralpak AD-H (5% IPA/hexanes, 1 mL min^{-1}, 254 nm, 30 °C).

The two enantiomers were isolated in high enantiomeric purity which was determined by chiral HPLC analysis using a Chiralpack AD-H column (Scheme 5.5B) and shown to induce an approximately equal and opposite optical rotation. The two enantiomers were subsequently tested by the Lain group for their effect on p53 activation and cell viability to determine if they were modulating a biological target capable of discriminating between the two enantiomers.

5.4.2 Biological analysis of the MJ05 enantiomers

Interestingly, the biological assessment of (-)-MJ05 (**1**) revealed that it does not activate p53 transcription and similarly had no effect on the viability of the ARN8 cancer cell line at concentrations up to 10 µM (Figure 5.6). In contrast, (+)-MJ05 (**1**) was shown to activate p53 transcription to a greater extent than (±) MJ05 (**1**) and also appeared to be nearly twice as potent (IC_{50} value of ~2.2 µM) as (±)-MJ05 (**1**) at killing the ARN8 cells (IC_{50} value of ~4.0 µM)(Figure 5.6). This promising result identified (-)-MJ05 (**1**) as a highly valuable control compound for further biological assays, and suggested that (+)-MJ05 (**1**) was targeting an enzyme or protein that is capable of discriminating between the two enantiomers. Most importantly these results identified (+)-MJ05 (**1**) as a more potent and promising lead for future biological testing and chemical development.

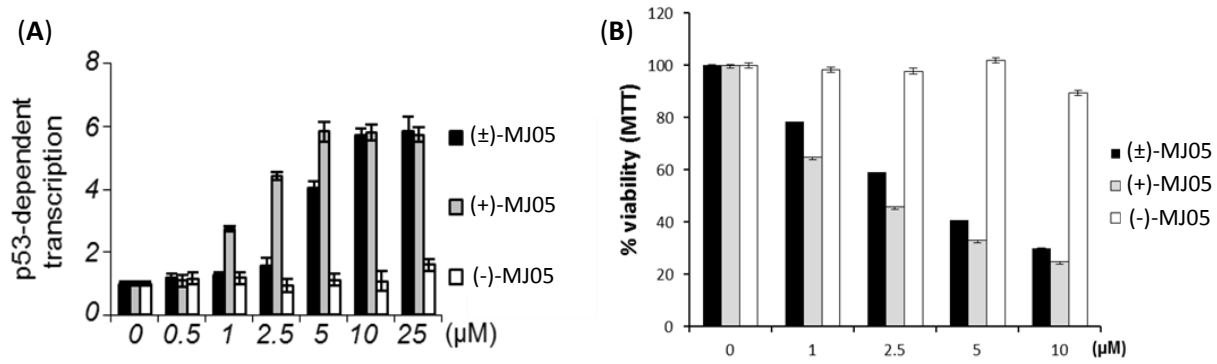

Figure 5.6. Effect of (+)- and (-)-MJ05 (1) on (A) p53 transcriptional activation and (B) cell viability (ARN8 cells). Data provided by the Lain group.

5.4.3 Large scale synthesis of (+)-MJ05 (1)

As a result of the very promising biological data collected for (+)-MJ05 (**1**), it was necessary to carry out a larger scale synthesis of (+)-**1** to enable further biological investigation and also verify if (+)-MJ05 (**1**) was the predicted (*R*)-enantiomer. To achieve this goal it was decided to use the opposite enantiomer of the chiral auxiliary **7**, (S_S)-*tert*-butanesulfinamide, as this would facilitate the use of L-Selectride as the reducing agent to furnish the desired (S_S,*R*)-sulfinamide product. The use of L-Selectride rather than $NaBH_4$ simplifies the reaction procedure, as it is added drop-wise directly to the sulfinyl-imine solution without the need to cannula the sulfinyl-imine solution onto a pre-formed

suspension of the reducing agent, as is the case with $NaBH_4$. Furthermore, in the original synthesis of (+)- and (-)-MJ05 (**1**) (Scheme 5.4), the L-Selectride reduction resulted in a small increase in diastereoselectivity and yield when compared to the $NaBH_4$ reduction, possible due to the slow addition of the reducing agent and the removal of the imine transfer step in addition to any inherent increase in selectivity associated with the change in transition state (Scheme 5.4). This increase in yield and selectivity would have a more significant impact on the large scale synthesis of (+)-MJ05 (**1**).

The synthesis was carried out from ketone **5** using the previously described procedures (Scheme 5.6). The ^{1}H NMR spectrum of the isolated (S_S,*R*)-sulfinamide diastereomer **17** was identical to that of the previously isolated (R_S,*S*)-sulfinamide diastereomer **13** as would be expected. Subsequent cleavage of the sulfinamide **17** yielded the 4-aminotetrahydroindazole **16**, which on coupling with 2-picolinic acid provided (+)-MJ05 (**1**). This was shown to have an equivalent positive optical rotation and chiral HPLC trace to that obtained for the previously synthesised sample of (+)-MJ05 (**1**).

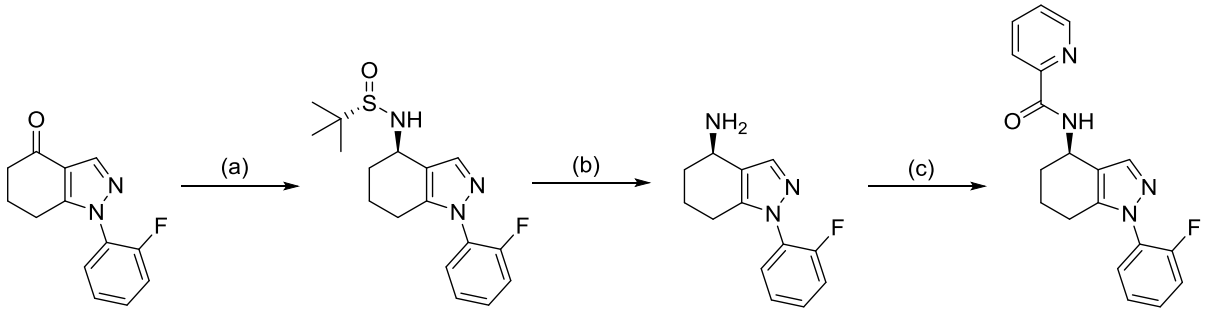

Scheme 5.6. Diastereoselective reductive amination. *Reagents & conditions*: (**a**) (i) (S_S)-**7**, $Ti(OEt)_4$, THF, 75 °C. (ii) L-Selectride, THF, -48 °C, 73%, dr 94:6 (**b**) HCl, MeOH, r.t., 90% (**c**) 2-picolinic acid, EDC.HCl, Et_3N, HOBt, DMAP, DCM, r.t., overnight, 91%, >98% ee, $[\alpha]_D^{20}$ = +72.1° (*c* 0.1, $CHCl_3$).

The diastereofacial control observed by Ellman *et al*. was confirmed for our substrate by X-ray crystallographic analysis of the isolated sulfinamide diastereomer **17** obtained by L-Selectride reduction of the (S_S)-*tert*-butanesulfinyl imine **7**. The X-ray structure of **17** confirmed the formation of the expected (S_S,*R*) diastereomer (Figure 5.7). This result confirms that (+)-MJ05 (**1**) was the predicted (*R*)-enantiomer.

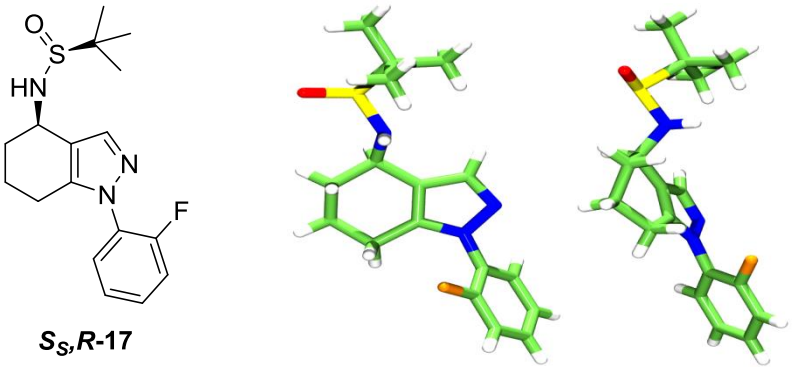

Figure 5.7. Two different views of the X-ray crystal structure of (S_S,*R*)-sulfinamide diastereomer 17. Hydrogens added after refinement for clarity. X-ray crystallographic data provided by Prof. Alexandra Slawin.

The large scale sample of (*R*)-(+)-MJ05 (**1**) was shown to have identical biological activity to the original (*R*)-(+)-MJ05 (**1**) sample and provided sufficient material (~5 g) for further comprehensive biological assessment and target identification.

5.4.4 (*R*)-MJ05 mediated induction of pro-apoptotic activity

The potential of (*R*)-MJ05 (**1**) as a novel selective anticancer agent is currently being extensively explored by a collaborative team involving the Lain group (Karolinska Institutet , Sweden), Bathia group (City of Hope National Medical Center, USA) and the McCormack group (Haukeland University Hospital, Norway). A summary of the main results to date are outlined below.

A greater than additive increase in toxicity was observed for (*R*)-MJ05 (**1**) in combination with p53-MDM2 inhibitor nutlin-3 (**2**) against the ARN8 melanoma cell line. This increase in cytotoxicity did not occur when (*R*)-MJ05 (**1**) was combined with other p53 activators such as tenovin-6 (**18**, Figure 5.8). Interestingly, (*R*)-MJ05 (**1**) did not have any effect on the viability of nutlin-3 (**2**) treated normal cells (HNDFs), highlighting this as a potential adjuvant therapy with reduced cytotoxicity against normal cells. It was observed that (*R*)-MJ05 (**1**) elicited physiological responses which are similar to those attributed to p14ARF, a tumour suppressor with both p53 dependent and independent effects.[360] The ability of (*R*)-MJ05 (**1**) to mimic p14ARF function is an interesting feature of this molecule, as it has been observed that p14ARF gene expression is inactivated in a high proportion of tumours that retain wild type p53, including chronic myelogenous leukaemia (CML).[361,362]

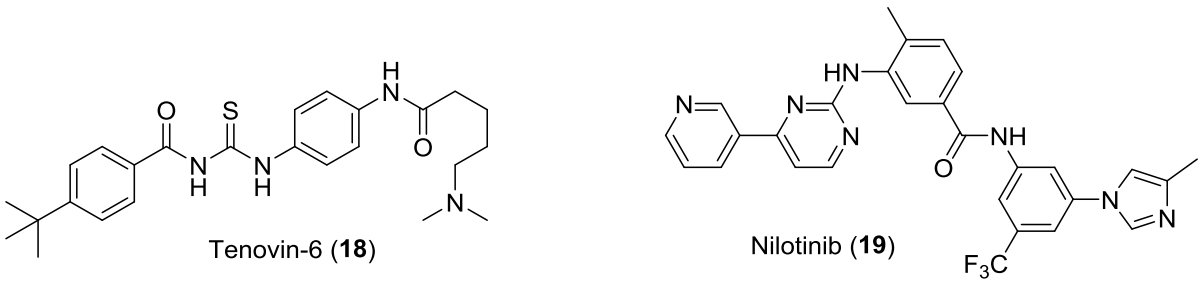

Figure 5.8. The chemical structures of Tenovin-6 (18) and Nilotinib (19).

Tyrosine kinase inhibitors (TKI) are the mainstay of CML treatment, but fail to eliminate leukaemia stem cells (LSC), leading to high risk of disease recurrence when treatment is stopped. There is considerable interest in the development of new strategies to target CML LSC. (*R*)-MJ05 (**1**)'s effect on primary normal cord blood (CB) or CML cells by itself, and in combination with TKI inhibitor Nilotinib (**19**, Figure 5.8) was assessed. Treatment with (*R*)-MJ05 (**1**) (5 and 10 μM) selectively induced expression of p53 target genes in CML but not normal CB cells as a single agent, or when combined with Nilotinib (**19**). (*R*)-MJ05 (**1**) (5 and 10μM) increased apoptosis and inhibited proliferation of CML cells without affecting normal CB cells. Combination of (*R*)-MJ05 (**1**) with Nilotinib (**19**) (1μM) resulted in a significant selective increase in apoptosis of CML cells.

In summary, (*R*)-MJ05 (**1**) shares the therapeutically relevant effects of p53 and p14ARF tumour suppressors. Treatment of (*R*)-MJ05 (**1**) in combination with nutlin-3 (**2**) resulted in a selective and significant increase in cytotoxicity against an ARN8 cancer cell line. In addition, studies indicate that (*R*)-MJ05 (**1**) is effective in selectively inducing apoptosis and inhibiting growth of primitive CML stem cells by itself and to an even greater extent in combination with Nilotinib (**19**), with significantly reduced effects on normal stem cells. Although the majority of (*R*)-MJ05 (**1**)'s physiological effects have been elucidated, its principal biological target has not yet been identified.

5.5 Conclusions and Future Work

(±)-MJ05 (**1**) was identified from a phenotypic screen of 20,000 drug-like molecules as a selective p53 activator with potent cytotoxic activity against an ARN8 cancer cell line. Further analysis showed that its cytotoxicity was highly selective for the cancer cell line over a human normal dermal fibroblast (HNDF) cell line. The promising therapeutic window obtained for **1** is a highly desirable property for new cancer chemotherapeutics. (±)-MJ05 (**1**) had also been previously identified as an inhibitor of the MDM2/MDM4 protein-protein interaction, which is central to cellular degradation of p53.

A versatile and high-yielding 4-step synthesis was developed to (±)-MJ05 (**1**), which facilitated the large-scale synthesis of **1** for biological assessment. Testing of (±)-MJ05 (**1**) in a mouse xenograft model showed that it significantly impaired tumour growth over a 15 day period. Based on this *in vivo* activity, a *tert*-butanesulfinamide diastereoselective reductive amination was utilised to access both enantiomers of (±)-MJ05 (**1**). The (+)-MJ05 (**1**) enantiomer proved to be more active than the original racemic (±)-MJ05 towards p53 transcriptional activation and had increased cytotoxicity, whilst (-)-MJ05 was inactive under the same conditions. This also identified (-)-MJ05 as a valuable control molecule, and revealed that (+)-MJ05's activity is likely as a result of modulation of a chirally discriminating biological target.

A large scale synthesis of (+)-MJ05 was then undertaken to provide material for further biological assessment. X-ray crystal structure analysis of the isolated diastereomer **17** revealed that it was the predicted (S_S,*R*) sulfinamide diastereomer, thus confirming that (+)-MJ05 was in fact (*R*)-(+)-MJ05.

Comprehensive biological assessment of (*R*)-MJ05 has revealed that it is a promising candidate for use in adjuvant therapy in the treatment of cancer. (*R*)-MJ05 resulted in a greater than additive cytotoxic effect against ARN8 cells in combination with nutlin-3 (**2**), with no concomitant increase in cytotoxicity against normal (HNDF) cells. Furthermore, an *ex-vivo* xenograft study using CML cells revealed that (*R*)-MJ05 selectively induced p53 target genes, increased apoptosis and inhibited proliferation of CML cells without affecting normal (CB) cells.

Current research is focused on the development of (R)-MJ05 as a preclinical drug lead. Assessment of (*R*)-MJ05's off-target effects revealed that it is highly selective, showing no activity against a panel of 146 purified kinases, 16 lipid kinases as well as 16 cyclin-dependent kinases. Preliminary *in vitro* pharmokinetic studies revealed that (*R*)-MJ05 has adequate chemical and metabolic stability. Future

synthetic optimisation of (*R*)-MJ05 will focus on improving its *in vitro* and *in vivo* pharmokinetic and pharmodynamic properties. Although, much of (*R*)-MJ05's physiological effects have been identified, its primary biological target has not been elucidated. The attachment of a photoaffinity tag containing a radioactive, fluorescent, or immunoreactive constituent or a biotin-linker to (*R*)-MJ05 (**1**) could provide a powerful chemical tool for target identification studies.

5.6 Experimental

5.6.1 General considerations

See Section 2.8.1 for general considerations.

HPLC analyses were obtained on a Gilson HPLC consisting of a Gilson 305 pump, Gilson 306 pump, Gilson 811C dynamic mixer, Gilson 805 manometric module, Gilson 401C dilutor, Gilson 213XL sample injector and sample detection was performed with a Gilson 118 UV/vis detector. Separation was achieved using a Chiralpak AD-H column.

5.6.2 General Methods

General Method A: *N*-acylation

To a solution of 2–picolinic acid (2 eq.), HOBt (1.5 eq.), EDC.HCl (1.5 eq.) and Et_3N (1.5 eq.) in DCM (20 mL/mmol) were added the appropriate 4-aminotetrahydroindazole (1 eq.) and DMAP (0.1 eq.). The resulting solution was stirred at room temperature for 16 hours. The solution was concentrated *in vacuo*; the residue was diluted with EtOAc and with a saturated aqueous solution of $NaHCO_3$ ($\times$3), brine, dried over $MgSO_4$, filtered and concentrated *in vacuo*. The crude product was purified *via* the Biotage SP4 (silica-packed SNAP; EtOAc/hexanes).

General Method B: *tert*-Butanesulfinyl cleavage

To a solution of the appropriate sulfinamide (1 eq.) in anhydrous methanol (10 mL/mmol) was added concentrated HCl (1 mL/mmol) dropwise. The solution was then stirred at room temperature for 4 hours. The reaction was quenched by addition of a saturated aqueous solution of $NaHCO_3$, and diluted with DCM and water. The organic layer was separated, washed with a saturated aqueous solution of $NaHCO_3$, brine, dried with $MgSO_4$, filtered and concentrated *in vacuo*. The obtained product did not require further purification.

5.6.3 Experimental Procedures

2-((Dimethylamino)methylene)cyclohexane-1,3-dione (4)[356]

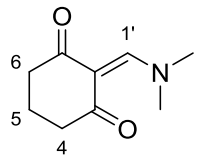

A solution of 1,3-cyclohexanedione **3** (5.0 g, 44.6 mmol, 1.0 eq.) in *N*,*N*-dimethylformamide dimethyl acetal (8.9 mL, 66.9 mmol, 1.5 eq.) was heated at reflux for 2 hours. Upon cooling, an orange solid precipitated, which was stirred in Et_2O (40 mL) and collected by filtration to give the title product **4** as an orange powder (5.3 g, 71%), which did not require further purification. **mp** 101-103 °C (lit. 117-119 °C);[356] **^{1}H NMR** (300 MHz, Chloroform-*d*) δ 8.04 (s, 1H, C1'-H), 3.38 (s, 3H, CH_3), 3.16 (s, 3H, CH_3), 2.46 (dd, *J* = 8.6, 4.3 Hz, 4H, C4-H_2, C6-H_2), 2.00 – 1.87 (m, 2H, C5-H_2); **^{13}C NMR** (75 MHz, Chloroform-*d*) δ 195.2 (C1, C3), 161.2 (C1'), 108.4 (C2), 47.5 (CH_3), 43.7 (CH_3), 37.2 (C4, C6), 18.6 (C5); ***m/z*** (ES^+) 168.04 ($[M+H]^+$, 100 %); Spectroscopic data are in agreement with the literature.[356]

1-(2-Fluorophenyl)-6,7-dihydro-1*H*-indazol-4(5*H*)-one (5)[357]

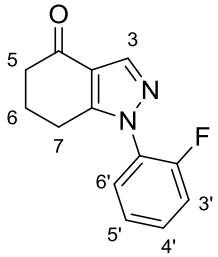

To a solution of 2-((dimethylamino)methylene)cyclohexane-1,3-dione **4** (1.67 g, 10.0 mmol, 1.0 eq.) in methanol (60 mL) and water (10 mL) were added 4-fluorophenylhydrazine hydrochloride (1.63 g, 10.0 mmol, 1.0 eq.) and sodium hydroxide (0.40 g, 10.0 mmol, 1.0 eq.). The resulting mixture was heated at reflux for 2 hours and concentrated *in vacuo*. To the residue were added AcOH (60 mL) and water (30 mL) and the corresponding mixture was heated at 110 °C for 2 hours. On completion of the reaction, the solution was concentrated *in vacuo*. The residue was diluted with EtOAc (100 mL) and washed with a saturated aqueous solution of $NaHCO_3$ (3 × 50 mL), brine (50 mL), dried over $MgSO_4$, filtered and concentrated *in vacuo*. The crude product was purified *via* the Biotage SP4 (silica-packed SNAP 50 g; 25-50% EtOAc/hexanes) to provide the title product **5** as a yellow solid (1.77 g, 77%). **mp** 104-106 °C (lit. 100-103 °C);[357] **IR** (KBr) ν_{max}: 2957, 1663 (C=O), 1508, 1408, 1226; **^{1}H NMR** (400 MHz, Chloroform-*d*) δ 8.10 (s, 1H, C3-H), 7.54 (td, *J* = 7.6, 1.7 Hz, 1H, C5'-H), 7.47 (dddd, *J* = 8.3, 7.6, 4.9, 1.8 Hz, 1H, C4'-H), 7.34 – 7.29 (m, 1H, C6'-H), 7.29 – 7.24 (m, 1H, C3'-H), 2.80 (td, *J* = 6.2, 1.5 Hz, 2H, C7-H_2), 2.57 – 2.53 (m, 2H, C5-H_2), 2.20 – 2.10 (m, 2H, C6-H_2); **^{13}C NMR** (101

MHz, Chloroform-*d*) δ 193.3 (C4), 156.1 (d, *J* = 252.0 Hz, C2'), 151.7 (C7a), 139.2 (C3), 131.0 (d, *J* = 7.7 Hz, C4'), 128.5 (C5'), 126.6 (br, C7'), 125.2 (d, *J* = 3.9 Hz, C6'), 120.3 (C3a), 116.9 (d, *J* = 19.7 Hz, C3'), 38.1 (C5), 23.5 (C6), 22.1 (d, *J* = 5.0 Hz, C7); ***m/z*** (ES^+) 252.89 ($[M+Na]^+$, 100 %); **HRMS** (ES^+) Calcd for $C_{13}H_{11}N_2OFNa$ $[M+Na]^+$: 253.0753, found 253.0757.

1-(2-Fluorophenyl)-4,5,6,7-tetrahydro-1*H*-indazol-4-amine (6)

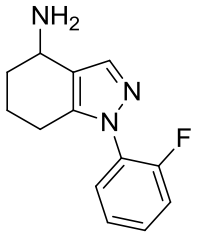

A solution of 1-(2-fluorophenyl)-6,7-dihydro-1*H*-indazol-4(5*H*)-one **5** (1.0 g, 4.3 mmol, 1.0 eq.) in 2-propanol (80 mL) was treated, under vigorous stirring, with ammonium acetate (3.3 g, 43.4 mmol, 10.0 eq.). After complete dissolution, molecular sieves (4 Å, 1.5 g) and $NaBH_3CN$ (1.3 g, 21.7 mmol, 5.0 eq.) were added and the reaction mixture was stirred for 12 hours at 70 °C. The solution was concentrated *in vacuo*. The residue was diluted with EtOAc (200 mL) and washed thoroughly with a 2 M aqueous solution of NaOH (20 mL) and brine (20 mL), dried over $MgSO_4$, filtered and concentrated *in vacuo*. Without further purification, the crude compound **6** was directly used in the next step. See **15** and **16** for the spectroscopic data for each enantiomer.

***N*-(1-(2-Fluorophenyl)-4,5,6,7-tetrahydro-1*H*-indazol-4-yl)picolinamide; (±)-MJ05 (1)**

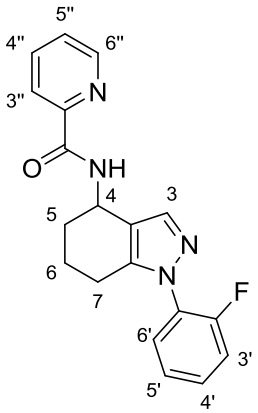

Prepared from 1-(2-fluorophenyl)-4,5,6,7-tetrahydro-1*H*-indazol-4-amine **6** (0.90 g, 3.9 mmol, 1.0 eq.) and 2–picolinic acid (0.48 g, 3.9 mmol, 1.0 eq.) using general method A. Purified *via* the Biotage SP4 (silica-packed SNAP column 10 g; 20-50% EtOAc/hexanes) to give the title product (±)-**1** as a white solid (0.92 g, 65% over 2 steps). **mp** 96-98 °C; **IR** (KBr) ν_{max}: 3288 (NH), 2945, 1661 (C=O), 1516; **^{1}H NMR** (500 MHz, Chloroform-*d*) δ 8.47 (dd, *J* = 4.7, 0.6 Hz, 1H, C6''-H), 8.19 (m, 2H, NH, C3''-H), 7.82 (td, *J* = 7.7, 1.6 Hz, 1H, C4''-H), 7.62 (s, 1H, C3-H), 7.45 – 7.27 (m, 3H, C5'-H, C4'-H, C5''-H),

7.29 – 7.16 (m, 2H, C6'-H, C3'-H), 5.37 – 5.25 (m, 1H, C4-H), 2.63 – 2.45 (m, 2H, C7-H_2), 2.18 – 2.03 (m, 1H, C5-H), 1.97 – 1.71 (m, 3H, C5-H, C6-H_2); **^{13}C NMR** (126 MHz, Chloroform-*d*) δ 163.7 (CO), 156.3 (d, *J* = 251.5 Hz, C2'), 149.9 (C2''), 148.1 (C6''), 141.8 (C7a), 139.4 (C3), 137.4 (C4''), 130.0 (d, *J* = 7.7 Hz, C4'), 128.6 (C5'), 127.4 (d, *J* = 11.8 Hz, C1'), 126.2 (C5''), 124.8 (d, *J* = 3.9 Hz, C6'), 122.3 (C3''), 118.0 (C3a), 116.7 (d, *J* = 20.1 Hz, C3'), 42.4 (C4), 30.1 (C5), 21.6 (C7), 20.1 (C6); ***m/z*** (ES^+) 358.86 ($[M+Na]^+$, 100 %); **HRMS** (ES^+) Calcd for $C_{19}H_{17}N_4OFNa$ $[M+Na]^+$: 359.1284, found 359.1283.

(*R*)-*N*-((*S*)-1-(2-Fluorophenyl)-4,5,6,7-tetrahydro-1*H*-indazol-4-yl)-2-methylpropane-2-sulfinamide (13)

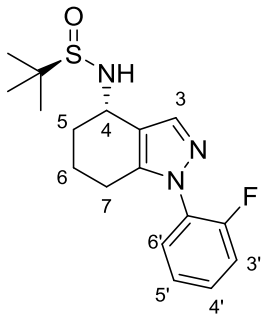

1-(2-Fluorophenyl)-6,7-dihydro-1*H*-indazol-4(5*H*)-one **5** (0.30 g, 1.30 mmol, 1.0 eq.) was added to a solution of (R_S)-2-methyl-2-propanesulfinamide **7** (189 mg, 1.56 mmol, 1.20 eq.) and $Ti(OEt)_4$ (0.55 mL, 2.6 mmol, 2.0 eq.) in THF (2.5 mL) at room temperature. The mixture was heated at 75 °C for 12 hours. The mixture was cooled to -48 °C and L-Selectride (3.9 mL, 1 M in THF, 3 eq.) was added dropwise. After 2 hours, the reaction was warmed to 0 °C and MeOH was added dropwise until gas evolution was no longer observed. The crude reaction mixture was poured into an equal volume of brine while being vigorously stirred. The resulting suspension was filtered through a plug of Celite, and the filter cake was washed with EtOAc. The filtrate was washed with brine (20 mL), and the brine layer was extracted with EtOAc (3 × 10 mL). The combined organic extracts were dried over $MgSO_4$, filtered, concentrated *in vacuo* and purified *via* the Biotage SP4 (silica-packed SNAP column 10 g; 20-70% EtOAc/hexanes) to give the title product **13** as a white solid (366 mg, 84%). **$[\alpha]_D^{20}$**= -30.0° (*c* 0.1, $CHCl_3$); **mp** 94-96 °C; **IR** (KBr) ν_{max}: 3418 (NH), 3220, 2921, 1667, 1460, 1194; **^{1}H NMR** (500 MHz, Chloroform-*d*) δ 7.65 (s, 1H, C3-H), 7.48 – 7.42 (m, 1H, C5'-H), 7.41 – 7.36 (m, 1H, C4'-H), 7.27 – 7.22 (m, 1H, C6'-H), 7.24 – 7.18 (m, 1H, C3'-H), 4.53 – 4.50 (m, 1H, C4-H), 3.37 (d, *J* = 9.4 Hz, 1H, NH), 2.59 – 2.44 (m, 1H, C7-H_2), 2.32 – 2.23 (m, 1H, C5-H_2), 2.00 – 1.91 (m, 1H, C6-H_2), 1.89 – 1.78 (m, 2H, C5-H_2, C6-H_2), 1.27 (s, 9H, (CH_3)$_3$); **^{13}C NMR** (101 MHz, Chloroform-*d*) δ 156.4 (d, *J* = 251.5 Hz, C2'), 141.5 (C7a), 139.4 (C3), 130.1 (d, *J* = 7.8 Hz, C4'), 128.7 (C5'), 127.4 (d, *J* = 11.7 Hz, C1'), 124.9 (d, *J* = 4.0 Hz, C6'), 119.2 (C3a), 116.8 (d, *J* = 19.9 Hz, C3'), 56.3 (C(CH_3)$_3$)), 50.8 (C4), 33.3

(C5), 22.9 (($\underline{C}H_3)_3$), 21.6 (d, *J* = 4.5 Hz, C7), 20.3 (C6); ***m/z*** (ES^+) 358.04 ($[M+Na]^+$, 100 %); **HRMS** (ES^+) Calcd for $C_{17}H_{22}N_3OSFNa$ $[M+Na]^+$: 358.1365, found 358.1367.

(*R*)-*N*-((*R*)-1-(2-Fluorophenyl)-4,5,6,7-tetrahydro-1*H*-indazol-4-yl)-2-methylpropane-2-sulfinamide (14)

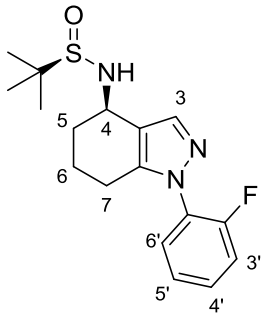

1-(2-Fluorophenyl)-6,7-dihydro-1*H*-indazol-4(5*H*)-one **5** (0.60 g, 2.60 mmol, 1.0 eq.) was added to a solution of (R_S)-2-methyl-2-propanesulfinamide **7** (0.38 g, 3.12, 1.2 eq.) and $Ti(OEt)_4$ (1.1 mL, 5.2 mmol, 2.0 eq.) in THF (5 mL) at room temperature. The mixture was heated at 75 °C for 12 hours. The mixture was cooled to -48 °C and then added dropwise *via* cannula to a -48 °C suspension of $NaBH_4$ (0.39 g, 10.4 mmol, 4.0 eq.) in a minimum amount of THF. The reaction mixture was warmed to 0 °C and stirred for 16 hours before the dropwise addition of MeOH until gas evolution was no longer observed. The crude reaction mixture was poured into an equal volume of brine while being rapidly stirred. The resulting suspension was filtered through a plug of Celite, and the filter cake was washed with EtOAc. The filtrate was washed with brine (20 mL), and the brine layer was extracted with EtOAc (3 × 10 mL). The combined organic extracts were dried over $MgSO_4$, filtered, concentrated *in vacuo* and purified *via* the Biotage SP4 (silica-packed SNAP column 10 g; 20-70% EtOAc/hexanes) to give the title product **14** as a white solid (0.7 g, 80%). $\mathbf{[\alpha]_D^{20}}$= +0.50° (*c* 0.42, $CHCl_3$); **mp** 106-108 °C; **IR** (KBr) ν_{max}: 3433 (NH), 3205, 2954, 1514, 1041; **^{1}H NMR** (300 MHz, Chloroform-*d*) δ 7.80 (s, 1H, C3-$\underline{H}$), 7.46 (td, *J* = 7.9, 1.8 Hz, 1H, C5'-$\underline{H}$), 7.43 – 7.35 (m, 1H, C4'-$\underline{H}$), 7.28 – 7.24 (m, 1H, C6'-$\underline{H}$), 7.24 – 7.18 (m, 1H, C3'-$\underline{H}$), 4.58 (dd, *J* = 9.6, 4.9 Hz, 1H, C4-$\underline{H}$), 3.32 (d, *J* = 4.9 Hz, 1H, N$\underline{H}$), 2.66 – 2.39 (m, 2H, C7-$\underline{H}_2$), 2.04 – 1.73 (m, 4H, C5-$\underline{H}_2$, C6-$\underline{H}_2$), 1.24 (s, 9H, ($C\underline{H}_3)_3$); **^{13}C NMR** (75 MHz, Chloroform-*d*) δ 156.7 (d, *J* = 251.5 Hz, C2'), 142.1 (C7a), 140.1 (C3), 130.4 (d, *J* = 7.8 Hz, C4'), 129.0 (C5'), 127.5 (br, C1'), 125.2 (d, *J* = 3.9 Hz, C6'), 119.2 (C3a), 117.0 (d, *J* = 20.1 Hz, C3'), 56.0 ($\underline{C}(CH_3)_3$)), 48.6 (C4), 31.8 (C5), 23.1 (($CH_3)_3$), 21.9 (d, *J* = 4.7 Hz, C7), 19.7 (C6); ***m/z*** (ES^+) 357.90 ($[M+Na]^+$, 100 %); **HRMS** (ES^+) Calcd for $C_{17}H_{22}N_3OSFNa$ $[M+Na]^+$: 358.1365, found 358.1358.

(*S*)-1-(2-Fluorophenyl)-4,5,6,7-tetrahydro-1*H*-indazol-4-amine (15)

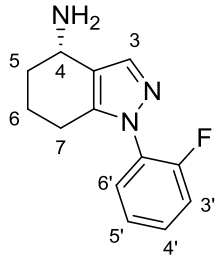

Prepared from (*R*)-*N*-((*S*)-1-(2-fluorophenyl)-4,5,6,7-tetrahydro-1*H*-indazol-4-yl)-2-methylpropane-2-sulfinamide **13** (1.06 g, 3.16 mmol, 1.0 eq.) using general method B. The title product **15** was obtained as a pale yellow oil (0.66 g, 91%), which did not require further purification. **^{1}H NMR** (400 MHz, Chloroform-*d*) δ 7.72 (s, 1H, C3-H), 7.45 (td, *J* = 7.6, 1.7 Hz, 1H, C5'-H), 7.42 – 7.34 (m, 1H, C4'-H), 7.27 – 7.18 (m, 2H, C6'-H, C3'-H), 4.09 – 4.02 (m, 1H, C4-H), 2.61 – 2.42 (m, 2H, C7-H$_2$), 2.12 – 1.99 (m, 1H, C5-H$_2$), 2.03 – 1.90 (m, 1H, C6-H$_2$), 1.81 – 1.68 (m, 1H, C6-H$_2$), 1.61 – 1.47 (m, 1H, C5-H$_2$); **^{13}C NMR** (101 MHz, Chloroform-*d*) δ 156.5 (d, *J* = 251.4 Hz, C1'), 140.8 (C7a), 139.0 (C3), 129.9 (d, *J* = 7.8 Hz, C4'), 128.8 (C5'), 127.7 (d, *J* = 11.6 Hz, C1'), 124.8 (d, *J* = 3.8 Hz, C6'), 121.7 (C3a), 116.7 (d, *J* = 20.1 Hz, C3'), 44.7 (C4), 34.2 (C5), 21.8 (d, *J* = 4.7 Hz, C7), 20.4 (C6); ***m/z*** (ES$^+$) 232.11 ([M+H]$^+$, 100 %).

(*R*)-1-(2-Fluorophenyl)-4,5,6,7-tetrahydro-1*H*-indazol-4-amine (16)

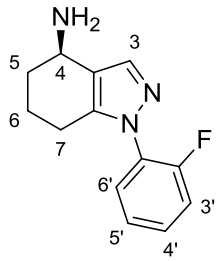

Prepared from (*R*)-*N*-((*R*)-1-(2-fluorophenyl)-4,5,6,7-tetrahydro-1*H*-indazol-4-yl)-2-methylpropane-2-sulfinamide **14** (1.4 g, 4.2 mmol, 1.0 eq.) using general method B. The title product **16** was obtained as a pale yellow oil (0.86 g, 90%), which did not require further purification. **^{1}H NMR** (500 MHz, Chloroform-*d*) δ 7.74 (s, 1H, C3-H), 7.51 – 7.41 (m, 1H, C5'-H), 7.42 – 7.34 (m, 1H, C4'-H), 7.25 – 7.18 (m, 2H, C6'-H, C3'-H), 4.12 – 4.03 (m, 1H, C4-H), 2.59 – 2.39 (m, 2H, C7-H$_2$), 2.10 – 2.02 (m, 1H, C5-H$_2$), 2.02 – 1.93 (m, 1H, C6-H$_2$), 1.82 – 1.69 (m, 1H, C6-H$_2$), 1.64 – 1.51 (m, 1H, C5-H$_2$); **^{13}C NMR** (101 MHz, Chloroform-*d*) δ 156.4 (d, *J* = 251.6 Hz, C1'), 140.9 (C7a), 139.0 (C3), 129.9 (d, *J* = 7.8 Hz, C4'), 128.7 (C5'), 127.7 (d, *J* = 11.6 Hz, C1'), 124.8 (d, *J* = 3.9 Hz, C6'), 121.7 (C3a), 116.7 (d, *J* = 20.0 Hz, C3'), 44.7 (C4), 33.9 (C5), 21.8 (d, *J* = 4.6 Hz, C7), 20.3 (C6); ***m/z*** (ES$^+$) 231.09 ([M+H]$^+$, 100 %).

(*S*)-*N*-(1-(2-Fluorophenyl)-4,5,6,7-tetrahydro-1*H*-indazol-4-yl)picolinamide; (-)-MJ05 (1)

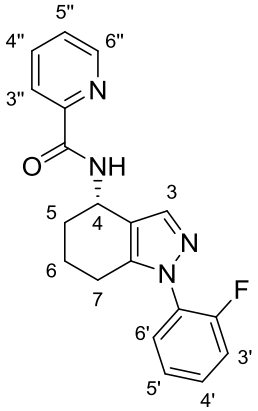

Prepared from (*S*)-1-(2-fluorophenyl)-4,5,6,7-tetrahydro-1*H*-indazol-4-amine **15** (0.66 g, 2.87 mmol, 1.0 eq.) and 2–picolinic acid (0.71 g, 5.74 mmol, 2.0 eq.) using general method A. Purified *via* the Biotage SP4 (silica-packed SNAP column 50 g; 20-50% EtOAc/hexanes) to give the title product (-)-MJ05 (**1**) as a white solid (0.84 g, 88%). **Chiral HPLC** analysis Chiralpak AD-H (5% IPA/hexane, 1 mL min^{-1}, 254 nm, 30 °C) t_R (major) 35.5, t_R (minor) 31.5, >99% ee; $[\alpha]_D^{20}$= -71.8° (*c* 0.1, $CHCl_3$); **mp** 116-118 °C; **IR** (KBr) ν $_{max}$: 3443 (NH), 3288, 2922, 1658 (C=O), 1530; **^{1}H NMR** (500 MHz, Chloroform-*d*) δ 8.47 (dd, *J* = 4.7, 0.6 Hz, 1H, C6''-H), 8.19 (m, 2H, NH, C3''-H), 7.81 (td, *J* = 7.7, 1.6 Hz, 1H, C4''-H), 7.62 (s, 1H, C3-H), 7.47 – 7.27 (m, 3H, C5'-H, C4'-H, C5''-H), 7.29 – 7.13 (m, 2H, C6'-H, C3'-H), 5.36 – 5.25 (m, 1H, C4-H), 2.63 – 2.42 (m, 2H, C7-H_2), 2.18 – 2.03 (m, 1H, C5-H_2), 1.97 – 1.73 (m, 3H, C5-H_2, C6-H_2); **^{13}C NMR** (126 MHz, Chloroform-*d*) δ 163.7 (CO), 156.3 (d, *J* = 251.5 Hz, C1'), 149.9 (C2''), 148.1 (C6''), 141.8 (C7a), 139.4 (C3), 137.4 (C4''), 130.0 (d, *J* = 7.7 Hz, C4'), 128.6 (C5'), 127.4 (d, *J* = 11.8 Hz, C1'), 126.2 (C5''), 124.8 (d, *J* = 3.9 Hz, C6'), 122.3 (C3''), 118.0 (C3a), 116.7 (d, *J* = 20.1 Hz, C3'), 42.4 (C4), 30.1 (C5), 21.6 (d, *J* = 4.7 Hz, C7), 20.1 (C6); ***m/z*** (ES^+) 358.89 ($[M+Na]^+$, 100 %); **HRMS** (ES^+) Calcd for $C_{19}H_{18}N_4ONa$ $[M+Na]^+$: 359.1284, found 359.1276.

(*R*)-*N*-(1-(2-Fluorophenyl)-4,5,6,7-tetrahydro-1*H*-indazol-4-yl)picolinamide; (+)-MJ05 (1)

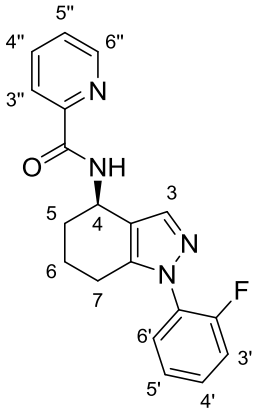

Prepared from (*R*)-1-(2-fluorophenyl)-4,5,6,7-tetrahydro-1*H*-indazol-4-amine **16** (0.86 g, 3.72 mmol, 1.0 eq.) and 2–picolinic acid (0.91 g, 7.44 mmol, 2.0 eq.) using general method A. Purified *via* the Biotage SP4 (silica-packed SNAP column 100 g; 20-50% EtOAc/hexanes) to give the title product (+)-MJ05 (**1**) as a white solid (1.16 g, 93%). **Chiral HPLC** analysis Chiralpak AD-H (5% IPA/hexane, 1 mL min^{-1}, 254 nm, 30 °C) t_R (minor) 35.9, t_R (major) 31.3, 98% ee; **$[\alpha]_D^{20}$**= +72.4° (*c* 0.1, $CHCl_3$); **mp** 117-119 °C; **IR** (KBr) ν $_{max}$: 3443 (NH), 3291, 2946, 1661 (C=O), 1530; **^{1}H NMR** (500 MHz, Chloroform-*d*) δ 8.47 (dd, *J* = 4.7, 0.6 Hz, 1H, C6''-H), 8.19 (m, 2H, NH, C3''-H), 7.81 (td, *J* = 7.7, 1.6 Hz, 1H, C4''-H), 7.62 (s, 1H, C3-H), 7.47 – 7.27 (m, 3H, C5'-H, C4'-H, C5''-H), 7.29 – 7.13 (m, 2H, C6'-H, C3'-H), 5.36 – 5.25 (m, 1H, C4-H), 2.63 – 2.42 (m, 2H, C7-H_2), 2.18 – 2.03 (m, 1H, C5-H), 1.97 – 1.73 (m, 3H, C5-H, C6-H_2); **^{13}C NMR** (126 MHz, Chloroform-*d*) δ 163.7 (CO), 156.3 (d, *J* = 251.5 Hz, C2'), 149.9 (C2''), 148.1 (C6''), 141.8 (C7a), 139.4 (C3), 137.4 (C4''), 130.0 (d, *J* = 7.7 Hz, C4'), 128.6 (C5'), 127.4 (d, *J* = 11.8 Hz, C1'), 126.2 (C5''), 124.8 (d, *J* = 3.9 Hz, C6'), 122.3 (C3''), 118.0 (C3a), 116.7 (d, *J* = 20.1 Hz, C3'), 42.4 (C4), 30.1 (C5), 21.6 (C7), 20.1 (C6); ***m/z*** (ES^+) 359.12 ($[M+Na]^+$, 100 %); **HRMS** (ES^+) Calcd for $C_{19}H_{18}N_4ONa$ $[M+Na]^+$: 359.1284, found 359.1281.

(*S*)-*N*-((*R*)-1-(2-Fluorophenyl)-4,5,6,7-tetrahydro-1*H*-indazol-4-yl)-2-methylpropane-2-sulfinamide (17)

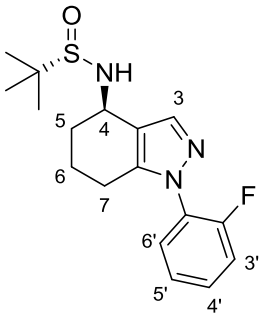

1-(2-Fluorophenyl)-6,7-dihydro-1*H*-indazol-4(5*H*)-one **5** (4.64 g, 20.1 mmol, 1.0 eq.) was added to a solution of (S_S)-2-methyl-2-propanesulfinamide **7** (2.44 g, 20.1 mmol, 1.0 eq.) and $Ti(OEt)_4$ (8.4 mL, 40.2 mmol, 2.0 eq.) in THF (40 mL) at room temperature. The mixture was heated at 75 °C for 12 hours. The mixture was cooled to -48 °C and L-Selectride (60.3 mL, 1 M in THF, 3.0 eq.) was added dropwise. After 2 hours, the reaction was warmed to 0 °C and MeOH was added dropwise until gas evolution was no longer observed. The crude reaction mixture was poured into an equal volume of brine while being vigorously stirred. The resulting suspension was filtered through a plug of Celite, and the filter cake was washed with EtOAc. The filtrate was washed with brine (30 mL), and the brine layer was extracted with EtOAc (3 × 20 mL). The combined organic extracts were dried over $MgSO_4$, filtered, concentrated *in vacuo* and purified *via* the Biotage SP4 (silica-packed SNAP column 180 g; 20-70% EtOAc/hexanes) to give the title product **17** as a white solid (4.89 g, 73%). **$[\alpha]_D^{20}$**=

+27.7° (*c* 0.35, $CHCl_3$); **mp** 112-114 °C; **IR** (KBr) ν $_{max}$: 3433 (NH), 3201, 2963, 1514, 1031; **^{1}H NMR** (500 MHz, Chloroform-*d*) δ 7.65 (s, 1H, C3-H), 7.47 – 7.42 (m, 1H, C5'-H), 7.42 – 7.36 (m, 1H, C4'-H), 7.27 – 7.24 (m, 1H, C6'-H), 7.24 – 7.18 (m, 1H, C3'-H), 4.53 – 4.49 (m, 1H, C4-H), 3.37 (d, *J* = 9.4 Hz, 1H, NH), 2.59 – 2.44 (m, 1H, C7-H_2), 2.34 – 2.23 (m, 1H, C5-H_2), 2.00 – 1.89 (m, 1H, C6-H_2), 1.89 – 1.76 (m, 2H, C5-H_2, C6-H_2), 1.26 (s, 9H, (CH_3)$_3$); **^{13}C NMR** (101 MHz, Chloroform-*d*) δ 156.4 (d, *J* = 251.5 Hz, C2'), 141.5 (C7a), 139.4 (C3), 130.1 (d, *J* = 7.8 Hz, C4'), 128.7 (C5'), 127.4 (d, *J* = 11.7 Hz, C1'), 124.9 (d, *J* = 4.0 Hz, C6'), 119.2 (C3a), 116.8 (d, *J* = 19.9 Hz, C3'), 56.3 (C(CH_3)$_3$)), 50.8 (C4), 33.3 (C5), 22.9 ((CH_3)$_3$), 21.6 (d, *J* = 4.5 Hz, C7), 20.3 (C6); ***m/z*** (ES$^+$) 357.84 ([M+Na]$^+$, 100 %); **HRMS** (ES$^+$) Calcd for $C_{17}H_{22}N_3OSFNa$ [M+Na]$^+$: 358.1365, found 358.1366.

6 Overall Conclusions

Protein-protein interaction modulation has developed as an attractive molecular target for novel cancer therapies and as a powerful research tool in chemical biology to advance our understanding of the underlying mechanisms involved in carcinogenesis. In this thesis, a range of screening approaches were utilised to identify modulators of PPIs which are implicated in oncogenesis.

The diverse range of multiprotein complexes involved in cellular regulation, signalling and pathophysiology mediated by the AAA+ protein reptin, has identified it as a promising but untapped therapeutic target. Virtual screening coupled with an *in vitro* PPI assay facilitated the identification of two modulators of the peptide binding function of reptin. A SAR optimisation study guided by molecular modelling and biological assessment provided Liddean (Figure 6.1), a promising chemical tool to study reptin's intricate protein interactome. A peptide phage display screen of Liddean (**48**) bound reptin identified the tumour suppressor protein p53 as a new interacting partner, which could potentially provide a novel therapeutic target for anticancer agents. Extensive research is continuing to dissect reptin's cellular functions and towards the optimisation of the cell permeable drug lead **13** (see Chapter 2) (Figure 6.1).

Nature's extensive repertoire of bioactive molecules has been underexploited in the hunt for PPI modulators due to the difficulties associated with screening the natural extract libraries against a target PPI. The increasing enthusiasm for PPI modulators combined with technological advances in screening methods has refocused attention on nature's plentiful store of drug leads. JBIR-22 (**4**) was identified from a screen of 123,599-natural product extract library as a potent inhibitor of PAC3 homodimerisation, a promising approach by which to inhibit the generation of the proteasomal machinery. JBIR-22 (**4**) is a member of a subfamily of the ubiquitous collection of bioactive natural products containing a tetramic acid core. A short asymmetric synthesis of the unnatural 4,4-disubstituted glutamic acid provided a synthetically versatile masked tetramic acid which could be modified by attachment of a range of side chains. Validation of this approach as a general route to this subfamily of tetramic acids was provided by the first total synthesis of the plant growth promoting agent harzianic acid (**19**) and its diastereomers (**19b**-**d**, see Chapter 3) with a longest linear sequence of only 6 steps (Figure 6.1). Subsequent utilisation of this synthetic approach facilitated the first total synthesis of JBIR-22 diastereomers **4a** and **4b** with a LLS of only 10 steps (Figure 6.1). Preliminary investigations indicate that the development of an alternative synthetic

approach containing a late stage chiral catalyst-controlled diastereoselective Diels-Alder reaction could be possible. This would provide the opportunity to access a diverse library of JBIR-22 (**4**) derivatives *via* a late stage Diels-Alder cyclisation of a range of polyene substituted tetramic acids.

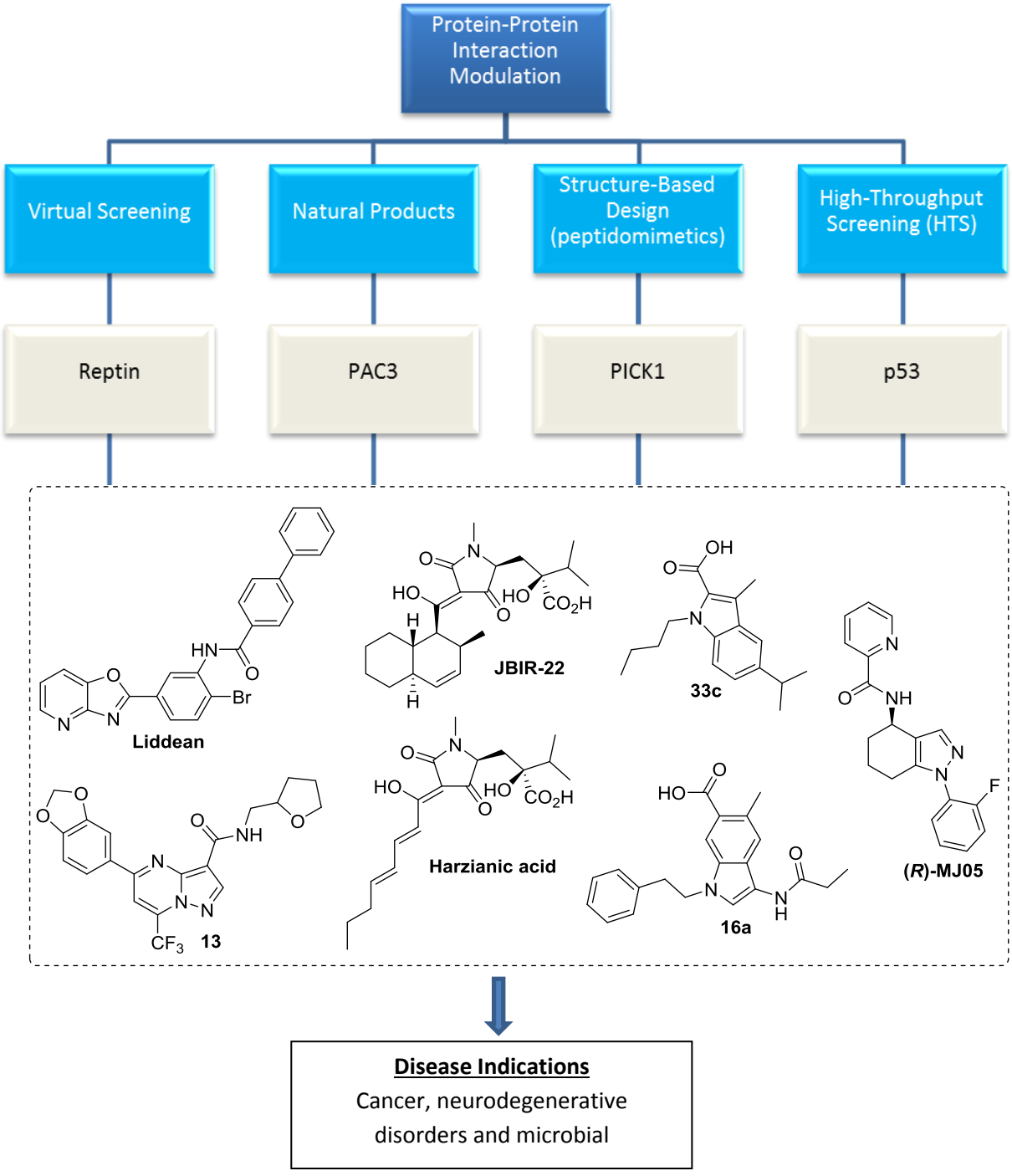

Figure 6.1. Summary of the PPI modulators developed in this thesis

The design of small molecule peptidomimetics of the binding epitope of one of the partners of a protein complex has been a fruitful source of PPI modulators. In particular, indole based peptidomimetics have been shown to successfully inhibit a range of PDZ domain mediated PPIs. A PDZ domain containing protein of significant therapeutic interest is PICK1, a scaffolding protein involved in the clustering and shuttling of its protein partners. Two series of peptidomimetic inhibitors of the PICK1 PDZ domain were designed by analysis of known PICK1-peptide coupling partners in conjugation with molecular modelling studies. Biological assessment of the 16 synthesised analogues identified **16a** and **33c** (see Chapter 4) (Figure 6.1), which had low micromolar binding affinities for the PICK1 PDZ domain. These novel peptidomimetics are on a par with the most active PDZ domain inhibitors in the literature, and provide a potential mechanism by which to investigate the PICK1's PPI with the dominant breast cancer drug target HER2. In addition, **16a** and **33c** are promising lead compounds for the development of nanomolar inhibitors of PICK1's PDZ domain, with potential as therapies for neurodegenerative disorders.

Mutation or unregulated degradation of the p53 tumour suppressor protein plays a pivotal role in cancer development and progression. As a result, modulation of the protein interactions involved in the regulation of the expression and degradation of p53 is thought to be a promising approach by which to target carcinogenesis. (±)-MJ05 (**1**) (see Chapter 5) was identified as a selective p53 activator from a forward chemical genetics screen of 20,000 drug-like compounds. (±)-MJ05 (**1**) was selected for further evaluation based on its promising therapeutic window and its potential mechanism of action *via* inhibition of the MDM2/MDM4 PPI complex involved in p53 degradation. An asymmetric synthesis of both enantiomers of (±)-MJ05 (**1**) revealed that (*R*)-MJ05 (**1**) was the active constituent of the racemate (Figure 6.1). (*R*)-MJ05 (**1**) is currently undergoing preclinical evaluation as a potential adjuvant therapy in combination with Nilotinib for the treatment of CML.

Despite their pivotal role in carcinogenesis, the interest in PPIs as drug targets has historically been tempered by the pervasive view that they are intractable drug targets. The urgent need for new, efficacious and non-toxic therapies for the treatment of complex diseases has highlighted the potential of PPI modulators as novel drug leads. The development of innovative screening methods has provided the opportunity to exploit this potentially rich source of drug leads. The application of a range of such screening approaches in this research, to successfully identify PPI modulators targeting a diverse range of proteins supports the changing perception regarding the druggability of disease relevant PPIs.

7 Bibliography

(1) Milroy, L.-G.; Grossmann, T. N.; Hennig, S.; Brunsveld, L.; Ottmann, C. *Chem. Rev.* **2014**, *114*, 4695–4748.
(2) Loh, S. N. *ACS Chem. Biol.* **2008**, *3*, 140–141.
(3) Zinzalla, G.; Thurston, D. E. *Future Med. Chem.* **2009**, *1*, 65–93.
(4) White, A. W.; Westwell, A. D.; Brahemi, G. *Expert Rev. Mol. Med.* **2008**, *10*.
(5) Hanahan, D.; Weinberg, R. A. *Cell* **2000**, *100*, 57–70.
(6) Martin, G. S. *Cancer Cell* **2003**, *4*, 167–174.
(7) Hanahan, D.; Weinberg, R. A. *Cell* **2014**, *144*, 646–674.
(8) Arkin, M. *Curr. Opin. Chem. Biol.* **2005**, *9*, 317–324.
(9) Ryan, D. P.; Matthews, J. M. *Curr. Opin. Struct. Biol.* **2005**, *15*, 441–446.
(10) Ivanov, A. A.; Khuri, F. R.; Fu, H. *Trends Pharmacol. Sci.* **2013**, *34*, 393–400.
(11) Nero, T. L.; Morton, C. J.; Holien, J. K.; Wielens, J.; Parker, M. W. *Nat. Rev. Cancer* **2014**, *14*, 248–262.
(12) Wells, J. A.; McClendon, C. L. *Nature* **2007**, *450*, 1001–1009.
(13) Arkin, M. R.; Wells, J. A. *Nat. Rev. Drug. Discov.* **2004**, *3*, 301–317.
(14) Falchi, F.; Caporuscio, F.; Recanatini, M. *Future Med. Chem.* **2014**, 343–357.
(15) Ferrari, S.; Pellati, F.; Costi, M. P. In *Disruption of Protein-Protein Interfaces: In Search of New Inhibitors*; Mangani, S., Ed.; Springer: Berlin, Heidelberg, 2013; Vol. Chapter 2, pp. 31–60.
(16) Jubb, H.; Higueruelo, A. P.; Winter, A.; Blundell, T. L. *Trends Pharmacol. Sci.* **2012**, *33*, 241–248.
(17) Tzakos, A. G.; Fokas, D.; Johannes, C.; Moussis, V.; Hatzimichael, E.; Briasoulis, E. *Molecules* **2011**, *16*, 4408–4427.
(18) Tanaka, T.; Rabbitts, T. H. *Cell cycle* **2008**, *7*, 1569–1574.
(19) Clackson, T.; Wells, J. A. *Science* **1995**, *267*, 383–386.
(20) Bogan, A. A.; Thorn, K. S. *J. Mol. Biol.* **1998**, *280*, 1–9.
(21) Van Roey, K.; Uyar, B.; Weatheritt, R. J.; Dinkel, H.; Seiler, M.; Budd, A.; Gibson, T. J.; Davey, N. E. *Chem. Rev.* **2014**.
(22) Thiel, P.; Kaiser, M.; Ottmann, C. *Angew. Chem. Int. Ed. Engl.* **2012**, *51*, 2012–2018.
(23) Lee, G. M.; Craik, C. S. *Science* **2009**, *324*, 213–215.
(24) Ray-Coquard, I.; Blay, J.-Y.; Italiano, A.; Le Cesne, A.; Penel, N.; Zhi, J.; Heil, F.; Rueger, R.; Graves, B.; Ding, M.; Geho, D.; Middleton, S. A.; Vassilev, L. T.; Nichols, G. L.; Bui, B. N. *Lancet Oncol.* **2012**, *13*, 1133–1140.
(25) Vu, B.; Wovkulich, P.; Pizzolato, G.; Lovey, A.; Ding, Q.; Jiang, N.; Liu, J.-J.; Zhao, C.; Glenn, K.; Wen, Y.; Tovar, C.; Packman, K.; Vassilev, L.; Graves, B. *ACS Med. Chem. Lett.* **2013**, *4*, 466–469.
(26) Gandhi, L.; Camidge, D. R.; Ribeiro de Oliveira, M.; Bonomi, P.; Gandara, D.; Khaira, D.; Hann, C. L.; McKeegan, E. M.; Litvinovich, E.; Hemken, P. M.; Dive, C.; Enschede, S. H.; Nolan, C.; Chiu, Y.-L.; Busman, T.; Xiong, H.; Krivoshik, A. P.; Humerickhouse, R.; Shapiro, G. I.; Rudin, C. M. *J. Clin. Oncol.* **2011**, *29*, 909–916.
(27) Yuriev, E.; Ramsland, P. A. *J. Mol. Recognit.* **2013**, *26*, 215–239.
(28) Villoutreix, B. O.; Bastard, K.; Sperandio, O.; Fahraeus, R.; Poyet, J.-L.; Calvo, F.; Déprez, B.; Miteva, M. *Curr. Pharm. Biotechnol.* **2008**, *9*, 103–122.
(29) Villoutreix, B. O.; Kuenemann, M. A.; Poyet, J.-L.; Bruzzoni-Giovanelli, H.; Labbé, C.; Lagorce, D.; Sperandio, O.; Miteva, M. A. *Mol. Inform.* **2014**, *33*, 414–437.
(30) Ewing, T. A.; Makino, S.; Skillman, A. G.; Kuntz, I. *J. Comput. Aided. Mol. Des.* **2001**, *15*, 411–428.
(31) Nikolovska-Coleska, Z.; Xu, L.; Hu, Z.; Tomita, Y.; Li, P.; Roller, P. P.; Wang, R.; Fang, X.; Guo, R.; Zhang, M.; Lippman, M. E.; Yang, D.; Wang, S. *J. Med. Chem.* **2004**, *47*, 2430–2440.
(32) Reddy, T. R. K.; Li, C.; Fischer, P. M.; Dekker, L. V. *ChemMedChem* **2012**, *7*, 1435–1446.

(33) Voet, A.; Zhang, K. Y. J. *Curr. Pharm. Des.* **2012**, *18*, 4586–4598.
(34) Phipps, K. D.; Surette, A. P.; O'Connell, P. A.; Waisman, D. M. *Cancer Res.* **2011**, *71* , 6676–6683.
(35) Shang, J.; Zhang, Z.; Song, W.; Zhou, B.; Zhang, Y.; Li, G.; Qiu, S. *Tumor Biol.* **2013**, *34*, 3785–3790.
(36) Jones, G.; Willett, P.; Glen, R. C.; Leach, A. R.; Taylor, R. *J. Mol. Biol.* **1997**, *267*, 727–748.
(37) Murali, R.; Cheng, X.; Berezov, A.; Du, X.; Schön, A.; Freire, E.; Xu, X.; Chen, Y. H.; Greene, M. I. *Proc. Natl. Acad. Sci. USA* **2005**, *102*, 10970–10975.
(38) Berezov, A.; Cai, Z.; Freudenberg, J. A.; Zhang, H.; Cheng, X.; Thompson, T.; Murali, R.; Greene, M. I.; Wang, Q. *Oncogene* **2012**, *31*, 1938–1948.
(39) McMillan, K.; Adler, M. *Proc. Natl. Acad. Sci.* **2000**, *97*, 1506–1511.
(40) Reynolds, K. A.; McLaughlin, R. N.; Ranganathan, R. *Cell* **2011**, *147*, 1564–1575.
(41) Motlagh, H. N.; Hilser, V. J. *Proc. Natl. Acad. Sci.* **2012**.
(42) Rosenbaum, J.; Baek, S.; Dutta, A. *Sci. Signal.* **2013**, *6*, 1–6.
(43) Jha, S.; Dutta, A. *Mol. Cell* **2009**, *34*, 521–533.
(44) Huen, J.; Kakihara, Y.; Ugwu, F.; Cheung, K. L. Y.; Ortega, J.; Houry, W. A. *Biochem. cell Biol.* **2010**, *40*, 29–40.
(45) Nano, N.; Houry, W. A. *Philos. Trans. R. Soc. B Biol. Sci.* **2013**, *368* .
(46) Shen, X.; Mizuguchi, G.; Hamiche, A.; Wu, C. *Nature* **2000**, *406*, 541–544.
(47) Jonsson, Z. O.; Dhar, S. K.; Narlikar, G. J.; Auty, R.; Wagle, N.; Pellman, D.; Pratt, R. E.; Kingston, R.; Dutta, A. *J. Biol. Chem.* **2001**, *276*, 16279–16288.
(48) Ikura, T.; Ogryzko, V. V; Grigoriev, M.; Groisman, R.; Wang, J.; Horikoshi, M.; Scully, R.; Qin, J.; Nakatani, Y. *Cell* **2000**, *102*, 463–473.
(49) Doyon, Y.; Selleck, W.; Lane, W. S.; Tan, S.; Cote, J. *Mol. Cell Biol.* **2004**, *24*, 1884–1896.
(50) Krogan, N. J.; Keogh, M. C.; Datta, N.; Sawa, C.; Ryan, O. W.; Ding, H.; Haw, R. A.; Pootoolal, J.; Tong, A.; Canadien, V.; Richards, D. P.; Wu, X.; Emili, A.; Hughes, T. R.; Buratowski, S.; Greenblatt, J. F. *Mol. Cell* **2003**, *12*, 1565–1576.
(51) Cai, Y.; Jin, J.; Florens, L.; Swanson, S. K.; Kusch, T.; Li, B.; Workman, J. L.; Washburn, M. P.; Conaway, R. C.; Conaway, J. W. *J. Biol. Chem.* **2005**, *280*, 13665–13670.
(52) Kanemaki, M.; Kurokawa, Y.; Matsu-ura, T.; Makino, Y.; Masani, A.; Okazaki, K.; Morishita, T.; Tamura, T. *J. Biol. Chem.* **1999**, *274* , 22437–22444.
(53) Izumi, N.; Yamashita, A.; Iwamatsu, A.; Kurata, R.; Nakamura, H.; Saari, B.; Hirano, H.; Anderson, P.; Ohno, S. *Sci. Signal.* **2010**, *3*, ra27.
(54) Wood, M. A.; McMahon, S. B.; Cole, M. D. *Mol. Cell* **2000**, *5*, 321–330.
(55) Bauer, A.; Chauvet, S.; Huber, O.; Usseglio, F.; Rothbacher, U.; Aragnol, D.; Kemler, R.; Pradel, J. *EMBO J.* **2000**, *19*, 6121–6130.
(56) Kim, J. H.; Kim, B.; Cai, L.; Choi, H. J.; Ohgi, K. A.; Tran, C.; Chen, C.; Chung, C. H.; Huber, O.; Rose, D. W.; Sawyers, C. L.; Rosenfeld, M. G.; Baek, S. H. *Nature* **2005**, *434*, 921–926.
(57) Venteicher, A. S.; Meng, Z.; Mason, P. J.; Veenstra, T. D.; Artandi, S. E. *Cell* **2008**, *132*, 945–957.
(58) Matias, P. M.; Gorynia, S.; Donner, P.; Carrondo, M. A. *J. Biol. Chem.* **2006**, *281*, 35918–35929.
(59) Gorynia, S.; Bandeiras, T. M.; Pinho, F. G.; McVey, C. E.; Vonrhein, C.; Round, A.; Svergun, D. I.; Donner, P.; Matias, P. M.; Carrondo, M. A. *J. Struct. Biol.* **2011**, *176*, 279–291.
(60) Petukhov, M.; Dagkessamanskaja, A.; Bommer, M.; Barrett, T.; Tsaneva, I.; Yakimov, A.; Quéval, R.; Shvetsov, A.; Khodorkovskiy, M.; Käs, E.; Grigoriev, M. *Structure* **2012**, *20*, 1321–1331.
(61) Torreira, E.; Jha, S.; López-Blanco, J. R.; Arias-Palomo, E.; Chacón, P.; Cañas, C.; Ayora, S.; Dutta, A.; Llorca, O. *Structure* **2008**, *16*, 1511–1520.
(62) López-Perrote, A.; Muñoz-Hernández, H.; Gil, D.; Llorca, O. *Nucleic Acids Res.* **2012**, *40*, 11086–11099.
(63) Hanson, P. I.; Whiteheart, S. W. *Nat. Rev. Mol. Cell Biol.* **2005**, *6*, 519–529.

(64) Cheung, K. L. Y.; Huen, J.; Houry, W. A.; Ortega, J. *Biochem. Cell Biol.* **2010**, *88*, 77–88.
(65) Maslon, M. M.; Hrstka, R.; Vojtesek, B.; Hupp, T. R. *J. Mol. Biol.* **2010**, *404*, 418–438.
(66) Niewiarowski, A.; Bradley, A. S.; Gor, J.; McKay, A. R.; Perkins, S. J.; Tsaneva, I. R. *Biochem. J.* **2010**, *429*, 113–125.
(67) Huber, O.; Ménard, L.; Haurie, V.; Nicou, A.; Taras, D.; Rosenbaum, J. *Cancer Res.* **2008**, *68*, 6873–6876.
(68) Grigoletto, A.; Lestienne, P.; Rosenbaum, J. *Biochim. Biophys. Acta* **2011**, *1815*, 147–157.
(69) Blanc, J. F.; Lalanne, C.; Plomion, C.; Schmitter, J. M.; Bathany, K.; Gion, J. M.; Bioulac-Sage, P.; Balabaud, C.; Bonneu, M.; Rosenbaum, J. *Proteomics* **2005**, *5*, 3778–3789.
(70) Rousseau, B.; Ménard, L.; Haurie, V.; Taras, D.; Blanc, J.-F.; Moreau-Gaudry, F.; Metzler, P.; Hugues, M.; Boyault, S.; Lemière, S.; Canron, X.; Costet, P.; Cole, M.; Balabaud, C.; Bioulac-Sage, P.; Zucman-Rossi, J.; Rosenbaum, J. *Hepatology* **2007**, *46*, 1108–1118.
(71) Etard, C.; Gradl, D.; Kunz, M.; Eilers, M.; Wedlich, D. *Mech. Dev.* **2005**, *122*, 545–556.
(72) Coste, A. de La; Romagnolo, B.; Billuart, P.; Renard, C.-A.; Buendia, M.-A.; Soubrane, O.; Fabre, M.; Chelly, J.; Beldjord, C.; Kahn, A.; Perret, C. *Proc. Natl. Acad. Sci.* **1998**, *95* , 8847–8851.
(73) Haurie, V.; Ménard, L.; Nicou, A.; Touriol, C.; Metzler, P.; Fernandez, J.; Taras, D.; Lestienne, P.; Balabaud, C.; Bioulac-Sage, P.; Prats, H.; Zucman-Rossi, J.; Rosenbaum, J. *Hepatology* **2009**, *50*, 1871–1883.
(74) Ménard, L.; Taras, D.; Grigoletto, A.; Haurie, V.; Nicou, A.; Dugot-Senant, N.; Costet, P.; Rousseau, B.; Rosenbaum, J. *J. Hepatol.* **2010**, *52*, 681–689.
(75) Matias, P. M.; Gorynia, S.; Donner, P.; Carrondo, M. A. *J. Biol. Chem.* **2006**, *281*, 38918–38929.
(76) Hann, M. M.; Oprea, T. I. *Curr. Opin. Chem. Biol.* **2004**, *8*, 255–263.
(77) Sauton, N.; Lagorce, D.; Villoutreix, B. O.; Miteva, M. *BMC Bioinformatics* **2008**, *9*, 184.
(78) Taylor, P.; Blackburn, E.; Sheng, Y. G.; Harding, S.; Hsin, K.-Y.; Kan, D.; Shave, S.; Walkinshaw, M. D. *Br. J. Pharmacol.* **2008**, *153*, S55–67.
(79) Wang, R.; Lu, Y.; Wang, S. *J. Med. Chem.* **2003**, *46*, 2287–2303.
(80) Houston, D. R.; Walkinshaw, M. D. *J. Chem. Inf. Model.* **2013**, *53*, 384–390.
(81) Neudert, G.; Klebe, G. *J. Chem. Inf. Model.* **2011**, *51*, 2731–2745.
(82) Thomas Sander (Actelion Pharmaceuticals Ltd.). OSIRIS Property Explorer http://www.organic-chemistry.org/prog/peo/.
(83) Brissette, R.; Goldstein, N. In *Cancer Genomics and Proteomics SE - 13*; Fisher, P., Ed.; Methods in Molecularbiology™; Humana Press, 2007; Vol. 383, pp. 203–213.
(84) Kehoe, J. W.; Kay, B. K. *Chem. Rev.* **2005**, *105*, 4056–4072.
(85) Smith, G. P.; Petrenko, V. A. *Chem. Rev.* **1997**, *97*, 391–410.
(86) Arap, M. A. *Genet. Mol. Biol.* **2005**, *28*, 1–9.
(87) Hertveldt, K.; Beliën, T.; Volckaert, G. In *Bacteriophages SE - 19*; Clokie, M. J.; Kropinski, A., Eds.; Methods in Molecular Biology™; Humana Press, 2009; Vol. 502, pp. 321–339.
(88) Molek, P.; Strukelj, B.; Bratkovic, T. *Molecules* **2011**, *16*, 857–887.
(89) Tompa, P. *Nat. Chem. Biol.* **2012**, *8*, 597–600.
(90) Tucker, T.; Marra, M.; Friedman, J. M. *Am. J. Hum. Genet.* **2009**, *85*, 142–154.
(91) Ten Bosch, J. R.; Grody, W. W. *J. Mol. Diagn.* **2008**, *10*, 484–492.
(92) Masoudi-Nejad, A.; Narimani, Z.; Hosseinkhan, N. In *Next Generation Sequencing and Sequence Assembly SE - 2*; SpringerBriefs in Systems Biology; Springer New York, 2013; Vol. 4, pp. 11–39.
(93) Grada, A.; Weinbrecht, K. *J Invest Dermatol* **2013**, *133*, e11.
(94) Bailey, T. L.; Williams, N.; Misleh, C.; Li, W. W. *Nucleic Acids Res.* **2006**, *34*, W369–73.
(95) Altschul, S. F.; Gish, W.; Miller, W.; Myers, E. W.; Lipman, D. J. *J. Mol. Biol.* **1990**, *215*, 403–410.
(96) Thompson, L. A.; Ellman, J. A. *Chem. Rev.* **1996**, *96*, 555–600.
(97) Waldmann, H.; Janning, P. *Chemical Biology*; Wiley, 2009; pp. 0–340.

(98) Gordon, E. M.; Kerwin Jr, J. F. *Combinatorial Chemistry and Molecular Diversity in Drug Discovery*; Wiley, 1998.
(99) Franzén, R. G. *J. Comb. Chem.* **2000**, *2*, 195–214.
(100) An, H.; Cook, P. D. *Chem. Rev.* **2000**, *100*, 3311–3340.
(101) Dalinger, I. L.; Vatsadse, I.; Shevelev, S.; Ivachtchenko, A. V. *J. Comb. Chem.* **2005**, *7*, 236–245.
(102) Katsuyama, I.; Ogawa, S.; Yamaguchi, Y. *Synthesis (Stuttg).* **1997**, 1321–1324.
(103) Danheiser, R. L.; Miller, R. F.; Brisbois, R. G.; Park, S. Z. *J. Org. Chem.* **1990**, *55*, 1959–1964.
(104) Recknagel, R. O.; Glende Jr., E. A.; Dolak, J. A.; Waller, R. L. *Pharmacol. Ther.* **1989**, *43*, 139–154.
(105) Evans, W. F. J.; Puckrin, E. *Geophys. Res. Lett.* **1996**, *23*, 1769–1772.
(106) Gutekunst, W. R.; Baran, P. S. *Chem. Soc. Rev.* **2011**, *40*, 1976–1991.
(107) Verrier, C.; Lassalas, P.; Théveau, L.; Quéguiner, G.; Trécourt, F.; Marsais, F.; Hoarau, C. *Beilstein J. Org. Chem.* **2011**, *7*, 1584–1601.
(108) Chen, X.; Engle, K. M.; Wang, D.-H.; Yu, J.-Q. *Angew. Chemie Int. Ed.* **2009**, *48*, 5094–5115.
(109) Ferrins, L.; Rahmani, R.; Sykes, M. L.; Jones, A. J.; Avery, V. M.; Teston, E.; Almohaywi, B.; Yin, J.; Smith, J.; Hyland, C.; White, K. L.; Ryan, E.; Campbell, M.; Charman, S. A.; Kaiser, M.; Baell, J. B. *Eur. J. Med. Chem.* **2013**, *66*, 450–465.
(110) Zhuravlev, F. A. *Tetrahedron Lett.* **2006**, *47*, 2929–2932.
(111) Holler, M. G.; Campo, L. F.; Brandelli, A.; Stefani, V. *J. Photochem. Photobiol. A Chem.* **2002**, *149*, 217–225.
(112) Myllymäki, M. J.; Koskinen, A. M. P. *Tetrahedron Lett.* **2007**, *48*, 2295–2298.
(113) Newman, D. J.; Cragg, G. M. *J. Nat. Prod.* **2012**, *75*, 311–335.
(114) Newman, D. J.; Cragg, G. M. *J. Nat. Prod.* **2007**, *70*, 461–477.
(115) Li, J. W.-H.; Vederas, J. C. *Science* **2009**, *325*, 161–165.
(116) Kodadek, T. *Chem. Commun.* **2011**, *47*, 9757–9763.
(117) Over, B.; Wetzel, S.; Grütter, C.; Nakai, Y.; Renner, S.; Rauh, D.; Waldmann, H. *Nat. Chem.* **2013**, *5*, 21–28.
(118) Koehn, F. E.; Carter, G. T. *Nat. Rev. Drug Discov.* **2005**, *4*, 206–220.
(119) Reindl, W.; Yuan, J.; Krämer, A.; Strebhardt, K.; Berg, T. *Chem. Biol.* **2008**, *15*, 459–466.
(120) Duncan, S. J.; Grüschow, S.; Williams, D. H.; McNicholas, C.; Purewal, R.; Hajek, M.; Gerlitz, M.; Martin, S.; Wrigley, S. K.; Moore, M. *J. Am. Chem. Soc.* **2001**, *123*, 554–560.
(121) Lepourcelet, M.; Chen, Y.-N. P.; France, D. S.; Wang, H.; Crews, P.; Petersen, F.; Bruseo, C.; Wood, A. W.; Shivdasani, R. A. *Cancer Cell* **2014**, *5*, 91–102.
(122) Hashimoto, J.; Watanabe, T.; Seki, T.; Karasawa, S.; Izumikawa, M.; Seki, T.; Iemura, S.-I.; Natsume, T.; Nomura, N.; Goshima, N.; Miyawaki, A.; Takagi, M.; Shin-Ya, K. *J. Biomol. Screen.* **2009**, *14*, 970–979.
(123) Izumikawa, M.; Hashimoto, J.; Hirokawa, T.; Sugimoto, S.; Kato, T.; Takagi, M.; Shin-Ya, K. *J. Nat. Prod.* **2010**, *73*, 628–631.
(124) Hirano, Y.; Hayashi, H.; Iemura, S.-I.; Hendil, K. B.; Niwa, S.-I.; Kishimoto, T.; Kasahara, M.; Natsume, T.; Tanaka, K.; Murata, S. *Mol. Cell* **2006**, *24*, 977–984.
(125) Finley, D. *Annu. Rev. Biochem.* **2009**, *78*, 477–513.
(126) Bonvini, P.; Zorzi, E.; Basso, G.; Rosolen, A. *Leukemia* **2007**, *21*, 838–842.
(127) Fenteany, G.; Standaert, R. F.; Lane, W. S.; Choi, S.; Corey, E. J.; Schreiber, S. L. *Science* **1995**, *268*, 726–731.
(128) Adams, J.; Palombella, V.; Sausville, E. *Cancer Res.* **1999**, 2615–2622.
(129) Murata, M.; Matsuoka, S.; Matsumori, N.; Paul, G. K.; Tachibana, K. *J. Am. Chem. Soc.* **1999**, *121*, 870–871.
(130) Royles, B. J. L. *Chem. Rev.* **1995**, *95*, 1981–2001.
(131) Jeong, Y.-C.; Moloney, M. G. *J. Org. Chem.* **2011**, *76*, 1342–1354.
(132) Schobert, R.; Schlenk, A. *Bioorg. Med. Chem.* **2008**, *16*, 4203–4221.
(133) Gromak, V. V; Avakyan, V. G.; Lakhvich, O. F. *J. Appl. Spectrosc.* **2000**, *67*, 205–215.

(134) Steyn, P. S.; Wessels, P. L. *Tetrahedron Lett.* **1978**, *19*, 4707–4710.
(135) Nolte, M. J.; Steyn, P. S.; Wessels, P. L. *J. Chem. Soc., Perkin Trans. 1* **1980**, 1057–1065.
(136) Athanasellis, G.; Igglessi-Markopoulou, O.; Markopoulos, J. *Bioinorg. Chem. Appl.* **2010**, *2010*, 315056.
(137) Schobert, R. *Naturwissenschaften* **2007**, *94*, 1–11.
(138) Fisch, K. M. *RSC Adv.* **2013**, *3*, 18228.
(139) Staunton, J.; Weissman, K. J. *Nat. Prod. Rep.* **2001**, *18*, 380–416.
(140) Sims, J. W.; Fillmore, J. P.; Warner, D. D.; Schmidt, E. W. *Chem. Commun. (Camb).* **2005**, 186–188.
(141) Campbell, C. D.; Vederas, J. C. *Biopolymers* **2010**, *93*, 755–763.
(142) Oikawa, H.; Tokiwano, T. *Nat. Prod. Rep.* **2004**, *21*, 321–352.
(143) Stocking, E. M.; Williams, R. M. *Angew. Chem. Int. Ed. Engl.* **2003**, *42*, 3078–3115.
(144) Kelly, W. L. *Org. Biomol. Chem.* **2008**, *6*, 4483–4493.
(145) Kim, H. J.; Ruszczycky, M. W.; Choi, S.; Liu, Y.; Liu, H. *Nature* **2011**, *473*, 109–112.
(146) Ose, T.; Watanabe, K.; Mie, T.; Honma, M.; Watanabe, H.; Yao, M.; Oikawa, H.; Tanaka, I. *Nature* **2003**, *422*, 185–189.
(147) Serafimov, J. M.; Gillingham, D.; Kuster, S.; Hilvert, D. *J. Am. Chem. Soc.* **2008**, *130*, 7798–7799.
(148) Watanabe, K.; Mie, T.; Ichihara, A.; Oikawa, H.; Honma, M. *J. Biol. Chem.* **2000**, *275* , 38393–38401.
(149) Guimarães, C. R. W.; Udier-Blagović, M.; Jorgensen, W. L. *J. Am. Chem. Soc.* **2005**, *127*, 3577–3588.
(150) Kaufmann, G. F.; Sartorio, R.; Lee, S.-H.; Rogers, C. J.; Meijler, M. M.; Moss, J. a; Clapham, B.; Brogan, A. P.; Dickerson, T. J.; Janda, K. D. *Proc. Natl. Acad. Sci. U. S. A.* **2005**, *102*, 309–314.
(151) Kaufmann, G. F.; Sartorio, R.; Lee, S.-H.; Mee, J. M.; Altobell, L. J.; Kujawa, D. P.; Jeffries, E.; Clapham, B.; Meijler, M. M.; Janda, K. D. *J. Am. Chem. Soc.* **2006**, *128*, 2802–2803.
(152) Waters, C. M.; Bassler, B. L. *Annu. Rev. Cell Dev. Biol.* **2005**, *21*, 319–346.
(153) Lowery, C. A.; Park, J.; Gloeckner, C.; Meijler, M. M.; Mueller, R. S.; Boshoff, H. I.; Ulrich, R. L.; Barry Clifton E.; Bartlett, D. H.; Kravchenko, V. V; Kaufmann, G. F.; Janda, K. D. *J. Am. Chem. Soc.* **2009**, *131*, 14473–14479.
(154) Sengoku, T.; Nagae, Y.; Ujihara, Y.; Takahashi, M.; Yoda, H. *J. Org. Chem.* **2012**, *77*, 4391–4401.
(155) Spengler, J.; Schedel, H.; Sieler, J.; Quaedflieg, P. J. L. M.; Broxterman, Q. B.; Duchateau, A. L. L.; Burger, K. *Synthesis (Stuttg).* **2001**, *2001*, 1513,1518.
(156) Lacey, R. N. *J. Chem. Soc.* **1954**, 850–854.
(157) Poncet, J.; Jouin, P.; Castro, B.; Nicolas, L.; Boutar, M.; Gaudemer, A. *J. Chem. Soc. Perkin Trans. 1* **1990**, 611.
(158) Burke, L. T.; Dixon, D. J.; Ley, S. V; Rodríguez, F. *Org. Biomol. Chem.* **2005**, *3*, 274–280.
(159) Burke, L. T.; Dixon, D. J.; Ley, S. V.; Rodríguez, F. *Org. Lett.* **2000**, *2*, 3611–3613.
(160) Kawada, M.; Yoshimoto, Y.; Kumagai, H. *J. Antibiot. (Tokyo).* **2004**, *57*, 2–4.
(161) Hazalin, N. A. M. N.; Ramasamy, K.; Lim, S. M.; Cole, A. L. J.; Majeed, A. B. A. *Phytomedicine* **2012**, *19*, 609–617.
(162) Yang, S.-W.; Mierzwa, R.; Terracciano, J.; Patel, M.; Gullo, V.; Wagner, N.; Baroudy, B.; Puar, M.; Chan, T.-M.; McPhail, A. T.; Chu, M. *J. Nat. Prod.* **2006**, *69*, 1025–1028.
(163) Yang, S.; Mierzwa, R.; Terracciano, J.; Patel, M.; Gullo, V.; Wagner, N.; Baroudy, B.; Puar, M.; Chan, T.; Chu, M. *J. Antibiot. (Tokyo).* **2007**, *60*, 524–528.
(164) Vinale, F.; Flematti, G.; Sivasithamparam, K.; Lorito, M.; Marra, R.; Skelton, B. W.; Ghisalberti, E. L.; School. *J. Nat. Prod.* **2009**, *72*, 2032–2035.
(165) Vinale, F.; Nigro, M.; Sivasithamparam, K.; Flematti, G.; Ghisalberti, E. L.; Ruocco, M.; Varlese, R.; Marra, R.; Lanzuise, S.; Eid, A.; Woo, S. L.; Lorito, M. *FEMS Microbiol. Lett.* **2013**.
(166) Daferner, M.; Anke, T.; Sterner, O. *Tetrahedron* **2002**, *58*, 7781–7784.

(167) Feng, Y.; Broder, C. C.; Kennedy, P. E.; Berger, E. A. *Science* **1996**, *272*, 872–877.
(168) Alkhatib, G.; Combadiere, C.; Broder, C. C.; Feng, Y.; Kennedy, P. E.; Murphy, P. M.; Berger, E. A. *Science* **1996**, *272*, 1955–1958.
(169) Palani, A.; Tagat, J. R. *J. Med. Chem.* **2006**, *49*, 2851–2857.
(170) Maeda, K.; Das, D.; Nakata, H.; Mitsuya, H. *Expert Opin. Emerg. Drugs* **2012**, *17*, 135–145.
(171) Gilliam, B. L.; Riedel, D. J.; Redfield, R. R. *J. Transl. Med.* **2011**, *9 Suppl 1*, S9.
(172) Sawa, R.; Mori, Y.; Iinuma, H. *J. Antibiot. (Tokyo).* **1994**, *47*, 731–732.
(173) Vinale, F.; Sivasithamparam, K.; Ghisalberti, E. L.; Marra, R.; Woo, S. L.; Lorito, M. *Soil Biol. Biochem.* **2008**, *40*, 1–10.
(174) Lorito, M.; Woo, S. L.; Harman Gary E.; Monte, E. *Annu. Rev. Phytopathol.* **2010**, *48*, 395–417.
(175) Barton, L. L.; Hemming, C. B. *Iron Chelation in Plants and Soil Microorganisms*; Academic Press, New York, 1993.
(176) Neilands, J. B. *J. Biol. Chem.* **1995**, *270* , 26723–26726.
(177) Hider, R. C.; Kong, X. *Nat. Prod. Rep.* **2010**, *27*, 637–657.
(178) Biersack, B.; Diestel, R.; Jagusch, C.; Sasse, F.; Schobert, R. *J. Inorg. Biochem.* **2009**, *103*, 72–76.
(179) Kaufmann, G. F.; Sartorio, R.; Lee, S.-H.; Rogers, C. J.; Meijler, M. M.; Moss, J. a; Clapham, B.; Brogan, A. P.; Dickerson, T. J.; Janda, K. D. *Proc. Natl. Acad. Sci. U. S. A.* **2005**, *102*, 309–314.
(180) Baldwin, S.; Long, A. *Org. Lett.* **2004**, *6*, 1653–1656.
(181) Helaine, V.; Bolte, J. *Tetrahedron: Asymmetry* **1998**, *9*, 3855–3861.
(182) He, V.; Rossi, È.; Gefflaut, T.; Alaux, Â.; Bolte, J. *Adv. Synth. Catal.* **2001**, 0–5.
(183) Polt, R.; Seebach, D. *J. Am. Chem. Soc.* **1989**, *111*, 2622–2632.
(184) Alderweireldt, F.; Jadot, J.; Casimir, J.; Loffet, A. *Biochim. Biophys. Acta - Gen. Subj.* **1967**, *136*, 89–94.
(185) Jadot, J.; Casimir, J.; Loffet, A. *Biochim. Biophys. Acta - Gen. Subj.* **1967**, *136*, 79–88.
(186) Meier, L. K.; Sorensen, H. *Phytochemistry* **1979**, *18*, 1173–1175.
(187) Bu'Lock, J. D. *Biosynthesis*; A specialist periodical report. Biosynthesis; Royal Society of Chemistry, 1980; pp. 155–178.
(188) Liu, G.; Cogan, D. A.; Ellman, J. A. *J. Am. Chem. Soc.* **1997**, *119*, 9913–9914.
(189) Robak, M. T.; Herbage, M. A.; Ellman, J. A. *Chem Rev* **2010**, *110*, 3600–3740.
(190) Xu, H.-C.; Chowdhury, S.; Ellman, J. A. *Nat. Protoc.* **2013**, *8*, 2271–2280.
(191) Trost, B. M.; Brindle, C. S. *Chem. Soc. Rev.* **2010**, *39*, 1600–1632.
(192) Evans, D. A.; Bartroli, J.; Shih, T. L. *J. Am. Chem. Soc.* **1981**, *103*, 2127–2129.
(193) Hajos, Z. G.; Parrish, D. R. *J. Org. Chem.* **1974**, *39*, 1615–1621.
(194) Gathergood, N.; Juhl, K.; Poulsen, T. B.; Thordrup, K.; Jørgensen, K. A. *Org. Biomol. Chem.* **2004**, *2*, 1077–1085.
(195) Kochi, T.; Tang, T.; Ellman, J. *J. Am. Chem. Soc.* **2002**, 6518–6519.
(196) Kochi, T.; Tang, T. P.; Ellman, J. *J. Am. Chem. Soc.* **2003**, *125*, 11276–11282.
(197) Reddy, L.; Gupta, A.; Liu, Y. *J. Org. Chem.* **2011**, 3409–3415.
(198) Zimmerman, H. E.; Traxler, M. D. *J. Am. Chem. Soc.* **1957**, *79*, 1920–1923.
(199) Colyer, J. T.; Andersen, N. G.; Tedrow, J. S.; Soukup, T. S.; Faul, M. M. *J. Org. Chem.* **2006**, *71*, 6859–6862.
(200) Robak, M. T.; Herbage, M. A.; Ellman, J. A. *Chem. Rev.* **2010**, *110*, 3600–3740.
(201) Gribble, G. W. *Org. Process Res. Dev.* **2006**, *10*, 1062–1075.
(202) W. Gribble, G. *Chem. Soc. Rev.* **1998**, *27*, 395.
(203) Borch, R. F.; Bernstein, M. D.; Durst, H. D. *J. Am. Chem. Soc.* **1971**, *93*, 2897–2904.
(204) Robak, M. T.; Herbage, M. A.; Ellman, J. A. *Chem. Rev.* **2010**, *110*, 3600–3740.
(205) Staunton, J.; Weissman, K. J. *Nat. Prod. Rep.* **2001**, *18*, 380–416.
(206) Ley, S. V.; Woodward, P. R. *Tetrahedron Lett.* **1987**, *28*, 3019–3020.
(207) Booth, P. M.; Broughton, H. B.; Ford, M. J.; Fox, C. M. J.; Ley, S. V.; Slawin, A. M. Z.; Williams, D. J.; Woodward, P. R. *Tetrahedron* **1989**, *45*, 7565–7580.

(208) Fox, C. M. J.; Ley, S. V; Slawin, A. M. Z.; Williams, D. J. *J. Chem. Soc., Chem. Commun.* **1985**, 1805–1806.
(209) Clarke, T.; Ley, S. V. *J. Chem. Soc., Perkin Trans. 1* **1987**, 131–135.
(210) Booth, P. M.; Fox, C. M. J.; Ley, S. V. *Tetrahedron Lett.* **1983**, *24*, 5143–5146.
(211) Booth, P. M.; Fox, C. M. J.; Ley, S. V. *J. Chem. Soc., Perkin Trans. 1* **1987**, 121–129.
(212) Ley, S. V.; Smith, S. C.; Woodward, P. R. *Tetrahedron* **1992**, *48*, 1145–1174.
(213) Ley, S.; Smith, S.; Woodward, P. *Tetrahedron Lett.* **1988**, *29*, 5829–5832.
(214) Ley, S.; Woodward, P. *Tetrahedron Lett.* **1987**, *28*, 345–346.
(215) Lipson, V. V; Gorobets, N. Y. *Mol. Divers.* **2009**, *13*, 399–419.
(216) Ivanov, A. S. *Chem. Soc. Rev.* **2008**, *37*, 789–811.
(217) Schreiber, S.; Claus, R.; Reagan, J. *Tetrahedron Lett.* **1982**, *23*, 3867–3870.
(218) Uchida, K.; Ogawa, T.; Yasuda, Y.; Mimura, H.; Fujimoto, T.; Fukuyama, T.; Wakimoto, T.; Asakawa, T.; Hamashima, Y.; Kan, T. *Angew. Chem. Int. Ed. Engl.* **2012**, *51*, 12850–12853.
(219) Thompson, S. K.; Heathcock, C. H. *J. Org. Chem.* **1990**, *55*, 3386–3388.
(220) Lambert, T. H.; Danishefsky, S. J. *J. Am. Chem. Soc.* **2006**, *128*, 426–427.
(221) Wilson, R. M.; Jen, W. S.; Macmillan, D. W. C. *J. Am. Chem. Soc.* **2005**, *127*, 11616–11617.
(222) Ahrendt, K.; Borths, C. J.; Macmillan, D. W. C. *J. Am. Chem. Soc.* **2000**, *122*, 4243–4244.
(223) Evans, D.; Chapman, K.; Bisaha, J. *Tetrahedron Lett.* **1984**, 7–10.
(224) Paintner, F. F.; Bauschke, G.; Polborn, K. *Tetrahedron Lett.* **2003**, *44*, 2549–2552.
(225) Merino, P.; Marqués-López, E.; Tejero, T.; Herrera, R. *Synthesis (Stuttg).* **2009**, *2010*, 1–26.
(226) Kumpulainen, E. T. T.; Koskinen, A. M. P.; Rissanen, K. *Org. Lett.* **2007**, *9*, 5043–5045.
(227) Jacobs, W. C.; Christmann, M. *Synlett* **2008**, *2*, 247–251.
(228) Gaich, T.; Baran, P. S. *J. Org. Chem.* **2010**, *75*, 4657–4673.
(229) Hendrickson, J. B. *J. Am. Chem. Soc.* **1975**, *97*, 5784–5800.
(230) Bertz, S. H. *J. Am. Chem. Soc.* **1982**, *104*, 5801–5803.
(231) Mulzer, J. *Nat. Prod. Rep.* **2014**, *31*, 595–603.
(232) Newhouse, T.; Baran, P. S.; Hoffmann, R. W. *Chem. Soc. Rev.* **2009**, *38*, 3010–3021.
(233) Könning, D.; Hiller, W.; Christmann, M. *Org. Lett.* **2012**, *14*, 5258–5261.
(234) De Figueiredo, R. M.; Voith, M.; Fröhlich, R.; Christmann, M. *Synlett* **2007**, *2007*, 391–394.
(235) Ma, S. M.; Li, J. W.-H.; Choi, J. W.; Zhou, H.; Lee, K. K. M.; Moorthie, V. a; Xie, X.; Kealey, J. T.; Da Silva, N. a; Vederas, J. C.; Tang, Y. *Science* **2009**, *326*, 589–592.
(236) Devos, M.; Patte, F.; Rouault, J.; Lafort, P.; Van Gemert, L. J. *Standardized Human Olfactory Thresholds*; Oxford Press, 1990; p. 118.
(237) Chen, M.; Roush, W. R. *Org. Lett.* **2012**, *14*, 426–428.
(238) Shimshock, S. J.; Waltermire, R. E.; DeShong, P. *J. Am. Chem. Soc.* **1991**, *113*, 8791–8796.
(239) DeShong, P.; Ramesh, S.; Elango, V.; Perez, J. J. *J. Am. Chem. Soc.* **1985**, *107*, 5219–5224.
(240) Pronin, S. V; Kozmin, S. a. *J. Am. Chem. Soc.* **2010**, *132*, 14394–14396.
(241) Du, H.; Ding, K. *ChemInform* **2010**, *1*, 1–57.
(242) Corey, E. J. *Angew. Chemie Int. Ed.* **2002**, *41*, 1650–1667.
(243) Takao, K.; Munakata, R.; Tadano, K. *Chem. Rev.* **2005**, *105*, 4779–4807.
(244) Furuta, K.; Kanematsu, A.; Yamamoto, H.; Takaoka, S. *Tetrahedron Lett.* **1989**, *30*, 7231–7232.
(245) Iwasawa, N.; Sugimori, J.; Kawase, Y.; Narasaka, K. *Chem. Lett.* **1989**, *18*, 1947–1950.
(246) Evans, D.; Miller, S.; Lectka, T.; von Matt, P. *J. Am. Chem. Soc.* **1999**, *121*, 7559–7573.
(247) Evans, D.; Johnson, J. *J. Org. Chem.* **1997**, *62*, 786–787.
(248) Corey, E. J.; Loh, T. P. *J. Am. Chem. Soc.* **1991**, *113*, 8966–8967.
(249) Simsek, S.; Horzella, M.; Kalesse, M. *Org. Lett.* **2007**, *9*, 5637–5639.
(250) Evans, D.; Miller, S.; Lectka, T. *J. Am. Chem. Soc.* **1993**, *12*, 6460–6461.
(251) Evans, D.; Kozlowski, M.; Tedrow, J. *Tetrahedron Lett.* **1996**, *37*, 7481–7484.
(252) Desimoni, G.; Faita, G.; Jørgensen, K. A. *Chem. Rev.* **2006**, *106*, 3561–3651.
(253) Owens, T.; Hollander, F. *J. Am. Chem. Soc.* **2001**, 1539–1540.
(254) Ellman, J. A.; Owens, T. D.; Tang, T. P. *Acc. Chem. Res.* **2002**, *35*, 984–995.

(255) Evans, D. a.; Johnson, J. S. *J. Org. Chem.* **1997**, *62*, 786–787.
(256) Corey, E.; Ishihara, K. *Tetrahedron Lett.* **1992**, *33*, 6807–6810.
(257) Raithby, P. R.; Shields, G. P.; Allen, F. H.; Motherwell, W. D. S. *Acta Crystallogr. Sect. B* **2000**, *56*, 444–454.
(258) Eya, B. K.; Toshikazu, O.; Isao, K.; Wood, D. L. *Tetrahedron* **1990**, *46*, 2695–2706.
(259) Snider, B. B.; Lu, Q. *J. Org. Chem.* **1996**, *61*, 2839–2844.
(260) Lygo, B.; Hirst, D. J. *Synthesis (Stuttg).* **2005**, 3257–3262.
(261) Grauer, A.; König, B. *European J. Org. Chem.* **2009**, *2009*, 5099–5111.
(262) Floris, M.; Moro, S. *Mol. Inform.* **2012**, *31*, 12–20.
(263) Kharb, R.; Rana, M.; Sharma, P. C.; Yar, M. S.; Delhi, N. *J. Chem. Pharm. Res.* **2011**, *3*, 173–186.
(264) Vagner, J.; Qu, H.; Hruby, V. J. *Curr. Opin. Chem. Biol.* **2008**, *12*, 292–296.
(265) Karatas, H.; Townsend, E. C.; Cao, F.; Chen, Y.; Bernard, D.; Liu, L.; Lei, M.; Dou, Y.; Wang, S. *J. Am. Chem. Soc.* **2012**, *135*, 669–682.
(266) Patel, A.; Vought, V. E.; Dharmarajan, V.; Cosgrove, M. S. *J. Biol. Chem.* **2008**, *283* , 32162–32175.
(267) Cao, F.; Townsend, E. C.; Karatas, H.; Xu, J.; Li, L.; Lee, S.; Liu, L.; Chen, Y.; Ouillette, P.; Zhu, J.; Hess, J. L.; Atadja, P.; Lei, M.; Qin, Z. S.; Malek, S.; Wang, S.; Dou, Y. *Mol. Cell* **2014**, *53*, 247–261.
(268) Rew, Y.; Sun, D.; Gonzalez-Lopez De Turiso, F.; Bartberger, M. D.; Beck, H. P.; Canon, J.; Chen, A.; Chow, D.; Deignan, J.; Fox, B. M.; Gustin, D.; Huang, X.; Jiang, M.; Jiao, X.; Jin, L.; Kayser, F.; Kopecky, D. J.; Li, Y.; Lo, M.-C.; Long, A. M.; Michelsen, K.; Oliner, J. D.; Osgood, T.; Ragains, M.; Saiki, A. Y.; Schneider, S.; Toteva, M.; Yakowec, P.; Yan, X.; Ye, Q.; Yu, D.; Zhao, X.; Zhou, J.; Medina, J. C.; Olson, S. H. *J. Med. Chem.* **2012**, *55*, 4936–4954.
(269) Moll, U. M.; Petrenko, O. *Mol. Cancer Res.* **2003**, *1* , 1001–1008.
(270) You, L.; Xu, Z.; Punchihewa, C.; Jablons, D. M.; Fujii, N. *Mol. Cancer Ther.* **2008**, *7*, 1633–1638.
(271) Vogrig, A.; Dorr, L.; Bouzidi, N.; Boucherle, B.; Wattiez, A.-S.; Cassier, E.; Vallon, G.; Ripoche, I.; Abrunhosa-Thomas, I.; Marin, P.; Nauton, L.; Thery, V.; Courteix, C.; Lian, L.-Y.; Ducki, S. *ACS Chem. Biol.* **2013**, *8*, 2209–2216.
(272) Fujii, N.; Shelat, A.; Hall, R. a; Guy, R. K. *Bioorg. Med. Chem. Lett.* **2007**, *17*, 546–548.
(273) Mahindroo, N.; Punchihewa, C.; Bail, A. M.; Fujii, N. *Bioorg. Med. Chem. Lett.* **2008**, *18*, 946–949.
(274) Mayasundari, A.; Ferreira, A. M.; He, L.; Mahindroo, N.; Bashford, D.; Fujii, N. *Bioorg. Med. Chem. Lett.* **2008**, *18*, 942–945.
(275) Hammond, M. C.; Harris, B. Z.; Lim, W.; Bartlett, P. *Chem. Biol.* **2006**, *13*, 1247–1251.
(276) Jeleń, F.; Oleksy, A.; Smietana, K.; Otlewski, J. *Acta Biochim. Pol.* **2003**, *50*, 985–1017.
(277) Pan, L.; Wu, H.; Shen, C.; Shi, Y.; Jin, W.; Xia, J.; Zhang, M. *EMBO J* **2007**, *26*, 4576–4587.
(278) Dev, K. K. *Nat. Rev. Drug Discov.* **2004**, *3*, 1047–1056.
(279) Dev, K. K. *Curr. Top. Med. Chem.* **2007**, *7*, 3–20.
(280) Wang, C. Extended PDZ Domain Database http://bcz102.ust.hk/pdzex/.
(281) Aarts, M.; Liu, Y.; Liu, L.; Besshoh, S.; Arundine, M.; Gurd, J. W.; Wang, Y.-T.; Salter, M. W.; Tymianski, M. *Science* **2002**, *298*, 846–850.
(282) Joshi, M.; Vargas, C.; Boisguerin, P.; Diehl, A.; Krause, G.; Schmieder, P.; Moelling, K.; Hagen, V.; Schade, M.; Oschkinat, H. *Angew. Chem. Int. Ed. Engl.* **2006**, *45*, 3790–3795.
(283) Fujii, N.; You, L.; Xu, Z.; Uematsu, K.; Shan, J.; He, B.; Mikami, I.; Edmondson, L. R.; Neale, G.; Zheng, J.; Guy, R. K.; Jablons, D. M. *Cancer Res.* **2007**, *67*, 573–579.
(284) Subbaiah, V. K.; Kranjec, C.; Thomas, M.; Banks, L. *Biochem. J.* **2011**, *439*, 195–205.
(285) Thorsen, T. S.; Madsen, K. L.; Rebola, N.; Rathje, M.; Anggono, V.; Bach, A.; Moreira, I. S.; Stuhr-Hansen, N.; Dyhring, T.; Peters, D.; Beuming, T.; Huganir, R.; Weinstein, H.; Mulle, C.; Strømgaard, K.; Rønn, L. C. B.; Gether, U. *Proc. Natl. Acad. Sci. USA* **2010**, *107*, 413–418.
(286) Bolia, A.; Gerek, Z. N.; Keskin, O.; Banu Ozkan, S.; Dev, K. K. *Proteins* **2012**, *80*, 1393–1408.

(287) Perez, J. L.; Khatri, L.; Chang, C.; Srivastava, S.; Osten, P.; Ziff, E. B. *J. Neurosci.* **2001**, *21*, 5417–5428.
(288) Zhang, B.; Cao, W.; Zhang, F.; Zhang, L.; Niu, R.; Niu, Y.; Fu, L.; Hao, X.; Cao, X. *Cancer Sci.* **2010**, *101*, 1536–1542.
(289) Dev, K. K.; Henley, J. M. *Trends Pharmacol. Sci.* **2006**, *27*, 574–579.
(290) Hanley, J. G. *Pharmacol Ther.* **2008**, *118*, 152–160.
(291) Xia, J.; Zhang, X.; Staudinger, J.; Huganir, R. L. *Neuron* **1999**, *22*, 179–187.
(292) Jaulin-Bastard, F.; Saito, H.; Le Bivic, A.; Ollendorff, V.; Marchetto, S.; Birnbaum, D.; Borg, J. P. *J. Biol. Chem.* **2001**, *276*, 15256–15263.
(293) Hudis, C. A. *N. Engl. J. Med.* **2007**, *357*, 39–51.
(294) Bach, A.; Stuhr-Hansen, N.; Thorsen, T. S.; Bork, N.; Moreira, I. S.; Frydenvang, K.; Padrah, S.; Christensen, S. B.; Madsen, K. L.; Weinstein, H.; Gether, U.; Strømgaard, K. *Org. Biomol. Chem.* **2010**, *8*, 4281–4288.
(295) Fujii, N.; Haresco, J. J.; Novak, K. a P.; Stokoe, D.; Kuntz, I. D.; Guy, R. K. *J. Am. Chem. Soc.* **2003**, *125*, 12074–12075.
(296) Fujii, N.; Haresco, J. J.; Novak, K. a P.; Gage, R. M.; Pedemonte, N.; Stokoe, D.; Kuntz, I. D.; Guy, R. K. *Bioorg. Med. Chem. Lett.* **2007**, *17*, 549–552.
(297) Vogrig, A.; Boucherle, B.; Deokar, H.; Thomas, I.; Ripoche, I.; Lian, L.-Y. Y.; Ducki, S. *Bioorg. Med. Chem. Lett.* **2011**, *21*, 3349–3353.
(298) Elkins, J. M.; Papagrigoriou, E.; Berridge, G.; Yang, X.; Phillips, C.; Gileadi, C.; Savitsky, P.; Doyle, D. A. *Protein Sci.* **2007**, *16*, 683–694.
(299) Madsen, K. L.; Beuming, T.; Niv, M. Y.; Chang, C.-W.; Dev, K. K.; Weinstein, H.; Gether, U. *J. Biol. Chem.* **2005**, *280*, 20539–20548.
(300) Shi, Y. *Biochemistry* **2010**, *49*, 4432–4439.
(301) Xu, J.; Xia, J. *Neurosignals.* **2007**, *15*, 190–201.
(302) Dougherty, D. A. *Science* **1996**, *271*, 163–168.
(303) Burley, S. K.; Petsko, G. A. *FEBS Lett.* **1986**, *203*, 139–143.
(304) Gallivan, J. P.; Dougherty, D. A. *Proc. Natl. Acad. Sci.* **1999**, *96* , 9459–9464.
(305) Crowley, P. B.; Golovin, A. *Proteins Struct. Funct. Bioinforma.* **2005**, *59*, 231–239.
(306) Zhong, W.; Gallivan, J. P.; Zhang, Y.; Li, L.; Lester, H. A.; Dougherty, D. A. *Proc. Natl. Acad. Sci.* **1998**, *95* , 12088–12093.
(307) Bissantz, C.; Kuhn, B.; Stahl, M. *J. Med. Chem.* **2010**, *53*, 5061–5084.
(308) Verdonk, M. L.; Cole, J. C.; Hartshorn, M. J.; Murray, C. W.; Taylor, R. D. *Proteins Struct. Funct. Bioinforma.* **2003**, *52*, 609–623.
(309) Eldridge, M. D.; Murray, C. W.; Auton, T. R.; Paolini, G. V; Mee, R. P. *J. Comput. Aided Mol. Des.* **1997**, *11*, 425–445.
(310) Salonen, L. M.; Bucher, C.; Banner, D. W.; Haap, W.; Mary, J. L.; Benz, J.; Kuster, O.; Seiler, P.; Schweizer, W. B.; Diederich, F. *Angew. Chem. Int. Ed. Engl.* **2009**, *48*, 811–814.
(311) Ma, J. C.; Dougherty, D. A. *Chem. Rev.* **1997**, *97*, 1303–1324.
(312) Jesús Ezquerra; Ezquerra, J.; Pedregal, C.; Lamas, C.; Barluenga, J.; Pérez, M.; García-Martín, M. A.; González, J. M. *J. Org. Chem.* **1996**, *61*, 5804–5812.
(313) Pelkey, E.; Gribble, G. *Synthesis (Stuttg).* **1999**, *7*, 1117–1122.
(314) Roy, S. S.; Gribble, G. W. *Tetrahedron Lett.* **2008**, *49*, 1531–1533.
(315) Çalimsiz, S.; Organ, M. G. *Chem. Commun. (Camb)* **2011**, *47*, 5181–5183.
(316) Han, C.; Buchwald, S. L. *J. Am. Chem. Soc.* **2009**, *131*, 7532–7533.
(317) Tamao, K.; Kiso, Y.; Sumitani, K.; Kumada, M. *J. Am. Chem. Soc.* **1972**, *94*, 9268–9269.
(318) Hayashi, T.; Konishi, M.; Kobori, Y.; Kumada, M.; Higuchi, T.; Hirotsu, K. *J. Am. Chem. Soc.* **1984**, *106*, 158–163.
(319) Dreher, S. D.; Dormer, P. G.; Sandrock, D. L.; Molander, G. A. *J. Am. Chem. Soc.* **2008**, *130*, 9257–9259.
(320) Joshi-Pangu, A.; Ganesh, M.; Biscoe, M. R. *Org. Lett.* **2011**, *13*, 1218–1221.

(321) Zhang, F.; Zhao, Y.; Sun, L.; Ding, L.; Gu, Y.; Gong, P. *Eur. J. Med. Chem.* **2011**, *46*, 3149–3157.
(322) Ray, S.; Patra, A.; Mal, D. *Tetrahedron* **2008**, *64*, 3253–3267.
(323) Nakamura, K.; Inoue, K.; Ushio, K.; Oka, S.; Ohno, A. *J. Org. Chem.* **1988**, *53*, 2589–2593.
(324) Roznyatovskiy, V.; Lynch, V.; Sessler, J. L. *Org. Lett.* **2010**, *12*, 4424–4427.
(325) Macarron, R.; Banks, M. N.; Bojanic, D.; Burns, D. J.; Cirovic, D. A.; Garyantes, T.; Green, D. V. S.; Hertzberg, R. P.; Janzen, W. P.; Paslay, J. W.; Schopfer, U.; Sittampalam, G. S. *Nat. Rev. Drug Discov.* **2011**, *10*, 188–195.
(326) Mayr, L. M.; Fuerst, P. *J. Biomol. Screen.* **2008**, *13* , 443–448.
(327) Liu, B.; Li, S.; Hu, J. *Am. J. Pharmacogenomics* **2004**, *4*, 263–276.
(328) Cesa, L. C.; Patury, S.; Komiyama, T.; Ahmad, A.; Zuiderweg, E. R. P.; Gestwicki, J. E. *ACS Chem. Biol.* **2013**, *8*, 1988–1997.
(329) Heeres, J. T.; Hergenrother, P. J. *Chem. Soc. Rev.* **2011**, *40*, 4398–4410.
(330) Lokey, R. S. *Curr. Opin. Chem. Biol.* **2003**, *7*, 91–96.
(331) Choi, H.; Kim, J.-Y.; Chang, Y.; Nam, H. In *Arabidopsis Protocols SE - 21*; Sanchez-Serrano, J. J.; Salinas, J., Eds.; Methods in Molecular Biology; Humana Press, 2014; Vol. 1062, pp. 393–404.
(332) Haggarty, S. J.; Schreiber, S. L. In *Chemical Biology*; Wiley-VCH Verlag GmbH, 2008; pp. 299–354.
(333) Das, R. K.; Samanta, A.; Ghosh, K.; Zhai, D.; Xu, W.; Su, D.; Leong, C.; Young-Tae, C. *Interdiscip. Bio Cent.* **2011**, *3*, 1–18.
(334) Ares, J.; Durán-Peña, M[a]j.; Hernández-Galán, R.; Collado, I. *Phytochem. Rev.* **2013**, *12*, 895–914.
(335) McCarthy, A. R.; Hollick, J. J.; Westwood, N. J. *Semin. Cancer Biol.* **2010**, *20*, 40–45.
(336) Berkson, R. G.; Hollick, J. J.; Westwood, N. J.; Woods, J. A.; Lane, D. P.; Lain, S. *Int. J. Cancer* **2005**, *115*, 701–710.
(337) Lain, S.; Hollick, J. J.; Campbell, J.; Staples, O. D.; Higgins, M.; Aoubala, M.; McCarthy, A.; Appleyard, V.; Murray, K. E.; Baker, L.; Thompson, A.; Mathers, J.; Holland, S. J.; Stark, M. J. R.; Pass, G.; Woods, J.; Lane, D. P.; Westwood, N. J. *Cancer Cell* **2008**, *13*, 454–463.
(338) Soussi, T. *EMBO Rep.* **2010**, *11*, 822–826.
(339) Lane, D. P. *Nature* **1992**, *358*, 15–16.
(340) Vogelstein, B.; Lane, D.; Levine, A. J. *Nature* **2000**, *408*, 307–310.
(341) Vousden, K. H.; Prives, C. *Cell* **2009**, *137*, 413–431.
(342) Zilfou, J. T.; Lowe, S. W. *Cold Spring Harb. Perspect. Biol.* **2009**, *1*, a001883.
(343) Marine, J. C.; Dyer, M. A.; Jochemsen, A. G. *J. Cell Sci.* **2007**, *120*, 371–378.
(344) Haupt, Y.; Maya, R.; Kazaz, A.; Oren, M. *Nature* **1997**, *387*, 296–299.
(345) Brooks, C. L.; Gu, W. *Mol. Cell* **2006**, *21*, 307–315.
(346) Brown, C. J.; Lain, S.; Verma, C. S.; Fersht, A. R.; Lane, D. P. *Nat. Rev. Cancer* **2009**, *9*, 862–873.
(347) Shangary, S.; Wang, S. *Annu. Rev. Pharmacol. Toxicol.* **2009**, *49*, 223–241.
(348) Wade, M.; Li, Y.-C.; Wahl, G. M. *Nat. Rev. Cancer* **2013**, *13*, 83–96.
(349) Khosravi, R.; Maya, R.; Gottlieb, T.; Oren, M.; Shiloh, Y.; Shkedy, D. *Proc. Natl. Acad. Sci. U S A* **1999**, *96*, 14973–14977.
(350) Vassilev, L. T.; Vu, B. T.; Graves, B.; Carvajal, D.; Podlaski, F.; Filipovic, Z.; Kong, N.; Kammlott, U.; Lukacs, C.; Klein, C.; Fotouhi, N.; Liu, E. A. *Science* **2004**, *303*, 844–848.
(351) Nigro, J. M.; Baker, S. J.; Preisinger, A. C.; Jessup, J. M.; Hostetter, R.; Cleary, K.; Bigner, S. H.; Davidson, N.; Baylin, S.; Devilee, P.; et al. *Nature* **1989**, *342*, 705–708.
(352) Hollstein, M.; Sidransky, D.; Vogelstein, B.; Harris, C. C. *Science* **1991**, *253*, 49–53.
(353) Lain, S.; Lane, D. *Eur. J. Cancer.* **2003**, *39*, 1053–1060.
(354) Muller, P. Y.; Milton, M. N. *Nat. Rev. Drug Discov.* **2012**, *11*, 751–761.
(355) Ma, Q.; Lu, A. Y. *Pharmacol. Rev.* **2011**, *63*, 437–459.
(356) Claramunt, R. M.; López, C.; Pérez-Medina, C.; Pinilla, E.; Torres, M. R.; Elguero, J. *Tetrahedron* **2006**, *62*, 11704–11713.

(357) Hoefle, M. L.; Short, F. Antiinflammatory 1-phenyl-1H-indazole-4-acetic acids. US 3657270 A, 1972.
(358) Tanuwidjaja, J.; Peltier, H. M.; Ellman, J. A. *J. Org. Chem.* **2007**, *72*, 626–629.
(359) Borg, G.; Cogan, D. A.; Ellman, J. A. *Tetrahedron Lett.* **1999**, *40*, 6709–6712.
(360) Weber, J. D. *Genes Dev.* **2000**, *14*, 2358–2365.
(361) Bai, Y.; Lu, Z.; Lin, Y.; Sun, B. *Oncol. Res. Featur. Preclin. Clin. Cancer Ther.* **2013**, *21*, 23–1.
(362) Williams, R. T.; Sherr, C. J. *Cold Spring Harb. Symp. Quant. Biol.* **2008**, *73* , 461–467.

Appendix A: The 31 hits selected for testing in the reptin-AGR2 peptide binding assay (Chapter 2).

Visual analysis of the top 100 hits identified the presence of 15 different groups of compounds. Groups 1-13 were classified based on a similar structural core. 1-3 analogues were purchased from each group for testing depending on the size and structural diversity of the group. Group 14 contained the remaining analogues that did not contain a common structural core, of which 7 were purchased for testing.

Group 1	Group 2	Group 3	Group 4	Group 5
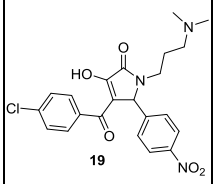 19	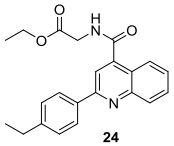 24	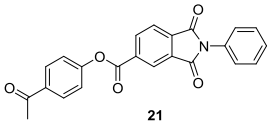 21	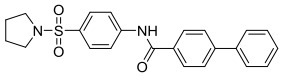 14	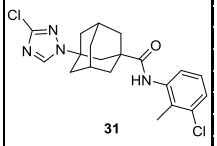 31
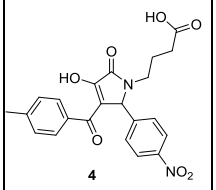 4	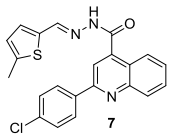 7	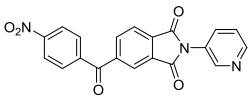 5	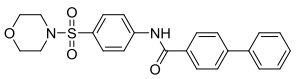 20	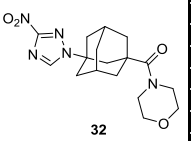 32
Group 6	**Group 7**	**Group 8**	**Group 9**	
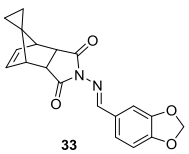 33	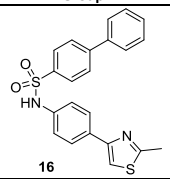 16	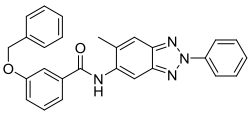 15	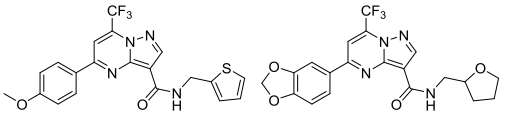 3 13	
Group 10	**Group 11**	**Group 12**	**Group 15 (singular)**	
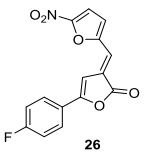 26	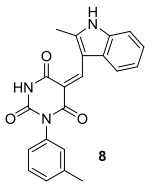 8	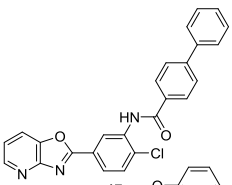 17	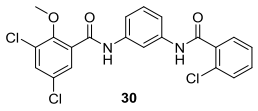 30	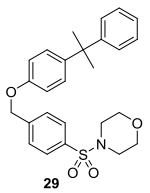 29
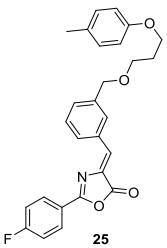 25	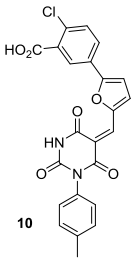 10	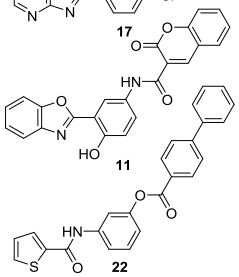 11 22	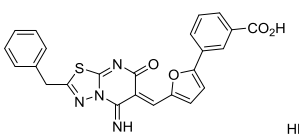 18	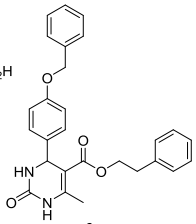 6
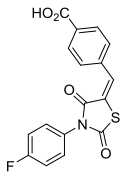 12	**Group 13**	**Group 14**	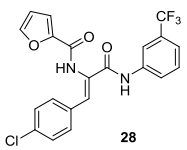 28	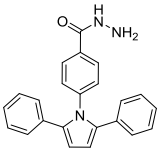 9
	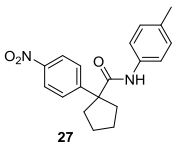 27	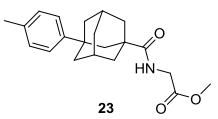 23		

Appendix B: ^{1}H NMR spectra provided for the purchased analogues of hits 17 and 13 (Chapter 2).

^{1}H NMR spectra provided by Chembridge.

Compound **37**:

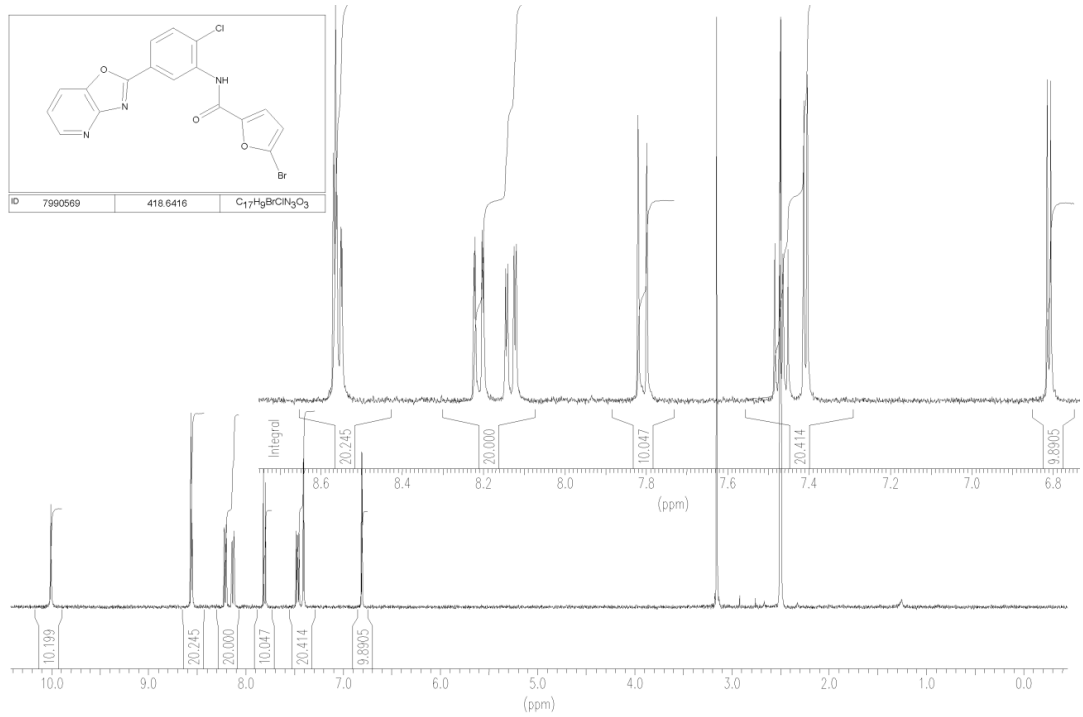

Compound **38**:

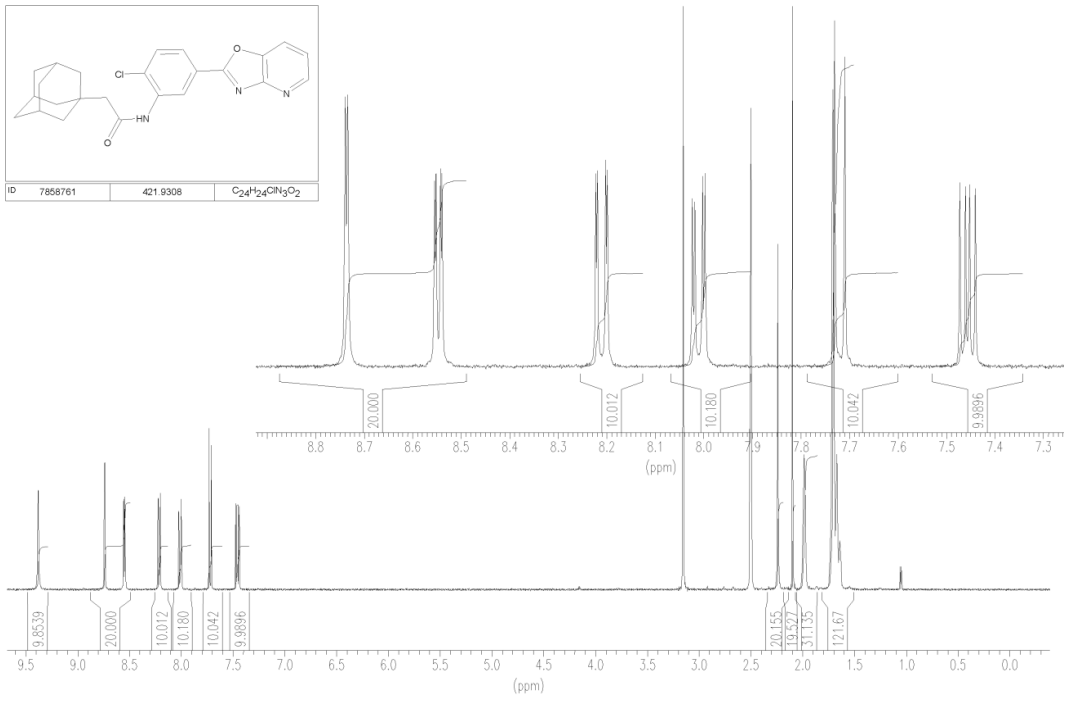

Compound **39**:

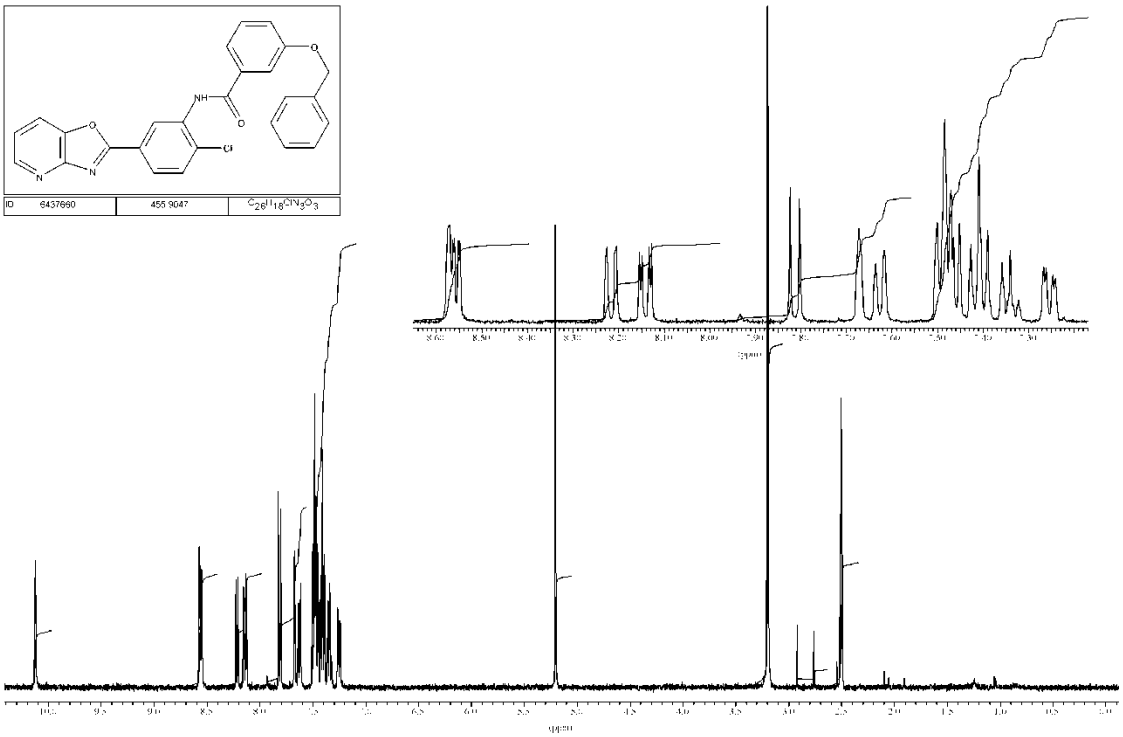

Compound **40**:

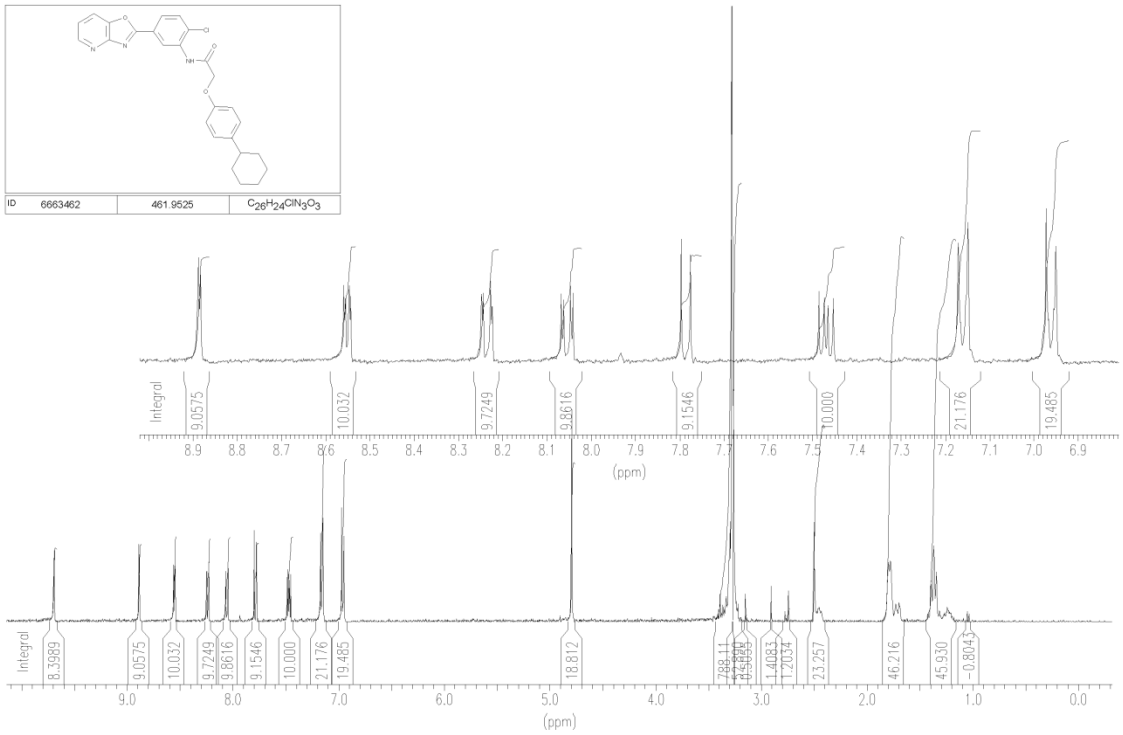

Compound **41**:

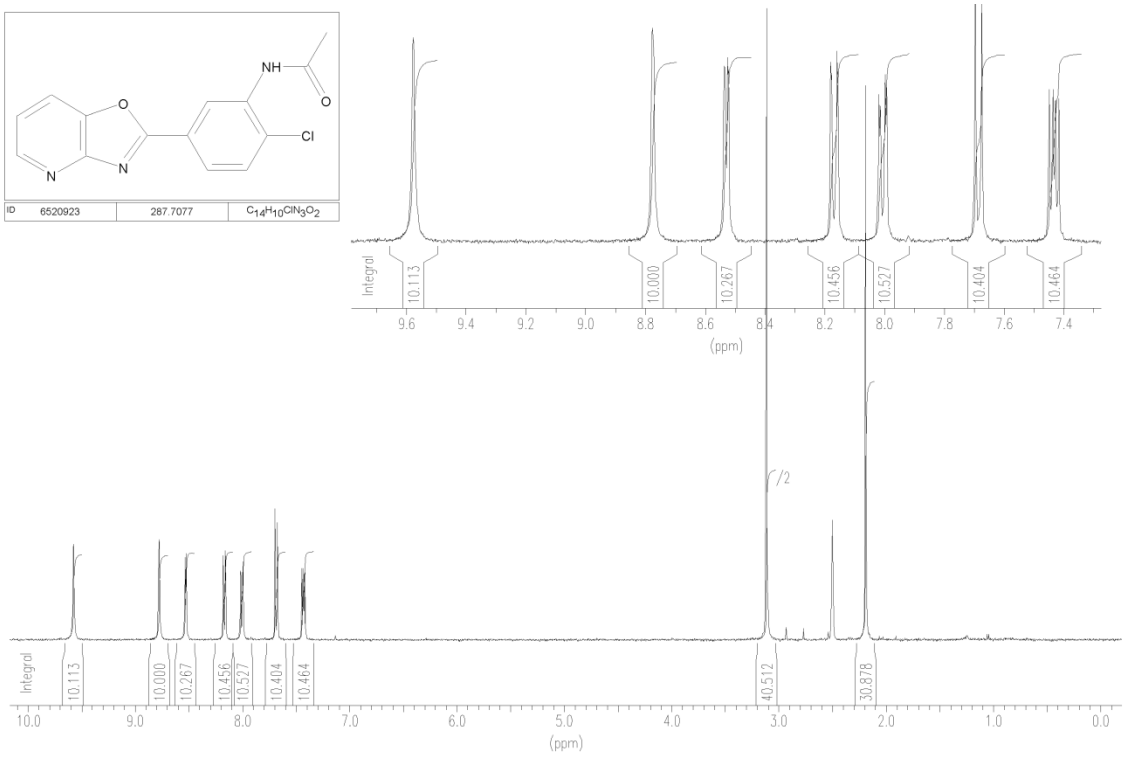

Compound **3**:

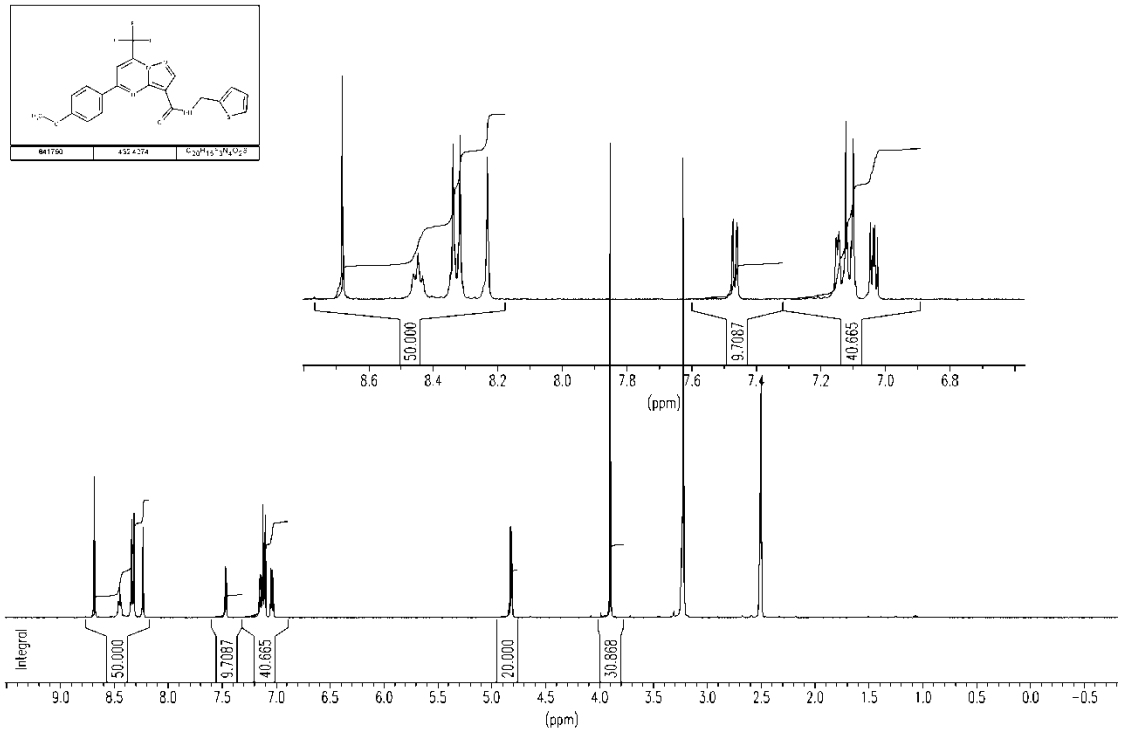

Compound **61**:

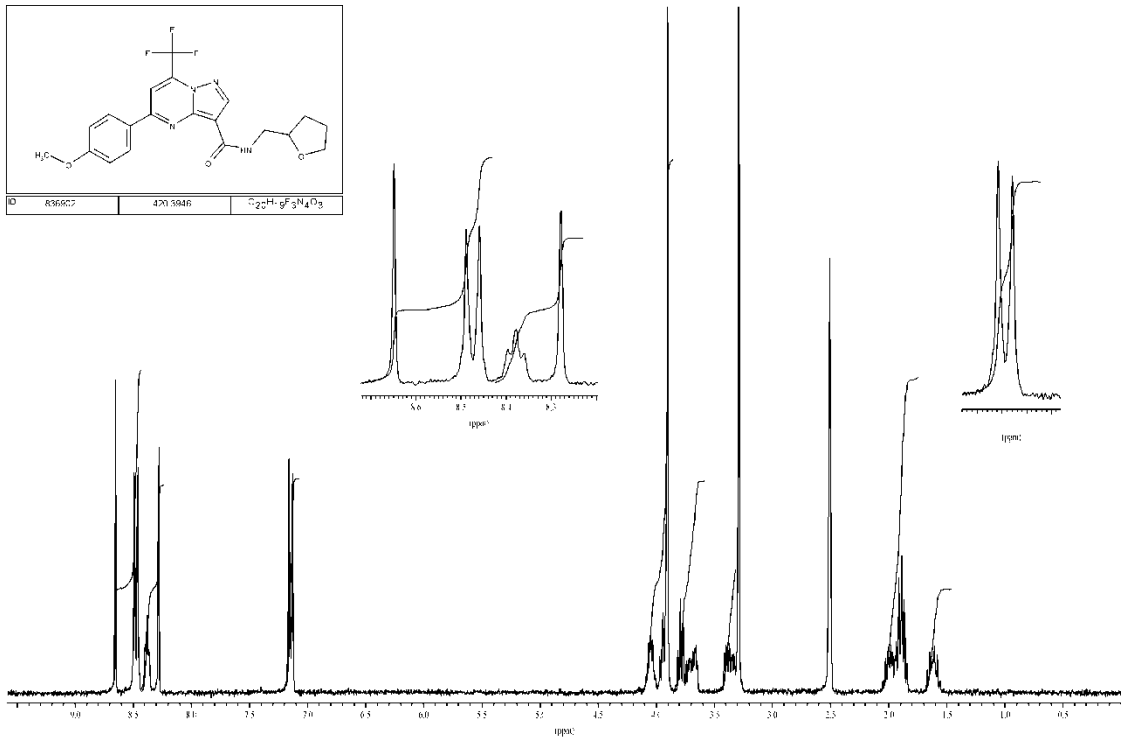

Compound **62**:

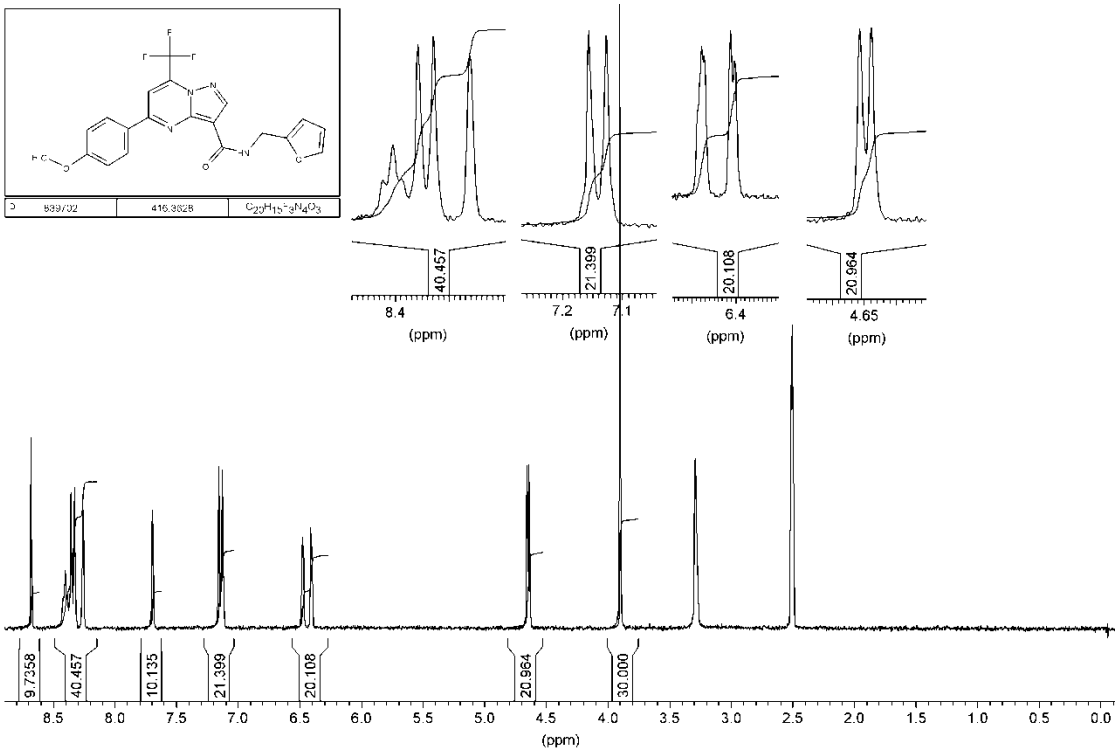

Appendix C: ^{1}H and ^{13}C NMR spectra of (*R*,*R*)-Harzianic acid (19) in $CDCl_3$ and MeOD (Chapter 3)

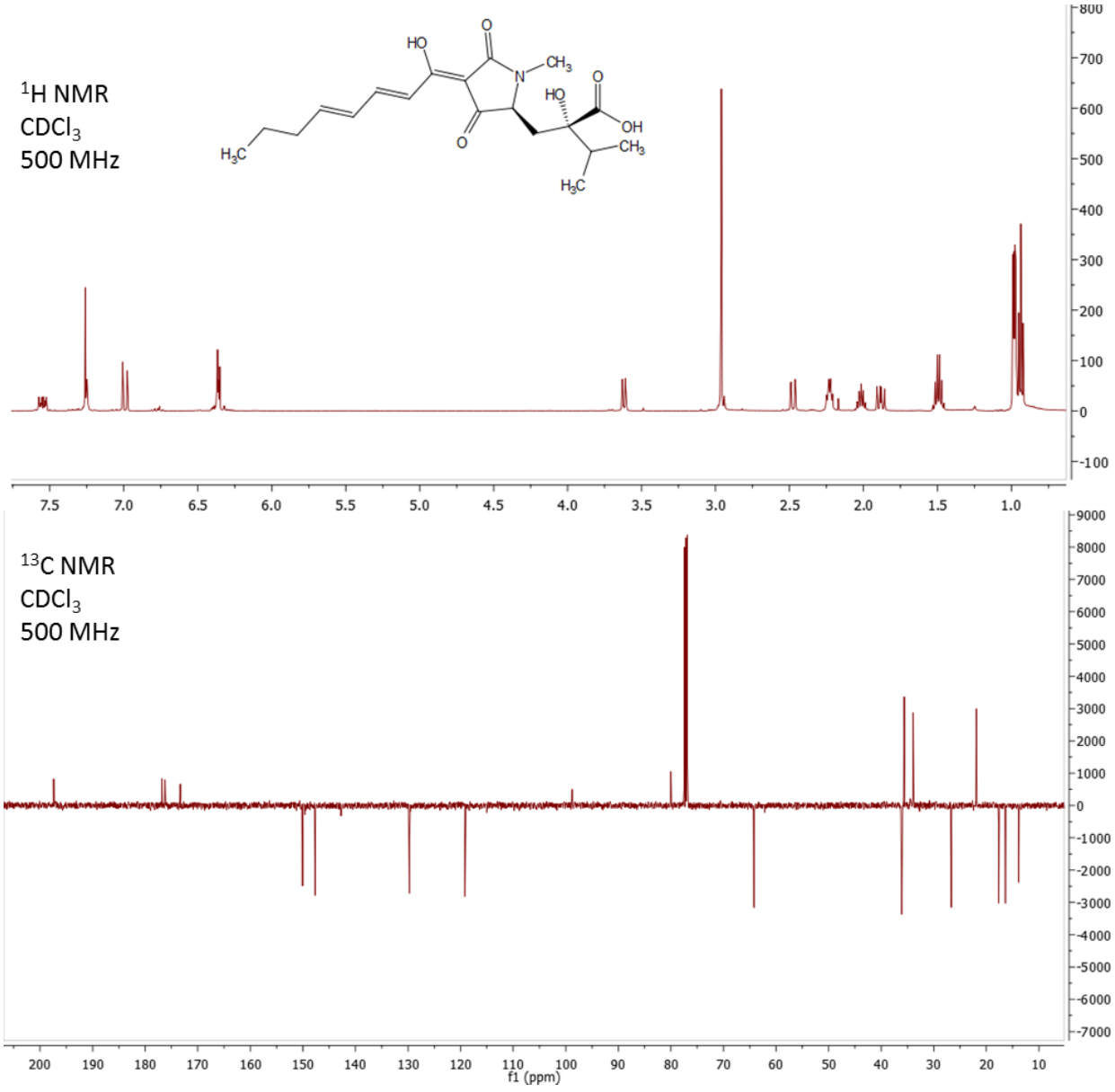

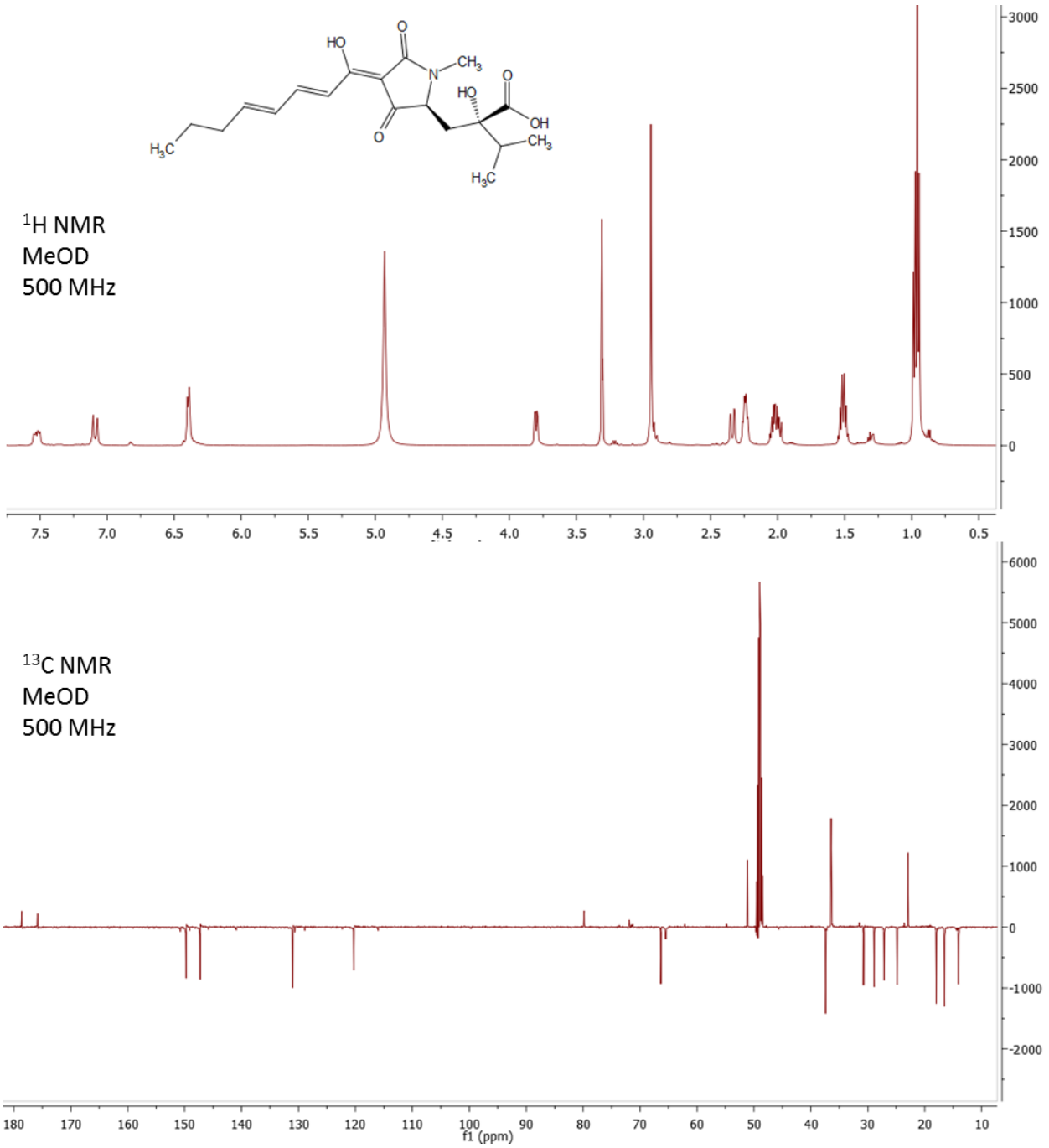
HO
O
N
CH3
O
HO
OH
CH3
H3C
O
H3C
1H NMR
MeOD
500 MHz
3000
2500
2000
1500
1000
500
0
7.5
7.0
6.5
6.0
5.5
5.0
4.5
4.0
3.5
3.0
2.5
2.0
1.5
1.0
0.5
13C NMR
MeOD
500 MHz
6000
5000
4000
3000
2000
1000
0
-1000
-2000
180
170
160
150
140
130
120
110
100
90
80
70
60
50
40
30
20
10
f1 (ppm)

Appendix D: ^{1}H and ^{13}C NMR spectra of (*S*,*R*)-5'*epi*Harzianic acid (19b) in $CDCl_3$ and MeOD (Chapter 3)

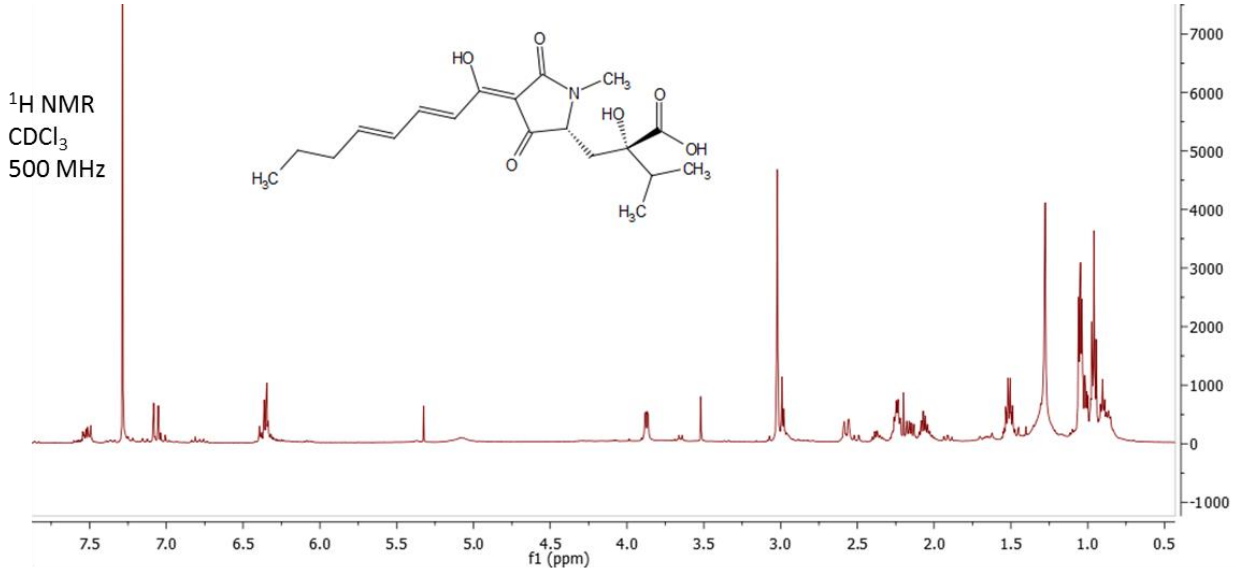

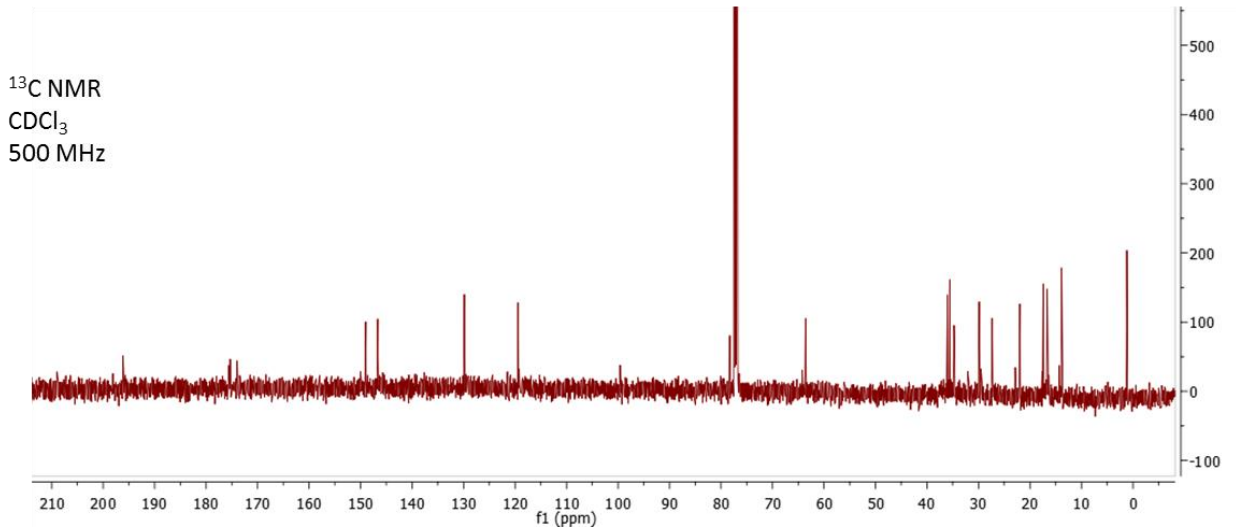

^{1}H NMR
MeOD
500 MHz

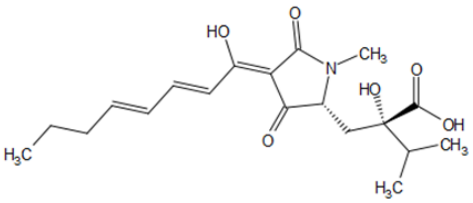

^{13}C NMR
MeOD
500 MHz

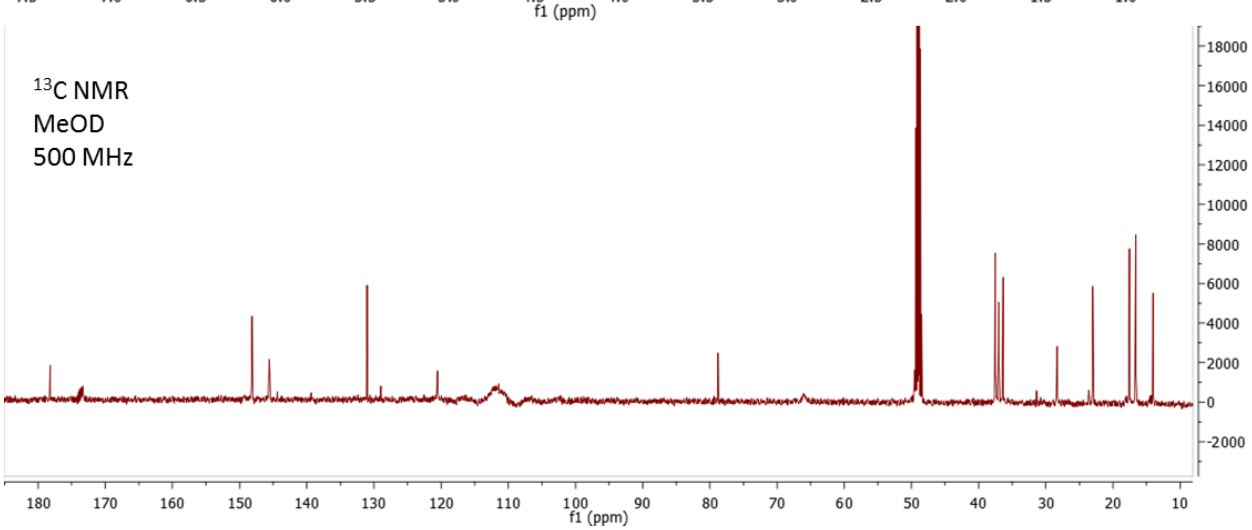

Appendix E: NOE analysis, ^{1}H and COSY NMR spectras of (±)-68 (Chapter 3)

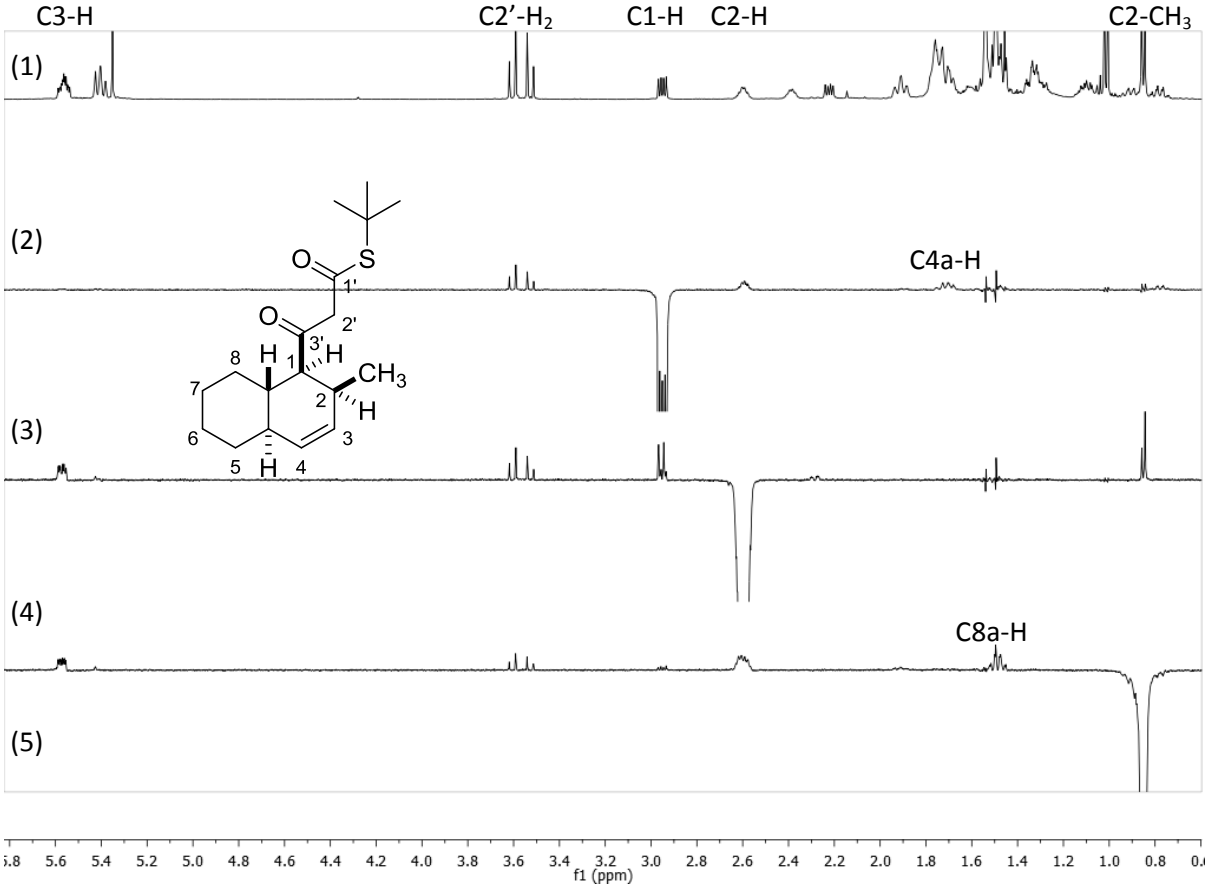

(1) In $CDCl_3$ at room temperature the (±)-**68** exists as a (3 : 1) *keto* : *enol* mixture. NOE analysis of the major *keto* tautomer is shown. (2) An NOE was observed between C1-H and C2'-H_2, C2-H and C4a-H, demonstrating C1-H, C2-H and C4a-H are cofacial. (3) An NOE was observed between C2-H and C1-H, C2'-H_2, C2-CH_3 and C3-H, confirming the presence of C1-H and C2-H on the same face of the decalin ring. (4) An NOE was observed between C2-CH_3 and C2-H, C2'-H_2, C8a-H and C3-H, demonstrating C2-CH_3 and C8a-H are cofacial. The NOE analysis confirms the formation of the predicted *endo*-diastereomer of (±)-**68**. Relative stereochemistry of (±)-**68** is shown.

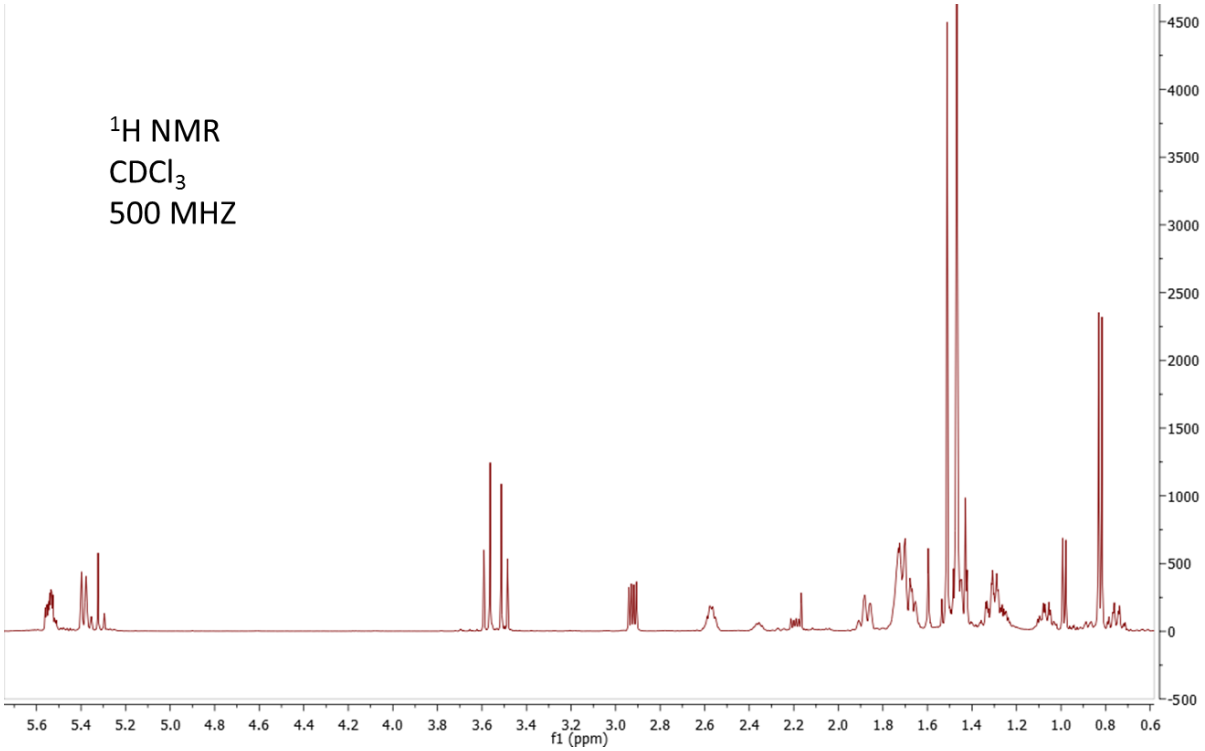

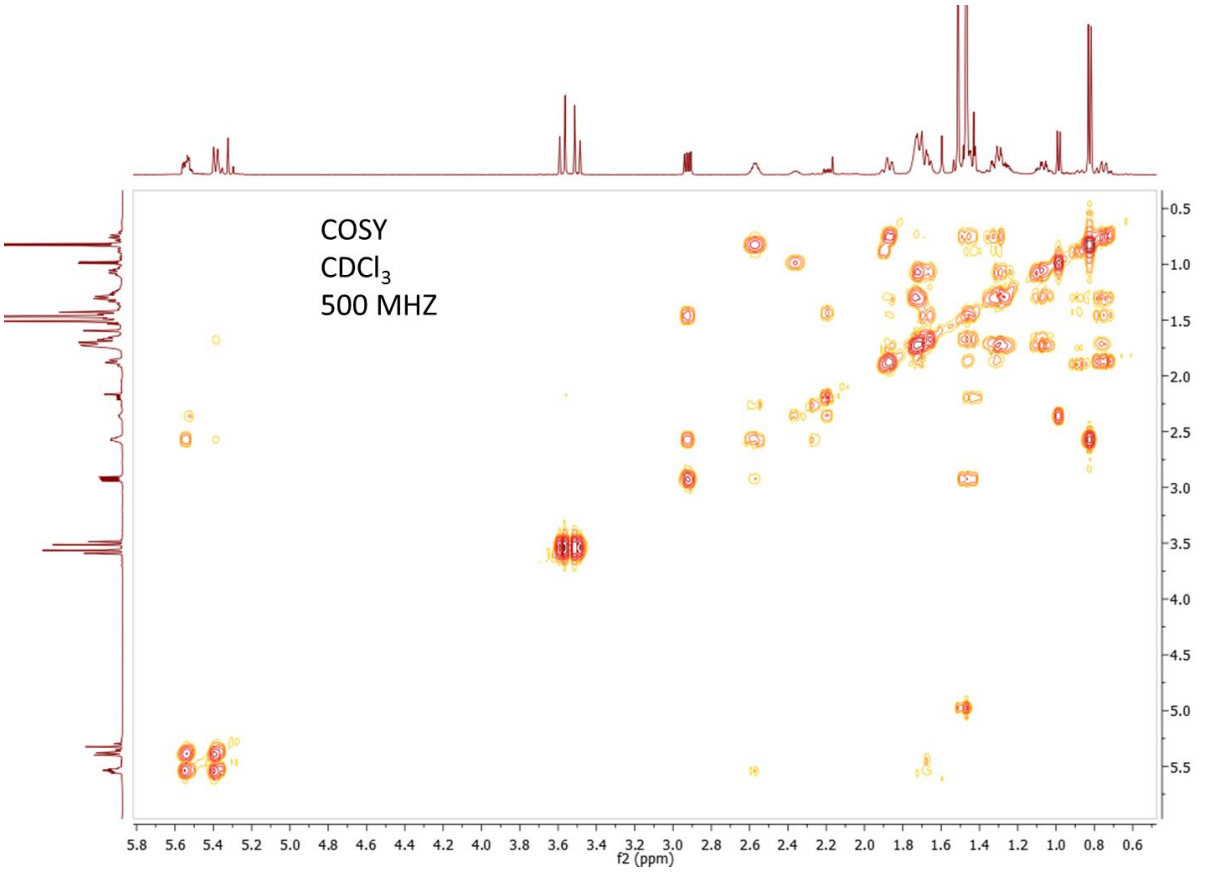

m.

Appendix F: ^{1}H and ^{13}C NMR spectra of JBIR-22 diastereomeric mixture 4a/b (Chapter 3)

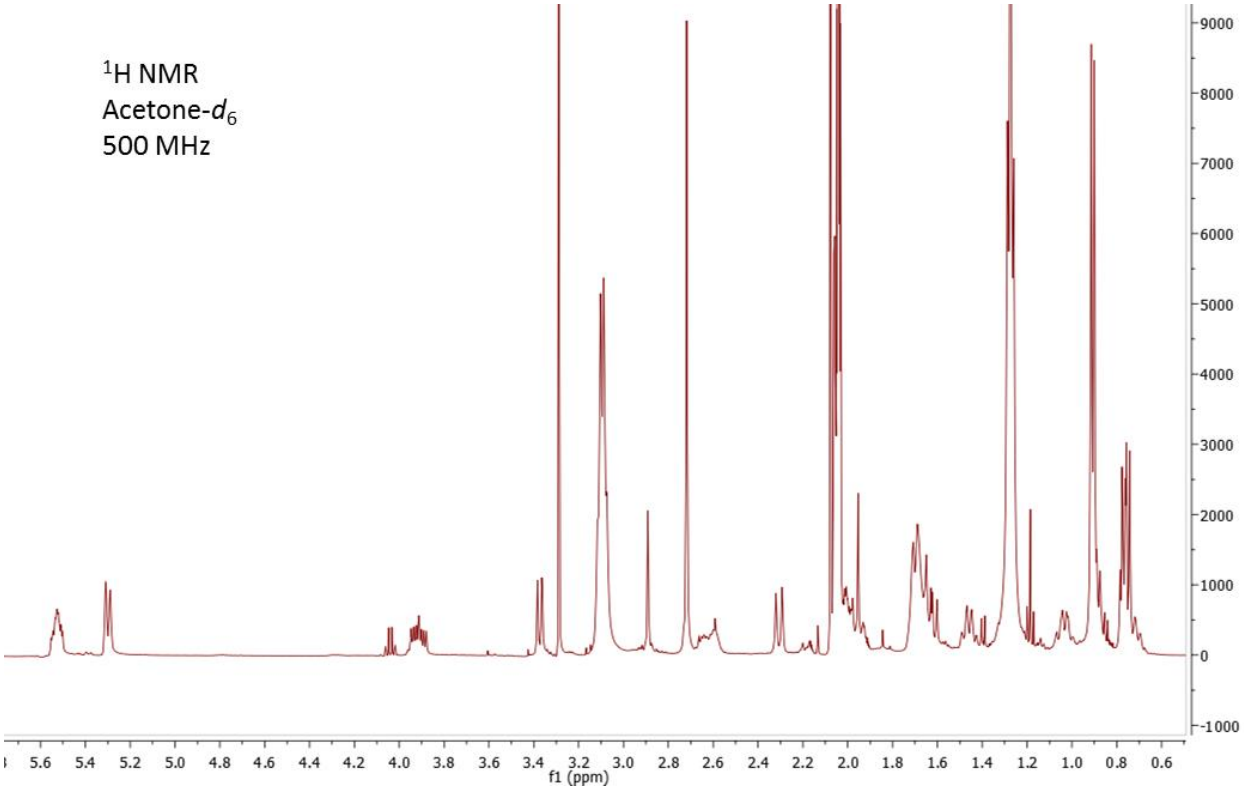

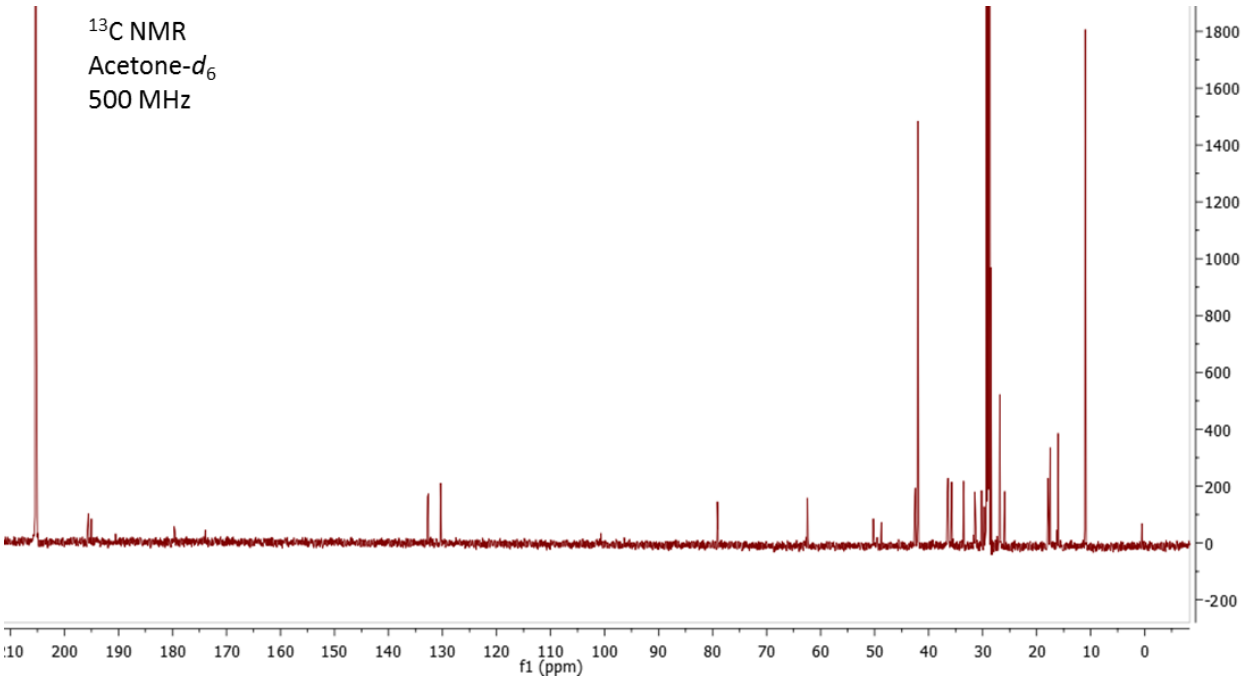

Appendix G: Full GC chromatograms of (±)-90, 90a and 90b (Chapter 3)

Full GC traces of (±)-**90**, **90a** and **90b**. GC analyses were obtained on a Shimadzu GC consisting of a Shimadzu AOC-20i auto injector and a Shimadzu GC-2025 gas chromatograph. Analysis was performed using Shimadzu GCsolution v2.41 software and separation was achieved using an Agilent Cyclosil-B column. The minor diastereomers of **90a** and **90b** can be observed with retention times between 20-22 minutes.

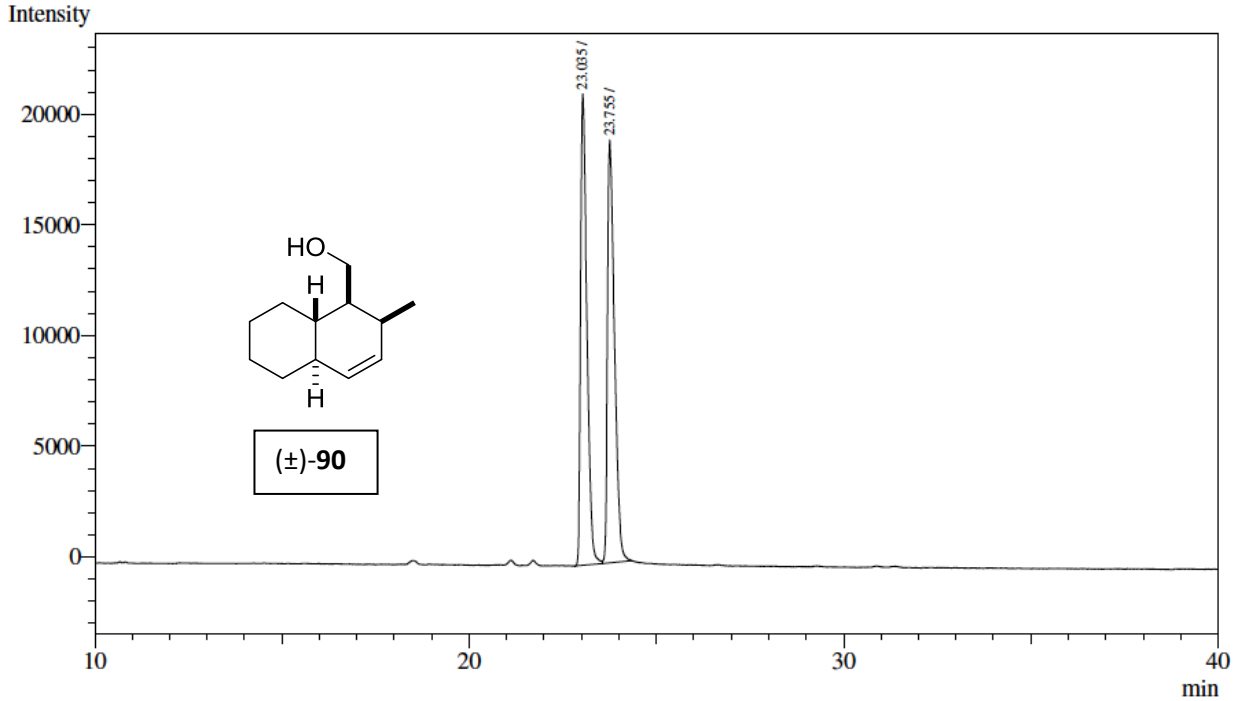

Peak#	Ret.Time	Area	Area%
1	23.035	247722	50.0871
2	23.755	246861	49.9129
Total		494583	100.0000

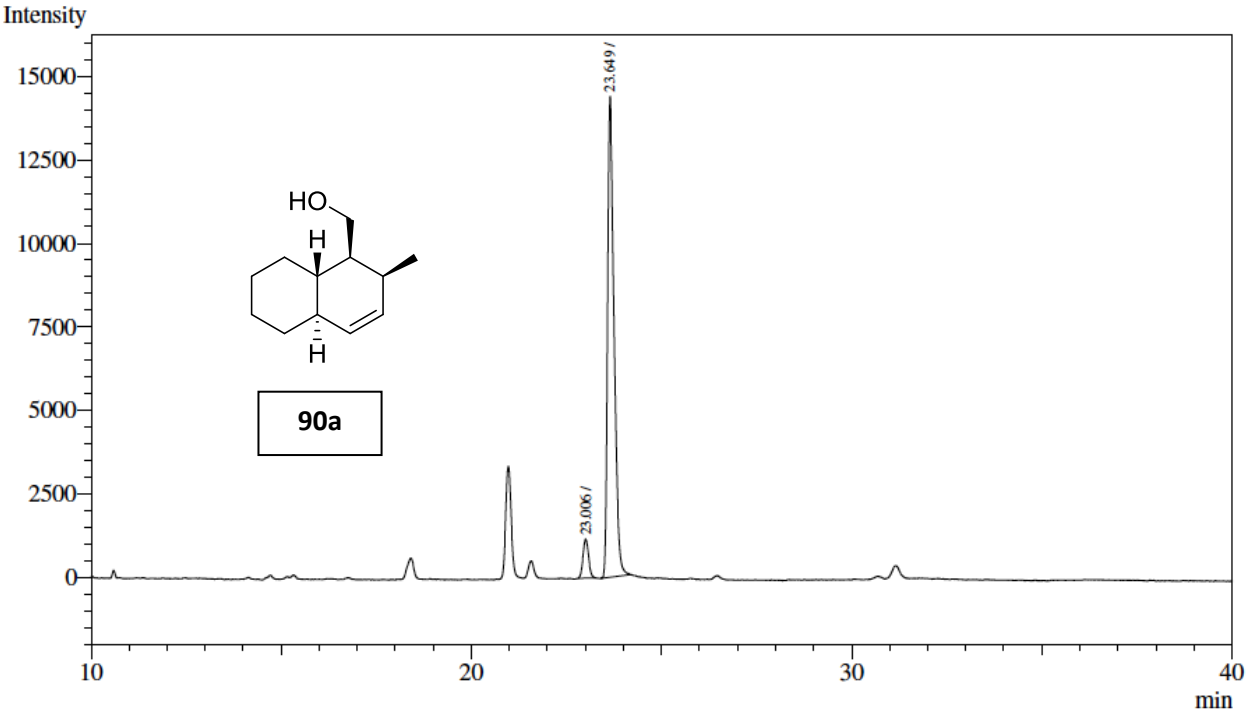

Peak#	Ret.Time	Area	Area%
1	23.006	11848	6.5768
2	23.649	168304	93.4232
Total		180152	100.0000

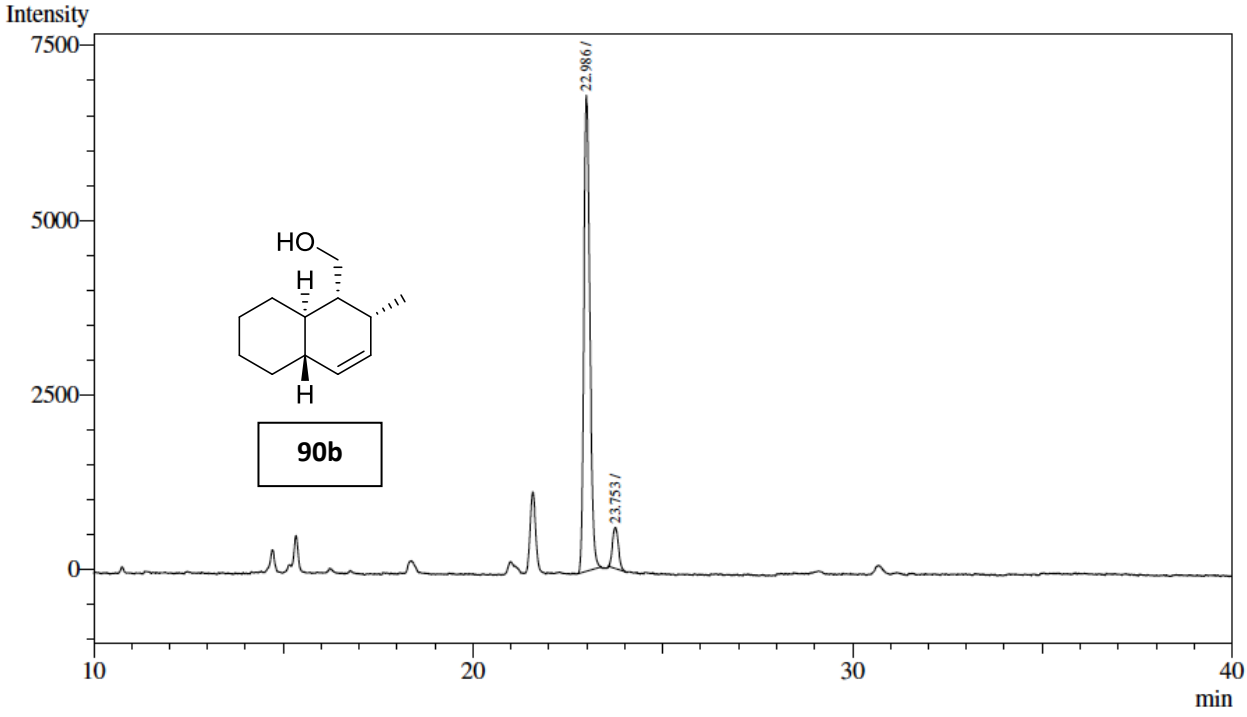

Peak#	Ret.Time	Area	Area%
1	22.986	74556	92.1743
2	23.753	6330	7.8257
Total		80886	100.0000

Appendix H: ^{1}H and ^{13}C NMR spectra of 4a and 4b (Chapter 3)

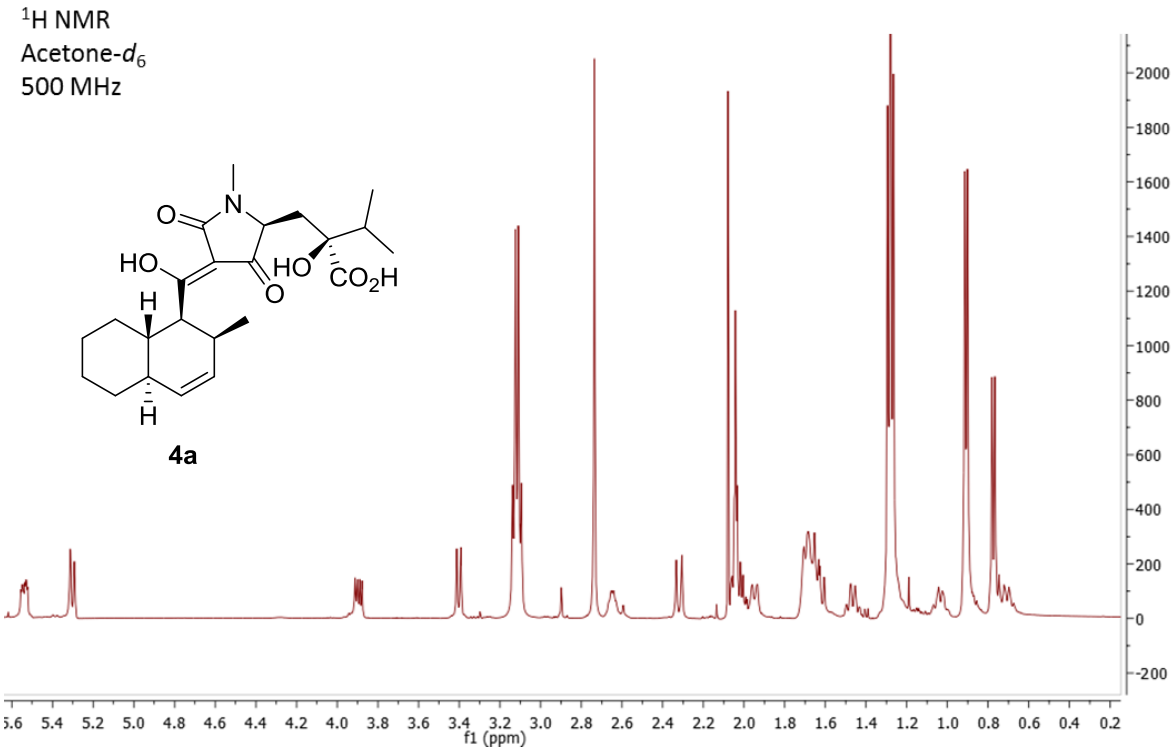

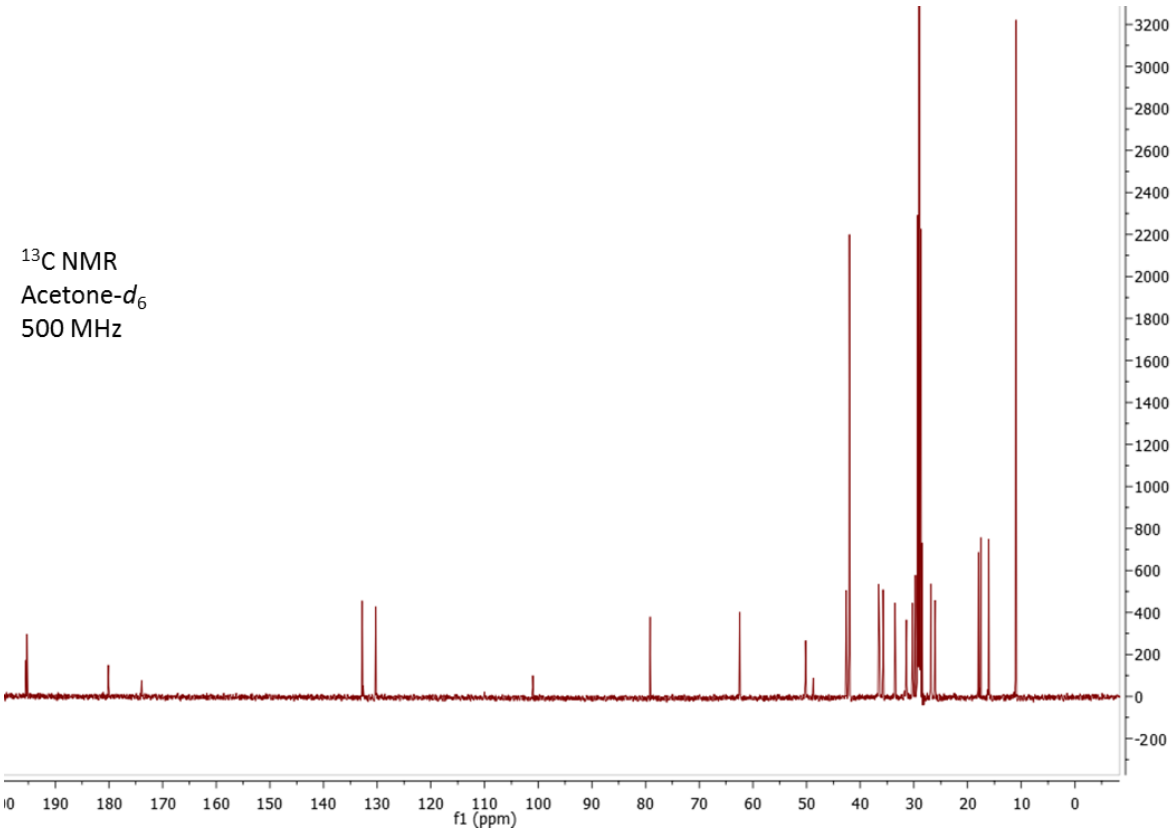

^{1}H NMR
Acetone-d_6
500 MHz

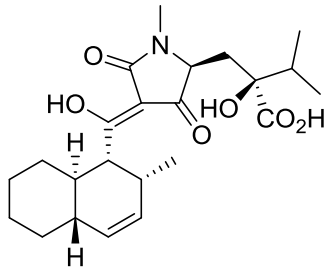

4b

^{13}C NMR
Acetone-d_6
500 MHz

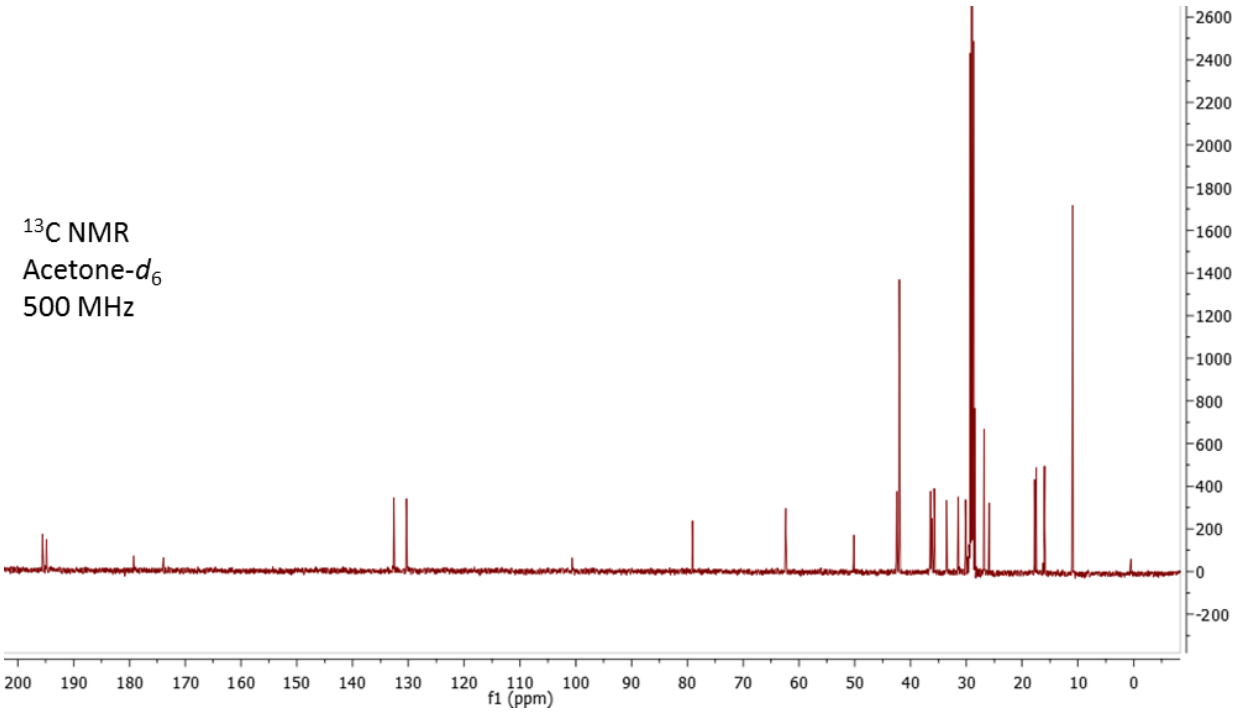

Appendix I: ^{1}H NMR spectrum of a sample of the isolated JBIR-22 (4) (Chapter 3)

^{1}H NMR spectrum of an authentic sample (~0.5 mg) of JBIR-22 (**4**) obtained from Dr Kazuo Shin-ya, National Institute of Advanced Industrial Science (AIST), Japan. Spectrum was obtained in acetone-d_6 using a 1.75 mm probe.

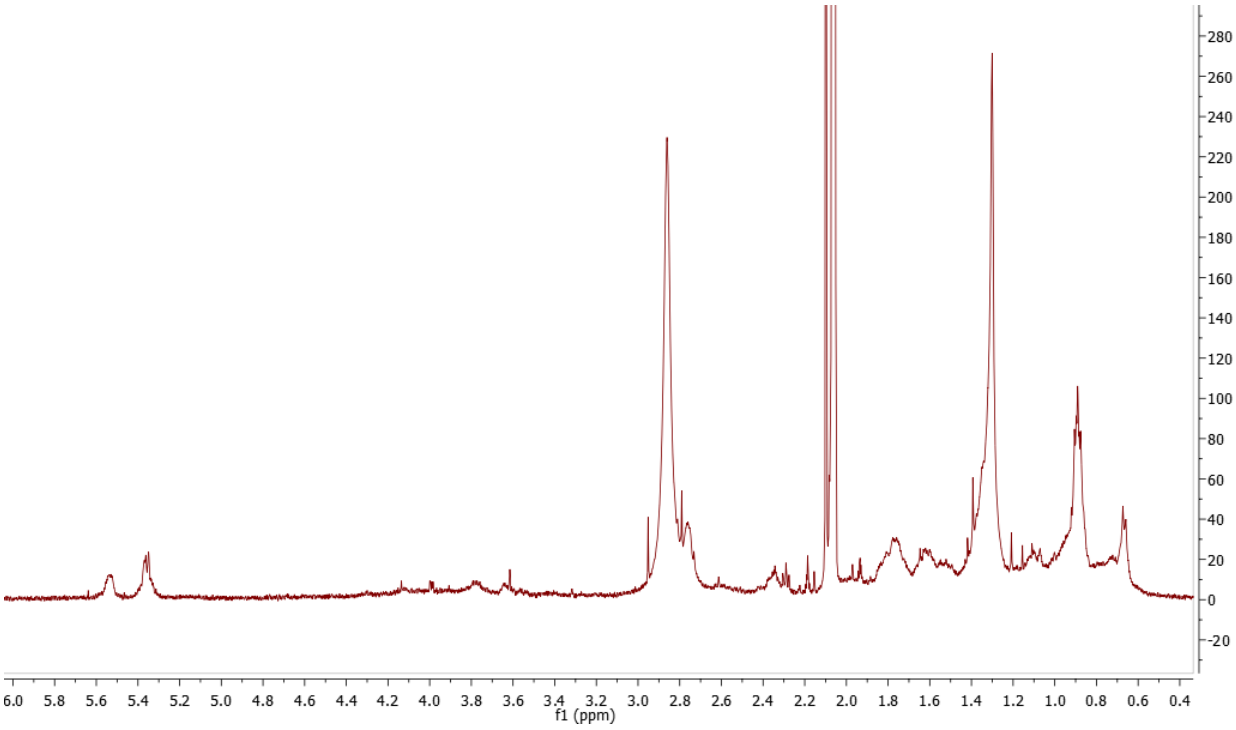

Appendix J: NMR spectra of the product resulting from the achiral catalysed cycloaddition of 65 (Chapter 3)

^{1}H NMR spectrum of the crude reaction mixture of the IMDA cycloaddition of **65**.

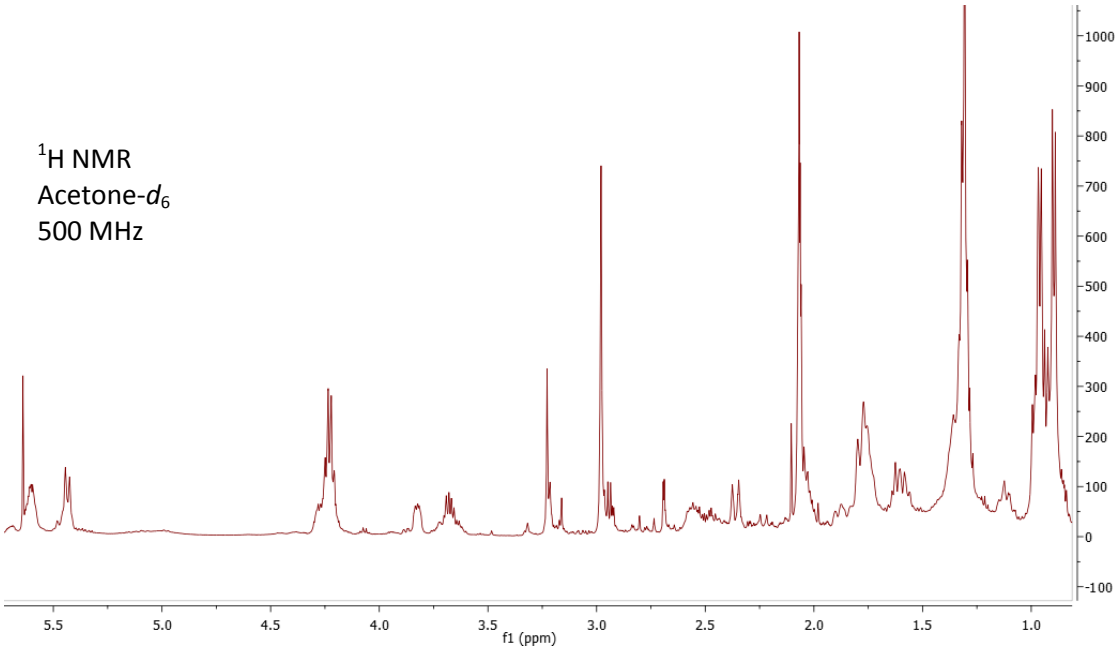

^{13}C NMR spectrum of crude reaction mixture in acetone-d_6. Two sections of the NMR spectrum are magnified to highlight the characteristic doubling of the carbon signals resulting from the formation of a mixture of diastereomers (**77a**/**b**).

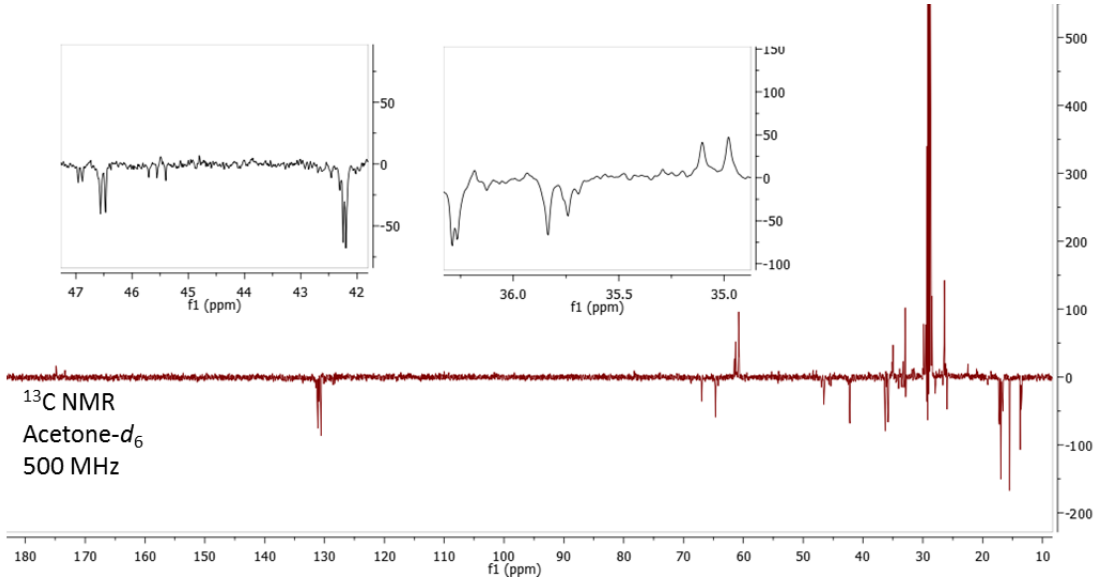

Appendix K: GoldScore of a selection of the docked PICK1 series 1 inhibitors (Chapter 4)

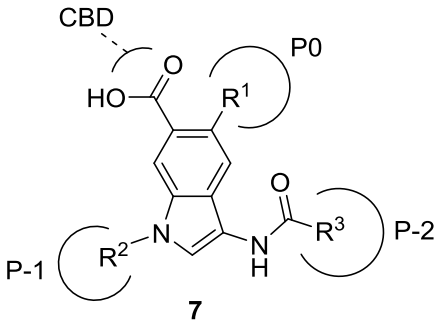

7

No.	R^1	R^2	R^3	GoldScore
1	methyl	ethylbenzene	ethyl	57.86
2	*sec*-butyl	ethylbenzene	propyl	57.75
3	2-methylpentane	ethylbenzene	ethyl	57.73
4	*sec*-butyl	ethylbenzene	cyclopropyl	57.74
5	*iso*-propyl	ethylbenzene	*iso*-butyl	58.79
6	methyl	*n*-butyl	ethylbenzene	58.18
7	*iso*-propyl	*n*-butyl	ethyl	54.95
8	methyl	*n*-butyl	benzyl	52.38
9	*iso*-propyl	*n*-butyl	*iso*-butyl	56.72
10	methyl	*iso*-butyl	ethylbenzene	55.17
11	*iso*-propyl	*iso*-butyl	*iso*-propyl	54.82
12	*iso*-propyl	*iso*-butyl	ethyl	53.97
13	methyl	*iso*-butyl	*iso*-butyl	48.68
14	methyl	*iso*-propyl	benzyl	48.32
15	*iso*-propyl	*iso*-propyl	ethyl	48.64
16	*iso*-propyl	*iso*-propyl	*iso*-propyl	49.57
17	methyl	benzyl	*iso*-propyl	50.31
18	*iso*-propyl	benzyl	ethyl	55.55
19	*iso*-propyl	benzyl	*iso*-butyl	56.65
20	methyl	ethyl	phenyl	49.72
21	*iso*-propyl	ethyl	ethyl	51.53
22	*iso*-propyl	ethyl	benzyl	58.92
23	*iso*-propyl	*N*,*N*-dimethylethylamine	ethylbenzene	62.74
24	*iso*-propyl	*N*,*N*-dimethylethylamine	ethyl	53.69
25	*iso*-propyl	*N*,*N*-dimethylethylamine	*iso*-butyl	57.67

A selection of the compounds docked into the PDZ domain of the X-ray crystal structure of PICK1 [PDB: 3HPK] after extraction of the GluR2 (-EVKI) ligand. Only compounds which docked in the PICK1 PDZ domain and mimicked the pose of the natural peptide (-VKI) are reported.

Appendix L: Crystal Data and Structural Refinement of Small Molecule X-ray of 46 (Chapter 3)

Empirical Formula	$C_{14}H_{23}NO_5S$
Formula Weight	317.40
Crystal Color, Habit	colorless, prism
Crystal Dimensions	0.120 X 0.050 X 0.050 mm
Crystal System	orthorhombic
Lattice Type	Primitive
Lattice Parameters	a = 5.5980(11) Å
	b = 15.959(4) Å
	c = 18.735(4) Å
	V = 1673.8(6) $Å^3$
Space Group	$P2_12_12_1$ (#19)
Z value	4
D_{calc}	1.259 g/cm^3
F_{000}	680.00
μ(MoKα)	2.124 cm^{-1}
Diffractometer	XtaLAB P200
Radiation	MoKα (λ = 0.71075 Å)
	multi-layer mirror monochromated
Voltage, Current	45kV, 66mA
Temperature	-180.0°C
Detector Aperture	83.8 x 70.0 mm
Data Images	439 exposures
Pixel Size	0.172 mm
$2\theta_{max}$	50.7°
No. of Reflections Measured	Total: 7588
	Unique: 3006 (R_{int} = 0.0403)
	Parsons quotients (Flack x parameter): 935
Corrections	Lorentz-polarization
	Absorption

	(trans. factors: 0.733 - 0.989)
Structure Solution	Direct Methods (SIR2011)
Refinement	Full-matrix least-squares on F^2
Function Minimized	Σ w $(Fo^2 - Fc^2)^2$
Least Squares Weights	$w = 1/ [\sigma^2(Fo^2) + (0.0000 \cdot P)^2$ + 0.0000 · P] where $P = (Max(Fo^2,0) + 2Fc^2)/3$
$2\theta_{max}$ cutoff	50.7^o
Anomalous Dispersion	All non-hydrogen atoms
No. Observations (All reflections)	3006
No. Variables	194
Reflection/Parameter Ratio	15.49
Residuals: R1 (I>2.00σ(I))	0.0239
Residuals: R (All reflections)	0.0273
Residuals: wR2 (All reflections)	0.0547
Goodness of Fit Indicator	0.542
Flack parameter (Parsons' quotients = 935)	0.03(4)
Max Shift/Error in Final Cycle	0.001
Maximum peak in Final Diff. Map	$0.18\ e^-/Å^3$
Minimum peak in Final Diff. Map	$-0.19\ e^-/Å^3$

Appendix M: Crystal Data and Structural Refinement of Small Molecule X-ray of 91a (Chapter 3)

Empirical Formula	$C_{12}H_{18}O_2$
Formula Weight	194.27
Crystal Color, Habit	colorless, platelet
Crystal Dimensions	0.150 X 0.150 X 0.010 mm
Crystal System	tetragonal
Lattice Type	Primitive
Lattice Parameters	a = 7.8129(11) Å
	c = 35.798(6) Å
	V = 2185.2(6) $Å^3$
Space Group	$P4_32_12$ (#96)
Z value	8
D_{calc}	1.181 g/cm^3
F_{000}	848.00
μ(CuKα)	6.232 cm^{-1}
Diffractometer	XtaLAB P100
Radiation	CuKα (λ = 1.54187 Å)
	multi-layer mirror monochromated
Voltage, Current	40kV, 30mA
Temperature	-100.0°C
Detector Aperture	83.8 x 33.5 mm
Data Images	3983 exposures
Pixel Size	0.172 mm
$2\theta_{max}$	136.3°
No. of Reflections Measured	Total: 23076
	Unique: 2000 (R_{int} = 0.0544)
	Parsons quotients (Flack x parameter): 692
Corrections	Lorentz-polarization
	Absorption
	(trans. factors: 0.800 - 0.994)

Structure Solution	Direct Methods (SIR2011)
Refinement	Full-matrix least-squares on F^2
Function Minimized	$\Sigma\ w\ (Fo^2 - Fc^2)^2$
Least Squares Weights	$w = 1/ [\ \sigma^2(Fo^2) + (0.0725 \cdot P)^2$ $+ 0.0550 \cdot P\ ]$ where $P = (Max(Fo^2,0) + 2Fc^2)/3$
$2\theta_{max}$ cutoff	136.3^o
Anomalous Dispersion	All non-hydrogen atoms
No. Observations (All reflections)	2000
No. Variables	132
Reflection/Parameter Ratio	15.15
Residuals: R1 (I>2.00σ(I))	0.0373
Residuals: R (All reflections)	0.0387
Residuals: wR2 (All reflections)	0.1000
Goodness of Fit Indicator	1.085
Flack parameter (Parsons' quotients = 692)	-0.04(9)
Max Shift/Error in Final Cycle	0.000
Maximum peak in Final Diff. Map	$0.21\ e^-/Å^3$
Minimum peak in Final Diff. Map	$-0.20\ e^-/Å^3$

Appendix N: Crystal Data and Structural Refinement of Small Molecule X-ray of 91b (Chapter 3)

Empirical Formula	$C_{12}H_{18}O_2$
Formula Weight	194.27
Crystal Color, Habit	colorless, platelet
Crystal Dimensions	0.300 X 0.140 X 0.030 mm
Crystal System	tetragonal
Lattice Type	Primitive
Lattice Parameters	a = 7.8135(7) Å
	c = 35.790(4) Å
	V = 2185.0(4) $Å^3$
Space Group	$P4_12_12$ (#92)
Z value	8
D_{calc}	1.181 g/cm^3
F_{000}	848.00
μ(CuKα)	6.232 cm^{-1}
Diffractometer	XtaLAB P100
Radiation	CuKα (λ = 1.54187 Å)
	multi-layer mirror monochromated
Voltage, Current	40kV, 30mA
Temperature	-100.0°C
Detector Aperture	83.8 x 33.5 mm
Data Images	3983 exposures
Pixel Size	0.172 mm
$2\theta_{max}$	136.2°
No. of Reflections Measured	Total: 23224
	Unique: 1994 (R_{int} = 0.0614)
	Parsons quotients (Flack x parameter): 703
Corrections	Lorentz-polarization
	Absorption
	(trans. factors: 0.755 - 0.981)

Structure Solution	Direct Methods (SIR2011)
Refinement	Full-matrix least-squares on F^2
Function Minimized	$\Sigma\ w\ (Fo^2 - Fc^2)^2$
Least Squares Weights	$w = 1/ [\ \sigma^2(Fo^2) + (0.0723 \cdot P)^2$ $+ 0.1083 \cdot P\ ]$ where $P = (Max(Fo^2,0) + 2Fc^2)/3$
$2\theta_{max}$ cutoff	136.2^o
Anomalous Dispersion	All non-hydrogen atoms
No. Observations (All reflections)	1994
No. Variables	132
Reflection/Parameter Ratio	15.11
Residuals: R1 (I>2.00σ(I))	0.0405
Residuals: R (All reflections)	0.0414
Residuals: wR2 (All reflections)	0.1063
Goodness of Fit Indicator	1.104
Flack parameter (Parsons' quotients = 703)	-0.03(9)
Max Shift/Error in Final Cycle	0.000
Maximum peak in Final Diff. Map	$0.24\ e^-/Å^3$
Minimum peak in Final Diff. Map	$-0.20\ e^-/Å^3$

Appendix O: Crystal Data and Structural Refinement of Small Molecule X-ray of (*SsR*)-17 (Chapter 5)

Empirical Formula	$C_{17}H_{22}FN_3OS$
Formula Weight	335.44
Crystal Color, Habit	colorless, prism
Crystal Dimensions	0.200 X 0.100 X 0.030 mm
Crystal System	hexagonal
Lattice Type	Primitive
Lattice Parameters	a = 11.3879(17) Å c = 22.909(4) Å V = 2572.9(7) $Å^3$
Space Group	$P6_5$ (#170)
Z value	6
D_{calc}	1.299 g/cm^3
F_{000}	1068.00
μ(MoKα)	2.060 cm^{-1}
Diffractometer	Mercury70
Radiation	MoKα (λ = 0.71075 Å)
Voltage, Current	50kV, 16mA
Temperature	-180.0°C
Detector Aperture	70.0 x 70.0 mm
Pixel Size	0.068 mm
$2\theta_{max}$	50.6°
No. of Reflections Measured	Total: 16327 Unique: 3130 (R_{int} = 0.0377) Parsons quotients (Flack x parameter): 1370
Corrections	Lorentz-polarization Absorption (trans. factors: 0.867 - 0.994)

Structure Solution	Direct Methods (SIR2004)
Refinement	Full-matrix least-squares on F^2
Function Minimized	$\Sigma w (Fo^2 - Fc^2)^2$
Least Squares Weights	$w = 1/ [\sigma^2(Fo^2) + (0.0517 \cdot P)^2$ $+ 0.5035 \cdot P]$ where $P = (Max(Fo^2,0) + 2Fc^2)/3$
$2\theta_{max}$ cutoff	50.6^o
Anomalous Dispersion	All non-hydrogen atoms
No. Observations (All reflections)	3130
No. Variables	212
Reflection/Parameter Ratio	14.76
Residuals: R1 (I>2.00σ(I))	0.0350
Residuals: R (All reflections)	0.0369
Residuals: wR2 (All reflections)	0.0902
Goodness of Fit Indicator	1.040
Flack parameter (Parsons' quotients = 1370)	-0.00(3)
Max Shift/Error in Final Cycle	0.000
Maximum peak in Final Diff. Map	$0.59\ e^-/Å^3$
Minimum peak in Final Diff. Map	$-0.24\ e^-/Å^3$